Extractive Metallurgy of Rare Earths

C. K. Gupta
N. Krishnamurthy

CRC PRESS

Boca Raton London New York Washington, D.C.

Library of Congress Cataloging-in-Publication Data

Gupta, C. K.
Extractive metallurgy of rare earths / C.K. Gupta, N. Krishnamurthy.
p. cm.
Includes bibliographical references and index.
ISBN 0-415-33340-7 (alk. paper)
1. Rare earth metals--Metallurgy. I. Krishnamurthy, N. (Nagaiyar) II. Title.

TN799.R37G87 2004
669'.291--dc22 2004047817

International Standard Book Number 0-415-33340-7
Library of Congress Card Number 2004047817
Printed in the United States of America 1 2 3 4 5 6 7 8 9 0
Printed on acid-free paper

Foreword

The field of the rare earths is fascinating. Important research and development work continues globally to explore and establish ways and means to put the rare earths to use, individually and collectively, in the service of humankind. In terms of rare earth reserves, India ranks among the top ten countries of the world. Indian rare earth research and industry date back to the 1950s and have been based on the monazite available in the beach sands of the eastern and the southern parts of the country.

Rare earth research, development, and production continue to be among the important activities of our Department of Atomic Energy. Our accomplishments in these areas have derived strength and continue to do so from the work emerging from the Materials Group of Bhabha Atomic Research Centre in Mumbai. In this context, Dr. C.K. Gupta and colleagues deserve special mention for their continuing significant contributions to rare earth research and development. Dr. Gupta and his colleague, Dr. N. Krishnamurthy, are eminently qualified to author this book. I am pleased to have been invited to write this foreword. The authors prepared in 1992 a comprehensive review of the state of the art of extractive metallurgy of the rare earths. This paper was published in the *International Materials Reviews* and was well received. The authors' abiding interest in this field has found expression now in the present comprehensive volume.

The authors have done a commendable job and deserve praise for being extremely successful in fulfilling the need for such a volume. The vast amount of information that has been brought together and organized in this book had remained scattered throughout the scientific and engineering literature. Everyone involved with the extraction of the rare earths and the preparation of their numerous derivatives for a variety of specific applications will welcome this comprehensive publication. It should be useful to both experienced professionals and neophytes in the rare earth field.

I would like to mention that Dr. Gupta has authored about a dozen books in the field of chemical metallurgy of special metals and materials. The present book is yet another important addition to this impressive list.

Anil Kakodkar
Chairman, Atomic Energy Commission
India

Preface

A chronological account of the chemistry and metallurgy of the rare earths arranges into three eras or ages. The basis of this division is the availability and purity of the rare earth metals and materials and the scientific and engineering information about them. The period prior to 1950 may be called the "Dark Age." The next two decades were the "Age of Enlightenment." The period after the early 1970s may be considered the "Golden Age." In the first three decades of this golden era a number of remarkable advances and discoveries were made in the field of rare earths, and these have left an indelible mark on the global materials scenario. It is widely perceived that the future of the rare earths will be glorious and full of excitement, be it in science, technology, or in commercial utilization.

The rare earths are a community of 17 metallic elements, all but one occurring naturally (14 lanthanides and 2 associated elements). They are found in combination in mineral deposits widespread throughout the world. Notably large reserves exist in China, the U.S., and Australia. The word "rare" in "rare earths" arises more from the historical difficulty in separating and obtaining them as individual pure elements than from their inherent nonavailability. There have been major developments in the technologies for the production of separated high purity rare earths. Highly efficient separation technologies have been key to the exploitation of the rare earths in a wide range of now commonplace applications that have slowly become an inseparable part of modern living.

The scientists at Bhabha Atomic Research Centre in Mumbai, India are proud to be in the global mainstream of the scientific and technological research and development activities in the field of rare earth chemicals, metals, and alloys. The Indian rare earth program also includes commercial scale manufacture of rare earth products for domestic and international markets. Our long association with rare earth research motivated us some time ago to produce a review on the extractive metallurgy of the rare earths. This was published in the *International Materials Reviews*. This review provided a concise guide to access and retrieve information from the vast rare earth literature. It was, however, no substitute for a comprehensive book, which would serve as a reference text that stands on its own with detailed information on selected topics. With the publication of the review in 1992 and our progressively increasing involvement with the rare earths, our thinking gradually transformed into a commitment to preserve the available information on the extractive metallurgy of the rare earths in the form of a book. This thinking gathered further momentum because we found that although a voluminous literature in the form of numerous conference proceedings, a highly rated series of volumes on the physics and chemistry of the rare earth

elements (edited by Gschneidner and Eyring), and important trade publications and newsletters is available, all of these publications have objectives different from that of our book. We are not aware of any other text that covers the subject in the manner we have attempted here. We have worked to bring together all relevant matters concerning the extractive metallurgy of the rare earths and related information that, at present, remains scattered in a variety of forms of published literature.

This book has been organized into seven chapters. Chapter 1, *The Rare Earths*, provides the background information on the properties and applications of the rare earths and highlights the links of these aspects to the totality of rare earth extraction and processing techniques. The interesting sequence of the discovery of the rare earths is first presented, followed by a listing and discussion of the currently accepted values and information pertaining to the various properties of the rare earths. A comprehensive account of all major applications of the rare earths is then provided.

Chapter 2, *Resources*, presents in detail all currently available information on the world's rare earth resources, their location, quality, and quantity. The resource utilization trends and patterns from the times when the rare earths were first produced as a commodity up to the present are presented. Factors leading to the unequal availability of the rare earths are highlighted, and the world's rare earth resources position is dealt with in the context of current and projected demands.

Chapter 3, *Resources Processing*, incorporates a detailed account of the techniques for the processing of the various rare earth resources and the separation of individual rare earth elements. While placing a strong emphasis on the modern methods of solvent extraction and ion exchange, the salient features of the classical methods of rare earth separation are covered in detail. Various options for the treatment of the as-mined rare earth resources by physical and chemical beneficiation methods prior to separation are discussed.

Chapter 4, *Reduction*, deals with the techniques for converting the pure rare earth oxide intermediates to the metals. The numerous scientifically interesting and technologically challenging procedures for rare earth metal reduction are described in considerable detail. Chemical as well as electrochemical reduction methods have been used and the variety in the actual processes has come about because of the different physical properties of the individual rare earth elements. Particularly, the melting and boiling points of the elements dictate the type of process best suited for reduction. These aspects are discussed.

Chapter 5, *Refining*, is devoted to the purification of the rare earth metals. Elucidation of the unique properties of the rare earth elements has been possible only with the availability of these elements in very pure forms; therefore, major efforts have gone into the development of suitable techniques such as pyrovacuum treatment, zone melting, and electrotransport to prepare metals of high purity levels. The chapter covers these refining techniques as applied to different rare earth metals.

Chapter 6, *Rare Earth Materials*, is concerned with the techniques for the preparation of the numerous rare earth alloys and compounds and rare earth bearing materials. Among the materials described are the traditional products like misch metal and rare earth–iron–silicon alloys, as well as new materials like lanthanum–nickel alloys, permanent magnet materials based on samarium and neodymium, magnetostrictive and magnetocaloric materials. The procedures followed by various manufacturers of rare earth materials are outlined. The presentation also covers methods under investigation for newer materials.

Chapter 7 is an overview — a sojourn for the reader in the world of the rare earths. While going through this chapter one can develop a brief but significant acquaintance with the rare earths in their entirety.

In all the chapters the text is liberally supported by tables and figures. Key property

values and results have been listed in the tables, and the figures comprise line drawings of equipment and flowsheets of processes. References to original papers are extensively made in the text and all the references are grouped in one place at the end of the book. The reference list will serve as a very useful guide for those who want to refer to the original sources for more information on specifics.

We hope this book will be useful to professionals involved with the extraction, separation, concentration, and production of the rare earth metals, alloys, and chemicals. They include process, production, and regulatory staff engineers; management as well as research and development professionals; graduate students; and libraries attached to universities and R&D establishments.

We would like particularly mention the contributions of certain people who have been especially involved, with the preparation of this book. The work pertaining to the production of the typed version of the manuscript in its finished form was very efficiently handled by Poonam Khattar. All figures for the book were drawn by Yatin Thakur. We are grateful to the editorial department of G+B, particularly to Catherine Bewick in the initial stages and to Sally Cheney, Lloyd W. Black, and Matt Uhler in the latter stages for support- ing and encouraging us in the project.

Finally, we wish to dedicate this book to our wives, Chandrima Gupta and Kusuma Krishnamurthy, in gratitude for their unique contributions towards the completion of this work.

Bhabha Atomic Research Centre
Mumbai, India

C.K. Gupta
N. Krishnamurthy

August 15, 2004

Acknowledgment

The effort to bring out this book on the extractive metallurgy of rare earths has been greatly supported by many wonderful people. The list is too long. However, there have been tremendous positive contributions to building this work from Mrs. Janie Wardle of Taylor & Francis Books and Mr. Victor D. Selivanov, Production Coordinator, Izdatelsky Dom FIAN, Moscow. We gratefully acknowledge their great cooperation and support.

It is our pleasure to acknowledge Mr. Chiradeep Gupta, Scientist from Bhabha Atomic Research Centre, and his wife Mrs. Nita Gupta, who contributed considerably to the proof correction work.

Several figures and tables that appear in this book have originally appeared in publications by Elsevier, The Electrochemical Society, John Wiley and Sons, Wiley-VCH, ASM International, The Minerals, Metals and Materials Society, The Institute of Materials, Minerals and Mining, American Powder Metallurgical Institute, National Technical Information Service, Metal Rare Earth Ltd. and American Chemical Society. We are grateful to these institutions and other authors who very graciously gave permission to reproduce matter from their publications in this book.

Bhabha Atomic Research Centre
Mumbai, India

C.K. Gupta
N. Krishnamurthy

Contents

Foreword
Preface
Acknowledgment

Chapter 1 **The Rare Earths**
1.1 INTRODUCTION
1.2 DISCOVERY
1.3 SPECIAL CHARACTERISTICS
1.3.1 Electronic Configuration
1.3.2 Lanthanide Contraction
1.3.3 Basicity
1.4 PROPERTIES
1.4.1 Melting Point
1.4.2 Boiling Point
1.4.3 Allotropes
1.4.4 Resistivity
1.4.5 Magnetic Properties
1.4.6 Spectral Properties
1.4.7 Mechanical Properties
1.5 REACTIVITY
1.5.1 Air/Oxygen
1.5.2 Refractories
1.5.3 Nitrogen
1.5.4 Hydrogen
1.5.5 Carbon
1.5.6 Silicon
1.5.7 Sulfur, Selenium, Phosphorus
1.5.8 Refractory Metals
1.5.9 Acids and Bases
1.5.10 Water
1.6 AQUEOUS SYSTEMS

1.6.1 The Trivalent State
1.6.2 Complexes
1.6.3 The Tetravalent State
1.6.4 The Divalent State
1.7 APPLICATIONS
1.7.1 Metallurgy
1.7.2 Magnets
1.7.3 Terfenol
1.7.4 Magnetic Refrigeration
1.7.5 Magnetooptic Materials
1.7.6 Ceramics
1.7.7 Electronics
1.7.8 Chemical
1.7.9 Optical
1.7.10 Phosphors
1.7.11 Nuclear
1.7.12 Hydrogen Storage
1.7.13 Superconductor
1.7.14 Miscellaneous
1.8 SUMMARY

Chapter 2 **Resources of Rare Earths**
2.1 INTRODUCTION
2.2 CRUSTAL ABUNDANCE
2.3 MINERALS
2.3.1 Bastnasite
2.3.2 Monazite
2.3.3 Xenotime
2.3.4 Allanite
2.3.5 Apatite
2.3.6 Brannerite
2.3.7 Eudialyte
2.3.8 Euxenite, Fergusonite, Florencite, Gadolinite, and Loparite
2.3.9 Perovskite
2.3.10 Pyrochlore
2.3.11 Zircon
2.3.12 Others
2.3.13 Scandium Minerals
2.3.14 Promethium
2.4 RARE EARTH DEPOSITS
2.4.1 Primary and Secondary
2.4.2 Carbonatites
2.4.3 Pegmatites
2.4.4 Hydrothermal Deposits
2.4.5 Weathered Deposits
2.4.6 Placers
2.4.7 Distribution
2.5 RESOURCES AND RESERVES

2.6 OCCURRENCES
2.6.1 Argentina
2.6.2 Australia
2.6.3 Bangladesh
2.6.4 Brazil
2.6.5 Canada
2.6.6 China
2.6.7 Germany
2.6.8 India
2.6.9 Indonesia
2.6.10 Japan
2.6.11 Malaysia
2.6.12 Malawi
2.6.13 Mozambique
2.6.14 Myanmar
2.6.15 New Zealand
2.6.16 Peru
2.6.17 South Africa
2.6.18 Sri Lanka
2.6.19 Taiwan
2.6.20 Thailand
2.6.21 Turkey
2.6.22 United States
2.6.23 Former USSR
2.6.24 Venezuela
2.6.25 Vietnam
2.6.26 Zaire
2.7 BY-PRODUCTS AND CO-PRODUCTS
2.8 WORLD RARE EARTH PRODUCTION AND AVAILABILITY
2.8.1 Brazil
2.8.2 India
2.8.3 United States
2.8.4 Australia
2.8.5 China
2.8.6 Former Soviet Union
2.8.7 South Africa
2.8.8 Canada
2.8.9 Malaysia
2.8.10 Thailand
2.8.11 Sri Lanka
2.8.12 Zaire and Madagascar
2.9 RARE EARTH PRODUCTION POTENTIAL
2.10 FORECAST
2.11 SUMMARY

Chapter 3 **Resource Processing**
3.1 INTRODUCTION
3.2 MINING

3.2.1 Hard Rock Deposits
3.2.2 Placer Deposits
3.3 PHYSICAL BENEFICIATION
3.3.1 Monazite
3.3.2 Bastnasite
3.3.3 Bayan Obo Ore
3.4 CHEMICAL TREATMENT
3.4.1 Monazite
3.4.2 Bastnasite
3.4.3 Chlorination
3.4.4 Xenotime
3.4.5 Elliot Lake Uranium Ore
3.4.6 Gadolinite
3.4.7 Euxenite
3.4.8 Loparite, Pyrochlore, Fergusonite, and Samarskite
3.4.9 Apatite
3.5 SEPARATION PROCESSES
3.5.1 Selective Oxidation
3.5.2 Selective Reduction
3.5.3 Fractional Crystallization
3.5.4 Fractional Precipitation
3.5.5 Ion Exchange
3.5.6 Solvent Extraction
3.6 SCANDIUM
3.7 SUMMARY

Chapter 4 **Reduction**
4.1 INTRODUCTION
4.2 FUNDAMENTALS
4.3 METALLOTHERMY
4.4 PREPARATION OF RARE EARTH CHLORIDES
4.4.1 Preparation of Hydrated Rare Earth Chloride
4.4.2 Dehydration of Hydrated Rare Earth Chlorides
4.4.3 Dry Methods
4.4.4 Purification of Rare Earth Chlorides
4.5 REDUCTION OF RARE EARTH CHLORIDES
4.5.1 Early Attempts
4.5.2 Reduction in a Refractory Bomb
4.5.3 Reduction in Tantalum Crucible
4.5.4 Intermediate Alloy Processes
4.5.5 Kroll Type Processes
4.6 PREPARATION OF RARE EARTH FLUORIDES
4.6.1 Wet Method
4.6.2 Dry Methods
4.6.3 Purification of Rare Earth Fluorides
4.7 REDUCTION OF RARE EARTH FLUORIDES
4.7.1 Lithium Reduction
4.7.2 Calcium Reduction (Ames Process)

4.7.3 Intermediate Alloy Process
4.7.4 Preparation of Scandium
4.7.5 Reduction of Samarium, Europium, and Ytterbium Halides
4.8 OXIDE REDUCTION PROCESSES
4.8.1 Reduction–Distillation—Lanthanothermy
4.8.2 Reduction–Distillation—Other Reductants
4.9 NEW REDUCTION PROCEDURES
4.9.1 Direct Preparation of Gadolinium Metal Powder
4.9.2 Metallothermic Reduction in Molten Salt
4.10 CARBOTHERMIC REDUCTION
4.11 ELECTROLYTIC PRODUCTION OF RARE EARTH METALS
4.11.1 Chloride Electrolysis
4.11.2 Electrowinning at Room Temperature
4.11.3 Electrowinning Solid Metal Deposits
4.11.4 *In situ* Preparation of Electrolyte
4.11.5 Commercial Electrowinning from Rare Earth Chlorides
4.11.6 Oxide–Fluoride Electrolysis
4.12 RECOVERY OF RARE EARTH METALS AS ALLOYS
4.12.1 Electrolysis of Chlorides
4.12.2 Electrolysis of Oxide–Fluoride Melts
4.13 CURRENT EFFICIENCY
4.14 SUMMARY

Chapter 5 **Refining Rare Earth Metals**
5.1 INTRODUCTION
5.2 ORIGIN OF IMPURITIES
5.2.1 Starting Materials
5.2.2 Crucible
5.2.3 Environment
5.3 METHODS FOR IMPURITY REMOVAL
5.4 PYROVACUUM TREATMENTS
5.4.1 Distillation
5.4.2 Removal of Halogens/Halides
5.4.3 Degassing
5.5 PYROVACUUM TECHNIQUES
5.5.1 Lanthanum, Cerium, Praseodymium, and Neodymium
5.5.2 Yttrium, Gadolinium, Terbium, and Lutetium
5.5.3 Scandium, Dysprosium, Holmium, Erbium, and Lutetium
5.5.4 Samarium, Europium, Thulium, and Ytterbium
5.6 ELECTROREFINING
5.6.1 Yttrium
5.6.2 Gadolinium
5.6.3 Cerium
5.7 ULTRAPURIFICATION METHODS
5.8 ZONE REFINING
5.8.1 Preliminary Studies
5.8.2 Lanthanum, Gadolinium, and Terbium
5.8.3 Lanthanum, Cerium, and Gadolinium

5.9 SOLID STATE ELECTROTRANSPORT
5.9.1 SSE System
5.9.2 Residual Resistivity Ratio
5.9.3 Lanthanum
5.9.4 Praseodymium
5.9.5 Neodymium
5.9.6 Gadolinium
5.9.7 Terbium
5.9.8 Yttrium
5.9.9 Dysprosium and Holmium
5.9.10 Erbium
5.9.11 Lutetium
5.9.12 Samarium
5.10 ZONE REFINING AND ELECTROTRANSPORT
5.10.1 Neodymium
5.10.2 Gadolinium
5.11 IODIDE REFINING
5.12 MISCELLANEOUS PROCESSES
5.13 SUMMARY

Chapter 6 **Rare Earth Materials**
6.1 INTRODUCTION
6.2 MISCH METAL
6.2.1 Preparation of Mixed Rare Earth Chlorides
6.2.2 Electrolysis of Chlorides
6.2.3 Electrolysis of Oxide–Fluoride Melts
6.2.4 Ames Process
6.2.5 Thermal Reduction Process
6.3 RARE EARTH–SILICON–IRON ALLOYS
6.3.1 Reno (USBM) Process
6.3.2 BARC Process
6.3.3 Baotou Process
6.4 RARE EARTH–MAGNESIUM–SILICON ALLOYS
6.5 RARE EARTH–ALUMINUM–ZINC ALLOY
6.6 YTTRIUM–ALUMINUM ALLOY
6.7 PERMANENT MAGNET MATERIALS
6.8 RARE EARTH–Co PERMANENT MAGNETS
6.8.1 Preparation
6.8.2 Preparation of Magnets
6.9 NEODYMIUM–IRON–BORON MAGNETS
6.9.1 Production of Nd–Fe–B Alloys
6.9.2 Production of Nd–Fe–B Magnets
6.10 Sm–Fe–N MAGNETS
6.11 NANOCOMPOSITE PERMANENT MAGNET MATERIALS
6.12 TERFENOL-D
6.13 MAGNETIC REFRIGERANTS
6.14 THIN FILM DEPOSITION PROCESSES
6.14.1 Bubble Domain Memory Materials

6.14.2 Magnetooptic Storage Media
6.15 $LaNi_5$
6.16 SUPERCONDUCTORS
6.17 SUMMARY

Chapter 7 **A Sojourn in the World of Rare Earths**
7.1 THE PERIODIC TABLE OF ELEMENTS
7.2 RADIATION
7.3 LANTHANIDE AND ACTINIDE ELEMENTS
7.4 PROCESSING RARE EARTHS
7.5 APPLICATIONS OF RARE EARTHS
7.6 METHODS OF PREPARING ELEMENTAL AND COMPOUND FORMS OF RARE EARTHS
7.7 CONCLUSION

REFERENCES

CHAPTER 1

The Rare Earths

1.1 INTRODUCTION

The term "rare earths" denotes the group of 17 chemically similar metallic elements, including scandium, yttrium, and the lanthanides (Spedding 1978). The lanthanides are the series of elements with atomic numbers 57 to 71, all of which, except promethium, occur in nature. The rare earth elements, being chemically similar to one another, invariably occur together in the minerals and behave as a single chemical entity. Thus, the discovery of the rare earths themselves occurred over nearly 160 years from 1788 to 1941 (Szabadvary 1988, Weeks 1956). Then followed the problem of separating them from one another for scientific study or industrial use. This has been one of the most challenging tasks of rare earth technology. While the attempts in separating the rare earths began with the work of Mosander during 1839–1841, much of the effort directed to the separation of various rare earths occurred from 1891 to 1940. During this period, from the available mixed and separated compound intermediates many rare earth alloys and metals were prepared and commercial applications were developed for mixed or roughly separated rare earths. The following two decades, 1940–1960, were the most productive in terms of effective process development. Most important were the development of modern separation methods, which resulted in the availability of sufficient quantities of pure individual rare earth compounds (Powell and Spedding 1959) for the investigation of reduction processes to prepare pure metals and alloys (Beaudry and Gschneidner 1978) and evaluation of their properties. Beginning in the 1960s, much progress was made in the large scale production of purer rare earths, in the identification of newer properties, and in their use in a variety of important commercial applications. The usable forms of rare earths encompass naturally occurring oxide mixtures, and products synthesized from them, high purity individual metals, alloys, and compounds. The current annual demand for rare earths is in the range of 80,000 to 100,000 metric tons calculated as rare earth oxides. It has also been estimated (Jackson and Christiansen 1993) that the world rare earth reserves are large and sufficient to support the present level of consumption for many centuries to come.

This chapter is a survey of the history, properties, and applications of the rare earths and highlights the background to their current status as materials of interest in the laboratory and products of use in technology and industry.

Table 1.1 Discovery of rare earth elements

Year	Mineral/element	Discovered by	Named by	Confirmed by	Origin of name
1784	Gadolinite	C.A. Arrhenius	A.G. Ekeberg		Person: J. Gadolin
1794	Yttria	J. Gadolin	A.G. Ekeberg	M. Delafontaine	Place: Ytterby
1751	Cerite	A.F. Cronstedt	J.J. Berzelius, W. Hisinger		Asteroid: Ceres
1804	Cerium	J J. Berzelius, W. Hisinger	J.J. Berzelius, W. Hisinger		Asteroid: Ceres
1839	Samarskite	M.H. Klaproth, G. Rose			Person: Col. Samarsky
1839	Lanthanum	C.G. Mosander	J.J. Berzelius		Chemical behavior: to escape notice
1842	Didymium	C.G. Mosander	C.G. Mosander		Chemical behavior: twins
1843	Erbium (known as terbium after 1864)	C.G. Mosander	C.G. Mosander	M. Delafontaine, J.L. Soret, H.E. Roscoe, A.J. Schuster, J.G. Marignac, J.L. Smith	Place: Ytterby
1843	Terbium (known as erbium after 1864)	C.G. Mosander	C.G. Mosander	M. Delafontaine, J.L. Smith	Place: Ytterby
1878	Ytterbium	J.C. Marignac	J.C. Marignac	M. Delafontaine, L.F. Nilson	Chemical behavior: between erbium and yttrium
1879	Samarium	P.E.L. De Boisbaudran	P.E.L. De Boisbaudran	P.T. Cleve	Mineral: samarskite
1879	Scandium	L.F. Nilson	L.F. Nilson		Place: Scandinavia
1879	Thulium	P.T. Cleve	P.T. Cleve		Place: Scandinavia ("Thule" is her ancient name)
1879	Holmium	P.T. Cleve	P.T. Cleve	J.L. Soret, P.E.L. De Boisbaudran	Place: Stockholm (medieval name)
1886	Dysprosium	P.E.L. De Boisbaudran	P.E.L. De Boisbaudran		Chemical behavior: difficult to access
1886	Gadolinium	J.C. Marignac	J.C. Marignac	M. Delafontaine, J.L. Soret	Person: J. Gadolin
1886	Praseodymium	C.A. von Welsbach	C.A. von Welsbach	A. Bettendorf	Chemical behavior: green twin
1886	Neodymium	C.A. von Welsbach	C.A. von Welsbach	A. Bettendorf	Chemical behavior: new twin
1901	Europium	E. Demarcay	E. Demarcay	G. Urbain	Place: Europe

Table 1.1 (continued)

Year	Mineral/element	Discovered by	Named by	Confirmed by	Origin of name
1907	Lutetium	G. Urbain, C.A. von Welsbach	G. Urbain		Place: Paris (Roman name of Paris)
1947	Promethium	J.A. Marinsky, L.E. Glendenin, C.D. Coryell	J.A. Marinsky, L.E. Glendenin, C.D. Coryell		Legend: Prometheus

1.2 DISCOVERY

The discovery of rare earth elements began in 1787 and went on for about 160 years to conclude in the 1940s (Szabadvary 1988, Weeks 1956). All the naturally occurring rare earths and all but one of all the rare earth elements had been discovered by the turn of the century and the discovery of the remaining one rare earth had to wait until the discovery of nuclear reactions.

The rare earth elements and their discoverers are listed in Table 1.1 and charted in Figure 1.1. The activity started at Ytterby, a village near Stockholm in Sweden. Ytterby is the site of a quarry that had been the source of many unusual minerals containing rare earths.

In 1787, Carl Axel Arrhenius, a lieutenant of the Swedish Royal Army and also an amateur mineralogist, found a black mineral, until then not mentioned by anyone, in Ytterby. The mineral was analyzed by the Finnish chemist Johan Gadolin in 1794. Gadolin found iron and silicate as constituents of the mineral and also a "new earth," which accounted for 30% of the mineral. The discovery of the new earth by Gadolin was confirmed by the Swedish chemist Anders Gustaf Ekeberg during the following year. Ekeberg found that the mineral also contained beryllium, a metal that had only just been discovered by the French chemist Nicolas Louis Vanquelin. The mineral found by Arrhenius turned out to be an iron–beryllium–silicate. Ekeberg gave the name "yttria" to the new earth discovered by Gadolin and also named the mineral "gadolinite."

Until the first decade of the nineteenth century, "earths" were universally considered to be elements. The fact that earths were not elements but compounds was first stated by the Hungarian chemist Antal Ruprecht but conclusively proved by Sir Humphrey Davy who electrolyzed melts of earths and obtained metals from them. In the first decade of the nineteenth century, Davy separated numerous metals such as calcium, strontium, and barium from alkaline earths and from then on the metals were distinguished from earths. For example, chemists began to name yttrium for the metal instead of yttria even though the metal itself had not been produced in the pure state.

Interestingly, another new mineral, which was later shown to contain an unknown earth, had been discovered by A.F. Cronstedt in the Bastnäsgrube mine close to Rydderhyatten in Sweden in 1751, before gadolinite was discovered in Ytterby. This mineral was investigated by Jöns Jakob Berzelius and Wilhelm Hisinger in Sweden and independently by Martin Heinrich Klaproth in Germany. They reported simultaneously, in 1804, the discovery of a new element in the mineral. Klaproth was still considering "earths" as elements and named the new earth "ochroite earth," while Berzelius and Hisinger stated

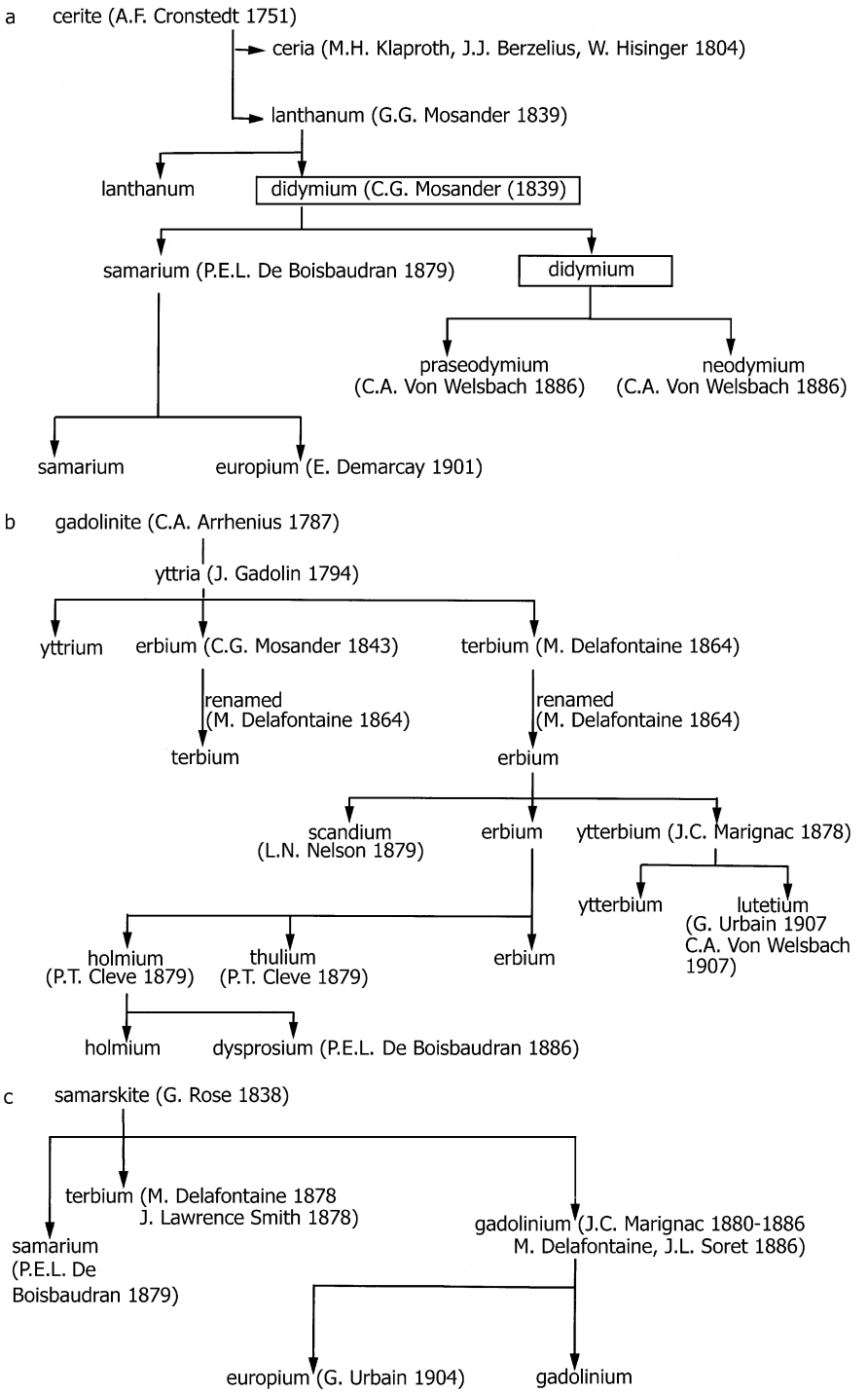

Figure 1.1 Discovery of rare earth elements: (a) cerite sequence, (b) gadolinite sequence, (c) samarskite sequence.

that the earth was the oxide of a new element. They named the element "cerium" after the asteroid Ceres that had been discovered only three years earlier, in 1801. The mineral that contained cerium was named "cerite."

Carl Gustaf Mosander, an associate of Berzelius, through his patient and painstaking investigations established that both yttria and ceria were complex in nature and contained new elements. In 1839 Mosander separated a new element from ceria. Berzelius suggested to Mosander the name "lanthanum" for the new element (in Greek "lanthano" means "to escape notice"). Mosander believed that the lanthanum separated by him was not a pure element but might contain yet another new element. Continuing his experiments, he succeeded in 1842 in detecting that new element. He named the new element "didymium." The element didymium, which was present in cerite, tracked lanthanum in some experiments while it tracked cerium in some other experiments. It therefore got the name from the Greek word "didymos," meaning twins, to denote that it accompanied cerium and lanthanum as a twin in the cerium mineral.

The possibility of gadolinite containing new elements in addition to yttrium was already indicated by the works of Heinrich Rose and Berzelius before Mosander turned his attention to this mineral. Reporting his results in 1843, Mosander mentioned not one but two more new elements in gadolinite. He named them "erbium" and "terbium."

Beginning in the 1850s a new analytical aid, spectral analysis, began to be used to identify and confirm the existence of new elements. In 1864, Marc Delafontaine, a Swiss-American chemist used spectroanalytical identification to unequivocally prove and confirm the existence of yttrium, terbium, and erbium. He interchanged, probably unintentionally, the names given by Mosander for terbium and erbium, and the interchanged names have persisted ever since. What was called erbium by Mosander became known as terbium and what was named terbium by Mosander came to be known as erbium.

There was considerable confusion surrounding terbium and erbium in the 1860s. Delafontaine himself became doubtful while O. Popp, Johan Fridrik Bahr, and Robert Wilhelm Bunsen denied the existence of terbium while accepting that erbium existed. Charles Augustus Young, a U.S. scientist, demonstrated in 1872 the existence of erbium in the solar spectrum, and the existence of erbium was doubted no more. The matter of terbium was finally resolved by Delafontaine and the Swiss chemist Jean Charles Marignac by 1877–78. Delafontaine separated the terbium oxide from the mineral "samarskite," which had been discovered in 1838 by the German mineralogist Gustav Rose. In 1878, J. Lawrence Smith, a U.S. chemist and mineralogist, also reported the existence of terbium in samarskite. In the same year Marignac confirmed the presence of terbium in gadolinite, the mineral in which Mosander had originally found the element. Further confirmations to the existence of terbium were provided by the spectral analysis reports of J.L. Soret in 1880 as well as by Sir Henry Enfield Roscoe and A.J. Schuster in 1882.

Delafontaine reported in 1878 that the absorption spectrum of didymium separated from samarskite was not fully identical with the absorption spectrum of didymium separated from cerite. He suspected that didymium was not a single element. Interestingly, in 1879, the French chemist Paul Emile Lecoq de Boisbaudran disproved Delafontaine's report on the spectra but did find a new element in samarskite. He named the element "samarium" after the mineral samarskite in which it was detected.

Investigating gadolinite, Marignac had not only confirmed the existence of terbium in it but also was looking for more new elements in the mineral. He worked on the erbium fraction obtained from the mineral and separated an oxide and salts that were different from

erbium in both chemical and spectral characteristics. In 1878 Marignac named the new element "ytterbium" because it stood between yttrium and erbium in its properties. In the same year, Marignac's ytterbium was also identified by Delafontaine in an yttrium niobate mineral called "sipylite," which had been discovered in Virginia (U.S.A.) by John William Mallet in 1877.

The experiments on erbium described by Marignac were repeated in Sweden by Lars Frederick Nilson, and he also confirmed the existence of ytterbium and the statements of Marignac regarding it. Proceeding further, through an exceedingly intricate fractioning procedure, Nilson finally obtained a basic nitrate from gadolinite. He dissolved the salt in nitric acid and the solution yielded a weak absorption line in the red and in the green spectrum. It also precipitated as an oxalate. Nilson considered this a new element and in 1879 named it "scandium," after Scandinavia.

In Sweden, Per Theodor Cleve investigated the erbium fraction remaining after the separation of ytterbium. Based on a spectrum taken by the Swedish physicist Tobias Robert Thalén, Cleve suspected that the erbium fraction could contain more elements. Proceeding by chemical separation and spectral analysis, he identified the existence of two new elements and named them "thulium," after the legendary old name of Scandinavia, and "holmium," after the medieval Latin name of Stockholm. Before Cleve reported his discovery of the new elements in 1879, the Swiss chemist Soret had indicated, on the basis of absorption spectrometry, the possibility that an unknown element was present in the erbium sample given to him by Marignac. Soret later stated that the unknown element mentioned by him corresponded to Cleve's holmium. The statements and discoveries of Soret and Cleve were confirmed in 1879 by Lecoq de Boisbaudran.

In 1886, Boisbaudran, following an elaborate, intricate, and wearisome method for the chemical separation and spectroscopic and fluorescence studies of gadolinite rare earth elements, concluded that the holmium discovered by Cleve contained another new element. He named it "dysprosium."

Earlier, in 1880, Marignac investigated samarskite by chemical separations. He obtained the nitrate of a substance that differed in many respects from the other elements then known. He tentatively named it "Yα" and after more investigations by him as well as by Delafontaine and Soret, in 1886, proposed the name gadolinium for Yα.

In 1885 Carl Auer von Welsbach, an Austrian chemist, began investigations on didymium. By then, it was already widely suspected that didymium might not be a single element, but chemical separation efforts to substantiate the presence of the new element were unsuccessful. Auer used fractional crystallization instead of the hitherto applied fractional precipitation, to separate didymium. In 1886, he succeeded in obtaining two fractions of didymium ammonium nitrate. He further investigated them by absorption and spark spectrometry and concluded that the fractions belonged to different elements. He named the elements "praseodidymium" and "neodidymium." In course of time, "di" disappeared from these names and they came to be known as praseodymium and neodymium. Mosander's naming of the "element" didymium, meaning twins, was indeed prophetic.

Auer's discovery of praseodymium and neodymium was questioned by Henry Becquerel in 1887, but in 1890 Auer's experiments were repeated by A. Bettendorf, and the existence of praseodymium and neodymium was confirmed. The unseparated mixture of praseodymium and neodymium, however, continued to be referred to by the name didymium.

Samarium, discovered in 1879 in the original didymium by Boisbaudran, was also confirmed as a new element by Cleve. In 1886, the French chemist Eugene Demarcay

announced that he separated a new element from samarium. He substantiated his claim only 15 years later in 1901 when he succeeded in preparing it as a pure substance in the form of the double nitrate with magnesium. He named the element "europium." In 1904, europium was also separated from gadolinium by the French chemist Georges Urbain.

In 1905 Auer mentioned that Marignac's ytterbium probably contained new elements. Two years later, he published experimental results supporting his doubt and stated that ytterbium consisted of two elements. He named them "aldebaranium" and "cassiopeium." Almost simultaneously, Urbain also reported that ytterbium consisted of two elements, which he named "neoytterbium" and "lutetium." In course of time the name ytterbium (for neoytterbium) and lutetium survived. The name lutetium was derived from the ancient Roman name of Paris.

With the discovery of lutetium, the story of the discovery of the naturally occurring rare earth elements, which lasted for well over a century, ended.

Even though all the naturally occurring rare earth elements had been discovered, the discoverers themselves did not realize that fact. For example, both Auer and Urbain continued to work on reporting new elements. But that was not to be. The theoretical explanation of the great similarity of the properties of the rare earth elements and also the maximum limit for their number came in later years with the development of the atomic theory. Atomic numbers were introduced by van den Broek in 1912, and Henry Growyn Jeffreys Mosley discovered in 1913 a mathematically expressible relationship between the frequency of x-rays emitted by the element serving as anticathode in the x-ray tube and its atomic number. Urbain subjected all the rare earth elements discovered in later times to the Mosley check, to determine their atomic numbers and thus confirm that they were true elements. The range of rare earth elements, from lanthanum with atomic number 57 to lutetium with atomic number 71, was established. Amongst these, the element with atomic number 61 was yet unknown.

In 1941, researchers at the Ohio State University irradiated praseodymium, neodymium, and samarium with neutrons, deuterons, and alpha particles and produced several new radioactivities, which were most probably those of element 61. The formation of element 61 was also claimed in 1942 by Wu and Segre (1942). Chemical proof of the formation of element 61 was provided in 1945 at the Clinton Laboratory (now the Oak Ridge National Laboratory) by Marinsky, Glendlin, and Goryell (1947), who used ion exchange chromatography to obtain the element from the products of fission of uranium and of neutron bombardment of neodymium. They named the element "promethium" after Prometheus, who stole fire from the Gods for man (Szabadvary 1988). Promethium does not occur in nature.

1.3 SPECIAL CHARACTERISTICS

The close chemical similarity of all the rare earth elements is, first of all, displayed in their occurring together in nature and further by the fact that it took nearly 160 years of efforts by many great names in science to isolate and identify them. It has been borne out by experimental evidence that striking similarities among the chemical properties of the elements and their compounds is the consequence of strikingly similar electronic configurations.

1.3.1 Electronic Configuration

The electronic configurations of the rare earth elements are listed in Table 1.2. Scandium, yttrium, and lanthanum are the elements that begin three successive series of transition elements. Their valence electron configurations are $ns^2(n-1)d^1$ with $n = 4$, 5, and 6, respectively. They have no *f* electrons. The 14 elements following lanthanum, namely, cerium to lutetium, are the lanthanides (lanthanum like) and have valence electron configurations represented by $6s^25d^14f^{n-1}$ or $6s^24f^n$. The 5*d* and 4*f* electrons have similar energies in the neutral rare earth atoms, and this is the reason for two typical electronic configurations. The elements cerium to lutetium constitute the series known as the "inner transition" elements or "*f*" elements. It must, however, be stated that the electronic configurations given are not known with complete certainty because of the great complexity of the electronic spectra of these atoms and the consequent difficulty in analysis.

The ionization potentials of rare earth elements are comparatively low. The elements are therefore highly electropositive and form compounds that are essentially ionic in nature. While all the rare earths form M^{3+}, some of them also occur in +2 and +4 states. These states are always less stable than the +3 state. The occurrence of +2 and +4 states in certain rare earths, which is of considerable importance in rare earths extractive metallurgy, is related to their electronic structures and ionization potentials. Special stability is apparently associated with an empty, half filled, and filled "*f*" shell configurations.

The rare earths scandium, yttrium, and lanthanum form only the M^{3+} ions because this results in the inert gas configuration. Lutetium and gadolinium form only the M^{3+} ions because they then attain the stable $4f^{14}$ and $4f^7$ configurations, respectively. The most stable M^{2+} and M^{4+} ions are formed by those rare earths that can thereby attain f^0, f^7, or f^{14} configuration. Thus, Ce^{4+} and Tb^{4+} attain the f^0 and f^7 configurations, respectively, and Eu^{2+} and Yb^{2+} attain the f^7 and f^{14} configuration, respectively. In other words, the special stability of the f^0, f^7, and f^{14} configurations is an important factor in determining the existence of oxidation states other than +3 in the rare earths. However, there could be other thermodynamic and kinetic factors that are of equal or greater importance in determining the stability of the oxidation states.

1.3.2 Lanthanide Contraction

The term "lanthanide contraction" is used to denote the significant and steady decrease in the size of atoms and ions with the increase in atomic number as the lanthanide series is crossed from lanthanum to lutetium. Thus, as given in Table 1.2 and Figure 1.2, lanthanum has the greatest and lutetium the smallest radius. The cause of the contraction is stated to be the imperfect shielding of one electron by another in the same subshell. As one proceeds from lanthanum to lutetium, both the nuclear charge and the number of 4*f* electrons increase by one at each element. Owing to the shape of the orbitals, the shielding of one 4*f* electron by another is very imperfect. Atomic nucleus is poorly shielded by the highly directional 4*f* electrons and, as a result, at each increase of the atomic number the effective nuclear charge experienced by the 4*f* electron increases, resulting in a reduction in the size or contraction of the entire 4*f* shell. With successive increase in atomic number, such contractions accumulate and result in the steady decrease in size. This is the famous lanthanide contraction.

Lanthanide contraction is the root cause of many features of the rare earths' chemistry. The chemistry of lanthanides is predominantly ionic and is determined primarily by the size

Table 1.2 Properties of rare earth elements

Properties	Scandium	Yttrium	Lanthanum	Cerium	Praseodymium	Neodymium	Promethium	Samarium	Europium
Atomic properties									
Atomic number	21	39	57	58	59	60	61	62	63
Atomic weight	44.95591	88.90585	138.9055	140.115	140.90765	144.24	(145)	150.36	151.965
Crystal structure	cph <1337 bcc >1337	cph <1478 bcc >1478	dcph <1478 fcc >310 and <865 bcc >865	fcc <−148 dcph >−148 and <139 fcc >139 and <726 bcc >726	dcph <795 bcc >795	dcph <863 bcc >863	dcph <863 bcc >890	rhomb <734 cph >734 and <922 bcc >922	bcc
Atomic volume, cm^3/mol at 24°C	15.059	19.893	22.602	17.2	20.803	20.583	20.24	20.000	28.979
Density, g/cm^3 at 24°C	2.989	4.469	6.146	8.16	6.773	7.008	7.264	7.520	5.244
Conduction electrons	3	3	3	3, 3.1	3	3	3	3	2
Valence in aqueous solution	3	3	3	3, 4	3	3	3	3, 2	3, 2
Color in aqueous solution, RE^{3+}	colorless	colorless	colorless	colorless	yellow green	rose	pink	yellow Sm^{2+} is deep red	colorless Eu^{2+} is pale yellow
Main absorption bands of RE^{3+} ion in aqueous solution in the range 200 to 1000 nm	–	–	–	210.5, 222.0, 238.0, 252.0	444.5, 469.0, 482.2, 588.5	354.0, 521.8, 574.5, 739.5, 742.0, 797.5, 803.0, 868.0	548.5, 568.0, 702.5, 735.5	362.5, 374.5, 402.0	375.5, 394.1
Color of oxide, RE_2O_3		white	white	off white (CeO_2)	yellow green black (Pr_6O_{11}) pale blue (Pr_2O_3)	pale blue	pink	cream	white
Number of isotopes: natural (artificial)		1 (14)	2 (19)	4 (15)	1 (14)	7 (7)	(15 to 18)	7 (11)	2 (16)

Table 1.2 (continued)

Properties	Scandium	Yttrium	Lanthanum	Cerium	Praseodymium	Neodymium	Promethium	Samarium	Europium
Thermal neutron absorption cross section: for naturally occurring mixture of isotopes, single isotopes (mass number of isotope), barns/atom		1.31	8.9	0.73	11.6	50	–	5600 66000 (149)	4300 9000(151) 5000(152) 420(153) 1500(154) 13000(155)
Ionization potential, eV/g·atom		6.6	5.61	5.65	5.76	6.31	–	5.6	5.67
Electronegativity		1.177	1.117	(+3) 1.123 (+4) 1.43	1.130	1.134	1.139	1.145	(+2) 0.98 (+3) 1.152
Thermal, electrical, and magnetic properties									
Melting point, °C	1541	1522	918	798	931	1021	1042	1074	822
Boiling point, °C	2831	3338	3457	3426	3512	3068	–	1791	1597
Heat of fusion, kJ/mol	14.1	11.4	6.20	5.46	6.89	7.14	(7.7)	8.62	9.21
Heat of sublimation at 25°C, kJ/mol	377.8	424.7	431.0	422.6	355.6	327.6	(348)	206.7	175.3
Allotropic transformation temperature, °C	cph-bcc 1337	cph-bcc 1478	dcph-fcc 310 fcc-bcc 865	fcc-dcph –148 dcph-fcc 139 fcc-bcc 726	dcph-bcc 795	dcph-bcc 863	dcph-bcc 890	rhomb-cph 734 cph-bcc 922	–
Heat of transformation, kJ/mol	cph-bcc 4.00	cph-bcc 4.99	dcph-fcc 0.36 fcc-bcc 3.12	fcc-dcph – dcph-fcc 0.05 fcc-bcc 2.99	dcph-bcc 3.17	dcph-bcc 3.03	dcph-bcc (3.0)	rhomb-cph 0.2 cph-bcc 3.11	–
Heat capacity at 298K, C_p, J/mol·K	25.5	26.5	27.1	26.9	27.4	27.4	(27.3)	29.5	27.7

Table 1.2 (continued)

Properties	Scandium	Yttrium	Lanthanum	Cerium	Praseodymium	Neodymium	Promethium	Samarium	Europium
Standard entropy, S^0_{298}, J/mol·K	34.6	44.4	56.9	72.0	73.9	71.1	(71.6)	69.5	77.8
Coefficient of thermal expansion, per °C	10.2×10^{-6}	10.6×10^{-6}	12.1×10^{-6}	6.3×10^{-6}	6.7×10^{-6}	9.6×10^{-6}	(11×10^{-6})	12.7×10^{-6}	35.0×10^{-6}
Thermal conductivity, W/(cm·K)	0.158	0.172	0.134	0.113	0.125	0.165	(0.15)	0.133	(0.139)
Magnetic moment (theoretical for 3+ ion), Bohr magnetons		0	0	2.5	3.6	3.6	–	1.5	3.5
Magnetic susceptibility, emu/g·atom		191×10^{-6}	101×10^{-6}	2430×10^{-6}	5320×10^{-6}	5650×10^{-6}	–	1275×10^{-6}	33100×10^{-6}
Curie temperature, °C		none	none	none	none	none	–	none	none
Néel temperature, °C		none	none	−260.6	none	−253	–	−258	−165
Superconducting transition temperature, K	0.050 (at 18.6 GPa)	1.3 (at 11 GPa)	5.10	0.022 (at 2.2 GPa)					
Electrical resistivity, μOhm·cm	56.2	59.6	61.5	74.4	70.0	64.3	(75)	94.0	90.0
Hall coefficient, V·cm/A·Oe	-0.13×10^{-12}	–	-0.35×10^{-12}	$+1.81\times10^{-12}$	+0.709	$+0\,971\times10^{-12}$	–	-0.21×10^{-12}	$+24.4\times10^{-12}$
Work function, eV	3.5	3.23	3.3	2.84	2.7	3.3	3.07	3.3	2.54
Density of liquid rare earth metal, g/cm^3	2.80	4.24	5.96	6.68	6.59	6.72	(6.9)	7.16	4.87

Table 1.2 (continued)

Properties	Scandium	Yttrium	Lanthanum	Cerium	Praseodymium	Neodymium	Promethium	Samarium	Europium
Heat capacity of liquid rare earth metal, C_p, J/mol·K	(44.2)	43.1	34.3	37.7	43.0	48.8	(50)	(50.2)	38.1
Mechanical properties									
Yield strength, 0.2% offset, MPa	173	42	126	28	73	71	–	68	–
Ultimate tensile strength, MPa	255	129	130	117	147	164	–	156	–
Uniform elongation, %	5.0	34.0	7.9	22	15.4	25.0	–	17.0	–
Reduction in area, %	8.0	–	–	30	67.0	72.0	–	29.5	–
Young's modulus, GPa	74.4	63.5	36.6	33.6	37.3	41.4	(46)	49.7	18.2
Shear modulus, GPa	29.1	25.6	14.3	13.5	14.8	16.3	(18)	19.5	7.9
Bulk modulus, GPa	56.6	41.2	27.9	21.5	28.8	31.8	33	37.8	8.3
Poisson's ratio	0.279	0.243	0.280	0.24	0.281	0.281	(0.28)	0.274	0.152
Recrystallization temperature, °C	550	550	300	325	400	400	(400)	440	300
Vicker's hardness, 10 kg load, kg/mm^2	85	38	37	24	37	35	–	45	17
Compressibility at 25°C, (cm^2/kg)	2.26×10^{-6}	2.68×10^{-6}	4.04×10^{-6}	4.10×10^{-6}	3.21×10^{-6}	3.00×10^{-6}	2.8×10^{-6}	3.34×10^{-6}	8.29×10^{-6}

Table 1.2 (continued)

Properties	Gadolinium	Terbium	Dysprosium	Holmium	Erbium	Thulium	Ytterbium	Lutetium
Atomic properties								
Atomic number	64	65	66	67	68	69	70	71
Atomic weight	157.25	158.92534	162.50	164.93032	167.26	168.93421	173.04	174.967
Crystal structure	cph <1235 bcc >1235	cph <1289 bcc >1289	cph <1381 bcc >1381	cph	cph	cph	cph <795 bcc >795	cph
Atomic volume, cm^3/mol at 24°C	19.903	19.310	19.004	18.752	18.449	18.124	24.841	17.779
Density, g/cm^3 at 24°C	7.901	8.230	8.551	8.795	9.066	9.321	6.966	9.841
Conduction electrons	3	3	3	3	3	3	2	3
Valence in aqueous solution	3	3	3	3	3	3,2	3,2	3
Color in aqueous solution, RE^{3+}	colorless	very pale pink	pale yellow green	yellow	pink	greenish tint	colorless Yb^{2+} is yellow	colorless
Main absorption bands of RE^{3+} ion in aqueous solution in the range 200 to 1000 nm	272.9, 273.3, 275.4, 275.6	284.4, 350.3, 367.7, 487.2	350.4, 365.0, 910.0	287.0, 361.1, 416.1, 450.8, 537.0, 641.0	364.2, 379.2, 487.0, 522.8, 652.5	360.0, 682.5, 780.0	975.0	none
Color of oxide, RE_2O_3	white	brown (Tb_4O_7)	yellowish white	yellowish white	pink	white, greenish tint	white	white
Number of isotopes: natural (artificial)	7(11)	1(17)	7(12)	1(18)	6(12)	1(17)	7(10)	2(14)
Thermal neutron absorption cross section: for naturally occurring mixture of isotopes, single isotopes (mass number of isotope), barns/atom	46,000 70,000(155) 180,000(157)	46	950 130(161) 680(161) 240(162) 220(163) 2780(164)	64	160	125	37	80
Ionization potential, eV/g·atom	6.16	6.74	6.82				6.25	5.0

Table 1.2 (continued)

Properties	Gadolinium	Terbium	Dysprosium	Holmium	Erbium	Thulium	Ytterbium	Lutetium
Electronegativity	1.160	1.168	1.176	1.184	1.192	1.200	(+2) 1.02 (+3) 1.208	1.216
Thermal, electrical, and magnetic properties								
Melting point, °C	1313	1356	1412	1474	1529	1545	819	1663
Boiling point, °C	3266	3223	2562	2695	2863	1947	1194	3395
Heat of fusion, kJ/mol	10.0	10.79	11.06	(17.0)	19.9	16.8	7.66	(22)
Heat of sublimation at 25°C, kJ/mol	397.5	388.7	290.4	300.8	317.1	232.2	152.1	427.6
Allotropic transformation temperature, °C	cph-bcc 1235	cph-bcc 1289	cph-bcc 1381				fcc-bcc 795	
Heat of transformation kJ/mol	cph-bcc 3.91	cph-bcc 5.02	cph-bcc 4.16				fcc-bcc 1.75	
Heat capacity at 298K, C_p, J/mol. K	37.1	28.9	27.7	27.2	28.1	27.0	26.7	26.8
Standard entropy, S^0_{298}, J/mol. K	67.9	73.3	75.6	75.0	73.2	74.0	59.8	51.0
Coefficient of thermal expansion, per °C	9.4×10^{-6} (at 100°C)	10.3×10^{-6}	9.9×10^{-6}	11.2×10^{-6}	12.2×10^{-6}	13.3×10^{-6}	26.3×10^{-6}	9.9×10^{-6}
Thermal conductivity, W/(cm.K)	0.105	0.111	0.107	0.162	0.145	0.169	0.385	0.164
Magnetic moment (theoretical for 3+ ion), Bohr magnetons	7.95	9.7	10.6	10.6	9.6	7.6	4.5	0
Magnetic susceptibility, emu/g.atom	$356{,}000\times10^{-6}$	$193{,}000\times10^{-6}$	$99{,}800\times10^{-6}$	$70{,}200\times10^{-6}$	$44{,}100\times10^{-6}$	$26{,}100\times10^{-6}$	71×10^{-6}	17.9×10^{-6}
Curie temperature, °C	17	−53	−185	−254	−253	(−241)	none	none
Néel temperature, °C	none	−43	−97	−143	−188	−216	none	none

Table 1.2 (continued)

Properties	Gadolinium	Terbium	Dysprosium	Holmium	Erbium	Thulium	Ytterbium	Lutetium
Superconducting transition temperature, K	–	–	–	–	–	–	–	0.022 (at 4.5 GPa)
Electrical resistivity, μOhm·cm	131.0	115.0	92.6	81.4	86.0	67.6	25.0	58.2
Hall coefficient, V·cm/A·Oe	-4.48×10^{-12} (at 77K)	–	–	–	–	-1.8×10^{-12}	3.77×10^{-12}	-0.535×10^{-12}
Work function, eV	(3.07)	(3.09)	(3.09)	(3.09)	(3.12)	(3.12)	(2.59)	(3.14)
Density of liquid rare earth metal, g/cm^3	7.4	7.65	8.2	8.34	8.6	(9.0)	6.21	9.3
Heat capacity of liquid rare earth metal, C_p, J/mol·K	37.2	46.5	49.9	43.9	38.7	41.4	36.8	(47.9)
Mechanical properties								
Yield strength, 0.2% offset, MPa	15	–	43	–	60	–	7	–
Ultimate tensile strength, MPa	118	–	139	–	136	–	58	–
Reduction in area, %	56.0	–	30.0	–	11.9	–	92.0	–
Young's modulus, GPa	54.8	55.7	61.4	64.8	69.9	74.0	23.9	68.6
Shear modulus, GPa	21.8	22.1	24.7	26.3	28.3	30.5	9.9	27.2
Bulk modulus, GPa	37.9	38.7	40.5	40.2	4.4	44.5	30.5	47.6
Poisson's ratio	0.259	0.261	0.247	0.231	0.237	0.213	0.207	0.261
Recrystallization temperature, °C	500	500	550	520	520	600	300	600
Vicker's hardness, 10 kg load, kg/mm^2	57	46	42	42	44	48	21	77
Compressibility at 25°C (cm^2/kg)	2.56×10^{-6}	2.45×10^{-6}	2.55×10^{-6}	2.47×10^{-6}	2.39×10^{-6}	2.47×10^{-6}	7.39×10^{-6}	2.38×10^{-6}

Table 1.2 (continued)

Properties	La	Ce	Pr	Nd	Pm	Sm	Eu
Electronic configuration							
Atom	$5d6s^2$	$4f^15d^16s^2$	$4f^36s^2$	$4f^46s^2$	$4f^56s^2$	$4f^66s^2$	$4f^76s^2$
M^{2+}	$5d$	$4f^2$	$4f^3$	$4f^4$	–	$4f^6$	$4f^7$
M^{3+}	[Xe]	$4f$	$4f^2$	$4f^3$	$4f^4$	$4f^5$	$4f^6$
M^{4+}	–	[Xe]	$4f$	$4f^2$	–	–	–
Radii, M^{3+}	1.061	1.034	1.013	0.995	0.979	0.964	0.95

Properties	Gd	Tb	Dy	Ho	Er	Tm	Yb	Lu	Se	Y
Electronic configuration										
Atom	$5f^75d6s^2$	$4f^96s^2$	$4f^{10}6s^2$	$4f^{11}6s^2$	$4f^{12}6s^2$	$4f^{13}6s^2$	$4f^{14}6s^2$	$4f^{14}5d6s^2$	$[Ar]3d4s^2$	
M^{2+}	$4f^75d$	$4f^9$	$4f^{10}$	$4f^{11}$	$4f^{12}$	$4f^{13}$	$4f^{14}$	–		
M^{3+}	$4f^7$	$4f^8$	$4f^9$	$4f^{10}$	$4f^{11}$	$4f^{12}$	$4f^{13}$	$4f^{14}$		
M^{4+}	–	$4f^7$	$4f^8$	–	–	–	–	–		
Radii, M^{3+}	0.938	0.923	0.908	0.894	0.881	0.869	0.858	0.848	0.68	0.88

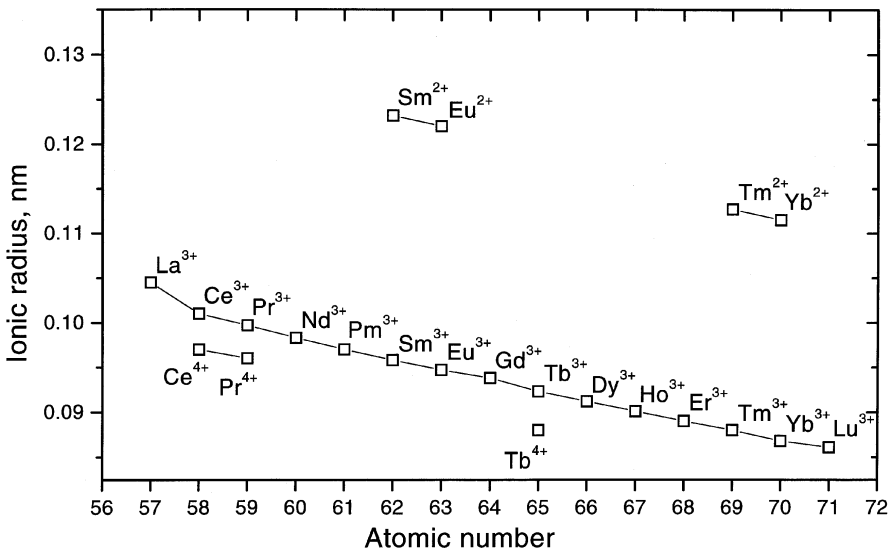

Figure 1.2 Lanthanide contraction.

of the M^{3+} ion. Even though the lanthanum atom and its tripositive ion are considerably larger in size than the corresponding yttrium species, the magnitude of lanthanide contraction is so much that the radii of the lanthanide species decrease to those of the yttrium species in the general holmium–erbium region. The similarity in the outermost electronic arrangement and the similarity in size due to lanthanide contraction explains the occurrence of yttrium in association with the heavier lanthanides. For essentially the same reason, it will be seen later that (i) yttrium compounds always concentrate with those of the heavier lanthanide elements in almost all fractionation procedures for the rare earths separation, (ii) considerable difficulty is experienced in separating yttrium from the heavier lanthanides, and (iii) yttrium exhibits general similarities in solubility, crystal structure, and in overall chemical properties with the heavier lanthanide metals. These factors, combined with the greater natural abundance of yttrium compared to the heavier rare earths led to these rare earths being popularly called the "yttrium earths." The chemistry of heavier rare earths is essentially the chemistry of yttrium.

The lanthanide contraction was sufficient for decreasing the atomic and ionic size of the heavier rare earths to those of yttrium but not to those of scandium. The atomic and trivalent ionic radii of scandium are far too small. Thus, scandium does not occur in rare earth minerals, and its chemistry is significantly different from that of the other rare earth elements.

1.3.3 Basicity

One of the important properties of rare earth elements, related to their ionic size, which is in turn related to lanthanide contraction, is basicity. Basicity determines, in one way or another, certain important chemical features of rare earths relevant to their extractive metallurgy. Basicity determines the extent to which cations hydrolyze in aqueous solution, the relative solubilities of salts of all types, the ease with which salts containing oxyanions

decompose when heated, and the stabilities of complex ions (Moeller 1961). A base tends to lose anions or electrons. Thus those cations with the least attraction for anion or electron are considered to be the most basic and those with the strongest attraction to be the least basic. Considering size relationships alone, the rare earth ions get arranged as follows in the order of decreasing basicity.

$La^{3+} > Ce^{3+} > Pr^{3+} > Nd^{3+} > Pm^{3+} > Sm^{3+} > Eu^{3+} > Gd^{3+} > Tb^{3+} > Dy^{3+} > Ho^{3+} > Y^{3+} > Er^{3+} > Tm^{3+} > Yb^{3+} > Lu^{3+} > Sc^{3+}$.

Cerium (IV) is less basic than any of the tripositive species, and all of the dipositive species are more basic than the tripositive species (Moeller and Kremers 1945).

The variation in basicity is the basis of most of the fractionation procedures for separating the rare earth elements from one another (Moeller 1961). In the so-called classical separation procedures, exploiting the differences in basicity, a large variety of fractional crystallization and fractional precipitation methods had been used. Later, the techniques of ion exchange and solvent extraction, which again ultimately operate exploiting basicity differences, have been used. The separations involving selective oxidation and reduction are also related to basicity because final removal from the contaminating tripositive species is usually effected by exploiting basicity differences between the different oxidation states of the element. Moeller (1961) emphasized that were it not for size induced alterations in basicity, the separation of the rare earth metal species would be a nearly insolvable problem.

A note of caution appears to be in order here. To readily achieve what has been stated in the previous paragraph, basicity differences should be large, the larger the better. Even though the size differences between the end members of the series or between two states of oxidation are substantial, the differences between adjacent members of the series in a given state of oxidation are at best very small. Therefore, generally, separations of adjacent members of rare earths are most difficult. However, there are exceptions like La^{3+}–Ce^{3+}.

1.4 PROPERTIES

In the elemental form, the rare earths are lustrous, iron gray to silvery metals. They are typically soft, malleable, ductile and usually reactive. Their reactivity is especially strong at elevated temperature or when finely divided.

The physical properties of the rare earth elements are listed (Cannon 1974, Gschneidner and Daane 1988, Gschneidner 1990, Gschneidner et al. 1995, McGill 1997) in Table 1.2.

1.4.1 Melting Point

The melting points increase in a regular manner across the series from lanthanum to lutetium with the exception of cerium, europium, and ytterbium. The melting point of lutetium is almost twice that of lanthanum. While considering the increase in the melting point by as much as 750°C, as the rare earth series is traversed from lanthanum to lutetium, as unusual for a group of nearly identical elements, Gschneidner and Daane (1988) attribute the change in the melting point to the extent of hybridization of the 4*f* and 5*d*6*s* orbitals. The hybridization is the largest for cerium (the lowest melting rare earth metal) and

decreases along the series from light lanthanides to heavy lanthanides. A lower melting point is associated with a greater amount of hybridization.

Various values have been reported for the melting points of the rare earth metals and this variety is traceable to the purity of the metal and the method used for the determination of the melting point. The temperature at which the rare earth metal melts depends on its purity. If appreciable quantities of oxygen, carbon, and nitrogen are present in the sample, the measured melting points are likely to be high (Spedding et al. 1968). In small quantities, these impurities can lead to lower readings of the melting point (Gschneidner and Daane 1988). For example, early reports on the melting point of lanthanum put it at 806°C, but the currently accepted value is 918°C. The determination of the La–C phase diagram by Spedding et al. (1959) revealed that the La–C eutectic melts at 806°C. Early samples of lanthanum metal were prepared by fused salt electrolysis using graphite electrodes, and melting point determinations using these samples, usually contaminated with carbon, led to the eutectic being reported as the pure metal's melting point. The availability of relatively large amounts of metallothermically prepared pure rare earth metals in the 1950s led to more accurate determination of their melting points. Melting point determined by thermal analysis using a refractory metal crucible also needs to be checked for the possibility of eutectic being reported as the melting point. In tantalum, however, the eutectic point and the actual melting point are very close to each other, differing by less than 1°C, in low melting rare earths but the difference may be appreciable in high melting rare earths (Garg et al. 1996). The difference between the eutectic temperature and the actual melting point is much smaller in the corresponding rare earth–tungsten systems (Krishnamurthy et al. 2000).

The melting point of the rare earth metal is an important parameter in determining the reduction process usable for metal production, both in metallothermic and electrolytic processes. Relatively inexpensive chloride reduction processes can be used for producing certain low melting rare earth metals, whereas more expensive fluoride reduction methods are needed for the high melting rare earth metals.

1.4.2 Boiling Point

The vapor pressures of all the rare earth metals were systematically determined at Ames in the 1950s using the Knudsen effusion technique for all the rare earth metals except promethium. Their data along with the values for promethium are included in Table 1.2.

The boiling points of rare earth metals do not exhibit a systematic variation, even to the extent that the melting points displayed, across the series. Lanthanum metal, which is among the four lowest melting point rare earths, has the highest boiling point. In other words, it has the lowest vapor pressure at its melting point for any rare earth metal. The most volatile rare earth metal is ytterbium. At 1000°C, for example, the vapor pressures of lanthanum and ytterbium differ by more than one billion (Gschneidner and Daane 1988). The heat of vaporization data for the rare earths are also listed in the table. Habermann and Daane (1961) noted certain correlations among the vapor pressure (boiling point), heat of vaporization, and electronic structure of the rare earth metals. For example, the divalent europium and ytterbium in the metallic state have no *d* electrons, resulting in weaker bonding. Consequently, vapor pressure is higher and the heat of vaporization lower. Later Gschneidner and Daane (1988) considered the electronic states of both the condensed phase and also the final gaseous atom in correlating the electronic structure to boiling point and heat of vaporization.

Like the melting point, the boiling point of the rare earth metal also strongly influences the method used for its preparation and purification. For example, the most volatile metals — europium, samarium, and ytterbium — are prepared by the reduction–distillation process, which is very similar to the Pidgeon process used for magnesium (Pidgeon and King 1948). In these and other metals, the high vapor pressures are also exploited for the purification of metal by sublimation or distillation (Beaudry and Gschneidner 1978). On the other hand, relatively high volatility of many of the rare earth metals has been a major limitation in the application of ultrapurification techniques like solid state electrotransport.

1.4.3 Allotropes

The crystal structures and lattice parameters of all the rare earth metals, except samarium, promethium, and holmium, were determined quite early by Klemm and Bommer (1937). Their work confirmed the existence of the lanthanide contraction, discovered the multivalency in cerium, europium, and ytterbium, and confirmed that the rare earths crystallize in at least three different structures: fcc, bcc, and hcp. Final and finer details of room temperature crystal structures of rare earth metals were established at Ames by various researchers between 1958 and 1971. The details of crystal structures, lattice parameter, and allotropic transformation temperatures of rare earths are summarized in Table 1.2.

Most of the rare earth metals crystallize in the close packed hexagonal structure. However, the stacking sequence along the *c*-axis is not identical for all. Lanthanum, cerium, praseodymium and neodymium crystallize with one stacking sequence; gadolinium to lutetium crystallize in another; and samarium has yet another arrangement. Most of the rare earth metals undergo allotropic transformation and the high temperature phase just below the melting point is invariably bcc. Europium, which is bcc even at room temperature, undergoes no transformation. Holmium, erbium, thulium, and lutetium also are monomorphic (cph) and do not undergo an allotropic transformation to the bcc phase before melting at atmospheric pressure. However, by application of pressure (~1 GPa), the bcc phase can be transformed in holmium and erbium. As regards the allotropic transformation temperatures, there is apparently no systematic trend across the lanthanide series (Gschneidner and Daane 1988).

The allotropic transformation is important in rare earth metal ultrapurification. The electrotransport mobilities of interstitial impurities in rare earth metals depend on the crystal structure of the metal. Mobility is higher in the bcc phase. Thus when no other complication crops up, electrotransport purification is best carried out in the bcc phase.

The light rare earths form solid solution with each other, and so do the heavy rare earths. The solid solution is not perfect and the liquidus and solidus lines are curved. When a light rare earth is alloyed with a heavy rare earth, two phases are likely to form.

1.4.4 Resistivity

The rare earth metals are poor electrical conductors. Among the rare earths, room temperature resistivities are highest in the center of the series. They also show anisotropy. Resistivity measured along the *c*-axis of a rare earth metal single crystal differs from that measured along the *a*- or *b*-axis in the basal plane. Rare earths are self-resistance heated during their purification by solid state electrotransport.

The resistivity of the metal at 4 K is sensitive to the presence of impurities, particularly oxygen, nitrogen, and hydrogen to the extent that it can be used for denoting the metal purity. A well-known method for estimating the total purity of a metal is to measure the ratio of resistivities at 298 K and at 4 K, or even 1 K. The impurities must be very low if the resistivity ratio obtained is very high. For certain rare earths, however, in spite of good purity, the resistivity ratio obtained may not be very high.

Among the rare earths, only lanthanum is superconducting at atmospheric pressure (Gschneidner and Daane 1988) and elemental lanthanum (fcc phase) is one of the better elemental superconductors ($T_c = 6.1$ K, $H_c(0) = 1600$ Oe) like lead ($T_c = 7.2$ K) and niobium ($T_c = 9.2$ K). At a high pressure of 20 GPa, lanthanum has the highest known elemental superconducting transition temperatures (13 K). Certain lanthanum-based ceramic compositions are, however, important superconducting materials.

1.4.5 Magnetic Properties

The 4*f* electrons determine the magnetic behavior of the rare earth metals. In the completed 4*f* subshell, the magnetic effects of different electrons cancel each other out, but in the incomplete 4*f* subshell, they do not. All rare earth metals, except scandium, yttrium, lanthanum, ytterbium, and lutetium are strongly paramagnetic. On cooling many of them become antiferromagnetic, and on cooling further a number of these elements become ferromagnetic. If a magnetic field of sufficient strength is applied, all paramagnetic rare earths become ferromagnetic at low temperatures. The rare earth metals display strong anisotropy; their magnetic behavior depends on the crystal axis.

The existence of ferromagnetism at room temperature in gadolinium was reported by and confirmed by Klemm and Bommer (1937). Much of the detailed studies on the magnetic behavior of the rare earth elements were carried out by the Ames group in the 1950s. Elucidation of the magnetic behavior of the rare earth metals, as has been the case with their many other properties, was greatly dependent on the availability of the rare earth metals in high levels of purity and in special forms such as large single crystals (Gschneidner and Daane 1988).

1.4.6 Spectral Properties

The trivalent rare earth ions, except Ce^{3+} and Yb^{3+}, exhibit very sharp absorption bands in the visible and ultraviolet regions. These bands are caused by *f*–*f* transitions and the sharpness comes because the electrons in the 4*f* inner shell of the rare earths are shielded from the chemical environment by the $5s^2p^6$ octet. Most of the rare earth salts display colors that are characteristic of the tripositive ions. The striking colors persist in aqueous and nonaqueous solutions and are unaffected by alterations of anions present or the addition of complexing agents (Moeller 1971). The absorption bands and colors are listed in Table 1.2.

In the rare earths with electronic configurations $4f^1$ and $4f^{13}$ no *f*–*f* transition is possible. Thus, Ce^{3+} and Yb^{3+} do not absorb in the visible region. They do, however, absorb in the ultraviolet region due to transitions of the type $4f^n - 4f^{n-1}5d$. The divalent ions of europium, samarium, and ytterbium display colors in aqueous solutions: Eu^{2+} is pale yellow, Sm^{2+} is deep red, and Yb^{2+} is yellow.

1.4.7 Mechanical Properties

Values for the elastic and mechanical properties of rare earth metals reported in the literature vary widely. This is because of the variation in the impurity levels of the metals. Generally the elastic property values increase with an increase in purity (Gschneidner and Daane 1988). The chosen values (Gschneidner 1990) are listed in Table 1.2. In the series, there is an increase in the elastic moduli with an increase in atomic number until a maximum is reached at thulium. Cerium, europium, and ytterbium have anomalously low values. The elastic constants of rare earths are similar in value to those of aluminum, zinc, cadmium, and lead.

The hardness and strength values of the rare earths (Gschneidner and Daane 1988, Gschneidner, 1990) follow the same periodic trend displayed by the elastic constants. Cerium, europium, and ytterbium have anomalously low values. Mechanical properties improve from the light rare earths to the heavy rare earths. In the lower range, the strengths of rare earth metals are similar to that of aluminum, and in the higher range the values correspond to levels between aluminum and titanium.

1.5 REACTIVITY

1.5.1 Air/Oxygen

At room temperature, all the rare earth metals are not affected by air the same way. Some corrode very rapidly while some remain bright and shiny for years. A solid block of europium tarnishes immediately on exposure to air at room temperature, particularly when the air is moist. If left in that condition, it will get converted to an oxide of europium in a few days or weeks. Massive blocks of lanthanum, under similar conditions, will undergo surface corrosion in a few days and will develop a thick crust of oxide in a few months. Neodymium behaves in the same way as lanthanum; however, most of the heavy rare earth metals will remain bright for a long time.

Increase in temperature and humidity accelerates oxidation of rare earth metals (Gschneidner and Daane 1988). The rate at which lanthanum oxidizes increases by more than a factor of ten when the relative humidity is increased from 1 to 75%. The oxidation of lanthanum at 1% humidity, which is 0.8 mg/cm^2 day at 35°C, increases to 5.1 mg/cm^2 day at 95°C, rising further to 32 mg/cm^2 day at 400°C, and to 130 mg/cm^2 day at 600°C (Love and Kleber 1960). The value at 75% relative humidity is 210 mg/cm^2 day at 95°C. Under the latter conditions, praseodymium oxidizes at the rate of 55 mg/cm^2 day, neodymium at 20 mg/cm^2 day, and samarium at 1 mg/cm^2 day. The corresponding values for the trivalent lanthanides gadolinium through lutetium, scandium, and yttrium are 0 to 0.35 mg/cm^2 day. The oxide products formed by the oxidation of the light rare earths, lanthanum through neodymium, are the hexagonal A form RE_2O_3 phase. Samarium through gadolinium form the monoclinic β form RE_2O_3 and the remaining rare earths form the cubic C form RE_2O_3 phase. The A form oxides react readily with water vapor in the air to form an oxyhydroxide, and this spalls exposing the fresh metal surface which undergoes oxidation. The C-type structure oxides form a tight coherent stoichiometric gray black coating, preventing further oxidation.

The rate of oxidation is sped up considerably if the metal contains one or more impurities such as fluorine, calcium, magnesium, carbon, iron, and many of the *p*-group elements such as zinc, gallium, germanium, and their congeners. Pure metals are attacked by oxygen and moisture slowly at first but once oxidation starts, the oxide apparently catalyzes the reaction and oxidation is fast.

1.5.2 Refractories

The reactivity of rare earth metals toward oxygen is due to the large negative free energy of formation of the oxide, and the free energy of formation of rare earth oxide is among the most negative of all the elements in the periodic table. In other words, the rare earth oxides are among the most stable of the oxides of all elements in the periodic table. At room temperature only calcia is more stable than the rare earth oxides. As a consequence, the rare earth metals could attack and reduce most of the refractory crucibles, including zirconia, alumina, and magnesia and such refractory linings (Kremers 1961). The attack on refractories is particularly relevant when containment of the liquid rare earth metal is considered. Rare earth metals form solid solutions with oxygen. These solutions have greater stability (Alcock 1976) and this leads to the rare earth metal picking up and dissolving oxygen from oxides of comparable (for example, MgO) or greater (for example, CaO) stability.

1.5.3 Nitrogen

Rare earth metals show strong affinity for nitrogen. The mononitrides of rare earths are comparable in stability to those formed by metals such as titanium or zirconium (Pankratz et al. 1984). They have high melting points and very low decomposition pressures. The metals also form solid solutions with nitrogen. For example, cerium dissolves up to 0.3 wt % nitrogen at 750°C. The equilibrium nitrogen pressures over these solutions will be still lower. Thus the rare earths are very good getters of nitrogen from the environment and do not easily degas with respect to nitrogen.

The reaction between rare earth metals and nitrogen is, however, slow. High temperatures are needed to observe any appreciable reaction. Besides, the formation of a nitride layer on the surface greatly retards further nitridation.

1.5.4 Hydrogen

Rare earth metals react with hydrogen and easily form hydrides at temperatures of 400 to 600°C. If hydriding is allowed to continue, when the metal is hydrided up to and beyond REH_2, the solid material fragments. When the hydrogen content is below REH_2, the material behaves like a metal and at certain concentrations of hydrogen conducts electricity better than even the pure metal. It is possible to load more hydrogen per unit volume in yttrium metal than in liquid hydrogen or water. The decomposition pressure of YH_2 is low even at fairly high temperatures and becomes 1 atm only at 1260°C (Spedding et al. 1968).

Unlike the yttrium hydride, several rare earth metal hydrides decompose and degas evolving hydrogen at relatively low temperatures. The brittleness and crumbling tendency

of the hydride, combined with the possibility of easy hydrogen removal by degassing has made hydriding–comminution–dehydriding a method to make rare earth metal powder. It is, however, likely that the effort to drive off last traces of hydrogen from the powdered hydride, by the use of high temperatures, will result in a partially sintered mass of powder (Gschneidner and Daane 1988).

1.5.5 Carbon

All rare earths are known to form dicarbides REC_2 and most of them (La–Sm, Gd–Ho, Y) form sesquicarbides, RE_2C_3. Monocarbides (e.g., ScC, LaC) and subcarbides (e.g., RE_3C_4, Sm, Gd–Lu) are also known (Goldschmidt 1967). The rare earth carbides are high melting and form extensive solid solutions with oxygen and nitrogen. The solid solubility of carbon in rare earth metals is also considerable (Massalski et al. 1990). For example, yttrium dissolves up to 1.3 wt % C at 1520°C and lanthanum takes up to 0.3 wt % C at 775°C. The high stability of the lower carbides of rare earths and also of the carbon–RE solutions make the attack of molten rare earth metals on graphite crucibles an important factor leading to contamination of rare earth metals with carbon. Besides, these characteristics have rendered carbothermic reduction a useless method for rare earth metal preparation.

1.5.6 Silicon

Silicon, like carbon, forms rare earth silicides and solid solutions. Rare earth silicides are generally all disilicides represented by the formula $RESi_2$, but silicides of other stoichiometry have also been reported (Goldschmidt 1967).

1.5.7 Sulfur, Selenium, Phosphorus

The rare earths react exothermically with sulfur, selenium, and phosphorus. On heating a mixture of rare earth metal with these elements, the reaction sets off and, if precautions are not taken, could seriously damage the crucible, furnace, vacuum enclosures, etc. On the other hand, at low temperatures, some of the rare earths, particularly heavy rare earths, hardly react with, for example, sulfur.

1.5.8 Refractory Metals

Among the refractory metals, niobium, molybdenum, tantalum, and tungsten are resistant to attack by liquid rare earth metals. The metals listed above are in order of decreasing solubility in the liquid rare earth metals at high temperatures, tungsten being the least soluble (Dennison et al. 1966, 1966a). About 1.5 at. % tantalum is soluble in lutetium at the eutectic temperature and the corresponding solubility of tantalum in scandium is about 3 at. %. When tungsten is used in place of tantalum, the solubility of tungsten in liquid rare earth metals is about one-third of the solubility of tantalum. This makes tungsten the most inert container for holding liquid rare earth metals. However, tungsten embrittles and has poor mechanical properties compared to tantalum. Thus tantalum is a more useful crucible

material for liquid rare earths in spite of its solubility in rare earths. The solubility of tantalum is a function of temperature, and for many rare earth metals it decreases from a high value at high temperatures to a very low value at temperatures just above the rare earth metal's melting point.

Commenting on the interaction of tantalum with liquid rare earth metals, Gschneidner and Daane (1988) have stated that the use of ceramic crucibles for metal preparation and purification puts an upper limit of 95–98 at % purity of the rare earth metals. The use of tantalum has allowed purity level to rise to 99 at % and higher.

1.5.9 Acids and Bases

All rare earth metals readily dissolve in dilute mineral acids and hydrogen is evolved. In a certain range the rate of dissolution is proportional to the acid concentration (Gschneidner and Daane 1988). Attack on the metal by concentrated sulfuric acid is somewhat less (Kremers 1953). Rare earth metals resist attack by hydrofluoric acid because REF_3 forms and coats the metal. This coating prevents further attack by the acid. A mixture of equal parts of concentrated nitric acid and 48% hydrofluoric acid attacks most rare earths only superficially and may be used to clean/pickle the rare earth metals. This acid mixture may be used to separate tantalum from the rare earths because only tantalum dissolves whereas the rare earths remain more or less intact (Gschneidner and Daane 1988). Rare earth metals react with common organic acids but at slower rates than with mineral acids of the same concentration.

Rare earth metals react, but slowly, with strong bases like sodium hydroxide. With a weak base like ammonium hydroxide no reaction occurs. The lack of reactivity may be due to the formation of an insoluble rare earth hydroxide coating on the metal surface.

1.5.10 Water

The reaction of rare earths with water varies depending on the metal. Generally light rare earth metals react with water, slowly at room temperature and vigorously at higher temperature. The heavy rare earths react very slowly. However, even with cold water, europium reacts to form $Eu(OH)_2 \cdot H_2O$, liberating hydrogen (Spedding et al. 1968).

1.6 AQUEOUS SYSTEMS

The standard oxidation potential data listed in Table 1.2 indicate that each of the rare earth elements is a powerful reducing agent in aqueous acidic solution and forms the tripositive ion readily. The special stability of empty, half filled, and completely filled $4f$ shells are reflected (Moeller 1967) in that the $4f^0$ cerium (IV) is much less readily reduced to the tripositive state than the $4f^1$ praseodymium (IV). For similar reasons, $4f^7$ europium (II) and $4f^{14}$ ytterbium (II) are weaker reducing agents than samarium (II).

1.6.1 The Trivalent State

The rare earths are characteristically trivalent. In aqueous solution, the tripositive rare earth cations have a strong ionic character and form salts with a large variety of anions. The solubilities of such salts vary widely.

Rare earth hydroxides are obtained as gelatinous precipitates from aqueous solutions by the addition of ammonia or dilute alkalies. Rare earth hydroxides are definite compounds and are not just hydrous oxides. As mentioned earlier, $La(OH)_3$ is the most basic of the rare earth hydroxides and the basicity decreases across the series with increase in the atomic number.

Rare earth salts containing thermally unstable anions such as OH^-, CO_3^{2-}, and $C_2O_4^{2-}$, when heated, yield first the basic derivatives and finally the oxides. The hydrated salts, regardless of the nature of the anion, undergo thermal hydrolysis at high temperatures. Anhydrous compounds of rare earths containing thermally stable anions such as O^{2-}, F^-, Cl^-, and Br^- melt without decomposition at relatively high temperatures. These solids are also highly ionic.

The chlorides, bromides, nitrates, bromates, and perchlorate salts of rare earths are all soluble in water. When their aqueous solutions are evaporated, they precipitate as hydrated crystalline salts. For example, the rare earth chlorides crystallize as hexahydrates. The light rare earths (La to Nd) can form heptahydrates. On heating, the hydrated chlorides lose HCl more readily than H_2O. The product is oxychloride. The bromides and iodides are quite similar to the chlorides. The iodides as well as the iodates and acetates are somewhat less soluble in water. The sulfates are sparingly soluble and their solubility decreases with increase in temperature. The rare earth oxides, sulfides, fluorides, carbonates, oxalates, and phosphates are insoluble in water. Among the halides only the fluorides are insoluble. The addition of hydrofluoric acid or fluoride ions to RE^{3+} solutions even in 3M nitric acid results in the precipitation of REF_3. This is a characteristic test for rare earth ions. Rare earths can also be precipitated as oxalates, another insoluble rare earth compound, from a dilute nitric acid solution. The precipitation is not only quantitative, but also specific to rare earths and is used for the determination of rare earths gravimetrically. Oxalate precipitation is also a useful procedure for rare earth purification. The oxalate is calcined to the oxide.

Double slats of rare earths are common. The most important are the double nitrates $2RE(NO_3)_3 \cdot 3MgNO_3 \cdot 24H_2O$ and $RE(NO_3)_3 \cdot 2NH_4NO_3 \cdot 4H_2O$, and the double sulfates $RE_2(SO_4)_3 \cdot 3Na_2SO_4 \cdot 12H_2O$ and $RE_2(SO_4)_3 \cdot MgSO_4 \cdot 24H_2O$. The cerium group double sulfates are only sparingly soluble in sodium sulfate whereas those of the yttrium group are appreciably soluble. This characteristic makes it possible to achieve a fairly rapid separation of the entire group of rare earths into two subgroups.

1.6.2 Complexes

The formation of complex species is an important feature of tripositive rare earth ions. It is improbable, however, that any hybrid *f* orbitals from the ions would take part in covalent bonding, and the large size of the RE^{3+} ions make it possible for only certain types of complexes to be formed (Moeller 1961). Thus, (i) the number of rare earth complexes is limited, (ii) only species that can attract the RE cations as a result of their own small size, large charge, and chelating abilities will yield complexes, (iii) stabilities of such complexes with respect to dissociation will be less than those of the tripositive transition metal ions,

and (iv) bonding in all complex species will be predominantly ionic. The coordination number is usually 7, 8, 9, or 10 and only in isolated cases it is 6. Properties that depend directly on the 4*f* electrons are not affected by complexation. The complexes formed by tripositive rare earth ions include complexes with citric acid, ethylene diamine tetraacetic acid (EDTA), and hydroxy ethylene diamine triacetic acid (HEDTA). The most important of the chelates are the species derived from the various polyamine polycarboxylic acids. Many of these have been isolated and characterized. These complexes are water soluble. However, the stabilities of the species in solution are of great importance because differences in the stabilities of the complexes have been used in conjunction with ion exchange techniques to effect separation of rare earths from one another (Powell 1979, Powell 1961). The complex formation is pH dependent and the stabilities of chelates are related to the ionic radii of the rare earth ion. The stabilities of complex species invariably increase from La^{3+} to Eu^{3+} or Gd^{3+} but for cations heavier than gadolinium, the stability may continue to increase, remain nearly constant, or pass through a maximum (Moeller 1967).

1.6.3 The Tetravalent State

Cerium(IV) is the only tetrapositive rare earth species that is stable in aqueous solution as well as in solid compounds (Moeller 1961). The III and IV valency states of cerium are often designated as cerous and ceric, respectively. The ceric oxide, CeO_2, hydrous ceric oxide, $CeO_2 \cdot nH_2O$, and ceric fluoride, CeF_4, are the only binary solid compounds of Ce(IV). Ceric oxide is obtained by heating cerium metal, $Ce(OH)_3$, or any of the several Ce(III) oxosalts such as the oxalate, nitrate, or carbonate in air or oxygen. CeO_2, white when pure, is quite inert and not attacked by even strong acids or alkalies. It can, however, be dissolved by acids in the presence of reducing agents to form Ce(III) solutions. Hydrous $CeO_2 \cdot nH_2O$ can be obtained as a yellow gelatinous precipitate, from Ce(IV) solutions on treatment with bases. The hydroxide is precipitated at pH 1. Ceric fluoride, CeF_4, is prepared by reacting anhydrous $CeCl_3$ or CeF_3 with fluorine at room temperature. Ceric fluoride is inert to cold water and is reduced to CeF_3 by hydrogen at 200–300°C.

Ce(IV) is obtained in solution by treatment of Ce(III) solution with strong oxidizing agents like ozone, peroxodisulfate, or bismuthate in nitric acid. Under alkaline conditions, oxidation of cerium to +4 state is readily effected by $OC1^-$, H_2O_2, and O_2. In solutions, Ce(IV) can also be obtained by electrolytic oxidation. Cerium(IV) forms phosphates insoluble in $4NHNO_3$ and iodates insoluble in $6NHNO_3$ as well as insoluble oxalate. Precipitation as phosphate or iodate can be used to separate Ce(IV) from trivalent rare earths. Ce(IV) is extracted more readily than the RE(III) ions into organic solvents like tributyl phosphate. Ce(IV) can be used as an oxidizing agent.

Ceric oxide dissolves, undergoing reduction, in acids such as hydrochloric acid. In acidic medium, reduction of cerium (IV) is effected by many reductants such as Fe^{2+}, Sn^{2+}, I^-, and H_2O_2. It dissolves in oxidizing acids such as nitric acid or sulfuric acid without undergoing reduction. The double ammonium nitrite of Ce(IV), the orange red soluble $Ce(NO_3)_4 \cdot 2NH_4NO_3$, crystallizes readily from a concentrated nitric acid solution. It is both an excellent source of Ce(IV) and a useful analytical oxidizing agent.

Pr(IV) is a powerful oxidizing agent and oxidizes water itself. Therefore, it does not exist in aqueous solution. When Pr(III) salt or oxide is heated in air, Pr_6O_{11} forms. Both Pr(III) and Pr(IV) are present in the oxide.

The chemistry of Tb(IV) is similar to that of Pr(IV). The oxide Tb_4O_7 is obtained on igniting Tb(III) oxosalts in air. Tb_4O_7 contains both Tb(III) and Tb(IV). TbO_2 is obtained by oxidation of Tb_2O_3 with atomic oxygen at 450°C. The colorless compound TbF_4 is obtained by treating TbF_3 with gaseous fluorine at 300–400°C.

1.6.4 The Divalent State

The divalent state of Sm, Eu, and Yb are well established both in solution and solid compounds. These species are obtained (Moeller 1967) by (i) thermal reduction of anhydrous halides or chalcogenides with metals or hydrogen. For example, solid oxide, chalcogenides, halides, carbonate, or phosphate of europium (II) may be obtained by reduction of the corresponding Eu(III) compound or from $EuCl_2$ by metathesis, (ii) electrolytic reduction in aqueous solution or in halide melts, for example, Eu(II) and Yb(II), (iii) chemical reduction in solution: Eu(II) using Zn in aqueous solution, Sm(II) using Mg in ethanol, (iv) thermal decomposition of anhydrous triiodides, and (v) controlled oxidation of free metals or their amalgams.

The divalent rare earth cations are strong reducing agents in acidic aqueous solutions and their reducing ability decreases in the order $Sm^{2+} >> Yb^{2+} >> Eu^{2+}$. Both Sm^{2+} and Yb^{2+} undergo instant oxidation to the tripositive species by the hydronium ion and also by air. The oxidation of Eu^{2+} is, however, slower and solutions containing Eu^{2+} can be readily handled. In acidic solution, all three ions are rapidly oxidized by elemental oxygen. The RE^{2+} ions resemble Group II ions, particularly Ba^{2+}. Thus the hydroxides are soluble and sulfates are insoluble. Eu^{3+} can be readily separated from the other rare earths by reduction with zinc to the dipositive state followed by the precipitation of the remaining tripositive rare earths as hydroxides by carbonate free ammonia. The water insoluble compounds, sulfates, carbonates, or fluorides of the divalent ions are relatively more resistant to oxidation. These ions have little tendency, compared to Ba^{2+} or Sr^{2+}, to form complex compounds.

1.7 APPLICATIONS

The rare earths have an ever growing variety of applications in the modern technology. They provide many an industry with crucial materials, and they provide many a customer with benefits (Molycorp Inc., 1993). The first application of the rare earths and the beginning of the rare earth industry date back to 1891 and were related to the inventions of the Austrian entrepreneur and scientist Carl Auer von Welsbach. He used the rare earths to solve what was at that time a major technical problem — the production of bright light. It was already known that a solid of suitable composition and large surface area when brought into the hot zone of a gas flame would glow, giving off the required bright light. The hitch was finding the suitable solid that would be the incandescent mantle. Auer solved the problem. First, he announced in 1866 the discovery of a gas mantle composed of zirconia doped with lanthana. That mantle was too brittle and produced cold blue light. Later, after persistent experimentation, Auer came up in 1891 with a gas mantle composed of 99% thoria and 1% ceria. The light from this mantle was not only white and bright and superior to electric light, but it was also cheaper. This situation remained for several decades until about 1935 and an estimated (Greinacher 1981) five billion gas mantles had been produced

and consumed in the world. The Auer mantle was produced by a simple process. A cotton sock was saturated with a salt solution which upon ignition resulted in a mixture of thorium–cerium oxides with large surface area. Even today, light production from gas mantles remains in use in remote areas where electricity is unavailable or erratic and in some railroad signal devices.

The next important application of the rare earths also came from Auer's inventions. The search for a simple ignition system for his gas mantle lamps led him to discover in 1903 a pyrophoric alloy called flintstone. Production of flintstones was the first major large scale use for rare earth metals which began in 1903. The flintstone, which is composed of 70% misch metal and 30% iron, was used in the lighters for the gas mantle. The name "misch metal" was coined by Auer for the alloy which contained lanthanum, cerium and didymium in the proportion in which they occurred in monazite. To produce misch metal, Auer founded in 1907 a company at Karinthia in Austria. The company came to be known as Treibacher Chemische Werke and was the first company involved in the commercial production of rare earths. Auer used the fused salt electrolysis method for the production of misch metal, and in 1908 over 800 kgs of misch metal–iron flints entered the market. Following Auer's discovery, production of lighter flints was started in about 1915 by Ronson Metals in the United States.

Greinacher (1981) has noted that in the 22 years between 1908 and 1930, about 1,100 to 1,400 metric tons of flints were produced from approximately 1,300 to 1,800 metric tons of rare earth oxides in the form of rare earth chlorides. During the same time, about 7,500 metric tons of thorium nitrate were used for Auer incandescent mantles. The lighter flints are still very common and account for the consumption of a substantial fraction of the misch metal produced. Pyrophoric alloys, which give tracer shells their distinctive fiery trail, also contain misch metal as a constituent.

The production of intense light by electric arc was developed by Beck in Germany in 1910. These electric arc lamps have been used for a wide range of lighting purposes, including search lights and for cinema projectors. Historically, the third major use of rare earths was the addition of rare earth fluoride as a wick in arc light carbons (Greinacher 1981). Even though the electric arc struck and maintained between carbon electrodes emits light, it is low in intensity. The brightness is greatly increased if a cored carbon, consisting of an outer shell of carbon and inner core made from carbon flour mixed with rare earth oxides and fluorides, is used. The enhanced brightness and color comes about because of the characteristic emission spectra of the core material (Bagchi 1988).

From these beginnings, and over many years, industrial applications of rare earths have developed in metallurgy, magnets, ceramics, electronics, chemical, optical, medical, nuclear technologies (Gschneidner 1981). The major uses of rare earths are summarized in Table 1.3.

1.7.1 Metallurgy

Rare earths have major applications as metallurgical alloys. The oldest of these alloys is misch metal which is, as mentioned earlier, an alloy consisting only of rare earth metals, with the individual rare earth elements present in the same proportion in which they naturally occur in bastnasite or monazite. Misch metal is the form in which the rare earths were introduced as constituents in numerous alloys for a variety of applications. A selection of alloys that benefit from rare earth additions is described below.

Table 1.3 Applications of rare earths

Rare Earth	Applications
RARE EARTHS	Rare earth primary products are mainly used as raw materials for high-purity individual rare earth chemicals, and in the making of petroleum and environment protection catalysts, misch metal, and polishing powders
LANTHANUM	Lanthanum-rich rare earth compounds have been extensively used as components in FCC catalysts, especially in the manufacture of low-octane fuel from heavy crude oil. Lanthanum-rich rare earth metals have an important role in hydrogen storage batteries. Lanthanum is utilized in green phosphors based on the aluminate $(La_{0.4}Ce_{0.45}Tb0_{.15})PO_4$. Lanthanide zirconates are used for their catalytic and conductivity properties and lanthanum stabilized zirconia has useful electronic and mechanical properties. Lanthanum is utilized in laser crystals based on the yttrium–lanthanum–fluoride (YLF) composition.
CERIUM	Commercial applications of cerium are numerous and include glass and glass polishing, phosphors, ceramics, catalysts and metallurgy: In the glass industry, it is considered to be the most efficient glass polishing agent for precision optical polishing. It is also used to decolorize glass by keeping iron in its ferrous state. The ability of cerium-doped glass to block out ultraviolet light is utilized in the manufacturing of medical glassware and aerospace windows. It is also used to prevent polymers from darkening in sunlight and to suppress discoloration of television glass. It is applied to optical components to improve performance. In phosphors, the role of cerium is not as the emitting atom, but as a "sensitizer." Cerium is also used in a variety of ceramics, including dental compositions and as a phase stabilizer in zirconia-based products. Ceria plays several catalytic roles. In catalytic converters it acts as a stabilizer for the high surface area alumina, as a promoter of the water-gas shift reaction, as an oxygen storage component and as an enhancer of the NOX reduction capability of rhodium. Cerium is added to the dominant catalyst for the production of styrene from methylbenzene to improve styrene formation. It is used in FCC catalysts containing zeolites to provide both catalytic reactivity in the reactor and thermal stability in the regenerator. In steel manufacturing, it is used to remove free oxygen and sulfur by forming stable oxysulfides and by tying up undesirable trace elements, such as lead and antimony.
PRASEODYMIUM	It is highly valued for ceramics use as a bright yellow pigment, in praseodymium doped zirconia, because of its optimum reflectance at 560 nm. Much research is being done on its optical properties for use in amplification of telecommunication systems, including as a doping agent in fluoride fibers. It is also used in the scintillator for medical CAT scans.
NEODYMIUM	Primary applications include lasers, glass coloring and tinting, dielectrics and, most importantly, neodymium–iron–boron ($Nd_2Fe_{14}B$) permanent magnets. The neodymium-based magnet was first introduced in 1982 simultaneously by Sumitomo Specialty Metals (Japan) and General Motors (U.S.) and commercialized in 1986. It is used extensively in the automotive industry with many applications including starter motors, brake systems, seat adjusters and car stereo speakers. Its largest application is in the voice coil motors used in computer disk drives. Neodymium has a strong absorption band centered at 580 nm, which is very close to the human eye's maximum level of sensitivity making it useful in protective lenses for welding goggles. It is also used in CRT displays to enhance contrast between reds and greens. It is highly valued in glass manufacturing for its attractive purple coloring to glass. Neodymium is included in many formulations of barium titanate, used as dielectric coatings and in multi-layer capacitors essential to electronic equipment. Yttrium–aluminum–garnet (YAG) solid state lasers utilize neodymium

Table 1.3 (continued)

	because it has optimal absorption and emitting wavelengths. Nd-based YAG lasers are used in various medical applications, drilling, welding and material processing.
SAMARIUM	Samarium is primarily utilized in the production of samarium–cobalt (Sm_2Co_{17}) permanent magnets. It is also used in laser applications and for its dielectric properties. Samarium-cobalt magnets replaced the more expensive platinum–cobalt magnets in the early 1970s. While now overshadowed by the less expensive neodymium–iron–boron magnet, they are still valued for their ability to function at high temperatures. They are utilized in lightweight electronic equipment where size or space is a limiting factor and where functionality at high temperature is a concern. Applications include electronic watches, aerospace equipment, microwave technology and servomotors. Because of its weak spectral absorption band samarium is used in the filter glass on Nd:YAG solid state lasers to surround the laser rod to improve efficiency by absorbing stray emissions. Samarium forms stable titanate compounds with useful dielectric properties suitable for coatings and in capacitors at microwave frequencies.
EUROPIUM	Europium is utilized primarily for its unique luminescent behavior. Excitation of the europium atom by absorption of ultraviolet radiation can result in specific energy level transitions within the atom creating an emission of visible radiation. In energy-efficient fluorescent lighting, europium provides not only the necessary red, but also the blue. Several commercial red phosphors are based on europium for color TV, computer screens and fluorescent lamps. Its luminescence is also valuable in medical, surgical and biochemical applications.
GADOLINIUM	Gadolinium is utilized for both its high magnetic moment and in phosphors and scintillated materials. When mixed with EDTA dopants, it is used as an injectable contrast agent for patients undergoing magnetic resonance imaging. With its high magnetic moment, gadolinium can reduce relaxation times and thereby enhance signal intensity. The particularly stable half full 4*f* electron shell with no low lying energy levels creates applications as an inert phosphor host. Gadolinium can therefore act as host for x-ray cassettes and in scintillated materials for computer tomography.
TERBIUM	Terbium is primarily used in phosphors, particularly in fluorescent lamps and as the high intensity green emitter used in projection televisions, such as the yttrium–aluminum–garnet (Tb:YAG) variety. Terbium responds efficiently to x-ray excitation and is, therefore, used as an x-ray phosphor. Terbium alloys are also used in magneto-optic recording films, such as TbFeCo.
DYSPROSIUM	Dysprosium is most commonly used as in neodymium-iron-boron high strength permanent magnets. While it has one of the highest magnetic moments of any of the rare earths, this has not resulted in an ability to perform on its own as a practical alternative to neodymium compositions. It is, however, now an essential additive in NdFeB production. It is also used in special ceramic compositions based on BaTiO formulations.
HOLMIUM	Holmium has the highest magnetic moment (10.6μB) of any naturally occurring element. Because of this it has been used to create the highest known magnetic fields by placing it within high strength magnets as a pole piece or magnetic flux concentrator. This magnetic property also has value in yttrium–iron–garnet (YIG) lasers for microwave equipment. Holmium lasers at a human-eye safe 2.08 microns allowing its use in a variety of medical and dental applications in both yttrium–aluminum–garnet (YAG) and yttrium–lanthanum–fluoride (YLF) solid state lasers. The wavelength allows for use in silica fibers designed for shorter wavelengths while still providing the cutting strength of longer wavelength equipment.

Table 1.3 (continued)

ERBIUM	Erbium has application in glass coloring, as an amplifier in fiber optics, and in lasers for medical and dental use. The erbium ion has a very narrow absorption band coloring erbium salts pink. It is therefore used in eyeware and decorative glassware. It can neutralize discoloring impurities such as ferric ions and produce a neutral gray shade. It is used in a variety of glass products for this purpose. It is particularly useful as an amplifier for fiber optic data transfer. Lasers based on Er:YAG are ideally suited for surgical applications because of its ability to deliver energy without thermal build-up in tissue.
THULIUM	Thulium products are mainly used in making crystals and lasers. An important application of thulium in the medicine area, and relatively independent of its high cost, is the production of portable x-ray sources. These sources are available for about one year, as tools in medical and dental diagnosis, as well as to detect defects in inaccessible mechanical and electronic components. This type of sources does not need excessive protection. Usually a small cap of lead is enough. Thulium can also be used in magnetic and ceramic materials (ferrite), similar to the yttrium–iron alloys, used in the microwave technologies.
YTTERTBIUM	Ytterbium is being used in numerous fiber amplifier and fiber optic technologies and in various lasing applications. It has a single dominant absorption band at 985 in the infrared making it useful in silicon photocells to directly convert radiant energy to electricity. Ytterbium metal increases its electrical resistance when subjected to very high stresses. This property is used in stress gauges for monitoring ground deformations from earthquakes and nuclear explosions. It is also used as in thermal barrier system bond coatings on nickel, iron and other transition metal alloy substrates.
LUTETIUM	Lutetium is the last member of the rare earth series. Unlike most rare earths it lacks a magnetic moment. It also has the smallest metallic radius of any rare earth. It is perhaps the least naturally abundant of the lanthanides. It is the ideal host for x-ray phosphors because it produces the densest known white material, lutetium tantalate ($LuTaO_4$). It is utilized as a dopant in matching lattice parameters of certain substrate garnet crystals, such as indium–gallium–garnet (IGG) crystals due to its lack of a magnetic moment.
YTTRIUM	Yttrium has the highest thermodynamic affinity for oxygen of any element; this characteristic is the basis for many of its applications. Some of the applications of yttrium include its use in ceramics as crucibles for molten reactive metals, in fluorescent lighting phosphors, computer displays and automotive fuel consumption sensors. Yttria-stabilized zirconium oxide is used in high temperature applications, such as in thermal plasma sprays to protect aerospace component surfaces at high temperatures. Crystals of the yttrium–iron–garnet (YIG) variety are essential to microwave communication equipment. The phosphor Eu:Y_2O_2S creates the red color in televisions. Crystals of the yttrium–aluminum–garnet (YAG) variety are utilized with neodymium in a number of laser applications. Yttria can also increase the strength of metallic alloys.
SCANDIUM	Scandium products are mainly used in ceramics, lasers, phosphors and in certain high performance alloys

Ductile Iron The rare earths played a leading part in the discovery and commercialization of nodular iron (Linebarger and McCluhan 1981). Nodular iron has properties similar to mild steel and is essentially a ductile cast iron. Nodular iron results when the graphite flakes in cast iron are converted to nodules. In the 1940s it was discovered that

spheroidal graphite could be routinely produced in the laboratory in irons containing 0.02% Ce. The rare earth elements cleanse the metal of elements that prohibit spherical graphite growth, and the compounds they then form provide heterogeneous substrates for graphite nucleation. Its good physical and foundry properties have made nodular iron an attractive engineering material, particularly in the automotive industry.

In the manufacture of nodular iron, rare earths are added as misch metal or mixed rare earth silicides and not as pure rare earth metals, mainly due to cost considerations (Davies 1981). Magnesium has emerged as a competition for rare earths for graphite nodularization in cast iron, threatening the continued use of misch metal for this purpose (Falconnet 1988).

Steels The deleterious effect of sulfur on the mechanical properties of freshly cast steel is well known. Iron sulfides form and concentrate at the boundaries between the grains of steel formed on solidification. Such steels are very brittle and fracture on working. Addition of rare earths to steel causes the sulfur content to be captured in the form of very stable compounds such as RE_2S_3 or RE_2S_2O. These compounds tend to form globular or spherical inclusions that do not concentrate at the grain boundaries, thus greatly enhancing ductility (Luyckx 1981). The sulfides and oxysulfides are very stable at steel making temperatures and, unlike other sulfides such as those of manganese, they neither deform nor elongate under processing conditions. As the rare earth concentration is increased, MnS inclusions are displaced by rare earth oxysulfides or sulfides. The stability of granular rare earth sulfides alleviates the detrimental effects of elongated MnS inclusions on toughness. Besides improvements in the toughness characteristics of HSLA steels, rare earth additions also improve fatigue, creep, and several other mechanical properties (Collins et al. 1961, Linebarger and McCluhan 1981) of steels. The rare earths react quite efficiently with hydrogen in steel and also lower the hydrogen diffusion coefficient.

Rare earths are added to steel as misch metal, rare earth silicides (RE content 30%), and alloys such as Fe–Si–10 RE, Mg–Fe–Si–0.1 to 0.2 RE. The effect of rare earth metals in steels, in whichever form they are introduced, is the same, and the amount of misch metal usually added to ferrous alloys is about 0.1 to 0.2%. Such small additions do lead to considerable beneficial effects in both nodular iron and steels. Starting in the late 1960s, rare earth additions to steel in the forms mentioned above became a widely accepted practice. The practice of adding rare earths to steel was reviewed by Wauby (1978). A few kilograms of misch metal were added to each metric ton of special steel used in the manufacture of an Alaska oil pipeline because misch metal improves the physical properties of steel under arctic conditions. Because of its use in the Alaska pipeline steel, a major increase in demand occurred for misch metal in the period 1971–1978. In spite of the fact that the major consumption of rare earths is in the iron and steel industry, the annual tonnage of that industry that is treated with lanthanides had indeed been very small (Haskin and Paster 1979). The use of rare earths in the form of rare earth silicides or misch metal in steels grew explosively in the 1970s and peaked around 1975. Since then the market for rare earth products dropped off, following the availability of cleaner steel and the use of calcium for ultimate desulfurization (Falconnet 1988).

Superalloys In the early 1960s, researchers at General Electric discovered that stainless steel containing both aluminum and yttrium possessed exceptional high temperature corrosion resistance. Beginning then and until about 1975, these alloys were produced for limited application in the nuclear industry (Davies 1981). This alloy, known as "fecralloy" to denote the presence of Fe, Cr, Al, and Y in it, has since been widely adopted for the fabrication of furnace heating elements and has been considered as a replacement for ceramic substrates in emission control catalysts for the automobile industry. Lanthanum is also used

in high temperature iron based alloys (Davies 1981). An alloy with 200 ppm lanthanum combines oxidation resistance to 1,100°C with good ductility and ease of fabrication.

Superalloys are essentially a class of heat-resistant alloys used in gas turbine engines, electric generators, jet engine exhaust nozzles, reaction vessels and, in general, as materials in intense high-temperature oxidizing environments. Certain rare earth elements are added to superalloys. Essentially, the rare earth elements are added to enhance their oxidation resistance. Yttrium is the active component in the M–Cr–Al–Y (Fe–Cr–Al–Y, Ni–Cr–Al–Y, Co–Cr–Al–Y) family of superalloys. The stability of alumina–chromia skin is enhanced by traces of yttrium. The alloys, even when applied by vapor deposition, form an oxide coating that exhibits remarkable adhesion because yttrium acts to prevent the formation of voids at the oxide/substrate interface. Lanthanum and cerium also play a similar role in certain nickel and cobalt superalloy compositions. Cerium is used in amounts ranging from 100 to 300 ppm in certain high strength nickel alloys to control sulfur and oxygen. Typically 200 to 400 ppm of lanthanum are added in nickel base and cobalt base high temperature alloys for gas turbine service. For example, lanthanum raises the operating temperature of nickel base Hastelloy-K from about 950°C to about 1,100°C. Without lanthanum, these alloys exhibit less resistance to cyclic oxidation, and lanthanum probably results in a firmly bound oxide layer. Misch metal in small concentrations (0.03–0.05%) added to electrical resistance alloys such as Ni–20 Cr causes the formation of dense and more adherent surface oxides, leading to a tenfold increase in service life, from 1,000 to about 10,000 h. The addition of cerium to the Cu78 high temperature aerospace alloy (Al–8Fe–4Ce) of Alcoa for enhancing its oxidation resistance was stated as the first major industrial use of cerium metal. Usually, less than 1 wt % of rare earths added in the form of individual metal leads to dramatic improvements in the performance of these superalloys.

Magnesium Alloys The beneficial effects of the addition of rare earths to magnesium alloys were discovered in the late 1930s by Haughten and Prytherch (1937). Sauerwald (1947) discovered the exceptional grain refining action of zirconium in magnesium. Murphy and Payne (1947) showed that the rare earth additives are compatible with zirconium, and enhanced properties could be obtained by incorporating both rare earths and zirconium. Subsequently, zinc (Emley 1966) or silver were also included as desirable additives to these alloys.

At high temperatures, as compared with conventional magnesium alloys, magnesium alloys containing about 3% misch metal and 1% Zr show enhanced creep strength (Kremers 1961). Significantly higher strength at all temperatures was obtained by using Di(Nd + Pr) in place of misch metal as the alloying constituent. The new generation magnesium alloys contain individual rare earths. One of the two magnesium alloys for use in high performance engines for aircraft, space rockets, and satellites, possibly as castings, contains 4% zinc and 1% misch metal and can be used in applications seeing temperatures as high as 160°C. The other, which contains 5.5% yttrium, 3.5% other rare earths, and 0.5% zirconium, is stable at temperatures up to 280°C (Jackson and Christiansen 1993). A Mg–Al–Zn–Nd alloy has good corrosion resistance in an aqueous saline solution and a Mg–Y–Nd–Zr alloy was shown to have good corrosion resistance, good castability, and stability up to 300°C. Rare earths refine the grain, improve strength, ductility, toughness, weldability, machinability, and corrosion resistance in the host alloy.

Improving upon the commercially available Mg–Y–Nd–Zr alloy, a lower weight high creep resistance quarternary alloy consisting of Mg–Sc–Mg–Zr has been developed by researchers at TU Clausthal, Germany (Hedrick, 2001).

It has also been found that a melt spun amorphous magnesium alloy containing 10 at % cerium and 10 at % nickel has good ductility, and in addition, a tensile fracture strength more than twice as large as conventional optimum age hardened alloy.

Aluminum Alloys A small amount of yttrium (100 ppm) in combination with zirconium was found to increase (by 50%) the conductivity of aluminum transmission lines (Davies 1981). The addition of misch metal to aluminum base alloys used for high tension transmission line has led to improved tensile strength, heat resistance, vibration resistance, corrosion resistance, and extrudability. An yttrium–magnesium– aluminum alloy has been developed in China for transmission cabling (McGill 1997).

The aluminum alloys 22Si–1MM and 2.5Cu–1.5Ni–0.8Mg–1.2Fe–1.2Si–0.15MM possess good high temperature properties and fatigue strength and are used in automobile industry, air craft, small engine, and other fields. A new aluminum alloy composed of aluminum, iron, and cerium is also under development as a replacement for titanium components in specific applications in the range of 90 to 315°C. Cerium imparts the required corrosion resistance at elevated temperatures (Jackson and Christiansen 1993). Significant improvements in high strength Al–Mg and Al–Li alloys have been obtained by the addition of scandium (McGill 1997).

The addition of scandium to aluminum increases the yield strength as it reduces the grain size. The scandium aluminum alloy has been used in a premier line of baseball and softball bats. The high strength alloy allows the bats to have thinner walls, less weight and greater rebound (Hedrick 1997).

A low density glassy alloy containing about 90 at % Al, up to 9 at % transition metals and about 5 at % rare earths has been under development (Kilbourn 1988). The transition metals considered were iron, cobalt, and nickel and the rare earths were cerium, neodymium, and yttrium. These materials, produced by melt spinning, have extremely high tensile strengths, about twice that of the best crystalline commercial alloy, good ductility in addition to low density. These characteristics are attractive for aerospace applications.

An Al–8 wt % Fe–4 wt % Ce alloy was made by the rapid solidification (RS) technique of melt spinning and processed further by powder metallurgy techniques. These alloys rely on the rapid gettering of oxygen by the rare earth. The stability of dispersed oxide particles thus formed improve the high temperature performance of the alloys (Kilbourn 1988), particularly creep resistance, elevated temperature tensile strength, thermal stability, and corrosion resistance. Compared to the heat-treatable ingot metallurgy products whose elevated temperature properties are limited to 175°C, the RS Al–Fe–Ce alloys retain good strength even up to 340°C.

About 1 to 3% misch metal in aluminum–carbon composite improves the wetting by carbon and hence the incorporation of graphite dispersoid in the metal matrix, resulting in a material with improved tensile strength.

Titanium Alloys Yttrium, in concentrations of approximately 200 ppm, was found to improve ductility and ease of fabrication of vacuum arc melted titanium alloys (Davies 1981). Microalloying of various commercial titanium alloys with rare earths has also resulted in improved strength, stress rupture, and oxidation resistance.

Rapidly solidified titanium alloys (the rare earth addition, particularly Y, Nd, Er, or Ce ranged from 1 to 2%) showed improvements by orders of magnitude in high temperature yield strength, stress rupture life, and creep resistance. The most important of the rare earth additives have been those with erbium or yttrium (Mahajan and Rama Rao 1988).

Copper Alloys The addition of misch metal or yttrium to oxygen-free high conductivity (OFHC) copper enhances oxidation resistance without affecting electrical conductivity.

For example, the oxidation resistance nearly doubled at 600°C when 0.1 wt % Y was added to the copper.

Misch metal additions have been used to improve the hot workability and deep drawing characteristics of bronzes containing less than 1 wt % lead, and also the wear resistance of highly leaded bronzes. Adding misch metal in leaded bearing bronze reduced the coefficient of friction by a factor of four.

Zinc Alloys Misch metal is a constituent in the alloy Galfan (Zn–5% Al–0.05% MM) used in galvanizing baths. This alloy, developed by the International Lead–Zinc Research Organization, is superior with respect to corrosion resistance and permeability to standard galvanized steel sheet and wire of equal coating thickness and has comparable paintability and weldability properties (Radtke and Herrschaft 1983).

Oxide Dispersion Strengthened (ODS) Alloys In ODS alloys the high thermal stability of the rare earth oxides such as Y_2O_3, CeO_2 impart desirable properties like high temperature strength, creep resistance, and resistance to cyclic corrosive oxidation (Kilbourn 1988). Yttria (0.25 to 1.3%) is introduced into the nickel–chromium and iron–chromium alloys by mechanical alloying. The mechanical alloying is a high energy ball milling process that permits solid-state processing and results in the biggest improvement in properties. After mechanical alloying, the alloy powder is processed by powder metallurgy techniques. The products are high temperature high strength ODS alloys, which have found use in gas turbine blades, combustors, and other such applications.

Long Range Ordered Alloys Long range ordered alloys such as $(Fe,Co)_3V$, $(Fe,Ni)_3V$, and $(Fe,Co,Ni)_3V$ have been materials with potential for high temperature applications. The addition of a small amount of Ce (<0.1%) together with titanium has been found to double the rupture ductility, substantially lower the creep rate, and considerably improve the rupture life of some of these alloys (Mahajan and Rama Rao 1988). In another application, mixtures containing Zr, Ce, and Y oxides of controlled particle morphology are plasma sprayed onto the metal surfaces to create barrier coatings for the protection of the metal substrates against high temperature degradation.

1.7.2 Magnets

Among the numerous applications of the rare earths, one of the most spectacular has been their use in the new generation permanent magnets. In the late 1960s, samarium alloyed with cobalt was first used in magnets, and in the 1980s the cheaper and more powerful neodymium–iron–cobalt magnets also became available (Wernick 1995).

Sintered magnets of the $SmCo_5$ type, the first of the rare earth magnets to be available commercially, possess specific magnetic properties much superior to the well-known and hitherto well-established ferrite and alnico magnets. This is shown by values in Table 1.4. The intermetallic $SmCo_5$, because of its hexagonal structure, exhibits a high degree of uniaxial anisotropy, resulting in extremely high coercivity, which in turn results in considerably greater energy product.

The magnetic strength of Sm–Co compounds is predominantly from the cobalt atoms. Samarium apparently helps define an anisotropic structure "locking" the cobalt moments in place and rendering demagnetization difficult (Molycorp, 1993).

The rare earth cobalt magnets can be extremely short and still provide adequate magnetizing force. The superior properties of rare earth magnets not only permitted

extensive miniaturization in a wide variety of consumer and industrial products, but also resulted in performance characteristics hitherto unattainable. The products in which rare earth magnets have been or are used include wrist watches, "hi-fi" equipment, high power DC motors, magnetic bearings, computer peripherals, microwave tubes, and so on.

Both samarium and cobalt are expensive and limited in supply and this made the $SmCo_5$ magnets expensive. The disadvantage of the high cost of samarium was sought to be offset by using misch metal in its place. The use of misch metal offers significant cost reduction particularly for large volume applications such as in electric machinery. The theoretical energy product of $PrCo_5$ is 30% higher than that of $SmCo_5$ but $PrCo_5$ has substantially weaker anisotropy compared with $SmCo_5$ (Wallace et al. 1988). Praseodymium, which is more abundant than samarium was considered to replace Sm in $SmCo_5$ materials (Kilbourn 1988). The use of praseodymium in magnets would give it application in a quantity it has never had before.

Table 1.4 Some properties of commercially available conventional and rare earth magnets

Magnet	Properties				
	$(BH)_{max}$, kJ/m^3	Br, T	H_cB, kA/m	H_cJ, kA/m	T_c,°C
Barium ferrite					
Plastic bonded	18	0.245	175	207	450
Sintered	25	0.365	175	180	450
AlNiCo					
Cast	35	1.15	50	50	860
$SmCo_5$					
Plastic bonded	60	0.570	390	600	725
Sintered	180	0.950	720	1800	725
Sm_2Co_{17}					
Sintered	210	1.050	770	1635	775
NdFeB					
Plastic bonded	80	0.680	460	820	340
Sintered	250	1.175	825	960	310

A new generation of samarium–cobalt magnets that not only permitted savings in raw material costs but also provided enhanced magnetic properties was based on the 2:17 alloy, Sm_2Co_{17}. The most widely used of the 2:17 alloys are of the type $Sm(Co, Cu, Fe, M)_x$, where M = Zr, Hf, or Ti, and x is in the range 7.0 to 7.85. These magnets have found use, particularly in Japan, as stepping motors for quartz analog watches, in high performance audio pick ups, and loudspeakers.

The discovery of $Nd_2Fe_{14}B$ magnets in 1984 ushered in a new era for the rare earth–transition metal based permanent magnets. The Nd–Fe–B magnets are high strength magnets with a magnetic energy of up to 50 MGOe, which is a factor 2.5 times greater than that of $SmCo_5$ magnets, with high remanence and coercive force. The highest magnetic strength commercial product available is rated at 42 MGOe (Hedrick 2001). There is a large potential for these magnets because iron, which is cheap and available in abundance (unlike the scarce and costly cobalt), is present as the main constituent (82.4 at %). Neodymium is also in ample supply, being the third most abundant rare earth and constituting 13% of bastnasite and 18.5% of monazite ores.

Nd–Fe–B magnets have extensively penetrated commercial markets. Initially used in Japan in data processing and audio-visual equipment in nonextreme thermal environments, their first large scale application was linked with the substitution of ferrite magnets by Nd–Fe–B magnets in small electric motors of automobiles, an application pioneered by General Motors. Another use of Nd magnets lies in the medical applications such as magnetic resonance imaging equipment. The worldwide production of neodymium magnets is and will be driven strongly by the electronic industry (especially the manufacture of computers and portable devices like cellular phones) as well as by automotive and industrial applications. Starting in about 1985, rare earth metal demand was greatest for neodymium metal used in high strength permanent magnet alloys (Hedrick 1997). World production of Nd–Fe–B magnets in 1999 was 13500 t for sintered magnets and 2740 t for bonded magnets (Hedrick 2000). Since 1990, the demand and hence production was gaining at 28.6% per year for the sintered and 25.7% for the bonded. The NdFeB magnet applications, currently growing at 15% overall annual growth rate (Tourre 1998) are roughly as follows: motors in electronics, particularly hard disc drive (HDD) applications are 69% of the global market, automotive and appliance motors constitute 14%, magnetic resonance imaging (MRI) another 10% and other applications, especially acoustics, make up the remaining 7%.

It was anticipated that with neodymium in ample supply the neodymium magnet cost would drop to a level where it would replace not only the Sm–Co magnets, but also the AlNiCo. The main limitation of the Nd–Fe–B magnets is their lower Curie temperature (about 300°C). This leaves the field open for Sm–Co magnets (Curie temperature 700 to 900°C) for uses where this property is of major importance.

The coercivity of Nd–Fe–B high strength permanent magnets is enhanced by using Dy as an additive. Dysporium probably substitutes into the magnetic phase, creating $Nd_{2-x}Dy_xFe_{14}B$ with higher anisotropy (hence higher coercivity) than the unsubstituted material (Molycorp, 1993).

The continuing search for new permanent magnet materials has led to the emergence of certain rare earth–iron intermetallic compounds modified by interstitials such as nitrogen and carbon, such as $Sm_2Fe_{17}N_{\approx 3}$ (Coey et al. 1991). Interstitial modification has been found to bring in advantages like an increase in Curie temperature and development of a strong uniaxial anisotropy (Collocott et al. 1999).

1.7.3 Terfenol

Magnetostriction is a property exhibited by certain materials and these materials are known as magnetostrictive materials. A magnetic field applied to a magnetostrictive material makes it expand or contract and, conversely, when stress is applied to the magnetostrictive material, a magnetic pulse is generated. The property of magnetostriction was discovered in 1971 but it took another 15 years before commercial application of the phenomenon became possible with the development of suitable materials (Jiles 1994). Iron alloys of rare earths such as Tb, Sm, and Dy exhibit properties of very large magnetostriction and find application as transducers for the conversion of magnetic pulse to mechanical energy. The Laves phase alloy $Tb_{0.3}Dy_{0.7}Fe_{1.9}$ (terfenol-D) in particular shows outstanding magnetostrictive properties and has attracted much attention for development (Clark 1979). The magnetostriction in an applied field exhibited by terfenol is approximately 100 times larger than that of nickel, the well-known metal exhibiting magnetostriction. Terfenol changes dimension

in a magnetic field instantaneously and this effect is essentially at the heart of advanced transducers and micropositioners. The uses of terfenol are also in areas of high power actuators, acoustic devices, broad-band sonar devices, micropositioners, fluid control valves and micropumps (Gschneidner and Daane 1988, McGill 1997).

Terfenol-D was also slated for use as the small material to control fluid flow in natural gas fuel injection in light duty diesel engines (Hedrick, 2000).

Dysporium–terbium–iron magnetostrictive alloys are also being developed for use as actuators to allow precision positioning of the next generation space telescope (NGST). This use is based on the alloys' ability to expand and contract accurately when subjected to a magnetic field (Hedrick 1998). Incidentally, NGST would have 6 to 12 times the surface area of the Hubble space telescope.

1.7.4 Magnetic Refrigeration

Gadolinium metal and alloys have been considered as the working substance in magnetic refrigeration cycles (Hashimoto et al. 1981). The underlying principle of magnetic refrigeration is that a gadolinium-based solid heats up in a strong magnetic field and cools when removed from the field. This system works even at room temperature but has greatest prospects in cryogenic applications. Initially GdPd was used, and later the gadolinium aluminum garnet (GAG) single crystal and intermetallics $(Dy_{0.5}Er_{0.5})Al_2$ and $TbNiO_2$ were used as magnetic refrigerants for cooling to as low as 4 K. The refrigerator using the magnetic refrigerant is called the active magnetic regenerative magnetic refrigerator AMR-MK (Hedrick 1985a). The main advantages of the magnetic refrigerator are the compactness and large refrigeration power per unit volume. It is also reliable, vibration free, and more efficient than most cryogenic cooling systems particularly below liquid nitrogen temperature (77 K). The novel magnetic properties of ^{141}Pr nuclei find use in a nuclear demagnetization refrigerator (Mueller et al. 1980). The intermetallic $PrNi_5$ has been used to obtain temperatures as low as 27 μK in conjunction with nuclear magnetic cooling of copper.

Gschneidner et al. (1999) have reported two major breakthroughs in magnetic refrigeration. They successfully demonstrated that sub-room temperature magnetic refrigeration is a viable and competitive technology vis-a-vis conventional gas cycle compression/expansion refrigeration. In a laboratory prototype refrigerator using 3 kg of Gd spheres as magnetic refrigerant in a magnetic field of 5 T, they achieved a cooling power of 600 watts, operating in a maximum temperature span of 30 K, while running the apparatus for more than 1,200 h over a 10-month period. They also reported the discovery of the giant magnetocalorific effect (MCE) materials $Gd_5(Si_xGe_{1-x})_4$, which have MCEs ranging from 25 to 200% of better than the known prototype magnetic refrigerants such as gadolinium. As an added attraction, their Curie temperatures are tunable from 40 to 290 K by changing the Si to Ge ratio in this material. These new materials can make magnetic refrigeration more efficient. Refrigeration systems based on the new material can have application in home and automobile air conditioning, and in household appliances like refrigerators, freezers and ice makers (Hedrick 1997).

1.7.5 Magnetooptic Materials

Amorphous $Tb_{25}(Fe_{0.9}Co_{0.1})_{75}$ thin films are RF or DC sputtered on a substrate and coated by a transparent ceramic film. A laser beam is used to write, read, or erase the information

on the amorphous alloy by making use of the Kerr rotation. Information storage densities, 15 to 50 times more than that usual in a conventional magnetic hard disc have been achieved. Gadolinium has been used instead of terbium in this application.

Information storage using cylindrical domains in a sheet of magnetized material was first reported in 1967. These domains were named bubble domains because they moved in a perturbing field much like bubbles move on a liquid surface. The stability of bubble domain is maximum when its diameter is approximately equal to or more than the thickness of the magnetic sheet in which it is situated. A high packing density requires domain diameters of three micrometers or less. Hence, the magnetic material in the bubble domain memory must be a thin film supported by a substrate. Rare earths are used in making bubble domain memories. The substrate is a nonmagnetic garnet, GGG (gadolinium gallium garnet), $Gd_3Ga_{15}O_{12}$, usually prepared by the well-known Czochralski, or pulling, technique. Magnetic garnet films are deposited on this substrate and the typical composition of the film for micrometer diameter bubble is $Y_{1.25}Lu_{0.45}Sm_{0.4}Ca_{0.9}Fe_{4.1}Ge_{0.9}O_{12}$. Both the substrate and the thin film in the bubble domain memory contain rare earths. The quantity of rare earths in the thin film is not very significant. However, substantial quantities of gadolinium have been consumed for making the substrates.

1.7.6 Ceramics

Rare earth oxides, particularly ceria and yttria, are used as sintering aids in powder metallurgical fabrication due to their ability to eliminate weakening voids (Jackson and Christiansen 1993). For instance, during the sintering of silicon nitride, the Si–Y–O–N liquid phase is formed. On cooling, the nitride grains regroup and the yttrium oxynitride cools into a microcrystalline intergranular bond between the grains, and this resists crack development. The silicon nitride thus obtained is used in hot zone engine parts and high speed cutting tools.

Yttria has a major use in the stabilization of the high temperature cubic phase of zirconia. The stabilized zirconia (YSZ) is one of the best high temperature, high strength, and thermal shock resistant refractory compositions that is stable under many conditions of oxidation and reduction at elevated temperatures. It has high thermal insulation properties and is used as a barrier coating to protect hot parts in jet engines. Due to the presence of oxygen defects, YSZ has an electrical resistivity that permits its use as an oxygen sensor in automobile exhaust systems. YSZ has also been adopted for use as SO_2 sensor (Hedrick 2000). The concentration range of SO_2 can be sensed from 1 ppm to 1000 ppm.

An integral part of the emission control system in automobiles is the exhaust oxygen sensor, which feeds back information for control of the air–fuel ratio. This is necessary to ensure that the exhaust gas composition is very near the stoichiometric point so that the catalytic converter system, which not only oxidizes the hydrocarbons and carbon monoxide in the exhaust gases but also reduces the nitrous oxide, operates efficiently (Kennard 1981). Stabilized zirconia is a key material in this sensor. The stabilizers used are calcia, magnesia, or yttria. While calcia or magnesia stabilization has cost advantages, yttria stabilization results in better ionic conductivity. Ytterbia is still better but more expensive. Oxygen sensors based on yttria-stabilized zirconia also have use in industrial furnaces and in the measurement of oxygen content in molten glass, molten steel, and other metals. They are also used in research in solid electrolyte galvanic cells. In medicine, YSZ is used for hip replacement parts, and in dentistry it is used for tooth filling. Yttria-stabilized zirconia has also been used as an electrode in the high temperature electrolysis of water. Yttria-stabilized

zirconia cells have been tested in certain advanced space programs for the production of O_2 from CO_2 (McCallum 1998).

The formation of solid solution of ceria with, for example, trivalent cations such as Y or La results in oxygen ion vacancies that are mobile. Oxygen diffusion is fast whereas the cation diffusion is slow. The defect fluorites then formed have good oxygen conductivity and are considered novel electrolytes for temperatures above ≈600°C.

A long life (>5000 h) ceramic heating element for use in air up to 1,900°C is based on $La_{0.84}Sr_{0.16}CrO_3$. This material combines electrical conductivity and structural rigidity in an oxidizing environment and has significantly extended the operating temperature range of compact furnaces in air.

The electrical conductivity of $CaCrO_3$ is fairly constant at around 0.1 $(\Omega\text{-cm})^{-1}$ in the range 500°C to 1900°C. The conductivity can be greatly increased by adding calcium and strontium at levels up to 20 mole % to give (LaM) CrO_3. Further, the conductivity of $Ca_{0.84}Sr_{0.16}CrO_3$, already > 2 $(\Omega\text{-cm})^{-1}$ at room temperature rises to > 10 $(\Omega\text{-cm})^{-1}$ above 300°C and remains close to this value up to 200°C. There are two important uses for (La,M) CrO_3. One is as furnace heating elements. The most important use will be as the crucial inter-cell conducting material in solid oxide fuel cells (SOFC) (Minh 1993).

Ceramic fuel cells, also called solid oxide fuel cells (SOFC's) generate electricity directly from the reaction of a fuel with an oxidant. Power is produced electrochemically by passing a hydrogen-rich fuel over the anode and air over the cathode and separating the two by an electrolyte. In producing electricity, the only byproducts of SOFC are heat, water and CO_2. A current government-industry partnership program in U.S.A. is aiming to ready a 1-megawatt fuel cell micro turbine power plant. These cells operate at 1000°C. $LaMnO_3$ is a P type conductor and Sr-doped $LaMnO_3$ has a high electronic conductivity in oxidizing atmospheres. It is the preferred cathode material for use in severe conditions of SOFC's.

Another perovskite, (La,M) CoO_3, has properties to be considered for use as possible catalytically active electrodes stable in high temperature aggressive environments for fuel cells and sensors (Molycorp 1993).

Many application possibilities have been indicated (McGill 1997) for rare earths in ceramics. These include the use of La_2O_3, Y_2O_3, and CeO_2 with Ni, Co, Cr or Zn as electrodes in fuel cells with zirconia–yttria solid electrolyte, and the use of $LaCrO_3$ and $LaCoO_3$ electrodes in magnetohydrodynamic generators. Rare earths containing perovskites have been considered for certain catalytic applications (Gunasekaran 1988).

In fact rare earth perovskites, represented generally by $REMO_3$ where M is a transition metal, are of continuing interest in many developing technologies. These are electrocatalysis, high temperature electrodes and electrolytes, and membranes for gas separation and sensors (Molycorp 1993). The wide range of application also results from potential for possible fine tuning of structure in these compounds.

Pure cerium oxide has been used as opacifier in ceramic glazes (Greinacher 1981). In the 1960s, praseodymium (Pr_6O_{11}, 90%) was used with zirconium oxide, in the ratio ZrO_2, 62–64%; SiO_2, 32–33%; Pr_6O_{11}, 3–6% (Kudo 1988), as a beautiful yellow pigment in ceramics. Praseodymium is built into the zirconium silicate lattice and thereby results in the full optical splendor. The praseodymium pigment is stable at high temperatures.

Cerium sulfide, CeS, and also yttria are also used as materials for making crucibles besides being used as high temperature materials (McGill 1993). CeS has one of the most negative free energies of formation for sulphides and has been proposed as a containment material for very reactive molten metals such as uranium and titanium (Krikorian and

Curtis, 1988). CeS has electrical conductivity like metal, high thermal conductivity, high melting point (2442°C), good thermal shock resistance and is also machinable like a metal (Molycorp, 1993). Samarium, europium, gadolinium, and dysprosium oxides are used in the nuclear industry in radiation-shielding ceramic compositions. Rare earths (Eu, Sm, Ce) oxides have also been used to improve light fastness of lead chromate and titanium dioxide pigments and also to impart natural fluorescence to artificial teeth.

In 1971, Heartling and Land (1971) first reported achieving optical transparency in a ferroelectric ceramic material, lanthanum modified lead zirconate titanate (PLZT) solid solution. The PLZT ceramics ($Pb_{1-x}La_x(Zr_{1-y}Ti_y)O_3$) have interesting applications in military and industrial devices. These applications include use in thermal/flash protection goggles, data display recorders, stereoviewing systems, eye safety devices such as electronic welding helmets, and in image storage devices (Heartling 1981). The basic operation of these devices relies on the change in the optical properties of the ceramic with the strength and direction of electric field applied to it, and the changes are brought about rapidly. The use of PLZT as electromechanical transducers and their piezoelectrical properties have also been studied (McGill 1993). The rare earth used in these applications is lanthanum, and the PLZT is made by conventional ceramic fabrication methods of hot pressing and polishing. Remarkable effects on optical transparency are achieved when the amount of lanthanum exceeds 7 at % in the ceramic.

The attractive thermionic properties of LaB_6 were identified by Laferty (1951) at General Electric Company, U.S.A. This compound, with the melting point above 2,500°C, also has a low vapor pressure, low work function, and excellent thermionic emission current. It is superior to tungsten but is more expensive. It is used in the electron gun of electron microscopes where high electron intensities are very desirable.

More than any other material LaB_6 shows resistance to attack by aggressive fluorine at very high temperatures. This property leads to many strategic applications involving fluorine gas. The resistance is conferred by the formation of an adherent fluoride film on the boride (Molycorp 1993, Holocombe et al. 1982).

Researchers in China have noted that when rare earths are incorporated in a cemented carbide, a 50 to 100% improvement in carbide tool life was observed. The improvement is, however, dependent on both the rare earth used and how it is incorporated in the mixture. (Hedrick 2001).

1.7.7 Electronics

The hexaborides of rare earths are a unique electric resistor material that has near zero temperature coefficient of resistance, a feature not provided by metals. Formation of glass frits and LaB_6 can be screen printed and fired to provide resistor components required in modern integrated circuitry (Molycorp 1993).

Rare earth materials find use in electronic devices that convert one form of energy to another (Jackson and Christiansen 1993). Both input and output are electricity in some cases, but the output variance is determined by thermal or radiation energy. The rare earths in these materials are added to synthetic garnet crystals such as yttrium–iron, yttrium–aluminum, and gadolinium–gallium. Yttrium–iron garnets or YIGs ($Y_3Fe_5O_{12}$) have found important uses in reactor and communication devices. Yttrium and gadolinium are also used in garnets for microwave applications. Besides use as microwave filters, yttrium aluminum garnet or YAG, ($Y_3Al_5O_{12}$) crystals when doped with small quantities of neodymium or erbium can be used for lasers. The YAG single crystal has many desirable

properties for use in high power solid state lasers. It is hard and optically isotropic and has sites suitable for trivalent rare earth ion substitution without charge compensation. The most common solid state laser is based on neodymium (Weber 1979). It is usually in a glass or YAG host. Nd, present at around 1 to 5 wt % in the host, is exposed to intense broad spectrum light, and the Nd atoms absorb the light and are pumped to an excited energy state. Then follows the lasing transition to a lower energy level and the production of light emission at or very close to 160 nm. The exact wavelength depends on the host. Neodymium doped YAG emits at 1064 nm, which is in the infrared region. This laser is quite popular in cutting, welding, and metal heat treating applications. The Ho–YAG and Er–YAG lasers emitting at 2000 nm and at 2900 nm respectively have been developed for use in microsurgery, in place of CO_2 lasers. Ho^{3+} ion lases at ≈2.08 microns, an eye-safe wavelength. Er–YAG lasers lasing at ≈2.9 microns have also been found useful in dental work (McCallum 1998). This wavelength is sharply absorbed by water. It is thus possible to effect energy delivery without thermal buildup in tissue. Single crystal gadolinium–aluminum–scandium garnet (GASG) doped with nickel and chromium is likely to be used in tunable and high power laser applications. Neodymium doped $Gd_3Ga_5O_{12}$ (GGG) crystals are used in high power pulsed lasers. A frequency doubled 532 nm neodymium doped YAG (Nd : YAG) laser with a green beam was approved for medical use by the U.S. Food and Drug Administration. Rare earths such as Pr, Nd, Ho, Er, and Tm used in a variety of hosts such as $CaWO_4$, YAG, and $LiFY_4$ are materials for optically pumped or activated solid state lasers with a wide variety of wavelengths. Multilayer capacitors essential to electronic equipment require dielectrics with a high electric constant and a capacitance invariable over a wide temperature range, −50 to +120°C. The so-called "NPO" dielectric material used in such capacitors contain neodymium barium titanate formulations. The components present probably include $Bao:Nd_2O_3:nTiO_2$ (n ≈ 3 to 5) (Molycorp 1993). Rare earths have also been used in the miniaturization of capacitors (La_2O_3, Gd_2O_3, Dy_2O_3) and in the production of thermistors (Haskin and Paster 1979). Gadolinium oxide has been used in making optical fibers.

Significant quantities, several hundred tons, of cerium are used annually, in the form of cerium ammonium nitrate solution for etching on substrates in the electronic manufacturing industry (Kudo 1988).

1.7.8 Chemical

The largest single application of rare earths, in which the naturally occurring rare earth mixture is useful, is in the manufacture of rare earth containing zeolite cracking catalysts required in the petroleum refining process (Wallace 1981, Venuto and Habib 1979). In petroleum refining, catalysts are used to increase the yield of gasoline obtained from the heavier oil fractions by cracking. In the early 1960s, it was discovered that incorporation of small amounts of zeolite in a silica–alumina matrix resulted in considerable enhancement in the performance of the catalyst in gas–oil cracking. From then on zeolite cracking catalysts have largely replaced the amorphous silica–alumina catalysts used previously. Zeolites are made catalytically more active and thermally more stable at the operating temperatures by replacing the sodium in them with rare earth ions. Rare earth exchanged zeolites are prepared by many methods and the rare earth content of the catalyst may vary from 0.5 to 5%. The rare earth starting material used commercially for the manufacture of these catalysts is usually a mixture of rare earth chlorides or nitrates. Rare earth usage in commercial petroleum cracking catalysts started in 1964.

Porous zeolite catalysts, having as much as 5% rare earth lining in their cavities, were particularly used in the production of leaded gasolines. Oil refineries, however, have been phasing out leaded gasolines since 1985 and phasing in higher octane varieties. Rare earths tend to lower octane rating and rare earth use is declining in this industry.

The rapid decline in the demand of rare earths for fluid cracking catalysts was also the result of environmental legislation reducing the amount of lead allowed in gasoline (Hedrick 1997). The refinery industry began substituting fluid cracking catalysts that used significantly lower amount of rare earths, particularly lanthanum concentrates and rare earth chlorides.

In the chemical process industry, rare earth elements have been used or considered for use as catalysts for ammonia synthesis, alkylation, isomerization, hydrogenation, dehydrogenation, dehydration, polymerization, refining of hydrocarbons, and oxidation (Molycorp 1964–1970, Molycorp 1971–1976, Rosynek 1977, Peters and Kim 1981). Methanation catalysts contain rare earths, the ability of rare earths to form hydrides being useful here (Coon et al. 1978). Rare earth chelates with diketones were considered for use as antiknock compounds (McGill 1993), as replacements for the well-known lead compounds.

The multivalency of europium and cerium have led to the exploration of some interesting possibilities of energy conversion in aqueous systems (McGill 1997).

Catalytic converters have been used in automobiles since the 1970s to convert hydrocarbons, carbon monoxide, and nitrogen oxides in the engine exhaust to water, carbon dioxide, and nitrogen. The catalysts comprise γ-alumina and small amounts of precious metals, and are activated by cerium, which is about 5% by weight. Cerium provides oxidation resistance at high exhaust temperatures, stabilizes rhodium and palladium dispersions, minimizes the interaction of rhodium with alumina, and enhances the oxidizing ability of the system. Efforts have also been made to substitute lanthanum-enriched palladium for the more expensive rhodium.

Actually the role of ceria in automotive exhaust catalysts is complex. In addition to enhancing the catalytic activity of precious metals deposited on it, its function is described as "an oxygen storage component" that enhances performance when the exhaust gases are fuel rich/air poor. Anyway, ceria is a crucial ingredient in the catalysts used to control vehicle exhaust emissions and an average catalytic convertor contains approximately 50 to 75 gms of CeO_2 (Molycorp 1993).

1.7.9 Optical

The optics industry encompasses a vast range from glasses through lasers and fiber optics to phosphors and fluorescent lights. Through the use of rare earths in these products, communication and vision have improved. The 4*f* electrons in the rare earth elements possess narrow and sharp absorption–emission lines in the visible range, and this plays a role in the use of rare earths in the optics and phosphor industries.

An early and continuing use of the rare earths is in the manufacture of glass. As in 1896, Dressback patented and manufactured a mixture containing cerium and other rare earth oxides for decolorizing glass (Riker 1981). This, incidentally, was the first commercial use of cerium. Iron oxide is always present as an impurity in glass and causes a yellow green color. If decolorizing is necessary due to iron contained in the glass, cerium is added to oxidize the iron. While a chemical decolorization of iron is achieved by oxidation to the trivalent state, physical decolorization is achieved by selective absorption by didymium

through optical compensation. A combination of chemical and optical decolorization may be used.

While small amounts of CeO_2 decolorize glass, ~1% CeO_2 makes glass yellow and larger amounts of CeO_2 make glass brown. Neodymium colors glass bright red, praseodymium colors glass green, and their mixture colors glass blue. Holmium also colors glass blue. Erbium oxide gives a pale pink color to the glass, and this color cannot be obtained by any other means (Riker 1981). Because of the stability of trivalent erbium, glass formulations with Er are colored pink. It is the only pink truly stable in glass melts. Pink coloration by erbium is used in ophthalmic materials like sunglasses as well as in decorative crystal glassware. Decoration in glass due to impurities such as ferric ions can be neutralized or complemented by erbium absorption, resulting in the formation of a neutral gray, colorless shade. Incidentally, this is the dominant use for erbium, and erbium oxide of ≈96% purity can be used for this purpose (Molycorp 1993). Further coloring effects are obtainable by combining rare earths with other elements, for example, titanium + cerium for yellow, selenium + neodymium for violet, and nickel + neodymium for red. Cerium is used only in conjunction with other coloring oxides.

In 1912, Crookes of England found cerium to be excellent for ultraviolet (UV) absorption without imparting color to the glass, a feature useful in protective eyeglasses. Crookes absorptive sunglasses contain the natural ratio of Nd/Pr together with a high amount of Ce to give a good UV cutoff. Glasses with 2 to 4% Ce_2O_3 (or Pr, Nd oxides) absorb UV and infrared (IR) radiation and are used in the production of glassblowing and welding goggles. Didymium oxide has long been used in welder's goggles because of a high concentration of Nd and Pr, which effectively absorb yellow sodium light.

A neodymium-doped glass light bulb has been introduced by GE for use in typical incandescent applications around home. The powder blue colored bulb uses neodymium to absorb the yellow spectrum, which is more prevalent in the emission from a tungsten filament than from natural sunlight, and provides a more sunlight-like light with richer colors and improved surface definition of the home environment (Hedrick 2001).

Neodymium oxide together with vanadium trioxide is used for making optical glass for photometers and nicol prisms. Most cathode ray tube face plates use Ce-stabilized glass. Cerium prevents browning/fogging of glass under nuclear radiation (γ rays and cathode rays). Large quantities of radiation-shielding windows, which provide very high transmission without darkening due to formation of color centers, were needed in the nuclear industry. As the result of much development work in the 1950s and 1960s, cerium is used in radiation-shielding windows. Cerium in container glass prevents colorization caused by UV radiation and protects the product.

Lanthanum was first used in the optical glass industry in 1935 by Morey (1938). Low silica glass containing lanthanum oxide possesses a high index of refraction and low dispersion and is extensively used in the manufacture of camera and other lenses (Greinacher 1981). Optical glass for camera lenses is made from a "lanthanum–flint" composition containing Ca_2O_3 and B_2O_3 (Molycorp 1993). Lanthanum oxide does not impart color to the glass. Optical glasses containing up to 40% lanthanum oxide are made and these are also corrosion resistant. Gadolinium is also added to optical glasses meant for use in magnetooptical and electrooptical systems. It is very important that the rare earth materials introduced into the optical glasses be 99.9–99.995% rare earth oxide in purity (Riker 1981) and that no radiation-absorbing oxides are present. In Japan, the world's largest manufacturer of optical glasses, consumption of La_2O_3 has been considerable because of large volume production of autofocus SLR cameras and video cameras.

Praseodymium is used for vacuum deposited antireflection coating on lenses and as a constituent in tinted glass filters for selective light absorption.

The rare earth elements act as activators in laser glasses. Neodymium is the most popular rare earth for this purpose (Greinacher 1981) and this use has already been described. Neodymium can be incorporated in very large glass rods and intense pulses (up to 10^{15} watts) can be generated from neodymium lasers (Singh 1988). A rare earth laser crystal neodymium (Nd^{3+}) doped lithium niobate ($LiNbO_3$) emits a continuous three-color beam: red, green and blue. The red and green emissions are obtained by frequency doubling and the blue emission is created by self-sum frequency doubling (Hedrick 2001). Glasses doped with rare earths such as Nd, Yb, Er, and Ho could possibly find future technological applications in the areas of luminescent solar concentrators and light sources for fiber optics in addition to use as laser materials. Luminescent solar concentrators have been prepared using a combination of Nd^{3+} and Yb^{3+} with UO_2^{2+} or Cr^{3+}. Fluoride glasses for fiber wave guide sources contain Er^{3+}. Glass fibers containing rare earths can transmit data over exceptionally long distances without booster stations. The glass for these fibers, which may be composed of fluorides of lanthanum, zirconium, barium, aluminum, sodium, and hafnium, is formed by chemical vapor deposition, rather than through a melt to minimize impurities (Jackson and Christiansen 1993). Erbium doped fiber amplifiers (EDFA) are used for optical communications in terrestrial long trunk and undersea cable applications (Auzel and Goldner 1999).

This is the current major high technology application of erbium. Optical telecommunications rely on signals transmitted down silica fibers. The signals use a wavelength of 1.55 microns which is a low-loss wavelength window in the fiber. Incidentally, erbium lases efficiently at this wavelength in the fiber and can be pumped by light of other wavelengths such as visible or near infrared, thus enabling a very efficient optical method of amplification.

Erbium-doped fiber amplifier (EDFA) contains lengths of fiber, doped with ppm levels of erbium spliced into the optical fiber at regular intervals. Along with the signal energy the pumping energy is also transmitted down the fiber. The Er in the EDFA lases, amplifying the longer wavelength light signal that also propagate down the complete fiber.

The first application of cerium oxide or cerium rich rare earth oxide mixture in glass polishing began in the European glass industry by about 1933, spread to the Canadian optical industry by about 1940, and to the United States in the following years (Horrigan 1981, Duncan 1970). Special REO compositions containing 50 to 90% cerium oxide, the remainder being other light rare earth elements, are used to polish glass surfaces without abrading. Polishing agents such as rouge, silica, and zirconia are slow and dirty and leave minute scratches. REO compounds are much faster and cleaner and provide a superior finish. Polishing with REO is mostly a chemical reaction and water plays an active role. According to the chemical–mechanical hypothesis (Horrigan 1981), in the ceric oxide polishing of glass, the formation of CeO–Si activated complex permits the rupture of O–Si–O bonds by hydrolysis. Subsequently, the complex CeO–Si breaks apart, the hydrated silica is swept away along with the alkalis released from the glass surface and the process repeats.

The quantity of cerium-based products used in the U.S. for polishing mirrors, plate glass, television tubes, ophthalmic lenses, and precision optics was approximately 340 metric tons in 1960. The advent of the Pilkington process in 1972–73 for large scale plate glass manufacture curtailed this market for cerium oxide; however, over 1000 metric tons of cerium-based products continued to be used for polishing in the U.S. by the 1980s.

1.7.10 Phosphors

The first application of a rare earth element in a sophisticated technology was in 1965, thanks to the work of Levine and Palilla (1965), when a material consisting of Eu doped in an yttrium-containing host $Eu^{3+}{\cdot}YVO_4$ was introduced as red phosphor in color television picture tubes, replacing the previously used Ag activated CdS red phosphor. The strong and sharp emission lines of europium at 610 nm without a yellow component, perceived by the eye as a wonderfully saturated red color tone, provided an evenly colored TV picture. Subsequently, YVO_4 was replaced by either Y_2O_3 or Y_2O_2S. Both these phosphors are better than the vanadate because their energy conversion efficiency is greater and their emission is a bit more orange. Color for television and computer screens is obtained through the use of three phosphors: a europium–yttrium compound for red, a terbium fluoride–zinc sulfide for green, and a cerium–strontium sulfide for blue. When activated by photons, these phosphors emit the luminescence that makes the screen attractively colorful. Each color TV screen requires approximately 5–10 g yttrium oxide and 0.5–1 g europium oxide (Jackson and Christiansen 1993). Since 1964, the TV industry has been using highly purified Y and Eu oxides in ton quantities. The purities required exceed 99.9% and many individual impurities in excess of 100 ppm may be deleterious. The TV face plate contains neodymium oxide which blocks ambient light from ruining the picture.

A new rare earth phosphor, lithium doped $Gd_2O_3{:}Eu^{3+}$, has been developed in Korea for flat panel field emission displays. This phosphor is said to have higher cathode luminescence than the widely used commercial phosphors, europium doped yttrium oxide and europium doped yttrium oxy-sulphide (Hedrick 2000).

Another phosphor with potential use for field emission arrays to produce compact lightweight displays that consume less electricity than CRTs is the green rare earth phosphor $SrGa_2S_4{:}Eu^{2+}$. This could potentially substitute for the use of the standard green CRT phosphor ZnS:Cu, Al (Hedrick 1998). Several CRT phosphors contain Tb. For example, Tb:YAG and $Tb{:}Y_2SiD_5$, a phosphor for high intensity green emission needed for projection TVs (Welker 1991, Ronda et al. 1997).

Rare earth based phosphors are composed of rare earth activators and host lattice. The optical spectral inertness of hosts such as lanthanum, gadolinium, yttrium, and lutetium, ensure that they do not interfere with the activator emission spectra. There is an added advantage of close chemical similarity, which makes substitutional incorporation of rare earth activators in these hosts possible. Besides, rare earth hosts such as oxides, oxysulfides, phosphates, vanadates, and silicates are rugged materials compatible with high temperature operations involved in tube processing and in their reclamation (McColl and Palilla 1981). Some more examples of cathode ray tube phosphors are $Ce_2O_2S{:}Tb^{3+}$, $CaS{:}Ce^{3+}$, and $SrGa_2S_4{:}Eu^{2+}$ for green, and $SrCl_5(PO_4){:}Eu^{2+}$ and $ZnS{:}Tm^{3+}$ for blue (McGill 1993).

An organolanthanide phosphor (OLP) for potential commercial use in flat panel displays has been developed by researchers at the University of Oxford, U.K. The polymer material is an organoterbium emitter. A high efficiency organic electroluminescent device that produced a green light with peak luminescence of 2000 candelas per square meter has also been fabricated (Hedrick 2001).

Ce (III) has no absorption bands in the visible but does absorb strongly just outside the visible spectrum, in the UV region. Solids with Ce(III) often show strong optical absorption and luminescence in the UV or near UV. Cerium is used in several CRT phosphors. In fluorescent lighting, phosphorous Ce is also used as a sensitizer for other lanthanide emitters.

A number of rare earth phosphors have been developed for conversion of x-radiation into visible light, which then strikes photographic film (Rabatin 1981). Phosphors that consist of Tb^{3+} – Gd_2O_2S or Yb^{3+} – La_2O_2S, Eu – BaFCl, Tm – LaOBr, and La_2O_3–Tb have allowed significant reduction in the x-ray dosage required for medical radiographic data. For example, Tb activated gadolinium oxysulfide, currently the most popular x-ray phosphor, enables up to 80% lower x-ray dosage to patients. In addition to reduced exposure to patients as well as to staff, the advantages of rare earth phosphors over the originally used calcium tungstate phosphor include need for less silver in the film and a sharper picture because of reduced patient movement within a shorter time interval (Jackson and Christiansen 1993). Eu-based phospho-luminable phosphors are in use for the automation of x-ray detection systems. The phosphor used is Eu doped BaFBr or variations of this material. The phosphor used absorbs the x-ray radiation. In a separate later processing step, upon stimulation by a small spot laser beam, the phosphor emits visible radiations proportional to the absorbed dose (Crawford and Brixner 1991). Gadolinium compounds act as hosts in scintillator materials such as Eu: $(Y, Gd)_2O_3$, Pr, Ce:Gd_2O_2S for computed tomography (Greskovich and Duklos 1997). The RE_2O_2S materials account for a significant fraction of the world's use of rare earth elements. Important among these are Y_2O_2S for TV phosphors and other oxysulphides for x-ray screens. The luminescence of Tm under x-ray excitation is in the near UV (= 375 nm) and blue (= 465 nm). This closely matches the sensitivity normal photographic film. Tm:LaOBr is a sensitive x-ray phosphor helpful in reduction of x-ray exposure of patients (Molycorp 1993).

In another application to films, CaF_2:Eu is placed in front of a solar cell to convert UV sunlight into the visible region where the solar cell can efficiently convert it into electricity (McCallum 1998).

Scintillation is a flash of light produced in a phosphor by absorption of an ionizing particle or photon, and a scintillation counter is a device for detecting and counting scintillations produced by ionizing radiation. Scintillation detectors are used to detect x-rays and gamma rays. A lanthanum chloride compound doped with 10% trivalent cerium emits at 330 nm and 350 nm. This compound may be used as a scintillation detector. The cerium-doped lanthanum chloride compound has better energy resolution and improved response times than the thalium-doped sodium iodide, the most commonly used scintillation detector material (Hedrick 2000).

Rare earths are also useful as lamp phosphors. The three spectral lines most important to human vision are blue-violet near 450 nm, green near 535 nm, and orange-red near 615 nm. Lamp phosphors activated by Eu^{2+} supply the blue-violet color. Commercial phosphors based on the broad emission of Eu^{2+} at just the right spectral position for the blue are Eu:$Sr_5(PO_4)_3$cl, Eu:Ba $Mg_2Al_{16}O_{27}$ and Eu:$Sr_4Al_4O_{25}$. Trivalent terbium, holmium, and erbium are candidates for pure green emission but had problems compared to the old trustworthy zinc silicate:Mn^{2+}. Thus, the addition of rare earths to the phosphors in fluorescent lamps makes the light appear more natural. Some of the phosphors employing terbium's green emission are Tb : $(La,Ca)PO_4$, Tb : $CaMgAl_{11}O_{19}$, Tb : $(Ca,Cd)MgB_5O_{10}$. Europium and terbium are used as activators with yttrium, lanthanum, or gadolinium as hosts. The resultant light is stronger and leads to approximately 25% savings in capital and operating costs (Jackson and Christiansen 1993). Energy-efficient illumination, ranking high in visual efficiency, is given by rare earth phosphors based on scandium also.

Scandium, in small amounts, has been widely used by the lighting industry in the manufacture of metal halide lamps. Because of the hygroscopicity of the scandium iodide, it is incorporated by a special process that forms the iodide *in situ* in the lamp by reacting

a small piece of scandium with elemental iodine. Scandium metal is used by lamp manufacturers in the form of uniform small discs (Davies 1981). Dysprosium is also used in metal halogen lamps to improve brightness (Kudo 1988).

The atomic emission spectra of dysporium at high temperature contains many lines in the visible spectrum. Dysporium is added as anhydrous halides, e.g., DyZ_3. The salts dissociate in the lamps hot center, absorb energy there and emit radiation efficiently producing high intensity illumination. The ions later recombine at the lamp's cooler wall surfaces (Molycorp 1993).

The role of rare earths in lamp phosphors was summarized by Thornton (1981) with this statement: the emission from rare earth phosphor is not only useful but made to order for the requirements of the human visual system for optimal seeing.

Rare earth silicates are useful as specialized phosphor hosts. Yttrium orthosilicates are commercial phosphors and also have potential for projection TVs. The high efficiency and very fast decay time of $Ce:Y_2Si_2O_7$ material makes it suitable for specialized CRT use. $Ce:Gd_2SiO_5$ is a potential scintillator for positron emission imaging and gamma ray detection (Molycorp 1993). A new class of luminescent materials represented by the blue-white phosphor Sr_2CeO_4, which has an unusual type of one-dimensional chain structure, is said to have a possible future use in flat panel displays, fluorescent lighting, television and computer CRT monitors, and temperature sensing (Hedrick 1998).

The samarium compound $SrB_4O_7 : Sm^{2+}$ is usable above 100 gigapascals and to a temperature of 800 K. This is the material in a new optical pressure gauge developed for diamond anvil cells. Pressure measurement is based on shift in the fluorescence line of the material. Traditionally, shift in the fluorescence line of ruby was used for pressure measurement, and samarium compound emits in the same range as the ruby line, but with higher intensity (Hedrick 1998).

1.7.11 Nuclear

Rare earths have found a variety of applications in nuclear energy. One of the largest uses of Gd oxide is in the nuclear power industry. It is used in General Electric Company's boiling water reactors (BWRs) as a burnable portion. Gadolinium oxide is mixed directly with uranium oxide, and its presence in the fuel helps in achieving a uniform neutron flux during the lifetime of the fuel element. Gadolinium not only has a high neutron absorption cross section but also a burn-up rate similar to that of ^{235}U. Besides Gd_2O_3 has physical and chemical properties very similar to UO_2. Gadolinium is used intimately mixed at ~5% with UO_2 in a pellet form. About 2 metric tons of Gd oxide were estimated to be in use in 26 operational BWRs in the U.S. A gadolinia burnable poison system for pressurized heavy water reactors (PHWRs) was under development at Babcock and Wilcox. Besides gadolinium, the elements Eu, Sm, and Dy have a large capture cross section for thermal neutrons, and dysprosium has also been considered as a burnable poison. Europium is unique because, like hafnium, it exhibits a high capture cross section. Not only is the cross section of the naturally occurring mixture of isotopes of europium high, but also each of the five isotopes of the uninterrupted series ^{151}Eu, ^{152}Eu, ^{153}Eu, ^{154}Eu, ^{155}Eu, each one forming on capture of a neutron by the one with one mass number less, has large capture cross sections. This property is valuable for the use of europium for control rods in compact nuclear reactors (Greinacher 1981), as, for example, in nuclear submarines. Europium hexaboride, EuB_6, has been considered as the neutron absorber material in fast breeder reactors. This boride

has both europium and boron as neutron absorbers, and the novel neutron absorbing properties of europium are combined with the hexaboride stability (Molycorp 1993, Pasto and Tennery 1977).

The neutron absorbing isotope ^{167}Er has properties that can provide an extremely long life time for nuclear fuels for specialized reactors. It has been used in a U–Zr–H fuel in research submersibles. Erbia, Er_2O_3, is also homogeneously mixed with UO_2 fuel, to enable pressurized water reactors to operate with a 2-year load recycle (Jonsson et al. 1992).

Yttrium has a low capture cross section for thermal neutrons and was considered as a material for tubing in molten salt nuclear reactors. Because of high hydrogen atom density and high temperature stability, Ce and Y hydrides are useful as neutron moderators (Greinacher 1981). The (n, β) reaction characteristic of Gd and Dy and their availability as thin foils have also greatly benefitted the nondestructive technique of neutron radiography (Davies 1981).

Neutron radiography is a useful practical tool for nondestructive testing in the aerospace, nuclear, and engineering industries, and its widespread use very much depends on the availability of gadolinium and dysprosium in the form of thin foils. In neutron radiography, like in x-ray radiography, an imaging beam is passed through the specimen and the attenuated beam is recorded to produce an image of the internal details of the specimen. The recording medium in neutron radiography is also a standard x-ray film. This film, however, is insensitive to neutrons and so needs an aid to produce the image. The aid is a 0.025 mm thick gadolinium foil placed in direct contact with the x-ray film. When exposed to the attenuated thermal neutron beam, the gadolinium absorbs neutrons and promptly emits beta radiation (electrons), and the x-ray file is sensitive to the beta radiation. Dysprosium is used for the same purpose but differently. In neutron radiography, dysprosium foil generally 0.1 mm thick is exposed to the attenuated neutron beam but in the absence of the x-ray film. The exposed dysprosium foil is then removed from the beam and its beta decay (nuclear transformation by emission of beta rays) is used to produce an autoradiograph in contact with the x-ray film. This technique, using dysprosium, has been particularly suitable for radiography of highly radioactive materials (Davies 1981).

Dysporium doped crystals, particularly $CaSO_4$ or CaF_2, have been used in dosimeters for monitoring exposure to ionizing radiation, such as gamma rays or neutrons (Molycorp 1993). Such a crystal on exposure to energetic radiation creates in situ and qualitatively excited Dy atoms. When the crystal is heated these atoms luminesce producing a glow peak. The magnitude of the glow peak is related to the radiation dose. Thalium doped in $CaSO_4$ is used in dosimeters for radiation measurements. This is used for precise measurements of low radiation doses in the range 0.1 mR to R, for example in personal badge detectors (Molycorp 1993).

The exceptional thermal stabilization of monazite and xenotime structures, possible single phase behavior up to their melting points, combined with limited chemical reactivity has led to the suggestion that rare earth phosphates be considered as hosts for the long storage of radioactive waste (Molycorp 1993).

1.7.12 Hydrogen Storage

An application for the rare earths that was identified in 1969–1970 concerns the hydrogen energy system. The ability of the intermetallics REM_5, where RE is the rare earth and M is iron, cobalt, or nickel, to absorb a large amount of hydrogen at room temperature was

identified in 1969 by Zijlstra and Westendorp (1969) of the Philips Research Laboratories, Eindhoven, The Netherlands. The following year, Van Vucht, Kuijpers and Brunning (1970), also from the same laboratory, revealed the remarkable hydrogen absorption properties of $LaNi_5$. This intermetallic absorbs hydrogen readily at room temperature to form the compound $LaNi_5H_6$, which has per cubic centimeter more hydrogen than even liquid hydrogen. It also gives off hydrogen at a higher temperature and the whole absorption and desorption process is essentially reversible with only a small hysteresis loop. Lanthanum nickel intermetallic can be used commercially as a hydrogen storage medium and for related technological applications. Solid state storage of hydrogen offers advantages in volume, weight, pressure, energy savings, and safety over cryogenic and compressed gas.

While $LaNi_5$ is most efficient in terms of both capacity and kinetics, it also remains more expensive than the majority of its rivals. Lanthanum in $LaNi_s$ can be partially replaced by cerium, praseodymium, neodymium, misch metal or thorium, and nickel by Al, Co, Cr, Cu, Fe, or Pt. It is thus possible to vary the hydrogen absorption–desorption properties for various commercial applications or for basic research studies (McGill 1997, Gschneidner and Daane 1988, Buschow 1984).

The world's largest hydrogen storage vessel was made by Kawasaki Heavy Metal Industry (Omachi 1988). The vessel has a capacity of 175 Nm^3 and carried a total 1000 kg charge of La-rich misch metal–nickel alloy for hydrogen storage, and is operated at 700 kPa (at 30°C) stage pressure. Compared to high pressure hydrogen storage of the same capacity, the vessel is 30% lighter and occupies only ~14% of the volume. Besides, in one cycle of absorption–desorption, hydrogen gas is upgraded in purity from 99.99% to 99.99999%. The Japanese also have been developing hydrogen fueled cars and even have successfully road tested a Toyota wagon (2000 cc, 4 cycles) driving a 200-km stretch at 100 km/h. In this, a La–MM–Ni–Al alloy was selected for hydrogen storage (Omachi 1988).

The hydriding reaction between hydrogen and lanthanum nickel alloy is specific and is usable as a method for separation of hydrogen and also for purification of hydrogen as mentioned in the previous paragraph. The metal hydride process for separation or recovery of hydrogen from industrial off-gas streams consists of two steps: hydrogen absorption and hydrogen desorption. The off-gas feed stream is passed through a packed bed containing the hydriding alloy while maintaining the hydrogen partial pressure in the stream at more than the equilibrium decomposition pressure (of the hydriding alloy) to enable absorption of hydrogen by the bed. In the second step, the absorbed hydrogen is recovered by desorbing the hydrogen from the bed either by increasing the bed temperature or by lowering the system pressure. This scheme has advantages such as reaction specificity (only hydrogen reacts), high hydrogen recovery, product purity (>99.9%) and energy efficiency (Huston and Sheridan 1981). The metal hydride process has been investigated for hydrogen recovery from ammonia purge gas stream generated during ammonia manufacture. When the objective is hydrogen purification, after absorbing residual gaseous impurities are expelled by simply desorbing a portion of the hydride.

The possibility of reversible hydrogen absorption–desorption over a range of temperatures has been used in hydride chemical compressors. Hydrogen is absorbed at low temperatures and pressures and desorbed at a higher temperature and pressure. At Brookhaven National Laboratory, U.S., a $LaNi_{4.5}Al_{0.5}$ alloy was used and hydrogen pressures up to 7600 kPa were attained in capsules. The unit also delivered 1.2 m^3 of hydrogen at 4250 kPa in a continuous operation (Huston and Sheridan 1981).

Hydride heat pumps have been devised on the basis of the reversibility of metal–hydrogen reaction and the heat of the chemical reaction. In these devices, which are

closed units comprising two or more hydride beds, hydrogen functions as the energy carrier. With no moving parts in the system, heat can be pumped over large temperature differentials by a suitable choice of hydriding alloys, heat sources, and heat sinks. These hydride pumps can operate with low grade heat. A demonstration unit made by Ergenics used $LaNi_5$ and $LaNi_{4.7}Al_{0.3}$. This unit generated hot water at 95–100°C from wastewater at 60°C and 20°C cooling water. In Japan, hydrogen heat pumps have been used to function as an air-conditioning system (Omachi 1988). The pump used 800 kg of MM–Ni–Ca–Al alloy and had a capacity of 630 MJ/h. This air conditioner, installed at an 18-room leisure house in a spa in Hokkaido, operated efficiently with energy input from the spa's hot water for cooling in summer and warming in winter. A large chemical heat pump using 3500 kg of MM–Ni–Co–Al alloy, having a capacity of 1300 MJ/h, was also developed in Japan (Omachi 1988). A hydride refrigerator that could cool to as low as –240°C (33 K) without using electricity has also been described (Jackson and Christiansen 1993). In a chamber, lanthanum nickel hydride was heated to 104°C. Stored hydrogen gas was released and this gas was passed through a heat exchanger and was then allowed to expand. The expansion cooled the gas considerably and some liquid hydrogen was also formed. The gas was conducted to another chamber where it was absorbed by more alloy to form the hydride. The cycle was then repeated using the new hydride until the cooling chamber attained the target temperature.

Two types of hydrogen-based rechargeable batteries containing rare earth elements have been proposed (Jackson and Christiansen 1993). Both offer good cycling life, high energy and power density, effective protection from over- and under-charging, and superior low temperature behavior. In the first type, electrodes composed of lanthanum, neodymium, nickel, cobalt, and silica are used. In the second type, which was made by the Sharp Corporation of Japan, in the form of 20 mm diameter buttons giving 1.2 V, the battery is composed of a nickel–oxide anode, a lanthanum–nickel–tin cathode, and a separator of polyamide resin containing caustic potash. When an electrical load is applied, the cathode releases contained hydrogen that consists of protons and electrons, the protons pass through the separator to the anode, and the electron generates electric current. For alkaline nickel–metal hydride batteries, two families of metal hydrides are widely used. They are the AB_5 and AB_2 intermetallic compounds where, in general, A is a late transition or a rare earth element, and B is one or more early transition elements (Züttel et al. 1999). A popular AB_5 alloy is $Lm(Ni_{3.6}Mn_{0.4}Al_{0.3}Co_{0.7})$, where Lm stands for lanthanum-rich misch metal (≈50 wt % La). The AB_5 type alloys, which form hydrides up to AB_5H_6, are currently replacing the cadmium electrodes in nickel cadmium batteries because they are environment friendly and have high energy density. The NiMH (nickel metal hydride) batteries are the leading rechargeable battery product, ahead of nickel–cadmium and lithium ion types. NiMH batteries are used in cellular phones, portable computers, personal data assistants (PDAs), camcorders and other portable devices (Hedrick 2001). These batteries are also recommended as midterm technology for electrical vehicles by the United States Automotives Battery Consortium (Vogt 1998). NiMH batteries are used in both hybrid electrical vehicles (HEV) and pure electric vehicles (PEV). By 2000, HEVs were commercially available in the U.S. The commercially available HEV Honda Insight with a NiMH battery outputs 144 volts and in the Toyota Prius, the battery produces 274 volts. The driving ranges of the PEVs range from 55 km to 240 km (Hedrick, 2000). In the 1990s demand has increased for rare earth metals used in nickel hydride rechargeable batteries.

1.7.13 Superconductor

A topic that has generated considerable worldwide interest in relatively recent times is high critical temperature (T_c) superconductivity. Until recently all the known high T_c materials contained either yttrium or one of the lanthanides (Kilbourn 1988). A ceramic compound of Y, Ba, Cu, and O exhibits zero resistance at 90–100 K, making it possible to replace expensive liquid helium with the cheaper liquid nitrogen as a refrigerant for the superconductor. These new superconductors have already been fabricated in thin films, the form used in electronic circuits, on a laboratory scale in the U.S. Large scale commercial use of these superconductors will depend on whether these materials can sustain the high currents necessary in applications such as electricity pylons, power generators, electric storage units, and electric motors. Another potential application area is in devices where power losses are usually significant but currents are small. The major developments in the field have been extensively reviewed (Wu et al. 1987, Hatfield and Miller 1988). As far as the rare earths are concerned, the practical realization of commercial high T_c superconductors would mean an unprecedented demand for several of the rare earths.

1.7.14 Miscellaneous

Rare earth metals have been useful as getter materials for removing residual oxygen in a small confined volume. The great affinity of the rare earths for oxygen is the basis of this application.

A remarkable application of cerium, developed in the 1980s, is in starch polyacrylonitrile copolymers, that absorb 500 to 1000 times their weight of water. These copolymers have been developed in Japan for making baby diapers (Kudo 1988). For this application, cerium is used in the form of oxide or hydroxide, in quantities of several hundred metric tons per annum. Cerium is used as a high pressure antiwear lubricant. Cerium fluoride is added to greases, pastes and suspensions used as lubricants (Molycorp 1993).

An interesting application of rare earths, widely practiced in the People's Republic of China, is to use the rare earth elements as trace nutrients in agriculture. The positive effects of rare earths on plant growth have also been claimed by Buckingham et al. (1999) in Australia while Diatloff et al. (1999) from the same country have not found a positive effect on plant growth.

Rare earths have also been used in radiopharmaceutical therapy (Turner 1998). For this application, β emitting radiolanthanides such as holmium-166 (half-life 26.8 h), samarium-153 (half-life 46.3 h), and lutetium-177 (half-life 6.7 days) have been suggested as suitable. These radionuclides also emit γ photons of suitable energies for quantitative imaging on conventional γ cameras. Their half-lives correspond to the required irradiation time for the tumor cells and thus minimize radiotoxicity to normal tissues. All these qualify them as tools for radiopharmaceutical treatment of cancer patients for whom conventional therapy has failed.

Rare earths are used in the paints and pigments industry (Desai 1988). Cerium compounds with or without the hydrous oxides of aluminum or silicon are used extensively to coat lead chrome paints to improve their light fastness. Titanium dioxide pigment is treated with cerous acetate to improve resistance to sunlight and outdoor durability particularly for the pigments applications in synthetic fibers, molding compositions of high polymers,

paints, powder coatings, and wire coatings. A water-based yttrium coating to provide corrosion resistance and a lead-free primer for paints has been developed (Hedrick 2001). Yttrium hydroxide coating is applied by electrodeposition from an yttrium salt and converted to yttrium oxide during heat curing.

Rare earth compounds also find use in the paint industry as dryers, in the textiles industry, as oxidizing agents for self-cleaning ovens and also in wastewater purification (McGill 1997). Lanthanide caroxylates are used as paint dryers. Cerium carboxylates addition in alloyed resin promote drying of the resin coating by accelerating the cross-linking reactions within the polymer skin. Cerium salts are used as combustion additions. These salts, soluble in hydrocarbon, promote the complete oxidation of diesel fuels (Molycorp 1993). Cerium stearate controls the labile hydrogen in PVC, limits the high temperature dehydrochlorination reactions and hence confers high temperature stability to PVC.

Cerium and titanium dioxide have been used to make an improved electrorheological (ER) fluid. The viscosity, stiffness and heat transference of the fluid can be varied using an electric field. Under the field, the particles in the ER fluid are polarized and organize into structures, thus increasing the viscosity. Cerium-doped titanium dioxide in dimethylsilicone oil had five to six times higher shear stress than pure titanium dioxide. Potential applications of the rare earth material are in viscous clutches, variable cushion shock absorbers and other variable coupling devices (Hedrick 2001). A process that allows cerium dioxide to be used as a sunscreen has been developed. Cerium dioxide particles are coated with a 10-nm layer of boron nitride which eliminated agglomeration, provided cerium catalytic activity and produced a slippery feel when incorporated into an organic thin film. The coated cerium particles had higher transparency and greater UV blocking than the common sunscreen ingredients such as titanium dioxide or zinc oxide. The improved sunscreen reduces sunburn, reduces skin aging and reduces potential causes of skin cancer (Hedrick 2000).

The total rare earth consumption can be distributed among many major end-use categories. The approximate distribution in the year 2001, in the U.S. (Hedrick 2002) by end use was as follows:

Glass polishing and catalysts = 34%

Petroleum refining catalysts = 16%

Automotive catalytic convertors = 15%

Metallurgical additives and alloys = 14%

Rare earth for lighting, television/computer monitors, radars and x-ray intensifying film = 9%

Permanent magnets = 8%

Other uses = 4%.

Although the rare earths occur abundantly in nature, they were never cheap materials. This has resulted in current rare earth users searching for a cheaper solution even for established applications of rare earths. The substitution of rare earths has been occurring in two ways. One is through the use of new processes and the other is through the use of new substances (Greinacher 1981, Falconnet 1988). These are listed in Table 1.5. It is, however, apparent that while substitution of rare earths occurred where metallurgical and magnetic

properties are involved, in those applications based on optical, chemical and certain special magnetic properties substitution appears less likely. Thus applications of rare earths in certain polishing applications, catalysts, phosphors, magnets, optical glass components, coloring and decoloring of glass, pigments, and intensifiers of x-rays will be long lasting.

Table 1.5 Alternatives to rare earths in applications.

Application	Rare Earth Material	Alternative
Metallurgy Nodular iron Steel	 Misch metal Misch metal, RE silicide	 Magnesium Calcium
Nuclear energy Control rod	 Europium	 Hafnium
Hydrogen storage	Lanthanum nickel alloy	Iron titanium alloy
Glass Polishing	 Cerium oxide	 Plate glass (Pilkington) process
Ceramics Glazed ceramic tiles	 Cerium	 Tin, zirconium
Catalysis	Mixed RE	High octane gasoline

Focusing on the scenario for the future demand of rare earths, the use of rare earths in applications such as automotive pollution catalysts, permanent magnets and rechargeable batteries will continue to increase with a growing demand for automobiles, electronic equipment, computers and portable equipment. Future growth is forecast for rare earths in applications such as rechargeable NiMH batteries, fiber optics and medical applications including magnetic resonance imaging (MRI) contrast agents, positron emission tomography (PET), scintillation detectors, medical isotopes, and dental and surgical lasers. Future growth is also expected for rare earths in magnetic refrigeration alloys (Hedrick 2001).

1.8 SUMMARY

What are rare earths? How were they all discovered and why did their discovery occur over an unusually long period of scientific endeavor? What are their properties? What types of interactions do they undergo? Apart from scientific curiosity, what had made researchers attempt to unravel the mystery surrounding the enigma called rare earths? These questions are briefly answered in this chapter. Notwithstanding the great scientific merit of studying the rare earths for their own unique characteristics, it is very clear that the rare earths are remarkably useful materials in an extensive range of technological fields. In many of these they are simply unsubstitutable. The rare earths are extremely useful materials and they are abundantly available in nature. The logical effort then will be to produce them cheaply in sufficient quantities and of required quality. This is not possible without a good understanding of the physics and chemistry of the rare earths. To study the physics and chemistry of the rare earths, in turn, the rare earths were needed in pure form. This "catch-22" situation, which persisted in the rare earth industry during the first four decades of the 20th century, was alleviated by the remarkable and highly rated research work conducted at

Ames Laboratory under the leadership of Professor Frank H. Spedding, starting from the late 1940s. Largely through these efforts, the technology became available that brought the rare earths within the reach of any scientist who wished to study them. Many research groups all over the world have investigated the rare earths and highlighted their scientific behavior and application possibilities.

This first chapter provides the backdrop needed to appreciate the remainder of the book. Specifically, this chapter provides the background necessary to understand the separation processes to isolate the rare earths from one another. Physical properties given are invariably related to their application potential in reduction and refining steps. Many of the applications listed also justify the necessity to take pains and obtain the required quantity of rare earth material.

CHAPTER 2

Resources of Rare Earths

2.1 INTRODUCTION

The rare earths are moderately abundant elements in the earth's crust that occur in a large number of minerals. Rare earths typically occur as carbonates, oxides, phosphates and silicides in the forming minerals. Rare earth minerals are found in hard rock and placer deposits located throughout the world, with unusually large deposits occurring in a few countries. Rare earth minerals in most of the deposits, however, are such that they can be recovered only as co-products or by-products of certain other minerals. In some important deposits, however, the rare earths can be recovered as the primary or main product. Even though there are a large number of rare earth minerals, much of the actual world rare earth supply comes from only a handful of sources. About a dozen more rare earth minerals also occur in deposits that can be used to supplement easily the rare earth supply. The total rare earths contained in world rare earth reserves is considered sufficient to meet the foreseeable demand for these elements, through the twenty-first century.

While the total rare earth content in world rare earth resources is large, the availability of individual rare earth elements has for long remained highly unequal. This situation is the culmination of many factors, both inherent and transient. The inherent factor is that while each of the rare earth minerals generally contains all the rare earth elements, the concentrations of individual rare earths in the mineral are, as a rule, highly unequal. In each mineral some rare earth elements are present in high concentrations while some others are in very low concentrations, and this, in turn, varies from mineral to mineral. Besides, there is a wide variation in the contents of different minerals in the rare earth deposits. The predominant mineral in world rare earth deposits is enriched with respect to rare earths of lower atomic numbers and highly depleted with respect to rare earths of higher atomic numbers. The next most important mineral is also similarly disposed, but to a lesser extent. As a result, the rare earths of lower atomic numbers are available more than the rare earths of higher atomic numbers. The transient factor relates to the by-product status of the rare earth minerals and the occurrence of the element thorium in some of them. These factors affect the current production of the minerals and hence the availability of individual rare earth elements present in them.

This chapter details the natural occurrence of the rare earth elements in several different minerals, the occurrence of the minerals in various deposits, and the location of the deposits in different countries of the world. The composition of the mineral and the

Table 2.1 Abundance of rare earth elements in the earth's crust

Element	Kleber and Love 1963	Jackson and Christiansen 1993	Sabot and Maestro 1995	McGill 1997	Lide 1997
Sc	10		10	5–10	22
Y	28	29	28	28–70	33
La	18	29	18	5–18	39
Ce	46	70	46	20–46	66.5
Pr	5.5	9	5.5	3.5–5.5	9.2
Nd	24	37	24	12–24	41.5
Sm	6.5	8	6.5	4.5–7	7.05
Eu	0.5	1.3	0.5	0.14–1.1	2.0
Gd	6.4	8.0	6.4	4.5–6.4	6.2
Tb	0.9	2.5	0.9	0.7–1	1.2
Dy	5.0	5.0	5.0	4.5–7.5	5.2
Ho	1.2	1.7	1.2	0.7–1.2	1.3
Er	4.0	3.3	4.0	2.5–6.5	3.5
Tm	0.4	0.27	0.4	0.2–1	0.52
Yb	2.7	0.33	2.7	2.7–8	3.2
Lu	0.8	0.8	0.8	0.8–1.7	0.8

distribution of individual rare earths in the mineral and the quantity of rare earths contained in the deposit are presented. The status of the rare earth deposits as a present or potential resource for rare earths is highlighted. An overall picture of the availability of rare earths, vis-à-vis their consumption, is given. The unequal availability of individual rare earth elements is mentioned, and estimates on the amounts of individual rare earth elements theoretically recoverable from world rare earth resources are provided.

2.2 CRUSTAL ABUNDANCE

The abundance or scarcity of an element is conveyed in a general way by its crustal abundance, which is its average concentration in the earth's crust. Many estimates of the crustal abundance of the rare earths have been made and values that differ considerably from one another have been reported. This is illustrated in Table 2.1. The values given by Lide (1997) represent the median of the various reported values. These values have been adopted for the present discussion. In terms of inherent abundance in the earth crust, the rare earths are not rare because the total rare earths abundance (220 ppm) is more than that of even carbon (200 ppm), and several rare earth elements are more abundant than many better known metals. This is presented in Table 2.1 and illustrated in Figure 2.1. Among the rare earths, the relative abundance varies widely. Those elements having even atomic numbers are more abundant than their odd numbered neighbors (Kilbourn 1988). The rare earths with lower atomic numbers (lighter rare earths), as will be described later, have larger ionic radii hence are more incompatible and therefore more strongly concentrated in the continental crust than the rare earths with larger atomic number (heavier rare earths). Thus lanthanum, cerium, praseodymium, and neodymium are the most abundant rare earths. The

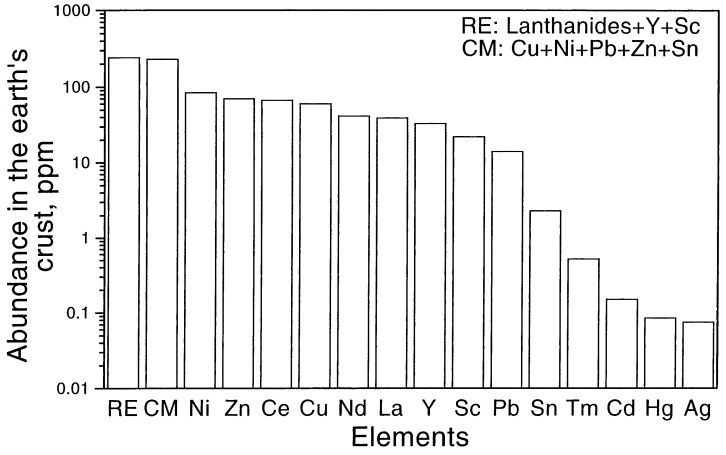

Figure 2.1 Abundance of rare earths and certain common elements in the earth's crust.

most abundant rare earth is cerium and the least abundant is thulium. In comparison it can be stated that cerium is more plentiful than copper; neodymium, yttrium, and lanthanum are more plentiful than cobalt or lead; praseodymium, samarium, gadolinium, dysprosium, and erbium are each more plentiful than tin; and ytterbium and thulium, the least abundant of the rare earths, are each more plentiful than mercury or silver.

The extent to which a metal is used in technology and is available commercially is determined not only by its crustal abundance but also by many other factors (Hampel 1961). These include (1) the degree of metal concentration by natural processes into ore deposits, (2) the relative ease of obtaining the ore from the environment, and (3) the feasibility of extracting the metal from the ore. Unlike the common metals like copper and lead, which form fairly concentrated natural deposits, the rare earths occur widely distributed in low concentrations. Added to this, the nature of their mineralization and the complexity of the processes needed for their extraction seems to justify the adage "rare" — even though considering crustal abundance alone they are not rare.

2.3 MINERALS

In nature the rare earths do not occur in the elemental state, nor do they occur as individual rare earth compounds. The rare earths, scattered dilutely in the earth's crust, occur as mixtures in many rock formations such as basalts, granites, gneisses, shales, and silicate rocks and are present in amounts ranging from 10 to 300 ppm (Sabot and Maestro 1995). Their strong affinity for oxygen has resulted in their being found mostly as oxidic compounds even though other combinations are possible. The rare earths occur in over 160 discrete minerals. Most of these minerals are rare but the rare earths content in them, expressed as oxide, can be as high as 60% rare earth oxide (REO). Many other minerals, in which the rare earths occur by atomic substitution, are also known (Aplan 1988). In total, nearly 200 minerals containing >0.01% rare earths are presently known (O'Driscoll 1991). As a rule, any rare earth mineral usually contains all the rare earth elements with some of them enriched and some others in very low concentrations.

Table 2.2 Important rare earth minerals

Mineral	Formula	Rare earth content, %	Other constituents, %
Aeschynite	$(Ce,Ca,Th)(Ti,Nb)_2O_6$	Ce_2O_3 15.5–19.5; $(Y,Er)_2O_3$ 0.9–4.5	TiO_2 21.2–24; Nb_2O_5 23.8–32.5; Ta_2O_5 0–7; ThO_2 11.2–17.5; CaO 2.3–2.7; FeO 2.2–4.3 also Sn, Mn, Mg
Bastnasite	$(Ce,La,Pr)(CO_3)F$	Ce_2O_3 36.9–40.5; $(La,Pr,..)_2O_3$ 36.3–36.6	CO_2 19.8–20.2 F 6.2–8.5
Euxenite	$(Y,Ce,Ca,U,Th)(Ti,Nb,Ta)_2O_6$	$(Y,Er)_2O_3$ 18.2–27.7 $(Ce,La,...)_2O_3$ 16–30	TiO_2 16–30; Nb_2O_5 4.3–47.4; Ta_2O_5 1.3–23; ThO_2 1–5; UO_2 0.4–12
Fergusonite	$(Y,Sr,Ce,U)(Nb,Ta,Ti)O_4$	Y_2O_3 31–42; $(Ce,La,..)_2O_3$ 0.9–6; Er_2O_3 0–14	$(Nb,Ta)_2O_5$ 46–57.5; ThO_2 1–3.4; UO_2 1.2–6; TiO_2 0–6; also ZrO_2, SnO_2, WO_3
Gadolinite	$(Y,Ce)_2FeBe_2Si_2O_{10}$	Y_2O_3 30.7–46.5 $(Ce,La,...)_2O_3$ 5.23	FeO 10–13.7; SiO_2 23–24.5; ThO_2 0.3–0.4; BeO 9–10.2; also Ca, Mg
Loparite	$(Na,Ca,Ce,Sr)_2(Ti,Ta,Nb)_2O_6$	$(Ce,La,...)_2O_3$ 32–34	TiO_2 39.2–40; $(Nb,Ta)_2O_5$ 8–11; CaO 4.2–5.2; Na_2O 7.8–9; also Sr, K, Si, Th
Monazite	$(Ce,La...)PO_4$	$(Ce,La,...)_2O_3$ 50–68	P_2O_5 22–31.5; ThO_2 4–12; U 0.1–0.3; ZrO_2 0 to 7; SiO_2 0 to 6
Orthite	$(Ca,Ce)_2(Al,Fe)_3Si_3O_{12}[O,OH]$	Ce_2O_3 0–6; La_2O_3 0–7 Y_2O_3 0–8	BeO 3.8; also ThO_2
Parisite	$Ca(Ce,La...)_2(CO_3)F_2$	Ce_2O_3 26–31; $(La,Nd,..)_2O_3$ 27.3–30.4 Y 8	CaO 10.4–11.4; CO_2 23–24.5; F 6–7
Priorite	$(Y,Er,Ca,Th)(Ti,Nb)_2O_6$	$(Y,Er)_2O_3$ 21.1–28.7 Ce_2O_3 3.7–4.3	TiO_2 21.8–34; Nb_2O_5 15–36.7; Ta_2O_5 0–1.3; CaO 1–4.1; ThO_2 0.6–7.9; UO_2 0.5–3; FeO 1.4–5.6; SnO_2 0–0.3; PbO 0.08; MnO 0–2
Samarskite	$(Y,Er,U,Ce,Th)_4(Nb,Ta)_6O_2$	Y_2O_3 6.4–14.5; Er_2O_3 2.7–13.4; Ce_2O_3 0.25–3.2; La_2O_3 0.37–1; $(Pr,Nd)_2O_3$ 0.74–4.2	Nb_2O_5 2.7–46.8; Ta_2O_5 1.8–27; ThO_2 0–4.2; UO_2 4–16 also Ti, Zr, Sn
Thorite	$ThSiO_4$		U_3O_8 10–16
Xenotime	YPO_4	Y_2O_3 52–62	ThO_2, UO_2 upto 5; ZrO_2 3; SnO_2, SiO_2 9
Yttrocerite	$(Ca,Y,Ce,Er)F_2$-$3H_2O$	Ce 8.5–11.5; Y 14.3–37.7	Ca 19.7–32.7 F 37.7–41.6

A listing of selected rare earth minerals from the point of rare earth extraction (Aplan 1988, Ferron et al. 1991, Jackson and Christiansen 1993) is given in Table 2.2. Even though the rare earth minerals are so many in number, about 95% of all the world rare earth resources occur in just three minerals, bastnasite, monazite, and xenotime. These three therefore are the principal ore minerals for rare earth extraction. Among these, again, bastnasite occurs most frequently, monazite is second, and xenotime is the distant third. Other

rare earth minerals that have been or are now used as resources of rare earth include apatite, brannerite, euxenite, gadolinite, loparite, and uraninite. The minerals allanite, apatite, and other phosphorite sources, eudialyte, fergusonite, floreneite, parisite, perovskite, pyrochlore, zircon, and a few other naturally occurring rare earth bearing materials are also considered potential rare earth resources.

The first eight rare earths, lanthanum to gadolinium, are often referred to as the cerium subgroup of the rare earth elements or light rare earth elements, and the remaining eight elements, terbium to lutetium, together with yttrium, are said to belong to the yttrium subgroup or heavy rare earth elements (Jackson and Christiansen 1993). Sometimes, the rare earths are divided into three subgroups. From lanthanum to neodymium are called "light rare earths," from samarium to dysprosium are known as "medium rare earths," and from holmium to lutetium, including yttrium, are called "heavy rare earths" (Sabot and Maestro 1995). In another classification (Kremers 1961), the light rare earths, from lanthanum to samarium, are called the "cerium group;" the middle rare earths, europium to dysprosium, are called the "terbium group;" and the heavies, holmium to lutetium and yttrium, are called the "yttrium group."

2.3.1 Bastnasite

The mineral bastnasite is a fluorocarbonate of the cerium group rare earth metals and hardly contains any thorium. As regards the geological environment, bastnasite is found in vein deposits, contact metamorphic zones, and pegmatites. Bastnasite occurs as veins or dissemination in a complex of carbonate–silicate rocks, occurring with and related to alkaline intrusives, for example, in California. Bastnasite occurs in quartz veins that cut micaceous schists and quartzite, in Burundi. It is in fluorite-bearing veins and breccia filings in Permian sandstone, for example, in New Mexico (Jackson and Christiansen 1993). The rare earth content of bastnasite is approximately 70% REO, mostly of the lighter elements. Bastnasite is a primary source of light REO in the enormous deposit in Bayan Obo in China (800 million metric tons; 6% REO) and at Mountain Pass, California in the U.S. (3.3 million metric tons; 7.7% REO). The rare earth content in bastnasite from these locations is given in Table 2.3 (Hedrick 1991). In addition, bastnasite is also the main REO mineral at Brockman in Australia, Pocos de Caldas in Brazil, Thor Lake in Canada, and Karonge in Burundi. Bastnasite is chemically susceptible to weathering and this causes REO to dissolve and combine with available phosphates.

2.3.2 Monazite

The mineral monazite is a phosphate, mainly of the cerium group rare earths and thorium. Monazite is found in many geological environments. It occurs as an accessory mineral in acidic igneous rocks, in metamorphic rocks, and in certain vein deposits. Due to its chemical stability it also develops into detrital mineral in placer deposits and beach sands (Aplan 1988). The primary monazite deposits have been useful as rare earth resources in a few instances. Notable among them are occurrences in Van Rhynsdorp and Naboomspruit (South Africa), in Colorado (U.S.) and in Bayan Obo (China). The most important monazite resources have been the beach placers. Alluvial, stream, and aeolian deposits have been much less significant. Beach sand deposits contain, in addition to monazite, other heavy minerals like ilmenite, rutile, and zircon. Sometimes monazite co-occurs with placer gold

Table 2.3 Rare earth element distribution in bastnasite (w.r.t. 100% REO)

Rare earth	Bastnasite, Mountain Pass, California, U.S.	Bastnasite, Bayan Obo, Nei Monggol, China
La	33.2000	23.0000
Ce	49.1000	50.0000
Pr	4.3400	6.2000
Nd	12.0000	18.5000
Sm	0.7890	0.8000
Eu	0.1180	0.2000
Gd	0.1660	0.7000
Tb	0.0159	0.1000
Dy	0.0312	0.1000
Ho	0.0051	trace
Er	0.0035	trace
Tm	0.0009	trace
Yb	0.0006	trace
Lu	0.0001	trace
Y	0.0913	0.5000

Table 2.4 Rare earth distribution in monazite from different locations

Rare earth	Australia, North Staradbroke Island, Queensland	Australia, Capel, Western Australia	Brazil, East coast	China, Nangang, Guang-dong	India	U.S., Green Cove Springs, Florida	U.S., Bear Valley, Idaho	Australia, Mount Weld
La	21.50	23.90	24.00	23.35	23.00	17.50	26.23	26.00
Ce	45.8	46.02	47.00	42.70	46.00	43.70	46.14	51.00
Pr	5.3	5.04	4.50	4.10	5.50	5.00	6.02	4.00
Nd	18.6	17.38	18.50	17.00	20.00	17.50	16.98	15.00
Sm	3.1	2.53	3.00	3.00	4.0	4.90	2.01	1.8
Eu	0.8	0.05	0.0550	0.10		0.16	1.54	0.4
Gd	1.8	1.49	1.00	2.03		6.60	0.77	1.0
Tb	0.29	0.04	0.1	0.70		0.26		0.1
Dy	0.64	0.69	0.35	0.80		0.90	Tb,Dy:0.31	0.2
Ho	0.12	0.05	0.035	0.12		0.11		0.1
Er	0.18	0.21	0.07	0.30		0.04		0.2
Tm	0.03	0.01	0.005	trace		0.03		trace
Yb	0.11	0.12	0.02	2.40		0.21		0.1
Lu	0.01	0.04		0.14		0.03	Ho-Lu:0.15	trace
Y	2.50	2.41	1.4	2.40	Eu-Y: 1.50	3.20	1.39	trace

or tin deposits (Aplan 1988). Monazite-bearing heavy mineral sand deposits are found in large quantities principally in Australia, Brazil, China, India, Malaysia, South Africa, and the United States. The rare earth content and individual rare earth element distribution in

monazite are variable, as is its thorium content, depending on the location (Hedrick 1985, Hedrick 1992). This is shown in Table 2.4. Usually monazite contains about 70% REO, and the rare earth fraction is constituted by 20 to 30% Ce_2O_3; 10 to 40% La_2O_3; significant amounts of neodymium, praseodymium, and samarium; and lesser amounts of dysprosium, erbium, and holmium. Yttrium content may vary from a trace to ~5% Y_2O_3, and thorium content of 4 to 12% is common. Some amount of uranium is also present in monazite.

2.3.3 Xenotime

Xenotime is an yttrium phosphate containing about 67% REO, mostly of the heavier elements. The mineral is a minor constituent of granite or gneiss (Aplan 1988). Having undergone a weathering, transportation, and concentration process similar to that of monazite, xenotime co-occurs with it in placer deposits, but such deposits are relatively few. Usually the content of xenotime may range from 0.5 to about 5% of the monazite present. An occurrence where the proportion of xenotime may be as high as 50% was identified in California (Sabot and Maestro 1995). Xenotime occurs in the placer cassiterite deposits in Malaysia and in certain Australian heavy mineral sands. Xenotime occurs also in the placer cassiterite deposits of Indonesia and Thailand and in the heavy mineral sands of China, as well as in the alluvial tin mines of Brazil (Highley et al. 1988). The rare earth distribution in xenotime is given in Table 2.5. In addition to the three major minerals, there are several other rare earth minerals that are, or could be, of importance in the economic recovery of rare earths.

2.3.4 Allanite

This mineral is a rare earth bearing member of the epidote group. Allanite occurs in igneous, hydrothermal, and metamorphic environments. It may be found as small or disseminated crystals throughout the pegmatitic body or as veins varying in width from a fraction of an inch to several feet. The rare earth content of allanite is normally limited to about 5% REO, but it may vary from 3 to 51%, depending on the source. The thorium content of allanite may vary from a trace up to 3%. It is the relatively low REO and thorium content and the usually scattered presence in the rock that has kept allanite from being processed on a large scale. However, allanite had been considered as a useful future resource (Nininger 1956) because it is available in very large quantities and might be produced at a lower cost per ton than monazite. At present three deposits are considered to have potential for allanite mining (Jackson and Christiansen 1993). They are the Mary Kathlean uranium tailings in Queensland, Australia, the Alice Springs prospect in the Northern Territory, Australia (1 million metric tons, 4% allanite, 20% REO), and the deposits in Hall Mountain Group in Idaho, United States. The rare earth distribution in allanite is given in Table 2.5.

2.3.5 Apatite

Apatite is a calcium fluorophosphate. It is found in carbonatites, alkaline igneous rocks, and some sediments. Apatite is not a rare earth mineral but a rare earth concentrating mineral (Aplan 1988). Rare earth ions proxy calcium ions in the lattice because of the similar size of the rare earth ions and calcium ions. The rare earth content of apatite is

highly variable and ranges from a trace to over 10% (as REO). The amount and distribution of rare earths are dependent on the nature of the host rock. The rare earth distribution in Kola apatite is given in Table 2.5.

Apatite may constitute a substantial resource for rare earths. Unlike most of the rare earth minerals, which are found only in small quantities in a potential ore body, apatite occurs in large quantities like bastnasite and monazite.

Large quantities of rare earth bearing apatites occur at Kola Peninsula (~1% REO) and in the Vishnevye Mountains (>1% REO) in the former Soviet Union (Hedrick 1985), in Phalaborwa in South Africa, and in the Mineville iron ore in New York State in the United States (Aplan 1988). Rare earth bearing apatites have also been located in California placers (Hedrick 1986) and in Florida (Altschuler et al. 1967). Phosphorites in the large phosphoria formation of Montana, Utah, and Wyoming contain rare earths (0.16%) (Aplan 1988). The quantity of rare earths contained in phosphate sources has been estimated to be over 8 million metric tons REO (Cross and Miller 1988).

2.3.6 Brannerite

The uranium ore brannerite contains rare earths and occurs in pegmatites and conglomerates. The major economic location for brannerite is the Precambrian quartz pebble conglomerate at Elliot Lake, Ontario, Canada (Adams and Staatz 1973). The distribution of rare earths in the deposit is given in Table 2.5. Brannerite also occurs in association with gold in the Witwatersrand deposit in South Africa (Highley et al. 1988) and at Radium Hill, Australia (Adams 1971).

2.3.7 Eudialyte

Eudialyte is a zirconium mineral that in some instances contains rare earths (1 to 3% REO) and could be rich in yttrium (0.2 to 1%) (Ferron et al. 1991). This silicate mineral occurs in nepheline syenite, for example, at the Ilimaussaq deposit in Greenland; and in peralkaline granite, for example, at Pajarito in New Mexico, United States (Jackson and Christiansen 1993). The rare earth contents of these deposits are 0.9% and 0.18% REO, respectively. Eudialyte deposits also occur in the former USSR and Canada. An advantage is that eudialyte tends to form as coarse grained euhedral crystals that are easily dissolved in acids.

2.3.8 Euxenite, Fergusonite, Florencite, Gadolinite, and Loparite

The minerals euxenite and fergusonite are complex tantaloniobates of titanium, rare earths, thorium and uranium. These co-occurring metal values and the heavy rare earth content make euxenite processing attractive (Dayton 1958). Euxenite occurs in the placer deposits of Idaho.

The mineral florencite is an aluminum phosphate. It occurs in the weathered zone of carbonatites. This mineral by itself can be relatively high in REO, but it is not known to occur in large quantities (Jackson and Christiansen 1993).

Gadolinite is a beryllium iron silicate mineral found in granites, granitic pegmatites, and placers. Gadolinite is a widespread but not abundant component of pegmatites and has been found in veins, lenses, and pockets in many locations, particularly in the United States

Table 2.5 Rare earth distribution in important rare earth minerals (% of total rare earth oxide)

Rare earth	Ion adsorption type ore		Uranium residues, Canada	Xenotime Malaysia	Xeno-time, Guandong, China	Gadoli-nite	Alla-nite	Apatite	Loparite , Kola
	Longnan	Xunwu							
La	1.82	43.4	0.80	0.50	1.20	1	20	25.78	27.8
Ce	0.40	2.40	3.70	5.00	8.00	2	40	46.22	57.1
Pr	0.70	9.00	1.00	0.70	0.60	2	10	4.00	3.7
Nd	3.00	31.70	4.10	2.20	3.50	5	20	14.4	8.7
Sm	2.80	3.90	4.50	1.90	2.20	5	2	1.6	0.91
Eu	0.10	0.50	0.20	0.20	0.20	trace	0.03	0.5	0.13
Gd	6.90	3.00	8.50	4.00	5.00	5	1	1.5	0.21
Tb	1.30	trace	1.20	1.00	1.20	0.5	0.1	0.1	0.07
Dy	6.70	trace	11.20	8.70	9.10	6	0.3	1.02	0.09
Ho	1.60	trace	2.60	2.10	2.60	1	0.1	0.10	0.03
Er	4.90	trace	5.50	5.40	5.60	4	0.3	0.15	0.07
Tm	0.70	trace	0.90	0.90	1.30	0.6	0.1	0.02	0.07
Yb	2.50	0.30	4.00	6.20	6.00	4	0.3	0. 08	0.29
Lu	0.40	0.10	0.40	0.40	1.80	0.6	<0.1		0.05
Y	65.00	8.00	51.40	60.80	59.30	60	3	4.40	0.14

(Kleber and Love 1963). Recently gadolinite deposits have been found in Quebec and Yellowknife, Northwest Territories (Canada) (Hedrick 1985). Gadolinite usually contains about 40% REO. The rare earth distribution (Foos and Wilhelm 1954, Spedding and Powell 1954) is given in Table 2.5.

Loparite is basically a niobium ore that contains titanium and the rare earths. A large deposit of loparite occurs in the Kola Peninsula of the former Soviet Union. The rare earth content is as much as 30% REO (Jackson and Christiensen 1993), from the cerium group. The rare earth distribution in loparite is given in Table 2.5.

2.3.9 Perovskite

Perovskite, which is a calcium titanate, is a rare earth concentrating mineral where the rare earths substitute calcium. Rare earth containing varieties, enriched essentially in the light rare earths, are mainly associated with alkalic igneous rock suites. A major prospect containing perovskite is at Powderhorn, Colorado, U.S. Here the rock contains 0.36% REO (Jackson and Christiensen 1993). Large quantities of rare earths are reportedly contained in various perovskite ore bodies (Haskin and Paster 1979).

2.3.10 Pyrochlore

Pyrochlore is another rare earth concentrating mineral (Aplan 1988, Highley et al. 1988). In this mineral, rare earths substitute in the alkali position. Large deposits of pyrochlore

occur at St. Honoré and Oka in Quebec (Noblitt 1965) and Araxa, Brazil (Adams 1971), and at various places along the Rift Valley in East Africa.

2.3.11 Zircon

Zircon is also known to accept a spectrum of rare earth elements in the mineral and can be considered as a probable source of yttrium and heavy lanthanides (Haskin and Paster 1979).

2.3.12 Others

It has been recently established that granite-like subalkaline rare metal metasomatites located near faults may serve as an important source of yttrium and other rare earths.

An unusual type of rare earth ore known as ion adsorption type ore is found at various locations in South China. This ore was formed by the weathering rare earth-rich primary granite-type rock or volcanic rock followed by adsorption of soluble rare earth species on clays. Mild, humid, rainy climatic conditions and tectonically stable environment are suitable for these processes to occur. In southern China, especially in the Jiangxi Province, where such conditions prevail, many ion adsorption-type rare earth deposits are found. Incidentally, the weathering process also modifies the proportion of the various lanthanides originally found in the source rock, as they ultimately end up as the ion adsorption ores. The composition of ion adsorption ores depend on location, but overall they are relatively rich in Y and the mid-rare earths such as Eu, Sm and Gd. The rare earth distribution on the ion adsorption ore are given in Table 2.5.

2.3.13 Scandium Minerals

The abundance of scandium in earth's crust is greater than even such well-known metals as lead, tin, mercury, and silver. Yet, scandium rarely occurs in concentrated quantities. The reason is that scandium does not combine with ore-forming anions.

The rare earth element scandium does not usually occur in the rare earth minerals. An important exception is the huge iron–niobium–rare earth deposit in Bayan Obo, China. This deposit contains scandium in concentrations ranging from 0.006 to 0.016% Sc_2O_3 in various ores and dispersed over the niobium and rare earth minerals (CREI 1998).

The major source of scandium is uranium ores, which contain about 0.1% scandium. Some scandium is also recovered from wolframite. Scandium content in wolframite is of the order of 500–800 ppm and this was considered an important potential resource in the U.S. (Kleber and Love 1963). The only mineral that contains a large percentage (33 to 45) of scandium is thortveitite. It is a scandium silicate in which variable amounts of yttrium and lanthanides, aluminum, iron, thorium, zirconium, and alkaline earths substitute for scandium. This mineral is very rare. Only two sources are known. It was found in the granite pegmatites in northern Norway, and a variety called befanamite was found in Madagascar. Thortveitite is not considered an important source of scandium. Slags from blast furnaces used in the production of cast iron and tin smelting are also sources of scandium.

2.3.14 Promethium

Several rare earths are among the elements formed in the fission of uranium and plutonium. The spent fuel from nuclear reactors is the only source of the rare earth element promethium (Wheelwright 1973).

2.4 RARE EARTH DEPOSITS

2.4.1 Primary and Secondary

The minerals of rare earths occur in a variety of geologic environments. Generally they are found in hard rock deposits or in placer sands. The hard rock deposits are of primary origin and the placer deposits are of secondary origin. The composition of the rare earth minerals in these deposits is strongly influenced by the presence of phosphates and carbonates (Jackson and Christiansen 1993).

2.4.2 Carbonatites

The most dominant sources of rare earths are carbonatites (Jackson and Christiansen 1993). These are deep-seated magmas, rich in carbon dioxide and low in silica, that intruded the earth's crust and solidified. Magmas forming closer to the surface usually lose their carbon dioxide and other volatile agents and do not bear rare earths. The rare earths in carbonatites are almost exclusively the light rare earth elements contained in minerals such as bastnasite, allanite, and apatite. Monazite, when present, contains the maximum amount of rare earths and a minimum amount of calcium and thorium.

2.4.3 Pegmatites

Pegmatites are a hard rock source of rare earths that begin as granitic magmas formed by remelting of crustal material (Jackson and Christiansen 1993). As the magma cools, crystals incorporating heavy rare earth elements form first. This is followed by crystallization of the residual liquid, which is relatively rich in lighter rare earth elements. Thus monazite and allanite in pegmatites tend to be richer in the heavy rare earths than when they are found in other rocks. The overall rare earth content of monazite is, however, decreased because it is likely to have more calcium and thorium.

2.4.4 Hydrothermal Deposits

Rare earth elements can be carried by hydrothermal solutions that are developed through the interaction of hot underground water with crustal material (Jackson and Christiansen 1993). The light rare earth elements are less soluble than the heavier elements, and they therefore tend to settle out first, leaving the liquid more concentrated in heavy elements. As

Table 2.6 Distribution of rare earth oxide deposits, mineral types, and production status of mines in those deposits by country (from Jackson and Christiansen 1993)

Country	Deposit type			Mineral			Production status		
	No. of deposits	Placer	Hard rock	Monazite	Bastnasite	Other[1]	Non-producer[2]	Producer	REO concentrates[3]
Argentina	1	1	0	1	0	0	1	0	0
Australia	35	28	7	30	2	3	21	14	11
Brazil	16	14	2	0	2	0	12	40	2
Burundi	2	0	2	0	2	0	2	0	0
Canada	5	0	5	0	1	4	2	3	1
China	4	3	1	3	1	0	0	4	4
Egypt	1	1	0	1	0	0	1	0	0
Gabon	1	0	1	0	0	1	1	0	0
Greenland	1	0	1	0	0	1	1	0	0
India	5	5	0	5	0	0	1	4	4
Kenya	1	0	1	1	0	0	1	0	0
Malawi	1	0	1	1	0	0	1	0	0
Mauritania	1	0	1	1	0	0	1	0	0
Mozambique	1	1	0	1	0	0	1	0	0
Namibia	1	0	1	0	1	0	1	0	0
New Zealand	2	2	0	2	0	0	2	0	0
South Africa	3	1	2	2	0	1	0	3	1
Sri Lanka	1	1	0	1	0	0	0	1	1
United States	40	13	27	32	3	5	32	8	2
Uruguay	1	1	0	1	0	0	1	0	0
Total	123	71	52	96	11	16	82	41	26

[1]Includes allanite, anatase, apatite, brannerite, davidite, eudialyte, florencite, gadolinite, perovskite and xenotime.
[2]Mines or deposits known or assumed to have no production.
[3]Number of mines or deposits of the known producers that generate REO concentrates for each country.

a result, hydrothermal deposits contain minerals such as xenotime, which are enriched in the heavy rare earths.

2.4.5 Weathered Deposits

Deep chemical weathering of carbonatites causes the dissolution of calcite, dolomite, and apatite. The rare earths released as a result of this activity have an affinity for the phosphate radical and form superzene monazite. Pyrochlore is converted to florencite and perovskite is converted to anatase by extreme lateritic weathering. Generally, the light rare earth minerals are converted to heavy rare earth minerals (Jackson and Christiansen 1993).

A peculiar type of rare earth deposit may be formed as a result of *in situ* lateritic weathering of igneous rocks. *In situ* weathering of REO rich host rocks occurring under conditions of prolonged weathering with limited erosion can result in ion adsorption type

deposits wherein a high Si, Al clay crust adsorbs rare earth ions from weathered minerals of a host rock (Clark and Zheng 1991).

2.4.6 Placers

Large amounts of rare earth minerals such as monazite and xenotime are contained in placers. These minerals are characterized by high specific gravity and chemical inertness. They are therefore stable during the erosion and transportation cycles of weathering. The major locations for placers are rivers, deltas, and coastlines. Heavy minerals are concentrated along the coast by a combination of tidal action, long shore currents, waves, winds, and natural traps such as a cape. Important placers for mining are recently formed beaches and dunes along the coastlines, as well as some older deposits that have become stranded due to land elevation or ocean withdrawal.

2.4.7 Distribution

According to a United States Geological Survey Circular (Jackson and Christiansen 1993), there are 123 important rare earth deposits in the world and they are located in 20 countries. The distribution is indicated in Table 2.6. Most of the deposits are located in the United States, followed by Australia, Brazil, Canada, India, and China. These deposits have been categorized either as placers or as hard rock type.

Numerically, placers are more in number. There are 71 placer deposits in the world and 52 hard rock deposits. Mostly the placers are found in recent or ancient shorelines and less frequently along present or former river banks. Monazite is the predominant rare earth mineral in the placers. The countries having major placer deposits are Australia, Brazil, the United States, India, China, and New Zealand. Placer deposits are also found in Argentina, Egypt, Mozambique, South Africa, Sri Lanka, and Uruguay. The data given in the U.S. Geological Survey Circular (Jackson and Christiansen 1993) do not include rare earths in the tin placers of Southeast Asia and deposits in the former Soviet Union.

As regards the hard rock deposits, the maximum number are found in the United States, followed by Australia, Canada, Brazil, Burundi, South Africa, and China. Monazite is the major mineral found in most of the hard rock deposits, in 96 out of the total 123; bastnasite is predominant at 11 sites. At the 16 remaining deposits, the leading minerals are allanite (3 sites), brannerite (3), apatite (2), and eudialyte (2), with anatase, davidite, florenite, gadolinite, perovskite, and xenotime limited to individual properties. The ion adsorption type ore deposits of China do not figure in the U.S. Geological Survey Circular (Jackson and Christiansen 1993).

2.5 RESOURCES AND RESERVES

The term *resources* has been generally used to denote the deposits of a commodity, in this context, the rare earths in or on the earth's crust in such forms and concentrations that economic extraction of the commodity is presently feasible. The term *reserve*, on the other hand, has been used to represent, in the present context, the specific bodies of rare earth

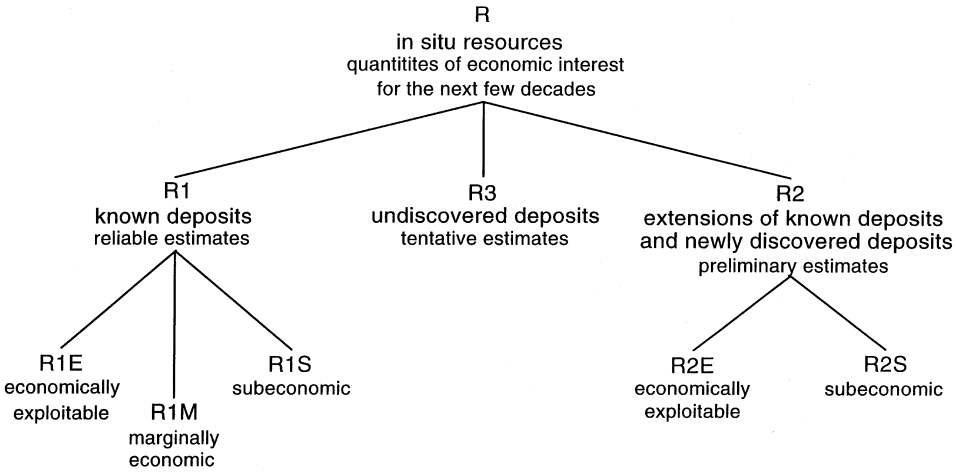

Figure 2.2 United Nations resource categories.

bearing material of known location, quality and quantity, from which the rare earth can be extracted presently. Resources of rare earths, therefore, include reserves (Bureau of Mines Staff 1975).

The total quantity of rare earths contained in world rare earth reserves had been estimated, for a long time, at 47.6 million metric tons of REO (Hedrick 1988, Clark and Zheng 1991, Sabot and Maestro 1995). Most of the rare earth reserves were located in China followed by the U.S. with important quantities also occurring in Australia, India, the former Soviet Union and South Africa. These data have been drastically revised with the discovery of a huge rare earth reserve in Namibia and major upward revision in the estimates of rare earth reserves in China, the United States, Australia, and India (Jackson and Christiansen

Table 2.7 Rare earth oxide resources in the world's major rare earth oxide deposits, by geologic type and resource category (from Jackson and Christiansen 1993)

Deposit type	Mineral	R1E			Other resources		
		Number of deposits	Million metric tons	%	Number of deposits	Million metric tons	%
REO ore resources							
Placer	Monazite	59	17,421	85	14	7,278	61
Hard rock	Monazite	21	991	5	14	1270	11
Hard rock	Bastnasite	10	1302	6	5	2815	23
Hard rock	Other	16	866	4	6	662	6
	Total	106	20580	100	39	12025	100
REO							
Placer	Monazite	57	6.732	7	10	3230	13
Hard rock	Monazite	21	11.605	12	13	1,987	8
Hard rock	Bastnasite	11	72.118	77	5	18936	76
Hard rock	Other	14	2.959	3	6	0.894	4
	Total	103	93.414	100	34	25,047	100

1993). Excluding the reserves in the former Soviet Union, the world rare earth reserves are presently estimated at 93.4 million metric tons REO. In 2001, U.S. Geological Survey estimated world resources of rare earths to be 100 million metric tons (Mt) of contained REO (Hedrick, 2001). However, new terms have been defined to describe the world rare earth resources.

A more detailed description of world rare earth resources has been made using the international classification system for mineral resources recommended by the United Nations Group of Experts on Definitions and Terminology for Mineral Resources (Jackson and Christiansen 1993). The United Nations resource classification is summarized in Figure 2.2. The whole of the *in situ* resources are divided into known deposits, extensions of known deposits, and newly discovered deposits and undiscovered deposits. The known deposits that are of greatest current interest are again divided into economically exploitable deposits (R1E), marginally economic (R1M), and subeconomic (R1S). The R1E deposits generally refer to the deposits known usually as reserves.

The details of rare earth ore resources in major world rare earth deposits as given by U.S. Geological Survey Circular (Jackson and Christiansen 1993) are summarized in Table 2.7. Worldwide rare earth resources of the R1E category (ore grade material in R1E resources) amount to a total of 20.6 billion metric tons, with the placer deposits constituting 85% of the total, and hard rock deposits constituting the remaining 15%. Dividing the total R1E resource tonnage in terms of minerals, 90% of it is monazite, 6% bastnasite, and 4% other rare earth minerals.

The quantities of rare earth oxides (REO) in R1E resources of the world are listed in Table 2.8. The total REO contained in R1E category world rare earth resources amounts to 93.4 million metric tons. Only 7% of this total REO tonnage are contained in placer deposits and 93% are in hard rock. Dividing in terms of minerals, 20% of the total REO tonnage is contained in monazite (present in both placer and hard rock), 77% in bastnasite, and 3% in other rare earth minerals.

The data in Table 2.8a present the familiar picture of China ranking first in the listing of world rare earth reserves. China, with 48 million metric tons of REO in bastnasite, is the country having the largest amount of REO. Namibia, which has 20 million metric tons of REO, also in bastnasite, is the second. The United States has 14 million metric tons of REO, 73% of it in monazite, and ranks third. Australia is fourth with 5.7 million metric tons of REO, 69% of it in monazite. India has 2.6 million metric tons of REO, all of it in monazite, and ranks fifth. South Africa and Canada, each having one million metric tons of REO, come next. These are the seven countries having major rare earth reserves.

The current status on world rare earth reserves and reserve base can be obtained through publications of the U.S. Geological Survey. The latest figures on world rare earth resources appearing in Mineral Commodity Summaries issued in January 2003 (USGS 2003) are reproduced in Table 2.8b. These data are based on revised reserve and known base estimates for China. The table also includes information on rare earth resources of the former Soviet Union. Estimates of reserves of almost all the countries are revised to relatively lower values.

2.6 OCCURRENCES

Rare earth deposits are found at various locations in the world. Current information on major rare earth deposits in the world, as given by the U.S. Geological Survey (Jackson and

Table 2.8a Metric tons of rare earth oxides in R1E resources, by continent and country, deposit type, and mineral (from Jackson and Christiansen, 1993)

Country	Deposit type thousand metric tons			Mineral (% of R1E resource)	
	Placers	Hard rock	Total	Monazite	Bastnasite and others
Africa					
Burundi	nr	2	2	nr	100
Egypt	122	nr	122	100	nr
Kenya	nr	13	13	100	nr
Malawi	nr	330	330	100	nr
Mauritania	nr	4	4	100	nr
Mozambique	6	nr	6	100	nr
Namibia	nr	20,000	20,000	nr	100
South Africa	630	405	1,035	87	13
Subtotal	758	20,755	21,513		
Percent of total				6	94
Asia					
China	nr	48,000	48,000	nr	100
India	2,560	nr	2,560	100	nr
Sri Lanka	1	nr	1	100	nr
Subtotal	2,561	48,000	50,561		
Percent of total				5	95
Austalasia					
Australia	2,797	2,918	5,715	69	31
New Zealand	nr	nr	nr	100	nr
Subtotal	2,797	2,918	5,715		
Percent of total				69	31
North America					
Canada	nr	1,047	1,047	nr	100
Greenland	nr	270	270	nr	100
United States	393	13,598	13,990	73	27
Subtotal	393	14,915	15,307		
Percent of total				67	33
South America					
Argentina	3	nr	3	100	nr
Brazil	219	95	314	70	30
Subtotal	223	95	318		
Percent of total				70	30
Total	6,732	86,682	93,414		
Percent of world total				20	80

Table 2.8b World rare earth reserves and reserve base

Country	Reserves (Mt REO)	Reserve base (Mt REO)
United States	13.0	14.0
Australia	5.2	5.8
Brazil	0.11	0.31
Canada	0.94	1.0
China	27.0	89.0
India	1.1	1.3
Malaysia	0.03	0.035
South Africa	0.39	0.4
Sri Lanka	0.012	0.013
Former Soviet Union	19.0	21.0
Other countries	21.0	21.0
World total (rounded)	88.0	150.0

Christiansen 1993), are summarized in Table 2.9. Details and additional information on these and other deposits are given below for various countries.

2.6.1 Argentina

A rare earth–uranium–thorium deposit is located in San Luis Province, Argentina. The project known as "Rodeo de los Molles" is located about 300 km southwest of Cordoba and 200 km northeast of San Luis. Minerals of economic significance include bastnasite, britholite (a rare earth silicon phosphate), and allanite with 2.0 to 2.5% rare earth content (RIC 1995).

2.6.2 Australia

Australia has major rare earth reserves. There are 30 monazite and 2 bastnasite deposits in Australia, and other rare earth minerals occur in 3 more deposits. Out of the total 35 REO deposits, 27 are placers (Jackson and Christiansen 1993). Heavy mineral sand placer deposits comprising ilmenite, rutile, zircon, monazite and, in a few cases, xenotime occur extensively along the Australian coast, particularly the east and west coasts. There are 15 placer deposits in western Australia, 7 in Queensland and 5 in New South Wales. The west coast deposits are mainly paleobeach placers and the principal deposits are located inland and 10 to 100 meters above sea level. The deposits on the east coast have been formed by waves and wind and their combination. Eight rare earth deposits in Australia are located inland. Three of them are in west Australia, two in south Australia, and one each in the Northern Territory, Queensland, and Victoria.

Eneabba The Eneabba mineral sands deposit on the west coast north of Perth has been the major source of monazite in Australia. Additional mineral sands reserves occur in the adjacent Eneabba West deposit. The mineral sands of Eneabba also contain useful quantities of xenotime (Taylor 1991).

.

Table 2.9 World rare earth deposits (Jackson and Christiansen 1993)

Location	Deposit type	Principal minerals	Average grade
Argentina			
Rio Tercero (Cardoba)	Placer, fluvial	Monazite	0.0173% monazite containing 60% REO and 3.8% ThO_2
Australia			
Agnes Waters (Rocky Point) (Queensland)	Placer, marine	Ilmenite, rutile, zircon, monazite, quartz	1.36% ilmenite, 0.18% rutile
Alice Springs (Northern Territory)	Magmatic	Allanite	4.0% allanite containing 20% REO
Australind (Western Australia)	Placer, marine	Ilmenite, rutile, zircon, leucoxene, monazite, quartz, garnet	15% heavy minerals, 0.03% monazite
Bowen (Abbot Point) (Queensland)	Placer, marine	Ilmenite, rutile, zircon, monazite, quartz	
Brockman (Western Australia)	Magmatic	Columbite, pyrochlore, bastnasite, xenotime, cassiterite, sphalerite	0.09% REO, 0.124% Y_2O_3
Busselton East (Western Australia)	Placer, marine	Ilmenite, rutile, zircon, leucoxene, monazite, quartz	
Byfield (Queensland)	Placer, marine	Ilmenite, rutile, zircon, monazite, quartz	1.14% heavy minerals, 0.05% monazite
Capel South (Western Australia)	Placer, marine	Ilmenite, rutile, zircon, leucoxene, monazite, quartz	0.06% monazite
Cataby (Western Australia)	Placer, marine	Ilmenite, rutile, zircon, monazite, quartz	7.7% heavy minerals, 0.1% monazite
Cooljarloo/Jurien Bay (Western Australia)	Placer, marine	Ilmenite, rutile, zircon, leucoxene, monazite, quartz	3.2% heavy minerals, 0.2% monazite
Coolooa (Queensland)	Placer, marine	Ilmenite, rutile, zircon, monazite, quartz	0.00846% monazite
Eneabba (Western Australia)	Placer, marine	Ilmenite, rutile, zircon, kyanite, monazite, quartz	0.05% monazite
Frazer Island (Queensland)	Placer, marine	Ilmenite, rutile, zircon, monazite, quartz	1.75% heavy minerals, 0.005% monazite
Gingin South (Western Australia)	Placer, marine	Ilmenite, rutile, zircon, kyanite, leucoxene, quartz	10.02% heavy minerals
Hamel (Waroona) (Western Australia)	Placer, marine	Ilmenite, leucoxene, zircon, kyanite, staurolite, monazite, quartz	
Higgins (Western Australia)	Placer, marine	Ilmenite, zircon	
Jangardup (Western Australia)	Placer, marine	Ilmenite, rutile, zircon, leucoxene, kyanite, staurolite, monazite, xenotime, quartz, garnet	6.8% heavy minerals, 0.0476% monazite, 0.0204% xenotime
Mary Kathleen (Queensland)	Magmatic		Former uranium mine

Table 2.9 (continued)

Location	Deposit type	Principal minerals	Average grade
Minninup, beach dunes (Western Australia)	Placer, marine	Ilmenite, leucoxene, zircon, monazite, xenotime, quartz	8.0% heavy minerals
Moreton Island (Queensland)	Placer, marine	Ilmenite, leucoxene, zircon, quartz	
Mount Weld (Western Australia)	Magmatic	Apatite, pyrochlore, magnetite, ilmenite, monazite, quartz	17% REO and yttrium
Munmorah (New South Wales)	Placer, marine	Ilmenite, rutile, zircon, monazite, quartz	0.81% heavy minerals, 0.006% monazite
Nobiac, Southeast (New South Wales)	Placer, marine	Ilmenite, rutile, zircon, leucoxene, monazite, quartz, garnet	0.0091% monazite
Newrybar (New South Wales)	Placer, marine	Ilmenite, rutile, zircon, monazite, tourmaline, quartz, garnet	1.1% heavy mineral, 0.0418% monazite
North Capel (Western Australia)	Placer, marine	Ilmenite, rutile, zircon, leucoxene, monazite, quartz,	0.080% monazite
North Stradbroke Island (Queensland)	Placer, marine	Ilmenite, rutile, zircon, monazite, quartz,	1.5% heavy minerals, 0.0015% monazite
Olympic Dam (South Australia)	Magmatic	Chalcocite, bornite, chalcopyrite, uraninite, brannerite, hematite, bastnasite, fluocerite	0.3285% REO associated with U_3O_8 in a major Cu/Au/Ag/U mine
Port Pirie (South Australia)	Magmatic	Uraninite, dvidite	Tails from radium hill
Stockton Bight (New South Wales)	Placer, marine	Ilmenite, rutile, zircon, monazite, quartz	
Tomago (New South Wales)	Placer, marine	Ilmenite, rutile, zircon, monazite, quartz, garnet	Dune and beach deposits
Viney Creek (New South Wales)	Placer, marine	Ilmenite, rutile, zircon, monazite, quartz	
Waroona, North and South (Western Australia)	Placer, marine	Ilmenite, leucoxene, zircon, monazite, quartz	15% heavy minerals
WIM-150 (Victoria)	Placer, fluvial	Ilmenite, leucoxene, zircon, anatase, monazite, xenotime, quartz	5.221% heavy minerals, 0.076% REO
Wonnerup Beach (Western Australia)	Placer, marine	Ilmenite, zircon, monazite, quartz, garnet	
Yangibana (Western Australia)	Magmatic	Monazite	3.09% monazite, 1.7% REO
Yoganup Extended (Western Australia)	Placer, marine	Ilmenite, rutile, zircon, leucoxene, monazite, quartz	13.3% heavy minerals, 0.056% monazite
Brazil			
Acobaca (Southern Bahia)	Placer, marine	Ilmenite, rutile, zircon, monazite, quartz	0.47% monazite

Table 2.9 (continued)

Location	Deposit type	Principal minerals	Average grade
Anchieta (Espirito Santo)	Placer, marine	Ilmenite, rutile, zircon, monazite, quartz	0.71% monazite
Aracruz (Espirito Santo)	Placer, marine	Ilmenite, rutile, zircon, monazite, quartz	1.05% monazite
Buena (Rio de Janeiro)	Placer, marine	Ilmenite, rutile, zircon, monazite, quartz	0.83% monazite
Camaratuba (Rio Grande do Norte)	Placer, marine	Ilmenite, rutile, zircon, tourmaline, monazite, xenotime, quartz, garnet	Elevated dunes at the base of an ancient sea cliff
Careacu (Minas Gerais)			
Cordislandia (Minas Gerais)			
Guarapari (Espirito Santo)			
Northeast dunes	Placer, marine	Ilmenite, rutile, zircon, monazite, quartz	0.033% monazite
Pocos de Caldas (Minas Gerais)	Magmatic		3.33% REO in bastnasite
Prado (Bahia)			
Sao Gancalo do Sapucai (Minas Gerais)	Placer, fluvial	Ilmenite, zircon, gold, monazite, garnet	0.066% monazite
Serra (Espirito Santo)	Placer, marine	Ilmenite, rutile, zircon, monazite, quartz	0.80% monazite
Tapira (Minas Gerais)	Magmatic	Anatase, apatite, perovskite, limonite, magnetite, garnet	0.03% REO in anatase overburden at a phosphate mine
Burundi			
Karonge	Magmatic	Fluocerite, cassiterite, monazite, barite, goethite, quartz	3.0% bastnasite, 1.50% REO
Kasagwe	Magmatic		3.0% bastnasite, 1.59% REO
Canada			
Elliot Lake (Denison) (Ontario)	Magmatic	Uraninite, brannerite, monazite, zircon, pyrite, quartz	0.0072% REO and yttrium in a uranium mine
Elliot Lake (Rio Algom, except Stanleigh) (Ontario)	Magmatic	Uraninite, brannerite, monazite, zircon, pyrite, quartz	0.0064% REO and yttrium in a uranium mine
Elliot Lake (Rio Algom, Stanleigh) (Ontario)	Magmatic	Uraninite, brannerite, monazite, zircon, pyrite, quartz	0.0071% REO and yttrium in a uranium mine
Strange Lake (Newfoundland/Quebec)	Magmatic	Zircon, monazite,allanite, gadolinite, pyrochlore, fluorite	1.3% REE and 0.66% Y_2O_3 in a primary beryllium property
Thor Lake (Northwest Territories)	Magmatic	Xenotime, gadolinite, allanite, columbite, amphibole, fluorite	REE and yttrium occur in a primary beryllium property

Table 2.9 (continued)

Location	Deposit type	Principal minerals	Average grade
China			
Bayan Obo (Inner Mongolia)	Magmatic	Hematite, magnetite, monazite, rutile, martite	6% REO in a major hematite mine
Beihai (Guangxi)	Placer, fluvial	Ilmenite, rutile, zircon, monazite, quartz	1.5% heavy minerals
Guangdong (Guangdong)	Placer, fluvial	Ilmenite, rutile, zircon, monazite, quartz	2.3% heavy minerals
Xun Jiang (Guangxi)	Placer, fluvial	Ilmenite, rutile, zircon, monazite, quartz	6.0% heavy minerals
Egypt			
Nile Delta—Rosetta	Placer, marine	Ilmenite, rutile, zircon, monazite, magnetite, garnet	0.5% monazite
Gabon			
Mabounie	Magmatic		A carbonatite with florencite; 2.52% REO in the ore
Greenland			
Ilimaussaq	Magmatic	Pyrochlore, eudialyte	0.9% Y_2O_3 in a carbonatite
India			
Chavara (IREL) (Kerala)	Placer, marine	Ilmenite, rutile, zircon, leucoxene, sillimanite, monazite, quartz, garnet	18% heavy minerals, 0.135% monazite
Chavara (KMML) (Kerala)	Placer, marine	Ilmenite, rutile, zircon, leucoxene, sillimanite, monazite, quartz, garnet	18% heavy minerals, 0.135% monazite
Manavalakurichi (Tamil Nadu)	Placer, marine	Ilmenite, rutile, zircon, leucoxene, sillimanite, monazite, quartz, garnet	2.5% monazite
Chatrapur (Orissa)	Placer, marine	Ilmenite, rutile, zircon, leucoxene, sillimanite, monazite, quartz, garnet	0.585% monazite
Ranchi and Purulia (Bihar)	Placer, fluvial	Ilmenite, rutile, zircon, monazite, apatite, columbite, magnetite, quartz	1.64% heavy minerals, 0.31% monazite, 0.03% apatite
Kenya			
Rangwa/Ruri/Homa	Magmatic	Monazite, barite, fluorite	5.6% monazite
Malawi			
Kangankunde	Magmatic	Staurolite, monazite	5.0% monazite
Mauritania			
Bou Naga	Magmatic	Monazite	4.4% REO in massive monazite
Mozambique			
Congolone	Placer, marine	Ilmenite, rutile, zircon, monazite, quartz	2.8% heavy minerals, 0.007% monazite

Table 2.9 (continued)

Location	Deposit type	Principal minerals	Average grade
Namibia			
Etaneno	Magmatic		Requires an effective separation process
New Zealand			
Barrytown (South Island)	Placer, marine	Ilmenite, rutile, zircon, magnetite, cassiterite, gold, monazite, scheelite	0.01% monazite
Westport (South Island)	Placer, marine	Ilmenite, rutile, zircon, magnetite, cassiterite, gold, monazite, scheelite	undergoing feasibility study
South Africa			
Buffalo Fluorspar (Transvaal)	Magmatic	Fluorite, monazite, apatite	1.0% monazite
Phalaborwa (Transvaal)	Magmatic	Bornite, chalcopyrite, apatite, pyroxene, hornblende, plagioclase	Major copper producer
Richards Bay (Natal)	Placer, marine	Ilmenite, rutile, zircon, magnetite, leucoxene, monazite, quartz, garnet	6.5% heavy minerals, 0.023% monazite
Sri Lanka			
Pulmoddai	Placer, marine	Ilmenite, rutile, zircon, sillimanite, monazite, garnet, quartz	70% heavy minerals, 0.15% monazite
United States			
Aiken County (South Carolina)	Placer, fluvial	Ilmenite, rutile, zircon, monazite, quartz, clay	0.031% monazite
Bald Mountain (Wyoming)	Magmatic	Ilmenite, zircon, monazite, magnetite, hematite, quartz	0.2% monazite, 0.011% ThO_2
Bear Lodge (Wyoming)	Magmatic	Monazite, xenotime, hematite, feldspar, quartz	1.306% REO, 0.034% ThO_2
Bear Valley (Idaho)	Placer, fluvial	Ilmenite, magnetite, monazite, garnet, quartz	0.0052% monazite
Big Creek (Idaho)	Placer, fluvial	Ilmenite, magnetite, zircon, monazite, garnet	0.04% monazite
Blackfoot Bridge (Idaho)	Magmatic	Collophane, vanadinite, uraninite, rare earth elements, pyrite, clay	0.1% rare earths at phosphate property
Brunswick—Altamaha (Georgia)	Placer, marine	Ilmenite, magnetite, zircon, monazite, quartz	0.0285% monazite
Caldwell Canyon (Idaho)	Magmatic	Collophane, vanadinite, uraninite, rare earth elements, pyrite, clay	0.1% rare earths at phosphate property
Champ (Idaho)	Magmatic	Collophane, vanadinite, uraninite, rare earth elements, pyrite, clay	0.1% rare earths at phosphate property

Table 2.9 (continued)

Location	Deposit type	Principal minerals	Average grade
Conda (Idaho)	Magmatic	Collophane, vanadinite, uraninite, rare earth elements, pyrite, clay	0.1% rare earths at phosphate property
Cumberland Island (Georgia)	Placer, marine	Ilmenite, rutile, zircon, leucoxene, monazite, quartz	Production unlikely
Diamond Creek (Idaho)	Magmatic	Monazite, xenotime, fluorite, hematite, feldspar, quartz	1.22% REO, 0.21% ThO_2
Gallinas Mountains (New Mexico)	Magmatic	Fluorite, rare earth elements, pyrite, quartz, clay	2.95% REO
Gay and South Forty (Idaho)	Magmatic	Collophane, vanadinite, uraninite, rare earth elements, pyrite, clay	0.1% rare earths at phosphate property
Gold Fork—Little Valley (Idaho)	Placer, fluvial	Ilmenite, magnetite, zircon, gold, monazite, quartz	0.009% monazite
Green Cove Springs (Florida)	Placer, marine	Ilmenite, magnetite, zircon, staurolite, monazite	0.0077% monazite
Hall Mountain Group (Idaho)	Magmatic	Gold, zircon, apatite, monazite, hematite, quartz	0.026% Y_2O_3, 0.668% ThO_2
Henry (Idaho)	Magmatic	Collophane, vanadinite, uraninite, rare earth elements, pyrite, clay	0.12% rare earths at phosphate property
Hicks Dome (Illinois)	Magmatic	Thorite, xenotime, rare earth elements, fluorite, barite, apatite, sulfides, hematite	0.42% REO, 0.15% ThO_2
Hilton Head Island (South Carolina)	Placer, marine	Ilmenite, rutile, zircon, staurolite, magnetite, monazite, quartz, clay, garnet	0.018% monazite
Husky (Idaho)	Magmatic	Collophane, vanadinite, uraninite, rare earth elements, pyrite, clay	0.1% rare earths at phosphate property
Iron Hill (Colorado)	Magmatic	Ilmenite, rutile, zircon, pyrochlore, apatite, monazite, fluorite, pyrite	Mining goal would be Nb_2O_5
Lehmi Pass (Idaho)	Magmatic	Monazite, thorite, rutile, quartz, hematite, pyrite	Mining goal would be ThO_2
Maxville (Florida)	Placer, marine	Ilmenite, zircon, staurolite, monazite, quartz	Extension of Green Cove Springs being developed
Maybe Canyon (Idaho)	Magmatic	Collophane, vanadinite, uraninite, rare earth elements, pyrite, clay	0.1% rare earths at phosphate property
Mineville Dumps (New York)	Magmatic	Magnetite, martite, apatite, quartz, feldspar	1.04% REO, 0.0136% ThO_2 in iron mine dumps
Mountain Fuel (Idaho)	Magmatic	Collophane, vanadinite, uraninite, rare earth elements, pyrite, clay	0.1% rare earths at phosphate property
Mountain Pass (California)	Magmatic	Allanite, monazite, barite, quartz	12% bastnasite, 7.68% REO in major rare earth producer

Table 2.9 (continued)

Location	Deposit type	Principal minerals	Average grade
Music Valley (California)	Magmatic	Xenotime, monazite, gold, biotite, quartz	RE value ranges from 3 to 14%
North Henry (Idaho)	Magmatic	Collophane, vanadinite, uraninite, rare earth elements, pyrite, clay	0.1% rare earths at phosphate property
North and South Carolina Placers (North and South Carolina)	Placer, fluvial	Ilmenite, rutile, zircon, sillimanite, staurolite, monazite, garnet, kyanite	Series of separate placers
Oak Grove (Tennessee)	Placer, fluvial	Ilmenite, rutile, zircon, leucoxene, staurolite, monazite, garnet, kyanite, tourmaline	0.09% REO
Pajarito (New Mexico)	Magmatic	Eudialyte, zircon	0.18% Y_2O_3 in major potential source of yttrium in the United States
Pearsol Creek (Idaho)	Placer, fluvial	Ilmenite, magnetite zircon, monazite, garnet, quartz	0.0185% monazite
Powderhorn (Colorado)	Magmatic	Perovskite, pyrochlore, apatite, biotite, feldspar	0.36% REO in 12% TiO_2 material
Silica Mine (Tennessee)	Placer, fluvial	Ilmenite, rutile, zircon, leucoxene, monazite, quartz	0.0105% monazite in sand, 0.07% monazite in heavy minerals dump
Smoky Canyon (Idaho)	Magmatic	Collophane, vanadinite, uraninite, rare earth elements, pyrite, clay	Phosphate mine
Trail Creek (Idaho)	Magmatic	Collophane, vanadinite, uraninite, rare earth elements, pyrite, clay	0.1% rare earths at phosphate property
Wet Mountains (Colorado)	Magmatic	Thorite, xenotime, barite, hematite, quartz	ThO_2:REO ratio 2.2:1.0
Wooley Valley (Idaho)	Magmatic	Collophane, vanadinite, uraninite, rare earth elements, pyrite, clay	0.11% rare earths at phosphate property
Uruguay			
Atlantida	Placer, fluvial	Monazite	3.2% monazite

Cooljarloo/Jurien Bay Mineral sands deposits occur at Jurien Bay and Cooljarloo in western Australia just south of Eneabba. Cooljarloo's deposits were estimated as 16 million metric tons of proven and 42 million metric tons of probable ore grading 3 to 5% heavy minerals, including monazite (Hedrick 1985a). Reserves at Jurien Bay were estimated at 25 million metric tons of proven and 1 million metric tons of probable ore grading 6 to 7% heavy minerals, including monazite. At Cooljarloo, the mined sand is composed of about 0.2% monazite, and at Jurien Bay the sand contains 0.7% monazite. Total reserves were equivalent to 64,000 metric tons REO at Cooljarloo, and 100,000 metric tons REO at Jurien Bay (Hedrick 1985a).

Jangardup Jangardup mineral sands deposit, located 60 km south of Nannup in southwestern Australia, has moderate quantities of xenotime.

WIM-150 This deposit was named after Wimmera Industrial Minerals and is a major deposit of heavy mineral sands near Horsham in western Victoria (Taylor 1991). The WIM-150 deposit contains an estimated 32 million metric tons of heavy minerals in an area of about 40 square km. This includes 580,000 metric tons of monazite and 170,000 metric tons of xenotime.

Murray Basin About six times the amount of rare earths in the WIM-150 deposit occur in the four other deposits of Murray Basin, western Victoria (RIC 1993). The monazite and xenotime content of the Murray Basin heavy mineral deposit, on the whole, has been estimated to be about seven times larger than the current proven reserves of rare earths in Australia. The deposit is a commercial source of zircon and titanium minerals in addition to monazite.

Olympic Dam The Olympic Dam deposit is a huge multimetal (copper, uranium, gold, and rare earths) resource (Taylor 1991). The hard rock ore body contains rare earth minerals at a typical concentration of 5000 ppm. The minerals found are bastnasite, monazite, and florencite with a very minor amount of xenotime. Significantly, the most abundant of the rare earth minerals in the deposit, bastnasite, is abnormally enriched in heavy rare earths and the usual europium depletion is absent.

Brockman The Brockman deposit is located in the East Kimberley region of western Australia. It is potentially a major source of yttrium and heavy rare earths that could be recovered along with other minerals (Taylor 1991). Up to 100 meters in depth, 8.97 million metric tons of resource grading, in percentage, 1.027 ZrO_2, 0.116 Y_2O_3, 0.437 Nb_2O_5, 0.026 Ta_2O_5, 0.038 HfO_2, 0.01 Ga, 12.1 Al_2O_3, and 0.105 REO have been indicated. Besides, up to a depth of 250 meters, 13.6 million metric tons of additional resources of similar grades have been inferred.

Toongi A deposit is located at Toongi, which is 20 km south of the large regional town Dubbo in central New South Wales approximately 410 km northwest of Sydney. To date only limited work has been done on the evaluation of this deposit, which has indicated 10 million tonnes of resources from 0 to 30 meters depth (Taylor 1991). The composition is 2.1% ZrO_2, 0.05% HfO_2, 0.14% Y_2O_3, 0.56% Nb_2O_5, 0.036% Ta_2O_5, and 0.75% REO. An additional 40 million tonnes of deposits of similar grade occur between 30 and 100 meters of depth.

The yttrium content of the deposit is notably high and the distribution of rare earth oxides indicates that several rare earth minerals contribute to the total rare earth content of the ore.

Mount Weld The Mount Weld rare earth deposit in western Australia ranks as one of the richest major rare earth resources in the world (Taylor 1991). The Mount Weld complex comprises world class rare earth oxide and niobium/tantalum deposits developed within the Mount Weld carbonatite, an intrusive pipe approximately three kilometers in diameter. The main deposits are hosted within the soil/regolith horizon that blankets the entire carbonatite and form shallow lenses and sheets within 60 m of the surface. The most important REO deposit, the Central Lanthanide Deposit, CLD, is located at the center of the carbonatite with the Nb/Ta and other deposits generally located towards the outer fringes. Discovered in 1988, the CLD represents a spectacular enrichment zone of REDS. The deposit is believed to be the largest and highest grade of its type in the world. The resource here is estimated at 1.69 million metric tons grading 26.1% REO, using a cut-off grade of 20% REO, and 6.2 million metric tons grading 17.22% REO, using a cut-off grade of 10% REO. It has also been stated that the rare earth contained in the Mount Weld deposit is sufficient to supply 15 to 20% of the present world demand for rare earths for over 20 years. The

principal rare earth mineral in the deposit is supergene monazite, and in some zones the mineralization is predominantly churchite — hydrated yttrium phosphate mineral. The europium content of monazite is unusually high. Most importantly, the Mount Weld deposit is low in the radioactive element thorium. Besides, the ore zones have low deleterious element levels in other elements such as fluorine and calcium, which is relevant in both metallurgical and operating environmental performance.

John Galt This is a hard rock deposit containing high grade veins of xenotime and is located in the Kimberley region of western Australia. The rare earth distribution in the ore is generally similar to xenotime, but the yttrium content as a proportion of total rare earths is higher than normal (Taylor 1991).

Yangibana This is a hard rock rare earth deposit in western Australia. In this deposit, the rare earth mineralization occurs over a distance of approximately 7 km with a width of several hundred meters. The estimated size of the resource is 3.5 million metric tons with an average grade of 1.7% REO (Taylor 1991). The ore probably has unusually high europium content.

2.6.3 Bangladesh

Heavy minerals including monazite occur in the Cox's Bazaar coastal area of Bangladesh. The beach sand deposits, located 100 km southeast of Chittagong along the coast and nearby islands, contain resources estimated at 5 million metric tons of heavy minerals (Hedrick 1985a).

2.6.4 Brazil

There are numerous beach sand deposits extending from the northern border of the state of Rio de Janeiro over the state of Espirito Santo to the state of Bahia, on the Atlantic coast. Monazite deposits also occur in the state of Parana. According to the United States Geological Survey Circular (Jackson and Christiansen 1993), there are 14 monazite deposits, one bastnasite deposit, and one deposit of other rare earth minerals in Brazil. The crude mineral sand of Brazil contains around 10% of heavy minerals of which between 10 and 15% is monazite. The monazite contains about 64% of the rare earth oxides, 5.5 to 6% of thorium oxide, and 0.15 to 0.2% of uranium oxide. The relative concentration of rare earths in monazite is given in Table 2.4.

The rare earth deposits at Sao Goncalo de Sapucai and Tapira are of considerable interest (Jackson and Christiansen 1993). The Sao Goncalo de Sapucai deposit is the first inland placer to be dredged in Brazil. It is located on the Sapucai River in Minas Gerais. At Tapira, which is an existing phosphate mine based on apatite, an anatase bearing overburden currently stockpiled contains recoverable titanium and rare earths. A hard rock deposit at Pocos de Celdas in Minas Gerais is a resource containing 1.5 million metric tons of bastnasite. The average rare earth content of bastnasite in the deposit is 3.3% REO. According to the latest estimates (Hedrick 2000) 42000 tons of monazite occur in marine alluvial deposits and 40000 tons occur in stream placers. The resources of marine origin are distributed in deposits primarily in the states of Rio de Janeiro (26730 tons), Bahia (10186 tons) and Espirito Santo (4136 tons). The stream placers occur in the states of Mines Gerais (24396 tons), Espirito Santo (11372 tons) and Bahia (3481 tons).

2.6.5 Canada

In terms of rare earth resources, Canada is one of the seven major countries in the world. Canada is unique in that its rich rare earth reserves are not constituted by placer monazite or a large hard rock deposit with bastnasite as the principal mineral. The "other minerals" make up for the large rare earth deposits in Canada.

According to the United States Geological Survey Circular (Jackson and Christiansen 1993), there are 5 rare earth deposits in Canada, all of which are hard rock deposits. Three of these deposits contain uraninite, brannerite, and monazite, while the remaining two deposits contain gadolinite, zircon, monazite, allanite, fluorite, and pyrochlore or columbite and xenotime. Rare earths occur with uranium in the uranium deposit at Elliot Lake, Ontario (Drew et al. 1991). An yttrium–beryllium–zirconium deposit at Strange Lake, northeast of Schefferville on the Quebec–Labrador border contains huge quantities of rare earths in addition to beryllium, pyrochlore, and fluorite (Argall 1980). The current estimate of the reserve is 25 million metric tons with 0.38% yttrium. Large deposits of rare earth bearing pyrochlore occur at St. Honoré and at Oka in Quebec (Noblitt 1965). The rare earth content of Oka pyrochlore averages almost 10% REO and ranges from 2.5 to 11.8% REO. Cerium, lanthanum, neodymium, and yttrium predominate in this pyrochlore, which also has 0.02 to 1.51% ThO_2 and 0.03 to 0.72% U_3O_8.

A specialty metals deposit at Thor Lake, 130 km southeast of Yellowknife in the Northwest Territories contains the rare earths yttrium and beryllium. Proven reserves of 431,000 metric tons of ore grading 0.2% Y_2O_3 have been reported (Hedrick 1985a). A major new source of rare earths has been discovered in southern Yukon, Canada. Over 1,500,000 metric tons of ore are contained in a wide fluorite-bearing vein, which has a mineral assemblage of monazite and xenotime. The following composition has been reported for a representative rock outcrop of the deposit: 0.15% yttrium oxide, 0.62% niobium oxide, 1.10% zircon, 0.02% hafnium oxide, and 1.37% lanthanides consisting mostly cerium, lanthanum, and neodymium oxides.

2.6.6 China

China is foremost among the seven major countries with 48 million metric tons of REO found in resources located in the country. It has also been stated (Jackson and Christiansen 1993) that China probably has more rare earth deposits than what has been reported. Some of these deposits are among the world's largest rare earth resources.

There are four main belts of rare earth mineralization in China (Clark and Zheng 1991). They are (1) Inner Mongolia belt, (2) Fuji, Jiangxi–Guangdong, Guangxi – Hunan belt, (3) Hubei-Sichuan belt, and (4) Southeast China beach placer belt. Each of these belts has a unique type of rare earth mineral occurrence. The Inner Mongolia belt contains the Bayan Obo rare earth–iron mine, which, with over 350 million metric tons of reserves, is the world's largest rare earth mine. The principal minerals are bastnasite and monazite in a dolomitic iron formation. The Fuji, Jiangxi–Guangdong, Guangxi–Hunan belt occurs along the borders of the provinces mentioned and contains the relatively recently discovered and currently exploited ion adsorption deposits. The deposits are lateritic zones containing bastnasite, synchysite, and allanite. The ore occurs in numerous small deposits. The Hubei–Sichuan belt occurs along the borders of these two provinces and consists of bastnasite and parisite occurring in barite and calcite veins associated with alkaline and

carbonatite rocks. In the southeast China beach placer belt, beach placer deposits containing monazite and xenotime occur along the coastal areas of west Guangdong Province and Haian Island.

Thus rare earth deposits occur throughout the eastern half of China. Among these the metasedimentary deposits, which include the Bayan Obo deposit and the ion adsorption type deposits of southeast China, are the most important.

Bayan Obo The Bayan Obo iron–rare earth–niobium ore bodies, discovered in the late 1920s, are located 135 km northwest of Baotou in the Nei Monggol autonomous region of northern China. The Bayan Obo iron–rare earth–niobium mine is China's largest iron mine with iron ore reserves of more than 1 billion metric tons. The rare earth reserves of Bayan Obo exceed 35 million metric tons REO.

The genesis of the Bayan Obo deposit has been explained in many ways (Kanazawa and Miyawaki 1991), as a marine sedimentary–diagenitic deposit, as a sedimentary–metamorphic–hydrothermal deposit, and as a marine facies volcanosedimentary deposit and as marine facies volcanosedimentary carbonatite. It has also been interpreted (Drew et al. 1991) that the Bayan Obo iron–rare earth–niobium ore bodies were formed by hydrothermal replacement of Middle Proterozoic dolomite in an intercontinental rift setting.

Clark and Zheng (1991) have described the Bayan Obo deposit as occurring in a severely folded and faulted sequence of middle Proterozoic slates, quartzites, dolomites, and limestones intruded by Hercynian granites and weakly metamorphosed. The main mineralization zones lie south of the Kuang Gow fault and occur primarily in what is known as the H8 dolomite.

The H8 dolomite occurs within a zone that extends 18 km in the east-west direction and is 2 km in width. The majority of the commercial deposits occur here. The H8 dolomite occurs throughout the zone and is more than 1000 meters thick. Within the H8 dolomite there are three main ore zones: the main ore body, the east ore body, and the west ore body. The main ore body and the east ore body have reserves of 20 million metric tons and 15 million metric tons of REO, respectively. There are 16 medium ore bodies in the west mine.

The main ore body consists of tubular and/or lenticular bodies of REO bearing magnetite and hematite iron ores. A high but variable amount of fluorite is associated with both the ore and the surrounding dolomitic host rock throughout the Bayan Obo deposits.

At Bayan Obo, the REO bearing iron ore as well as the host H8 dolomitic rocks are the sources of rare earths. The main ore body has an average REO content of 6.19%, the east ore body 5.17%, and the west ore body approximately 1% (Argall 1980). Dolomitic type ores in the main and east ore bodies also contain a considerable amount of rare earths (2 to 4% REO).

The primary rare earth bearing minerals in the Bayan Obo ore bodies are bastnasite and monazite. These two together constitute approximately 80% of the REO occurring in the deposit. A total of 29 individual rare earth minerals have been reported to be intergrown in the Bayan Obo deposit. Among these, 13 are stated to be new minerals (Clark and Zheng 1991).

The rare earths in the ore at Bayan Obo occur as individual minerals and less than 10% is dispersed isomorphically in other minerals. In the ore bodies (Clark and Zheng 1991), bastnasite and monazite are closely associated and their ratio (bastnasite to monazite) varies depending on the ore type. Usually the quantity of bastnasite is 20 to 100% more than the quantity of monazite in the ore.

Monazite in the ores of Bayan Obo contains an average of only 0.26% of ThO_2. The REO and P_2O_5 together account for 98% of the monazite composition. The low thoria

content and high REO content make this a highly desirable mineral for rare earth production. The thoria content of bastnasite varies in the range 0.02 to 0.28%, making this also a favorable mineral for rare earth production. Fluorine occurrence is widespread in the mine but more than 98% of the fluorine in the deposits occurs primarily as fluorite and as a minor component in bastnasite.

Ion Adsorption Ore An unusual type of rare earth deposit known as the ion-adsorption type occurs in southern China (Clark and Zheng 1991). The deposits were initially discovered in southern Jiangxi Province, which to date remains the principal region for ion adsorption type deposits. Additional ion adsorption deposits have been discovered in the provinces of Guangdong, Fujian, Hunan, Guangxi, and Southern Anhui.

The ion adsorption deposits form as the result of *in situ* weathering of REO rich host rocks, most commonly granitic or volcanic rocks. For their formation, therefore, there must be sufficient quantity of rare earth-bearing host rock occurring within the zone of weathering, and the weathering or lateritic process must be balanced so that prolonged weathering is possible but with limited erosion. The rare earth cations from the host rocks are mobilized onto the aqueous phase and migrate downwards. Simultaneously with the weathering, various aluminosilicate minerals, such as kaolimite clays, form and these in turn adsorb the RE^{3+} cations. Such weathering requires a mild, rainy, humid and tectonically stable environment over a long period of time. All these conditions are met in southern China, and hence a large number of ion adsorption type REO deposits occur there.

Even though the reserve estimate of rare earths in ion adsorption type deposits in China is placed at one million metric tons REO, Clark and Zheng (1991) state that it is likely to be several million metric tons REO. Over 100 individual mineralized occurrences have been identified in Jiangxi Province alone, and geologic studies have shown granitic outcrops, which are potential sources of ion adsorption deposits, occupy very extensive areas in southern Jiangxi, western Fujian, and Guangdong provinces. The rare earth content of ion adsorption type ores in several major deposits of southern Jiangxi and western Fujian provinces are given in Table 2.5. These deposits are special in that they are characterized by low cerium and high neodymium, samarium, europium, gadolinium, and terbium or high yttrium contents. So, depending on the rare earth element required, the deposits may be selectively mined. The grades of ion adsorption type deposits are the lowest (0.05 to 0.2% REO) among the various rare earth deposits in China. This however is offset by the easier mining and beneficiation of these deposits.

Placers Placer deposits containing monazite and xenotime occur at many locations in China (Clark and Zheng 1991). The principal placer deposits are located along the coastal areas of west Guangdong and Hainan Island. The Nanshanhai deposit of Guangdong extends from the east to the west for about 9 km. It is 1.4 km wide and has an average thickness of 3.24 m. In addition to monazite (44,000 metric tons) and xenotime (8200 metric tons), zircon and ilmenite occur in the deposit. Reserves of monazite, equal in extent to that mentioned above, occur in fluvial and lacustrine placer deposits found widespread in Hunan, Hubei, Sichuan, and Jiangxi provinces. The average grade of placer deposits in China is 0.5 to 1.0% REO.

Other Deposits Rare earth-bearing carbonatite deposits associated with alkaline rocks have been found in Taohualashan, Northern Nei Monggol, Zhushan, northwestern Hubei, Weishan, southern Shandong, and Xichang, Sichuan (Clark and Zheng 1991). The main producing mine among these is the Weishan mine in Shandong Province. The principal ore mineral in this mine is bastnasite.

A massive alkaline igneous type rare earth deposit has been discovered recently in Mianning county, southwestern Sichuan. The ore body consists of mainly bastnasite with small amounts of parisite, chernovite, and xenotime. The metals lead, molybdenum, and bismuth occur in association with the rare earth minerals. This deposit is considered attractive because it is easy to beneficiate and low in thorium content.

Apatites enriched in rare earths occur over the western part of China. The levels of REO are, however, too low for commercial recovery.

2.6.7 Germany

Heavy mineral sands deposits, similar to those in the east coast of Australia, occur at Cuxhaven in the North Sea coast, Germany. Reserves have been estimated at 10 million metric tons of heavy minerals, including ilmenite, rutile, zircon, and possibly monazite (Hedrick 1985a).

2.6.8 India

A large variety of rare earth deposits occur in India of both the hard rock and placer types.

Hard Rock Deposits Rare earth minerals in large concentrations occur in pegmatites in the states of Bihar, Rajasthan, and Andhra Pradesh, and in hydrothermally altered formations, particularly those associated with carbonatites, in the states of Rajasthan, Tamilnadu, and Gujarat.

Vast occurrences of allanite within the granitic rocks are known in the districts of Madurai and Tirunelveli in Tamilnadu and in parts of Mayurbhanj and Koraput districts of Orissa. Allanite, even though it contains much less total REO (10 to 30%) than many other minerals, may best be reckoned in India as a potential source of rare earths in view of their extensive occurrence. Many of the allanites from parts of Bihar and Tamilnadu have been found to contain small amounts of europium and samarium. The Kanyaluka deposit in the Singhbhum district of Bihar contains pegmatites rich in xenotime. The deposits of uranium ore from Jaduguda contain appreciable amounts of dysprosium and gadolinium. Gadolinite occurs in the Mayurbhanj district of Orissa, and in the Madurai and Salem districts of Tamilnadu. Chevkinite occurs in parts of Orissa and Karnataka; uranothorite occurs in parts of Karnataka, Tamilnadu, and Uttar Pradesh; and rare earth-bearing pyrochlore and zircon occur in the north Arcot district of Tamilnadu and in the sandstones of Madhya Pradesh, respectively.

Yttrium occurs in association with lanthanides and like them is characteristic of granite pegmatites. These deposits occur in the (1) Rajasthan and Bihar pegmatite belt; (2) Kanyaluka, and Singhbhum district of Bihar; (3) Syenite pegmatites and alkali rocks like the carbonatites of Rajasthan, Gujarat, and Tamilnadu and, possibly, (4) in certain locations in Andhra Pradesh.

Placers The most important rare earth deposits of India are the beach sand deposits that contain monazite in addition to ilmenite, rutile, zircon, sillimanite, and garnet. India occupies an important place in the reserves of beach sand deposits and ranks second only to Australia. There are five major rare earth placer deposits, of which four are in coastal areas. The fifth placer, yet unworked, is inland. The rare earths in the Indian placer deposits have been estimated at 2.7 million metric tons REO, placing India in the fifth position after

China, Namibia, the United States, and Australia in the order of countries having the largest amounts of REO.

The rare earth placer deposits in India are found in the southwestern coast of the peninsula at Manavalakurichi in Tamilnadu, Chavara in Kerala, and on the eastern coast in Gopalpur in Orissa. The Chavara beach deposits extend over a stretch of 22 km from Kayamkulam in the north to Neendakara in the south. The Manavalakurichi beach deposits extend to about 2 km in length from the mouth of the river Valliar touching Kadiapatnam village to the village Chinnavilai. Apart from the rich seasonal washings on the beach, the dunes containing relatively higher percentage of silica form an important source. Extensive dune sand deposits occur along the south Orissa coast over a stretch of about 150 km. Of the several deposits located, the one close to Chatrapur is an extensive single deposit with the highest grade of heavy minerals. It runs over a coast length of nearly 18 km, covering a total area of over 26 square km between Gopalpur in the south and the Rushikulya river in the north. In addition to the main deposits described above, extensive heavy mineral deposits also occur on the coasts of Andhra Pradesh and Maharashtra. It is reported (Jackson and Christiansen 1993) that resources on the coastal placers of India may be underestimated because the beach sands are replenished by annual monsoons. Rare earths also occur in the inland placer deposits at Ranchi in Bihar state and at Purulia in West Bengal state.

2.6.9 Indonesia

In Indonesia, the important rare earth resource is xenotime, occurring in the cassiterite rich placers in the Tin Islands, Belitung, Bangka, Tujuh Archipelago, Singkap, Kundur and Karimun, which form part of the southern extension of the Tin belt of southeast Asia. The deposits of the Belitung island are the most important. The total reserves of monazite and xenotime in cassiterite placers of the Tin islands have been estimated at approximately 5000 metric tons. No actual mining or processing for rare earth recovery appears to have been carried out.

2.6.10 Japan

In Japan the titanium mineral sphene, containing rare earths, has been found (Ito 1991) in the syenitic rocks around the periphery of the Kamioka lead–zinc mine. The deposit is a holocrystalline syenitic rock that is composed essentially of diopside, feldspar, quartz with accessory sphene, apatite, epidote, calcite, amphibole, sphalerite, and others. The sphene content of the deposit is approximately 4 to 7% and the total rare earth content of the sphene is ~1.1% REO. Sphene is not commercially processed at present anywhere. It is a refractory and chemically stable silicate mineral.

2.6.11 Malaysia

Alluvial tin deposits in Malaysia contain cassiterite as the main economic mineral and, in addition, several other minerals such as ilmenite, monazite, xenotime, and zircon. Cassiterite and the associated minerals usually occur as free grains liberated from one

another due to the natural breakdown process from the primary ore body. Monazite, xenotime, ilmenite, and zircon's contents are highly variable and depend on the location of the deposit. Data are available usually for the composition of tin tailings generated in mineral benefication for cassiterite, known locally as "amang."

Alluvial tin deposits occur in various states in Malaysia, and the deposits in the Kinta valley of the Perak state are considered important. Analysis of an amang sample from this valley is given (Hussin et al. 1991) in Table 2.10.

Table 2.10 Analysis of an "amang" sample from Kinta Valley, Malaysia (Hussin et al. 1991)

Minerals	Percentage
Ilmenite	59.6
Hydroilmenite	7.9
Quartz	12.2
Topaz	7.7
Tourmaline	4.6
Siderite	2.5
Rutile	2.4
Garnet	1.3
Pyrite	0.7
Xenotime	0.5
Zircon	0.4
Monazite	0.2
Cassiterite	trace

The highest percentage of xenotime is found in the deposits at Jelepang (5%) and at Batu Gajah (3%) in the Kinta valley. The monazite content in the amang from Batu Gajah is 10% whereas no monazite is present in the amang from Jelepang. Similarly the deposit in the state of Terengganu contains about 2% monazite but no xenotime. Even in some areas of Perak, as well as in the state of Selangor, xenotime presence does not exceed trace levels. By and large, monazite occurrence is more prevalent in amang but useful quantities of xenotime are present. On average, Malaysian monazite (Sulaiman 1991) contains 25% Ce_2O_3, 2% Sm_2O_3, 2% Y_2O_3, 27% phosphate, 6% ThO_2, and 0.2% U_3O_8. A typical analysis of Malaysian xenotime is 35% Y_2O_3, 4% Dy_2O_3, 4% Yb_2O_3, 29% phosphate, 0.7% ThO_2, and 1.6% U_3O_8. Total rare earth reserves in Malaysia have been estimated (Kanazawa and Miyawaki 1991) at a modest 30,000 metric tons REO.

2.6.12 Malawi

Many rare earth minerals, including the common monazite and bastnasite and the less common synchysite and florencite, are found in Malawi. They occur in carbonatites in the Chilwa province of southern Malawi (Malunga et al. 1991).

Kangankunde Monazite in exploitable quantities occurs in Kangankunde carbonatite. Monazite is found as a pale green to colorless mineral disseminated throughout the carbonatite, in carbonatized fledspathic rocks, and in the surrounding eluvial soils. The monazite is poor in thoria. The rare earth content in the carbonatite ranges from 1.6 to 16.2% REO

with an average content of 10% REO. The mean percentage concentrations of Sm_2O_3 (1.43), Eu_2O_3 (0.17), and Y_2O_3 (0.10) compare favorably with Mountain Pass bastnasite. An estimated 13,000 metric tons of monazite occur to a depth of 30 meters.

Nanthace Hill The minerals synchysite and bastnasite occur in Nanthace Hill as disseminated needles, 0.2 to 1 mm long, in sideritic carbonatite. The grade is 1 to 3.6% REO. Three mineralized zones, more than 10 m thick, within the apatite and carbonatite contain 600,000 metric tons of ore with 1.7% REO up to a depth of 50 m.

The apatite carbonatite of Nanthace Hill bears higher concentrations of yttrium and europium. The total REO content of apatite crystals ranges from 0.5 to 1.25%.

Songwe In the Songwe carbonatite, the main mineralization is that of synchysite or bastnasite. Mineralized zones with thicknesses of more than 10 m show an REO content of more than 1%. Within 50 m depth, 1.4 million metric tons with 1.7% REO has been proved.

Chilwa Island The minerals synchysite and florencite occur as disseminated fibrous aggregates in the Chilwa Island carbonatite. In the central core of the sideritic carbonatite, the rare earth content is 5% REO. The mean Sm_2O_3, Eu_2O_3, and Y_2O_3 contents are 2.20, 0.47, and 1.64%, respectively.

The sideritic carbonatite of the Chilwa island contains apatite and pyrochlore. This apatite contains lanthanum (7.12%) and cerium (13.7%), while pyrochlore contains cerium (1.3–2.76%).

2.6.13 Mozambique

Placer deposits of heavy minerals including monazite occur in Mozambique at Congolone, which is on the coast, 15 km north of Angoche. The deposit consists of dredgeable reserves of 167 million metric tons grading 3.25% heavy minerals. The 5.42 million metric tons of heavy minerals in the reserve include 11,000 metric tons of monazite (RICI 1990).

2.6.14 Myanmar

In Myanmar monazite and xenotime occur associated with placer cassiterite and wolframite deposits. Columbite and tantalite also occur in these deposits, which are found in the Dawei and Myeik areas of southern Myanmar (Jackson and Christiansen 1993).

2.6.15 New Zealand

There are two placer deposits on the west coast of south island at Westport and Barrytown. These deposits contain ilmenite, rutile, zircon, and monazite like many other marine placers. Additionally, they contain magnetite, cassiterite, gold, and scheelite (Jackson and Christiansen 1993). The monazite reserves are considered modest.

2.6.16 Peru

An alluvial mineral sands ore body that contains cerium, lanthanum, neodymium, and other rare earths occurs near Tacna in Peru. This ore body contains titanomagnetite and associated minerals (RIC 1997).

2.6.17 South Africa

With more than 1 million metric tons of REO contained in South African rare earth deposits, the country potentially is a major producer of rare earths. There are three deposits; two of them are hard rock type and one is a placer. All three deposits are very large. At the Phalaborwa complex, the fluorapatite, $3Ca_3(PO_4)_2 \cdot CaF_2$, deposits contain a significant amount of rare earths, typically 0.5–1.0% REO. The proportions of europium, samarium, and neodymium are considerably higher in Phalaborwa apatite (Eu 1.1, Sm 5.0 and Nd 13%). An advantage of apatite as a source of rare earth products is the absence of thorium. The safe disposal of the radioactive element thorium is a vexation to monazite-based processes. Monazite occurs in the fluorspar deposit at Buffalo fluorspar. Richards Bay beach sand deposit contains ilmenite, rutile, zircon, and magnetite in addition to monazite. The hard rock monazite deposits at Van Rhynsdorp and Naboomspruit have been notable among the world's primary monazite deposits.

2.6.18 Sri Lanka

Substantial deposits of heavy mineral sands occur concentrated along the beach on the northeast coastline centered at Pulmoddai, 56 km north of the Trinconamalee port (Panditharatna 1991). The deposits occur over a stretch 9 km long, and 360 m wide. The mineral reserves of Pulmoddai have been estimated to be approximately 3.7 million metric tons. The Sri Lankan mineral sands have the distinction of being the richest in heavy minerals content. The heavy mineral content is in the range 60–75%, and the constituent minerals are ilmenite 70–80%, rutile 8–10%, zircon 8–10%, and monazite 0.2%. Interestingly, Pulmoddai's offshore deposits have been estimated to be between 0.95 and 1.34 million metric tons. It has also been estimated that about 14 to 16% of the quantity of heavy minerals mined are added to the deposits by accretion due to wave action during the monsoon season every year.

2.6.19 Taiwan

Heavy mineral sands deposits occur along the southwest coast of Taiwan. About 550,000 metric tons of mineral sands, containing about 10% black monazite, have been reported in this deposit (Miao and Horng 1988). The black monazite is primarily composed of rare earth phosphate and silica and also contains zirconium, titanium, uranium, and thorium as minor constituents. The Taiwan black monazite is particularly low in thorium, containing only 0.41% ThO_2. The composition of this monazite vis-à-vis the minerals from Australia and India is shown in Table 2.11. The main difference between the black and yellow monazite are the silica and thorium contents.

2.6.20 Thailand

Rare earth mineral deposits of both primary and secondary origins occur in Thailand in a wide range of geological environments. Monazite is the most common rare earth mineral in Thailand, and the occurrences of xenotime and microlite are also important. Significant quantities of monazite and small amounts of xenotime are invariably associated with tin and tungsten deposits.

Table 2.11 Composition of monazite, wt %

	Taiwan black monazite	Taiwan yellow monazite	Australian monazite	Indian monazite
REO	48.62	63.22	58.50	58.60
P_2O_5	20.14	30.27	27.50	30.1
SiO_2	18.66	1.62	2.83	1.7
ThO_2	0.41	3.21	6.40	8.8

Australian monazite from Eneabba Co., Australia.
Indian monazite from Indian Rare Earths Ltd., India.

Both hard rock and placer deposits occur in Thailand. The hard rock deposits include "disseminated" rare earth-bearing lithophile granitoids and stockworks, rare earth-bearing tin pegmatites, rare earth-bearing quartz veins and rare earth-bearing skarns and skarnoids. The placer deposits include alluvial placer deposits, recent and old beach sand deposits, near and offshore deposits, and weathering crust deposits. The grades of rare earth ores in these deposits have been estimated to vary from low (<0.001% RE minerals) for most primary deposits, and intermediate (0.01–0.001%) for pegmatite and alluvial placer deposits, to high (>0.01%) for weathering crust and placer deposits. The ore tonnages are considered to be small for the quartz vein, skarn type, and weathering crust deposits, intermediate for alluvial placer deposits, and large for disseminated granitic–pegmatitic and near offshore deposits.

Much of the cassiterite deposits of the Thai Peninsula are located in the western granitic belt (Pungrassami and Sanguansai 1991). The primary sources of tin, tungsten, and associated heavy minerals are pneumatolytic granite, pegmatite, apatite, and hydrothermal quartz veins. Beach sand deposits occur in Changwat Prachuap, Khiri Khan, and Changwat Chumphon. Monazite–cassiterite ratio in these deposits ranges 0.0011–0.5203 and the xenotime–cassiterite ratio ranges 0.00–0.0194. The reserves of cassiterite, monazite, and xenotime from the mines in the granitic belts and from offshore are only modest.

2.6.21 Turkey

A bastnasite deposit is in midwest Turkey near Eskisehir. This deposit also contains barytes and fluorite and is large enough to support an annual output of 12,000 metric tons REO.

2.6.22 United States

Before the discovery of the huge rare earth deposits at Bayan Obo, China, the United States was ranked first as the country with the greatest amount of REO in its resources. With the identification of massive quantities of bastnasite deposits in Namibia, the African country took the second rank, and presently the United States ranks third among the seven major countries in terms of REO contained in their resources.

In the United States there are 32 monazite and 3 bastnasite deposits in addition to 5 deposits containing other rare earth minerals (Jackson and Christiansen 1993). Rare earth deposits occur distributed across the United States from inland California to the lower east coast.

Deposits of monazite occur in the United States in Florida, South Carolina, Idaho, Georgia, Alabama, Virginia, Wyoming, California, and Alaska. Out of the 40 rare earth deposits in the United States, only 13 are placer deposits of which 8 are fluvial placers and 5 are marine placers. Monazite occurs with ilmenite, zircon, magnetite, and other minerals in these deposits. Monazite from stream placers in Idaho are relatively low in thorium. The composition of a commercial monazite concentrate from Idaho was given in Table 2.4. Monazite from Florida contains about 4% ThO_2 which is much less than the thorium contents of monazite from Brazil (6% ThO_2) and India (8% ThO_2). Recently, beach sand deposits at Green Cove Springs, Florida, have been important. Most of the monazite deposits in the United States are, however, hard rock deposits. On the other hand, the mineral euxenite occurs in a placer deposit at Bear Valley, Idaho (Kremers 1961, Jackson and Christiansen 1993).

Mineralized zones containing monazite and xenotime, containing an estimated combined REO equivalent tonnage of 2.5 million tons for every 30 meters of mining, with the structure reportedly 120 meters deep to the base of the synclinal trough, occur throughout Music Valley located in Riverside County, California.

Bastnasite was not a well-known rare earth mineral until the discovery in 1949 of a large bastnasite deposit in Mountain Pass, California (Olson et al. 1952, Evans 1966). The Mountain Pass ore body is located near the west center of a block of pre-Cambrian metamorphic rocks composed of granite–biotite–garnet–hornblende–gneisses and schists that are cut by pegmatites and other dikes. Large areas of potash-rich igneous rocks, syneite, and shonkinite intrude into this complex, and next to these is the intrusion of rare earth-bearing carbonatite, which is also of pre-Cambrian age. Three principal rock types, namely, calcite — pink barite, dolomite, and silicified carbonate, form the carbonatite ore body. The minerals contained are, approximately, calcite/dolomite/ankerite, 50%; barite/celesite/ strontianite, 3%; bastnasite, 12%; and silica, 8%.

The bastnasite ore body at Mountain Pass extends 750 m along a NW-SE strike, and dips 40 SW with an average thickness of 60 m. The deposit contains over 30 million metric tons proven and probable ore based on a 5% cut-off. The average rare earth content is 8.9% REO (Wilson 1991).

In the United States, rare earth-bearing apatites occur at several locations (Altschuler et al. 1967, Hedrick 1986), including the iron ores of Mineville, New York, California (placers), and Florida. The rare earth-containing apatite at Mineville occurs associated with magnetite ore in metamorphosed sedimentary and igneous rocks. The rare earth content of the apatite averages 11.1% REO (range 3–35%). It also contains thorium (average 0.15%, range 0.01–0.33%) and uranium (average 0.032%, range 0.015–0.2%) (McKeown and Klamic 1959). In the same way that RE^{3+} is substituted, the Ca^{2+} in the apatite crystal lattice can also be proxied by Th^{4+} and U^{4+}. The rare earths in the apatite include all elements except Pm and Tb. The contents of Ce, La, Nd, and Y are especially higher.

The sedimentary phosphate rocks of Florida contain about 0.024% Y_2O_3 and in total 0.05% total rare earths (Weterings and Janssen 1985). These rocks also contain uranium and vanadium. Phosphorite samples from the large phosphoria formation of Idaho, Montana, Utah, and Wyoming average 0.16% rare earths (~0.06% La, Nd etc., and 0.1% Y) (Aplan 1988).

In the United States a deposit occurs near Mescalero, New Mexico, that contains not only yttrium, but also zirconium in a silicate mineral called eudialyte (Kilbourn 1990). The lanthanide elements are contained in complex mineralizations, such as in the eudialyte, in many of the hard rock resources identified in the United States and elsewhere in the world.

2.6.23 Former USSR

Phosphate rocks of magmatic origin occurring at the Kola Peninsula of the former Soviet Union hold a considerable amount of yttrium and other rare earths. The yttrium content of Kola apatite averages 0.04% Y_2O_3 in the total rare earth content averaging 1% REO. Rare earth-bearing apatite deposits also occur at Vishnevye Mountains, and the rare earth content is more than 1% REO. Uraniferous phosphates containing rare earths occur at Schevchenko in Kazakhsthan. The reserves, however, are limited. A fluorocarbonate rich in yttric rare earths, yttrosynchisite, occurs in Kutessiak deposit, but reserves are limited. Deposits of rare earths are also found in Dnieprodzerzhinsk in the Ukraine, but the nature of this deposit is not known.

Large deposits of the mineral loparite occur in Russia's Kola Peninsula adjacent to Finland. Loparite ores are rich in light rare earths, and the rare earth content is 32–34% REO. In addition, loparite contains 39 to 40% TiO_2, 8–10% $(Nb, Ta)_2O_5$, 4–5% CaO, and 8–9% Nb_2O_3. Loparite supplies the bulk of the CIS demand for the rare earth (Kosynkin et al. 1993).

2.6.24 Venezuela

Usable deposits of rare earths and niobium have been reported at Cerro Impacto (Hedrick 1985a), 190 km southwest of Cindad Bolivar, Bolivar state. Intense weathering, as a result of the country's tropical climate, has leached the original carbonatite source rock to result in thick lateritic beds enriched in rare earths and other elements. Rare earth contents range from 0.1 to 11%.

2.6.25 Vietnam

In Vietnam, the most important rare earth deposit occurs at Nam Nam Xe situated at the northwestern part of the country (Tirnh 1991). The Nam Nam Xe rare earth deposit belongs to the hydrothermal–metasomatic type. The deposit occurs as a series of barite–barito-celestite rare earth carbonate veins. These veins vary in thickness from a few centimeters up to about four meters. They are 200 to 1000 meters long. The rare earth content varies from 1.2 to 36.2% with an average of 9–13%. In addition to rare earths, the deposit contains significant amounts of minerals such as baritocelestite and barite.

There are more than 35 minerals in the Nam Nam Xe deposit. The main minerals are bastnasite, parisite, synchisite, baritocelestite, barite, and the secondary minerals are calcite, ankerite, monazite, ortite, siderite, pyrite, galena, apatite, fluorite, phlogopite, limonite, magnetite, chlorite, and monmorrillonite. All the minerals are closely intergrown.

The ore is reported to be easy to process for recovery of rare earth, strontium, and barium; however, no actual mining and processing for rare earth appears to have been carried out.

2.6.26 Zaire

Monazite is found in several tin and gold deposits in the Kivu region (Hedrick 1985a), Zaire. Reserves of monazite in the Obaye mining sector occur in two separate deposits. The

Kabengelwa deposit contains about 2000 metric tons of monazite (equivalent to about 600 metric tons of REO) in ore grading 2.8 kg of heavy mineral sands per cubic meter. The Mashabuto deposit reportedly contains 45 metric tons of monazite (equivalent to 25 metric tons of REO) in ore grading 3 kgs of heavy minerals per cubic meter.

2.7 BY-PRODUCTS AND CO-PRODUCTS

In spite of the large identified world resources of rare earths, their production and supply have been strongly influenced by the nature of rare earths mineralization. Commercial mine production of rare earths is feasible in most of the cases only as a co-product or by-product of some other mineral value. The reason for this is that the concentration of rare earths in its reserves is so low that the extraction of rare earths alone is not economical since the current market value of the rare earths cannot support entirely the mining and production costs involved in such an operation.

When rare earth is extracted as a co-product, the market value of the main product supports the cost of extraction of the rare earth, and the recovery of rare earths in turn makes the recovery of the main product economically more attractive. There is a sharing of mining and production costs between a co-product and a main product, the latter carrying a major share of the overall cost burden. When rare earths are recovered as a by-product, the situation is the same as that of its recovery as a co-product except that the recovery and sale of by-product rare earths is not a necessary condition for making the recovery and the sale of the main product economically viable.

The recovery of rare earths as the primary product has been carried out from the Mountain Pass, CA, bastnasite deposit. In fact the Mountain Pass mine is the only active mine in the western world operated exclusively for the recovery of rare earths as no commercial co-products or by-products are reclaimed (Wilson 1991). There is a possibility of recovering rare earth as the main product in at least three deposits in Australia: Mt. Weld, Yangibana, and John Galt (Taylor 1991).

Historically, the only country where monazite recovery has been the purpose of mining beach sand deposits is Brazil. The principal attraction is the thorium content of monazite. In fact, all over the world monazite was formerly mined solely for its thorium content (3–9%). Since 1920, however, the rare earth content of the ore has been of greater importance. From placer deposits of heavy mineral sands, rare earth has been invariably recovered as a by-product of ilmenite production in most of the cases, and as a by-product of cassiterite mining in southeast Asia, and in some cases as a by-product of placer gold (Aplan 1988).

Rare earths have been recovered as a by-product of uranium extraction at Denison Mines, Elliot Lake in Canada. Much of the world's rare earth production comes from its recovery as a by-product of iron ore mining at Bayan Obo, China. In the former Soviet Union, the supply of rare earth bearing mineral loparite is associated with the large titanium recovery operations in the Kola Peninsula. A large potential exists for the recovery of rare earths from apatite as a by-product of phosphoric acid production from various locations in the world. Rare earths can be by-products if perovskites are ever processed for titanium recovery. True to its status as a by-product, the recovery of rare earths has not been a constant feature of the main product recovery in most of the cases, resulting in rare earth rich tailings being accumulated for possible future recovery. These tailings may in the future be processed for rare earth recovery, which would then assume the status of a pseudo main product.

The extraction of rare earths from anatase concentrates in Brazil has been cited as an example of possible new by-product sources of rare earths. Another example is the possibility of by-product rare earths production from the Olympic Dam copper–uranium–gold mine in South Australia.

The recovery of rare earths as a co-product could be carried out in the processing of two of the Australian resources. The ore minerals of the Brockman deposit are very fine grained and not amenable to physical beneficiation to obtain concentration of any of the valuable minerals. Processing would therefore involve fine milling and chemical dissolution and separation by solvent extraction. There is the possibility therefore of recovery of values like ceramic grade alumina and zirconia with the production of yttrium and rare earths as co-products. The Toongi deposit in New South Wales is another suitable project for recovery of rare earths as co-product along with zirconia, tantalum, and niobium.

2.8 WORLD RARE EARTH PRODUCTION AND AVAILABILITY

The status of world rare earth deposits and production from these are shown in Table 2.12 (Jackson and Christiansen 1993). Commercial production of rare earths began in the 1880s with the mining in Sweden and Norway of the rare earth thorium phosphate mineral monazite. This was to provide material for the production of the incandescent lamp mantle invented by Welsback in 1884. Initially the oxides of zirconium, lanthanum and ytterbium were used. Later, improvements in the mantle required oxides of thorium and cerium for the mantle with small amounts of neodymium and praseodymium for marking an indelible brand name label in the mantle (Hedrick 2000).

The published data on world rare earth production over the past 100 years are plotted in Figure 2.3. The picture during the thirty years (1965–1995) when world rare earth production was derived from many countries is given in Figure 2.4. Global rare earth production over the fifty year period, 1950 to 2000, showing the dominance of different type of resources, appears in Figure 2.5. The most recent ten year mine production details appear in Table 2.13. Regular commercial mining of rare earth reserves began approximately 100 years ago (Parker and Baroch 1971). India and Brazil were the principal sources of world rare earth supply, with the United States occasionally contributing, until the late 1940s, when Australia and Malaysia also started regular production. Much of the world rare earth supply between 1950 and 1985 came from the United States, which was the leading producer, and from Australia, which was the second. By 1985, however, China rose to second place, and by 1988 it overtook the United States to become the world's leading producer. China, the United States, the former Soviet Union, Australia, India, Brazil, and Malaysia have all been major rare earth producing countries with South Africa, Canada, Thailand, Sri Lanka, Madagascar, and Zaire contributing occasional or smaller amounts to world rare earth production (Jackson and Christiansen 1993, Hedrick 1995, Hedrick 1997).

Monazite was the major rare earth resource from the beginning of the industry until 1965. Thereafter bastnasite production equaled or exceeded monazite production. At present, bastnasite is the world's major source of rare earths. It constituted 62% of world output of rare earth minerals in 1989 and the proportion rose to very high levels starting in 1994–1995 (Hedrick 1995, Hedrick 1997). Incidentally, no bastnasite was produced before the 1950s.

Table 2.12 Present status of world rare earth deposits

Location	Year of discovery (Year of first production)	Mining method	Commodities	Production, kt Annual [year] (Cumulative)	Resources, kt [year]	Status
Argentina						
Rio Tercero (Cardoba)	1957 (Not producing)	None	Monazite	None (None)	Ore: 31700; Monazite: 5.48	No current production plans
Australia						
Agnes Waters (Rocky Point) (Queensland)	1956 (Not producing)	None	Ilmenite, rutile, zircon	None (None)	Ore: 217,800	Estimate of resources is proprietary
Alice Springs (Northern Territory)	1987 (Not producing)	None	Allanite	None (None)	Ore:1,000 Allanite: 40	Remote location may preclude development
Australind (Western Australia)	Unknown (Not producing)	None	Ilmenite, rutile, zircon, leucoxene, monazite	None (None)	Ore: 6,000 HM: 901 Ilmenite: 662 Rutile: 3,6 Zircon: 61 Leucoxene: 50 Monazite: 1.8	Mining to be by surface sluice
Bowen (Abbot Point) (Queensland)	Unknown (Not producing)	None	Ilmenite, rutile, zircon, monazite	None (None)	Proprietary	This is a prospect
Brockman (Western Australia)	1973 (Not producing)	None	Columbite, pyrochlore, cerianite, bastnasite, xenotime, cassiterite	None (None)	Ore: 9,290 REO: 20	Undergoing feasibility study
Busselton East (Western Australia)	Unknown (Not producing)	None	Ilmenite, rutile, zircon, leucoxene, monazite	Proprietary	Proprietary	Potential reserve
Byfield (Queensland)	1956 (Not producing)	None	Ilmenite, rutile, zircon, monazite	None (None)	Ore: 2,400,000 HM: 27360 Monazite: 14	Awaiting feasibility study
Capel South (Western Australia)	1954 (1956)	Dredge	Ilmenite, zircon, leucoxene, monazite, xenotime	Monazite conc: 0,5		

Table 2.12 (continued)

Location	Year of discovery (Year of first production)	Mining method	Commodities	Production, kt Annual [year] (Cumulative)	Resources, kt [year]	Status
Cataby (Western Australia)	1976 (Not producing)	None	Ilmenite, rutile, zircon, monazite		Ore: 8,974 HM: 700 Ilmenite:490 Rutile: 49 Zircon: 84 Monazite: 10.5	Mining would be by open pit
Cooljarloo/Jurien Bay (Western Australia)	1971 (1975)	Dredge	Ilmenite, rutile, zircon, leucoxene, monazite	Ore: 12,000 Monazite concentrate: 2.5 [1988] (Unknown)	Ore: 589,980 Monazite: 55.3 [1990]	Cooljarloo is operating; Jurien Bay is on standby
Cooloola (Queensland)	1948 (1956)	Not producing	Ilmenite, rutile, zircon, monazite	Ore: 23,760 Ilmenite: 170 Rutile: 42 Zircon: 32 Monazite: 0.7 [in 1975] (Unknown)	Proprietary	Mining ceased in 1975; area is now a national park
Eneabba (Western Australia)	1968 (1974)	Dredge, Open pit	Ilmenite, rutile, zircon, monazite	Monazite concentrate: 8.9 [in 1987] (Monazite concentrate: 35.4, during 1984–1987)	Proprietary	
Frazer Island (Queensland)	1948 (1971)	Dredge	Ilmenite, rutile, zircon, monazite	Ore: 14,400 Ilmenite: 223 Rutile: 35 Zircon: 40 Monazite: 1 [in 1976] (Unknown)	Proprietary	Mining ceased in 1976; area is now a national park

Table 2.12 (continued)

Location	Year of discovery (Year of first production)	Mining method	Commodities	Production, kt Annual [year] (Cumulative)	Resources, kt [year]	Status
Gingin South (Western Australia)	Unknown (None)	Not producing	Ilmenite, rutile, zircon, leucoxene, monazite	None (None)	Ore: 29,200 HM: 2,931 Ilmenite: 1,434 Rutile: 156 Zircon: 147 Leucoxene: 210 [as of 1982]	Monazite content is not reported
Hamel (Waroona) (Western Australia)	Unknown (1989)	Open pit	Ilmenite, rutile, zircon	Proprietary (Unknown)	Proprietary	Monazite content is low and is not recovered
Higgins (Western Australia)	Unknown (None)	Not producing	Ilmenite, rutile, zircon	Proprietary (None)	Proprietary	Future open pit will replace Hamel
Jangardup (Western Australia)	1986 (None)	Not producing	Ilmenite, rutile, zircon, leucoxene, monazite, xenotime	HM concentrate: 270 [in 1990] (None)	Ore: 30,000 HM: 2,040 Ilmenite: 1,679 Rutile: 51 Zircon: 171 Leucoxene: 61 Monazite: 14 [as of 1990]	Potential reserve
Mary Kathleen (Queensland)	Unknown (Unknown)	Undergro und	Uraninite, REO	None (Unknown)	Ore: 6,800 REO: 272 [1990]	Underground uranium mine closed in 1963; rare earths could be recovered from tails
Minninup, beach dunes (Western Australia)	1973 (1986)	Not producing	Ilmenite, leucoxene, zircon, monazite, xenotime	Included in Waroona figures (Unknown)	Proprietary	Production and plant was to shift to Busselton East
Moreton Island (Queensland)	1950s (1957)	Not producing	Ilmenite, leucoxene, zircon	None (Unknown)	Proprietary	Closed by government

Table 2.12 (continued)

Location	Year of discovery (Year of first production)	Mining method	Commodities	Production, kt Annual [year] (Cumulative)	Resources, kt [year]	Status
Mount Weld (Western Australia)	1948 (None)	Not producing	Apatite, pyrochlore	None (None)	Ore: 6,300 REO: 1,085 [R2E, 1990]	Could commence at 20,000–50,000 t/y of ore
Munmorah (New South Wales)	1950 (1969)	Not producing	Ilmenite, rutile, zircon, monazite	None (None)	Ore: 71,200 Monazite: 4.3 [R2E, 1990]	Closed by government in 1977
Nobiac, Southeast (New South Wales)	Unknown (None)	Not producing	Ilmenite, rutile, zircon, monazite	None (None)	Ore: 2,000 HM: 27 Rutile: 8 Zircon: 13 Monazite: 0,1 [1990]	
Newrybar (New South Wales)	1935 (1990)	Dredge	Ilmenite, rutile, zircon	Ore: 3500 Rutile: 12 Zircon: 10 [1990] (None)	Ore: 22,000 HM: 242 [1990]	
North Capel (Western Australia)	Unknown (Unknown)	None	Ilmenite, zircon, leucoxene, monazite, xenotime	None (None)	Proprietary	Property closed in 1987, resumed operation in 1990
North Stradbroke Island (Queensland)	1947 (1949)	Dredge	Ilmenite, rutile, zircon, monazite	Ore: 46,093 [1989] Monazite concentrate: 400 [1988] (Ore: 195,750 [1966–1981] Monazite concentrate: 2.3 [1975–1987])	Proprietary	Consolidated Rutile Ltd., purchased Associated Minerals Consolidated leases in 1985

Table 2.12 (continued)

Location	Year of discovery (Year of first production)	Mining method	Commodities	Production, kt Annual [year] (Cumulative)	Resources, kt [year]	Status
Olympic Dam (South Australia)	1975 (1988)	Under-ground	Chalcocite, bornite, chalcopyrite, uraninite, bastnasite, fluorite	Ore: 1,500 Cu: 45 U_3O_8: 1.5 [1988] (Unknown)	Ore: 450,000 Cu: 11,250 U_3O_8: 360 REO: 1,478 [1988]	REO in uranium is not recovered
Port Pirie (South Australia)	Not applicable (None)	Not producing	Davidite	None (None)	Ore: 200 [1989]	Plans to reprocess uranium tails
Stockton Bight (New South Wales)	Unknown (1985)	Dredge	Ilmenite, rutile, zircon, monazite	Proprietary (Unknown)	Proprietary	HM concentrate goes to Hawk's Nest plant
Tomago (New South Wales)	1965 (1978)	Dredge	Ilmenite, rutile, zircon, monazite	Proprietary (Unknown)	Proprietary	
Viney Cree (New South Wales)	Unknown (1986)	Dredge	Ilmenite, rutile, zircon	Proprietary (Unknown)	Proprietary	HM concentrate goes to Hawk's Nest plant
Waroona, North and South (Western Australia)	1970 (1984)	Open pit	Ilmenite, leucoxene, zircon, monazite, xenotime	Ore: 590 Monazite: 0,235 [1988] (Unknown)	Proprietary	South operation replaced North one in 1988
WIM-150 (Victoria)	1987 (None)	Not producing	Ilmenite, leucoxene, zircon, monazite, xenotime	None (None)	Ore: 2,474,707 HM: 129,204 Monazite: 3,407 [1990]	Studies and tests are underway but scaled down in 1992
Wonnerup Beach (Western Australia)	Unknown (1959)	Open pit	Ilmenite, zircon, monazite	Proprietary (Unknown)	Proprietary	Beach resources depleted, mining dunes
Yangibana (Western Australia)	Unknown (None)	Not producing	Monazite	None (None)	Ore: 3,500 Monazite:108 [1989]	Feasibility study concluding
Yoganup Extended (Western Australia)	1954 (1972)	Not producing	Ilmenite, zircon, leucoxene, monazite	Monazite: 1.7 [1986]; 1.75 [1987]; 1.8 [1988] (Unknown)	Proprietary	HM concentrate goes to North Capel plant

Table 2.12 (continued)

Location	Year of discovery (Year of first production)	Mining method	Commodities	Production, kt Annual [year] (Cumulative)	Resources, kt [year]	Status
Brazil						
Alcobaca (Southern Bahia)	1970s (None)	Not producing	Ilmenite, rutile, zircon, monazite	None (None)	Monazite: 3.44 [1987]	
Anchieta (Espirito Santo)	1900s (Unknown)	Not producing	Ilmenite, rutile, zircon, monazite	None (Ore: 271 Monazite: 2.3 [1982–1987]	Ore: 57 Monazite: 0.407 [1987]	Probably mined out already
Aracruz (Espirito Santo)	1970 [None]	Not producing	Ilmenite, rutile, zircon, monazite	None (None)	Ore: 282 Monazite: 2.964 [1987]	No production planned yet
Buena (Rio de Janeiro)	1960s (Unknown)	Open pit	Ilmenite, rutile, zircon, monazite	Monazite: 3.8 [1987] (Unknown)	Monazite: 0.3	Probably mined out already
Camaratuba (Rio Grande do Norte)	1970s (Unknown)	Open pit	Ilmenite, rutile, zircon, monazite	Ore: 3,160 [1981] (Unknown)	Ore: 44,724 Monazite: 246 [1987] Ore: 490,000 R2E [1981]	
Careacu (Minas Gerais)	Unknown (None)	Not producing	Monazite	None (None)	Monazite: 2.5 [1987]	
Cordislandia (Minas Gerais)	Unknown (None)	Not producing	Monazite	None (None)	Monazite: 8.2 [1987]	
Guarapari (Espirito Santo)	Unknown (None)	Not producing	Monazite	None (None)	Monazite: 0.95 [1987]	
Northeast Dunes	Unknown (None)	Not producing	Ilmenite, rutile, zircon, monazite	None (None)	Ore: 145,000 Ilmenite: 1,700 Rutile: 59 Zircon: 398 Monazite: 48 [1990]	

Table 2.12 (continued)

Location	Year of discovery (Year of first production)	Mining method	Commodities	Production, kt Annual [year] (Cumulative)	Resources, kt [year]	Status
Pocos de Caldas (Minas Gerais)	Unknown (None)	Not producing	Bastnasite	None (None)	Bastnasite: 1,500 REO: 50 [1990]	Average REO content of 3.33 percent in bastnasite
Prado (Bahia)	Unknown (None)	Not producing	Monazite	None (None)	Monazite: 4.6 [1987]	
Sao Gancalo do Sapucai (Minas Gerais)	Unknown (None)	Not producing	Ilmenite, zircon, gold, monazite, garnet	None (None)	Ore: 75,600 Ilmenite: 630 Zircon: 115 Garnet: 33 Gold: 1.4 Monazite: 50 [1990]	Potential reserve
Sao Sebastio de Bela Vista (Minas Gerais)	Unknown (None)	Not producing	Monazite	None (None)	Monazite: 4.1 [1987]	
Serra (Espirito Santo)	1960 (None)	Not producing	Ilmenite, rutile, zircon, monazite	None (None)	Ore: 436 Monazite: 3.5 [1982]	Potential open pit
Tapira (Minas Gerais)	1966 (1983)	Open pit	Anatase, apatite, perovskite, columbite	Ore: 2,000 Anatase concentrate: 200 REO: 1.0 [1988]	Ore: 150,000 TiO_2: 33,000 REO: 45 [1988]	REO occurs in overburden of operating phosphate mine
Burundi						
Karonge	1940s (1948)	Not producing	Bastnasite	None (Ore: 141, bastnasite concentrate: 2.8) [1967–1987]	Ore: 2.2 Bastnasite: 1.9 REO: 1.2 [1983] Ore: 3.2 R2E [1983]	Mineable ore is 60,000 t at 3% bastnasite

Table 2.12 (continued)

Location	Year of discovery (Year of first production)	Mining method	Commodities	Production, kt Annual [year] (Cumulative)	Resources, kt [year]	Status
Kasagwe	Unknown (None)	Not producing	Bastnasite	None (None)	Ore: 67 Bastnasite: 2 REO: 1 [1990]	
Canada						
Elliot Lake (Denison) (Ontario)	1953 (1957)	Under-ground	Uraninite, brannerite, monazite	Ore: 4,766 [1983] (Ore: 37,212 U3O8: 44 [1957–1981] REO: 101 [1974–1976])	Ore: 105,681 REO: 10.8 [1989] Ore: 223,800 R2E [1983]	REO was produced sporadically
Elliot Lake (Rio Algom, except Stanleigh) (Ontario)	1953 (1956)	Under-ground	Uraninite, brannerite, monazite	Ore: 3,272 [1983] (Ore: 24,793 [1967–1981]	Ore: 68,197 REO: 5 [1989] Ore: 149,200 R2E [1983]	Closed in 1990
Elliot Lake (Rio Algom, Stanleigh) (Ontario)	Unknown (Unknown)	Under-ground	Uraninite, brannerite, monazite	Ore: 1,559 [1983] (Unknown)	Ore: 48,877 REO: 4.3 [1989] Ore: 59,700 R2E [1983]	Potential for 152 t/yr REO
Strange Lake (Newfoundland/Quebec)	1980 (None)	Not producing	Zircon, monazite,allanite, gadolinite, pyrochlore, fluorite	None (None)	Ore: 52,000 R1S [1981]	Could be started as a beryllium project
Thor Lake (Northwest Territories)	1979 (None)	Not producing	Xenotime, monazite, gadolinite, allanite, columbite, zircon	None (None)	Ore: 510 REO: 2.3 R1M [1987]	Essentially a Nb_2O_5-Ta_2O_5 project

Table 2.12 (continued)

Location	Year of discovery (Year of first production)	Mining method	Commodities	Production, kt Annual [year] (Cumulative)	Resources, kt [year]	Status
China						
Bayan Obo (Inner Mongolia)	1951 (1957)	Open pit	Hematite, magnetite, monazite, bastnasite, martite	Fe_2O_3 ore: 7,000 REO: 15 [1990] (Unknown)	Fe_2O_3 ore: 1,500,000 REO ore: 800,000 REO: 48,000 Nb: 1,000 [1990]	The largest known RE deposit
Beihai (Guangxi)	Unknown (1966)	Open pit	Ilmenite, rutile, zircon, monazite	Ore: 3,385 HM: 33 Ilmenite: 30 Zircon: 0,4 Monazite: 0,07 [1982] (Unknown)	Ore: 529,920 [1989]	HM recovered from sands manually
Guangdong (Guangdong)	1950s (1960s)	Open pit	Ilmenite, rutile, zircon, monazite	Ore: 6,085 Ilmenite: 15 Zircon: 0,6 Monazite: 0,075 [1982] (Unknown)	Ore: 385,320 [1989]	Covers five separate mines and plants
Xun Jiang (Guangxi)	1975 (None)	Not producing	Ilmenite, rutile, zircon, monazite	None (None)	Ore: 66,700 [1982]	–
Egypt						
Nile Delta — Rosetta	1920s (1965)	Open pit	Ilmenite, rutile, zircon, monazite, magnetite	None (Ilmenite: 29 Magnetite: 10 Zircon: 2 [1965–1968])	Ore: 44,393 Monazite: 222 [1989]	Also worked in 1929
Gabon						
Mabounie	Unknown (None)	Not producing	Fluocerite	None (None)	Unknown	2.52% REO

Table 2.12 (continued)

Location	Year of discovery (Year of first production)	Mining method	Commodities	Production, kt Annual [year] (Cumulative)	Resources, kt [year]	Status
Greenland						
Ilimaussaq	Unknown (None)	Not producing	Pyrochlore, eudialyte	None (None)	Ore: 30,000 ZrO_2: 330 Y_2O_3: 270 [1990]	One of three reported properties
India						
Chavara (IREL) (Kerala)	1920s (1932)	Open pit	Ilmenite, rutile, zircon, leucoxene, sillimanite, monazite	Ore: 219 Ilmenite: 135 Rutile: 6 Zircon: 3 Sillimanite: 5 Monazite: 0,8 [1982] (Ore: 1,245 Ilmenite: 813 Rutile: 31 [1960–1980])	Ore: 118,029 Monazite: 189 REO: 101 [1989]	Sands mined manually
Chavara (KMML) (Kerala)	1920s (1932)	Open pit	Ilmenite, rutile, zircon, leucoxene, sillimanite, monazite	Ore: 1,152 Ilmenite: 100 Rutile: 10 Zircon: 6 Leucoxene: 1,4 Monazite: 0,5 [1989] (Ore: 567 Ilmenite: 232 Rutile: 22 [1966–1980])	Ore: 114,752 Monazite: 184 REO: 101 [1989]	Sands mined manually

Table 2.12 (continued)

Location	Year of discovery (Year of first production)	Mining method	Commodities	Production, kt Annual [year] (Cumulative)	Resources, kt [year]	Status
Manavalakurichi (Tamil Nadu)	1900s (1911)	Open pit	Ilmenite, rutile, zircon, leucoxene, sillimanite, monazite, garnet	Ore: 285 Monazite concentrate: 3.8 [1982] (Ore: 1,933 [1966–1981])	Ore: 103,656 Monazite: 2,591 REO: 1,425 [1989]	Sands mined manually
Chatrapur (Orissa)	1958 (1983)	Open pit	Ilmenite, rutile, zircon, monazite	Ore: 2,280 [1989] (Unknown)	Ore: 224,397 Monazite: 1,418 REO: 780 [1989] Ore: 350,000 R2E, [1982]	
Ranchi and Purulia (Bihar)	1956 (None)	Not producing	Ilmenite, rutile, zircon, monazite, sillimanite, magnetite	None (None)	Ore: 86,480 Ilmenite: 330 Rutile: 64 Zircon: 146 Sillimanite: 379 Magnetite: 147 Monazite: 272 [1989]	Inland alluvium
Kenya						
Rangwa/Ruri/Homa	1940s (None)	Not producing	Bastnasite, Monazite, barite, fluorite	None (None)	Ore: 375 Monazite: 24 REO: 13 [1989] Ore: 3,750 R2E, [1982]	Potential open pit

Table 2.12 (continued)

Location	Year of discovery (Year of first production)	Mining method	Commodities	Production, kt Annual [year] (Cumulative)	Resources, kt [year]	Status
Malawi						
Kangankunde	1907 (None)	Not producing	Staurolite, monazite	None (None)	Ore: 11,000 Monazite: 550 Staurolite: 1,430 [1983] Ore: 22,000 R2E, [1983]	Monazite is low in thorium
Mauritania						
Bou Naga	Unknown (1968)	Open pit	Monazite	None (Ore: 1,4 [1968–70])	Ore: 100 Monazite: 8 REO: 4,4 [1970]	Operations limited to six months per year
Mozambique						
Congolone	Unknown (1992)	Open pit	Ilmenite, rutile, zircon, monazite	Ore: 17,558 Ilmenite: 422 Rutile: 8 Zircon: 38 Monazite: 1 [1990] (None)	Ore: 166,800 Ilmenite: 4,190 Rutile: 90 Zircon: 373 Monazite: 11 [1990]	Potential reserve
Namibia						
Etaneno	Unknown (None)	Not producing	Monazite	None (None)	REO: 20,000 [1989]	
New Zealand						
Barrytown (South Island)	1960s (None)	Not producing	Ilmenite, rutile, zircon, magnetite, cassiterite, gold, monazite	None (None)	Ore: 73,300 Monazite: 0.7 REO: 0.4 [1989]	Pilot plant study stage

Table 2.12 (continued)

Location	Year of discovery (Year of first production)	Mining method	Commodities	Production, kt Annual [year] (Cumulative)	Resources, kt [year]	Status
Westport (South Island)	Unknown (None)	Not producing	Ilmenite, rutile, zircon, gold, monazite	None (None)	Ore: 850,200 R2E, [1989]	Undergoing feasibility study
South Africa						
Buffalo Fluorspar (Transvaal)	1943 (1948)	Open pit	Fluorite, monazite, apatite	Ore: 1,800 Fluorite: 177 [1989] (Ore: 12,120 [1972–1980]	Ore: 50,000 CaF_2: 6,500 Monazite: 500 [1989]	Monazite is not reclaimed
Phalaborwa (Transvaal)	1912 (1932)	Open pit	Bornite, chalcopyrite, vermiculite, apatite, apatite, zircon, uraninite	Ore: 29,231 Cu concentrate: 294 U_3O_8: 87 zircon: 13 [1988] (Ore: 528,382 [1964–1988])	Ore: 123,840 Apatite: 1,858 REO: 130 [1989]	REO is not reclaimed
Richards Bay (Natal)	1967 (1977)	Dredge	Ilmenite, rutile, zircon, leucoxene, monazite, magnetite	Ore: 20,000 Ilmenite: 1,750 Zircon: 200 Monazite: >1 [1988] (Unknown)	Ore: 4,980,000 Monazite: 1,145 REO: 1.3 [1989]	Mines having three dredges and wet plants

Table 2.12 (continued)

Location	Year of discovery (Year of first production)	Mining method	Commodities	Production, kt Annual [year] (Cumulative)	Resources, kt [year]	Status
Sri Lanka						
Pulmoddai	1920s (1961)	Open pit	Ilmenite, rutile, zircon, monazite,	Ore: 220 Ilmenite: 150 Rutile: 13 Zircon: 13 Monazite: 0.7 [1990] (Ore: 1,963 Ilmenite: 1,141 Rutile: 87 Zircon: 24 Monazite: 0,7 [1966–1982])	Ore: 1,593 Monazite: 2.4 REO: 1.3 [1989] Ore: 55,967 HM: 7,141 R2E, [1982]	HM replenished by annual monsoons
United States						
Aiken County (South Carolina)	1950s (1955)	Open pit	Ilmenite, rutile, zircon, monazite	None (None)	Ore: 19,000 Monazite: 7.8 REO: 4.9 [1983]	Closed in 1958
Bald Mountain (Wyoming)	1951 (None)	Not producing	Ilmenite, zircon, monazite, magnetite	None (None)	Ore: 18,144 Monazite: 23 REO: 14 [1983]	Potential open pit
Bear Lodge (Wyoming)	Unknown (None)	Not producing	Monazite, xenotime, thorite	None (None)	Ore: 726,000 REO: 9,480 [1978]	Potential open pit; high thorium

Table 2.12 (continued)

Location	Year of discovery (Year of first production)	Mining method	Commodities	Production, kt Annual [year] (Cumulative)	Resources, kt [year]	Status
Bear Valley (Idaho)	1950 (1955)	Dredge	Ilmenite, magnetite, monazite, garnet, xenotime	None (None)	Ore: 109,900 Monazite: 17 REO: 11 [1982] Ore: 1,232,150 Monazite: 64 REO: 40 R2E [1982]	Mining ceased in 1959
Big Creek (Idaho)	1940's (1950)	Dredge	Ilmenite, magnetite, zircon, monazite, garnet	None (None)	Ore: 116,100 Ilmenite: 341 Magnetite: 5 Zircon: 16 Garnet: 39 Monazite: 47 [1982]	Date of shut down unknown
Blackfoot Bridge (Idaho)	Unknown (None)	Not producing	Collophane, monazite	None (None)	Ore: 5,900 P_2O_5: 1,534 Monazite: 9.4 [1984]	Mining to start in 2023 at close of Caldwell Canyon
Brunswick-Altamaha (Georgia)	1959 (None)	Not producing	Ilmenite, rutile, zircon, monazite	None (None)	Ore: 65,850 Ilmenite: 1,087 Rutile: 75 Zircon: 213 Monazite: 19 [1982]	Mining would be by dredge
Caldwell Canyon (Idaho)	Unknown (None)	Not producing	Collophane, monazite	None (None)	Ore: 11,000 P_2O_5: 2,574 Monazite: 17 [1984]	Mining to start in 2035 at close of Trail Creek

Table 2.12 (continued)

Location	Year of discovery (Year of first production)	Mining method	Commodities	Production, kt Annual [year] (Cumulative)	Resources, kt [year]	Status
Champ (Idaho)	Unknown (1982)	Open pit	Collophane, monazite	None (Ore: 2,716 [1982–1986])	Unknown	Mining ceased in 1986
Conda (Idaho)	1906 (1920)	Open pit	Collophane, monazite	None (Ore: 17,583 [1922–1982])	Unknown	Mining ceased in 1984
Cumberland Island (Georgia)	1940s (None)	Not producing	Ilmenite, rutile, zircon, leucoxene, monazite	None (None)	Ore: 241,000 Monazite: 43 REO: 27 [1982]	Partially in a national park
Diamond Creek (Idaho)	Unknown (None)	Not producing	Monazite, xenotime, thorite	None (None)	Ore: 235 Monazite: 4.6 REO: 2.9 [1978]	Would be an underground mine
Gallinas Mountains (New Mexico)	About 1885 (1943)	Open pit, under-ground	Fluorite, galena, malachite, bastnasite	None (Bastnasite concentrate: 0,06 [1954–1955])	Ore: 46 CaF_2: 28 REO: 1.4 [1983] Ore: 18 R2E, [1983]	Fluorite mine closed in 1956
Gay and South Forty (Idaho)	Unknown (1946)	Open pit	Collophane, monazite	Ore: 1,800 [1984] (Ore: 35,959 [1946–1982])	Ore: 18,000 P_2O_5: 4,590 Monazite: 18 [1989]	Not known
Gold Fork — Little Valley (Idaho)	1880s (1880s)	Dredge	Ilmenite, magnetite, zircon, gold, monazite, garnet	None (None)	Ore: 296,317 Monazite: 46 REO: 29 [1981]	Originally a gold placer

Table 2.12 (continued)

Location	Year of discovery (Year of first production)	Mining method	Commodities	Production, kt Annual [year] (Cumulative)	Resources, kt [year]	Status
Green Cove Springs (Florida)	1950s (1972)	Dredge	Ilmenite, rutile, zircon, leucoxene, monazite	Ore: 9,405 Ilmenite: 135 Rutile: 48 zircon: 57 Leucoxene: 8 Monazite: 1 [1989] (Ore: 19,842 [1986–1988])	Ore: 110,079 Monazite: 8 REO: 5 [1989]	The only placer REO producer in the United States
Hall Mountain Group (Idaho)	1930s (1930s)	Open pit, under-ground	Thorite, magnetite, gold, zircon, apatite, allanite, monazite	None (None)	Ore: 71 [1983]	Mining ceased in 1940s
Henry (Idaho)	Unknown (1969)	Open pit	Collophane, monazite	None (Ore: 13,322 [1969–1985])	Ore: 847 P_2O_5: 231 Monazite: 1.6 [1989]	Mining halted in 1990
Hicks Dome (Illinois)	1954 (None)	Not producing	Thorite, xenotime, fluorite, apatite, sulfides, bastnasite	None (None)	Ore: 14,700 REO: 62 [1978] Ore: 658,000 R2E [1978]	No production plans
Hilton Head Island (South Carolina)	1954 (None)	Not producing	Ilmenite, rutile, zircon, monazite	None (None)	Ore: 759,300 Ilmenite: 2,020 Rutile: 911 Zircon: 524 Monazite: 61 [1983]	Mining unlikely; active resort community

Table 2.12 (continued)

Location	Year of discovery (Year of first production)	Mining method	Commodities	Production, kt Annual [year] (Cumulative)	Resources, kt [year]	Status
Husky (Idaho)	Unknown (1993)	Open pit	Collophane, monazite	None (None)	Ore: 23,000 P_2O_5: 5,750 Monazite: 37 [1987]	Start in 1993 at 1,358,000 t/y
Iron Hill (Colorado)	1880s (None)	Not producing	Rutile, zircon, pyrochlore, apatite, monazite, fluorite	None (None)	Ore: 655,622 REO: 2,603 [1989]	Mainly a Nb_2O_5 property
Lehmi Pass (Idaho)	1949 (None)	Not producing	Monazite, thorite, rutile	None (None)	Ore: 39,009 Monazite: 316 REO: 199 [1989] Ore: 491 R2E [1989]	Would be mined underground for ThO_2
Maxville (Florida)	Unknown (1992)	Dredge	Ilmenite, zircon, staurolite	None (None)	Unknown	Expansion of Green Cove Springs
Maybe Canyon (Idaho)	Unknown (1966)	Open pit	Collophane, monazite	Ore: 910 [1985] (Ore: 21,148 [1966–1984])	Ore: 6,350 P_2O_5: 1,562 Monazite: 10 [1989]	Not known
Mineville Dumps (New York)	1700s (1824)	Open pit	Magnetite, martite, apatite	None (Unknown)	Ore: 15,672 REO: 163 [1983]	Dumps from former iron ore mine
Mountain Fuel (Idaho)	Unknown (1986)	Open pit	Collophane, monazite	Ore: 1,358 [1989] Ore: 4,074 [1986–1989]	Ore: 5,432 P_2O_5: 1,358 Monazite: 9 [1989]	Not known

Table 2.12 (continued)

Location	Year of discovery (Year of first production)	Mining method	Commodities	Production, kt Annual [year] (Cumulative)	Resources, kt [year]	Status
Mountain Pass (California)	1949 (1965)	Open pit	Barite, bastnasite, allanite, monazite	Ore: 308 REO: 24.7 (REO: 293 [1972–1989])	Ore: 28,123 bastnasite: 3,375 REO: 2,503 [1989] Ore: 156,877 R2E [1989]	The major REO producer in the United States
Music Valley (California)	1949 (None)	Not producing	Xenotime, monazite, gold	None (None)	Ore: 50 REO: 4.3 [1983]	Ore is highly radioactive
North Henry (Idaho)	Unknown (1991)	Open pit	Collophane, monazite	None (None)	Ore: 3,200 P_2O_5: 867 REO: 3.8 [1985]	To operate through 1994
North and South Carolina Placers (North and South Carolina)	1880s (1887)		Ilmenite, rutile, zircon, monazite	None (None)	Monazite: 90 REO: 57 [1978]	No plans for production
Oak Grove (Tennessee)	1960s (None)	Not producing	Ilmenite, rutile, zircon, monazite	None (None)	Ore: 174,600 Monazite: 271 REO: 157 [1982]	No plans for production
Pajarito (New Mexico)	1984 (None)	Not producing	Eudialyte	None (None)	None (None)	Ore: 2,400 Zircon: 29 REO: 4 [1989]
Pearsol Creek (Idaho)	1940s (1950)	Dredge	Ilmenite, magnetite zircon, monazite, garnet	None (None)	Ore: 172,471 Ilmenite: 376 Monazite: 32 [1982]	Unknown shutdown date

Table 2.12 (continued)

Location	Year of discovery (Year of first production)	Mining method	Commodities	Production, kt Annual [year] (Cumulative)	Resources, kt [year]	Status
Powderhorn (Colorado)	1980s (None)	Not producing	Perovskite, pyrochlore, apatite	None (None)	Ore: 246,000 REO: 886 [1982]	Potential open pit
Silica mine (Tennessee)	1930s [1942]		Ilmenite, rutile, zircon, leucoxene, monazite	Ore: 1,000 [1982] (Ore: 3,923 [1972–1982]	Ore: 26,700 Monazite: 3.6 REO: 2.1 [1989]	Only sand produced; HM stockpiled
Smoky Canyon (Idaho)	Unknown (1984)	Open pit	Collophane, monazite	Ore: 1,861 [1984] (Ore: 9,895 [1984–1989])	Ore: 35,455 P_2O_5: 9,573 Monazite: 56 [1989]	Production will continue through 2005
Trail Creek (Idaho)	Unknown (None)	Not producing	Collophane, monazite	None (None)	Ore: 27,000 P_2O_5: 6,750 Monazite: 43 [1984]	Production will start in 2005
Wet Mountains (Colorado)	1960s (None)	Not producing	Thorite, xenotime, barite	None (None)	Ore: 13,957 REO: 141 [1989]	No plans for production
Wooley Valley (Idaho)	Unknown (1955)	Open pit	Collophane, monazite	None (Ore: 11,453 [1955–1987])	Unknown	Mining ceased in 1987
Uruguay						
Atlantida	Unknown (None)	Not producing	Monazite	None (None)	Ore contains 3.2% monazite	Meager data

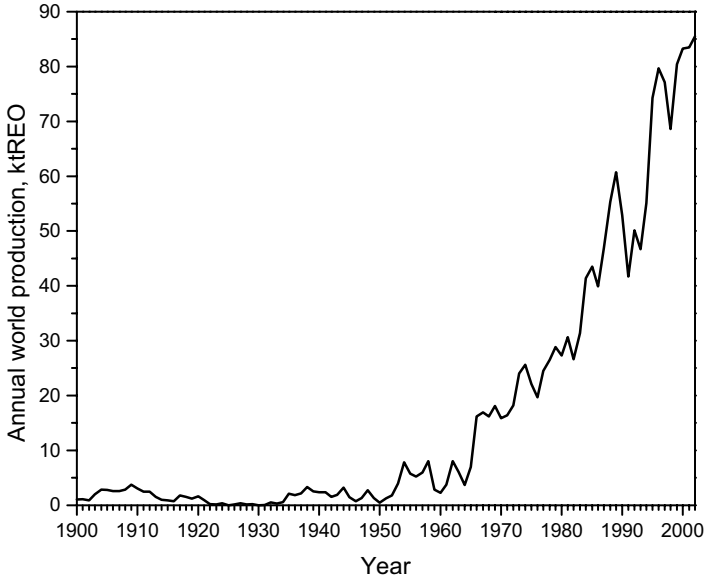

Figure 2.3 World rare earth production: annual total production (1900–2002).

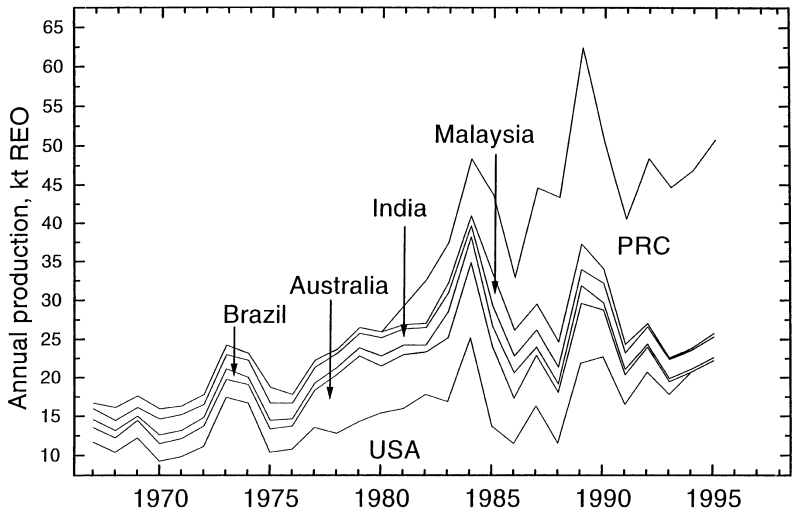

Figure 2.4 World rare earth production: contributions of the U.S., Australia, Brazil, India, Malaysia and China.

Monazite contains typically 50% REO as phosphate and the light lanthanide fraction (La, Ce, Pr, Nd) constitutes more than 90% of the total rare earth content while the other rare earth elements make up 5 to 10%. The rare earth content of bastnasite concentrate is constituted by as much as 99% of light rare earths (La–Nd), almost no heavy rare earths, and very little yttrium. Up to 60% of the rare earth content of xenotime is yttria, and it also has a higher proportion of the other heavy rare earths than monazite. Even though bastnasite

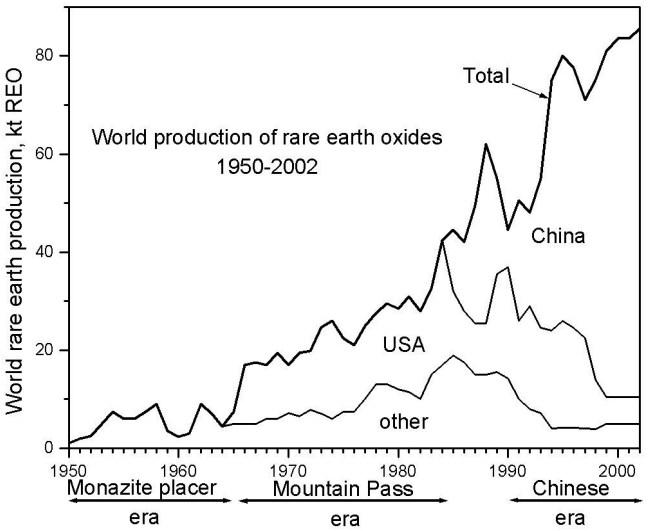

Figure 2.5 World rare earth production: production from 1950 through 2002, in four eras. Transitional era: 1984 to 1991.

and monazite contain predominantly cerium, lanthanum and neodymium (and only trace amounts of yttrium, 0.1% and 2.1% respectively), because these minerals have been processed in much larger quantities as compared to the heavy lanthanide sources, such as xenotime, they remain the principal sources of heavy lanthanides as well. This picture started changing somewhat in the 1980s with the ion adsorption type ores from China also contributing to world rare earth production and becoming the principal source for heavy metals.

Taylor (1991) estimated the world rare earth production in 1989 at 50,000 metric tons of REO with 50% of this total constituted by bastnasite, 40% by monazite, and the balance mainly from the ion adsorbing clay ores found in China. By 2000, the quantity of REO produced from monazite source is less than 5% of the total REO produced from all sources. By 2002 over 80% of all REO produced is from bastnasite, about 10% from ion adsorption ores, 5% from monazite and the remaining from other sources such as xenotime, loparite and brannerite. In the 1990s, however, monazite was a declining source of rare earths with production practically coming to a halt in Australia — the principal monazite producer in the world (Hedrick 1997). The declining importance of monazite as a raw material has been due to growing supplies of bastnasite from China and also due to problems associated with the disposal of the radioactive element thorium contained in monazite. There is similarly a decline in the production of xenotime, as well, from the main producer Malaysia. The decreased supply of traditional minerals enhanced the importance of the "other ores" and their contribution to world production of mid and heavy rare earths.

2.8.1 Brazil

In Brazil, out of 16 rare earth deposits, only 4 are known to be operating at present and 2 of these are making monazite concentrates. The status of the other 12 projects is not known (Jackson and Christiansen 1993). The heavy mineral sand mining in Brazil is conducted

Table 2.13 World mine production of rare earths (metric tons of REO equivalent)

Country	1986	1987	1988	1989	1990	1991	1992	1993	1994	1995	1996	1997	1998	1999	2000	2001	2002
U.S.	11094	16710	11533	21875	22700	16500	20700	17800	20700	22200	20400	100000	5000	5000	5000	5000	5000
Australia	5820	6600	6530	7700	6050	3850	3300	1650	–	–	–	–	–	–	–	–	–
Brazil	3300	1100	1100	2280	911	719	396	400	256	103	–	–	–	–	–	200	200
India	2200	2200	2200	2060	2500	2200	2200	2500	2500	2700	2700	2700	2700	2700	2700	2700	2700
Malaysia	3300	3300	3300	3300	1830	1090	427	224	234	448	340	418	202	625	446	450	450
China	6750	15100	18660	25220	16500	16150	21340	22100	30700	48000	55000	53000	60000	70000	73000	73000	75000
Former USSR			8500	8500	8500	8500	8000	4500	2000	2000	2000	2000	2000	2000	2000	2000	2000

primarily for the thorium content of monazite rather than for ilmenite, rutile, or zircon. This is in contrast to the objectives of placer mining in other countries where monazite is considered only as a by-product with ilmenite the primary product. The rare earth production in Brazil started declining significantly in the 1990s and no significant production was reported from 1996 onwards. Annual production of a modest 200 tons REO has been reported from the year 2001. It is produced in the states of Espirito Santo, Parana, and Rio de Janeiro (Hedrick 1985). Production was also started in the heavy mineral sands deposit at Cumuruxatiba in Bahia state, where monazite along with ilmenite, rutile, and zircon was recovered.

Monazite was first produced in 1885 in Brazil from beach sand deposits. These deposits occurring over a stretch of 200 km on the southeast coast of Brazil were at places so rich in monazite that their exploitation was possible and actually easily performed using primitive technical resources. Such rich deposits were only a small fraction of total rare earth occurrence in Brazil and these were exhausted even before 1950. In 1950, systematic exploitation of sands, which are relatively poorer in monazite and more complex in composition, started.

The new projects underway in Brazil include the dredging operation on the Sapucai River, which would be producing 1600 metric tons per year of monazite, equivalent to 900 metric tons per year of REO, and the phosphate mine at Tapira where the rare earth recovery plant would be producing 253 metric tons per year of REO.

2.8.2 India

Mining of Indian beach sand deposits for recovering monazite values started in 1911. Prior to World War II, much of world rare earth supply was derived from Indian deposits in addition to Brazilian sources.

Out of the five major rare earth mineral bearing placer deposits in India, four are in production and all of these are in coastal areas. The fifth placer, yet unworked, is inland and removed from the necessary infrastructure. Three of the operating projects, Chavara in Kerala, Manavalakurichi in Tamil Nadu, and Chatrapur in Orissa, are owned by the Government of India and another project at Chavara is owned by the Government of Kerala. Almost all of the minerals in the beach sands, ilmenite, rutile, zircon, garnet, sillimanite, leucoxene, magnetite, and monazite, are recovered. Currently, the annual REO production in India is about 3000 metric tons (Hedrick 1997).

2.8.3 United States

Production of rare earths started in the United States in 1887, two years after the beginning of world rare earth production in Brazil, from placer deposits in Burke County, North Carolina (Overstead et al. 1959) and continued until 1910. Since that time the only domestic production of monazite has been from placer deposits in Idaho and Florida. The production was not very significant between 1910 until the time of World War II because during that period the U.S. imported almost all the monazite it processed principally from India and Brazil. Due to the war, both India and Brazil had restricted export of monazite, possibly for preserving the nuclear fuel material thorium for their own future energy requirements and also for building domestic rare earth processing industries (Kleber and Love 1963). This cut-off of major supplies led to exploration in the U.S., and to identification and development of several large deposits. The U.S. emerged as a major

producer of rare earths with the discovery and development of the Mountain Pass bastnasite deposit in 1949. Monazite production also restarted in 1948 with the recovery of monazite as a by-product of mining Florida beach sands for titanium minerals and zircon. Since the early 1950s, monazite production was a part of very large scale operations for the separation of gold and ilmenite. Mining for rutile, garnet, zircon, and other minerals was conducted in the states of California, Colorado, Georgia, Florida, Idaho, and the Carolinas. In recent times, these operations have been mainly confined to Florida and South Carolina.

The U.S. emerged as the major producer of rare earths with the discovery of the Mountain Pass bastnasite deposit in 1949 and its subsequent development. Since that time the Mountain Pass mine has been the major and most important provider of rare earths in the U.S., and until the mid 1980s the only source of commercial bastnasite in the world. The only domestic source of REE for the U.S., the mine at Mountain Pass has operated below capacity and only intermittently over the past several years. This has been caused to a certain extent by local environmental and regulatory problems but to a large extent by global rare earth market factors which pose a threat to the long-term viability of Mountain Pass as a supplier of REE for high technology applications. By 1999 and 2000 nearly all (more than 90%) of separated REE used in the U.S is from Chinese rare earth resources.

Up to the end of 1994, monazite was produced in Florida at Green Cove Springs by RGC (U.S.) Minerals Inc., a subsidiary of the Australian company Renison Goldfields Consolidated Ltd. (RGC) as a by-product of ilmenite production from beach sands. The recovery of monazite ceased at the end of 1994 as world demand for radioactive thorium-bearing rare earth ores decreased, primarily due to increased thorium disposal cost.

The first U.S. source known to have produced commercial quantities of xenotime is the Marion, North Carolina, gold mine (RICI 1990). The mixed heavy minerals sands concentrate produced in the mine contains monazite as its major constituent with lesser amounts of zircon and xenotime. Production started in 1989; however, no current production is indicated (Hedrick 1997).

An increase in rare earth production by new sources is linked to the development of the eudialyte deposit at Pajarito in New Mexico and production of monazite from the placer deposit at Maxville in Florida. Apatite rich tailings of the iron ore at Mineville, New York, can be developed into a large source of yttrium and other rare earths (Sabot and Maestro 1995).

2.8.4 Australia

Australia has been the primary producer of monazite in the world. Regular monazite production started in the country in the late 1940s. Since 1967 Australian beach sand deposit was the major source of supply and until the late 1980s Australia continued to dominate, contributing nearly 37% of world monazite output. Australia has been the fourth largest producer of rare earths in the world after China, the United States, and the former Soviet Union (Hedrick 1997).

Monazite was recovered in Australia in various localities as a by-product of beach sand mining for ilmenite, rutile, and zircon. In 1983, the proportion of by-product monazite production in Australia was 16,963 tonnes per million tonnes of ilmenite. In 1988, only 7373 tonnes of monazite was produced per million tonnes of ilmenite. Over the same period the annual monazite production in Australia decreased from 15,000 to 12,000 tonnes (Taylor 1991).

In the 1990s, however, there was a decline in the Australian monazite production. Eneabba mineral sands deposit was the principal source of monazite in Australia. In 1991 it was described as a declining source by Taylor (1991), who, however, stated that the development of additional mineral sands reserves in the adjacent Eneabba west deposit could sustain the Eneabba production level in the immediate future. A major reason for the decrease in monazite production leading to near zero production from 1994 onwards was the decreased world demand for thorium-bearing rare earth concentrate.

At Eneabba potential exists for the recovery of substantial quantities of xenotime from existing mineral sands operations (Taylor 1991). Actual production, however, has been very little because of limited industrial requirements of unprocessed xenotime.

Notwithstanding the current status of no rare earth production, Australia remains one of the world's major sources of rare earth elements from its heavy mineral sands and rare earth laterite deposits. A briefing on this is given in Section 2.9 on rare earth production potential.

2.8.5 China

Mining has been going on in several rare earth deposits in China. Currently, Chinese rare earth supply comes from the Bayan Obo deposit of iron rare earth ore, bastnasite-bearing carbonatite comes from Mianning in Sichuan Province and Weishan in Shangdong Province, ion adsorption type clays are mined in the south China provinces of Jiangxi, Guangdong, Hunan, and Fujian. Placer monazite and xenotime deposits at Guangdong and Hunan provinces are also probably operational (Hedrick 1997). Amongst all these, the Bayan Obo deposit contributes to the major chunk of Chinese rare earth production and also supports the frequent large increases in the country's rare earth production levels.

Mining of the Bayan Obo deposit began in 1957 even though no rare earth production was reported from China prior to 1980. In the 1980s, China emerged as the major producer of rare earths. Chinese mine production capacity was about 6000 metric tons REO in 1982 and rose phenomenally to over 20,000 metric tons REO in 1985. Actual rare earth production itself increased fourfold between 1983 and 1989, from 6000 metric tons REO to 25,220 metric tons REO. Significant new production from 1987 onward was realized from the ion adsorption type REO deposits of southern China.

Rare earth production in China remained relatively low during 1990–1992 but started increasing, beginning in 1994. In 1994 production was 30,650 metric tons REO, which was 39% more than the 1993 level of 22,100 metric tons REO. The production was mainly from the Bayan Obo mine. There was another sharp increase in rare earth production between 1994 and 1995. In 1995 China was the leading producer of rare earths, producing a record 48,000 metric tons REO, an increase by about 57% of the previous level. In 1995 production of rare earths at Baotou was 26,905 metric tons REO, while Sichuan Province and Shangdong Province produced 8500 metric tons REO and 963 metric tons REO, respectively. The production of rare earths from ion adsorption type clays in southern China's provinces of Jiangxi, Guangalong, Hunan, and Fujian was 9770 metric tons REO (Hedrick 1997).

The significant annual increased levels continued through 1996 to 2002, with only a slight decrease from the previous year's level in 1997. Production picked up in 1998 crossing 60000 t REO, and the production of rare earth concentrates in China was 70,000 t REO in 1999. By 2000 rare earth content of the iron ore mined at Bayan Obo ranged from 40,000 to 50,000 t/yr REO, and it usually accounts for the bulk of the frequent increase in

the production level as well. Annual levels in 2000 and 2001 were 73000 t REO and the figure for 2002 is 75000 t REO. Regional production in 1997 was as follows: Baotou, Inner Mongolia Autonomous Region 35000 t REO; Shangdong Province 1200 t REO; Sichuan Province, 11000 t REO; Monazite concentrate production, all regions, 50 t REO, and ion adsorption clays, all regions, 6000 t (Hedrick 1997).

The Baotou Iron and Steel Company (BISC) is by far the largest and most important rare earth producer in China. The ore dressing plant of BISC splits the ore from Bayan Obo into two usable fractions — one for rare earth extraction and the other for iron smelting. Canadian-based Advanced Material Resources Ltd. (AMR), in a joint venture, produces rare earths from bastnasite-bearing carbonatite at Mianning, Sichuan Province. AMR is also involved in rare earth processing plants at Jiangyin, Jiangsu Province, and Zibo, Shangdong Province. In southern China, the major rare earth producer is the Zhujiang smelter. The raw materials for this plant are xenotime and monazite from Guangdong placer deposits. Monazite is also available from the Xun Wa and Long Nan mines near Nanchung in Kiangsi. Monazite, which is easily available in southern China, is used as the principal raw material in the Yao Lung chemical plant (Zhang et al. 1982). Alluvial placer deposits of monazite in the Hunan Province are processed by the Taojiang smelter. Ion adsorption type deposits are processed by the Jiangxi Rare Earth Company, Nanchang Rare Earth and the Ganjia Rare Earth Company. Ion adsorption ore of the Xunwu mine is processed by the Jiangnan Rare Earth material.

There are many placer and ion adsorption clay deposits in China which could be mined. The Bayan Obo mine accounts for 95% of REO reserves in China with the ion adsorption ores and other types representing 3% and 2%, respectively. While the Bayan Obo mine is essentially a producer of light rare earths, the ion adsorption ores are basically producers of both light and heavy rare earths. This factor can have a bearing on the production starting on these new projects.

2.8.6 Former Soviet Union

The former Soviet Union is a major producer of rare earths and ranks fourth in the world in terms of annual rare earth output, after China, United States and India. Annual production that used to be in the range of over 8000 t REO until the early 1990s decreased to the 2000 t REO per year level by 1994 and has remained so ever since.

The main sources of rare earths in the former Soviet Union are loparite ores, yttrosynchisite, and uraniferous phosphates. Rare earths were first derived from loparite in 1934 and commercial mining of loparite started in 1951 at the Karnasurk mine of the Lovosersk Enrichment Works, Murmansk Oblast. Current production is by the Lovosersk Mining and Benefication Complex near Revda, Murmansk Oblast, Russia. (Hedrick et al. 1997). Loparite mined from the Kola Peninsula is treated at the Irtysh Chemical Metallurgical Plant in east Kazakhstan Oblast in Kazakhstan and the Sillamjee Chemical Metallurgical United Works in Estonia. Uraniferous phosphates are mined at Schevchenko in Kazakhstan, but decrease in demand for uranium will lead to reduced supply from this source. The yttrosynchisite ores come from the Kutessiak deposit and are treated at the Kirgiz works. The other rare earth sources in the country are apatite and monazite. In the former Soviet Union a considerable quantity of monazite occurs, possibly at Samotkanskii and probably is produced but no production data are available. The status of apatite is similar. The recovery of rare earths from apatite of the Kola Peninsula is likely to gain importance as these ores are a potential source of yttrium and europium.

Apart from the six major rare earth-producing countries mentioned above, world rare earth production is contributed to by South Africa, Canada, Malaysia, Thailand, Sri Lanka, Zaire, and Madagascar (Jackson and Christiansen 1993, Hedrick 1997).

2.8.7 South Africa

A unique vein deposit was discovered in 1950 at Van Rhynsdorp in the Republic of South Africa. This remained a major source of monazite for the decade 1953–1963. A certain amount of rare earths has also been recovered from the Witwatersrand uranium deposit in South Africa (Highley et al. 1988). At present, in South Africa, there are three important major mines for REO ore minerals. At Buffalo fluorspar monazite occurs associated with fluorite and apatite, at the Phalaborwa complex apatite is rare earth bearing, and Richards Bay placer deposit contains monazite. Although all three mines are operating, monazite is not recovered at Buffalo fluorspar. Rare earths are not extracted from the apatite at Phalaborwa and only Richards Bay is recovering a monazite by-product. Richards Bay is a major beach dredging operation producing zircon. The annual rare earth production in South Africa in 1994 was a modest 400 metric tons of REO (Hedrick 1995).

2.8.8 Canada

In Canada rare earth has been produced as a by-product of uranium mining at Elliott Lake. A rare earth recovery plant had been in operation intermittently between 1967 and 1978 and, after modernization, has been in operation since 1986 at the Denison Mines, Elliott Lake, Ontario, for the recovery of yttrium and heavy rare earths from uranium leach solutions (Hedrick 1985). In 1988 nearly 100 metric tons of contained Y_2O_3 was produced from the source (Robjohns 1989). No significant production was reported in the 1990s (Hedrick 1995).

A remote possibility exists for increasing the rare earth production in Canada by development of the Strange Lake deposit. This deposit, developed for its beryllium content, would yield about 4700 metric tons per year of REO as a by-product (Jackson and Christiansen 1993).

2.8.9 Malaysia

Malaysia has been a rare earth producer from the late 1940s. Monazite and more particularly xenotime have been obtained as by-products of placer cassiterite mining. Placer cassiterite deposits at Perak have been worked by Beh minerals/Mitsubishi Chemical Industries Ltd. for monazite and xenotime production. Deposits at Perak and at Selangor, west Malaysia, have been mined to produce monazite and xenotime. The annual mine production of monazite and xenotime during the best of times in Malaysia is given in Table 2.13. Annual production of rare earths in Malaysia, which was only 187 metric tons REO in 1983, increased to 2563 metric tons REO in 1984 and to 3300 metric tons REO in 1985. Production remained steady until 1989, decreased to 1830 metric tons REO in 1990, 1090 in 1991, 427 in 1992, and down to 224 metric tons REO in 1993. The declining production was to culminate in the closure of the Asian Rare Earth Sdn. Btd. Plant in Ipoh, Perak State, in the face of overwhelming competition from China (Mining Journal 1994).

2.8.10 Thailand

In Thailand monazite and xenotime are recovered as by-products from alluvial tin mining and offshore tin dredging. Approximately 80–90% of the country's production of tin concentrates is from the Thai Peninsula (Pungrassami and Sanguansai 1991). From 1971 to 1989 the total production of monazite and xenotime in Thailand was 6400 metric tons, and 655 metric tons respectively. Almost 99% of this production was from the Thai Peninsula. Monazite is produced mainly from deposits of Changwat Phuket, Phangnga, Ranong, Surat Thani, Chumphon and Prachuap Khirikhan. Xenotime is produced mainly from deposits at Changwat Phuket, Phangnga, Ranong Trang, and Prachuap Khirikhan.

Annual production was less than 100 metric tons REO in 1983 but was about 150 metric tons REO during 1984 to 1986, and it increased to a steady 800 metric tons REO between 1987 and 1989. Production decreased to about 230 metric tons REO beginning in 1990 (Hedrick 1997).

2.8.11 Sri Lanka

In Sri Lanka there is one placer deposit of heavy minerals in Pulmoddai, and this is an operating monazite property that produces monazite concentrate. Monazite is recovered as a by-product during the processing and recovery of ilmenite, rutile, and zircon from this deposit.

Production has been going on for many years at a modest level of about 110 metric tons of REO per annum. Production was approximately three times this quantity in 1989. Production could be stepped up to 500 metric tons REO per year (Jackson and Christiansen 1993).

2.8.12 Zaire and Madagascar

Zaire and Madagascar are the two countries reporting rare earth production in small quantities. Monazite is produced in Zaire, and both monazite and bastnasite are produced in Madagascar (Jackson and Christiansen 1993).

In addition to the countries mentioned above, rare earth minerals are probably produced in Indonesia, North Korea, Mozambique, and Vietnam even though the regularity and extents are unknown.

The Congolone beach placer in Mozambique was considered a monazite deposit that could begin production immediately (Jackson and Christiansen 1993).

2.9 RARE EARTH PRODUCTION POTENTIAL

Actual world rare earth production is much less than the world production potential. For example, for 1989 (the latest year for which such data are available) potential REO production was 1,38,096 metric tons if the currently operating mines had all produced REO instead of discarding or stockpiling it. Actual world rare earth production in 1989 was only 66,990 metric tons REO (Jackson and Christiansen 1993). Even in 1994, the actual world mine production was 56,800 metric tons REO.

The principal potential rare earth producers are those placer operations where the objective is to recover titanium minerals and discard the other minerals. Recovery of rare earth oxides was not carried out in hard rock operations either. For example, the Olympic Dam underground mine in Australia could potentially produce about 5000 metric tons per year REO as a by-product of uranium recovery but has no plans to do this. Similarly, Canadian underground uranium mines have the potential for producing 610 metric tons per year of REO but actually produce only about 150 metric tons per year. About 41,000 metric tons per year of REO could be obtained from the Buffalo fluorspar mine and Phalaborwa copper–apatite mines in South Africa. In the United States about 7000 metric tons per year of REO could be recovered from the operating open pit phosphate mines, if the producers considered it economical.

In addition to considering the potential of the specific resources mentioned above, if the overall potential of all important resources is considered, the country having the greatest potential for REO production is South Africa. As compared to an actual annual production of about 400 metric tons REO, South Africa could produce about 41,300 metric tons per year. This would be an increase of approximately 100 times its present production. The U.S. has the potential to produce about 32,800 metric tons REO per year, which is more than 50% over the average annual production in the best of times. China could undoubtedly produce more REO than is reported, for example, by successfully treating Bayan Obo steel slag. Australia could produce about 11,500 metric tons REO per year, representing a more than 50% increase over the average annual production in better times, if Olympic Dam and some other placer operators introduced rare earth mineral recovery plants. In Brazil also, the rare earth output could be easily raised by a factor of five, and in India output could go up by nearly 100%. This status with respect to important rare earth producers is given in Figure 2.6 (Jackson and Christiansen 1993). Another aspect to be considered when dealing with potential and actual production is the deposit type. Of the actual 1989 world rare earth production, 41% came from placer sands and 59% from hard rock deposits. If the other operating mines that have potential for rare earth production are included, the relevant values become 27% of total production from placer sands and 73% from hard rock deposits. In other words, actual rare earth production from placer deposits could be raised by over 40% and the production from hard rock deposits could be increased by nearly 170%.

On the one hand the actual world rare earth production can be raised far beyond the current levels by fully realizing in practice the potential of each deposit currently worked. On the other hand, the exploitation of new deposits for actual production can be a more attractive alternative for increasing the tonnage of REO produced.

Worldwide there are many new projects that could start rare earth production within a few years. The highest number of such projects is in Australia.

Many placer and hard rock projects are pending in Australia (Taylor 1991). One of them is the WIM-150, an inland dredging property. The development of the WIM-150 deposit poses a number of technical challenges relating to the separation of fine grain minerals. The projected mining rate of 20 million metric tons per year of this deposit could result in the production of 12,000 metric tons per year of monazite and potentially up to 3000 metric tons per year of xenotime. The size of this resource is sufficient to support an operation on this scale for more than 30 years (Taylor 1991).

The WIM deposit is potentially a major source of rare earth minerals; however, these minerals can be recovered only as by-products from the production of titanium minerals and zircon from this deposit.

The Olympic Dam multimetal deposit in South Australia for the production of copper,

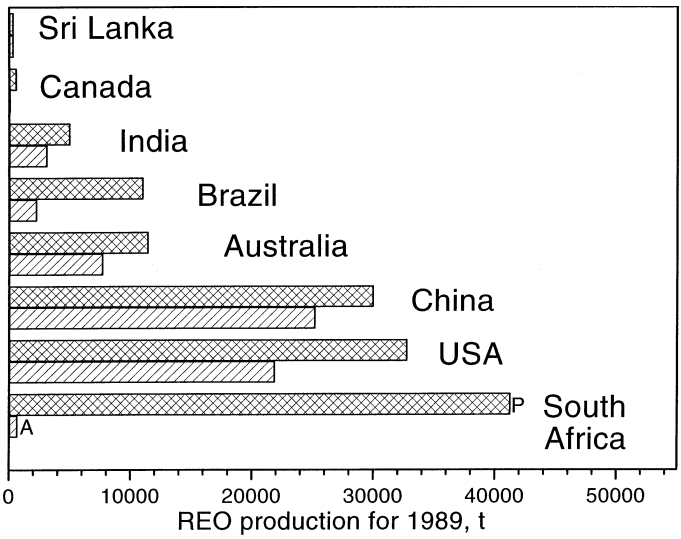

Figure 2.6 Potential (P) and actual (A) rare earth production of important rare earth producing countries.

uranium, and gold is a major resource with a potential operating life of more than 100 years. At the best average scale of operation, the quantity of rare earths mined in the ore may be of the order of 10,000 metric tons per year of REO content. The advantage of this situation is that the rare earths are already being mined and the major economic minerals will support a long-term operation. Besides, the environmental problems of processing rare earth ores are circumvented in this operation because it already involves disposal of radioactive wastes. The key factor, however, is the development of technology to economically extract the rare earths from the existing process streams.

Mining and processing of the Brockman Australia deposit would lead to co-production of high purity alumina, zirconia, yttria/rare earth concentrate, niobium, and tantalum pentoxide. Although xenotime mineral has not been found, the distribution of yttrium and the rare earth oxides in the deposit is similar to the distribution found in xenotime. The minerals in this deposit are very fine grained, and it is not possible to produce a physical concentrate of any of the valuable minerals. All the minerals have to be first obtained in solution and then processed for separation. The feasibility of obtaining the ore in the solution has been demonstrated in a pilot plant. A mining rate of 300,000 metric tons per year has been considered for the deposit. At this rate, the production of REO concentrate would be 450 metric tons per year which includes 275 metric tons per year of yttrium oxide. The resource is sufficient to support this level of production for over 100 years.

The Brockman deposit is a large potential source of yttrium and the other rare earth oxides. Current development of the source is hindered by remote location and high processing costs.

Other candidates for development are the Mount Weld rare earth deposit in Western Australia, with a grade of 26% REO and yttrium, the deposit at Yangibana with a grade of 1.7%, the allanite deposit at Alice Springs at 0.8% REO, and the placer deposit at Cataby, which has a potential for 4000 metric tons per year of monazite (Jackson and Christiansen 1993).

In addition there are a few dedicated resources in Australia which could be developed. These include tailings from the processing of Radium Hill uranium ore at Port Pirie, South Australia, tailings from old uranium extraction operations at Mary Kathleen, Queensland, and a carbonatite deposit at Cummins Range in Western Australia.

Australia has been a major producer of the rare earth raw materials monazite and xenotime. New mineral sands projects in Vidoria and Western Australia can support increased future production of these minerals. In addition there are a number of other potential sources of rare earths, some of them large and/or with attractively high europium and yttrium contents.

2.10 FORECAST

Published forecasts for rare earth production expect a growing demand and a continuously rising market for rare earths. The world consumption of rare earths was estimated at 45,000 metric tons REO in 1990, rising to 80,000 by the year 2000. Growing by 4 to 9 tons per year (tpy) the world demand is set to exceed the milestone of 100,000 tpy REO for the first time by 2004. With these anticipated consumption rates, there should be no difficulty in ensuring the supply of rare earths. In some of the working deposits, the reserves are sufficient for many years and adjacent resources will extend their operating periods. Those projects that could recover REO, but do not, could easily install rare earth circuits in their existing beneficiation plants. Several world class rare earth deposits, especially in Australia and China, have yet to be developed as world demand is currently satisfied by existing production, which itself is much less than the existing production potential. Considering that new deposits will continue to be located, world resources should be adequate to fulfill the demand for the foreseeable future.

The estimated long-term rare earth availability is presented in Figure 2.7. In relation to the cumulative world production until the year 2002 (1,721,000 metric tons REO), world rare earth reserves (93 million metric tons of contained REO) appear to be very substantial. Since this is the picture when only R1E resources are taken into account, the inclusion of other R1 resources and R2 resources will make natural availability of rare earths adequate to fulfill the world demand easily through the twenty-first century.

Even though in terms of total REO content the world rare earth reserves amount to an impressive figure of about 93 million metric tons, the amount of individual rare earths theoretically recoverable from this vast reserve varies greatly.

The rare earth element distribution in bastnasite and monazite qualitatively reflect the relative abundance of rare earths in nature. This is illustrated in Figure 2.8. The proportion of heavier rare earths (Sm–Lu, Y) content in bastnasite is considerably less than in monazite, which itself is less than that anticipated from crustal abundance data. Heavier rare earths are present in higher proportion in xenotime. While the minerals bastnasite and monazite are abundantly available in nature, xenotime occurrence and availability is small in comparison. Hence the rare earth composition in xenotime does not have much impact on overall rare earth availability. Large differences, therefore, are inherent in the availability of different rare earth elements. This status remains practically undisturbed even after the discovery of substantial quantities of ion adsorption type ores that are particularly enriched in middle and heavy rare earths because their extent as compared to bastnasite and monazite is still small.

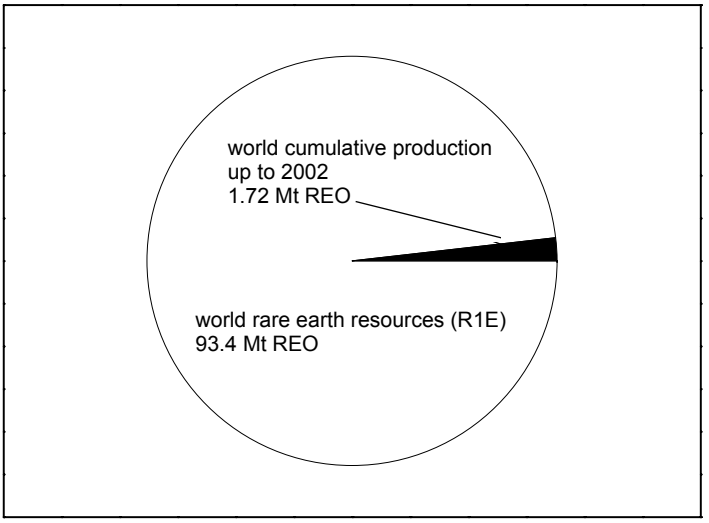

Figure 2.7 Estimated long term availability of rare earths.

Earlier the theoretically recoverable rare earth content from world reserves was estimated at 47.6 million metric tons REO, assuming (Hedrick 1988) one half of the world rare earth reserves are in bastnasite and one-half are in monazite, and these ores could be mined and separated without any mining, milling, and refining losses. More recent estimates (Jackson and Christiansen 1993), however, place world reserves at 93 million metric tons REO, with only 20% in monazite and 80% in bastnasite and certain other minerals. Assuming again that these ores could be mined and separated without any mining, milling, and refining losses, the theoretically recoverable rare earths from world rare earth reserves has been recalculated and given in Figure 2.9. The unequal availability of individual rare earths becomes more strongly highlighted in this estimate because bastnasite is poorer in heavy rare earth content than monazite, and bastnasite is the more predominant mineral in world rare earth resources. Latest estimates (USGS 2003) on world rare earth reserves place it at 88 million tons REO, and this would bring down the values shown in Figure 2.9 by approximately 5%.

Currently there is a trend among rare earth processes to shift away from radioactivity bearing rare earth ores. This trend has led to an adverse impact on monazite-producing mineral sands operations everywhere in the world. However, the favorable aspects of monazite as the rare earth resource, namely higher concentration of heavy rare earths, abundant supply, and recovery as a low cost by-product, will ensure a future long-term demand for monazite. However, the cost and space to dispose of the radioactive waste products will also rise and remain a problem to be tackled as this can result in severely limiting the use of monazite. In fact, several other current rare-earth raw-material resources are also constrained by environmental concerns, including the production of bastnasite in California and ion adsorption clays in Southern China.

Hedrick (1997) predicted that in the foreseeable future the top three rare earth producers, China, the U.S., and Australia, would remain significant rare earth suppliers and stated that the economic restructuring of Eastern Europe and Asia indicated a large potential for both new sources as well as new consumers.

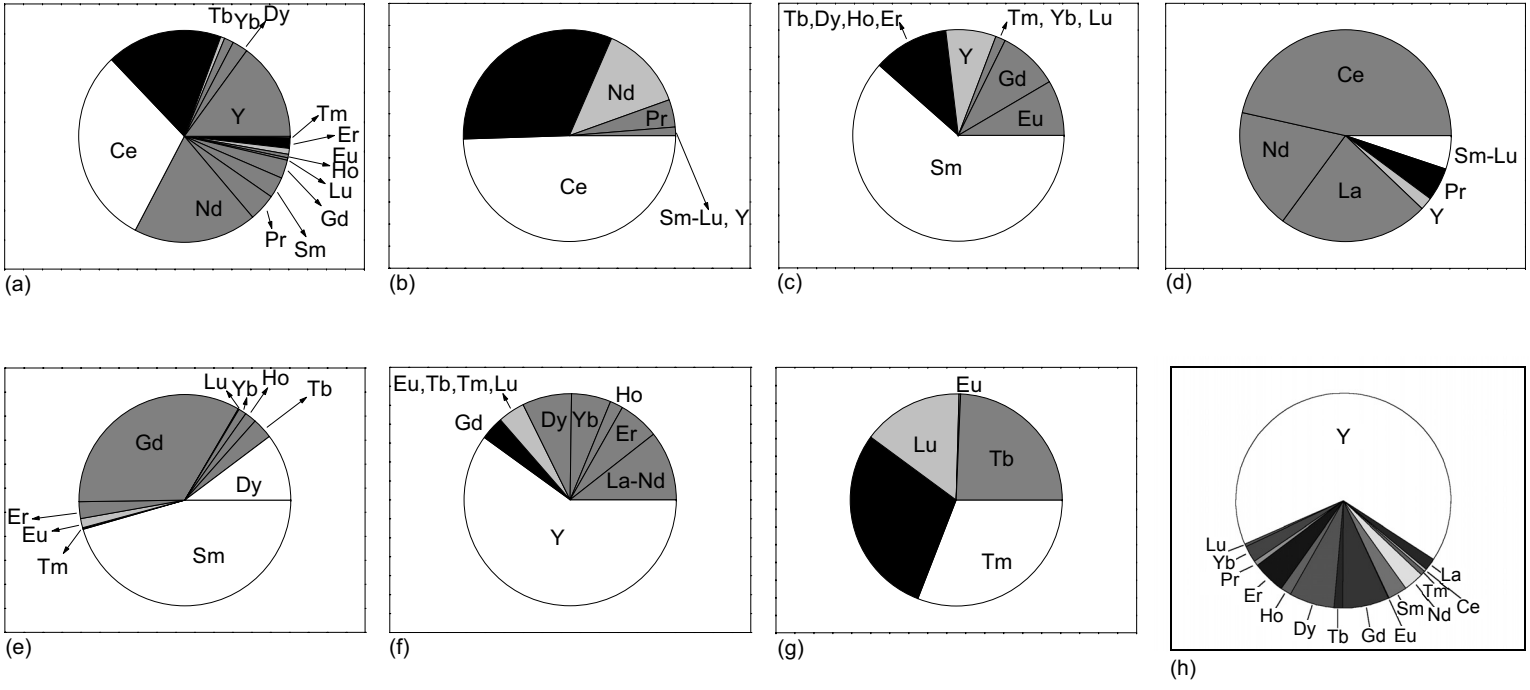

Figure 2.8 Relative contents of individual rare earths in major minerals:
(a) crustal abundance; (b) bastnasite; (c) Sm–Lu in bastnasite; (d) monazite; (e) Sm–Lu in monazite; (f) xenotime; (g) Sm–Lu in xenotime; (h) ion adsorption ore (rare earth laterite, Longnan, China).

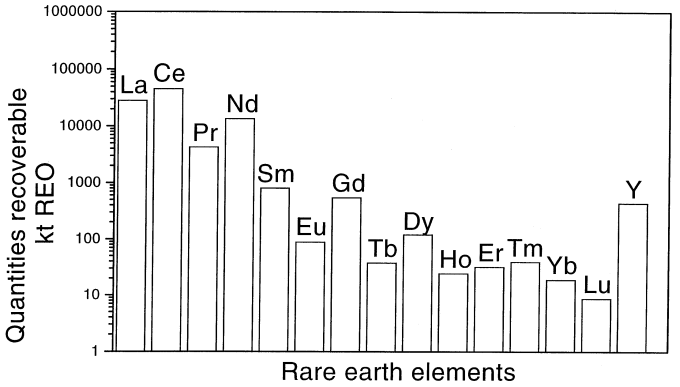

Figure 2.9 Theoretically recoverable rare earth contents from world reserves.

2.11 SUMMARY

All rare earths except promethium occur in nature. The rare earths are a relatively abundant group of metallic elements in the earth's crust, occurring in over 200 minerals. As a rule, any rare earth mineral usually contains all the rare earths, some of them enriched and some in very low concentrations. Although the minerals are numerous, about 95% of all world rare earth resources occur in just three minerals: bastansite, monazite, and xenotime. A dozen other minerals also have been or could be used as rare earth resources.

Rare earth deposits contain one or more rare earth minerals. They are broadly divided into hard rock deposits and placer sands. Bastnasite is found only in hard rock deposits, whereas monazite and xenotime occur in both hard rock and placer deposits. Deposits that have been traditionally considered as reserves correspond approximately to the "R1E resources" in the United Nations Resource Classification System.

World reserves (R1E resources) of rare earths have been estimated at 93.4 million metric tons REO in place, of which 93% occur in hard rock (primary) deposits and 7% occur in placer (secondary) deposits. These resources occur as follows: 20% in monazite and 80% in bastnasite and other minerals. Geographically, 52% of world REO resources are located in China, 22% in Namibia, 15% in the United States, 5% in Australia, 3% in India, and the remainder in several other countries. According to latest estimates, world rare earth reserves are 88 million tons.

There are as many as 40 rare earth deposits in the United States. The most important is Mountain Pass bastnasite deposit, which has over 3 million metric tons of REO and the distinction of being the only rare earth deposit in the world worked exclusively for the recovery of rare earths. Numerous other deposits of present and future relevance are in the United States. These include placer monazite deposits in the states of Florida, South Carolina, and Alaska, and deposits of other rare earth minerals such as euxenite, eudialyte, apatite, and other phosphorites, and perovskites.

There are 35 rare earth deposits in Australia, 28 are placers and 7 hard rock. Heavy mineral sand placer deposits containing monazite are widely distributed along the east and west Australian coasts. Major deposits at and near Eneabba have been the most important. The most promising and large reserves of monazite and xenotime are the WIM-150 deposit

and four other deposits in Murray Basin. Other major deposits include the Olympic Dam multimetal deposit, the Brockman deposit, the Toongi deposit, and for recovery of rare earths as a main product, the deposits at Mt. Weld, Yangibana, and John Galt.

Brazil has many placer deposits along the Atlantic coast and the only inland placer at Sao Goncalo de Sapucai on the Sapucai River. Monazite is the mineral in all these deposits. One of the two hard rock deposits occur at Tapira, an existing apatite mine where rare earths occur in anatase overburden, and the other hard rock bastnasite deposit occurs at Pocos de Caldas.

Many rare earth deposits, hard rock and placers, occur in India. The hard rock deposits, however, have been completely overshadowed by the extensive placer deposits of monazite-containing heavy minerals in the southwestern and eastern coasts.

In Canada there are large rare earth deposits that together contain more than 1 million metric tons REO. They include rare earth occurring in uranium ores at Elliot Lake, Ontario, a gadolinite deposit at Strange Lake, Quebec and a columbite–gadolinite deposit at Thor Lake, Northwest Territories.

China has numerous rare earth deposits, some of them unusual and some of them among the world's largest. The world's largest known rare earth deposit, containing 48 million metric tons REO, occurs at Bayan Obo. It is a iron–rare earth–niobium resource. Bastnasite and monazite account for about 70% and 30%, respectively, in the rare earth fraction. Monazite and xenotime placers occur at Guangdong, Guangxi, Hunan, Hubei, and Hainan Provinces in south China. The unusual ion adsorption type ore occurs at Jiangxi, Guangdong, Fujian, Hunan, Guangxi, and southern Anhui Provinces. Bastnasite also occurs in Sichuan and Shangdong. The rare earth deposits of China are great in quantity, and taken together are relatively better balanced as regards light, middle, and heavy rare earths content.

South Africa has more than 1 million metric tons of REO in its deposits, which include placer monazite at Richards Bay, rare earth bearing apatite at Phalaborwa complex, and monazite co-occurring with apatite and fluorite at Buffalo fluorspar.

In the former Soviet Union large deposits of the rare earth mineral loparite and rare earth bearing phosphate rocks of magmatic origin occur in the Kola Peninsula.

Heavy mineral sands containing monazite and, most importantly, xenotime, occur in the placer cassiterite deposits in the southeast Asia tin belt in Malaysia, Thailand, and Indonesia.

An enormous hard rock carbonatite deposit containing bastnasite occurs at Etaneno in Namibia. This deposit, containing an estimated 20 million metric tons REO, is second in size only to the Bayan Obo deposit in China. Besides this and the deposits at South Africa, rare earth resources are found in Africa at Malawi (hard rock monazite, Kangankunde), Mozambique (placer monazite, Congolone), Burundi (hard rock bastnasite, Karonge and Kasagwe), Kenya (hard rock monazite, Rangwa/Ruri/Homa), Egypt (placer monazite, Nile Delta–Rosetta), Mauritania (hard rock monazite, Bou Naga), and Gaban (hard rock florencite, Mabounie).

Rare earth deposits also occur in Argentina (placer monazite, Rio Tercero (Colorado)), Greenland (hard rock pyrochlore and eudialyte, Ilimaussaq), New Zealand (placer monazite, Barrytown and Westport in South Island), Sri Lanka (placer monazite, Pulmoddai), Uruguay (placer monazite, Atlantida), Bangladesh (placer monazite, Cox Bazzar coastal area), Germany (placer monazite, Cuxhaven), Indonesia (placer monazite, Tin Islands), Japan (hard rock sphene, Kamioka lead–zinc mine), Myanmar (placer monazite, Dawei and Myeik), Taiwan (placer monazite, Southwest coast), Turkey (hard rock bastnasite,

Eskisehir), Venezuela (lateritic beds, Cerro Impacto), Vietnam (hard rock bastnasite, Nam Nam Xe), and Zaire (placer monazite, Kivu region).

In spite of the large identified world resources for rare earths, their production and supply have been affected because, except at Mountain Pass, the rare earth minerals can be produced only as a by-product or co-product of some other mineral value.

Monazite was the principal rare earth source from the beginning of the rare earth industry 100 years ago until 1965. Thereafter production of bastnasite exceeded monazite production. In the 1990s, the status of monazite as a rare earth resource diminished and the production of bastansite and to a certain extent that of other resources such as ion adsorption ores have been increasing.

India and Brazil were the principal sources of world rare earth supply until the late 1940s, when Australia and Malaysia also started regular production. Much of the world rare earth supply during 1950 to 1985 came principally from the United States and secondly from Australia. By 1985 China rose to second place and by 1988 it overtook the United States to become the world's leading producer. Rare earth production in both China and the United States is primarily from bastnasite.

In 2002, world rare earth production was 98,300 metric tons REO. The leading producer was China (88,000 metric tons REO), followed by the United States (5000 metric tons REO), India (2700 t REO), and former USSR (2000 t REO). In 2003, while the world mine production reached 95,000 metric tons REO, no production was reported from U.S. Mountain Pass deposit (Hedrick 2004). China produced 90,000 metric tons REO, with India and Commonwealth of Independent States contributing 2700 and 2000 tons, respectively. In 1995, monazite started losing its importance due to problems associated with thorium disposal (probably only temporarily). While the total world REO production remained practically at the same level, the contributions from two major countries — Australia and Malaysia — declined substantially. This has been made up by enhanced Chinese production.

Actual world rare earth production is much less than the world production potential. If the presently operating mines had all produced REO instead of discarding or stockpiling it, the total world production could be more than double the actual world production. The status as regards individual countries is vastly variable. Further enhancement in rare earth production is possible by exploiting new reserves. Worldwide there are many new projects that could begin rare earth production within a few years.

Forecasts for rare earth production expect a growing demand and a continuously rising market for rare earths. The world rare earth consumption in the year 2000 was 80,000 metric tons REO and is set to exceed 100,000 t REO by the year 2004. There could be no difficulty in ensuring the supply of rare earths to meet such demand. Besides, undiscovered resources are thought to be very large relative to expected demand (Hedrick 2004). In relation to the world cumulative production in the year 2003 (1,816,000 metric tons REO), world rare earth reserves (93,000,000 metric tons REO) were very substantial. While the total REO content is an impressive figure of 93 million metric tons, the amount of individual rare earths theoretically recoverable from this vast reserve varies greatly because only 20% of the total reserves are in monazite and almost 80% are in bastnasite, with minor quantities in other rare earth minerals. Bastnasite is poorer in heavy rare earth content when compared to monazite. The individual rare earth availability is strongly tilted toward the light rare earths.

CHAPTER 3

Resource Processing

3.1 INTRODUCTION

In the extractive flowsheet of a metal, the term "resource processing" usually refers to the group of unit operations, involving both physical and chemical processing, which convert the as-mined ore to a compound that is either an end product by itself or an inter-process intermediate for the subsequent production of the metal or alloy or another compound. The processes, in the majority of the cases, are directed to the removal of impurity compounds from the material being processed. In the case of rare earths, the resource processing involves not only the operations that result in such impurity removal, but also special operations that achieve the difficult task of separating the considerable number of naturally co-occurring rare earth elements from one another.

Rare earth minerals are numerous and even those minerals shortlisted as sources for extraction are more than a dozen in number. However, much of the actual extraction of rare earths is principally from the two minerals monazite and bastnasite. As described in the preceding chapter, all the rare earths generally occur together in all the minerals with large variations in relative proportions. Such occurrence is the culmination of their similar chemical behavior, and it is this chemical similarity that has in the past made separation of rare earths from one another a daunting task.

The nature of the occurrence and distribution of the rare earth minerals has generally ensured that they could be recovered only as by-products or co-products. Therefore, except in one important case, Mountain Pass bastnasite, the physical beneficiation of the rare earth mineral is the same as that used for the main product of the resource. The Mountain Pass bastnasite has a unique process for physical beneficiation.

Chemical beneficiation or chemical processing of the concentrate obtained after physical beneficiation usually involves hydrometallurgical and sometimes pyrometallurgical operations. That the rare earth minerals will undergo chemical beneficiation by hydrometallurgy techniques is guided by the need for applying hydrometallurgical separation processes for isolating rare earths from one another. The chemical properties of rare earths permit their ready dissolution and easy precipitation. Subtle and systematic differences in the basicity of the rare earth elements have been used in developing possibilities for their chemical separation. The sheer number of rare earth elements that occur together ensured that the separation procedures, if feasible, would be laborious. However, the exhibition of

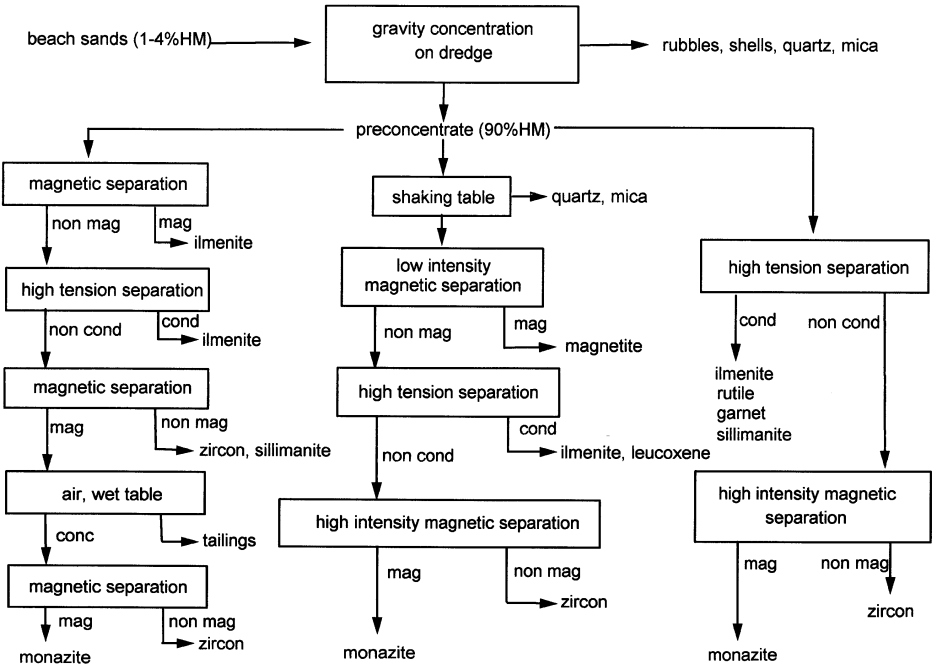

Figure 3.1 Physical beneficiation of beach sand minerals.

stable multivalence in the most abundant and also in one of the least abundant rare earths simplified to some extent the separation procedures. With the development of techniques like ion exchange and solvent extraction it became possible to work upon the inherent differences in rare earths chemical behavior, however small they are, to effect their separation from one another.

This chapter deals with the various aspects of rare earth resource processing. First, a brief description of the mining methods is presented. Then the procedures used for physical beneficiation to obtain the rare earth mineral concentrate and the procedures used to chemically treat the concentrates to a mixed rare earth oxide product are given. Next, the key feature of rare earth extractive metallurgy, separation of the rare earths from one another, is covered. All important processes and those that have been rated as suitable for industrial operation are covered. Essentially, resources processing comprises breaking down the mineral, recovering the rare earth values, and separating the individual rare earths. These operations are preceded by mining and beneficiation to obtain the concentrate for processing.

3.2 MINING

3.2.1 Hard Rock Deposits

Hard rock rare earth deposits are mined by open pit and underground methods (Jackson and Christiansen 1993). At two of the world's largest rare earth mines, Bayan Obo in China and Mountain Pass in the United States, the open pit operations are the standard drill, blast, load,

and haul to the mill procedures. At the Canadian uranium properties where rare earths could be recovered as by-product, underground room and pillar mining have been conducted.

3.2.2 Placer Deposits

Mining of placer sands that are under water or affected by a high water table is conducted by dredges. Shallower sands are mined using bucket wheel units, while bucket line and suction dredges are used for deeper material. Where water is not available, variations of open pit excavation methods, such as scrapers, front-end loaders, shovels, and draglines, are used. Usually drilling and blasting are not required but are useful when the sand is cemented by ferruginous or calcarenous precipitates. In countries where inexpensive, manual labor is available, the labor has been used to fill head-carried baskets or to work hand-operated sluices.

The as-mined ore is subjected to a physical beneficiation process after crushing and milling in the case of hard rock ore, and in the as-mined condition in the case of placer sand.

3.3 PHYSICAL BENEFICIATION

3.3.1 Monazite

In placer deposits, monazite occurs as a minor constituent along with sillimanite, garnet, and magnetite, while the major minerals are ilmenite, rutile, zircon, and quartz. Cassiterite occurs as the major mineral in the placer deposits of the Southeast Asia tin belt. Occasionally, trace quantities of other minerals, such as chromite, picotite, baddeleyite, and cinnabar, and native metals such as gold and platinum are also present. The beach sand deposits exhibit a considerable variation in mineralogy and chemical composition depending on the location (Hedrick 1985). The flowsheets for their beneficiation are therefore variable in detail. However, as the task is essentially to separate the already finely divided minerals with quite similar physical properties, the flowsheets have several features in common. An outline of the major steps in processing by physical beneficiation is given in Figure 3.1.

The highest concentrations of heavy minerals (HMs) in beach sand are found in the Manavalakurichi (70–80% HMs and 4–7% monazite) and Chavara deposits (70–80% HMs and 0.7–1% monazite) of India. Preconcentration by wet gravity methods is generally not required for these deposits. The same is true of the Pulmoddai deposit (Panditharatna 1991), which has 60–75% HMs, 70–80% ilmenite, 8–10% rutile, 8–10% zircon, and 0.02% monazite. With the Orissa deposit of India (20% HMs and 0.4% monazite), and for most other deposits throughout the world, bulk concentration of HMs is needed before actual separation of individual minerals is carried out (Bashir 1988). For example, a lean deposit containing 2–5% HMs is first concentrated to 20–30% HMs on cone concentrators. This product is then fed into spirals, which give a concentrate of more than 80% HMs.

The separation of heavy minerals is then achieved by exploiting small gravimetric differences or the slight differences in magnetizability and surface ionization potential among the various co-occurring minerals (Aplan 1988, Bashir 1988, Anderson 1986, Parker and Baroch 1971). Among the beach sand minerals, specific gravity of monazite is the

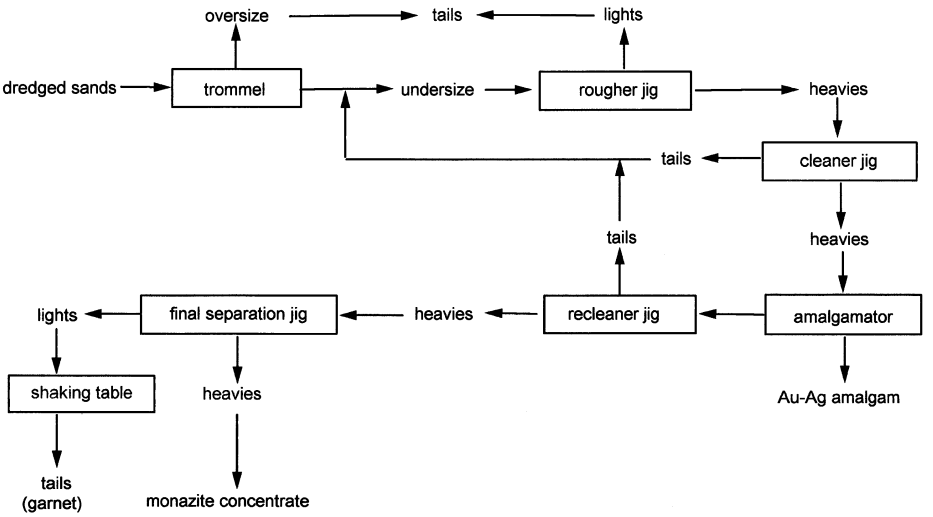

Figure 3.2 Concentration of placer minerals on board a dredge (Aplan 1988, Ferron et al. 1991).

highest. Ilmenite, garnet, xenotime, and monazite, in decreasing order of magnetizability, behave as magnetic minerals. In electrostatic separation, ilmenite and rutile behave as conducting minerals and at other times behave as nonconducting. Xenotime is more strongly magnetic than monazite and in magnetic separation concentrates with ilmenite. A poor electrical conductor, xenotime is electrostatically separated from ilmenite. Leucoxene, when present, can cause problems in the separation of monazite from ilmenite. A reduction roast at 600°C converts free hematite in leucoxene into magnetite and enables easy separation.

One of the simplest flowsheets for the production of a monazite concentrate from a placer deposit is shown in Figure 3.2. This figure outlines the process used to recover gold and monazite from a placer deposit in Idaho (Hill 1951, Jackson and Christiansen 1993). Gravity is the only method needed to produce a REO concentrate. Gold was removed earlier by amalgamation.

The dredging operations formerly operated in the gold placers in Idaho and tin placers of Southeast Asia are similar. Before separation of the heavy minerals concentrate, just as the gold was removed by amalgamation in Idaho, cassiterite was recovered using a series of jigs in placer tin beneficiation, Figure 3.3 (Fujita and Leepawpanth 1991, Meechumna 1991). Further separation of heavy mineral dredge concentrate is achieved using a combination of high intensity magnetic separation, high tension separation, and dry and wet tabling to obtain the clean concentrate of REO minerals and other minerals (Sulaiman 1991). As mentioned earlier, the beach sands of Manavalakurichi in India and Pulmoddai need not be preconcentrated. It is directly put in for separation into its constituents using electrostatic and magnetic methods. Some of the mineral beneficiation practices for obtaining monazite concentrate are outlined in Figures 3.4 to 3.7.

A combination of physical and flotation methods have been used for recovery of monazite concentrate from fine heavy mineral beach sand deposits (Ferron et al. 1991). When the valuable constituents of heavy mineral deposits are in a finer size range (between 15 and 100 microns), standard gravity methods are not very efficient and heavy losses of the valuable finer size constituents were observed. Flotation as useful.

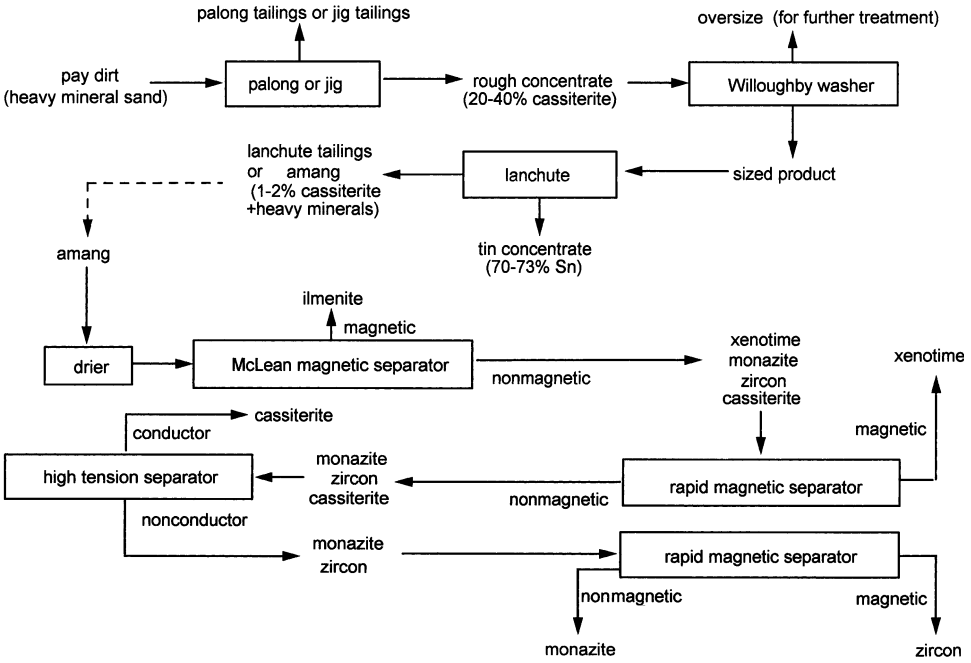

Figure 3.3 Physical beneficiation of cassiterite-bearing mineral sands of Southeast Asia.

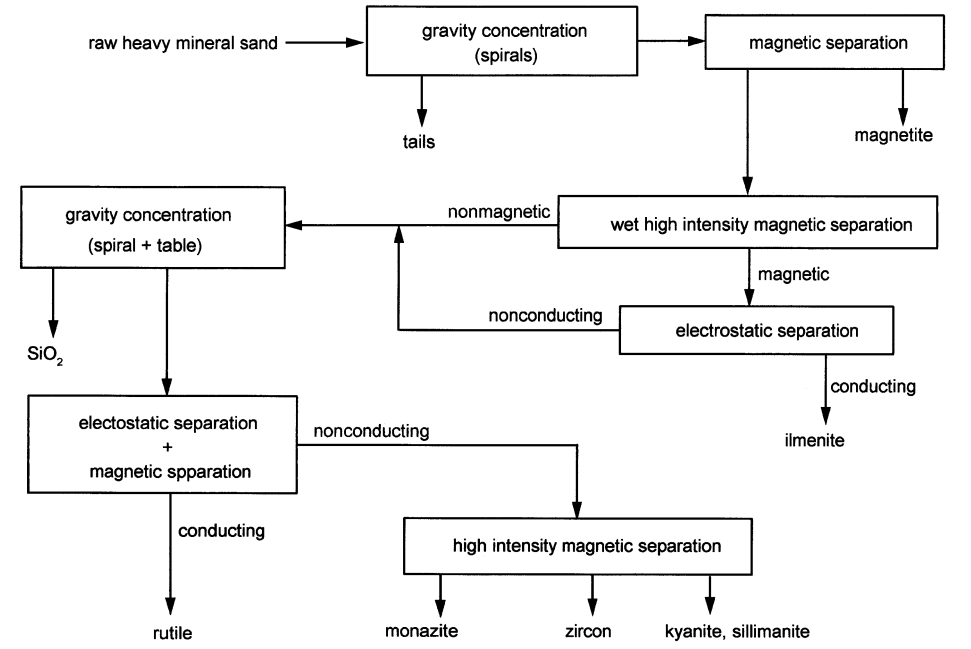

Figure 3.4 Beneficiation of coarse heavy mineral sand from Congolone, Mozambique (Ferron et al. 1991).

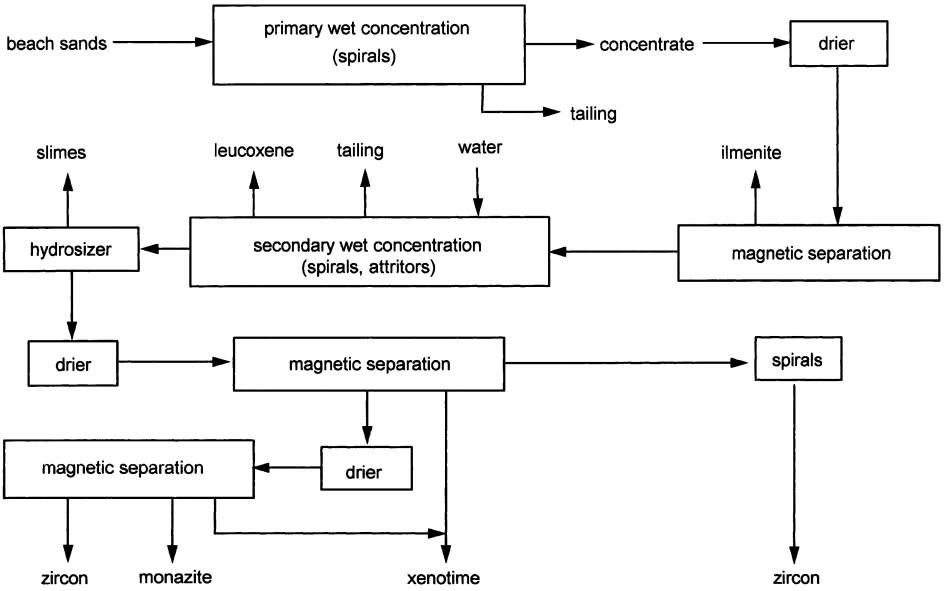

Figure 3.5 Beneficiation flowsheet at Cable Sands Pty Ltd plants, Australia (Houot et al. 1991).

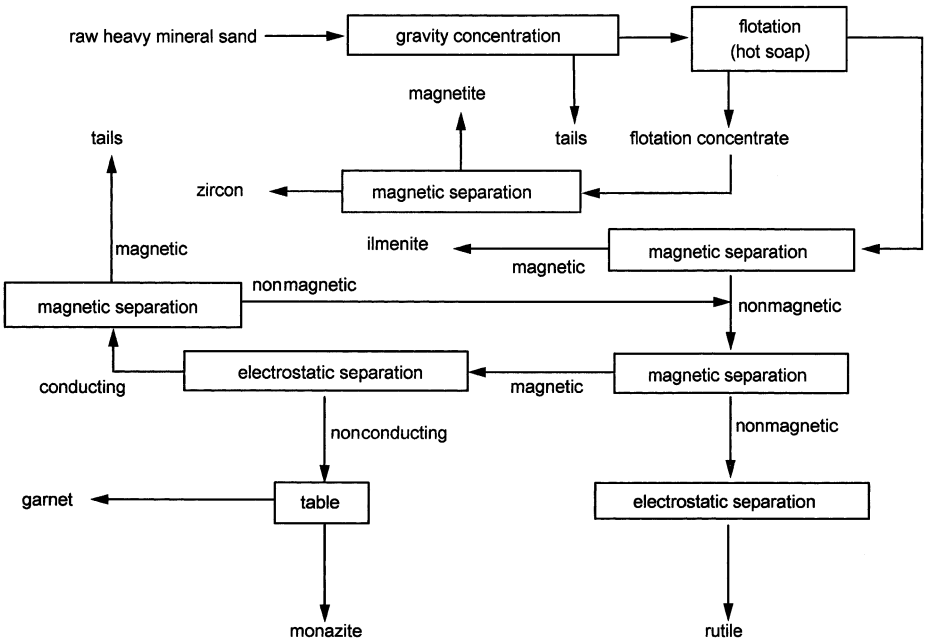

Figure 3.6 Beneficiation flowsheet at Zircon Rutile Ltd., Australia (Ferron et al. 1991).

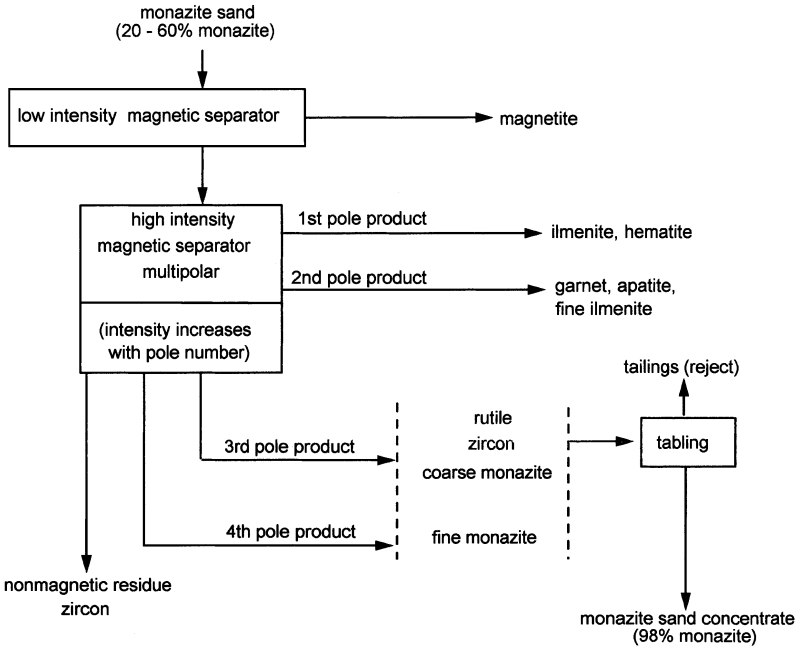

Figure 3.7 Flowsheet of the beneficiation of beach sand minerals in India.

In the former Soviet Union, for the production of bulk heavy mineral concentrate from fine grained beach sand deposits, flotation using fatty acid collectors was used (Zadorozhnyi 1965, 1967). Ferron et al. (1991) found that bulk mineral flotation can be performed efficiently using fatty acids or phosphoric acid esters as collectors. When separation of individual heavy minerals by flotation is involved, collector selection is dependent upon the ease of desorption prior to separation.

The dressing of South African monazite deposits occurring in association with copper minerals (Hill 1951) was done by flotation to recover both monazite and copper concentrates. Beneficiation by flotation had also been developed for Indian monazite (Viswanathan 1957) and for the recovery of monazite from molybdenum flotation tailings at the Climax Co. mine of Amax (Aplan 1988, Cuthbertson 1952). The flowsheet of the Climax Molybdenum Company's Byproducts Plant, CO is shown in Figure 3.8.

3.3.2 Bastnasite

The bastnasite ore of Mountain Pass has a distinctive beneficiation process. The process, in a simplified form, is shown in Figure 3.9. The blasted bastnasite rock is crushed and the crushed ore is built in layers to average 7% REO in blending piles, to be reclaimed and fed to the mill fine ore bin. The ore is withdrawn from the bin and conveyed to a ball mill where the particle size is reduced to 100% passing 150 mesh. The ground ore is beneficiated by hot froth flotation.

The flotation characteristics of bastnasite are fairly well established (Aplan 1988, Fuerstenau and Pradip 1986). Various collectors such as fatty acids (oleic) (Morrice and Wong

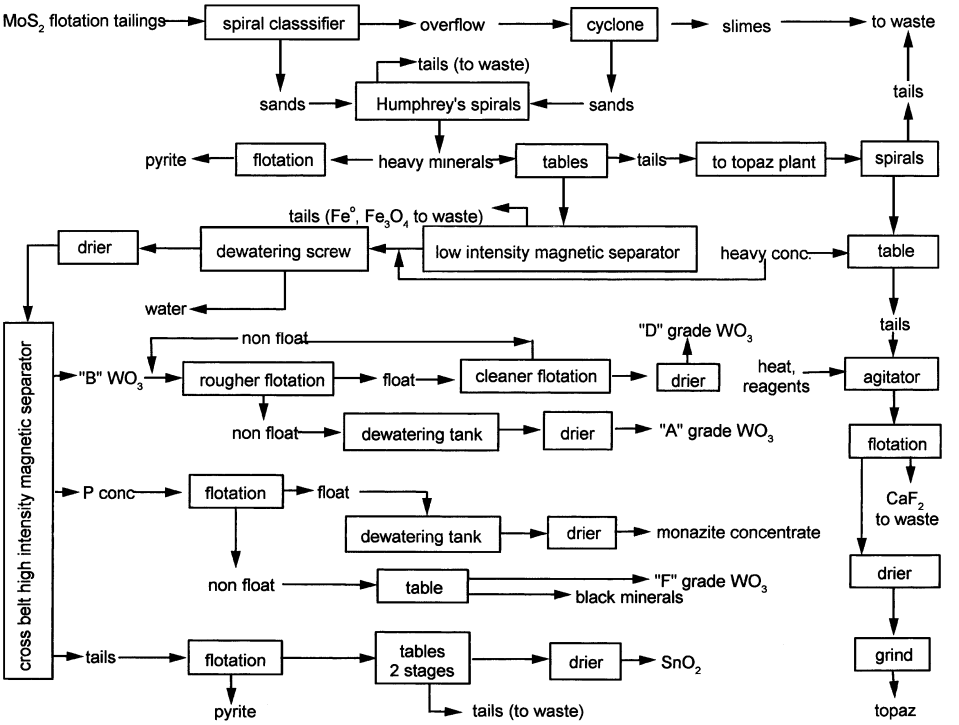

Figure 3.8 Flowsheet of Climax Molybdenum Company's Byproducts Plant, CO (Aplan 1988).

1982), hydroxamates (Aplan 1988, Pradip and Fuerstenau 1988), and dicarboxylic acids (Xuefang 1985) have been proposed and/or used. Some of the gangue minerals associated with bastnasite, such as calcite, barite, and celesite, have flotation properties similar to bastnasite and their separation by conventional fatty acid flotation is difficult.

Mountain Pass ore contains the gangue minerals barite, calcite, strontianite, and quartz. Prior to rougher flotation, the ore undergoes as many as six different conditioning treatments. Conditioning is carried out in large tanks (1800 mm by 2700 mm) with steam being bubbled through the pulp. The reagents are added step-wise in the pulp heated to 70 to 90°C, and the six-stage conditioning lasts for about 2 h. In the first stage, the ore slurry is mixed with soda ash, sodium fluosilicate, and steam. The next step is steam conditioning. In the third stage, ammonium lignin sulfonate is added in the presence of steam. In the fourth stage, the pulp is conditioned with steam, in the fifth stage with steam-distilled tall oil C-30, and in the sixth stage again with steam. The conditioned slurry, which contains 30–35% solids, is pumped to a rougher flotation circuit. Rougher flotation is carried out in 12 flotation cells, each with a capacity of 1700 liters. The tailings from rougher flotation average 1–2% REO. The rougher concentrate, which assays approximately 30% REO, is transported to cleaner cells for four-stage cleaning. These cells operate at 50% solids. Within the cleaning circuit the tailings are recirculated. Only the tailings from the first cleaner are put through a scavenger flotation circuit. The tailings from the scavenger circuit are combined with rougher tailings and constitute the flotation plant tailings which average 2% REO. The concentrate from the scavenger is reground and reverted to the rougher cells.

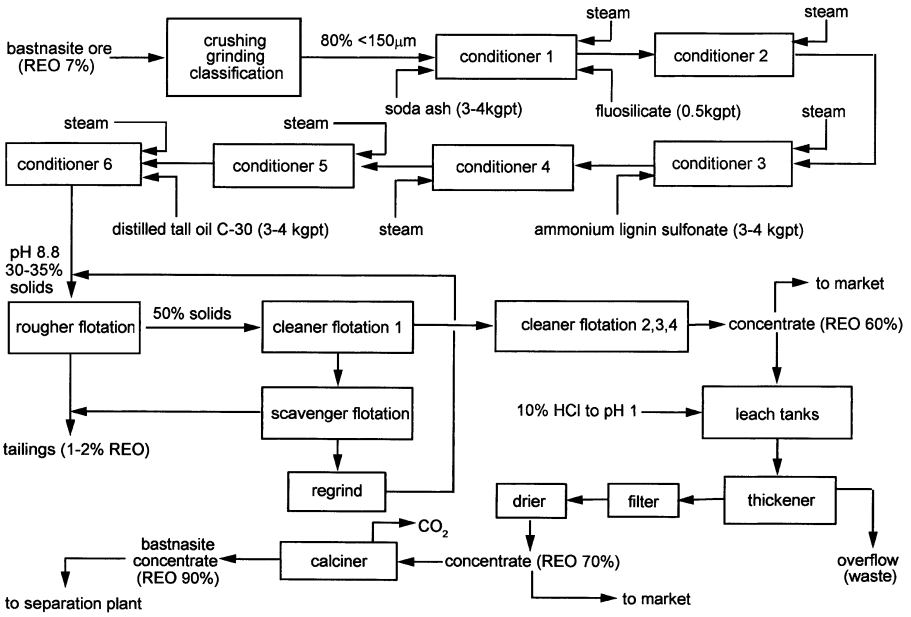

Figure 3.9 Simplified flowsheet for the recovery of bastnasite at the Molycorp plant (Aplan 1988).

After four-stage cleaning, the final concentrate from the flotation circuit is thickened, filtered, and dried. The final dried concentrate of Mountain Pass contains 60% REO and the overall recovery is 65–70% (Pradip and Fuerstenau 1988).

A higher recovery of 88% was obtained in a scheme (Ferron et al. 1991) shown in Figure 3.10. The complex bastnasite ore was beneficiated using a double reverse gangue flotation followed by bastnasite flotation. A specially developed collector was used.

3.3.3 Bayan Obo Ore

Numerous minerals occur intimately intergrown in the rare earth-bearing Bayan Obo iron ore (Aplan 1988, Fangji et al. 1988). In physical beneficiation, in addition to the rare earths, magnetite, fluorite, hematite, and niobium oxide are recovered as valuable by-products.

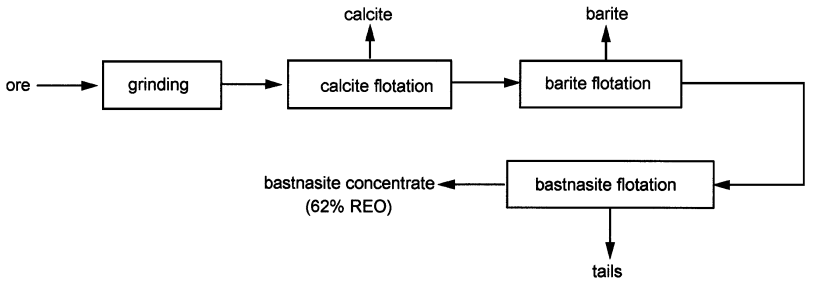

Figure 3.10 New scheme for the treatment of complex bastnasite ore (Ferrron et al. 1991).

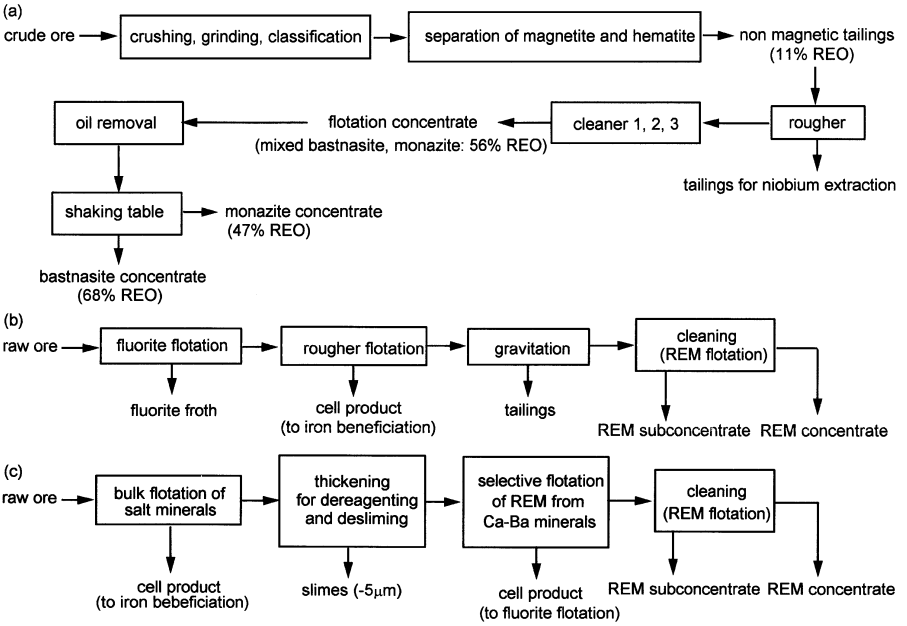

Figure 3.11 Schemes for the physical beneficiation of Bayan Obo ore (Anderson 1986, Houot et al. 1991).

Three schemes for the processing flowsheet of Bayan Obo ore (Luo and Clin 1988, 1985, Houot et al. 1991) are shown in Figure 3.11. The initial bulk flotation is carried out after grinding the ore to 90% <74 μm, with Na_2CO_3 as pH regulator, Na_2SiO_3 as depressant of iron minerals and silicates, and sodium salt of oxidized petroleum (paraffin soap) as collector. Depressed iron minerals and silicates remain at the bottom of the flotation cells and are taken for iron beneficiation and niobium recovery. After eliminating the surplus fatty acid collector by thickening and desliming at 5 μm, selective rare earth flotation is carried out with Na_2CO_3 as pH regulator, Na_2SiO_3 and Na_2SiF_6 as gangue depressants, and hydroxamic acid as collector at a pH between 5 and 6. Depressed calcite, fluorite, and barite settle to the flotation cell bottom. After selective flotation, the rougher concentrate contains approximately 45% REO. It contains both monazite and bastnasite. The recovery of rare earth as the concentrate at this stage is ~80%. After the final treatment by cleaning or high intensity magnetic separation, two concentrate fractions — the primary 68% REO concentrate and a secondary monazite concentrate containing 36% REO concentrate — are obtained at recoveries of 25% and 36%, respectively. The total recovery of rare earths from the ore is 61%.

3.4 CHEMICAL TREATMENT

3.4.1 Monazite

The recovery of mixed rare earths and removal of thorium from monazite are accomplished by a variety of methods (Bril 1964), after chemically attacking the mineral with sulfuric acid or sodium hydroxide.

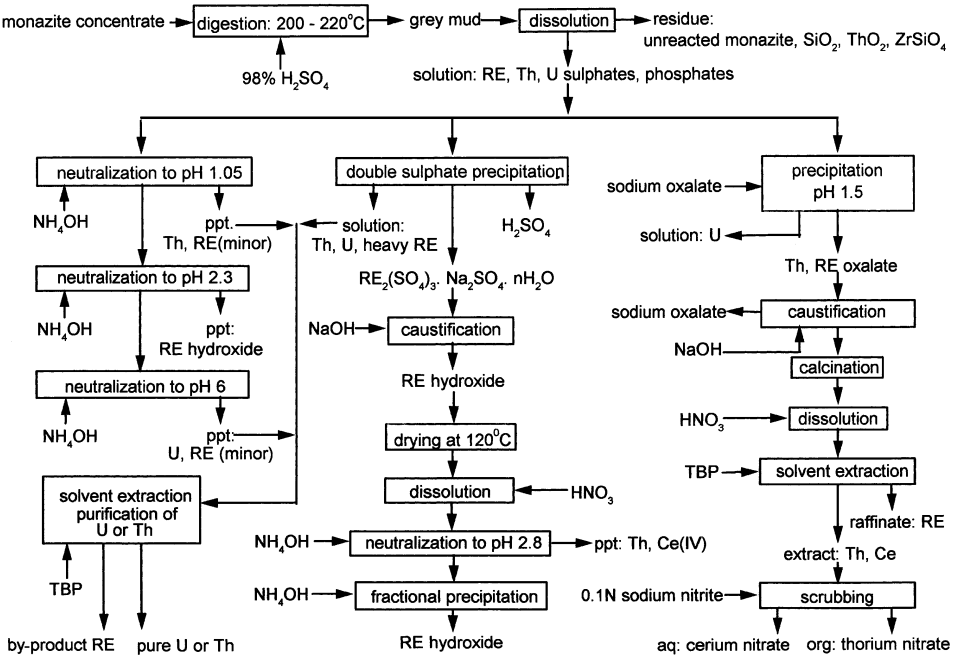

Figure 3.12 Monazite processing by acid treatment.

Acid treatment The sulfuric acid method had been used most extensively in the United States (Parker and Baroch 1971). With this method (Shaw et al. 1954), depending on the acid/ore ratio, temperature and concentration, either thorium or the rare earths can be selectively solubilized or both thorium and rare earths totally solubilized. Rare earths and thorium are subsequently recovered from the solution. The processes available are shown in Figure 3.12. The process of rare earth recovery based on rare earth double sulfate precipitation was largely developed by Pilkington and Wylie (1952) and has found industrial application. Yttrium and the heavy rare earth double sulfates are quite soluble and go with thorium. Even in the stepwise neutralization procedure investigated at Ames (Smutz et al. 1954, Barghusen and Smutz 1958), yttrium and the heavy rare earths are precipitated along with thorium as a basic compound. The rare earths, however, are recoverable from the thorium fraction during solvent extraction for the purification of thorium and uranium. Solvent extraction with tributyl phosphate (TBP) from an aqueous 8 N nitric acid solution of thorium and mixed rare earths permits the recovery of thorium, uranium, cerium, and cerium-free rare earths. Other commercially significant processes essentially involve precipitation of thorium pyrophosphate or basic salts from the leach liquor and subsequent recovery of the rare earth in solution as double sulfates, fluorides, or hydroxides or even selective solubilization of thorium in the ore treatment stage itself, as originally developed by Société des Produits Chimiques des Terres Rares (Powell 1939). The sulfuric acid process does not yield pure products and is no longer in commercial use.

Alkali treatment The flowsheet for the present commercial process for monazite treatment using caustic soda is given in Figure 3.13. The phosphate content of the ore is recovered as a marketable by-product, trisodium phosphate, at the beginning of the flowsheet, and this has been a major attraction for the commercial use of this process. The practical development of caustic soda treatment for rare earth processing is credited to

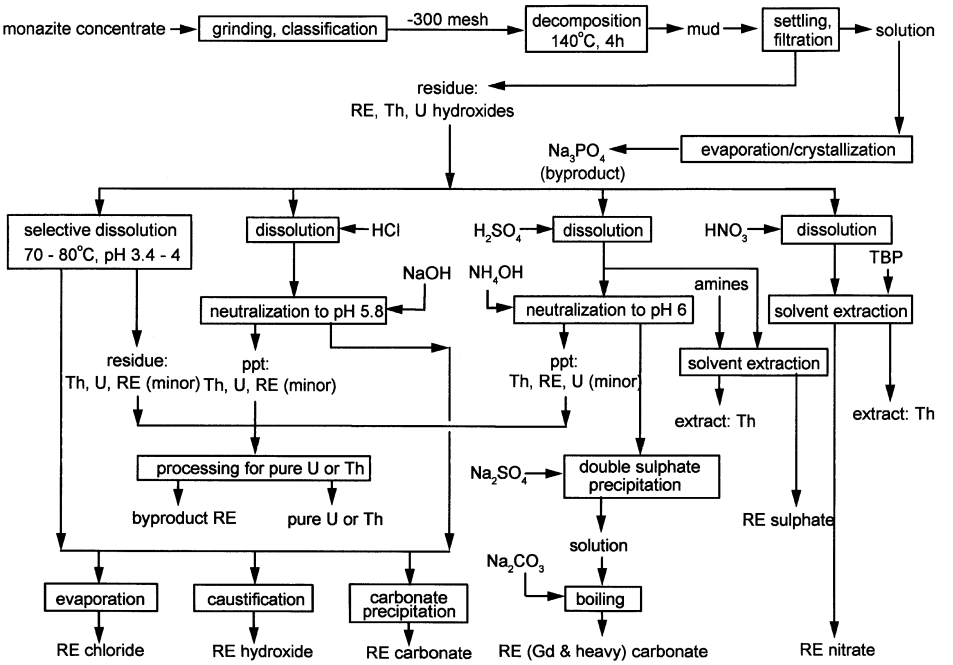

Figure 3.13 Monazite processing by alkali treatment.

de Rhoden and Peltier (1957), and considerable work on the process was carried out at the Battelle Memorial Institute. In the usual industrial practice, fine ground monazite is attacked with a 60–70% sodium hydroxide solution at 140–150°C (Krumholz 1957). In the Soviet practice, the grinding and caustic digestion are performed in one step and this enables about 50% savings in caustic soda consumption. Krumholz (1957) achieved a clean separation by digesting the ore with caustic soda at 170°C under a pressure of several atmospheres. The mixed rare earth thorium hydroxide cake is processed for rare earths and thorium recovery by a variety of methods.

The direct dissolution of mixed rare earth hydroxide in nitric acid and the separation of rare earths by extracting thorium and uranium with TBP is attractive but complicated because of interference arising from partial oxidation of cerium. An effective process for removing thorium completely and in a high state of purity is solvent extraction with higher amines. The amines function well with a sulfate solution (Kaczmarek 1981).

IRE practice The Indian Rare Earths Ltd. plant at Alwaye in Kerala uses the caustic soda treatment for the decomposition of monazite sands, and the process has four major stages: (1) Reaction of finely ground monazite sand with hot concentrated aqueous caustic soda solution, to convert the rare earth and thorium contained in the ore into their respective hydroxides. (2) Separation of the insoluble hydroxides from the dissolved phosphate and excess caustic soda. (3) Recovery of trisodium phosphate, and (4) Separation of rare earths from thorium by leaching with hydrochloric acid. An outline of the flowsheet at the IRE plant is shown in Figure 3.14.

The monazite sand is ground in a ball mill to finer than 300 mesh size in a closed circuit system using an air classifier. The ground sand in 1/2 ton batches is mixed with 50% caustic solution and the resulting mass is fed to a conical mild steel tank and heated to

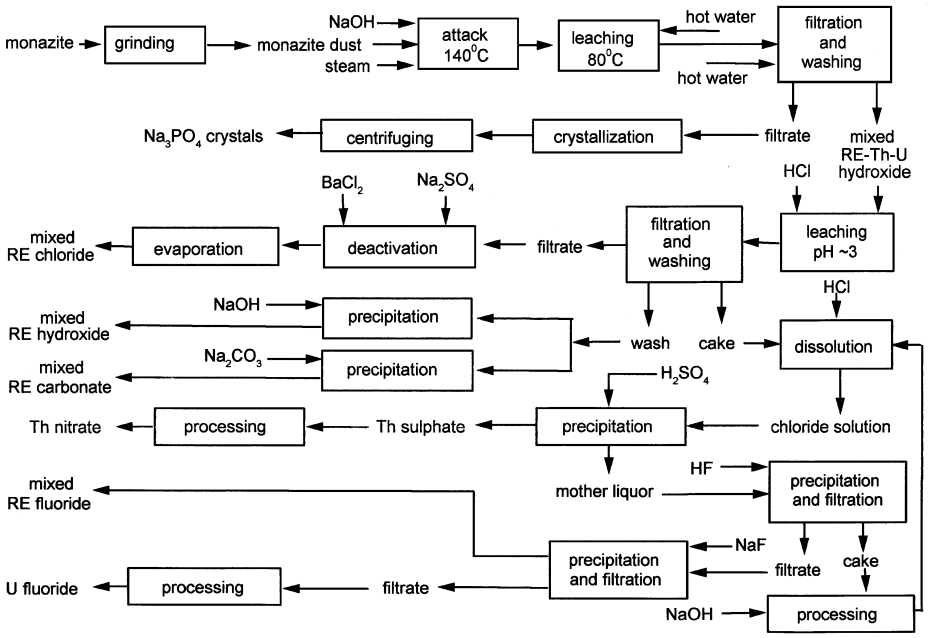

Figure 3.14 IRE process for caustic soda treatment of monazite.

approximately 150°C with the addition of fresh caustic soda at a ratio of about 1:1. The final concentration of caustic soda to give a monazite sand caustic soda is about 65 to 70%. The mixture is agitated during the reaction, which lasts for about 3 to 4 h. Most of the monazite is decomposed during this period.

The hydroxides–trisodium phosphate mixture is dumped into a tank containing dilute wash liquors from a previous decantation, and the slurry is heated to approximately 90°C and the density adjusted to about 30°Be. The slurry is allowed to settle for about 12 h when the supernatant liquid containing most of the trisodium phosphate and excess caustic soda is drawn off and sent to the trisodium phosphate recovery section. The hydroxides are washed once again with hot water and allowed to decant, and the supernatant liquid is drawn off to be reused for a subsequent extraction of trisodium phosphate.

By this means, the free alkalinity in the hydroxides is reduced from about 70 gms per liter (expressed as free NaOH) to about 15 gms per liter. The mixture of hydroxides is then fed to a vacuum leaf filter and washed to reduce the alkalinity before being treated for the separation of rare earths from thorium.

The solution of trisodium phosphate and caustic soda from the decantation tanks is filtered and fed to a vacuum for crystallization. In the crystallizer, the solution is cooled in two stages from about 70°C to 20°C, at which temperature most of the trisodium phosphate crystallizes out. The mixture of trisodium phosphate crystals and dilute caustic soda solution is fed to a continuous centrifuge and the centrifuged trisodium phosphate is dried in a hot air conveyor drier. The dry trisodium phosphate contains approximately 19% P_2O_5, and is purer than the trisodium phosphate manufactured by the usual process of neutralization of phosphoric acid.

The washed hydroxide cake is treated in a rubber lined tank with 21 to 22°Be hydrochloric acid. Sufficient quantity of hydrochloric acid is added to dissolve only the rare

earths while the thorium remains undissolved. Iron is precipitated by oxidizing it to the ferric stage, and suitable precautions are taken to prevent oxidation of cerium to the ceric stage. The pH of this slurry is in the neighborhood of 3. The slurry is pumped to a plate and frame type filter press using rubber lined equipment.

The filtrate after removal of lead is converted to the fused mixed rare earth chloride by heating it in an enameled cast iron vessel to the boiling point of approximately 145°C and then pouring it into steel drums where it solidifies on cooling.

The thorium hydroxide is washed and the wash waters are converted either to the mixed rare earth carbonate by the addition of sodium carbonate or to the mixed rare earth hydroxide by the addition of caustic soda. Both of these rare earth compounds are dried in a rotary drier before packed in steel drums.

The cake contains all the thorium present in the monazite and most of the uranium. It also contains a certain percentage of rare earths and other insoluble impurities.

The crude thorium hydroxide cake is dissolved in an excess of hydrochloric acid, and the resulting chloride solution is filtered on a plate and frame type filter press to remove insoluble impurities like ilmenite, zircon, etc. The clear filtrate is treated with an excess of 50% sulfuric acid. Most of the thorium is precipitated as a sulfate, while most of the rare earths and most of the uranium remain in solution. The thorium sulfate is centrifuged in a rubber lined centrifuge and the solution is sent for recovery of thorium, rare earths, and uranium that are in solution. The sulfate is not pure enough and is further purified by re-precipitating with 50% sulfuric acid to give a purer thorium sulfate.

The pure thorium sulfate is converted to hydroxide by reacting it with ammonium hydroxide. This is filtered and washed on filter presses to remove all the water soluble impurities. The thorium hydroxide is then dissolved in chemically pure nitric acid to give a solution of thorium nitrate, which is filtered and evaporated to the required strength in a glass lined evaporator. The molten nitrate is allowed to solidify in aluminum dishes and then packed in glass bottles or steel lined drums.

The solution obtained from the precipitation of thorium sulfate is treated for the recovery of thorium, rare earths, and uranium by fractional precipitation with hydrofluoric acid.

Monazite breakdown practices The conditions for monazite processing by alkali treatment have remained essentially unchanged for the past 40 years, except for minor variations. Recent summaries (Mackey 1986, Hart and Levins 1988, Koch 1987) of alkali digestion practices note that monazite can be very fine ground (to less than 10 micron) and cracked with a 70% NaOH solution under pressure for 2 h at 150°C to form an insoluble hydroxide residue of rare earths and thorium. Subsequently, the hydroxide residue is leached in nitric, sulfuric, or hydrochloric acid to prepare rare earth solutions for solvent extraction. Studies on the decomposition of an Australian monazite concentrate (48.6% rare earths, 6% thoria, 31% phosphate, and 14% residue of mostly zircon) pointed out that the extraction reached 98% only by digesting fine ground (less than 45 micron) monazite concentrate in 80% w/v (NaOH:monazite weight ratio 1.5:1) at 140°C for 3 h. Studies on Brazilian monazite have also confirmed the necessity of fine grinding (less than 45 micron) and high temperature (140–200°C) for effective decomposition. In their investigations on chemical treatment of Taiwanese black monazite, Miao and Horng (1988) used both "hydrothermal" and soda fusion methods. In the hydrothermal process, ground monazite (95% within 80 to 100 mesh) was cracked with 45 wt % of aqueous alkali solution at 170°C and 5 atmospheres in an autoclave for 3 h. As an alternative they fed unground monazite into fused caustic soda at 400°C in an open cylindrical stainless steel tank and reacted the

mass for 2.5 h with low speed agitation. In each of these operations, 90% of the rare earths contained in the monazite was recovered in the product. The product was rare earth hydroxide slurry with sodium phosphate in the first case and rare earth hydrous oxide with sodium phosphate hard mass rock in the second. In either case, the product was converted to the chloride by dissolving in HCl, and thorium was selectively precipitated as hydroxide from the RE chlorides by pH adjustment.

Caustic soda digestion is the process followed in the monazite cracking plant established in Malaysia in 1979, by Asian Rare Earth Sdn Bhd (ARE) at Bukit Merah in Perak State (Sulaiman 1991). Caustic soda digestion yields trisodium phosphate and the hydroxides of rare earths and thorium. The phosphate is separated from the hydroxides by dissolving it in water. From this solution it is crystallized out or converted to tricalcium phosphate. Thorium and rare earths are separated by a selective dissolution method. Rare earths are dissolved in concentrated HCl, and the undissolved thorium is filtered and produced as thorium cake waste. The rare earth fraction is separated into light and heavy rare earths by solvent extraction with HDEHP and the rare earths are finally precipitated as carbonates.

Rhône-Poulenc uses caustic soda digestion for chemical treatment of monazite at its plants in La Rochelle (France) and Freeport (Texas, U.S.). Monazite concentrate is reacted with sodium hydroxide to break the phosphate matrix. The rare earth hydroxides recovered in the process are leached with nitric acid to produce nitrate solutions for solvent extraction. Rhône-Poulenc separates all the rare earths by solvent extraction.

High temperature process A process involving high temperature reaction of monazite with calcium chloride and calcium carbonate has been suggested by Merritt (1990). In this process monazite is decomposed by reacting it with calcium chloride and calcium carbonate in an environment that is both reducing and sulfidizing, at temperatures between 980 and 1190°C. The products formed are rare earth oxysulfides, oxychlorides, a thorium rich oxide solid solution, and a calcium chlorophosphate (chloropatite). From the product, the rare earth elements are removed by leaching with 3% HCl. Filtration is used to separate the leach liquor from the gangue minerals that remain as the residue. The thorium rich oxide residue is resistant to acid attack and is probably suitable for disposal by burial. The process apparently has the following attractions.

(1) Effectively all the monazite is decomposed in 45 min compared to 3–4 h for the caustic digestion process.
(2) Grinding of monazite to ~50 μm is not necessary.
(3) The thorium oxide residue from the dilute acid leach is readily filtered, and, because it is more resistant to acid attack than thorium hydroxide, the residue is more suited for disposal by burial.

The high temperature reaction process, however, has certain limitations. They are (i) the maximum overall recovery of rare earth elements is only 89% compared to 94.5% for the sodium hydroxide digestion process, (ii) the recovery of phosphate value is not addressed, and (iii) the method does not offer improved rare earth element–thorium separation.

Another process (Merritt 1990a) used sodium carbonate as the reactant for attacking monazite but conducted the process in an environment that is both reducing and sulfidizing at 900°C. The product obtained consisted of rare earth element oxysulfide, a thorium rich oxide, and γ-trisodium phosphate and a mixed sodium rare earth element phosphate. From the reacted monazite, most of the phosphate can be separated by leaching it with water at room temperature. From the water-leached residue, the rare earth elements can be extracted

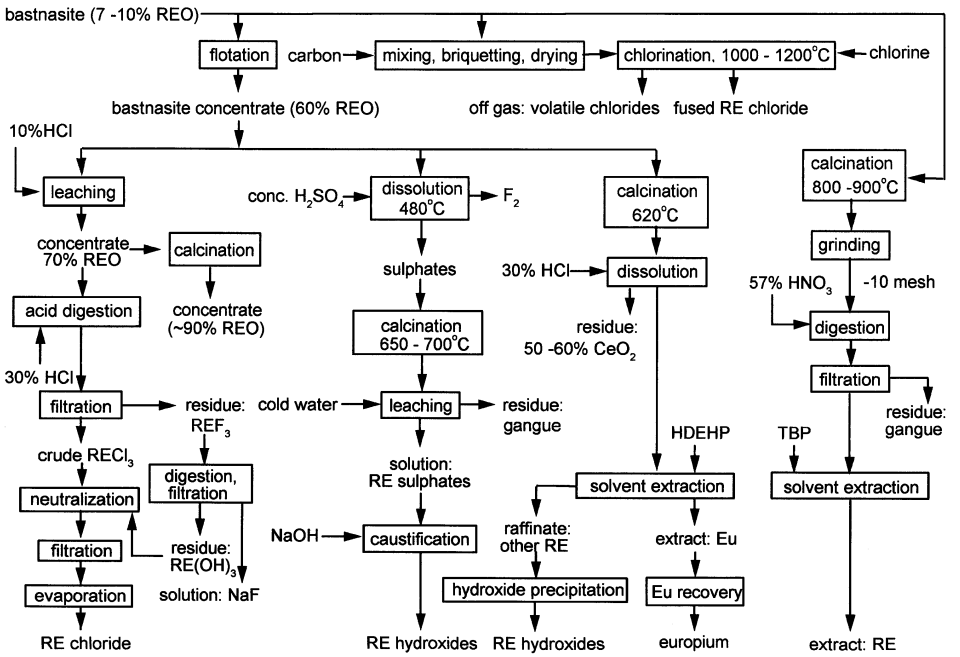

Figure 3.15 Chemical processing of bastnasite.

by selectively leaching the oxysulfide phase with 3.5% hydrochloric acid. In the present process, decomposition of monazite is rapid (complete in only 2 h), grinding is not necessary and the separation of rare earths from thorium is simple because unlike the present commercial process, careful control of pH is not necessary for separation. The better recovery of rare earth elements, 94.5% in the sodium hydroxide digestion process, apparently makes it superior, but in that process 10% of the original thorium remains with the rare earth elements. In the sodium carbonate process the corresponding figures are 91.5% recovery and only 6.6% of the original thorium left with the rare earths.

Merritt (1990, 1990a) conducted the experiments for these investigations using very small changes in a tube furnace. It is probably too early to compare this process extensively with a process of multiton batch size. Another disadvantage of the present high temperature process is the high temperature itself.

Chlorination A method of preparing anhydrous rare earth chlorides by high temperature chlorination of monazite was investigated (Hartley 1952). Pelletized mixtures of monazite and charcoal were heated in chlorine at over 900°C in a silica reactor. At this temperature over 85% of the rare earths in monazite were recovered as anhydrous rare earth chlorides, virtually free from thorium chloride and phosphorus compounds. In a later investigation by Brugger and Greinacher (1967) on the chlorination of bastnasite, it was emphasized that the process was applicable to monazite chlorination also.

3.4.2 Bastnasite

Chemical treatment of bastnasite can start with either crude ore or bastnasite concentrate. The methods available are summarized in Figure 3.15. The 60% REO bastnasite obtained

as the end product of physical beneficiation can be upgraded to about 70% REO by leaching with hydrochloric acid to remove calcium and strontium carbonates. The 70% REO concentrate can be upgraded to 85–90% REO by calcining it to remove the carbon dioxide.

The decomposition of bastnasite has been extensively investigated at Ames and at the U.S. Bureau of Mines (Rice 1959, Shaw 1959, Berber et al. 1960). A process was described, involving nitric acid digestion and solvent extraction in which over 98% of the original rare earth content was recovered starting from the crude bastnasite ore containing 7–10% REO. Starting with bastnasite concentrate, Shaw (1959), Berber et al. (1960) have described a process in which the concentrate was dissolved in warm concentrated sulfuric acid and the rare earths were recovered as water soluble sulfates. The sulfuric acid process has found commercial application (Kaczmarek 1981) for purifying rare earths from common elements such as Fe, Pb, Si, and Ba occurring in the ore.

In the Molycorp process (World Mining 1966) the flotation concentrate, containing 60% REO, is roasted in air at 620°C to drive off carbon dioxide and oxidize cerium to a tetravalent state. The calcine is treated with 30% HCl to dissolve the noncerium rare earths, yielding a marketable cerium concentrate containing 65–70% REO with 55–60% CeO_2. The solution is processed further for the recovery of europium and also to obtain other rare earths contained in it.

The ceria residue also contains mixed rare earth fluorides. The process of extraction of rare earths from bastnasite by leaching with hydrochloric acid is also patented. In this process, the fluorides in the ore are not removed completely. The fluorides are, however, decomposed by treatment in the caustic soda (Parker and Baroch 1971). The rare earth hydroxides are then leached with HCl.

The bastnasite concentrates are processed in China by heating with 98% sulfuric acid at 500°C in a rotary kiln. By this, the fluorocarbonate matrix is destroyed, carbon dioxide and hydrofluoric acid gases are released, and the rare earths are converted to their sulfates. The rare earths are precipitated as a double sodium sulfate by leaching with water and adding sodium chloride. Subsequently, the rare earth sulfates are converted to hydroxides by digestion in a strong caustic solution and the hydroxides are then dissolved in hydrochloric acid. Separation and purification of the rare earths is done using solvent extraction (Hart and Levins 1988, Koch 1987).

In the process followed at the Thorium Ltd. plant in the U.K., the bastnasite concentrate was treated with caustic soda to convert the fluoride component to hydroxide. Following this with dissolution in hydrochloric acid, a rare earth chloride solution was obtained from which the hexahydrate $RECl_3 \cdot 6H_2O$ was crystallized or the solution was processed further for recovering individual rare earths.

Direct alkaline roasting of the ore to convert the fluoride in the ore into soluble alkali fluoride, then water leaching, followed by separation of unconverted barite by flotation was a process investigated by Kasey (1959).

Kruesi and Duker (1965) of Molycorp developed the process, shown in Figure 3.16, for the production of rare earth chloride from bastnasite. The process essentially consists of three steps in which the following reactions are conducted.

$$REF_3{-}RE_2(CO_3)_3 + 9HCl \rightarrow REF_3 + 2RECl_3 + 3HCl + 3H_2O + 3CO_2$$

$$REF_3 + 3NaOH \rightarrow RE(OH)_3 + 3NaF \qquad \text{and}$$

$$RE(OH)_3 + 3HCl \rightarrow RECl_3 + 3H_2O$$

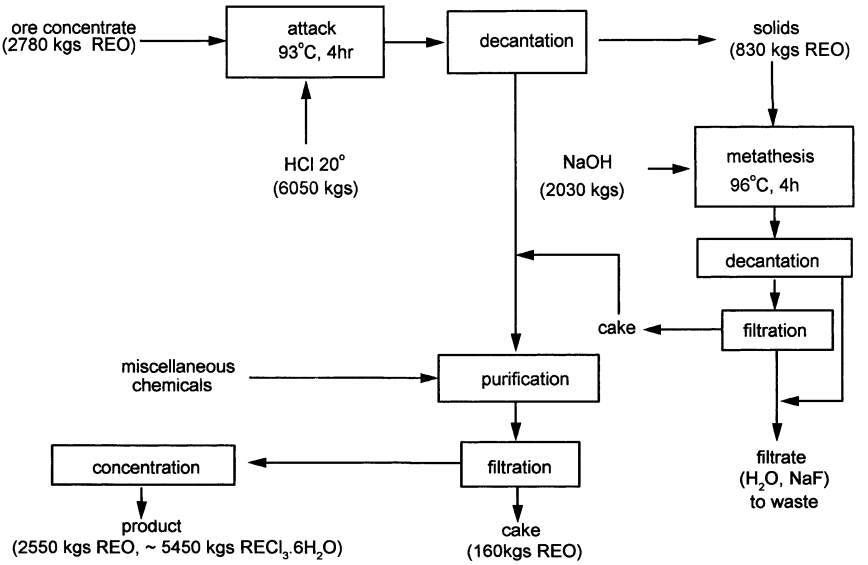

Figure 3.16 Production of rare earth chlorides from bastnasite (Kruesi and Duker 1965).

The bastnasite concentrate (70% REO, 65% minus 325 mesh) was attacked with minimum amount of hydrochloric acid (1.8 kg of 20° Be acid/kg of ore or 2.5 kg/kg of RE_2O_3) for 4 h at 200°F. Solid–liquid separation of the leach liquor was done by decantation. In the next step, rare earth fluoride in the solid residue was metathetically converted to rare earth hydroxide using 500 kg of NaOH per 1000 kg of concentrate feed (or 0.73 kg of NaOH per kg of REO feed). Reaction duration was 4 h. The metathesis cake was thoroughly washed with water to a low sodium content.

The next step consisted of neutralization and purification. Substantial amounts of free hydrochloric acid contained in the mother liquor were neutralized by addition of the rare earth hydroxide obtained in the metathesis step, until a pH of about 3 was obtained. The pH control was necessary to remove impurities. Small amounts of hydroxide were added to the heated solution to completely precipitate iron hydroxide. A small amount of sulfuric acid was added to precipitate lead sulfate, and then barium chloride was added to precipitate excess sulfate and to act as a carrier in the removal of any thorium daughter product originally present in the ore. At this pH, thorium hydroxide is also insoluble and traces of it were removed. On filtration, a sparkling clear solution of rare earth chlorides was obtained with all the impurities remaining in the cake. The cake was washed repeatedly to a low rare earth content and discarded. The rare earth chlorides solution was concentrated by evaporation into either a solution or cast in solid form. The analyses of the bastnasite concentrate starting material and rare earth chloride end products are given in Table 3.1.

3.4.3 Chlorination

Goldschmidt process A high temperature direct chlorination process was developed and used by the Goldschmidt AG in Germany (Brugger and Greinacher 1967) to directly obtain an anhydrous rare earth trichloride product well suited for the production of the

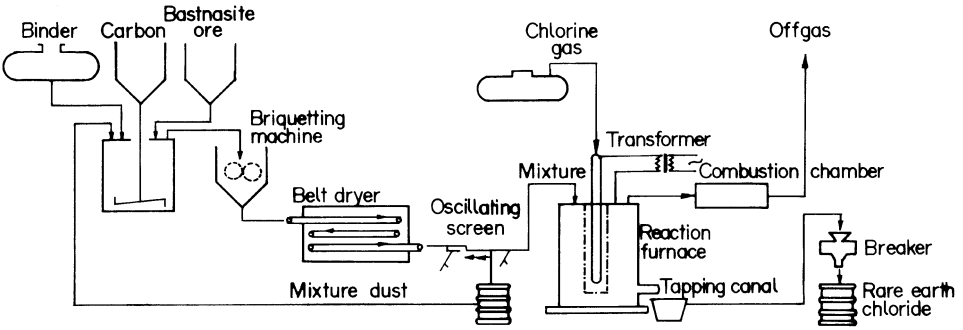

Figure 3.17 Goldschmidt process for bastnasite chlorination (Brugger and Greinacher 1967).

corresponding metal directly from bastnasite ore. The process is suitable for use in a variety of ores like monazite, xenotime, allanite, cerite, euxenite, fergusonite, and gadolinite. The flowsheet of a complete rare earth chlorination process given by Brugger and Greinacher (1967) is shown in Figure 3.17.

The bastnasite ore was ground to less than 80 mesh. Regrinding, obviously, was not necessary if the flotation concentrate was used. The ground ore was thoroughly mixed with a binder like sulfite liquor, sugar, starch, etc., and some water. The relatively dry brew was compacted into pellets through a briquetting machine and the pellets were passed through

Table 3.1 Typical analyses (%) of bastnasite concentrate and rare earth chlorides obtained

	Concentrate[a]		Chloride I[b]		Chloride II[c]
$BaSO_4$	1.0–0.5			$BaCl_2$	2.6–4.2
CaO	1.0–0.5	CaO	1.00	$CaCl_2$	3.4–3.6
F	5.0–5.5	MgO	1.00	acid insoluble fluoride	13–15
Fe_2O_3	0.5–0.3	Fe	0.005	Fe_2O_3	<0.01
SiO_2	1.0–0.5	SiO_2	0.05	$SrCl_2$	0.4–0.6
ThO_2	<0.01	radioactivity	absent	$MgCl_2$	0.1–0.2
REO	68–72	REO	46.0	REO	66.0
CeO_2	50.0			CeO_2	49–50
La_2O_3	31.0			La_2O_3 (including rare earths not listed)	32–35
Pr_6O_{11}	5.0			Pr_6O_{11}	3.8–4.3
Nd_2O_3	12.9			Nd_2O_3	11–12
Sm_2O_3	0.62			Sm_2O_3	0.6–1
Eu_2O_3	0.11				
Gd_2O_3	0.2				
Y_2O_3	0.05				
Other heavies	0.02				

[a]Typical analyses of Mountain Pass bastnasite concentrate.
[b]Chloride I was obtained by the wet method (Kruesi and Duker 1965).
[c]Chloride II was obtained by the dry method (Brugger and Greinacher, 1967).

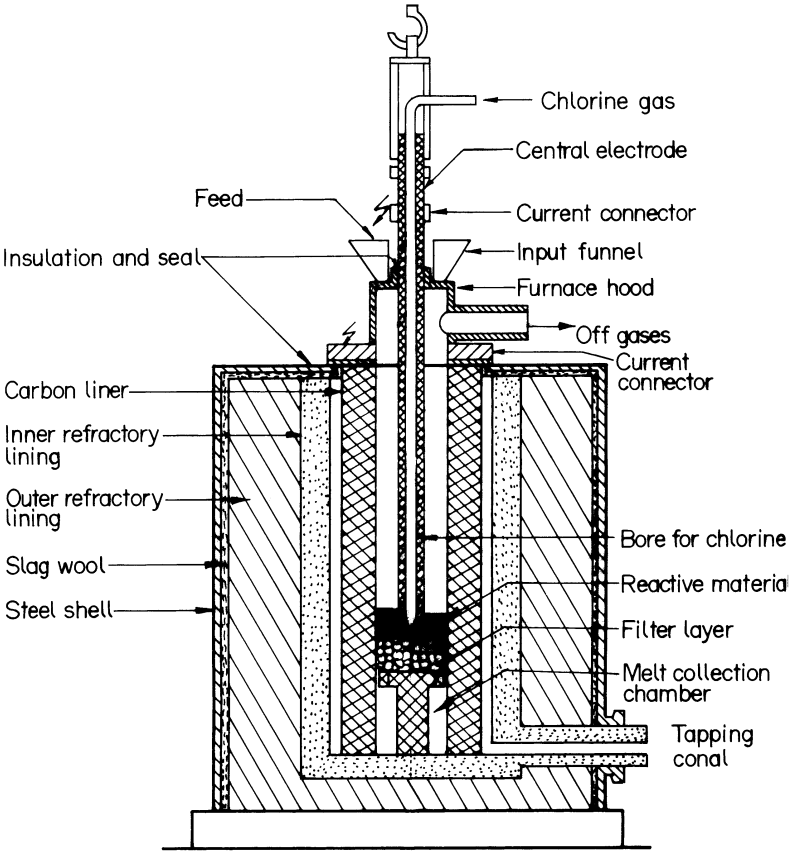

Figure 3.18 Diagram of chlorination furnace (Brugger and Greinacher 1967).

a band drier. Fine fraction was screened off and reverted to the mixer because it would be blown out of the furnace due to high gas velocity. The pellet passed continuously or batch-wise into the chlorination furnace.

The chlorination furnace is shown in Figure 3.18. The key requirement for complete chlorination is a temperature in the reaction zone of the furnace in the range of 1000 to 1200°C. Practically all metals and refractory materials react with chlorine and carbon and/or carbon monoxide. Natural graphite and amorphous carbon are resistant to the attack but not for a long time. Hence special furnace inserts of amorphous carbon, which could be rapidly replaced, were developed and used.

In the furnace, the ore–carbon mixture was completely converted to chlorides by gaseous chlorine. The chlorides were separated according to their volatility. The rare earth chlorides were tapped from the bottom of the furnace periodically as a nonvolatile fluid melt. The tapped chloride was allowed to solidify. The alkali and alkaline earth chlorides likewise collected in the melt chamber. All other reaction products were carried off by the off gases. The important reactions occurring during chlorination are listed in Table 3.2. The analysis of the rare earth chloride obtained is given in Table 3.1.

The chlorination furnace was operated with alternating current at low voltage (10–20 V) and high currents (2000–3000 A) with the loose layers of coke and of the

Table 3.2 Important reactions in the high temperature chlorination of bastnasite (Brugger and Greinacher 1967)

Exothermic reactions

$RE_2O_3 + 3C + 3Cl_2 = 2RECl_3 + 3CO$
$CeO_2 + 2C + 1.5Cl_2 = CeCl_3 + 2CO$
$CaO + C + Cl_2 = CaCl_2 + CO$
$Fe_2O_3 + 3C + 3Cl_2 = 2FeCl_3 + 3CO$
$FeO + 2C + 1.5Cl_2 = FeCl_3 + 2CO$

Endothermic reactions

$SiO_2 + 2C + 2Cl_2 = SiCl_4 + 2CO$
$P_2O_5 + 3C + 1.5Cl_2 = POCl_3 + 3CO$
$P_2O_5 + 5C = 2P + 5CO$
$CO_2 + C = 2CO$

ore–carbon briquettes functioning as the electrical resistance. The furnace was designed for high thermal loads and had a capacity of 100 tons/month of rare earth chloride. It consumed chlorine at the rate of 0.9–1.0 kg/kg $RECl_3$ and the energy consumption was 0.4–0.6 kWh/kg $RECl_3$.

The process was described (Brugger and Greinacher 1967) as suitable for chlorination of not only bastnasite, but also ores like monazite, allanite, cerite, xenotime, euxenite, fergusonite, gadolinite, etc. When monazite or xenotime is chlorinated, regrinding of the ore before mixing with carbon and compacting is not necessary. The required temperature of chlorination is higher for silicates and phosphates than for oxidic ores or niobates and tantalates.

Brugger and Greinacher (1967) cite several advantages of the process. The economic advantages include simplicity, low labor component, small space requirement, and low capital costs. Energy costs are also very small. The process yields anhydrous chlorides of the rare earths without oxide or oxychloride content, clearly separated from impurities, at a very high specific throughput.

Chlorination of Baotau concentrates A process essentially similar to that described by Brugger and Grenaicher (1967) was used to chlorinate Baotau rare earth concentrate on a production scale. The concentrate consisted mainly of bastnasite and monazite, and certain other minerals that could be chlorinated in the presence of carbon at high temperatures.

A laboratory experiment has been described (Li et al. 1986) as follows. The rare earth concentrate (60 to 70% REO) was mixed with charcoal (ratio of concentrate to fixed carbon in charcoal = 1 : 0.065–0.070) and pressed into briquettes which were dried at 120–140°C and then chlorinated. Chlorination was carried out in a 90 mm dia and 300 mm long graphite reactor at 950–1100°C. The chlorides with lower boiling points, like $FeCl_3$, $SiCl_4$, $ThCl_4$ were removed from the high temperature zone with the off gas, while the low vapor pressure chlorides like $CaCl_2$, $BaCl_2$ remained with the rare earth chloride. By this process over 91% of the rare earths contained in the concentrate was recovered as the chloride. The chlorine consumption was 0.84 kg/kg $RECl_3$ and energy consumption was 1 kWh/kg $RECl_3$. Apparently the Chinese runs, which have been tried only on a laboratory scale, were slightly more economical in chlorine consumption and slightly more expensive in energy consumption as compared to the Goldschmidt runs. The chlorination product

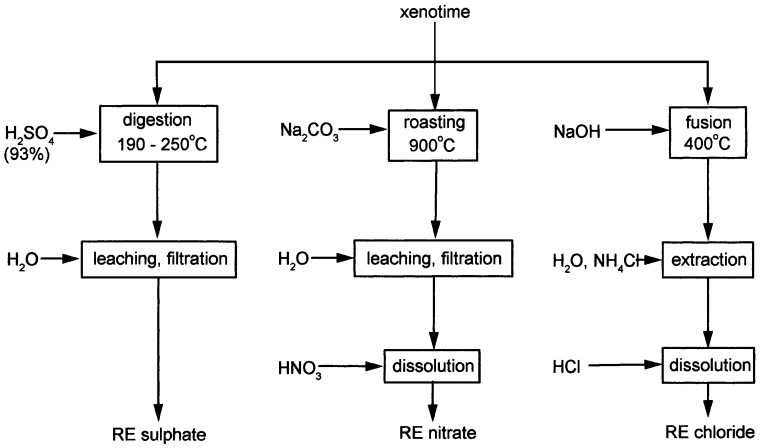

Figure 3.19 Chemical processing of xenotime.

consisted of 60% REO, 4–5% Ca+Ba, <0.2%, Fe < 4% F and <0.05% P. The rare earth chlorides have been used for electrowinning of metals.

3.4.4 Xenotime

The process options for treating xenotime are shown in Figure 3.19. The acid process for xenotime breakdown (Banks et al. 1959, Powell and Spedding 1959) involves attacking with concentrated (93%) sulfuric acid. The rare earth phosphates are converted to water soluble sulfates by leaching xenotime concentrates in conc. H_2SO_4 at 250–300°C for 1–2 h. Such leaching was uneconomical for concentrates containing less than 10% xenotime. These are treated by wetting the solids with sufficient acid and heating the mass at 300°C followed by water leaching. About 80–90% of the rare earths are solubilized. The recovery of rare earths by processes such as double sulfate precipitation is not possible because yttrium and the heavy rare earth sulfates are quite soluble. The sulfate solution is directly taken for separation. In the alternative process, the fine ground xenotime is treated by fusing it with molten caustic soda at 400°C (Topp 1965) or by mixing it with sodium carbonate and roasting at 900°C for several hours (Lever and Payne 1968). After leaching

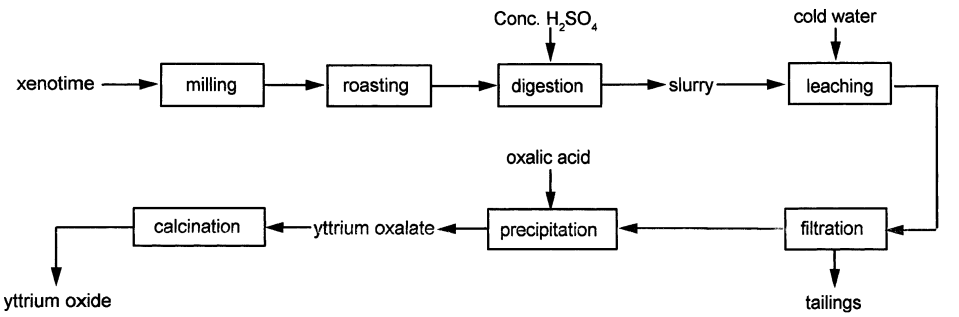

Figure 3.20 Xenotime processing in Malaysia.

out the phosphates, the hydroxide residue is dissolved in a minimum amount of hydrochloric acid and filtered from impurities such as silica, cassiterite, etc. The rare earths are recovered by precipitation as oxalates.

The xenotime processing plant of the Malaysian Rare Earth Corporation (MAREC) is located at Bukit Merah in Perak state, Malaysia. The process used in the plant for the production of yttrium oxide concentrate from xenotime is outlined (Sulaiman 1991) in Figure 3.20.

The xenotime is first milled to a required particle size and then roasted in a furnace. These operations ensure that good recovery is obtained in the next stage, which is sulfuric acid digestion of the roasted material. By sulfuric acid digestion, YPO_4 in the xenotime is converted to the water soluble sulfate. Cold water is used as the leachant for better recovery. Oxalic acid is added to the yttrium sulfate solution to precipitate yttrium oxalate. The final stage is the calcination of yttrium oxalate to the oxide.

The plant has a capacity to produce 200 tons of yttrium concentrate (60% Y_2O_3) per annum.

3.4.5 Elliot Lake Uranium Ore

The Elliot Lake uranium mines in Canada, upon demand, produce 60 to 70% REO concentrate from barren uranium leachate (Jackson and Christiansen 1993). At the Elliot Lake uranium mines, a large volume of barren liquor, relatively free from uranium but containing lanthanides and thorium, is generated. The liquor is generated from sulfuric acid leaching of uranium ores followed by removal of uranium from the filtered leach liquor by ion exchange. The minerals brannerite, uraninite, and uranothorite from which uranium was leached contain lanthanum, yttrium, ytterbium, cerium, praseodymium, neodymium, samarium, thorium, and lesser quantities of dysprosium and erbium. In the leaching process currently used, even though only about 20% of total rare earths in the ore is leached, approximately 75% of yttrium in the ore is leached along with uranium and thorium. Thus, after the removal of uranium by ion exchange, the barren liquor contains considerable amounts of yttrium and other rare earths, which can be recovered (Ritcey and Ashbrook 1979).

The barren acid solutions are treated with lime and air in Pachuka tanks to a pH of about 8.5. The resultant oxidized slurry is thickened. The thickener underflow is recovered for further treatment and the clear overflow is sent to the tailings. The underflow is acidified with H_2SO_4 to a pH of about 4.2 to redissolve yttrium and the rare earths and is filtered off from the iron, thorium, aluminum etc., in the solids. The rare earths are then precipitated with ammonia gas, thickened, and dried. The concentrate contains approximately 8–15% Y_2O_3 and 12–30% total REO, including yttrium.

3.4.6 Gadolinite

The processes for chemical treatment of gadolinite are outlined in Figure 3.21. The rare earths have been recovered from gadolinite by leaching the ground ore with nitric or hydrochloric acid and precipitating the rare earths as oxalates, thus effecting the separation from associated iron and beryllium (Foos and Wilhelm 1954). Concentrated sulfuric acid or a mixture of sodium hydroxide and sodium peroxide have also been used to attack the ore.

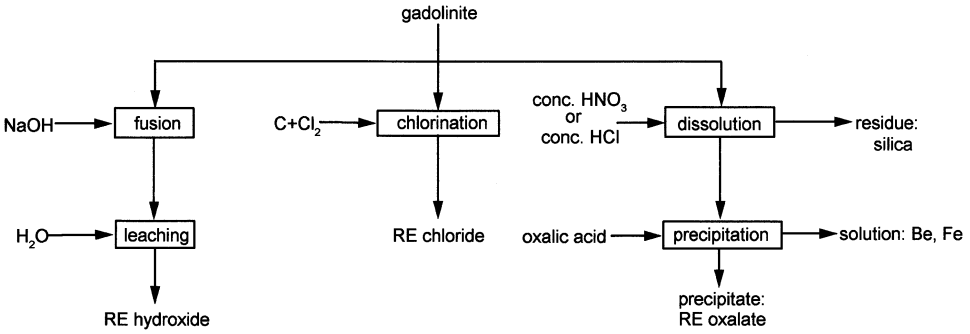

Figure 3.21 Chemical processing of gadolinite.

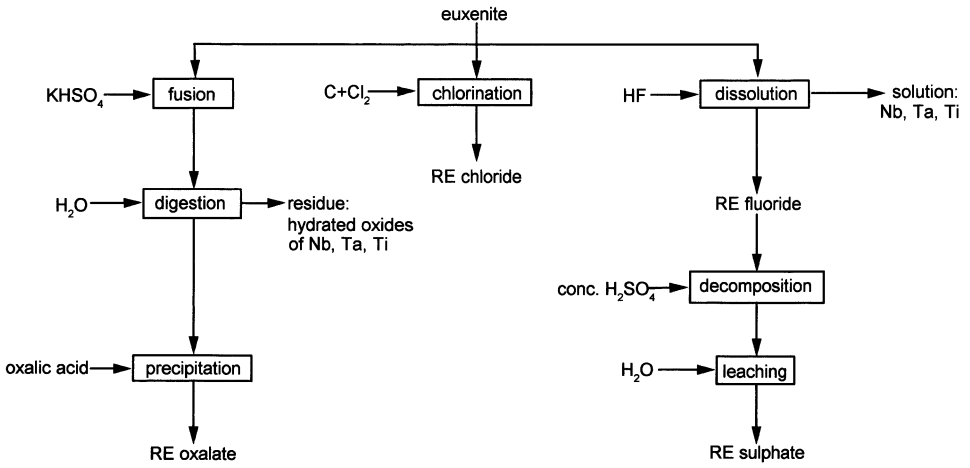

Figure 3.22 Chemical processing of euxenite.

3.4.7 Euxenite

Euxenite has been treated by reductive chlorination followed by distillation of the chlorides to separate rare earths, titanium, niobium, and tantalum fractions (Henderson et al. 1958). The processes for chemical treatment of euxenite are shown in Figure 3.22. Solvent extraction has also been used to remove tantalum–niobium chlorides and the rare earth metals from the chlorination residue. The ore is also amenable to treatment by fusion with ammonium bisulfate or caustic soda or by digestion with hydrofluoric or sulfuric acid or mixtures of the two (Shaw 1959, Shaw and Bauer 1959). The ore has also been processed by digestion in hot sodium hydroxide solution. The hydroxides of rare earths uranium, thorium, and iron formed are dissolved in diluted hydrochloric acid (Hedrick 1985). Soda ash is added to this solution to form a complex carbonate precipitate. The precipitate is leached with a dilute sulfuric acid to selectively solubilize the rare earths. From the leach liquor, rare earths are precipitated as oxalates by adding oxalic acid. Euxenite was considered as a potential future source of rare earths (Jackson and Christiansen 1993).

3.4.8 Loparite, Pyrochlore, Fergusonite, and Samarskite

Loparite is decomposed on an industrial scale by chlorination in the former Soviet Union. Pyrochlore can be processed to yield a niobium rich rare earth concentrate. The process described by Villani (1980) begins with digestion of pyrochlore ore in hydrofluoric acid, followed by solvent extraction of niobium by MIBK (methylisobutylketone). In another process, the ore is first digested with hot concentrated sulfuric acid. Niobium and rare earths are then selectively precipitated by gradual reduction of acid concentration and temperature (Charlot 1976).

Rare earths are recoverable from fergusonite and samarskite by a hot caustic digestion followed by an acid dissolution process. The process is similar to that described for euxenite.

3.4.9 Apatite

The apatite deposit at Phalaborwa in South Africa contains significant amounts of rare earth metals and is a feed material to a wet process phosphoric acid plant in the same locality. In the process for phosphoric acid production, the apatite concentrate is dissolved in a mixture of sulfuric acid and recycled dilute phosphoric acid. Bulk of the rare earth values, 70–85% of that contained in the feed, end up in the copious amount of phosphogypsum ($CaSO_4 \cdot 2H_2O$) formed in the dissolution reaction. The remainder of the rare earth values dissolve in the crude dilute phosphoric acid (27% P_2O_5) but eventually precipitate in the form of sludges that settle out when the dilute acid is concentrated to commercial grade (54% P_2O_5). These sludges consist mainly of calcium sulfate hemihydrate ($CaSO_4 \cdot 1/2H_2O$) but also 2–8% of rare earths (REO). The amount of sludge produced is very substantial (~10,000 t/a) at the Phalaborwa plant alone, and it represents a valuable source of the rare earth metals.

The sludge was washed and leached with dilute nitric acid to which calcium nitrate was added. Leaching was carried out in a mechanically agitated flat bottomed stainless steel pachuka, and over 85% of rare earths contained in them were solubilized. From the leach liquor that contains nitric acid, calcium nitrate, and added ammonium nitrate, the rare earths were recovered by solvent extraction and finally precipitated as rare earth oxalates from the strip solution. The oxalates were calcined in a rotary furnace to yield mixed rare earth oxide of 89–94% purity. Rare earth oxides have also been recovered from apatites in the former Soviet Union and Finland during the production of phosphoric acid for fertilizer. The ore is leached with nitric acid and from the leach liquor the silicic and fluorsilicic salts are precipitated by sodium nitrate. On partial neutralization of the leach liquor with ammonia, the rare earth phosphates are precipitated. From the phosphates, the rare earths are redissolved in nitric acid and are precipitated in a purer form as oxalates by the addition of oxalic acid.

In all the processes described, the products obtained after chemical processing of rare earth minerals contain the rare earths in essentially the same ratio in which they were originally present in the ore. This is because of the similar chemical behavior of the various rare earth elements in the reactions involved in these treatments. Operations such as double sulfate precipitation used for separating thorium result in partial rare earth separations in the two fractions, one enriched in the cerium group rare earths and the other enriched in the yttrium group rare earths. The separation of cerium is also accomplished during chemical

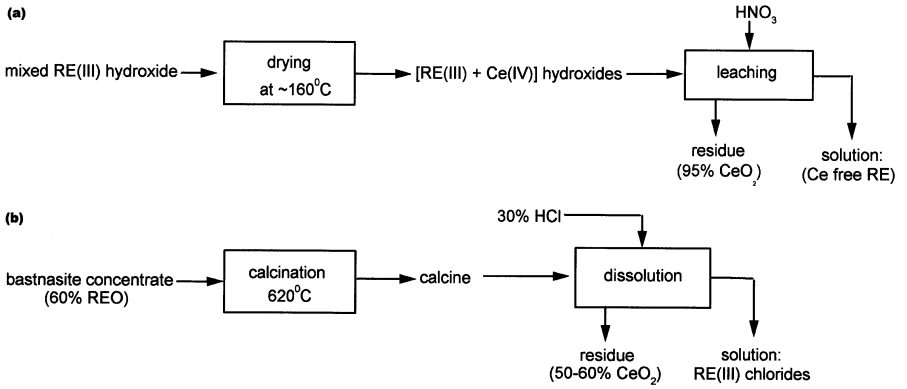

Figure 3.23 Separation of cerium by selective oxidation.

processes, involving its oxidation to Ce(IV). The subject of separation of rare earths is covered in the following section. Perhaps no other branch of rare earths extractive metallurgy has attracted so much attention and research effort as the separation of naturally occurring rare earth mixtures into pure individual compound intermediates.

3.5 SEPARATION PROCESSES

The various processes for separating individual rare earths from naturally occurring rare earth mixtures essentially utilize the small differences in basicity resulting from decrease in ionic radius from lanthanum to lutetium. The basicity differences influence the solubility of salts, the hydrolysis of ions, and the formation of complex species, and these properties form the basis of separation procedures by fractional crystallization, fractional precipitation, ion exchange, and solvent extraction. In addition to a trivalent oxidation state, Ce, Pr, and Tb can also occur in the tetravalent state, and Sm, Eu, and Yb also exhibit divalency. Selective oxidation or reduction of these elements is useful in effective separation because in the divalent and tetravalent states the elements exhibit markedly different chemical behavior compared to that in the trivalent state.

3.5.1 Selective Oxidation

The most abundant rare earth, cerium, can be separated relatively easily and early in the separation sequence. This simplifies the subsequent separation of the less abundant rare earths. Cerium is removed from the rare earths mixture after oxidation of naturally occurring Ce(III) to Ce(IV). This valence change occurs, for example, when bastnasite is heated in air at 650°C or when the rare earth hydroxides are dried in air at 120–130°C. In aqueous hydroxide suspensions, oxidation is effected by chlorination or electrolysis (Bauer et al. 1960, Douglas and Bauer 1959). An effective method of cerium removal from a complex lanthanides solution was suggested by an oxidation–precipitation process using ozone as the oxidizing agent. Once oxidized, Ce(IV) is separated (Bril 1964) from the trivalent components in the rare earth hydroxide–oxide mixtures either by selective

dissolution of trivalent species with dilute acid (Powell 1939) or by complete dissolution in concentrated acid followed by selective precipitation. The precipitation of even 99.8% pure ceric salts does not completely remove cerium from solution and additional cerium removal steps are necessary to prepare rare earths free from cerium. A process considered particularly effective for cerium recovery from any acid leachate solution containing rare earths uses air oxidation and solvent extraction as shown in Figure 3.23. A number of reagents have been studied for the solvent extraction of Ce(IV) nitrate and TBP is the preferred extractant for large scale operations (Bauer et al. 1960, Douglas and Bauer 1959).

Unlike Ce(IV), both Pr(IV) and Tb(IV) are not stable in aqueous solution. The higher oxides PrO_2 and Tb_4O_7 precipitate when a solution of rare earth hydroxides in fused potassium hydroxide is oxidized either by anodic oxygen or by potassium chlorate. The oxides are recovered by decantation or by dissolving away the melt.

3.5.2 Selective Reduction

Samarium, europium, and ytterbium can be easily separated from the trivalent rare earths mixture after reducing them to a divalent state. Unlike cerium, these elements are much less abundant, and separation using reduction is carried out only after they have been enriched by other procedures. The first application of selective reduction for the separation of a rare earth was by Yntema (1930). Using a mercury cathode he electrolytically reduced Eu(III) to Eu(II). Lithium amalgam electrodes were used for separation of Sm from Eu, and Yb by selective reduction. Recently, the continuous electrolytic reduction of Eu(III) to Eu(II) in rare earth chloride solutions derived from monazite was demonstrated in a redox flow cell. Marsh (1942, 1943, 1957) had separated samarium, europium, and ytterbium from rare earth mixtures in a buffered acetate solution by reductive extraction into dilute sodium amalgam. The separation is clear and complete and the method is amenable to counter current operation. It has been used commercially (Lever and Payne 1968) for the recovery of samarium and ytterbium. The recovery of pure europium from such amalgams is achieved by treatment with cold concentrated hydrochloric acid, which causes precipitation of the sparingly soluble $EuCl_2 \cdot 2H_2O$. Both Sm and Yb are rapidly oxidized to very soluble trihalides, whereas the oxidation of Eu proceeds very slowly in the absence of oxygen.

On an industrial scale, the method developed by McCoy (1936, 1941) has found acceptance. In a chloride solution, Eu(III) is reduced to Eu(II) by zinc, and the divalent Eu is recovered as sulfate. The process is shown in Figure 3.24. Zinc does not reduce Sm or Yb. When Eu is present only in a low concentration, $EuSO_4$ is recovered by coprecipitation with $BaSO_4$. The mixed sulfate precipitate is washed with an oxidizing acid solution to reoxidize and dissolve Eu(III), leaving $BaSO_4$ undissolved. The purity of Eu recovered in this process can be improved to 99.9% by precipitating $EuCl_2 \cdot 2H_2O$ from concentrated HCl. Recently, the separation of Eu has been achieved by photochemical means.

Europium can be separated from other rare earths by a photochemical reduction to the divalent stage followed by precipitation of the divalent europium as sulfate or chloride (Shastri et al. 1988). The photochemical separation was investigated using a low pressure mercury lamp with no filter at 185 nm, and with a Vycor filter at 254 nm and an ArF excimer laser operating at 193 nm. Equimolar mixtures (0.01 M) of binary and ternary lanthanide perchlorates and 0.05 M K_2SO_4 in 10% isopropanol were irradiated. The separation factor for Eu/RE varied from 1 for Eu/Pr and >200 for Eu/Tm. The process is represented by

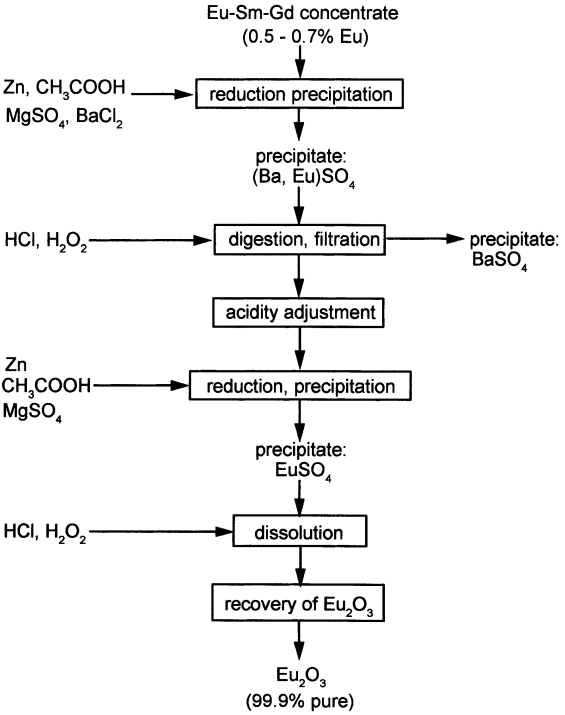

Figure 3.24 Separation of europium by selective reduction.

$$Eu^{3+}(H_2O) \xrightarrow{190\ nm} Eu^{2+} + H^+ + {}^{\cdot}OH$$

The OH radical was scavenged by isopropanol as

$$(CH_3)_2CHOH + {}^{\cdot}OH \rightarrow H_2O + (CH_2)_2{\cdot}COH$$

The sulfate ion present in solution causes precipitation of Eu^{2+} as $EuSO_4$. Besides, the presence of sulfate ions makes possible the shift of the charge transfer band to the longer wavelength light at 240 nm. Eu^{2+} is also reduced by the organic radicals by the reaction

$$(CH_3)_2{\cdot}COH + Eu^{3+} \rightarrow Eu^{2+} + H^+ + (CH_3)_2C{=}O$$

The precipitate of $EuSO_4$ is formed homogeneously during the photolysis.

Qui et al. (1991) studied the separation of Eu from a solution mixture of $SmCl_3$, $EuCl_3$ and $GdCl_3$, in a rare earth saturated ethanol–isopropanol system. The photo reduction of Eu was carried out with a high pressure mercury lamp. From the alcohol mixture, $EuCl_2$ was produced by photoreduction and precipitation. The precipitated $EuCl_2$ was 92% pure and the yield of Eu(II) was 95%. The whole separation process is represented as follows:

Dissolution and complexion

$$(Sm, Eu, Gd)Cl_3{\cdot}nH_2O + 3EtOH \rightarrow (Sm, Eu, Gd)Cl_3{\cdot}3EtOH + nH_2O$$
$$(Sm, Eu, Gd)Cl_3{\cdot}nH_2O + 3(isopropanol) \rightarrow (Sm, Eu, Gd){\cdot}Cl_3{\cdot}3(isopropanol) + nH_2O$$

Photoexcitation

$$(Sm, Eu, Gd)Cl_3 \cdot nH_2O + 3EtOH \xrightarrow{h\nu} (Sm, Eu, Gd)Cl_3 \cdot 3EtOH$$

$$(Sm, Eu, Gd)Cl_3 \cdot nH_2O + 3(isopropanol) \xrightarrow{h\nu} (Sm, Eu, Gd)Cl_3 \cdot 3(isopropanol)$$

Electron transition

$EuCl_3 \cdot 3EtOH \rightarrow EuCl_2 + 2EtOH$ + organic oxidation products

$EuCl_3 \cdot 3(isopropanol) \rightarrow EuCl_2 + 2(isopropanol)$ + organic oxidation products.

Even though Sm(III), Eu(III), and Gd(III) are all excited during photoreduction, only the reduction of Eu(III)–Eu(II) is possible and occurs because the reduction potential of Sm(III) and Gd(III) are more negative than that of Eu(III)/Eu(II).

Precipitation

The solubility of $EuCl_2$ in an ethanol–isopropanol mixture is low. This leads to the precipitation and hence separation of $EuCl_2$ from the other rare earths in the mixture. In order to precipitate $EuCl_2$, the water content of the alcohol mixture must be kept low.

A method of separating samarium, europium, and ytterbium is based on the fact that Sm, Eu, and Yb metals cannot be obtained by metallothermic reduction of their halides. During the reduction of a mixture of anhydrous rare earth halides with calcium, the halides of Sm, Eu, and Yb are not reduced and remain in the slag from which they are subsequently separated.

Samarium, which only reduces to the divalent state, also accumulates in the fused salt slag when the mixed rare earth chloride is electrolytically reduced to misch metal. The slag has been an inexpensive source of samarium for some time (Gschneidner and Daane 1988).

Before 1950, in addition to the separation procedures based on selective oxidation or reduction, the methods based on fractional crystallization and fractional precipitation were widely used for rare earth separations. The considerable effort spanning over 100 years that was applied to the problem of separation using these techniques has been extensively reviewed (Little 1921, Yost et al. 1947, Kremers 1953, Moeller 1963).

3.5.3 Fractional Crystallization

In fractional crystallization, a part of the salt in solution is precipitated by a change in temperature or by evaporation of a saturated solution. If the solubility of various components in the solution differ, the composition of the crystal crop will be different from that of the original solution. While the crystal crop becomes enriched in the less soluble component, simultaneously, the more soluble components will be enriched in the liquor.

More than half a dozen salts and double salts have been used for the separation of rare earth elements by fractional crystallization. This method has been considered as the best of the classical separation procedures for producing individual elements in high purity (Parker and Baroch 1971). The most suitable compounds have been the double ammonium nitrates $RE(NO_3)_3 \cdot 2NH_4NO_3 \cdot 4H_2O$ for the removal of lanthanum and separation of praseodymium and neodymium, and the double magnesium nitrates $2RE(NO_3)_3 \cdot 3Mg(NO_3)_2 \cdot 24H_2O$ for obtaining concentrates containing the middle rare earths samarium, europium, and gadolinium. The double manganese nitrates $2RE(NO_3)_3 \cdot 3Mn(NO_3)_2 \cdot 24H_2O$ have also been used in the separation of the ceric group. In the separation of the yttric group, the bromates $RE(BrO_3)_3 \cdot 9H_2O$ and ethyl sulfates $RE(C_2H_5SO_4)_3 \cdot 9H_2O$ have been found useful.

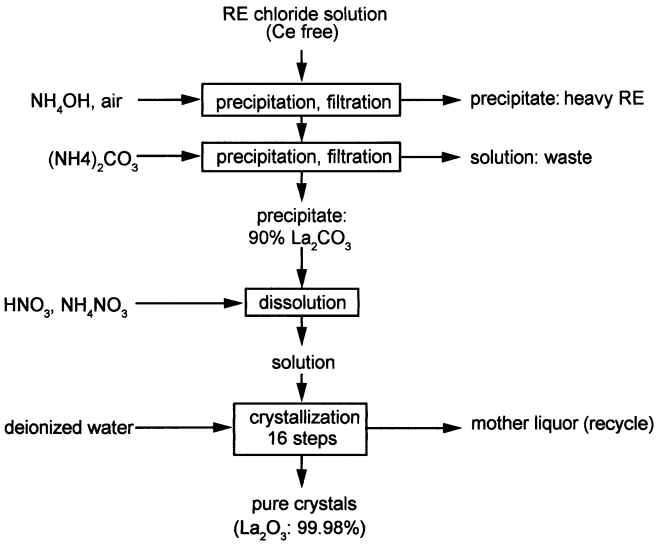

Figure 3.25 Separation of lanthanum by fractional crystallization.

Erbium, thulium, lutetium, and yttrium have been separated using a rare earth hexa-antipyrine iodide salt. A sodium rare earth EDTA salt has also been useful (Marsh 1955) for separating gadolinium, terbium, dysprosium, and yttrium by fractional crystallization. The separation by fractional crystallization of these salts has been used commercially (Lever and Payne 1968) to separate and raise to 99% purity, oxides of Gd, Tb, and Dy.

The lanthanum end of the series, where the differences in cationic radius are the greatest, is the most amenable for separation by fractional crystallization. Lanthanum forms the least soluble double nitrate. Starting from a cerium-free rare earth concentrate, a procedure for separating lanthanum in high purity involves the steps shown in Figure 3.25. From the rare earth concentrate solution, 90% La_2O_3 can be precipitated out using an air–ammonia mixture. From this product high purity lanthanum is then obtained by purification using countercurrent crystallization of the double nitrates $RE(NO_3)_2 \cdot 2NH_4NO_3 \cdot 4H_2O$.

The fractional crystallization is particularly slow and tedious for the heavy rare earths and in the Sm(III)–Gd(III) region, because the property difference between rare earths decreases as the atomic number increases. For example, a bromate salt of a thulium fraction recrystallized 15,000 times still contained ytterbium and erbium. The rare earth bromate had to be crystallized every day for 4 years to obtain good holmium.

3.5.4 Fractional Precipitation

Fractional precipitation denotes the removal of part of the rare earths from solution by the addition of a chemical reagent to form a new, less soluble compound. The rare earths still remaining in solution are recovered either by further precipitation as the same compound or by complete precipitation as the oxalate, hydroxide, or other compound.

As with fractional crystallization, a number of compounds have been studied for the separation of rare earths by fractional precipitation. The hydroxides and double sulfate, in particular, have been widely used. Double chromate precipitation has also been used to

separate rare earths from yttrium. Among the rare earth elements, hydrolysis occurs least extensively with lanthanum, which remains mostly in solution. For large scale operation, ammonia is used for carrying out hydroxide precipitation from the nitrate or chloride (Berber et al. 1960) solutions. The preliminary enrichment of yttrium-group rare earths and the extraction of yttrium from yttrium concentrates are also possible by this method. Lever and Payne (1968) have used fractional precipitation of basic nitrates to separate a high proportion of yttrium from a heavy rare earth concentrate.

The double sulfates $RE_2(SO4)_3 \cdot Na_2SO_4 \cdot nH_2O$ are usually precipitated by the addition of sodium sulfate to the rare earth solution. The elements La, Ce, Pr, Nd, and Sm form sparingly soluble double sulfates where as those of Ho, Er, Tm, Yb, Lu, and Y are soluble; Eu, Gd, and Dy form double sulfates of intermediate solubility. Generally, the use of this method is confined to crude separation of the rare earth mixture into three groups. However, the elements La and Y can also be readily separated.

Yttrium (Powell 1961) exhibits interesting behavior in fractional precipitation and is amenable to purification by a combination of hydroxide and double sulfate precipitations. The separation factor, however, is very small. In double sulfate precipitation, yttrium behaves like holmium, and in basic precipitation it behaves like neodymium. By the first method, the elements La–Dy can be removed and in the second method the elements Eu–Lu are removed.

A method in which the mixture to be separated was partially complexed with EDTA and the uncomplexed part was precipitated with sodium sulfate was also used. Earlier, a similar method had been proposed using oxalic acid as precipitating agent and nitrilotriacetic acid as the complexing agent.

Double chromates of rare earths with ammonium or potassium, precipitated from chloride solutions have been found suitable for the industrial production of high purity yttrium. For the separation of the heavy rare earths a method based on fractional thermal decomposition of fused nitrates has also been investigated.

In the years preceding 1947, the methods outlined thus far were the techniques available for separating the rare earths. For most of the rare earths elements, these procedures were relatively inefficient and laborious. The purity of the end products obtained was also not comparable with that subsequently achieved in the modern methods of ion exchange and solvent extraction, which have dominated the commercial separation of rare earths starting in the 1950s.

3.5.5 Ion Exchange

Method An ion exchange resin or ion exchanger can be considered as an ionic salt in which one of the ions is attached to an insoluble organic matrix (Kleber and Love 1963). In an anion exchange resin or anion exchanger the charge on the ion is negative. Similarly, the charge on the ion is positive in a cation exchanger.

When the ion exchange resin comes into contact with a salt solution, the mobile ion in the resin matrix may be displaced. Generally, (1) an ion of higher charge displaces an ion of lower charge, (2) between similarly charged ions, that with a larger radius displaces the one with the smaller radius, and (3) the displacement occurs according to the law of mass action.

The technique of ion exchange essentially involves the adsorption stage in which the ions from the solution get loaded or adsorbed on the exchanger and an elution stage during

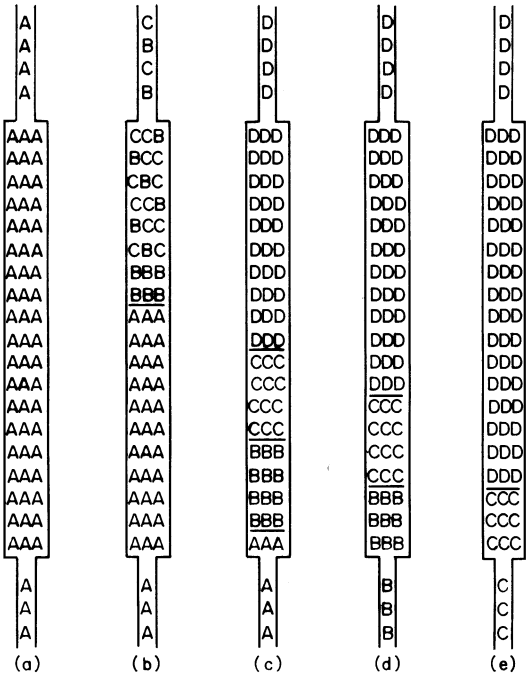

Figure 3.26 Simplified representation of events in displacement chromatography. (a) Column charged initially with A ions. (b) Column charged with a mixture of B and C ions — the order of increasing affinity is A, B, C; since C has greater affinity for the resin than B, some separation of B and C occurs during loading. (c) Bands of B and C being developed with an eluant containing D ions which are more strongly attracted to the resin than A, B or C ions. (d) Developed band of B ions passing off the column. (e) Developed band of C ions passing off the column (Powell 1961).

which, by a change of conditions, the ions desorb from the exchanger and enter into solution. In either step, an exchange between the ions in solution and those on the exchanger occurs. When more than one anion or cation is present in the solution and if certain selectivity is exhibited in these exchanges, the ion exchange process becomes an ion exchange separation.

According to the distribution law or partition law (Kleber and Love 1963) under equilibrium conditions, when a substance is distributed between two phases, the ratio of the concentration of the substance in two phases will have a constant value. For instance if the equilibrium concentration of the substance A in phase 1 is C_{A1} and in phase 2 is C_{A2} then DA, called the distribution coefficient, is

$$D_A = \frac{C_{A1}}{C_{A2}}$$

If there is another substance B which is similarly distributed, then

$$D_B = \frac{C_{B1}}{C_{B2}}$$

Usually the values of D_A and D_B are different. Comparison of D_A and D_B values gives information as to which of the two substances concentrates preferably, for example, in phase 1. In ion exchange, phase 1 can be taken as the resin phase, and in solvent extraction phase 1 can be taken as the organic phase. The other phase, phase 2, is the aqueous phase in both techniques. The ratio of the distribution coefficients, α,

$$\alpha_B^A = \frac{D_A}{D_B}$$

is called the separation factor. If α is close to 1, no separation can be achieved and separation is achievable if α is either very much more or less than unity.

The term "ion exchange chromatography" was used (Powell 1961) to describe the technique for separating mixtures of ions based on sorption (adsorption) of the ions on a suitable ion exchanger followed by differential displacement of the individual ions with an eluant. Two kinds of behaviors were observed. One has been named "displacement chromatography" and the other "elution chromatography."

The events in displacement chromatography are shown in Figure 3.26. Two ionic species B and C are sorbed on top of an exchange bed on which was loaded originally a third ionic species A, which has less affinity for the exchanger than either B or C. When this system is eluted with a simple salt solution containing ion D, which has greater affinity for the resin than even B and C, each ion tends to displace that having lesser affinity and banding develops as shown in Figure 3.26. The sequence in which the ions come out of the exchanger is shown (Powell 1961) in Figure 3.27. There is separation.

In elution chromatography, the ion sorbed initially and the eluant ion are usually the same. The eluant ion has a lesser affinity for the resin than the ions being separated. The equivalent concentration of the ions being eluted is less than the concentration of the eluant ion. Thus the eluant ion displaces the sorbed ions inefficiently and overruns them. Under the influence of the eluant and having different affinities for the resin, the sorbed ions progress down the exchange beds at different rates. The type of elution curve (Powell 1961) shown in Figure 3.28 is then obtained.

Application The first attempt on ion exchange separation of rare earths dates back to the late nineteenth century, when it was demonstrated in 1893 that yttrium and gadolinium

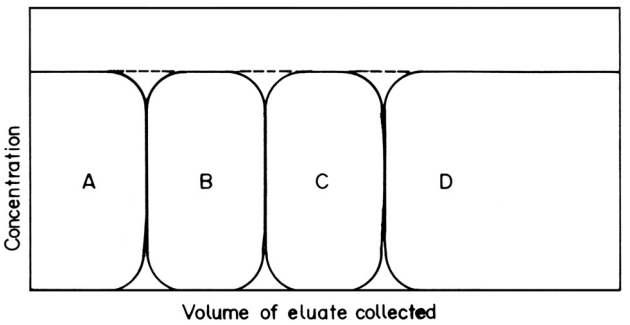

Figure 3.27 Typical elution plot in displacement chromatography. Some overlapping of bands is inherent, but regions of considerable extent are obtained within which the equivalent concentration of each ion is equal to the equivalent concentration of the driving ion in the eluant (Powell 1961).

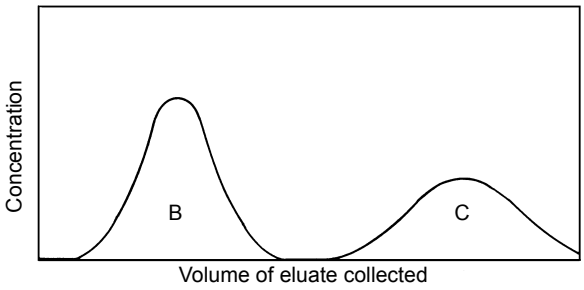

Figure 3.28 Typical elution plot obtained by elution chromatography. Eluent ions overrun and accompany the B band and the C band as they issue from the column (Powell 1961).

could be purified by adsorption on activated carbon. After over a half-century gap it was shown that the simple procedure of adsorption of tripositive rare earth ions on an ion exchanger and their removal by elution with sodium chloride effected no greater separation than fractional crystallization or precipitation. This was subsequently found true for most cation exchange media. While there is a decrease in the affinity of the rare earths for the resin from La(III) to Lu(III); i.e., as the size of the hydrated ion is decreased, the affinities of the various rare earth elements for the resin are not sufficiently different to result in satisfactory separation because the separation factors for adjacent rare earths undergoing simple cation exchange are close to unity.

This situation was changed by the use of complexing agents to enhance separation factors. The successful separation of rare earths by ion exchange was subsequently demonstrated at Ames and at Oak Ridge National Laboratory by using a citric acid–ammonium citrate eluant at regulated pH and was reported in a series of papers in the *Journal of the American Chemical Society* (Ketelle and Boyd 1947). The separation was achieved as a result of the different stabilities of the citrate complexes formed by the individual rare earths in the mixture (Powell and Spedding 1959, 1956, Powell 1964, Powell 1979). The citrate elution has been performed successfully under a wide range of conditions (Powell 1964) and has proved effective for the separation of up to several hundred grams each of the light rare earth elements. The differences between complex formation constants of adjacent heavy rare earths are not as large as those between the light rare earths, and the citrate process has not been very successful in separating bulk quantities of heavy rare earths. The extreme dilution of the eluant was also an economic disadvantage.

Besides the citrate, a number of eluting agents and process conditions have been actively evaluated, and they have been reviewed by Powell (1961, 1964, 1979). The use of amino polyacetic acids such as NTA and ethylene diamine tetra acetic acid (EDTA) as eluants was investigated but was unsuccessful due to the problem of aqueous insolubility. This and many other limitations of the elution process were solved in the band displacement technique developed by Spedding et al. (1954), using the resin in a special cation state. Compared with citrates, complexing agents such as EDTA and 2-hydroxy ethylene diamine triacetic acid (HEDTA) not only form 1:1 chelates of greater stability over wider pH ranges, but also give greater differences in stability between adjacent rare earths and allow higher concentrations to be used. Commercially, the most useful complexing agents are EDTA and HEDTA. The acids diethylene triamine pentacetic acid (DTPA) and 1,2-diamine cyclohexane tetraacetic acid (DCTA) also provide high separation factors

(Powell 1964, 1979). Powell (1979) has discussed the separation potential of each of these chelating agents and ranks EDTA and HEDTA as the most useful. EDTA can effectively separate all of the rare earths and yttrium from each other with the exception of Eu–Gd and Yb–Lu pairs because of the small difference in the separation factor and adverse kinetic effects, respectively. The Dy–Y separation is also very slow with EDTA because of the small difference in the stability of the two complexes. There is, however, a large difference between the stabilities of HEDTA–Dy and HEDTA–Y complexes, and so this pair can be separated by HEDTA. Besides, HEDTA is particularly useful in the separation of the Tm–Yb–Lu fraction, and good separations are possible with either La–Ce–Pr–Nd–Y–Sm or Ho–Er–Tm–Yb–Lu mixtures. The separation of Sm–Eu–Gd–Tb–Dy–Ho mixture with HEDTA is poor because of small differences in chelate stabilities. An advantage of HEDTA elution is that hydrogen ion retaining beds can be used because H_3(HEDTA) is considerably more soluble in cold water than H_4(EDTA). This permits easy recycling of reagent. The HEDTA complexes of heavy rare earths such as Tm, Yb, and Lu show only limited solubility and restrict the eluant concentration.

For the rapid separation of yttrium, a two-stage procedure that makes use of the different positions of yttrium in the elution sequence with different chelating agents was reported. In the EDTA system, yttrium elutes between Tb and Dy, whereas in HEDTA it elutes between Nd and Sm. The heavy rare earths are first separated by elution with HEDTA leaving yttrium in the Nd fraction. This fraction is then eluted with EDTA to separate yttrium from neodymium.

Temperature plays a crucial part in ion exchange separations. Kettele and Boyd (1947) first reported the shifting in the position of yttrium during elutions with 5% citrate. This was followed by investigations (Lindstrom and Winget 1962) on elutions at 87–90°C with citrate, lactate, and also EDTA, particularly for the separation of Y, Sm, Eu, and Tm. Lindstrom and Winget (1962) showed that the hydrogen ion could be used as retaining iron in rare earth separations with EDTA if the system is operated at 90–95°C when H_4(EDTA) becomes more soluble. Powell (1964, 1979) pointed out several other advantages of operation at 92°C. These include improved HETP (height equivalent of a theoretical plate) values and an increase in Gd–Eu and Eu–Sm separation factors. At all temperatures with EDTA, Y elutes between Tb and Dy, but with an increase in temperature to 92°C, Tb separation improves and there is a decrease in the Dy–Y separation. The rise in temperature also makes EDTA elution more effective for rare earth separation from non rare earth impurities, as, for example, in the case of the Tb–Pb–Yb–Lu mixture, which is difficult to separate at room temperature.

As pointed out above, HEDTA gives poor separation of the elements Sm–Ho at room temperature. A much better separation becomes possible at 92°C because of improvement in the adjacent element separation factor with rise in temperature (Powell 1979). The solubilities of species Tm(HEDTA), Yb(HEDTA), and Lu(HEDTA) increase with an increase in temperature, and eluant concentrations up to 0.072 M have been successfully used at 92°C compared with the maximum concentration of only 0.018 M at room temperature. In HEDTA elutions, there is a considerable shift in the position of yttrium with change in temperature (Morton and James 1967). The isolation of yttrium on a large scale as a result of this shift has been studied. Powell (1979) has also pointed out that the poor kinetics observed in ion exchange elution with DTPA could be countered to some extent by an increase in temperature.

The development of band displacement with ammonium ethylene diamine tetraacetate as the complexing agent established ion exchange as the main commercial process for rare

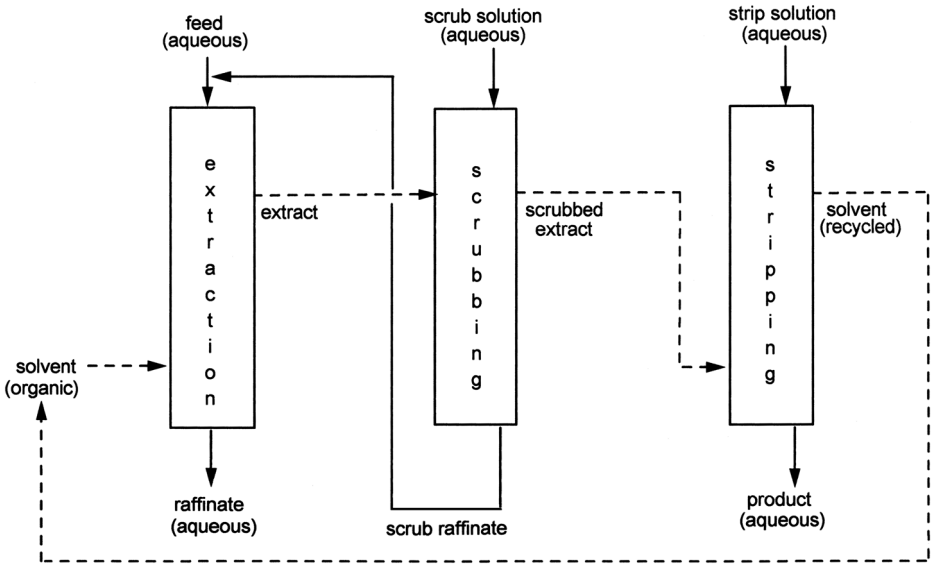

Figure 3.29 Typical solvent extraction flowsheet.

earth separation from the mid-1950s. The fact that it is feasible to separate a mixture of 15 rare earths into components exceeding 99.99% purity in one pass through the system and that the process can be scaled up to multi-tonne quantities, with possibilities of recovering and recycling water, and retaining ion and complexant, has led to the continued commercial use of ion exchange even after the entry of solvent extraction in the field. A major limitation of the band displacement technique or of displacement ion exchange chromatography is that the technique is inherently a batch process. Taniguchi et al. (1988) have succeeded in adopting fixed column band displacement chromatography to the continuous annular chromatograph (CAC). This technique, called continuous displacement chromatography (CDC), combines the processing capabilities of fixed column batch displacement chromatography with continuous operation of CAC and is applicable to any displacement chromatography separation that can be performed using conventional batch fixed column chromatography.

3.5.6 Solvent Extraction

Method The separation of rare earths by solvent extraction depends upon the preferential distribution of individual rare earths (either in the cationic form or as complex anions or as a neutral species) between two immiscible liquid phases that are in contact with each other. One of the liquid phases is an aqueous solution and the other is a non-aqueous phase in the organic phase. The expressions given for the distribution coefficient and separation factor, earlier in connection with ion exchange separation, can also be used for solvent extraction separation also. In ion exchange, phase 1 was taken as the resin phase and in solvent extraction, phase 1 can be taken as the organic phase. Phase 2 is the aqueous phase in both cases.

There are many advantages to using solvent extraction as the process for rare earth separation. One of them is that the rare earth loading in the solvent/extractant can be very high (~180 g REO/L). Therefore aqueous solutions with concentrations of 100–140 g

REO/L can be used. These make the equipment required for the process very compact (McGill 1993).

The organic phase used in solvent extraction usually consists of two or more substances. The extractant proper is responsible for collecting the rare earth species into the organic phase, however, the extractant is usually too viscous to be used in a practical system. It is dissolved in a suitable solvent to ensure a good contact with the aqueous phase. The solvents are kerosene and certain aromatics. A substance known as a modifier is also usually added to the organic phase to improve the hydrodynamics of the system.

The schematic of the solvent extraction process (Shibata 1991) is shown in Figure 3.29. Usually the transfer of metal ions from the aqueous to the organic phase does not occur completely in one contact. Multiple contacts are necessary. This also holds true for scrubbing (contacting the loaded organic phase with an aqueous solution to collect back the impurities extracted by the solvent) and stripping (contacting the scrubbed organic phase with an aqueous solution to recover the main extracted species from the organic phase, back to the aqueous phase).

The beginning of solvent extraction separation of rare earths was made in the 1930s by the observations of Hopkins and Quill (1933) and a few years later by Fischer et al (1937). They found differences in the distribution of various rare earth chlorides between water and partially miscible alcohols and ketones. Appleton and Selwood (1941) found a separation factor of 1.06 for the partition of lanthanum, neodymium thiocyanate between water and *n*-butyl alcohol and suggested that a continuous counter current extraction might be effective for separations. Higher separation factors of 1.29–1.55 depending on experimental conditions were obtained for the lanthanum–neodymium pair by Templeton and Peterson (1948), Templeton (1949) for the distribution of the nitrates between water and *n*-hexyl alcohol. The important observation that Ce(IV) can be separated readily and completely from the trivalent cations in an aqueous nitric acid solution by extraction with tributyl phosphate (TBP), first made by Warf (1949) marked the beginning of practical application of solvent extraction to rare earth separations. The TBP extraction of Ce(IV) was later investigated by Bauer (1959). A flowsheet for the purification of cerium and recovery of cerium nitrate by TBP extraction is given in Fig. 3.30. Cerium(IV) is stripped from the organic phase best by its reduction to cerium(III) using, for example, hydrogen peroxide (Warf 1949).

$$2[Ce(NO_3)_4(TBP)_2]_{org} + [H_2O_2]_{aq} = 2[Ce^{3+}]_{aq} + 8[NO_3^-]_{aq} + 2[H^+]_{aq} + O_2 + 4[TBP]_{org}$$

In such processes cerium dioxide products of high purity (>99.99%) are obtained from the strip liquors. The extractability of rare earths with TBP from concentrated hydrochloric and nitric acid solutions has been studied at Argonne National Laboratory (Peppard et al. 1953, 1958). The studies showed that extractions with TBP are more effective in nitrate systems and that the TBP– nitric acid system could be used to separate the trivalent rare earths from one another. In 1953 Oak Ridge National Laboratory isolated the first kilogram of pure Gd_2O_3 (98% Gd_2O_3) by using TBP–nitric acid solvent extraction using a mixed rare earth feed containing 25% Gd_2O_3 (Weaver et al. 1953). Using a similar technique, Weaver (1974) obtained better than 98% pure Sm_2O_3. The separation of rare earths from monazite using TBP (Ritcey and Pouskouleli 1987) was investigated by Bochinski et al. (1953, 1958). Foos and Wilhelm (1954) extended this work to study the separation of yttrium and heavy rare earths. A complete scheme for the separation of all the rare earths by solvent extraction was proposed by Callow (1967). However, the separation of rare earths beyond terbium with TBP has been difficult (Powell 1979).

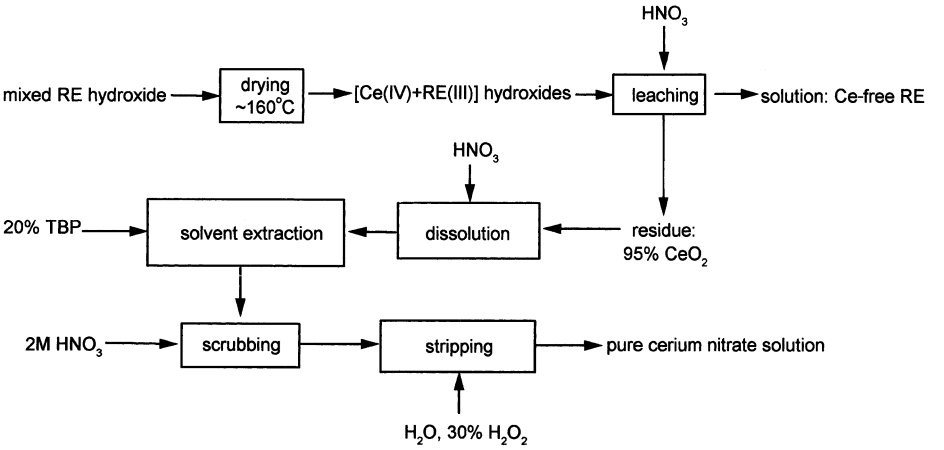

Figure 3.30 Separation and purification of cerium.

Peppard et al. (1957) first suggested the use of HDEHP for rare earth separations. HDEHP may be used either in chloride or sulfate systems both for obtaining rare earth concentrates from complex mixtures and to isolate individual rare earths in high purity. 99.8% pure lanthanum oxide was obtained using HDEHP in a 14-stage countercurrent extraction from a didymium chloride feed containing 45% La_2O_3, 35% Nd_2O_3, 10% Pr_6O_{11}, and 5% Sm_2O_3. By selective stripping of a preloaded solvent, Bauer and Lindstrom (1971) recovered >99% pure samarium oxide. The organic solvent (1 M HDEHP in kerosene) was loaded with a RE mixture 60% in Sm_2O_3, and the aqueous scrubbing solution contained 1.5% HCl and 20% NH_4Cl.

Many amines have also been examined for use in rare earth separations. Of these, tertiary amine extraction has received particular attention. An euxenite concentrate containing 47% yttria was processed using tri-*n*-butyl-amine solvent in 3-methyl-2-butanone and an aqueous phase of 8 M HNO_3 (Gruzensky and Engel 1959). The product obtained was 83% yttrium oxide. Other amine types such as tri-*iso*-octylamine (TIOA), methyl-dioctyl-amine (MDOA), dodecyl-amine (DDA) and alamine have also been used for the separation of rare earths (Rice and Stone 1962).

These early and experimental works were followed by many investigations in later years, and solvent extraction developed as a major technique for rare earths separation. The solvent extraction of rare earths has been reviewed by Peppard (1964), Weaver (1974), Sherrington (1983), Preston and Du Preez (1990), and Bautista (1995).

Numerous extractants have been used for analytical or experimental separation of rare earths from one another; however, only a relatively few are used in industrial practice. They include cation exchange extractants such as organophosphorus acids and carboxylic acids, neutral extractants such as tri-*n*-butyl-phosphate, and anion exchange extractants such as the amines. Among these, the primary industrial extractants used for the separation of rare earths by solvent extraction are di-2-ethyl-hexyl-phosphoric acid (HDEHP), 2-ethyl-hexyl-2-ethyl-hexyl-phosphonic acid (EHEHPA), tributyl-phosphate (TBP), versatic acid, versatic 10, and Aliquat 336. These are listed in Table 3.3. Even though considerable published information is available on the extraction behavior of these solvents, the details of solvent extraction processes actually practiced in the industry are well-kept secrets.

Table 3.3 Commercially used extractants for rare earth separation (Thakur 2000)

Extractant	Molecular formula
Tributyl-phosphate (TBP)	$(C_4H_9O)_3PO$
Di-2-ethyl-hexyl-phosphoric acid (HDEHP)	$(C_8H_{17}O)_2POOH$
2-ethyl-hexyl-2-ethyl-hexyl-phosphonic acid (EHEHPA) Trade names: PC88A, Ionquest 801	$(C_8H_{17}O)C_8H_{17}$ POOH
Versatic acid Versatic 10	$(R_1.R_2.R_3).C.COOH$ $C_9H_{19}C.COOH$; $(R_1.R_2.R_3 = C_8H_{19})$
Trialkyl-methyl-ammonium-chloride Trade name: Aliquat 336	$R_3CH_3N^+Cl^-$

Organophosphorus acids Monobasic organophosphorus acids include the well-known phosphoric, phosphonic, and phosphinic acids. Di-2-ethyl-hexyl-phosphoric acid, HDEHP, is the most investigated and most readily available organophosphorus acid. The organophosphorus acids are typical cation exchange extractants. The extraction by cation exchange involves most commonly the displacement of a hydrogen ion from the extractant by the extracted metal, resulting in the formation of an electrically neutral, organic soluble complex. In organic solvents of low polarity, the organophosphorus acids exist in the dimeric form H_2A_2, and the extraction is, therefore, represented by

$$[RE^{3+}]_{aq} + [3(HA)_2]_{org} \rightarrow [RE(HA_2)_3]_{org} + 3[H^+]_{aq}$$

As indicated by this reaction, the extraction is strongly pH dependent, inversely proportional to the third power of hydrogen ion concentration. As a consequence, in nitric or hydrochloric acid solutions, the minimum value of distribution coefficient is reached at an acid concentration of 3 N. For any given organophosphorus acid, the extraction efficiency of rare earths increases with an increase in atomic number. This could possibly result from the increase in the strength of the electrostatic attraction between the extractant anion (HA_2^-) and the rare earth cation, as the size of the cation decreases. The extraction of yttrium lies in the dysprosium–holmium–erbium region as could be anticipated on the basis of its cationic radius. On the same basis, it would also be anticipated that Ce(IV) is more preferentially extracted than the trivalent rare earth ion, and Eu(II) is not extracted when RE^{3+} is present. These characteristics could be used to separate cerium and europium from the rare earths mixture.

The distribution coefficient in HDEHP–rare earth systems increases with an increase in atomic number (and decreases in trivalent ionic radii), and the variation in the system HDEHP/perchloric acid is shown in Figure 3.31. HDEHP gives good separation factors for all rare earth elements. The average separation factor for adjacent rare earth elements is ~2.5. The separation factors in the system HDEHP/HCl are listed in Table 3.4.

HDEHP can extract from a variety of aqueous media, including nitrate, sulfate, chloride, and perchlorate, and the influence of the anion of the rare earth salt on the separation is considered to be generally small. The anion, however, apparently plays a role in certain cases. Even though HDEHP can extract from both chloride and nitrate solutions, it is considered to extract better from the chloride than the nitrate medium. Chlorides or sulfates are preferred for the separation of neodymium and samarium. Besides, sulfates are

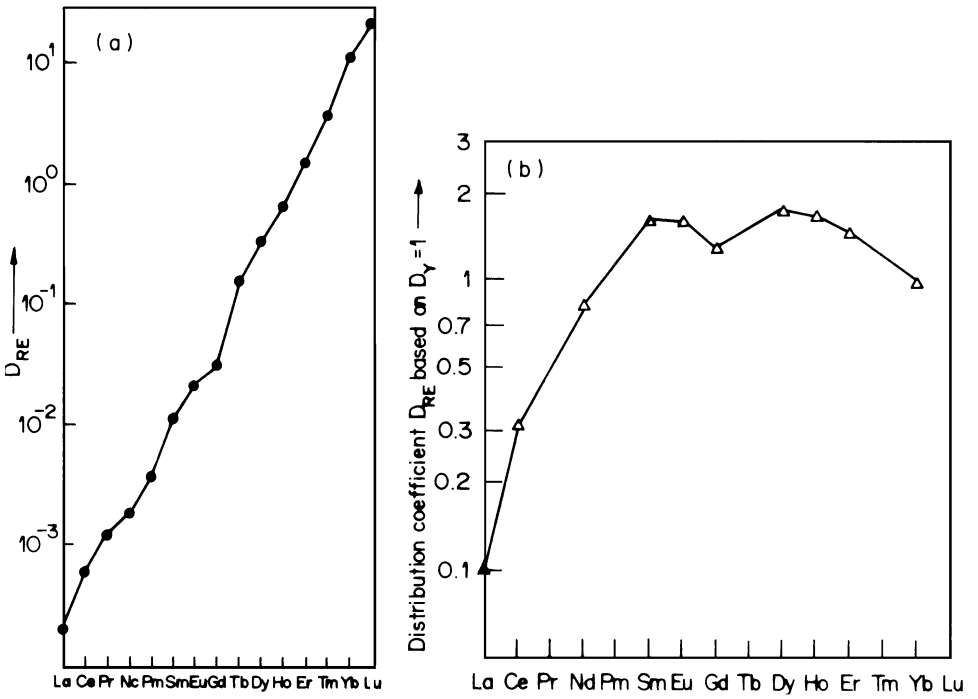

Figure 3.31 Distribution coefficient k_{RE} relative to $k_Y = 1$ in the system (a) HDEHP/perchloric acid; (b) TBP with 50% kerosene/rare earth nitrates (REO 450 gpl) (Pierce and Peck 1963, McGill 1993).

apparently more selective for the separation of cerium earths from the other rare earth elements (McGill 1993).

Generally, the separation factor is not greatly influenced by the total concentration of the rare earth element and also not by the relative concentrations of the various elements (McGill 1993). The distribution coefficients of rare earths decrease with an increase in temperature, and the effect of temperature is greater for the heavy rare earths. The distribution coefficient has been found to be dependent on the diluent for the organophosphorus acid and decreases in the order kerosene > cyclohexane > CCl_4 > xylene > benzene. HDEHP in kerosene is usually chosen as the extractant.

In HDEHP extractions there is also a possibility that separations can be enhanced by the use of scrubbing circuits in which exchange reactions, which are pH independent, like the following, occur:

$$[Sm^{3+}]_{aq} + [Nd(HA_2)_3]_{org} \rightarrow [Sm(HA_2)]_{org} + [Nd^{3+}]_{aq}$$

The extraction of rare earths by di-2-ethyl-hexyl-phosphinic acid in toluene was investigated by Preston and Du Preez (1990). They found that the distribution coefficient increased in the order La < Ce < Pr < Nd < Sm < Eu < Gd < Tb < Dy < Ho < Y < Er < Tm < Yb < Lu. Based on these data, they concluded that the organophosphorus acids could be particularly useful for separating the rare earth mixture into light, middle, and heavy

Table 3.4 Separation factor $(\alpha_B^A)^*$ of the rare earth elements in the extraction systems RE(III)-HCl-HDEHP (Bautista 1995)

A	B												
	Ce	Pr	Nd	Sm	Eu	Gd	Tb	Dy	Ho	Er	Tm	Yb	Lu
La	2.14	2.28	2.43	11.8	26.3	44.6	71.1	101	125	212	319	414	425
Ce		1.07	1.14	5.2	12.3	20.9	33.3	47.2	58.4	99.1	149	193	199
Pr			1.06	5.16	11.5	19.5	31.1	41.1	54.7	92.7	139	181	186
Nd				4.86	10.8	18.3	29.2	41.5	51.3	87.1	131	170	175
Sm					2.23	3.75	6.02	8.55	10.6	17.9	27.0	35.1	36.0
Eu						1.69	2.70	3.83	4.74	8.04	12.0	15.7	16.2
Gd							1.60	2.26	2.80	4.75	7.15	9.30	9.55
Tb								1.42	1.76	2.98	4.48	5.83	5.90
Dy									1.24	2.10	3.16	4.11	4.22
Ho										1.70	2.55	3.31	3.41
Er											1.50	1.90	2.01
Tm												1.30	1.34
Yb													1.03

$^*\alpha_B^A = D_A/D_B$, in the extraction from 0.1 mol dm^{-3} hydrochloric acid solution with 0.2 mol dm^{-3} HDEHP in kerosene.

fractions. The light and middle fractions could be conveniently split between neodymium and samarium, and the separation of middle and heavy fractions could be advantageously made between gadolinium and terbium.

The extraction of lanthanide chlorides by 2-ethyl-hexyl-2-ethyl-hexyl-phosphonic acid (EHEHPA), also known as PC88A, in kerosene was also reported. The separation factors are listed in Table 3.5. The extraction efficiency for the rare earths in EHEHPA also increases with atomic number but is lower in comparison with HDEHP under the same conditions. EHEHPA, however, is more selective for the separation of heavy rare earths from light rare earths. EHEHPA is preferred as an extractant for the separation of rare earth elements due to the high separation factors between any two adjacent rare earth elements compared to HDEHP. In the past decade, PC88A has practically replaced HDEHP in many of the applications where HDEHP was originally used for the industrial solvent extraction separation of rare earths.

As mentioned earlier, the organophosphorus acids are liquid cation exchangers and liberate hydrogen ion during the loading of the extractant with the rare earth ions. This liberated hydrogen ion, i.e., the increase in the solution acidity, adversely affects metal extraction. This problem is circumvented by saponifying the extractant with NaOH. The degree of saponification is restricted, however, to avoid gel formation due to excessive loading of rare earths and to avoid solubility of saponified solvent in the aqueous phase. The organic phase typically containing 1.0 M PC88A in kerosene (mainly paraffinic and naphthenic hydrocarbon in the $C_{10}-C_{14}$ range), containing 5% (v/v) isodecanol, after 20% saponification with NaOH, has been used for extraction of rare earths from a chloride aqueous solution (Koppiker 1990).

Table 3.5 Separation factor (α_B^A)* of the rare earth elements in the extraction systems RE(III)-HCl-EHEHPA (Bautista 1995)

A	B												
	Ce	Pr	Nd	Sm	Eu	Gd	Tb	Dy	Ho	Er	Tm	Yb	Lu
La	1.30	1.42	1.67	3.33	6.52	9.52	22.5	36.4	93.9	117	156	175	199
Ce		1.09	1.28	2.57	5.02	7.36	17.3	28.0	72.3	90.5	120	135	152
Pr			1.17	2.35	4.59	6.72	15.8	64.2	66.0	82.7	110	123	140
Nd				2.00	3.94	5.74	13.5	21.8	56.3	70.5	93.7	105	119
Sm					1.96	2.87	6.74	10.9	28.2	35.3	46.8	52.6	59.5
Eu						1.46	3.45	6.39	14.4	18.0	24.0	26.9	30.4
Gd							2.35	3.81	9.82	12.3	16.3	18.3	20.7
Tb								1.62	4.18	5.23	6.95	7.81	8.83
Dy									2.58	3.23	4.29	4.82	5.45
Ho										1.25	1.66	1.87	2.11
Er											1.33	1.49	1.69
Tm												1.12	1.26
Yb													1.13

* $\alpha_B^A = D_A/D_B$, in the extraction from 0.1 mol dm^{-3} hydrochloric acid solution with 0.2 mol dm^{-3} EHEHPA in kerosene.

Carboxylic acids Carboxylic acids (C_7–C_{15}) are soluble in hydrocarbons and, like the organophosphorus acids, extract by cation exchange. The extraction, represented by

$$3[R_3C\cdot COOH]_{org} + [RE^{3+}]_{aq} \rightarrow [(REC\cdot COO)3RE]_{org} + 3H^+$$

is conducted in a neutral or weakly acidic medium. Carboxylic acids are commercially available and are relatively inexpensive.

The most widely used among the carboxylic acids for rare earth extraction are the versatic acids $R_1R_2(CH_3)C\cdot COOH$, where R_1 and R_2 are branched chain alkyl groups. Versatic 911 has 9 to 11 carbon atoms and versatic 10 has 10 carbon atoms. These two are the most important and widely used. The separation factors for versatic 911 are listed in Table 3.6. The separation factors for La–Ce and Ce–Pr are 3 and 1.6, respectively, and these values are higher than those for TBP extraction. For Nd–Pr onward, the separation factors are similar to the TBP system (Brown and Sherrington 1979). Versatic acid extracts

Table 3.6 Separation factors between rare earths for extraction by Versatic 911/Shellsol A from a nitrate or chloride medium (McGill 1993)

Ce/La	Pr/Ce	Nd/Pr	Sm/Nd	Gd/Sm	Dy/Gd	Ho/Dy	Er/Ho	Yb	
3.00	1.60	1.32	2.20	1.96	1.94	1.17	1.28	1.49	
La/Y	Ce/Y	Pr/Y	Nd/Y	Sm/Y	Gd/Y	Dy/Y	Ho/Y	Yb/Y	Er/Y
0.028	0.085	0.14	0.18	0.39	0.77	1.50	1.75	2.25	3.35

similarly from both nitrate and chloride media. This reagent also extracts the heavy rare earths.

Naphthenic acids are represented by the general formula RCOOH, where R is a radical derived predominantly from cyclopentane or a homolog of cyclopentane. Naphthenic acid with diethyl ether or *n*-hexanol as a diluent was used with some success as an extractant for rare earth sulfates (Bauer and Lindstrom 1964). Rare earth extraction was dependent on pH, naphthenic acid concentration, and the mol ratio of naphthenic acid and the rare earth. The separation factor was enhanced to 2.2 for adjacent yttrium group elements by the addition of an aqueous phase chelating agent such as EDTA. Similarly, the addition of DTPA enhanced the separation factor to 3.5 for adjacent yttrium group elements (Bautista 1995).

Solvating extractants In extraction by solvation, the extractant replaces some or all of the coordinated water molecules from the aquated metal ion to form a species that is soluble in the organic phase. The most important solvating extractant for rare earth refining is tri-*n*-butyl-phosphate (TBP) and the extraction of a trivalent rare earth by TBP (see Table 3.7) can be represented by the general reaction

$$[RE(NO_3)3\cdot xH_2O]_{aq} + 3[TBP]_{org} \rightarrow [RE(NO_3)_3(TBP)_3]_{org} + xH_2O$$

Under a given set of conditions, the lanthanide stabilities of the complexes and hence their extractabilities might be expected to increase through the series from La^{3+} to Lu^{3+}, as the cationic radius decreases because the electrostatic interaction between the cation and ligand should be proportional to the reciprocal of cationic radius. Once the cationic radius is beyond a certain size, however, steric considerations overrule electrostatic effects. This is indicated by the existence of a maxima, as given in Figure 3.32, in the extractions by neutral organophosphorus compounds. In the TBP system, the extraction of yttrium usually lies between that of erbium and thulium.

The separation of yttrium from lighter lanthanides, e.g., lanthanum, increases markedly with an increase in nitrate concentration; however, there is no such change on yttrium separation from the heavier rare earths, e.g., thulium.

Rare earth nitrates up to a concentration of 0.5 mol/L (~170–190 g REO/L) can be loaded in pure TBP. The effect of temperature is small. Rare earth element salts such as

Table 3.7 Separation factors for various rare earth pairs in TBP extraction (McGill 1993)

REO concentration in aqueous phase, g/L	Separation factor							
	Ce/Y	Nd/Y	Sm/Y	Gd/Y	Dy/Y	Ho/Y	Er/Y	Yb/Y
60		4.08	5.71	4.44	3.96	3.03	2.13	
125	0.75	1.77	2.79	2.29	2.10	1.75	1.25	0.83
220	0.60	1.30	2.02	1.99	2.15	1.91	1.48	0.83
460		0.39	0.88	0.89	1.30	1.20	1.15	0.93
	Sm/Nd	Gd/Sm	Dy/Gd	Ho/Dy	Er/Ho	Yb/Er		
60	1.40	0.18	0.89	0.77	0.70	0.63		
125	1.58	0.82	0.92	0.83	0.72			
220	1.55	0.99	1.08	0.89	0.78			
460	2.26	1.01	1.45	0.92	0.96	0.81		

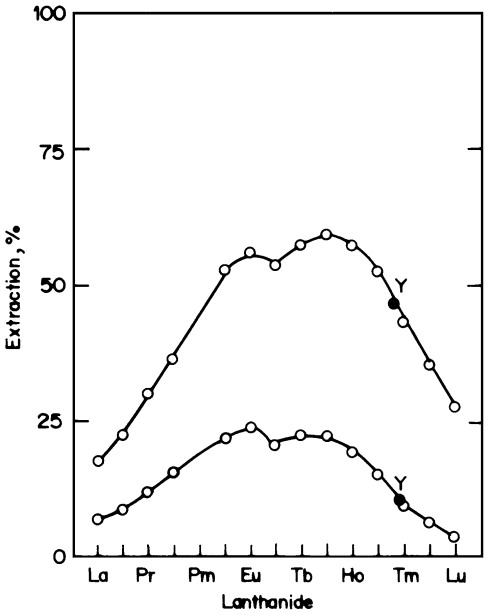

Figure 3.32 Extraction of trivalent lanthanides and yttrium from nitrate media by 2.0 M TBP in toluene at 20°C. Aqueous phases 0.01 M metal nitrates in 1 M HNO_3/2 M NH_4NO_3 (lower curve) and 1 M HNO_3/5 M NH_4NO_3 (upper curve) (Preston and Du Preez 1990; McGill 1993).

perchlorates, chlorides, and thiocyanates have poor distribution coefficients and/or selectivities in TBP.

It was observed by Preston and Du Preez (1990) that TBP and other neutral organophosphorus compounds are useful in the bulk recovery of the rare earth product from nitrate liquors, but they are less useful in separations among the trivalent lanthanides because the separation factors for adjacent rare earth pairs are generally small, in the range 1.2 to 2.2. This may be compared to the average separation factor of ~2.8 for HDEHP extraction from a nitrate medium.

Amines Long chain quaternary ammonium salts, $R_3CH_3N^+X^-$, in which R represents C_8–C_{12} groups and X represents nitrate or thiocyanate, are useful for the separation of rare earths (Preston and Du Preez 1988). Amines extract by anion exchange. In an extraction by anion exchange, a simple inorganic anion from an ion pair type extractant, such as a quaternary ammonium salt, is replaced by a complex metallic anion, in reactions such as

$$[R_4N\cdot NCS]_{org} + [RE^{3+}]_{aq} + 3[NCS^-]_{aq} \rightarrow [R_4N\cdot RE(NCS)_4]_{org}$$

$$[R_4N\cdot NO_3]_{org} + [RE^{3+}]_{aq} + 3[NO_3^-] \rightarrow [R_4N\cdot RE(NO_3)_4]_{org}$$

The extraction of different rare earths in the thiocyanate and in the nitrate systems exhibit interesting results. This is shown in Figure 3.33. In the thiocyanate system, the extraction of a rare earth increases within its atomic number. In the nitrate system, on the other hand, the extraction decreases with an increase in atomic number. Preston and Du Preez (1990) have attributed this behavior to the interplay of electrostatic and steric effects

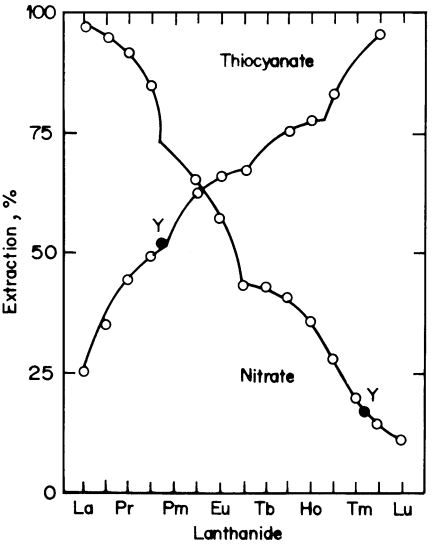

Figure 3.33 Extraction of trivalent lanthanides and yttrium (0.02 M as nitrates) from 4.0 M $NaNO_3$ by 0.5 M solutions of Aliquat 336 nitrate in xylene at 20°C and from 2.0 M KNCS by 0.25 M solutions of Aliquat 336 thiocyanate in toluene at 30°C (Preston and Du Preez 1990).

in the stability of the various complexes, and hence their extractability. The extraction behavior of yttrium is particularly important. In the thiocyanate system, yttrium behaves as a light rare earth lying between neodymium and samarium. In the nitrate system, on the other hand, yttrium behaves like a heavy rare earth lying between thulium and ytterbium. This indicates the possibility of separation of the yttrium in thiocyanate media from the fraction containing dysprosium, holmium, and erbium to which it reports in extraction with organophosphorus acids (Preston and Du Preez 1990). The separation factors for extraction with the typical anion exchange extractant, Aliquat 336, is compared with the values for extractions with HDEHP and EHEHPA in Table 3.8.

A large number of metal ions in the form of anionic complexes are extracted by long chain amines. For rare earth elements, however, primary and secondary amines are relatively weak extractants and need high concentrations of salts and acids for a useful separation effect. These amines preferentially extract rare earth sulfates and their poor selectivity is enhanced by the presence of EDTA and DTPA. In any case, these extractions are strongly dependent on pH and concentration and are difficult to control (McGill 1993). Tertiary amines are also poor extractants.

Synergistic effects The distribution coefficient can be considerably more than the sum of the distribution coefficients of individual extraction agents when the mixture of extractants is used. Such systems commonly used in many metal extraction operations have not been developed to levels of industrial application for rare earth extractions (McGill 1993).

Industrial processes Rare earth producers all over the world follow almost identical routes for solvent extraction separation of rare earths. Mixer settler assemblies involving hundreds of stages of mixing are the standard contacting equipment. These routes are based on the following overall scheme: (i) separation of rare earth generally in trivalent state, (ii)

Table 3.8 Separation factors for Aliquat 336 compared with HDEHP and EHEHPA (Preston 1996)

Rare earth metal		Separation factor[a]		
A	B	Aliquat[b]	EHEHPA[c]	HDEHP
La	Ce	1.67	4.55	2.70
Ce	Pr	1.72	2.12	1.50
Pr	Nd	2.04	1.27	1.25
Nd	Sm	2.97	4.00	4.26
Sm	Eu	1.42	1.78	1.78
Eu	Gd	1.75	1.35	1.50
Gd	Tb	1.02	3.00	
Tb	Dy	1.08	1.94	
Dy	Ho	1.24	1.53	
Ho	Er	1.43	1.90	
Er	Tm	1.59	1.78	
Tm	Yb	1.47	2.12	
Yb	Lu	1.34	1.44	

[a]Separation factors are expressed as α_B^A $(= k_A/k_b)$ for Aliquat and as α_A^B $(= k_b/k_A)$ for organophosphorus acids.

[b]For extraction of 0.02 M individual rare earths from 4.0 M sodium nitrate by 0.50 M Aliquat 336 nitrate in xylene.

[c]For extraction of 0.02 M individual rare earths from 4.0 M sodium nitrate by 0.20 M organophosphorus acid in toluene.

fractionation of the rare earths into three or four groups, (iii) preferential separation of yttrium, (iv) selective extraction of cerium and europium using their valence states Ce^{4+} and Eu^{2+}, and (v) separation of the desired individual rare earth of required purity.

For a solvent extraction system to be attractive for industrial application, there are several relevant factors (McGill 1993). The choice of the extractant and aqueous phase may be influenced by cost considerations of all the chemicals involved. In the extraction of rare earth salts by neutral extraction media or when the rare earths are extracted as an anionic complex, the reactive chemicals requirement is less. When the rare earths are extracted using cationic complexes, the reactive chemicals requirement is more because a base is required for extraction from the aqueous phase and an acid is required for selective washing and reextraction from the organic phase. In other words cationic extraction is considerably more expensive than anionic or neutral extraction. Cationic extraction is, however, characterized by high selectivity and is preferred when this characteristic is of major importance.

The first step in industrial solvent extraction is usually the separation of the rare earth elements from other elements. A solvent whose distribution coefficient for the rare earth elements as a group is markedly different from that of the other element in the aqueous solution (leach liquor) is chosen. HDEHP is a suitable extractant for this. This extractant is also suitable for concentrating the rare earth elements because of its high extraction ability for the rare earth elements, which enables it to extract them from dilute and often acidic solutions. A classic example for the industrial solvent extraction in rare earths processing is the Molycorp process for the production of europium.

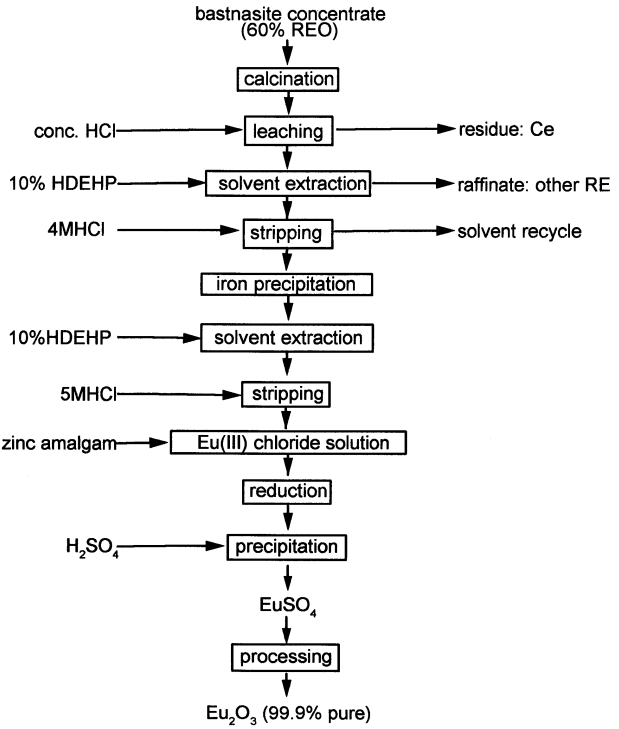

Figure 3.34 Molycorp process for europium oxide.

Molycorp The schematic flowsheet for the Molycorp process for the processing of Mountain Pass bastnasite (Harrah 1967) is shown in Figure 3.34. At the end of physical beneficiation and chemical treatment procedures, a chloride solution (100 g REO/L and 200 mg Eu_2O_3/L) containing all the rare earths (except Ce) originally contained in the ore is obtained. This solution is clarified, pH adjusted to 1.0 with soda ash, steam heated to 60°C, clarified again, and put through to the europium recovery circuit.

The chloride solution described in the previous paragraph contains 0.2 g Eu_2O_3 per liter. The solvent is 10% HDEHP in kerosene and the extraction is performed in 5 mixer settler stages. More than 98% of europium in the solution is extracted. The loaded organic is stripped with 4 M HCl. The strip solution, which contains 10 to 20 grams europium per liter, also contains iron as an impurity and this is precipitated out with soda ash at pH 3.5. Following iron removal, the Eu-bearing solution is subjected to a second solvent extraction with HDEHP in five mixer settler stages. This second extraction further purifies europium and the light rare earth fraction is left in the raffinate, which is reverted to the first SX circuit. Europium loaded in the organic is stripped with 5 M HCl. The aqueous strip solution is passed through a column of zinc amalgam to reduce Eu(III) to Eu(II). Sulfuric acid is added to the divalent europium solution to precipitate europium sulfate. Reduction and selective precipitation purifies europium from the heavy rare earths. More than 99.99% pure Eu_2O_3 is obtained by calcination.

In the second SX circuit, along with europium, other heavy rare earths are loaded in the organic. After europium removal, the strip solution still contains samarium, the heavy rare earths, and yttrium. Gadolinium is extracted from the europium barren solution by HDEHP in a 10-stage extraction circuit followed by 5 stages of stripping. The raffinate is

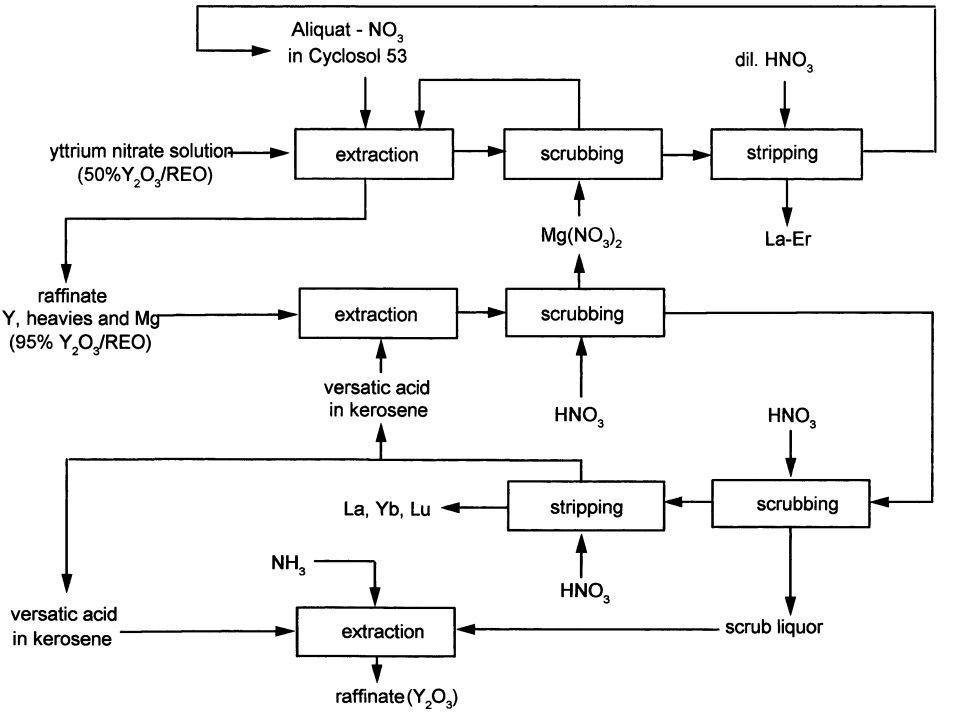

Figure 3.35 Molycorp process for pure yttrium oxide (McGill 1993).

neutralized with soda ash to precipitate samarium and the heavy rare earths. Raffinate from the europium (first solvent extraction) circuit contains La, Pr, and Nd, which are precipitated with ammonia and sodium hydrosulfide. Molycorp rare earth processing facilities at Louviers, Colorado, produce Gd, Tb, Dy, Ho, Er, Tm, Tb, Lu, and Y.

The Molycorp process for the preparation of pure yttrium oxide is shown in Figure 3.35. Starting from a concentrate containing 52% Y_2O_3 in the REO mixture, pure yttrium is produced is two consecutive cycles. The rare earths are separated into La–Er and Y–Lu fractions by Aliquat–NO_3^- with recycle using $Mg(NO_3)_2$ for stripping. Yttrium is finally purified by extraction with versatic acid, including a double recycle.

Denison Mines The recovery of rare earths from sulfate solutions resulting from uranium processing at Denison Mines, Elliot Lake, Ontario, has been done using solvent extraction with HDEHP. The flowsheet is shown in Figure 3.36. An yttrium-rich concentrate (~60% REO) is produced from sulfuric acid solutions containing 150 mg Y_2O_3/L.

The uranium barren solution at pH 2 from the ion exchange circuit is treated with lime and air in pachuka tanks. The pH is controlled to precipitate iron, some amount of thorium and other impurities. These are removed from solution using thickeners, filters, and clarifiers. The clarified solution is acidified with sulfuric acid and fed to the solvent extraction circuit. The solvent used is 10–12 vol % HDEHP in kerosene with no modifier and the extraction takes place in a countercurrent centrifugal extractor. Under extraction conditions used at present, all the rare earths and yttrium are loaded in the organic phase. The loaded solvent is stripped with nitric acid in a centrifugal contactor. Thorium and uranium present in the aqueous solution are loaded into the solvent together with the rare earths. The rare earths are separated from thorium and uranium during stripping. The

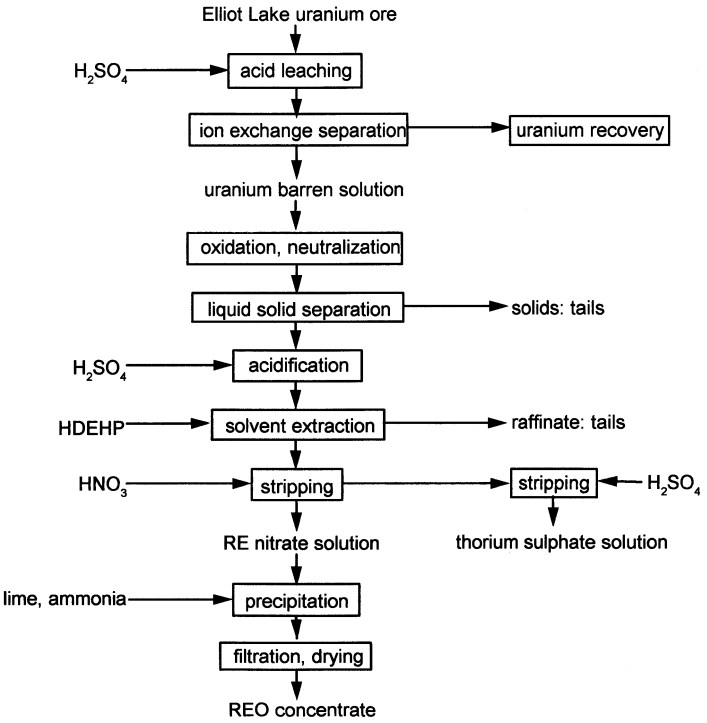

Figure 3.36 Denison Mines process for yttrium rich rare earth concentrates (Lucas and Ritcey 1975, McGill 1993).

yttrium–rare earth containing nitric acid solution is treated for precipitation. Slaked lime is added to the solution to consume all the free acid. Ammonia gas was then added to the solution to precipitate yttrium and other rare earths. The dried precipitate contains 30–35% Y_2O_3 and 60–70% RE_2O_3 including yttrium.

Indian Rare Earths The mixed rare earth chloride solution obtained in the course of chemical treatment of monazite contains less than 1% of any of the heavy rare earths. At the Alwaye Plant of Indian Rare Earths Ltd., solvent extraction with HDEHP was used for a quick initial concentration of the heavy rare earths and for the production of concentrates of various individual rare earths such as Sm, Eu, Gd, and Y with purities ranging from 60 to 95%. The schematic flowsheets are shown in Figures 3.37 and 3.38.

The flowsheets outlining the Indian practice for the fractionation of rare earths and for the separation of Nd and Pr using PC88A are shown in Figures 3.39 to 3.41. The flowsheets for the separation and purification of Sm, Eu, Dy, and Y are given in Figures 3.42 to 3.45 (Thakur 2000).

In the Indian practice (Koppiker 1990), from the RE chloride solution containing 200–240 g REO/L and about 0.05 M HCl, the rare earths are extracted with 1 M PC88A in kerosene. Extraction parameters are so chosen that the solvent extracts Sm and other heavy rare earths (HRE) and also yttrium, leaving the light rare earth (LRE) in the raffinate. The extract is then selectively scrubbed with 3 M HCl at a O/A phase ratio > 20 to remove the LRE. From the scrubbed loaded solvent, Sm, Eu, and Gd (MREs) are selectively stripped with 1–1.5 M HCl. The extract, presently containing only the HREs is then stripped with 3.5 M HCl.

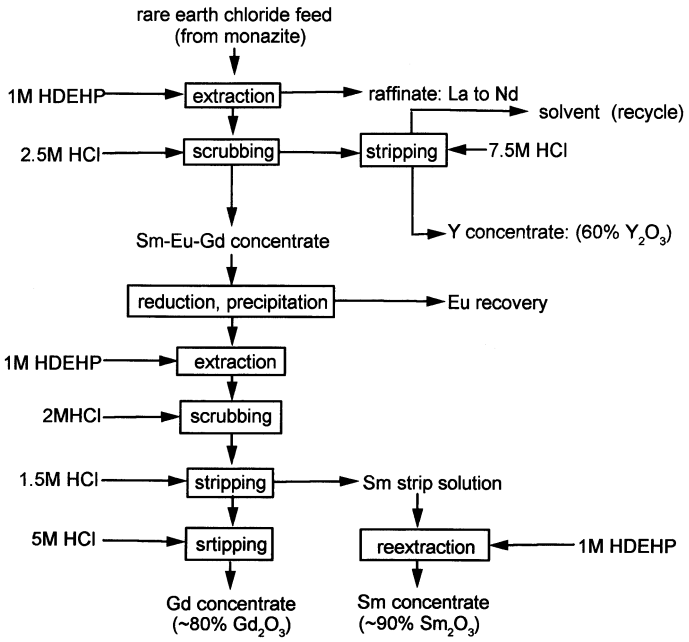

Figure 3.37 Flowsheet of rare earth separations by solvent extraction at Indian Rare Earths-I.

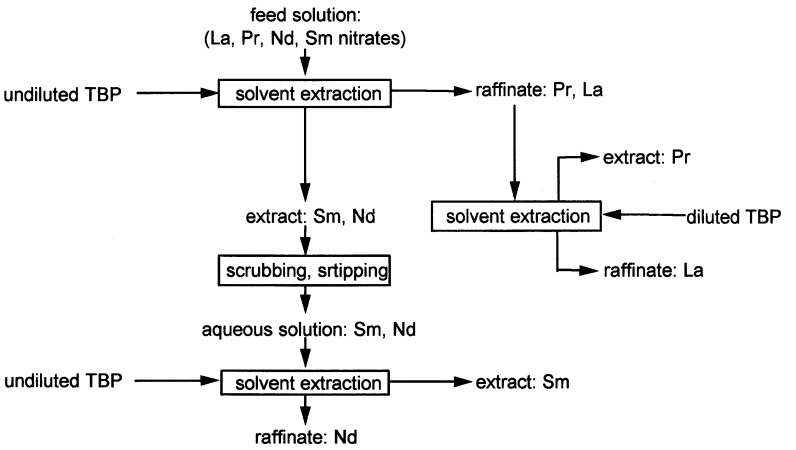

Figure 3.38 Flowsheet of rare earth separations by solvent extraction at Indian Rare Earths-II.

The first strip solution containing the middle RE fraction (40–50 g REO/L) is then processed to precipitate Eu as $EuSO_4$ after reduction with zinc dust. The Eu free solution, now containing all Sm and Gd is put through one more cycle of solvent extraction with PC88A or HDEHP as extractant to produce > 95% pure Sm_2O_3 and 80–90% pure Gd_2O_3.

The HRE fraction assaying around 60% Y_2O_3 and 15% Dy_2O_3 is treated further to obtain 93% Y_2O_3 in the first cycle of a two-cycle solvent extraction process. In the first

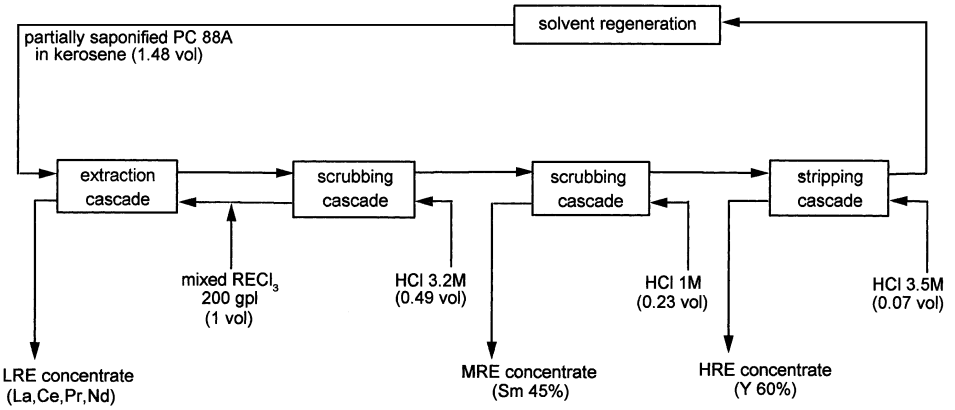

Figure 3.39 Flowsheet for the fractionation of rare earths using partially saponified PC88A (Thakur 2000).

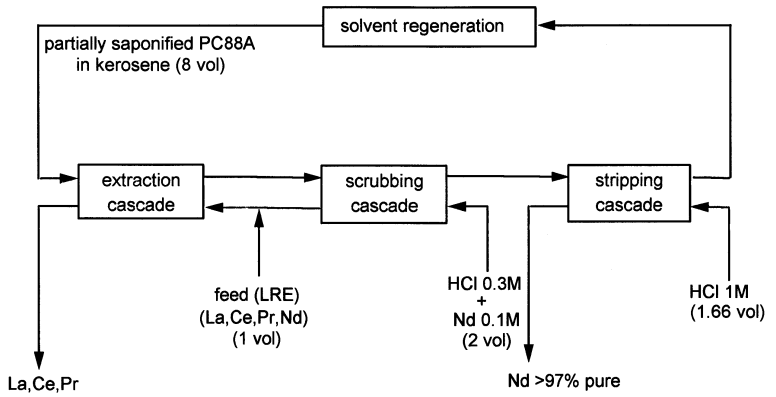

Figure 3.40 Flowsheet for the recovery of neodymium from LRE concentrate using partially saponified PC88A.

cycle the aqueous solution assaying ~25 g REO/L (60% Y_2O_3) and 0.4 M HCl is brought into contact with the solvent in eight stages. The solvent is 1.0 M PC88A in kerosene. The loaded solvent/extract is scrubbed with dilute HCl in six stages. Yttrium and HREs preferentially extracted by the solvent are finally stripped with strong HCl in four stages at a high phase ratio. The final strip solution would assay about 40 g REO/L (93% Y_2O_3) and about 1.0 M HCl. This solution is neutralized with NH_4OH to a pH of 4.0 and NH_4CNS is added to make it 1 M NH_4CNS. The solution is put through the second cycle of solvent extraction with 50% TBP in kerosene. The treatment is done in 16–18 stages of extraction and 18–20 stages of scrubbing with water, and eight stages of final stripping of the loaded extract with water. All REs other than Y are preferentially extracted by TBP leaving Y in the aqueous raffinate as high purity product at above 90% recovery. The final strip solution containing HRE would assay about 50% Er_2O_3 and forms the source for further separation of Er_2O_3.

In the Indian practice, the 60% Y_2O_3 concentrate upgraded to 93% Y_2O_3 by PC88A extraction is also purified further to obtain 99.99% Y_2O_3 by extraction using the Aliquat 336–thiocyanate system in a chloride medium.

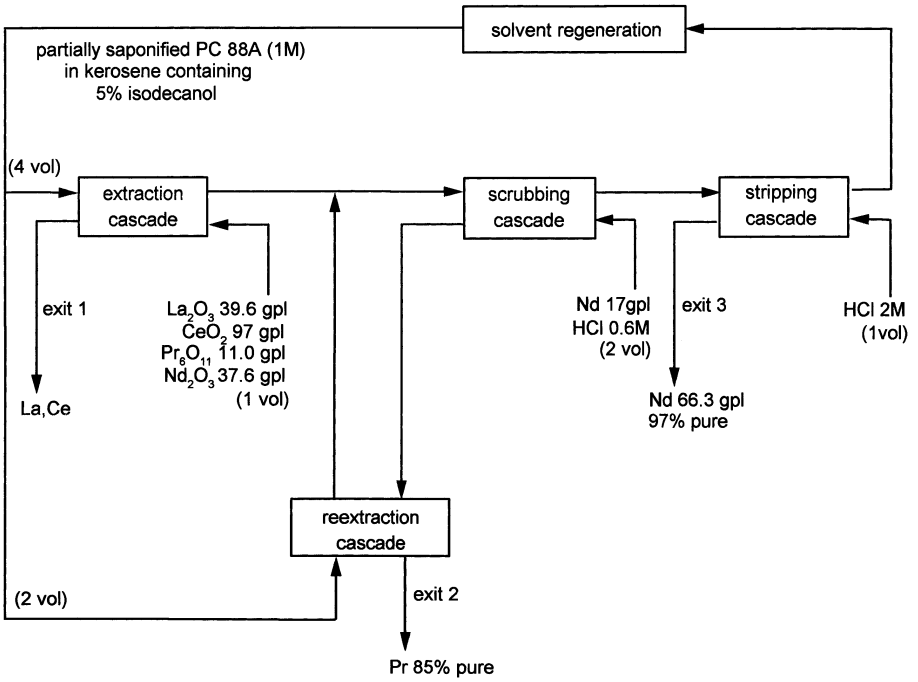

Figure 3.41 Flowsheet for 3 exit solvent extraction process for simultaneous purification of neodymium and praseodymium by PC88A.

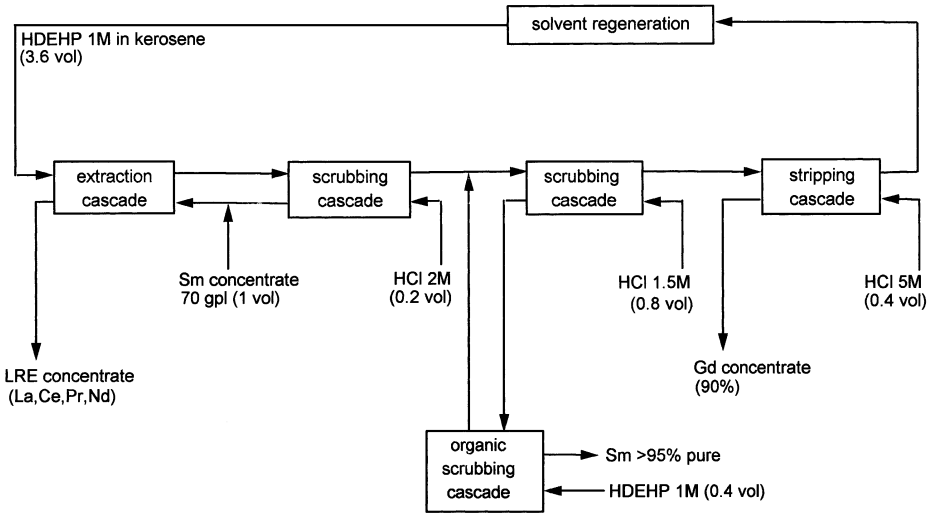

Figure 3.42 Flowsheet for the recovery of samarium from the MRE concentrate using HDEHP.

The aqueous raffinate obtained from the first cycle of SX for Y separation using PC88A assaying about 5 g REO/L has the composition Dy_2O_3 (55–60%), Tb_4O_7 (15%), Gd_2O_3 (8–12%), Ho_2O_3 (1–2%), Y_2O_3 < 10% and is treated for the recovery of Dy and

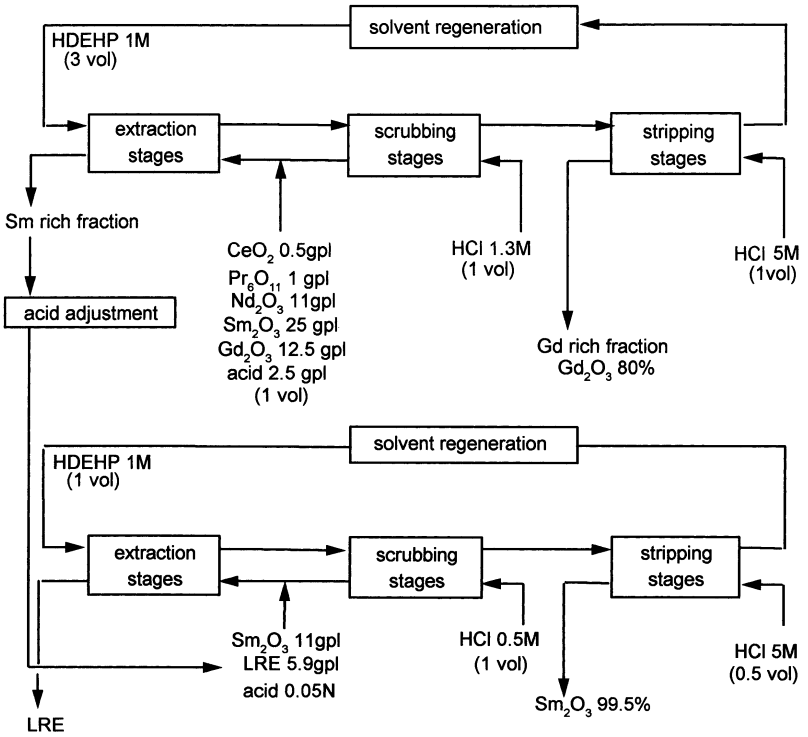

Figure 3.43 Flowsheet for the recovery of high purity samarium.

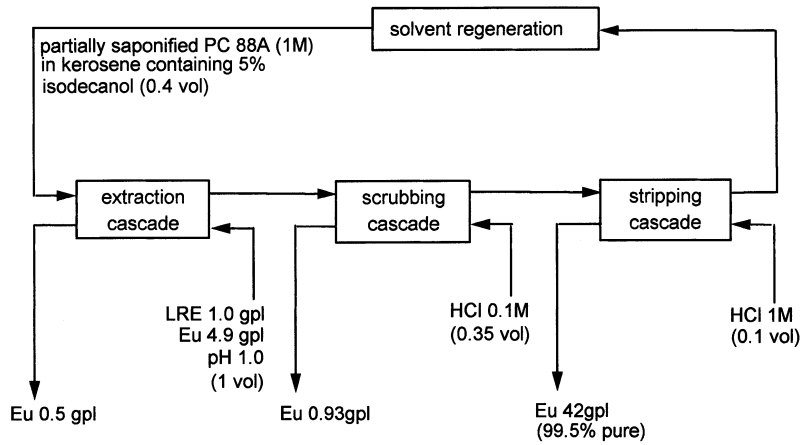

Figure 3.44 Flowsheet for the purification of europium by PC88A from the feed containing 83% Eu obtained after initial zinc reduction process (Thakur 2000).

Tb. This solution would have about 1 M HCl and is processed with 1 M HDEHP in kerosene. Keeping the phase ratio 1 in extraction and 4 in scrub Dy, the HREs are extracted preferentially and thus separated from LRE. The loaded extract is then stripped with HCl to preferentially strip Dy. The product Dy_2O_3 is about 97% pure.

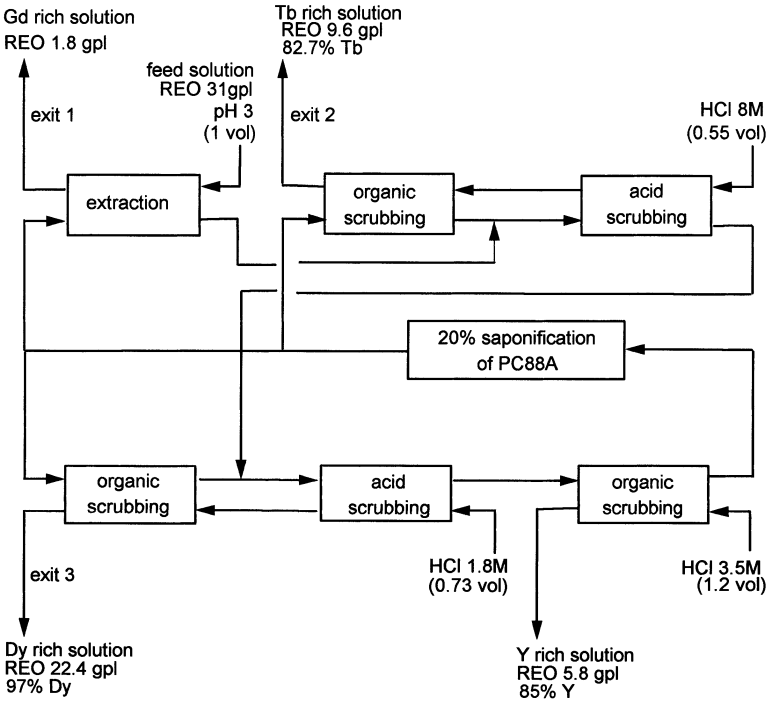

Figure 3.45 Flowsheet of the four exit solvent extraction process for the simultaneous purification of dysprosium, terbium, gadolinium and yttrium using PC88A.

In the processing of monazite ore at Indian Rare Earths Ltd., caustic digestion dissolves the phosphate and leaves a hydrated mixed metal oxides cake containing thorium, uranium, and rare earths. By leaching the cake with hydrochloric acid at pH 3.0, the bulk of the rare earths are preferentially removed and separated as mixed rare earth chloride. The slurry after removal of the major portion of rare earths contains all the thorium and uranium present in the monazite feed. In addition, this slurry also contains substantial quantities of rare earths. This rare earth content is recovered by solvent extraction using PC88A as the extractant. The flowsheet is shown in Figure 3.46 (Narayanan et al. 1988). The RE–Th slurry obtained after decantation of $RECl_3$ solution is dissolved in HCl and after clarification, its acidity is adjusted to 1.5 M. The aqueous feed solution is contacted in the extraction circuit with the solvent PC88A (Ionquest-801) in two stages. During this step uranium and all the thorium in the aqueous feed solution are completely picked up by the extractant leaving only the trivalent rare earths in the aqueous phase. Thorium and uranium are recovered separately from the loaded solvent, and the rare earths are recovered from the raffinate.

Mintek Solvent extraction has been used for recovering rare earths from rare earth carrying calcium sulfate sludge obtained in the manufacture of phosphoric acid from Phalaborwa apatite in South Africa (Preston et al. 1996, 1996a). The processing involved extensive application of solvent extraction using TBP, HDEHP, and Aliquat 336 in obtaining first a mixed rare earth oxide concentrate, as shown in Figure 3.47, followed by separation of this mixed oxide into heavy, middle, and light fractions as well as preparation of pure cerium, europium, and neo- dymium oxides (Preston 1996).

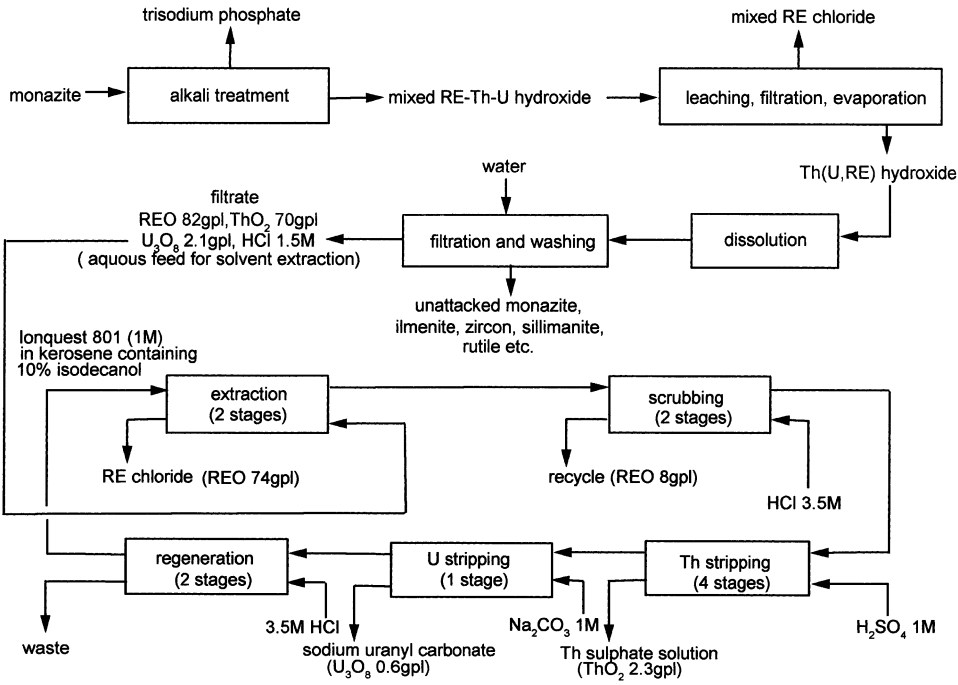

Figure 3.46 Process for the separation of rare earths, thorium and uranium by solvent extraction using 2-ethyl hexyl phosphonic acid mono 2-ethyl hexyl ester (Ionquest-801) (Narayanan et al. 1988).

As mentioned earlier, the rare earth values were leached from the sludge by dilute nitric acid and calcium nitrate. From the leach liquor, the rare earths were recovered by solvent extraction using 33 vol % dibutyl-butyl-phosphonate (DBBP) in Shellsol 2325. The loaded organic phase was stripped with water to yield a solution of mixed rare earth nitrates from which mixed rare earth oxide (98% pure) was obtained by the addition of oxalic acid and calcination of the oxalate precipitate. In later trials, the organic phase was changed to 40 vol % tributyl phosphate for an aqueous rare earth bearing leach liquor containing 1 M nitric acid and 3 M calcium nitrate. The mixed rare earth oxide obtained was 89–94% in purity and contained middle rare earths, particularly neodymium, samarium, europium, and gadolinium in considerably higher proportions than the commercially available mixed oxides from usual commercial rare earth resources.

A solvent extraction was used for the recovery of high purity cerium dioxide and a heavy rare earth oxide concentrate from the mixed rare earth oxide. The mixed oxide was dissolved in concentrated nitric acid to yield solutions in which up to 95% of the cerium was present as Ce(IV). From this solution, after dilution with water, Ce(IV) was extracted with high selectivity into a 15 vol% solution of TBP in Shellsol K in four extraction stages. After four stages of scrubbing with 3 M nitric acid, stripping of the organic phase was accomplished by reduction of Ce(IV) to Ce(III) with dilute H_2O_2 in two stages. Oxalic acid was added to the strip solution and the oxalate precipitated was calcined to 99.8% pure cerium dioxide, which was obtained in about 70% yield.

The raffinate from the cerium recovery circuit was extracted with 5 vol % solution of HDEHP in Shellsol AB in six stages followed by stripping in four stages to give strip

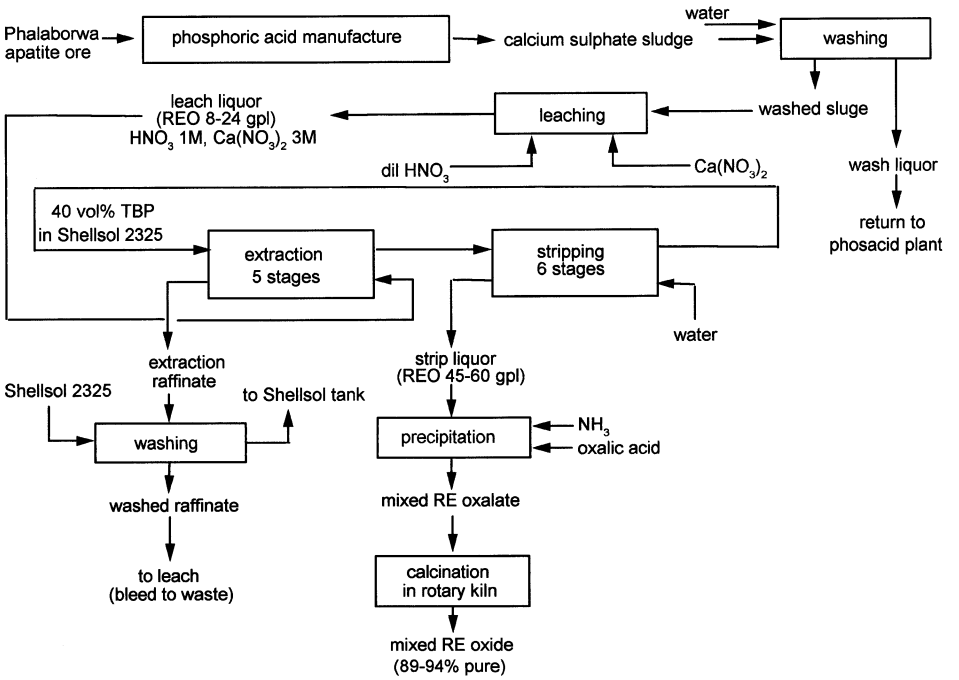

Figure 3.47 Schematic diagram of the pilot plant leaching and solvent extraction circuits for rare earth recovery from Phalaborwa apatite source (Preston 1996).

liquors, which on oxalate precipitation and calcination yielded mixed heavy rare earth oxide (99.4–99.8% REO). This contained 41–63% Y_2O_3, 17–31% Dy_2O_3, 4% HoO_3, 4–5% Er_2O_3 together with smaller amounts of other rare earths.

The raffinate from heavy rare earth extraction was processed for the separation of middle and light rare earth fractions. The processing consisted of extraction into a 15 wt % solution of HDEHP in Shellsol AB in eight countercurrent stages, followed by scrubbing with 1 M nitric acid in two to four stages and stripping with 1.5 M hydrochloric acid in six to eight stages. Addition of oxalic acid to the strip liquors, and calcination of the precipitated oxalate yielded mixed middle rare earth oxide product containing 45% Sm_2O_3, 29% Gd_2O_3, 13% Eu_2O_3, and 6% Nd_2O_3.

From the remaining light rare earth nitrate liquor containing Nd, Pr, Ce, and La, 0.50 M solution of Aliquat 336 nitrate (tricaprylmethyl ammonium nitrate) in Shellsol AB was used to selectively extract La, Ce and Pr in two extraction circuits. Purified neodymium solution was remaining as raffinate. Extraction was carried out in eight extraction and six scrubbing stages. Loaded solvent was stripped with water in six stages. From the solutions thus obtained, rare earth oxides were obtained by oxalate precipitation and calcination. From the raffinate, 75% of neodymium present in the original feed was obtained as 95–96% pure (magnet grade) Nd_2O_3. The impurities were 2% Pr_6O_{11}, 1.5% Sm_2O_3, 0.7% CeO_3, and 0.2% La_2O_3. From the first circuit strip liquor, lanthanum concentrate (51% La_2O_3, 36% CeO2, 7% Pr_6O_{11}, and 6% Nd_2O_3) and from second circuit strip liquor, praseodymium concentrate (32% Pr_6O_{11}, 41% Nd_2O_3, 22% CeO_2, and 4% La_2O_3) were obtained.

Megon The Megon Company in Norway, founded in 1969, processes xenotime to recover yttrium concentrate and high purity yttrium oxide. The flowsheet is shown in

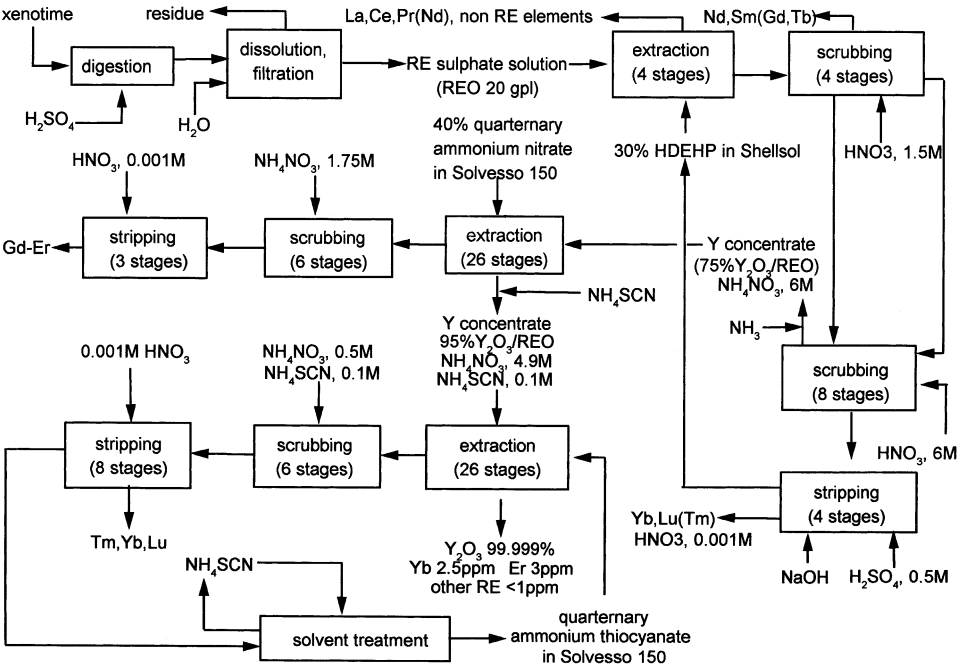

Figure 3.48 AS Megon process for high purity yttrium oxide (McGill 1997).

Figure 3.48. There are three extraction cycles (Ritcey and Ashbrook 1979, McGill 1993). From the rare earth sulfate solution obtained after chemical treatment of xenotime concentrate, a 30% solution of HDEHP in Shellsol T diluent is used to achieve an intermediate type of separation. In four mixer settler stages, some Nd, and all the heavier rare earths including yttrium are extracted while La, Ce, and Pr remain in the raffinate. Stripping the extract with 1.5 N HNO_3 in four stages removes the Nd–Tb fraction, which includes large amounts of samarium and gadolinium. Stripping the extract with 6 N HNO_3 in eight stages of mixer settlers removes yttrium with most of the heavy lanthanides. Ytterbium and lutetium are only partially stripped by HNO_3. They are, however, removed in a single stage with 10% NaOH. Instead of 10% NaOH, either 20% HF or 50% H_2SO_4 could also be used for an equally effective stripping. The caustic treatment also removes any Fe or Th present. The solvent phase is acidified with sulfuric acid and reverted to extraction.

The concentrated yttrium nitrate solution obtained by stripping with 6 N HNO_3 is processed further to high purity in many stages of extraction using the quaternary ammonium compound Aliquat 336. The separation of high purity yttrium is based, quite obviously, on the different extraction behavior of yttrium in nitrate and thiocyanate systems. Using 43% quaternary ammonium nitrate (nitrate of tricapryl-methylamine) in Solvesso 250, the lighter rare earths Gd–Er are extracted leaving yttrium in the raffinate along with thulium, ytterbium, and lutetium. The yttrium content of this rare earth mixture is 95%. Ammonium thiocyanate was added to this raffinate and using quaternary ammonium thiocyanate (tricapryl-methyl-ammonium-thiocyanate) in Solvesso 150, the rare earths Tm, Yb, Lu were extracted leaving yttrium in the raffinate. Yttrium is recovered from the raffinate by direct precipitation with oxalic acid and calcination to an oxide product. To enhance the purity of the yttrium product further, an additional solvent extraction stage is also carried out (mainly

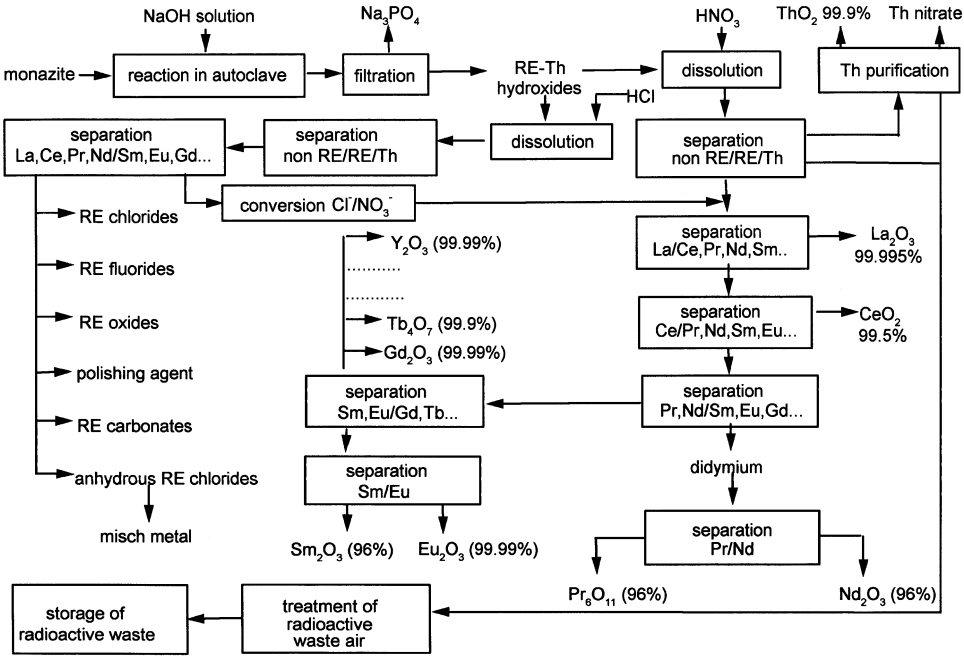

Figure 3.49 Rhône-Poulenc solvent extraction process for the separation of rare earth elements (McGill 1993).

to separate yttrium from non-rare earth impurities) ahead of the precipitation. From an aqueous solution containing ammonium thiocyanate, yttrium is extracted into the SCN form of Adogen 464. Yttrium is stripped from the solvent by water, and from the strip solution yttrium is precipitated as oxalate. The above process has been used by MCI–Megon, Norway for commercial production of 99.995% purity Y_2O_3. In addition to Aliquat 336, the solvent Adogen 464 in Solvesso 100 has also been used as the extractant (Ritcey and Ashbrook 1979) by Megon.

Rhône-Poulenc In Rhône-Poulenc all the rare earth elements with purities of >99.999% are produced almost entirely by solvent extraction. For certain rare earth elements, separation by solvent extraction alone would turn out to be very expensive. They are still produced in kilogram quantities by ion exchange. The outline of the Rhône-Poulenc separation scheme is shown in Figure 3.49 (McGill 1993).

Monazite, which is the source mineral, is digested with NaOH, and from the mixed RE–Th hydroxide obtained after trisodium phosphate separation, a rare earth chloride solution and a rare earth nitrate solution are produced. The unwanted elements are removed from each of these solutions. The solvent extraction stream in the chloride medium yielded nonseparated rare earth compounds, such as dehydrated rare earth chlorides, which are useful for electrolysis to misch metal. The solvent extraction stream in the nitrate medium is used to yield separated rare earth oxides. Lanthanum (99.995% La_2O_5) is left in the aqueous phase while the mixture of Ce, Pr, Nd, Sm, Eu, Gd, Tb, Y etc., goes into the organic phase. Similarly CeO_2 (99.5%) is separated in the Nd–Sm stream. After primary Ce removal, following the sequence shown in the figure, Pr, Nd, Sm, Eu, Gd, Tb, and Y oxides are recovered. The purification and isolation of individual rare earths is carried out

in a variety of extractants that include acidic and neutral organophosphorus compounds, amines, and carboxylic acids.

The solvent extraction separation of each rare earth element is carried out in multi-stage batteries of mixer settlers. At least 50 mixture settler stages per stream are needed to obtain a product with four to 99.9999% purity.

Rhône-Poulenc produces high purity separated rare earth oxides starting from not only monazite, but also from bastnasite or euxenite. The Rhône-Poulenc solvent extraction flowsheet has been regarded as the standard for all industrial producers (Bautista 1995).

Thorium Ltd. In the erstwhile practice at Thorium Ltd. in the U.K., a bastnasite concentrate was processed first by leaching the rare earth carbonates by HCl followed by caustic treatment of the leached concentrate, to break the fluoride bond. The rare earth hydroxides thus obtained were then leached with HCl. The mixed rare earths chloride solution was processed by solvent extraction. First, the rare earths samarium to yttrium were extracted by an unnamed extractant, and europium was reduced to the divalent state and recovered (Ritcey and Ashbrook 1979). Subsequently, gadolinium, samarium, and yttrium were recovered in a separate process. The raffinate contained La, Ce, Pr, and Nd. Sodium hypochlorite was used to oxidize Ce in the raffinate to Ce^{4+} which precipitated as cerium hydroxide on the addition of ammonia. The solution, containing La, Pr and Nd, was precipitated with sodium carbonate and the precipitate was redissovled in nitric acid.

Thorium Ltd. used TBP as extractant for the separation of individual rare earths from the nitrate solution. The process was a batch extraction in which equilibrium was attained by a total recycle on the extraction stages as well as total recycle on the scrubbing stages until the desired solutes had been concentrated. Water was used to strip the rare earths from the loaded solvent and from the strip liquor. The rare earths were precipitated as hydroxides or carbonates. The precipitates were dissolved once again in acid and the solution was recycled. Even though this process finally yielded the desired product purity, it is costly relative to a continuous process and is also not attractive for use in large plant installations.

For the extraction and separation of yttrium, Thorium Ltd. used Versatic 911. They developed the technique of total recycle in two consecutive systems. The first was a 25-stage process operated with versatic acid and the second was a 50-stage process operated with TBP as the extractant. By these, Y_2O_3 of 99.999% purity was obtained starting from a 47% Y_2O_3 concentrate (Brown and Sherrington 1979, McGill 1993).

Yao Lung chemical plant The Yao Lung chemical plant in Shanghai was the first of the rare earth processing plants in China. It went into production in 1964 and operates a similar process for the digestion of monazite as Rhône-Poulenc. The simplified flowsheet of this plant for extraction and separation of rare earth oxides from monazite (Zhang et al. 1982) is given in Figure 3.50.

A flowsheet for the simultaneous purification of yttrium and other heavy rare earths is shown in Figure 3.51. This flowsheet, believed to be used in Japan for commercial production (Thakur 2000), comprises solvent extraction operations with versatic acid, PC88A and TBP.

3.6 SCANDIUM

Solvent extraction has been the process used for the recovery and isolation of scandium from its resources, which are essentially non-rare earth minerals. In the processing of uranium,

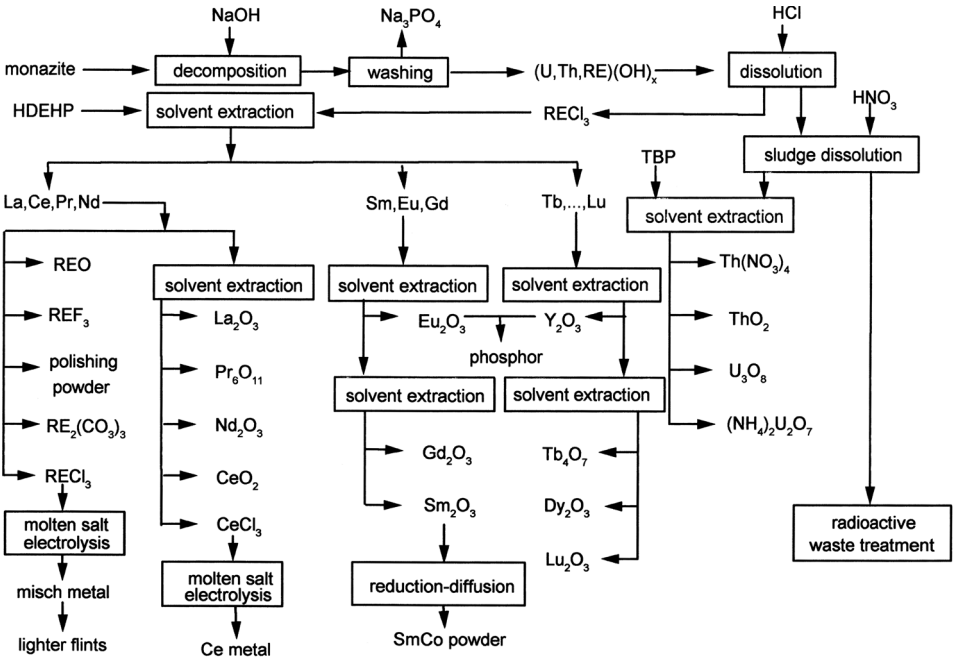

Figure 3.50 Simplified flowsheet of Yao Lung chemical plant (Zhang et al. 1982).

during solvent extraction, scandium is extracted and concentrated together with uranium. In the subsequent purification of the uranium, the scandium is separated. Three processes for accomplishing this separation and recovery of 99% pure scandium have been reviewed by Gschneidner (1975). In the processes likely to be used for large scale, high purity scandium recovery from wolframite use solvent extraction for separation. The processes employed for opening thortveitite use chlorination (Iya 1953, Vickery 1955) or fluorination (Spedding et al. 1958) to obtain a scandium-rich material which is subsequently dissolved and the scandium recovered in pure form by using ion exchange and solvent extraction.

3.7 SUMMARY

The by-product status of one of the two principal minerals of rare earths, monazite, carries it through the processing steps from as-mined condition to the status of a mineral concentrate. Even though monazite mining and processing are carried out in different parts of the world, the processes applied for beneficiating the mineral are essentially the same: gravity, electrostatic and electromagnetic separations and flotation. For beneficiating the bastnasite ore from Mountain Pass and the iron–rare earth–niobium ore from Bayan Obo, flotation is the key process and it works. Both acid and alkali digestion methods have been applied to monazite processing and the alkali treatment technique that yields trisodium phosphate by-product is used commercially. Chemical treatment of bastnasite is less extensive. Usually the processes applied for chemical attack of monazite and bastnasite or their minor variations work well on the remaining resources such as xenotime, gadolinite, and euexenite. As far

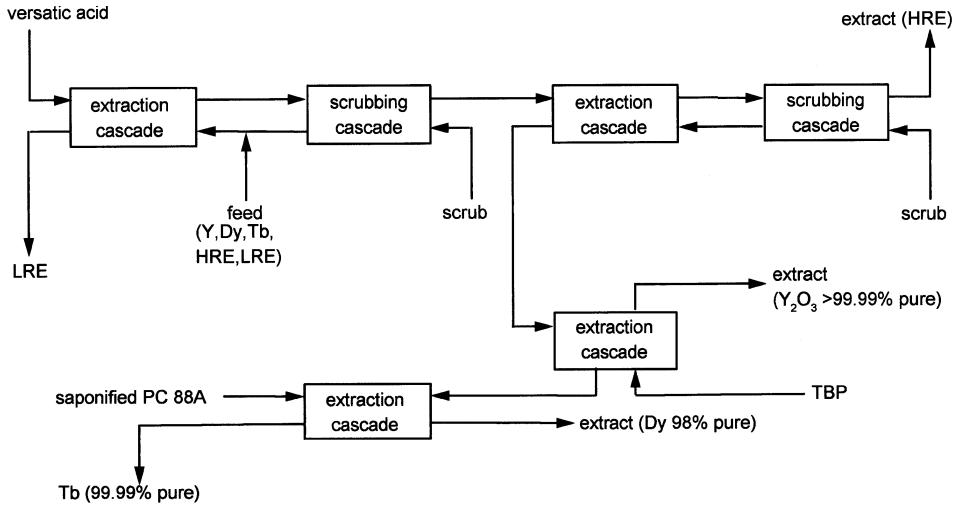

Figure 3.51 Flowsheet for the simultaneous purification of yttrium, terbium and dysprosium using versatic acid, TBP and PC 88A (Thakur 2000).

as chemical treatment of rare earth resources is concerned, direct chlorination in the presence of carbon has been the widely effective technique with every type of mineral.

The celebrated chemical similarity of the rare earth elements has a built-in bug in the slow and steady change in basicity, as the elements lanthanum to lutetium and yttrium are considered. This difference has been exploited directly and indirectly in devising procedures for separating rare earths from one another, both by the classical methods of fractional crystallization and fractional precipitation and also by the modern methods of ion exchange and solvent extraction. Exploitation of multivalency, particularly in cerium and europium, is obvious from the basis of methods for effecting their separation. These techniques have remained timeless and continue to be used even in current procedures as part of the overall technique of separation either preceding or following ion exchange or solvent extraction. Both ion exchange and solvent extraction rely on the availability of suitable complexing agents and solvents, respectively. EDTA and HEDTA are the mainstay for ion exchange. In solvent extraction TBP, DEHPA, PC88A, versatic acid and Aliquat 336 have been very useful.

Among the two modern separation techniques, ion exchange and solvent extraction, solvent extraction has the advantages that it is fast, continuous, and works on more concentrated solutions, and it is economical for handling large quantities of materials. Ion exchange is, however, regarded as superior for the production of extremely pure materials. However, commercial production of materials at 99.9% or even 99.99% purity with solvent extraction has been possible (Bautista 1995). Although the details of actual procedures, sequence of various operations, and identities of certain organic solvents are usually not disclosed in publications, the solvent extraction technology has been expanded in the three decades starting from the mid-1960s to commercial scale separation/ purification of at least 11 of the 15 rare earths that occur in bastnasite, monazite, and xenotime ores. Solvent extraction would not be the method of choice in at least two instances: (1) when product purity exceeding 99.9% is required, and (2) when the lesser abundant rare earths such as Tm, Yb, and Lu are to be isolated in a commercial solvent extraction circuit.

CHAPTER 4

Reduction

4.1 INTRODUCTION

The rare earth oxides are the end products of the ore processing and separation operations. They are therefore the natural starting material for conversion to metal by reduction. These oxides are extremely stable and their reduction to metal is, therefore, very difficult. The difficulties in reduction are usually compounded but occasionally alleviated by the physical properties such as the melting point and vapor pressure of the rare earth metals. Conversion of the rare earth oxide to a rare earth halide and reduction of the halide to the metal is a useful procedure because of certain inherent characteristics of the halide reduction processes. Fused salt electrolysis as applied to the production of reactive metals also holds relevance for rare earth metals preparation. The relatively low melting point of many of the rare earth metals is an advantage here. The preparation of rare earth metals by a method in which an alloy is prepared first and the metal is then recovered from the alloy is another interesting possibility. In this route both chemical and electrolyte methods of reduction may be used.

Every method of rare earth metal preparation has certain advantages and limitations with respect to applicability to individual rare earths, purity of product, yield of the metal, batch size, operational convenience, and economy. In spite of their celebrated chemical similarity in their trivalent states, the rare earths do display considerable variation in properties like melting point and vapor pressure. This variation largely comes in the way of applying certain reduction methods uniformly for the preparation of all the rare earth metals. Another factor is the possibility of a stable divalency in some of the rare earth elements. This frustrates attempts to produce them by the usual chemical or electrolytic reduction processes. Special processes, however, circumvent the limitation.

4.2 FUNDAMENTALS

The process of liberation of a metal from its compound or "reduction" is represented by the following general reaction:

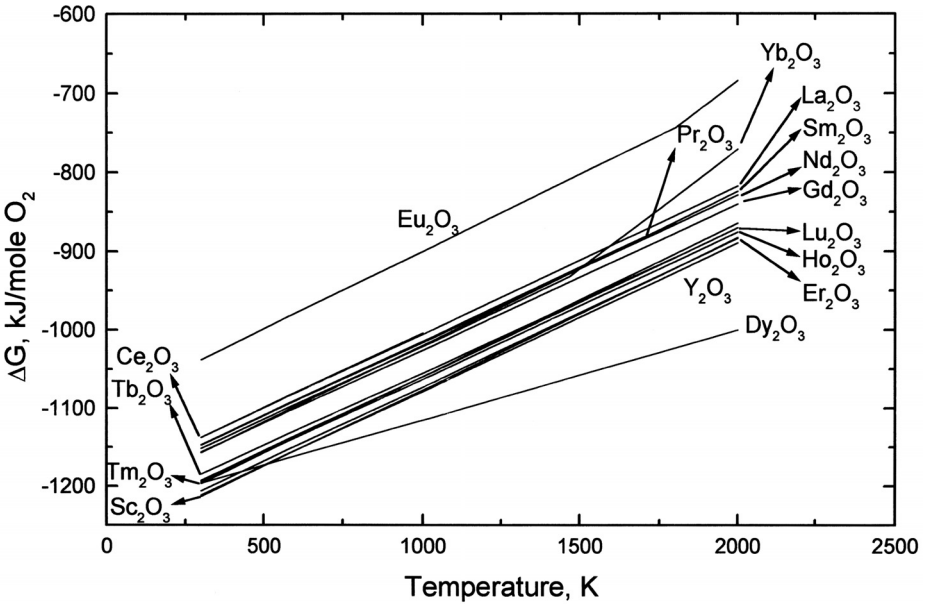

Figure 4.1 Standard free energy of formation of rare earth oxides as a function of temperature.

$$MX_n + iR = M + iRX_{n/i} \tag{1}$$

where M is the metal to be obtained; X is oxygen, fluorine, or chlorine; and R is the reducing element which, in general, may be hydrogen, carbon, or metals such as lithium, sodium, potassium, magnesium, calcium, or aluminum, in most of the cases. It is fundamental knowledge that metallurgical thermodynamics provides the answer to the question if reaction (1) can occur at all. The reaction is possible only when at a chosen reaction temperature the difference between the free energies of formation, ΔG, of the starting compound, MX_n, and the corresponding compound of the reductant element, $RX_{n/a}$, is negative. In other words, if the condition

$$i\Delta G(RX_{n/i}) - \Delta G(MX_n) < 0 \tag{2}$$

is satisfied. Therefore the free energies of formation of the metal as well as reductant oxides, fluorides, and chlorides, and their dependence on temperature determine which element can function as R for a given compound MX_n to release the metal M. The data on the free energies of formation of compounds were presented as straight line plots with temperature as abscissa and standard free energy of formation as ordinate first by Ellingham (1944) and later by Richardson and Jeffes (1948). The Ellingham diagrams of compounds relevant to the reduction of rare earths are given in Figures 4.1 to 4.5. Data from the U.S. Bureau of Mines Publications (Pankratz et al. 1984) have been used in preparing these diagrams.

Even as the first approximation, the number of elements that can function as reducing agents for the rare earths is very limited. Under standard conditions, the order of stability

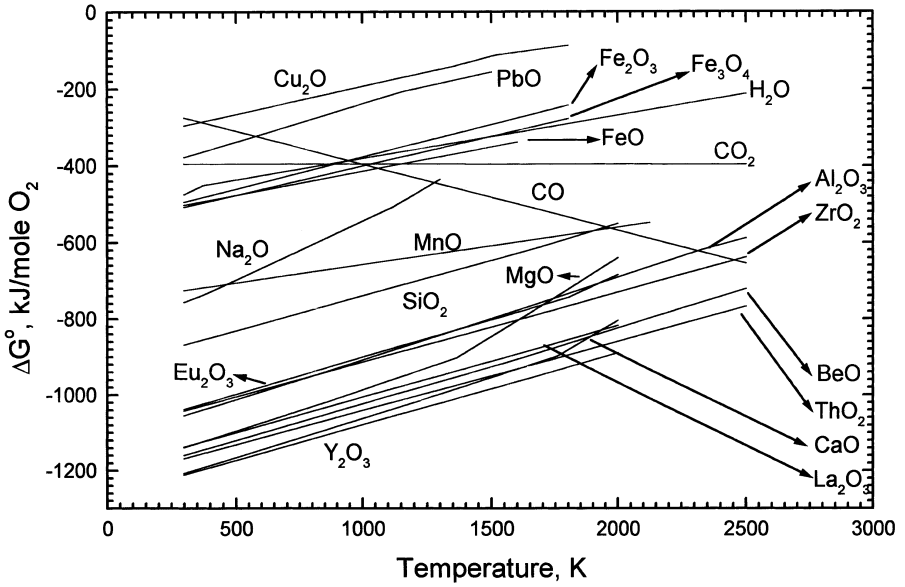

Figure 4.2 Standard free energy of formation of selected oxides of rare earths and certain common metals as a function of temperature.

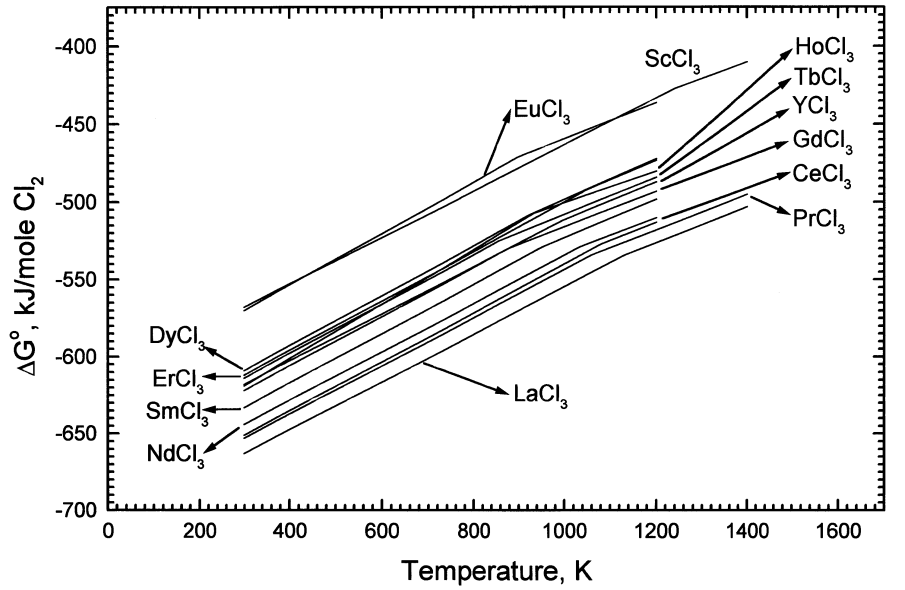

Figure 4.3 Standard free energy of formation of rare earth chlorides as a function of temperature.

among the oxides is $CaO > RE_2O_3 > MgO > Al_2O_3 >> SiO_2$. The situation is similar among the fluorides. Here again, the order of stability is $CaF_2 > REF_3 > LiF > NaF > MgF_2 > AlF_3$. There appears to be, however, a choice of many metals to reduce the rare earth chlorides

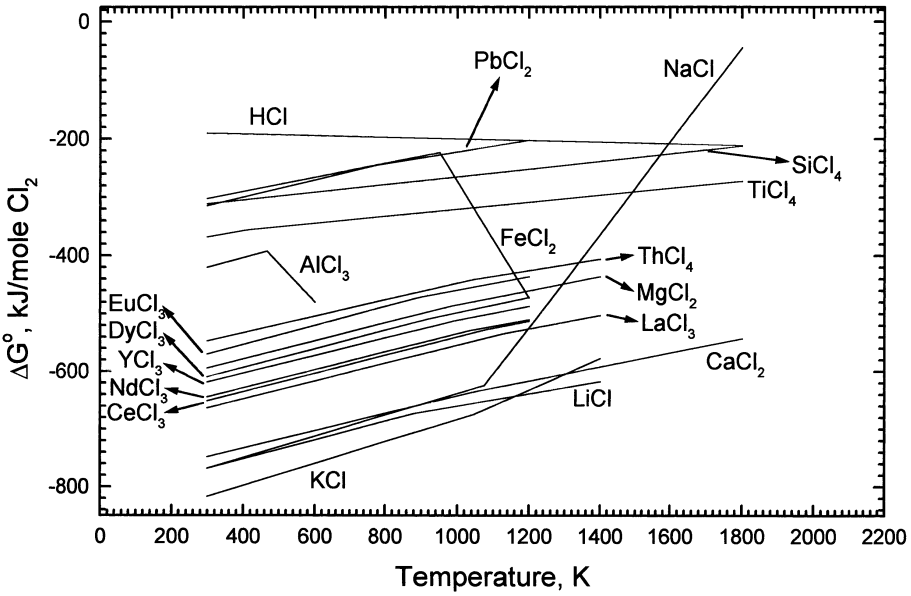

Figure 4.4 Standard free energy of formation of selected chlorides of rare earths and certain common metals as a function of temperature.

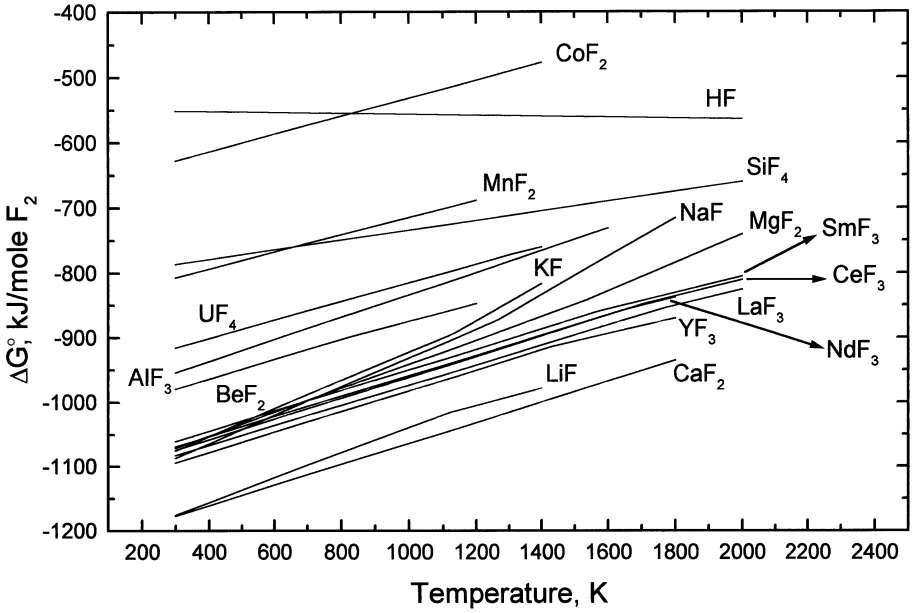

Figure 4.5 Standard free energy of formation of selected fluorides of rare earths and certain common metals as a function of temperature.

because the order of stability here is KCl > NaCl ≈ LiCl ≈ $CaCl_2$ > $RECl_3$ > $MgCl_2$ >> $AlCl_3$. Thus under standard conditions, which in effect means MX_n, R, M, and $RX_{n/i}$ given

in equation (1) are all pure and at one atmosphere pressure, only calcium can reduce the rare earth oxides and fluorides. However, the chlorides can be reduced by potassium, sodium, and lithium in addition to calcium. Among the nonmetals, hydrogen cannot reduce the rare earth chlorides at temperatures normally used for conventional reduction. Carbon, forming carbon monoxide, can reduce the rare earth oxide at high temperatures.

The picture under nonstandard conditions that, more often than not, more closely approximates the real reduction process condition is somewhat different. Here the reaction mixture need not be composed of only pure constituents MX_n, R, M and $RX_{n/i}$ under 1 atmosphere pressure. In other words, the activity, a, of each of the constituents, a_R, etc., need not be kept equal to 1. The use of conditions where a_R etc., of one or more of the components is made less than 1 alters the value of the free energy of the reaction and creates a more favorable environment for the reaction to proceed. The typical methods to effect the activity change are the formation of a product metal having a low boiling point and hence vaporizing in the metallothermic reaction ($p_M < 1$ atm and $a_M < 1$), recovery of the reduced metal as an alloy ($a_M < 1$), and trapping the compound formed by the reductant in a complex slag ($a_{RX_{n/i}} < 1$). It may also be mentioned here that carbothermic reduction under vacuum, which makes $p_{CO} << 1$ (or $a_{CO} << 1$) becomes an efficient method of reduction at high temperatures. Even after circumventing the reaction feasibility factor by tailoring the reaction component activities, there are other considerations that influence the practical implementation of the reduction process. In rare earth metal preparation, the choice of reducing agents being mainly confined to metals, certain factors relating to the practicability of metallothermic reductions merit consideration.

4.3 METALLOTHERMY

The metallothermic reduction reaction may be generally represented by the equation

$$M(I)\,X_n + iM(II) = M(I) + iM(II)X_{n/i}$$

where M(I) is the metal to be produced, X is the anion, and i, n are the stoichiometric coefficients. While the feasibility of the metallothermic process is determined by the free energies of formation of the compounds involved in the above reaction, the practicability of the metallothermic reduction is determined by several other properties such as melting point, boiling point, vapor pressure, density, viscosity (for liquid components), and characteristics such as chemical reactivity and alloying behavior of the various participants (reactants and products) of the reaction. The computation of the standard free energy of the reaction, therefore, presents only a limited picture on the reaction practicability. A more complete picture is obtained by considering the various properties of the reaction participants listed above.

The desirable characteristics of the metallothermic reduction have been summarized by Herget (1985) as: (i) the reaction should occur quickly and give product metal in high yields, (ii) the reaction products must be obtained in compact forms — metal as an ingot and the slag as a well-separated layer, (iii) the reaction should be self-sustaining and once initiated should proceed without the need for additional external heating, (iv) the product metal must be of high purity, (v) the reaction proceeds in an open atmosphere, (vi) the

reaction should proceed safely without risk, and (vii) the reaction should be amenable to being carried out in commercially available reactors using readily available refractories as containers.

Metallothermic reductions are generally exothermic reactions, and by a suitable choice of reactants, materials, and process conditions it has been possible to realize many of the characteristics listed above and obtain the metal from its compound. The use of reactants in a powder or particulate form favors better reagent contact and, once initiated, a quicker reaction. If the heat generated during the reaction is sufficient to raise the temperature of both slag and metal to above their melting points, and if they remain molten for a sufficient length of time, so that the molten metal (denser) settles by gravity with the immiscible slag layer (lighter) remaining on its top, a metal ingot topped by a solidified slag results on cooling. Slag and metal are then separable by mechanical means. When the heat of reaction is insufficient to result in an all liquid reaction mixture, other types of products can form. If the reduction occurs but the slag does not melt, the metal is formed as a powder dispersed in the slag matrix. The slag in this case is leached away to separate the metal powder. Metal in the form of powder can result even if the slag melts if the melting point of the metal is very high and the metal is not sintered at the temperatures involved. When the reduction to metal occurs with only the slag melting, but not the metal, the metal particles usually coalesce and undergo partial consolidation into what is called a sponge. Here the metal and sponge are separated either by aqueous leaching or by vacuum distillation.

By a suitable choice of reductants, reactors, and reaction conditions, the metal can usually be obtained in the chosen form. The rare earth metals have been prepared by metallothermic reduction in the form of an ingot, sponge, or powder. Metal ingot has been prepared usually by metallothermic reduction of rare earth fluorides as well as some of the rare earth chlorides using calcium as reductant. Rare earth metal in the form of sponge has been obtained from the chloride using lithium as the reductant. Rare earth metal powder has been directly obtained by reducing rare earth oxide with calcium. Instead of the elemental metal product certain rare earth alloys can also be directly prepared in ingot, sponge, or powder form. Metal is subsequently obtained from the alloy by distillation in vacuum.

In the earliest successful attempt on rare earth metal preparation, metallothermic reduction was used and this technique, to date, remains the most widely used. The purity of the metallothermic reduction product depends, among other things, on the purity of the starting materials, pure oxides, anhydrous chlorides and fluorides, and that of reductants. While the purity of rare earth oxides is essentially determined by the separation step, the purities of chlorides and fluorides are determined by the method of their preparation, usually starting from the oxides.

4.4 PREPARATION OF RARE EARTH CHLORIDES

The preparation of rare earth chlorides for use as intermediate for reduction to metal has been accomplished by two routes (Block and Campbell 1961). One, known as the wet route, involves dehydration of hydrated rare earth chloride and in the other, the dry route, the oxide is directly converted to anhydrous chloride.

4.4.1 Preparation of Hydrated Rare Earth Chloride

The basic procedure was described by Spedding et al. (1952). The rare earth oxide was dissolved in hydrochloric acid and the solution was evaporated to a syrup, which boiled at 128°C. This solution was then poured into a large porcelain disc and stirred while it cooled forming the hydrated chloride crystals.

Spedding and Daane (1952) also prepared hydrated cerium chloride by dissolving cerium ammonium nitrate in 6N hydrochloric acid and evaporating the resulting solution to a boiling point of 125−130°C. On cooling, the hydrated chlorides crystallized.

Nolting et al. (1960) prepared yttrium chloride by digesting yttrium oxide in concentrated hydrochloric acid and by evaporating the solvent until the yttrium chloride hexahydrate crystallized.

Mixed hydrated rare earth chloride was produced in the past (Hirschhorn 1967) by wet chemical treatment of bastnasite and monazite. The process used for bastnasite at the York, PA, plant of Molycorp (Kruesi and Duker 1965) was described in Chapter 3.

4.4.2 Dehydration of Hydrated Rare Earth Chlorides

An old and popular method for the preparation of anhydrous rare earth chlorides involves dehydration of the hydrated chloride under an atmosphere of dry HCl (Kleirheksal and Kremers 1928). Dehydration involves heating the hydrated chloride, and in many of the investigations (Block and Campbell 1961) it has been reported that the temperature should be below the melting point of partially dehydrated chloride to prevent it from reacting with the liberated water and forming oxychlorides. Harrison (1952), however, has observed that in the final stages of dehydration, temperatures above the melting point are necessary to prepare rare earth chlorides free of oxychlorides. An increase in dehydration temperature can result in quicker dehydration. While several days are required to dehydrate a single batch of chloride when the temperature is kept at well below 100°C, complete dehydration could be affected in half a day if the hydrates were slowly heated to 250°C under a reduced pressure of approximately 3 kPa. During dehydration a small flow of HCl is maintained over the salts to prevent hydrolysis.

The tendency to hydrolyze appears to depend on the temperature and the particular rare earth chloride (Koch 1953). The stability of oxychlorides increases with increase in temperature and with increase in atomic number. Thus heavier rare earth chlorides would be more difficult to prepare by dehydration of hydrated chlorides.

The following overall procedure has been used at Ames laboratory to prepare anhydrous rare earth chlorides on a fairly large scale (Block and Campbell 1961). Rare earth oxides were dissolved in hydrochloric acid and the solution was heated to drive off uncombined water. When the solution had been heated to about 130°C and had become viscous, it was poured into an evaporating dish and was allowed to cool. While cooling, the salt was stirred continuously to make it crystallize as a powder. The hydrated salt powder was then dehydrated by heating in a 75 to 100 mm diameter pyrex tube through which purified HCl was passed while the pressure was maintained at 550−650 Pa. Heating was done gradually, raising the temperature from below 80 to 400°C over a period of 10 to 30 h. The product was anhydrous rare earth trichloride free of oxychlorides.

Nolting et al. (1960) prepared anhydrous yttrium chloride in an apparatus shown schematically in Figure 4.6. The hydrated chloride was dehydrated by passing anhydrous

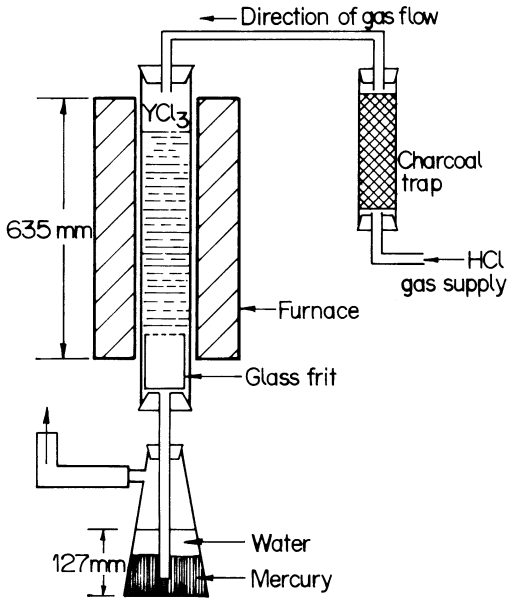

Figure 4.6 Setup for dehydrating yttrium chloride (Nolting et al. 1960).

hydrogen chloride gas under slight positive pressure downward through the dehydrating tower containing the yttrium chloride. Starting at 110°C hydrogen chloride was passed (~0.5 l/min) through the column for 24 h by which time no more water was collecting downstream outside the tower. The water collected until it then corresponded to 80% of the water of hydration of the yttrium chloride. The temperature was then raised to 350°C for another 24 h. Dehydrated yttrium chloride was removed from the tower after cooling. It was melted in a platinum crucible at 1000°C in an inert atmosphere to remove hydrogen chloride and cast into rods (25 mm diameter by 75 mm long) in a copper mold. The yield was quantitative.

In another method, the hydrated chloride was dehydrated in the presence of an excess of ammonium chloride (Jantsch et al. 1930, 1931, Gray 1951). The temperature of the salt was gradually raised keeping it under a stream of HCl or vacuum. As the heating continued, ammonium chloride was also evolved and this helped to prevent the formation of oxychlorides. Block and Campbell (1961) have reported that better results were obtained when the hydrated salts were dehydrated in the presence of ammonium chloride at a very low pressure than when the hydrated salts were treated under a reduced pressure of HCl. This happens because ammonium chloride is a more effective chlorinating agent than HCl. The pressure during dehydration with ammonium chloride should be less than 60 Pa to minimize oxygen contamination. Such an operation, because of low ambient pressure, requires several days for completion. The following description given by Block and Campbell (1961) pertains to the preparation of anhydrous yttrium chloride in 20 kg batches.

Yttrium oxide was slowly dissolved in concentrated hydrochloric acid and the insoluble matter was filtered out. Four moles of ammonium chloride per mole of yttrium was added to the filtrate. The solution was heated to evaporate water. Heating was continued until the normal boiling point of the solution reached 132°C and at this point the solution was a thick syrupy liquid. Upon cooling, this liquid solidified to a crystalline mass

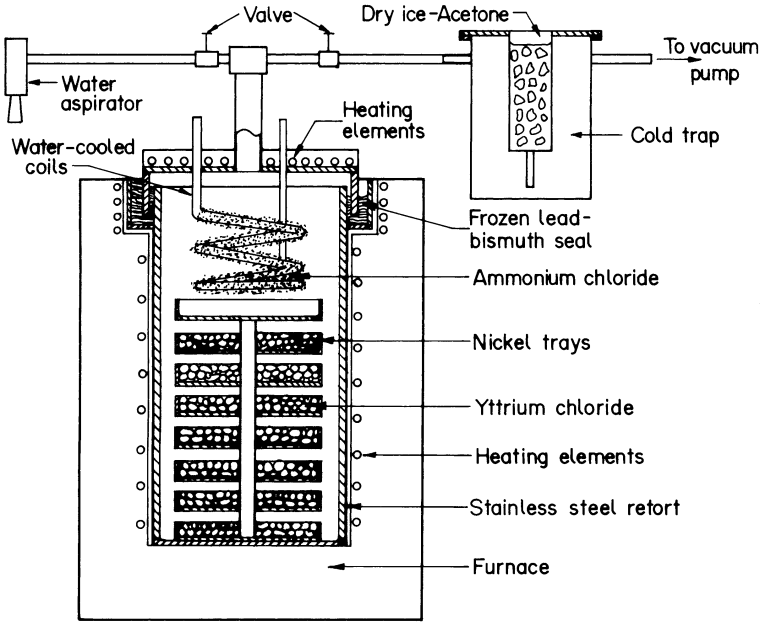

Figure 4.7 Yttrium chloride dehydration assembly (Block et al. 1960).

containing a mixture of ammonium chloride and hydrated yttrium chloride. This salt was dehydrated in a nickel vacuum retort (Block et al. 1960) shown in Figure 4.7.

The hydrated salt was loaded into a series of circular nickel trays to a depth of about 50 mm. Initially the retort was evacuated with a water aspirator and heated to 100–120°C. The bulk of the water was thus removed. After reaching 120°C and after the evolution of water had stopped, the valve to the aspirator was closed and the retort was connected to a rotary vacuum pump. A dry ice–acetone cold trap between the retort and the pump collected the water. The temperature of the retort was raised slowly to 350°C in such a way that the pressure within the retort remained at 3 to 70 Pa. During this operation, whatever water remained in the hydrated salt was removed and collected in the cold trap, and ammonium chloride was sublimed and collected by condensation on the water-cooled coils suspended from the top flange of the retort. Six to seven days of operation were required to handle a charge of 20 kgs, and 95 to 98% of yttrium originally present in the yttria was converted to anhydrous yttrium chloride.

Croat (1969) used the apparatus shown in Figure 4.8 for vacuum dehydration of a mixture of NH_4Cl and the hydrated rare earth trichloride. This apparatus consisted of an inconel furnace tube or retort (130 mm in diameter and 915 mm in length) in series with a dry ice and acetone trap and a pumping system. The face plate of the retort contained a water-cooled cold finger made of inconel for freezing out part of the NH_4Cl. The chloride was contained in a platinum boat with a loose fitting lid. Croat (1969) used this apparatus to prepare anhydrous chlorides of dysprosium, holmium, and erbium. The hydrated chlorides were heated for 4 h at 90°C while evacuating the retort with a water aspirator. The bulk of the uncombined water was thus removed. The charge was then gradually heated to 335°C while evacuating to 1 Pa. The bulk of the removed NH_4Cl was collected on the water-cooled cold finger. The anhydrous chlorides were vacuum cast in the apparatus

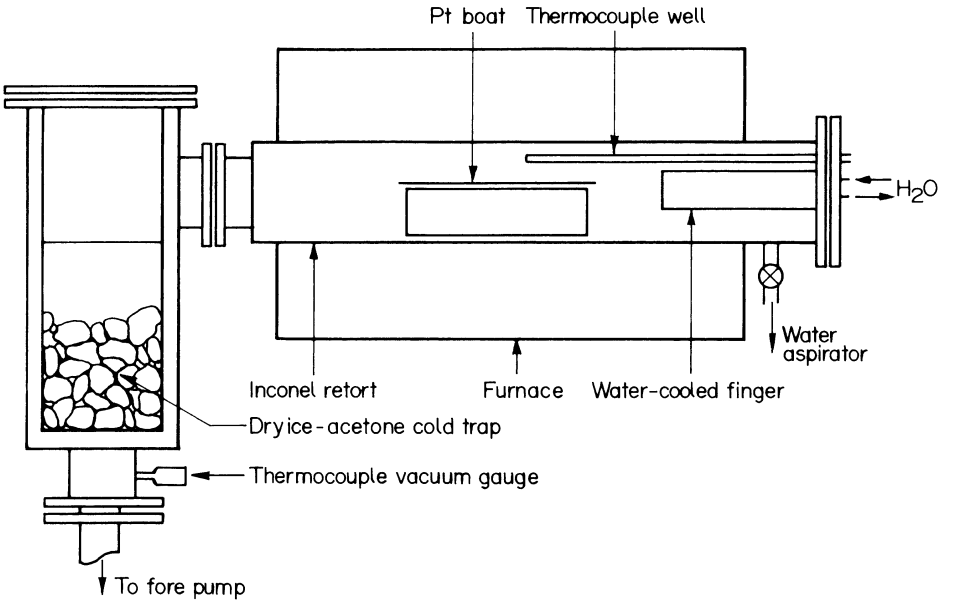

Figure 4.8 Schematic drawing of the apparatus for dehydrating hydrated rare earth trichloride (Croat 1969).

shown schematically in Figure 4.9. In the 62 mm diameter and 250 mm long tantalum crucible, approximately 600 g of the anhydrous chloride could be vacuum cast. The 6 mm tantalum tube extending upward from the bottom of the crucible was useful for venting volatile products during the casting process. The crucible lid made of a tantalum sheet was welded in place after the chlorides were loaded with the crucible. The chlorides were heated slowly under 0.001 Pa to approximately 100°C higher than their melting point and held for a few minutes only. The loss of chlorides by volatilization was negligible because the chloride vapor pressure at vacuum casting temperatures was less than about 10 Pa.

In a recent investigation, Chambers and Murphy (1988) used a glass-lined reactor, shown in Figure 4.10, for dehydration of neodymium chloride hexahydrate in a vacuum in the presence of ammonium chloride.

Hirschhorn (1967) has summarized the methods for dehydrating hydrated rare earth chloride as used industrially in the 1940s. The hydrated chloride obtained by wet chemical treatment of monazite or bastnasite contained about 30% H_2O. It was dehydrated using methods that minimize oxidation or hydrolysis. The technique typically included heating in vacuum or heating in air with the admixture of a salt, to reduce hydrolysis. The Auergesellschaft in Berlin used a rotary iron vacuum drum drier, steam heated to 350°C at a vacuum of 90 kPa. The product had an oxychloride content of 1.5%. In Bavaria, Prometheus used a process involving heating a mixture of rare earth chloride with $CaCl_2$ in air for 2 to 2.5 h. The yield was typically 62%, indicating that the dehydrated chloride contained substantial amounts of oxychloride. Treibacher Chemische Werke of Austria used a two-stage vacuum drying process in which the hydrate was heated first at 170°C and then at 350°C. While many dehydration techniques involve the addition of ammonium chloride to reverse hydrolysis, some commercial producers use sodium or calcium chloride to retard hydrolysis on the basis of common ion mass action effect.

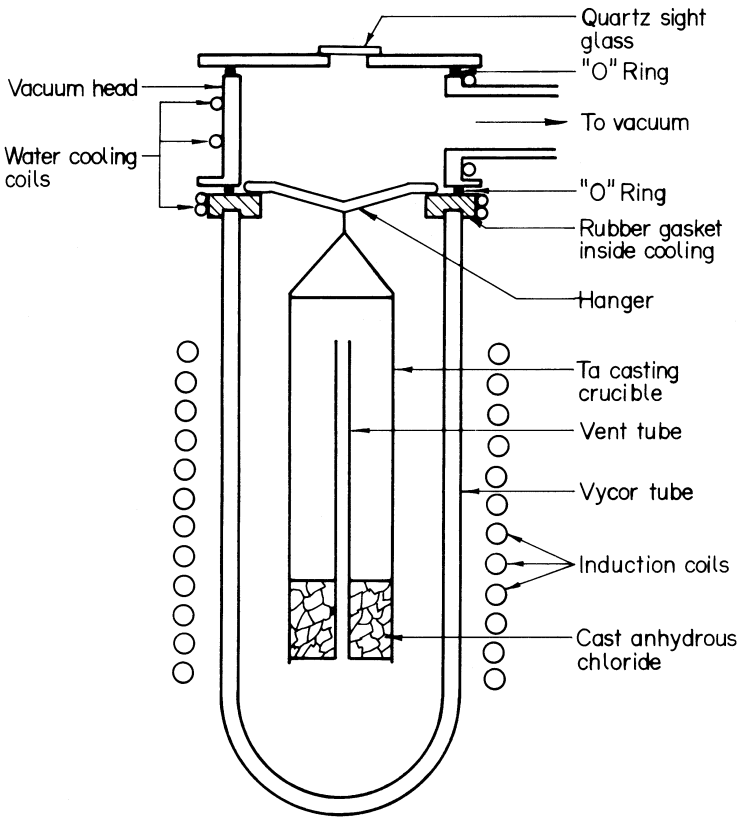

Figure 4.9 Apparatus for vacuum casting the anhydrous rare earth trichlorides (Croat 1969).

4.4.3 Dry Methods

There are many dry methods to directly prepare anhydrous rare earth chlorides. The method reported by Reed et al. (1935, 1939) involves the solid state reaction of rare earth oxide with ammonium chloride. By heating rare earth oxide with twice the theoretically required quantity of ammonium chloride at about 190°C, complete conversion of the rare earth oxide to rare earth chloride occurred. Excess ammonium chloride was removed from the product by heating to 300–320°C under vacuum. About 85 to 95% of the rare earth present in the oxide was converted to the anhydrous chloride.

Another dry method involves the use of thionyl chloride in a sealed pressure vessel. Conversion was usually incomplete even after the temperature between 150 and 300°C was maintained and the treatment was continued for three days (Hecht et al. 1947).

Other dry methods for the preparation of anhydrous rare earth trichloride involved direct reaction of the metal carbide or the rare earth oxide–carbon mixtures with a gaseous chlorinating agent, e.g., elemental chlorine. The method of directly chlorinating the rare earth minerals–carbon mixture by chloride was described earlier in Chapter 3 for monazite (Hartley 1952) and bastnasite (Brugger and Greinacher 1967). Actually, the process

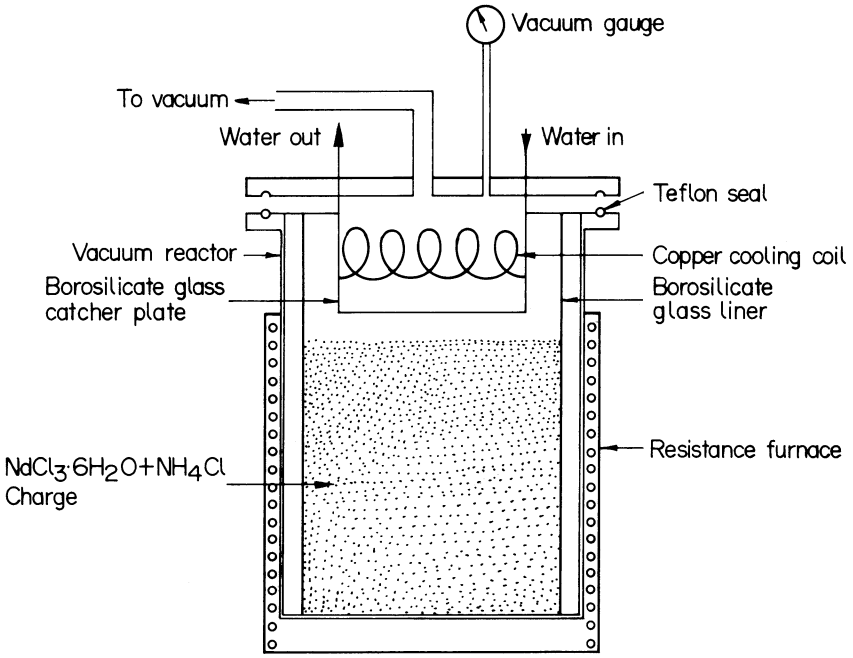

Figure 4.10 Apparatus for dehydrating neodymium chloride (Chambers and Murphy 1988).

described for bastnasite by Brugger and Greinacher (1967) has been used on a production scale at Th. Goldschmidt AG. This process has also been useful for chlorinating other rare earth ores like monazite, allanite, cerite, xenotime, euxenite, fergusonite, gadolinite, etc. The fused anhydrous chlorides of the rare earths obtained as final product are devoid of thorium chloride and any oxychloride. They are suitable for the production of corresponding metals. Using the same chlorinating procedure, one can convert pure rare earth oxide to the corresponding anhydrous chloride.

Block and Campbell (1961) have described a method for chlorinating cerium and yttrium oxides, with a mixture of chlorine and carbon tetrachloride, in the presence of carbon. The oxides were mixed with an excess of carbon and a small amount of dextrin (binder) and were formed into pellets or nodules. The nodules were loaded into a vertical quartz tube in the apparatus shown in Figure 4.11 (Block et al. 1960) and heated to 600°C in the absence of air, to decompose the dextrin. Either chlorine alone or carbon tetrachloride mixed with a small amount of chlorine was then passed up through the charge while it was heated to a temperature just below the melting point of the chloride. If the chlorides melt, they coat the unreacted particles of the charge. For cerium, temperatures between 750 to 800°C were found to be optimum, and for yttrium best results were obtained at 650°C. Approximately 95% of the rare earth present as the oxide was converted to the chloride in the above procedure. The product in these procedures was impure because of the presence of unreacted oxide and excess carbon and so needed a purification step.

Block et al. (1960) have also used yttrium oxalate in place of yttrium oxide–carbon mixture for chlorination. Yttrium oxalate was dried at 300°C for 8 h in the apparatus shown in Figure 4.11 and then was heated to 575°C while carbon tetrachloride was passed up

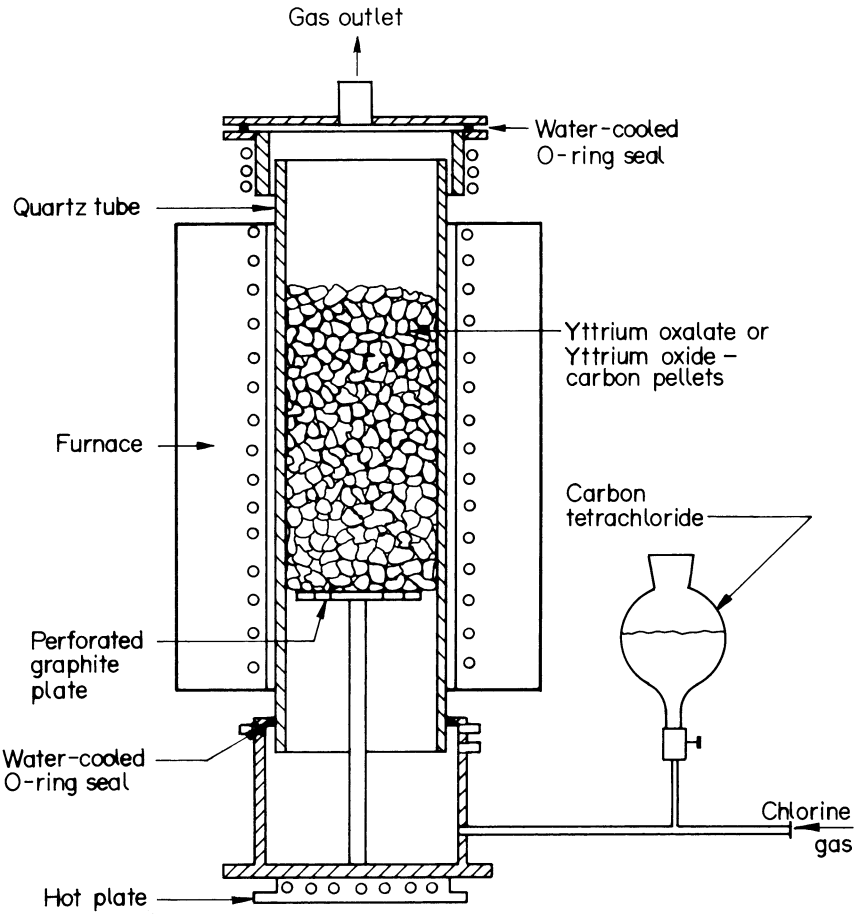

Figure 4.11 Yttrium chlorination apparatus (Block and Campbell 1961).

through the charge. Chlorine was used as a carrier gas to sweep the carbon tetrachloride through the tube. Overall yttrium recoveries of only 75% were obtained by this procedure. Even though no carbon remained in the product from the reaction, it needed to be purified to separate it from unreacted yttrium compounds.

4.4.4 Purification of Rare Earth Chlorides

The major impurity in a prepared rare earth chloride is oxygen. It is present either as unconverted oxide or oxychloride. Carbon is another impurity, particularly when the chloride is prepared by a carbothermic reduction. Vacuum distillation and filtration are the two methods used for freeing the rare earth chloride of oxygen-containing compounds, carbon, and several other impurities.

Purification by distillation was accomplished by Block et al. (1960) in an apparatus shown in Figure 4.12. The raw yttrium chloride obtained after dehydration was loaded into the nickel container shown in the bottom of the retort. The pressure inside the retort was

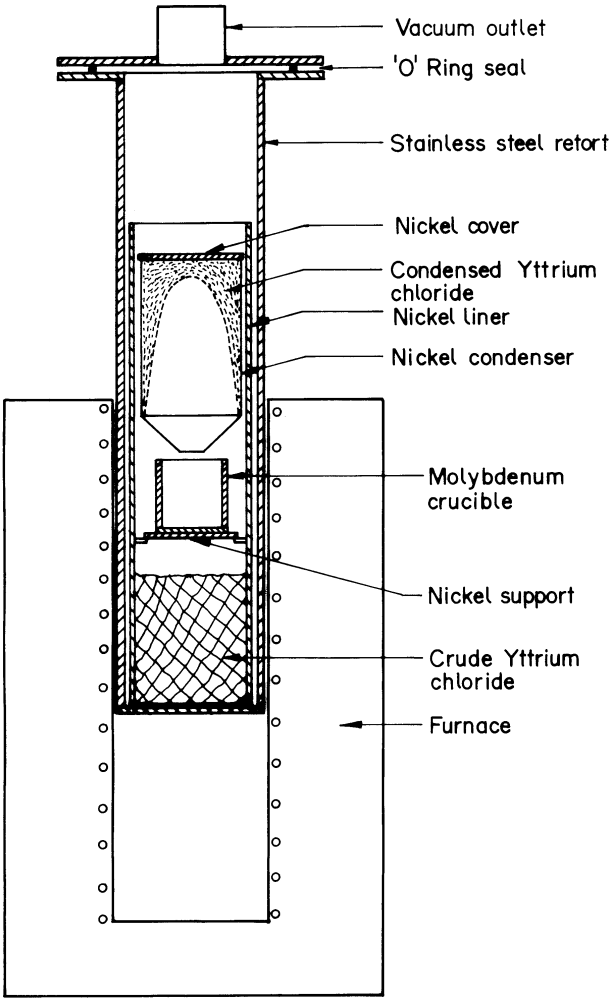

Figure 4.12 Yttrium chloride purification assembly (Block and Campbell 1961).

maintained between 5 and 50 mPa by continuous evacuation while the lower end of the retort containing the charge was heated to between 850 and 950°C. Yttrium chloride distilled and condensed in the upper cooler region of the retort. Distillation lasted 72 h to collect 20 kg of yttrium chloride. The retort was then backfilled with argon and the furnace was repositioned to heat the upper section of the retort to 900°C. Heating was continued for 1 h to allow the yttrium chloride to melt and run down into the molybdenum crucible which was placed midway between the charge container and condenser. Thus yttrium chloride was cast directly into the crucible, with minimum exposure to the atmosphere. Double distillation was done if an unusually large amount of impurities were present in the chloride. After the first distillation, the chloride was chipped off the nickel condensing shield and was loaded back into the lower container. The distillation was repeated. Between 90 and 95% of yttrium chloride charged to the retort was recovered in the purified product after vacuum distillation.

By vacuum distillation, not only the oxygen compounds are separated from the rare earth chloride, but also the rare earth chloride powder charge is converted into a dense crystalline mass. Even though the rare earth chlorides are extremely hygroscopic, less hydration occurred when the crystalline mass was handled as it exposed considerably less surface to the atmosphere (Moriarty 1968).

It is more difficult to separate carbon than oxygen by vacuum distillation. A second distillation is usually necessary to bring down the carbon level to less than 0.2%. Repeated distillation is necessary if the rare earth chloride is grossly contaminated. Solid impurities tend to entrain in the evaporating gas stream and are carried over to the condensate. Repeating the distillation results in their complete removal. As regards the overall recovery of rare earth chloride after preparation and purification, Block et al. (1960) noted that better recoveries (~90%) were obtained when an initial wet procedure was followed by distillation.

Filtration of the molten chloride is another method useful for the purification of rare earth chlorides (Block and Campbell 1961). This method was found to be especially effective for the separation of carbon from yttrium chloride. The molten chloride was allowed to drain through a pad of molybdenum wool and the entire operation was carried out in an argon atmosphere. As long as there was no moisture in the system, molybdenum or nickel containers could be used to contain the molten chloride. Filtration was more effective than distillation for removing gross contamination. However, if the impurities were present in lower levels, distillation was more effective.

4.5 REDUCTION OF RARE EARTH CHLORIDES

4.5.1 Early Attempts

The first recorded attempt at the preparation of a rare earth metal is credited to C.G. Mosander (1827). As early as 1826, he reduced cerium trichloride by heating it with potassium in a stream of hydrogen to obtain cerium metal powder. The product was, however, obtained in poor yields and was contaminated with excess reductant and reaction products. Following Mosander, several early attempts were made to reduce the rare earth chlorides by sodium and other alkali metals (Trombe 1957). The product obtained was invariably a metal powder in poor yield, dispersed in alkali chloride slag. However, successful preparation of several light rare earths was reported by reduction of their chlorides with potassium and sodium vapor (Kremers 1925, Zintl and Neumayr 1933). To remove the excess reductant and its products, the as-reduced metal was then vacuum annealed. Klemm and Bommer (1937) produced powder metals of all the rare earths except promethium. They carried out their reduction after sealing the rare earth trichloride with potassium in quartz ampoules to avoid atmosphere contact. The ampoules were heated at 350–400°C and the rare earth chlorides were reduced by potassium vapor. They succeeded in obtaining the rare earth metals as small crystals intermixed with excess potassium reductant and potassium chloride slag. Even though they never compacted their metal into an ingot, the metals were pure and they measured fairly accurate lattice constants for most of the rare earth metals.

The major investigations in the metallothermic reduction of rare earth chlorides are summarized in Table 4.1. A powder product dispersed in slag results from insufficient heat

Table 4.1 Chloride reduction processes

Year	Reactants	Process	Results	Reference
1827	$CeCl_3$–K	Heated in hydrogen flow	Ce metal powder in slag matrix	Mosander 1827
1952	$RECl_3$–Ca; (La, Ce, Pr, Nd)	Heated in Ta crucible under vacuum	Consolidated RE separated from slag	Spedding and Daane 1952
1959	YCl_3–Na or Li	Heated in Mo/Ta crucible under inert gas	Y sponge; slag distilled off	Block and Campbell 1961
1960	YCl_3–Li	Li vapor reduction of YCl_3 in Ta crucible inside a steel bomb	Y crystals; slag distilled off	Nolting et al. 1960
1967	YCl_3–Ca, Mg	Heated to 950°C	Low melting RE–Mg alloy; Mg distilled off	Carlson and Schmidt 1967
1968	$RECl_3$–Li; (La, Ce, Pr, Nd, Gd, Dy, Ho, Tb, Er, Lu, Y)	Li vapor reduction of $RECl_3$ in Ti crucibles inside steel bomb	RE crystals; slag distilled off	Moriarty 1968
1969	$RECl_3$–Li or Li–Ca; (Dy, Ho, Er)	Li vapor reduction of $RECl_3$	RE crystals; slag distilled off	Croat 1969

of reaction to melt the reaction products. Product melting and better slag–metal separation can be achieved primarily by (i) the use of a booster reaction to supplement the enthalpy of the main reaction, and (ii) forming a low melting reaction product such as the alloy and a multicomponent low melting slag. Cerium, neodymium, and gadolinium were obtained by reduction of their trichlorides with magnesium. As a result, a magnesium rare earth alloy was obtained. On removal of magnesium by vacuum distillation, rare earth metals with purities of 99.5–99.8% were obtained.

Following the earlier work of Moldenhauer (1914) and Karl (1934) calcium was also used to reduce cerium trichloride. Calcium in dolomite-lined steel bombs was used to reduce cerium trichloride securing kilogram levels of production of cerium metal. Here, additional heat necessary to melt and hence separate the reaction products was provided by using a calcium–iodine booster reaction. At the completion of the reduction, the slag was removed and the metal was vacuum melted to remove any excess calcium or calcium chloride slag. The purity of cerium thus obtained was greater than 98% and the yields were approximately 95%. This technique was also used to prepare lanthanum, praseodymium, and neodymium metals apart from cerium metal.

4.5.2 Reduction in a Refractory Bomb

The schematic of the reactor used by Spedding et al. (1952) for carrying out the reduction is shown in Figure 4.13. The bomb (reactor) was constructed from standard black steel pipe by welding a bottom of 6 mm steel plate on one end and threading the top to receive a standard steel or cast iron pipe cap. To prevent contact of the reaction mixture with the steel wall of the bomb a smooth surfaced refractory oxide liner was provided. The liner was a sintered lime or dolomitic oxide crucible inserted into the bomb and held in place by filling the narrow annular space between the crucible and the bomb walls with loose lime. On the top of the bomb, insulation was provided by a layer of lime held in place by a sintered lime lid. The threads of the bomb were sealed effectively by plumbers seal.

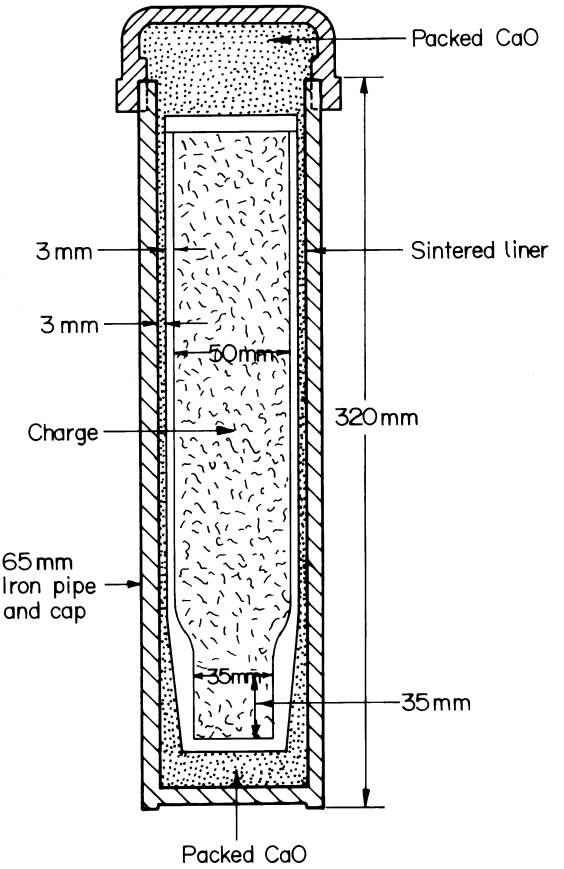

Figure 4.13 Loaded bomb for calciothermic reduction of rare earth chloride (Spedding et al. 1952).

The bomb was filled with a thoroughly mixed charge of the powdered anhydrous rare earth chloride, 20 mesh vacuum distilled calcium, and iodine in the ratio of 0.63 mole of iodine per mole of cerous chloride ($CeCl_3$) with 15% more calcium than the stoichiometric amount needed for the reaction. Reaction was initiated by placing the loaded and sealed bomb in a gas fired furnace held at 650 to 750°C. As the bomb temperature reached about 400°C, the reaction began and was going to completion in a matter of seconds, which was indicated by the sudden rise of the bomb temperature. The heat of reaction was found to be sufficient to melt both the slag and the metal and allow the metal to collect in the form of a massive cylinder in the bottom of the bomb. The bomb was removed from the furnace as soon as it fired and was allowed to cool before being opened.

The ingot obtained was invariably very clean with smooth sides and top and contained 1 to 5% calcium and 0.1 to 1% magnesium. Average yield of the metal in the ingot weighing 150 to 175 g per run was approximately 94%. The contaminants in the as-reduced metal were brought down to less than about 200 ppm each by remelting the metal in a magnesia or beryllia crucible in vacuum.

Spedding et al. (1952) carried out much of the initial experiments with cerium but noted that with respect to yields, contamination by calcium and magnesium, and quality of

ingots, the results of cerium were duplicated by lanthanum, neodymium, and praseodymium. Kilogram quantities of these metals in high purity were prepared by this technique in addition to over 500 kgs of 95–99% pure cerium on a 1.5 kg per batch scale.

Spedding and Daane (1954) noted that this method was capable of producing very pure metals if sufficient care was taken to introduce only pure rare earth chloride, pure calcium, and pure iodine into a pure liner because, in the entire system, which was closed, no impurities could get into the metal other than calcium, magnesium, or oxygen. Both calcium and magnesium could be distilled out on remelting but oxygen remained. To prevent the introduction of oxygen, the calcium was handled in an inert atmosphere and the bomb was loaded in an argon atmosphere glove box. Considerable care had to be taken to ensure that the chlorides were completely anhydrous and free of oxychlorides because even small amounts of these materials could lead to high oxygen content in the metal and also poor yields. If too much moisture was present it would invariably lead to explosions of the sealed bomb.

When only rare earth chloride and calcium were used in the charge, the heat liberated by the reaction (on this scale, namely ~170 g) was not sufficient to heat the resulting rare earth metal and calcium chloride slag to above their melting points. As a result the rare earth metal could not agglomerate into a massive ingot. Iodine was added as the booster and the extra heat liberated by the Ca–I exothermic reaction was sufficient to heat the reaction products to beyond their melting temperatures and hence enabled the rare earth metal to collect into a fused mass. Iodine also served to form a lower melting slag of $CaCl_2$–CaI_2. In an effort to find a substitute for the iodine, which was expensive, sulfur and potassium chlorate were also investigated as boosters (Spedding et al. 1952). The use of sulfur generated considerable heat, but no separation of the metal and slag occurred. Potassium chlorate, even under the best conditions, did not produce cerium metal in yields comparable to that obtained with iodine, either externally with respect to adhering slag or internally with respect to inclusions.

The method described above for the preparation of cerium, lanthanum, praseodymium, and neodymium metals by reduction of their chlorides by calcium with iodine as booster was also tried for yttrium (Spedding et al. 1952). Although the reaction proceeded vigorously enough to permit complete slag collection, apparently sufficient heat was not generated to fuse the metal, and the yttrium produced was intimately mixed with the slag. The unsuccessful attempt was attributed to the high melting point (1522°C) of yttrium. This procedure was not successful with even the relatively low melting gadolinium (1313°C). It turned out that the method could not be applied to metals melting at a temperature above the melting point of neodymium (1021°C).

4.5.3 Reduction in Tantalum Crucible

Two major problems confronted the attempts made to prepare high melting rare earth metals by chloride reduction. At high temperatures, the calcium chloride frothed and thus prevented clean slag–metal separation, and the oxide liners were attacked by the metal and impurities were introduced. Subsequently, Spedding and Daane (1952) attempted the reduction in a tantalum crucible was attempted. The procedure was as follows.

In a typical run, 70 g of rare earth chloride and 18.5 g of calcium were thoroughly mixed in an inert atmosphere and either jolt packed into a tantalum crucible or compacted in a powder press into cylinders that were then placed in the tantalum crucible. This charge contained 10% more calcium than was required by the stoichiometry of the reaction

$$2MCl_3 + 3Ca \rightarrow 3CaCl_2 + 2M$$

in which M represents a rare earth element. The loaded, outgassed crucible was covered with a tantalum lid, perforated to permit gas to enter or leave the vessel, and was placed inside a covered magnesia crucible (50 mm in diameter and 175 mm long). This was in turn placed inside a silica tube (58 mm diameter) one end of which was fused shut and the other end ground to serve as the inner half of a 55/50 standard taper joint. The silica tube was sealed onto a vacuum system evacuated to 0.1 Pa and then filled to 1 atm with argon which was purified by passing it over hot uranium turnings. The tantalum crucible was heated by means of a 6 kW induction furnace. At 550 to 600°C, the exothermic reaction between calcium and the rare earth chloride occurred as evidenced by the sudden increase in the temperature of the reaction crucible. In about 5 minutes, the final holding temperature could be reached, and at this temperature the crucible was held for 13 min to permit complete agglomeration of the product metal. The final holding temperature was 1000°C for lanthanum, cerium, praseodymium, and neodymium and 1350°C for gadolinium. After cooling to room temperature, the tantalum crucible was soaked in water to remove the calcium chloride slag and most of the excess calcium, leaving in the crucible bottom a layer of fused rare earth metal containing from 1 to 3% calcium. This impurity could be removed by remelting the metal under 0.1 Pa or better in the same crucible and vacuum apparatus. The remelting temperature was 1200°C for lanthanum, cerium, praseodymium, and neodymium and 1350°C for gadolinium.

Lanthanum, cerium, praseodymium, and gadolinium metals were prepared by this technique in 40 g lots with yields consistently exceeding 99%. Calcium content in the remelted product metal was not over 150 ppm. The use of booster reaction was not necessary because external heating was used, and tantalum was more resistant to molten rare earth metal attack than any refractory material.

4.5.4 Intermediate Alloy Processes

The chloride reduction as described for the five metals could not be applied to the higher melting metals because of excessive chloride volatilization and decreased yields. The main problem was the need to use high temperatures so that the metal would be molten at the reaction temperature. The need for high temperatures for reaction was overcome by preparing the metal as a low melting alloy. Carlson and Schmidt (1967) investigated the preparation of yttrium metal as an yttrium–magnesium alloy by calcium reduction of yttrium trichloride in the presence of magnesium. The excess calcium and magnesium were removed from the yttrium product by a heat treatment in vacuum.

A similar process was used by Schmidt and Carlson (1974) to prepare scandium metal by reducing scandium trichloride with calcium and/or magnesium. The calcium and magnesium from the as-reduced scandium were removed by vacuum heat treatment. Yttrium and scandium from alloys with magnesium will become molten at reaction temperatures that are considerably lower than the melting points of yttrium and scandium. Clean slag–metal separation was therefore possible.

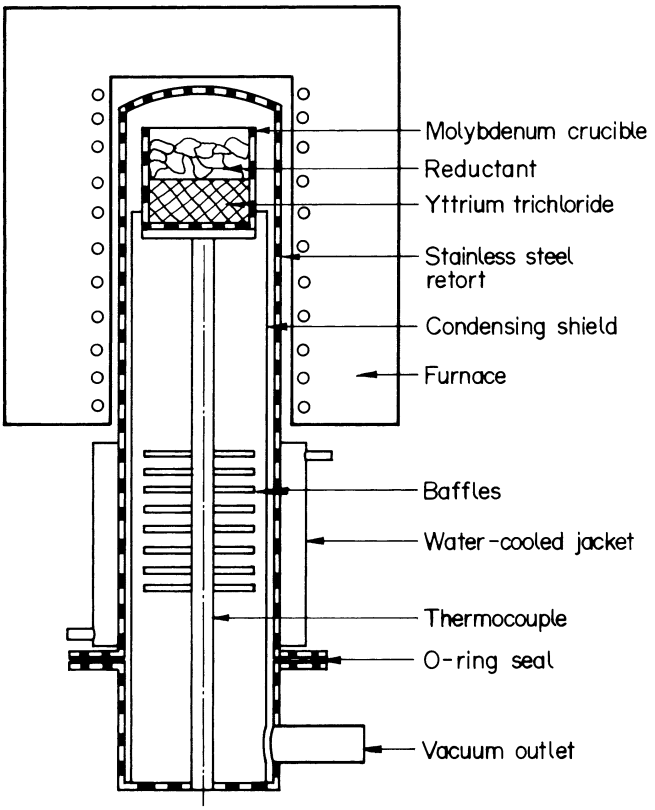

Figure 4.14 High vacuum reduction distillation assembly (Block et al. 1960).

4.5.5 Kroll Type Processes

An effective method for rare earth metal preparation at reaction temperatures less than the metal's melting point is to obtain the metal in a sponge form, as in the Kroll process for titanium (Kroll 1959).

Lithium/Sodium Reduction of Yttrium Chloride Block et al. (1960) prepared large quantities of high purity yttrium metal by reducing the chloride with both lithium and sodium. The stainless steel vacuum retort used for lithium reduction is shown in Figure 4.14. Both lithium and yttrium chloride react with moisture in the atmosphere. Hence handling operations, as far as possible, were performed in an inert atmosphere glove box. High purity lithium, 10 to 15% more than the stoichiometric amount required for reaction, was added to the molybdenum crucible containing yttrium chloride. The loaded crucible was transferred to the reduction distillation assembly. The retort was then evacuated to 0.01 Pa and backfilled to 35 kPa with argon. The charge was heated to 850°C for 1 h to complete the reaction, and thereafter the retort was evacuated again while it was heated to 900°C for 16 h to remove the excess lithium and lithium chloride from the yttrium sponge. Block et al. (1960) used batch sizes of up to 1 kg of yttrium chloride in the assembly shown and yttrium recoveries were between 95 and 100%.

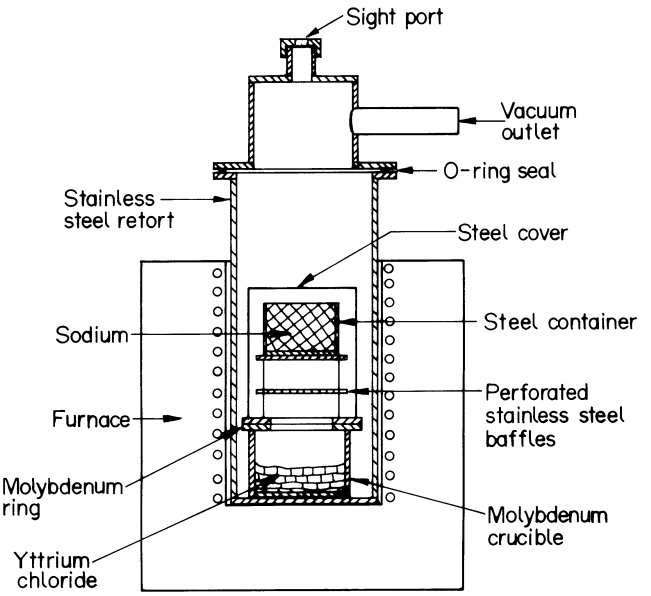

Figure 4.15 Metallic reduction assembly (Block et al. 1960).

This procedure was also carried out in a larger assembly designed for preparing up to 9 kg of yttrium sponge per batch. The reduction temperature was 900°C and holding time was maintained for 4 h and 45 min. After reduction, the crucible was inverted before the by-products were removed by vacuum distillation at 950°C for 24 h. Inverting the crucible allowed bulk of the excess lithium and lithium chloride to melt and run out of the crucible, thereby minimizing the time required for vacuum distillation.

The apparatus shown in Figure 4.15 was used by Block et al. (1960) for carrying out the sodium reduction of yttrium chloride. The batch size was 0.7 kg of yttrium chloride. Purified yttrium chloride was charged into a molybdenum crucible in the bottom of the stainless steel retort and excess sodium was placed in the steel container in the upper section of the retort. The loaded reduction retort was evacuated and filled with argon to between 7 and 15 kPa above atmospheric pressure. The lower section of the retort was heated to 850°C to melt the yttrium chloride, after which the section containing the sodium was heated at a temperature high enough to vaporize sodium, allowing the sodium vapors to react with the yttrium chloride until the reaction was complete, which took 5–7 h. This procedure, which is very similar to the Kroll process for zirconium, has the advantage of combining distillation purification of sodium with a facility for controlling the reaction. After the reaction was complete, the retort was rotated slightly beyond 90° from the vertical position and the bulk of the excess sodium and sodium chloride were poured out of the crucible. The retort was then evacuated and heating was continued to 850°C to remove the last traces of sodium and sodium chloride. Vacuum distillation without first pouring out the bulk of sodium invariably led to reverse reaction in which yttrium reduced the sodium chloride. As an alternative, after reduction, the retort could be cooled, the crucible inverted and vacuum separation done as with the large batch lithium reduction procedure.

Metal yields were between 95 and 99% in lithium reductions and between 61 and 85% in sodium reductions. The representative analysis of yttrium prepared by both lithium and

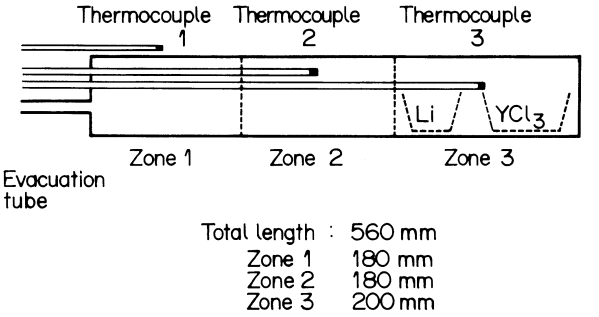

Figure 4.16 Reduction bomb assembly (Nolting et al. 1960).

sodium reduction are listed in Table 4.2. Yttrium produced by sodium reduction was lower in both carbon and oxygen impurities than that obtained by lithium reduction.

Nolting et al. (1960) and Moriarty (1968) have also used lithium vapor reduction of rare earth trichloride to prepare yttrium and other high melting rare earth metals.

Lithium Reduction of Yttrium Chloride Nolting et al. (1960) carried out the reductions in the reactor shown schematically in Figure 4.16. The stainless steel reactor was 75 mm in diameter and 560 mm long. The reactor was lined with 0.25 mm thick molybdenum foil. Two 100-mm tantalum boats (reduction crucibles) containing lithium and yttrium chloride were placed as shown in the figure. The reduction crucibles were shaped to conform to chamber geometry and they were placed on a tray constructed from 0.5 mm tantalum sheet. A 0.125 mm titanium foil was used as additional liner and as a getter for gaseous contaminants.

Table 4.2 Analysis of arc melted yttrium buttons (Block et al. 1960)

Reductant	Impurity content, ppm										
	O	N	C	Al	Na	Li	Fe	Cr	Ni	Si	Mo
Lithium	270	40	260	80	150	<1	400	100	70	<10	90
Sodium	125	60	120	30	100	<1	200	100	200	10	62

Purified anhydrous yttrium chloride weighing 305 g and clean lithium weighing 40 g were placed in the respective containers and positioned adjacent to each other in zone 3 of the bomb chamber, after which the reactor was closed by welding the face plate into position and the chamber was evacuated to 6 Pa. The reduction was initiated by placing the evacuated chamber in a preheated reduction furnace in a horizontal position. The bomb heated to 950°C in 15 min, and this temperature was maintained for 2 h over the entire length of the bomb. Within 5 min of exposure to temperature, the evacuation tube sealed due to condensation of lithium vapor. Lithium vapor reduced yttrium trichloride and the reduction was complete in 2 h. At the end of 2 h, the bomb was positioned so that the face plate protruded out of the furnace opening and an airblast was directed at the face plate. The furnace temperature was raised so that within 30 min, the temperature was steady at 1000°C in zone 3, 950°C in zone 2, and 400–500°C in zone 1. This gradient was maintained for 12 h to ensure complete removal of lithium chloride slag and excess lithium from the as-reduced yttrium crystals. The slag and excess reductant distilled off to the cooler surface.

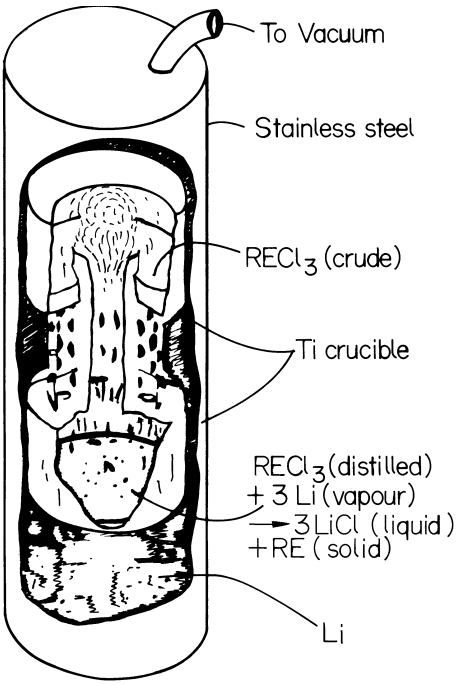

Figure 4.17 Reduction crucible used for lithium reduction of rare earth chlorides (Beaudry and Gschneidner 1978).

The reactor was then removed from the furnace and cooled. The bomb chamber was cut open in zone 2 at the thermocouple position and argon gas was flushed into the chamber. The product was 125 g of bright crystalline yttrium sponge, representing over 90% yield. Some of the crystals adhered to the tantalum crucible. Yttrium thus obtained was 99.8% pure with 0.16% oxygen as the major residual impurity. Nitrogen, carbon, and chloride contents were 0.006, 0.007, and 0.01%, respectively. The total nonmetallic content in the yttrium thus obtained was reported by Nolting et al. (1960) to be only 0.17%. The yttrium crystals were consolidated by arc melting.

Lithium Reduction of Rare Earth Chlorides Lithium reduction of rare earth trichlorides was adopted on a commercial scale by Moriarty (1968). The reactor used for this purpose is shown (Beaudry and Gschneidner 1978) in Figure 4.17. Crude rare earth chloride was placed in a titanium crucible with a tube down the center. A second titanium crucible was placed below it and they were separated by a spacer. Both crucibles were placed on a pedestal inside a stainless steel chamber. Chunks of commercial grade lithium were placed around the pedestal. The chamber was evacuated and the upper titanium crucible was heated to distill the rare earth trichloride into the lower crucible. After distilling the chloride, the entire steel chamber was heated to 800–1000°C. The lithium vapor filled the chamber and some of the lithium condensed in the vacuum line, sealing the chamber. The lithium vapor reacted with the molten rare earth chloride, reducing it to rare earth metal and forming lithium chloride slag. After the reduction was complete, the steel chamber was partially removed from the furnace and the lithium chloride slag was distilled from the reduction crucible to that part of the steel chamber that was outside the furnace

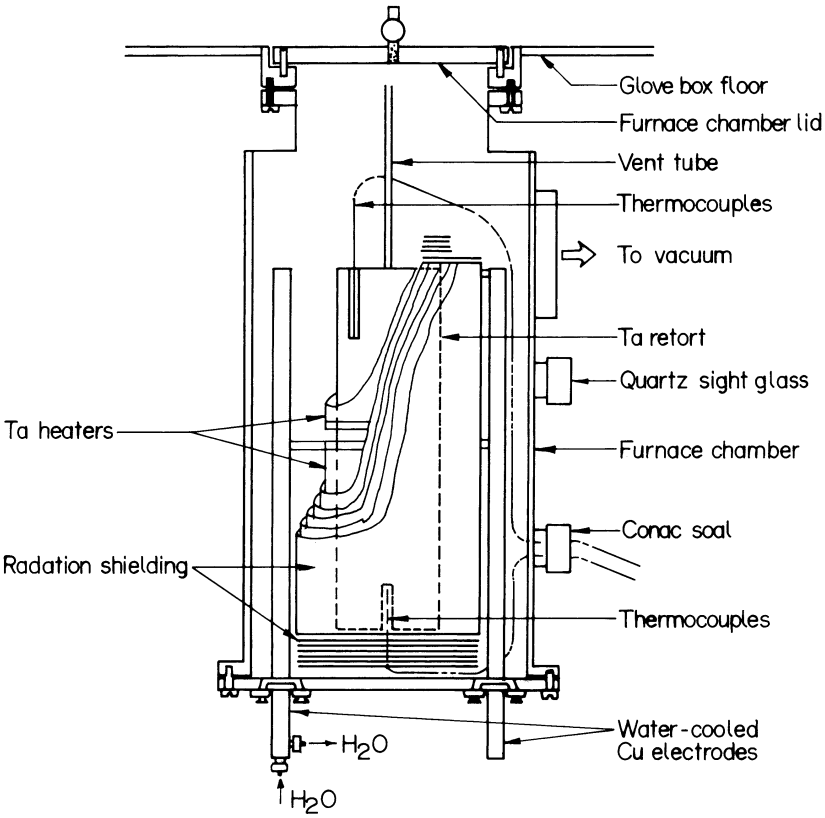

Figure 4.18 Schematic diagram of the glove box furnace used for rare earth metal reduction (Croat 1969).

and hence colder. After completing the distillation, the sealed steel chamber was opened and the rare earth metal crystals were consolidated by arc melting or induction melting. Moriarty (1968) reported the preparation of all of the rare earth metals except promethium, samarium, europium, and ytterbium, using the lithium vapor reduction method described. The relatively low temperature of the reduction (800 to 1000°C) ensured that the contamination of the reduced rare earth metal crystal with the crucible material was very low. The major impurity in these metals was oxygen, which ranged from 225 ppm for holmium to 1600 ppm for terbium. The nitrogen content was below 40 ppm for all the metals. The yields of recoverable metals were between 77 and 86% after reduction at 1000°C.

Lithium Reduction of Dysprosium, Holmium and Erbium Chlorides The reduction of dysprosium, holmium, and erbium trichlorides with lithium was studied by Croat (1969). The anhydrous chlorides were reduced at 900°C using lithium–5% calcium or pure lithium as the reductant. The liquid–vapor reduction was carried out in two steps: (1) distillation of the lithium vapor into liquid rare earth chloride at the reduction temperature and (2) distillation of the lithium chloride slag and excess reductant away from the product on completion of the reduction. Prior to reduction, the rare earth chloride was purified by one or more distillation operations. As regards the lithium reductant, approximately 5% calcium was added to the reductant in order to make the lithium vapor purer during distillation.

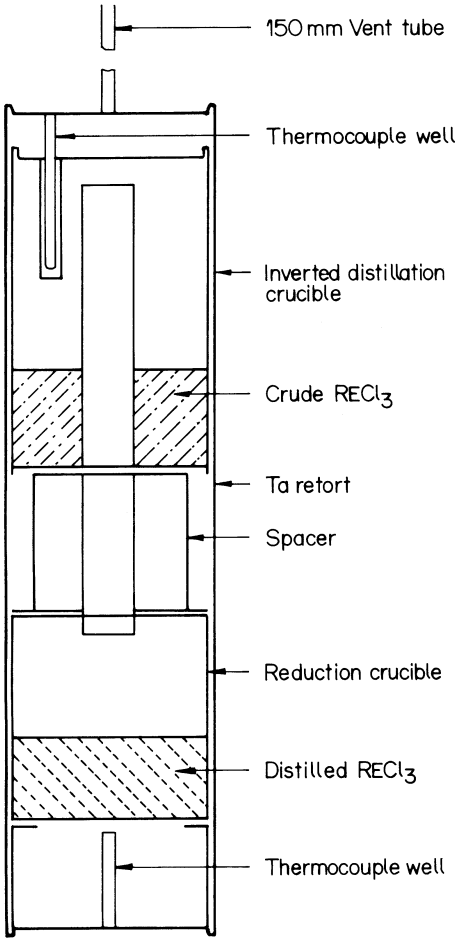

Figure 4.19 Schematic diagram of the distillation apparatus (Croat 1969).

During the liquid–vapor reduction process a certain amount of calcium also distilled and reduced the rare earth chloride. Excess calcium and calcium chloride slag were easily removed along with the lithium chloride and excess lithium.

The reduction was entirely carried out in tantalum crucibles and retort. All operations beyond the initial preparation of the chlorides were carried out inside a controlled atmosphere glove box.

The reduction was carried out inside the glove box furnace as shown in Figure 4.18. The tantalum retort used both for distilling and reducing the rare earth chloride is also shown positioned in the furnace in the figure. The retort measuring 300 mm in length and 83 mm in diameter was made of 0.75 mm thick tantalum. The bottom and top ends of the retort were of 0.25 mm thick tantalum and contained thermocouple wells for measuring the interior temperature. The retort lid also contained a tantalum vent tube extending up through a hole in the top radiation shielding. This tube allowed the retort to be welded shut in the glove box and then evacuated and maintained under a dynamic vacuum during the distillation of the chlorides. This vent tube sealed itself with lithium during reduction.

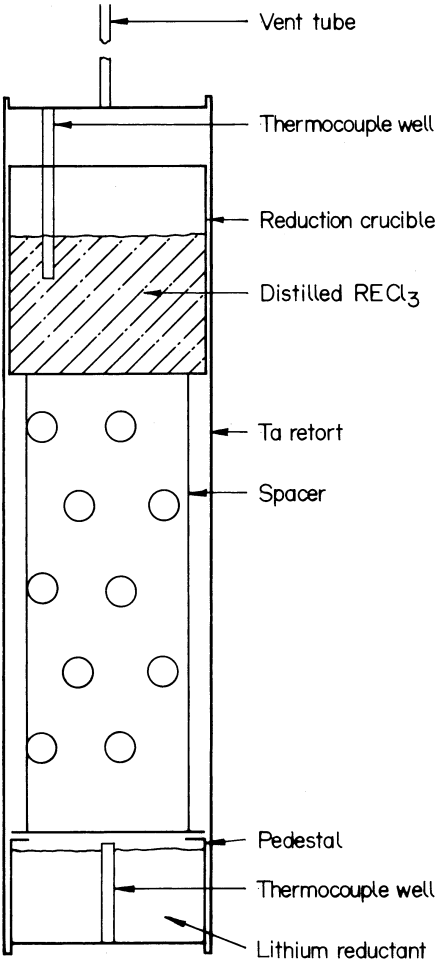

Figure 4.20 Schematic diagram of the reduction apparatus (Croat 1969).

The rare earth chloride was purified by distillation and only the purified chloride was used for reduction. The distillation assembly shown schematically in Figure 4.19 was made of tantalum and consisted of an inverted crucible, a spacer, and a reduction crucible resting on a pedestal at the bottom of the retort. During distillation, the chloride vapor passed from the inverted crucible by way of a tube welded in the bottom and extending upward to within 13 mm of the lid and downward to a point approximately 13 mm inside the reduction crucible.

The reduction apparatus, shown schematically in Figure 4.20, had a reduction crucible and a spacer placed on a pedestal at the bottom of the retort. Essentially, the distillation apparatus becomes the reduction apparatus by removing the distillation crucible and positioning the reduction crucible at the top rather than at the bottom of the retort.

Prior to reduction, the chlorides were purified by distilling them in the distillation assembly shown in Figure 4.19. The distillation crucible was loaded with cast chlorides and covered with a tight fitting crucible lid. The loaded distillation crucible, reduction crucible, and spacer were loaded in the tantalum retort and the lid of the retort was welded in place.

The assembly was placed into the furnace, which was then evacuated to a maximum pressure of 10^{-4} Pa. The retort was evacuated simultaneously through the vent tube. The required temperature gradient for distillation was provided by heating only the top of the retort by the upper heating element of the furnace. Dysprosium chloride was distilled at 850°C, holmium chloride at 875°C, and erbium chloride at 910°C, and the distillation rate was 1 gram per minute. For some runs the distillation was repeated once more and doubly distilled chloride was used for reduction.

The same retort in which the chlorides were distilled was also used for reduction. The reductant, lithium–5% calcium, was loaded into the bottom of the retort, the spacer was inserted, and the reduction crucible containing the distilled chlorides was loaded in the top as shown in Figure 4.20. The lid of the retort was rewelded and the retort was positioned in the furnace. The bottom of the retort was first heated to 300°C to outgas the reductant and allow the formation of the less volatile CaO at the expense of volatile Li_2O. The entire retort was then heated to 900°C to carry out the reduction. The temperature was maintained for 2 h for every 100 g of chloride. After the reduction was complete, the bottom furnace was turned off and the top furnace was maintained at 900°C to distill the lithium chloride slag and any excess calcium out of the reduction crucible to the bottom of the retort. For every 100 g of rare earth chloride reduced, the LiCl distillation temperature was maintained at 900°C for 1 h followed by 550°C for 2 h and 450°C for 2 h. The corresponding temperatures at the bottom of the retort were 640°C, 360°C, and 290°C, respectively. After completion of the reduction schedule, the retort was opened by cutting off the welded flange, and the reduction crucible containing the as-reduced metal was removed from the retort and placed on a pedestal inside the vacuum furnace. It was then heated at 7×10^{-5} Pa and 950°C for several hours to insure complete removal of any traces of lithium chloride and excess lithium reductant. The product, as reduced metal, was then recovered as bright, loosely packed crystals. The purity of as reduced metals from singly distilled anhydrous chlorides averaged 99.94 wt % or 99.2% atomic. Oxygen and hydrogen contents were quite high; approximately 500 and 15 ppm, respectively. The oxygen and hydrogen contents of metals prepared from doubly distilled chlorides are much lower, as shown in Table 4.3. The

Table 4.3 Analysis of as reduced dysprosium–holmium and erbium obtained by chloride reduction. Chlorides were doubly distilled before reduction (Croat 1969)

	Content, ppm		
Impurity	Dysprosium	Holmium	Erbium
H	6	5	10
Li	nd	nd	nd
C	39	17	11
N	7	3	7
O	135	81	109
F	<3	<3	<3
Cl	<3	<3	<3
Cr	2	<1	1.5
Fe	2	11	2
Ni	0.4	1	2

nd: not detected

purity of a reduced metal prepared from doubly sublimed chlorides was 99.9% atomic. Less than 3 ppm each of F and Cl were present in the as-reduced metal and no lithium was detected. The tantalum contents were below 30 ppm.

Croat (1969) carried out the reductions in batches ranging from 0.2 to 1 kg and 20% excess reductant was used. The average yields of reduced metal from the chloride were approximately 96%, whereas the overall yields of oxide to as-reduced metal were approximately 79%.

The method of producing pure rare earth metals by the chloride reduction route, though feasible for most of the metals, is usually an elaborate procedure requiring great procedural care and experimental facilities, particularly on account of their hygroscopicity and volatility. These two limitations are, to a large extent, circumvented by the use of fluorides in place of chlorides in the metal reduction procedures. As will be seen shortly, it turned out that the fluoride reduction method is technically more perfect than the chloride route for most of the rare earth metals in that the fluoride route satisfies more criteria as stated by Herget (1985) for a good metallothermic reduction method.

The preparation of rare earth metals through the fluoride route essentially has two major steps. One is the preparation of anhydrous rare earth fluoride starting from the oxide, and the other is the reduction of the fluoride to the metal.

4.6 PREPARATION OF RARE EARTH FLUORIDES

The preparation of rare earth fluorides for use as intermediates for reduction has been accomplished by two routes. One, known as the wet route, involves the precipitation of fluoride from aqueous solution followed by dehydration of the hydrated rare earth fluoride. In the other, known as the dry route, the oxide is directly converted to anhydrous fluoride.

4.6.1 Wet Method

This method consists of precipitation of hydrated rare earth fluoride from an aqueous solution followed by a dehydration step. The reactions involved are as follows:

$$RE_2O_3 + 6HCl\ (aq) \rightarrow 2RECl_3 \cdot xH_2O$$

$$RECl_3 \cdot xH_2O + HF\ (48\%\ aq) \rightarrow REF_3 \cdot x'H_2O$$

$$REF_3 \cdot x'H_2O \xrightarrow[\text{or } 600^\circ C \text{ in HF gas}]{300^\circ C \text{ in vacuum}} REF_3 + H_2O$$

In the above equations, x is usually 6 and x' is ½ or 1. The rare earth oxide is dissolved in hydrochloric or nitric acids. Addition of aqueous hydrofluoric acid to this solution results in the precipitation of hydrated fluoride (HF), which is recovered by decantation or filtration. The product is dried at 100 to 150°C in air to remove adhering moisture and then heated at 300°C in a vacuum or at 600°C in an anhydrous HF stream to thermally decompose the hydrate.

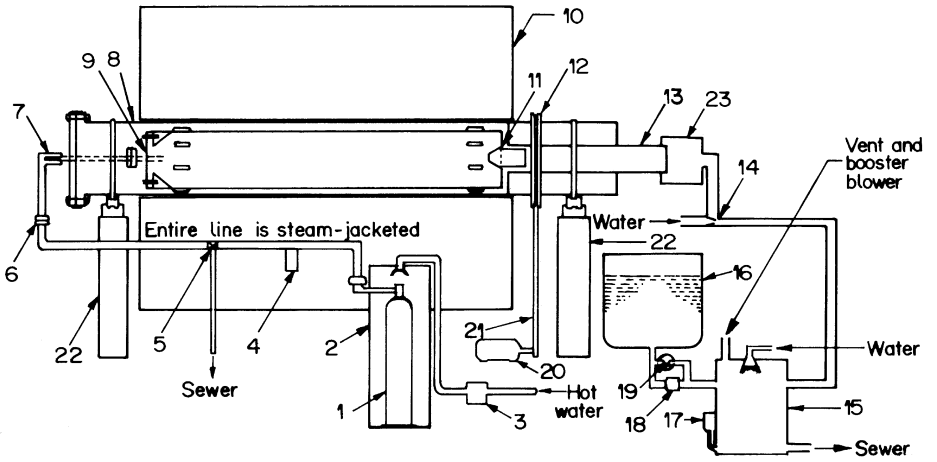

Figure 4.21 Furnace and rotary equipment for hydrofluorination of yttrium oxide (Banks et al. 1959).
1. hydrogen fluoride cylinder; 2. spray chamber; 3. solenoid chamber; 4. manometer; 5. check valve; 6. union; 7. Teflon universal seal (inlet); 8. inconel outer tube; 9. inconel inner tube; 10. electric furnace; 11. dust trap; 12. chain sprocket; 13. nickel exit tube; 14. water aspirator; 15. neutralizing tank; 16. soda ash neutralizing solution; 17. Beckman pH meter; 18. valve to pH controller; 19. by-pass valve; 20. AC motor (1 HP); 21. chain; 22. bearing supports; 23. teflon universal seal (outer).

For the aqueous hydrofluorination of rare earth solutions and to handle aqueous hydrofluoric acid and fluoride chloride solutions, plastic reaction vessels and filtration units are used. Carlson et al. (1956) have used this method of precipitation, filtration, and air drying to prepare 50 kg quantities of lanthanum, cerium, and yttrium fluorides. Treatment in an anhydrous HF stream has been carried out in equipment normally used for the dry hydrofluorination process, which will be described in the next section.

Minor variations from the general procedure could be found in specific cases of rare earth fluoride preparation by the aqueous route. In one approach, yttria was dissolved in hydrochloric acid and the solution was concentrated by evaporation to obtain $YCl_3 \cdot 6H_2O$ crystals. The addition of 70% HF to these crystals results in the formation of $YF_3 \cdot \frac{1}{2}H_2O$. In another approach, liquid anhydrous HF was used. Liquid HF can be obtained by condensing the vapors in a copper coil immersed in a dry ice bath. Dripping of liquid HF into a YCl_3 solution at 100°C results in the precipitation of $YF_3 \cdot \frac{1}{2}H_2O$ which is readily filterable. It must be mentioned here that generally the hydrated fluoride precipitates are gelatinous and difficult to filter from the aqueous solution.

Carlson et al. (1956) have noted that aqueous methods yield YF_3 with slightly more oxygen content than the dry methods. The oxygen content could, however, be lowered by the purification step.

4.6.2 Dry Methods

Reaction of Rare Earth Oxide with Anhydrous HF The method involves passing anhydrous HF gas directly over the oxide at elevated temperatures. The overall reaction is as follows:

$$RE_2O_3 + 6HF \rightarrow 2REF_3 + 3H_2O$$

For most rare earths, good fluoride conversion was achieved at 700°C in 8 h. A stationary bed type of furnace was quite adequate for preparing RF_3 in quantities of 500 to 1000 g (Carlson and Schmidt 1961). The reactor consisted of a horizontal inconel tube having an inlet line for anhydrous HF and an outlet line for the gaseous products. The rare earth oxide was placed in a platinum tray inside the inconel tube, which may also be lined with platinum. The tube was heated to 700°C by an electrical resistance furnace. At this temperature, to produce a high quality product in an 8-h period, an excess of approximately 200% of HF gas was required. The product (fluoride) was allowed to cool, and any HF gas adhering to it was removed by vacuum flushing with helium.

Lanthanum, cerium, neodymium, samarium, europium, gadolinium, terbium, dysprosium, holmium, erbium, thulium, ytterbium, lutetium, and yttrium fluorides have been prepared using this method. The fluoride conversion achieved in this process ranged from 99.90 to 99.98%.

The production of rare earth fluorides on a larger scale by direct reaction of Y_2O_3 with HF gas has been carried out by the (i) rotary batch method, (ii) fluidized bed method, and (iii) vibrating tray method.

Rotary batch method

A sketch of the unit used for hydrofluorination by the rotary batch method (Banks et al. 1959) is shown in Figure 4.21. High purity yttrium oxide was loaded into the inconel inner tube, which was then inserted into another inconel tube that could be rotated. The tube was closed and the HF gas lines were connected to the system. The HF gas was turned on when the temperature of the furnace reached 150°C. The temperature was gradually raised to 750°C over a period of about 6 h. After a lapse of about 1 h at 750°C, the inconel tube was rotated for 5-min periods at 10-min intervals. This rotation sequence was continued for a 2 h period after which the furnace and HF flow were turned off. The fluoride was cooled in the furnace for 12 h after which the liner containing YF_3 was removed and flushed with helium. The fluoride was removed from the liner, evacuated, flushed, ground, and stored in polyethylene bags inside metal containers.

A critical parameter in the method described was the amount of draft on the fluoride bed produced by the exhaust system. This draft ensured adequate sweep of HF over the salt. The amount of HF used was approximately 250% over the stoichiometric amount. About 25 kgs of high purity Y_2O_3 was loaded in each batch in the reactor and the yttrium fluoride product had an oxygen content in the range of 400 to 1000 ppm. Using this method, over 30,000 kgs of high quality YF_3 was prepared at Ames Laboratory over a two-year period.

In the above method the rotary motion of the reactor eliminates the problem of formation of yttrium fluoride crust on the surface of unreacted yttrium oxide. For example, in a static bed, where 25 kgs or more of Y_2O_3 were hydrofluorinated, the increase in the depth of the oxide bed and formation of crust inhibit the diffusion of HF gas into the unreacted oxide and resulted in poor conversions.

Fluidized bed method

Fluidized beds offer advantages such as enhanced reactants contact, high heat transfer coefficients, and good temperature control and hence absence of local overheating and sintering in the charge. The use of a fluidized bed for the preparation of YF_3 by hydrofluorination was investigated by Knudsen and Levitz (1959) at Argonne National Laboratory. The

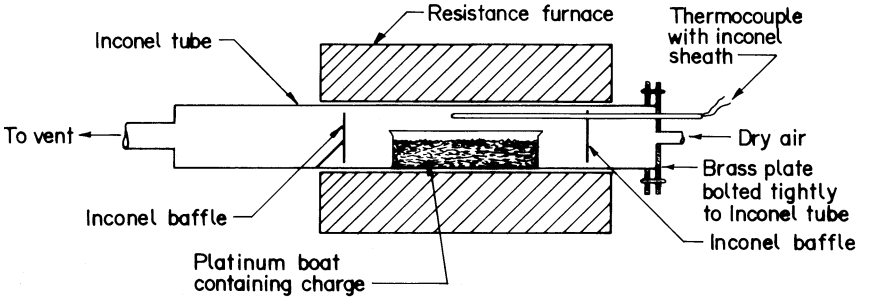

Figure 4.22 Apparatus used for the preparation of rare earth trifluorides by the ammonium bifluoride process (Carlson and Schmidt 1961).

reactor was a 75 mm diameter and 1070 mm high monel column with a porous monel plate distributor. The reactor was heated externally.

The charge consisted of 1 to 2 kgs of Y_2O_3. Nitrogen was used as the fluidizing gas initially, and the superficial gas velocities were kept at 0.15 to 0.2 meters per second, which were about 50% more than the minimum fluidizing velocity of the bed. Anhydrous HF was combined with the nitrogen stream when the bed temperature reached 150°C. The gases were preheated in a packed tube inside a furnace. As the bed temperature rose, the rate of HF flow was adjusted to control the bed temperature and limit the reaction at a desired level. In runs of 7 to 10 h duration at 600 to 700°C, good conversion of Y_2O_3 to YF_3 was obtained. The nickel contamination in the product was less when the temperature was lower, e.g., 600°C. Even though scaling up the batch size from the small 2 kg charge might be feasible, this method was not used to prepare large quantities of fluorides (Carlson and Schmidt 1961).

Vibrating tray method

The vibrating tray reactor (Fisher and Olson 1959) consisted of four inclined vibrating trays fixed in a cascade arrangement, so that Y_2O_3 would flow at a controlled rate countercurrent to the flow of HF gas. Conversions to >99% were obtained in a single pass at 700°C. Even though certain aspects of this unit appeared attractive, completely satisfactory performance was not achieved.

Reaction of Rare Earth Oxides with Ammonium Bifluoride Spedding and Daane (1956) developed a method in which ammonium hydrogen fluoride is used to convert the rare earth oxide to rare earth fluoride. The reaction is

$$RE_2O_3 + 6NH_4F\cdot HF \xrightarrow{300°C} 2REF_3 + 6NH_4F + 3H_2O$$

and the apparatus used for carrying out this reaction in batch sizes of 100 to 1000 g is shown in Figure 4.22.

The charge was a mixture of rare earth oxide and high purity ammonium bifluoride. The quantity of bifluoride was 30% more than the amount needed by the stoichiometry of the above equation. The charge was heated to 300°C for 12 h under a stream of dry air that swept away from the system volatile reaction products and excess $NH_4F\cdot HF$. The inconel baffles prevent plugging of the gas line because of condensation of NH_4F and $NH_4F\cdot HF$.

The conversion of rare earth oxide to the fluoride occurs quantitatively. Oxygen content in yttrium fluoride made by this process was approximately 400 to 1000 ppm.

4.6.3 Purification of Rare Earth Fluorides

Rare earth fluorides containing appreciable amounts of oxide or oxyfluoride could be purified by the following procedure in certain cases. The impure fluoride was combined with LiF (fluxing agent) to form a low melting salt mixture. This mixture was contained in a platinum crucible and heated to 1000°C. Anhydrous HF was passed through the molten salt to effect purification. The purified fluoride mixture was used as feed for metallothermic reduction (Carlson and Schmidt 1961). The fluorides of gadolinium, dysprosium, and yttrium have been purified by this method.

Another method applied mainly for the purification of yttrium fluoride (Carlson and Schmidt 1961) is as follows. Yttrium–magnesium alloy is a suitable intermediate product in the preparation of yttrium metal. A mixture of YF_3 and MgF_2 is first prepared by direct hydrofluorination of their oxides at 600°C in a static bed. In this step the conversions are usually 95 to 99%. For purification, LiF was added to the YF_3–MgF_2 mixture in a nickel vessel, degassed at room temperature and then melted under an anhydrous HF atmosphere. Hydrogen was bubbled through the molten mixture for 1 h while its temperature was raised to 850°C. Anhydrous HF was then bubbled through the melt for 3 h, and then the mixture was again treated with hydrogen for approximately 16 h to decrease the contamination by iron, chromium, nickel, and sulfur. The molten salt was then transferred to a storage container through a sintered nickel filter. Oxygen content in the fluoride had decreased, and by extending the duration of hydrofluorination from 3 to 8 h further decrease in oxygen content was achieved.

A process, known as topping, was extensively used at Ames to obtain purer rare earth fluorides. This is the second part of the two-step process described by Spedding and Henderson (1971) for quantitative conversion of the rare earth oxide to the fluoride. In the first step, a mixture of anhydrous HF and 60% Ar was passed over the rare earth oxide at 700°C for 16 h. The inconel furnace tube was lined with platinum, and the oxide was contained in a platinum boat to prevent contamination of the fluoride. The oxygen content of the fluoride thus obtained was 300 ppm. This residual oxygen was lowered further to less than 20 ppm, by topping. Topping involves heating the fluoride in a platinum crucible to approximately 50°C above its melting point under a dynamic HF–60% Ar atmosphere. Usually the time required for topping is 1 h at temperature for every 20 g of fluoride. A graphite resistance furnace is used.

In addition to lowering the oxygen content, topping also brings down the levels of impurity elements: aluminum, silicon, chromium, iron, nickel, and copper (Beaudry et al. 1983). The fluorides of these impurities have vapor pressures approximately 10^6 times greater than those of the rare earth fluorides at their melting points.

4.7 REDUCTION OF RARE EARTH FLUORIDES

Historically, the investigations on the metallothermic reduction of fluorides started much later than those using the chlorides. The important investigations on fluoride reduction

Table 4.4 Fluoride reduction processes

Year	Reactants	Process	Results	Reference
1951	REF_3–Li–I; (Ce, La, Nd)	Heated to 1200°C in a Mo crucible enclosed in a steel bomb	Consolidated Ce; separated from slag	Gray 1951
1953	REF_3–Ca; (Gd and all RE except Sm, Eu, Yb)	Heated in Ta crucible under argon	Consolidated RE metal well separated from slag	Daane and Spedding 1953
1956	YF_3–ZnF_2–Ca	Bomb reduction	Low melting Y–Zn alloy; Zn distilled off	Carlson and Schmidt 1961
1956	YF_3–$CaCl_2$–Ca–Mg	Heated in Zr or Ti crucible under argon	Low melting Y–Mg alloy; Mg distilled off	Carlson and Schmidt 1961
1961	YF_3–Li–Ca–Mg YF_3–Li–Mg	Heated in Ti crucible	Low melting Y–Mg alloy; Mg distilled off	Haefling et al. 1961

methods for rare earth metals preparation are summarized in Table 4.4. In one of the earliest attempts of fluoride reduction, Eyring and Cunningham (1948) prepared metallic praseodymium by passing barium vapor over praseodymium fluoride at 1100°C, under reduced pressure. Later, Gray (1951) developed a technique in which the rare earth fluoride was reduced with lithium in a molybdenum crucible enclosed in a steel bomb. Iodine was added to lower the slag melting point. Reductions were conducted up to 1200°C and cerium, lanthanum, and neodymium metals were prepared. Within a couple of years, a most enduring and successful process for the reduction of fluorides was developed at Ames. In the Ames process, calcium was used as the reducing agent and the greater stability and lower vapor pressure of calcium fluoride permitted reduction temperatures as high as 1700°C, higher than the melting point of any rare earth metal. It was thus possible to prepare all the rare earth metals (except those exhibiting stable divalency) irrespective of their melting point.

The first major investigation on fluoride reduction for rare earth metal preparation, which was usable for commercial level preparation of the metal, was by Gray (1951). The process was initially adopted by Johnson and Mathey (Lever and Payne 1968) for the production of lanthanum, cerium, and neodymium metals.

4.7.1 Lithium Reduction

Gray (1951) chose lithium as a suitable metal for reducing cerium trifluoride since it had a fairly high heat of reaction, produced the lowest melting fluoride, and did not alloy with cerium. However, as the heat of the reaction

$$CeF_3 + 3\,Li \rightarrow 3\,LiF + Ce$$

was not sufficient, in real conditions, to effect a rise in temperature sufficient for melting all the components, Gray provided iodine in the charge not only for Li–I booster reaction, but also for the fluxing action of LiI on LiF slag.

The reactants cerium trifluoride, iodine, and lithium were loaded into the reactor shown in Figure 4.23. This reactor was constructed of mild steel and lined on the inside with molybdenum. The reactants were pressed into pellets only slightly smaller in diameter

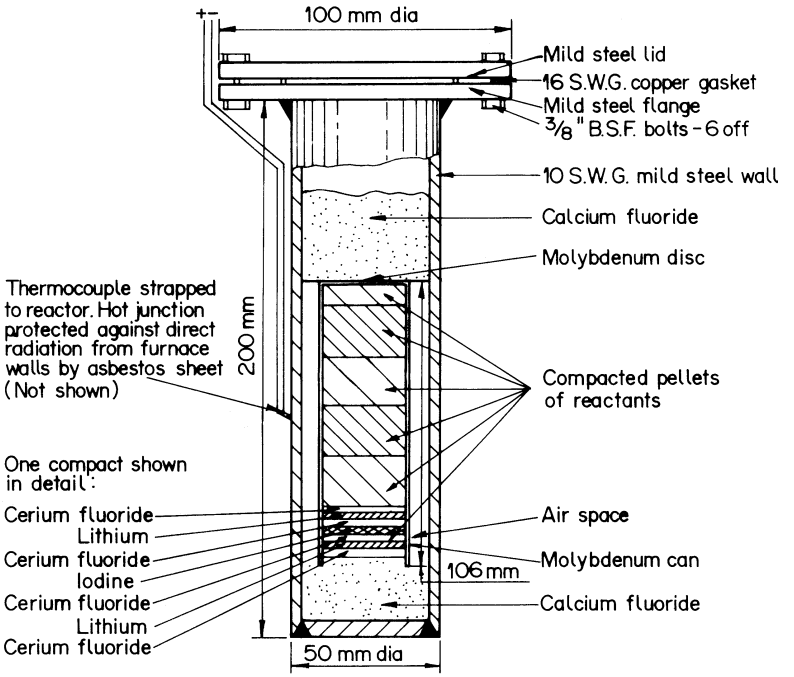

Figure 4.23 Reactor loaded for fluoride reduction (Gray 1951).

than the internal diameter of the crucible and loaded in the crucible in layers as shown at the bottom of the figure. A typical charge consisted of 110 g cerium trifluoride (≡79 g cerium), 20 g iodine, and 14.1 g lithium (11.7 g to react with CeF_3, 1.1 g to react with iodine and 10% excess).

The loaded reactor was put in a pot furnace heated to 1300°C. When, after about 15 min the outer wall of the reactor reached 1100°C, the furnace temperature was adjusted so that the reactor remained at 1100°C for 30 min, after which the reactor was removed from the furnace and allowed to cool.

In the reactor, cerium had collected at the bottom with the flux on top of it but cleanly separated from it. The metal yield was at best 82.5% and the purity was consistently 99.92–99.93%. The main impurities were molybdenum (up to 0.06%) and iron (0.01–0.03%). Interstitial impurities were not analyzed, and, incidentally, no precautions were taken to exclude air from the reactor. The purity given was obtained by difference.

Small quantities of rare earth metals, relatively low in oxygen content and also pure with respect to most nonmetallic impurities have been prepared (Daane 1961) using the apparatus shown in Figure 4.24. The rare earth halide to be reduced and the reductant metal are placed in separate refractory metal crucibles in a tantalum container. The lid of the container is welded on, and it has a small diameter tantalum tube that extends out of the furnace heating assembly. The system is evacuated while it is slowly heated to a temperature at which the reductant metal begins to volatilize and the vapors permeate the assembly. The metal vapors also condense in the cooler portions of the tantalum tube extending outside the furnace and seal off the system by the time the system has been outgassed and gettered. During the reduction, which lasts several hours, the system thus remains free of gases that would have otherwise diffused back into the reaction chamber

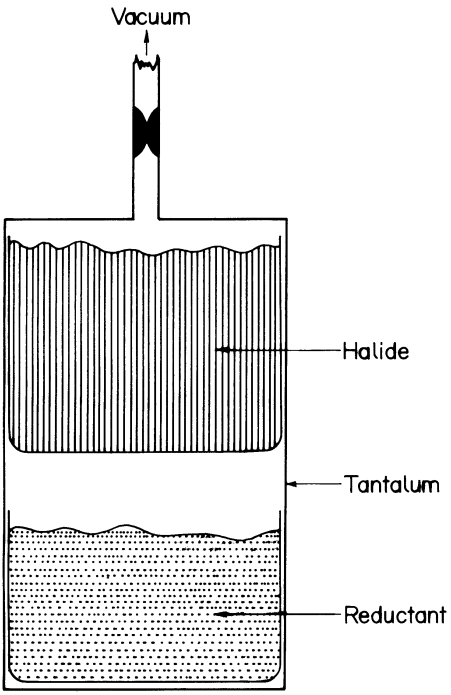

Figure 4.24 Rare earth metal reduction apparatus (Daane 1961).

from the vacuum pumping system. Heating is done at such temperature that the salt phase in which the reduction takes place is liquid, and equilibrium is promoted between the reductant metal vapor and the halide undergoing reduction. The required temperature is less if sodium or potassium is used as the reductant or if a rare earth chloride is being reduced than if calcium is the reductant and a rare earth fluoride is being reduced.

4.7.2 Calcium Reduction (Ames Process)

In the Ames process (Daane and Spedding 1953), the reductions were carried out by mixing the calcium and rare earth fluorides in a tantalum crucible in an argon environment. The fluorides were previously treated by vacuum sintering or fusion to remove the adsorbed gases from the very large surface area of the salt and also to reduce this surface area. Vacuum distilled calcium ground to 10 mesh particle size and stored in an inert atmosphere was used for these reductions. Mixing the reactants under inert gas cover decreases contamination by atmospheric gases. The quantity of calcium was 10% more than that required by the stoichiometry of the reaction

$$3Ca + 2REF_3 = 3CaF_2 + 2RE$$

The charge was loaded into a vacuum-outgassed tantalum crucible that was then covered with a perforated tantalum lid. The arrangement is shown schematically in Figure 4.25. The crucible was placed in a silica tube vacuum induction furnace and heated

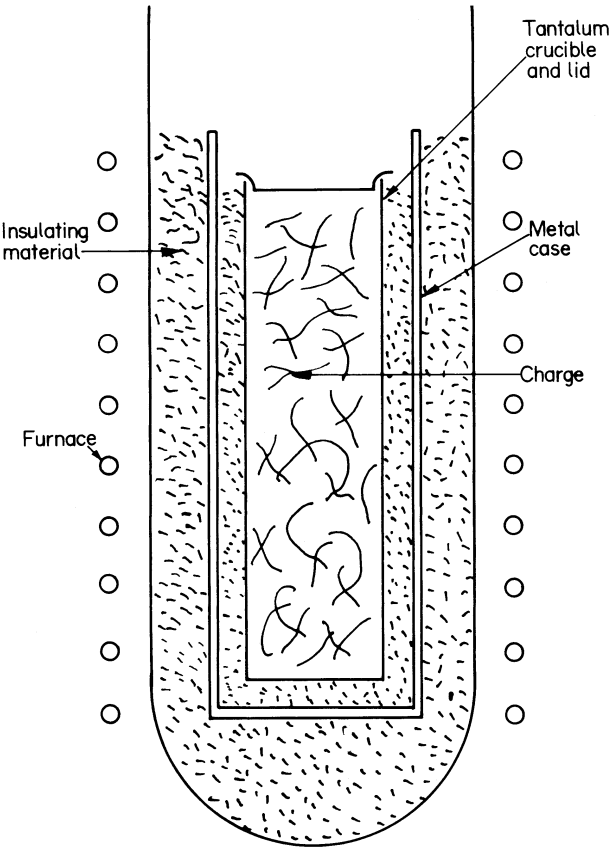

Figure 4.25 Schematic of the setup for the calciothermic reduction of rare earth trifluorides (Topp 1965).

slowly to 600°C to outgas the charge. Purified argon was admitted into the furnace at this temperature to a pressure of 70 kPa and the heating was continued further. The reaction started between 800 and 1000°C, depending on the particular rare earth, and the exothermicity of the reaction resulted in a distinct increase in the temperature of the charge to above the temperature of the furnace. The reaction was not violent and the external heating was continued to a temperature where both the products, slag and metal, were molten. The chosen temperature was 50°C above the melting point of calcium fluoride or 50°C above the melting point of the metal being prepared, whichever was higher. These reductions go to completion within a few minutes after reaching the chosen temperature, and holding for 15 minutes at the maximum temperature was sufficient to achieve good separation of metal and slag. Once the reductions had taken place and the furnace had cooled to room temperature, the crucible was removed from the furnace in air, and the slag layer that had formed on top of the metal ingot was knocked out of the crucible, leaving a clean ingot of rare earth metal in a 97 to 99% yield with 0.1 to 2% calcium as the principal impurity. Daane (1961a) had described that in a 50 mm diameter by 200 mm high tantalum crucible, 300 g of the rare earth metal could be made per batch. The crucibles were made of 0.25 mm thick tantalum sheets for such a batch size, whereas 0.76 mm thick tantalum

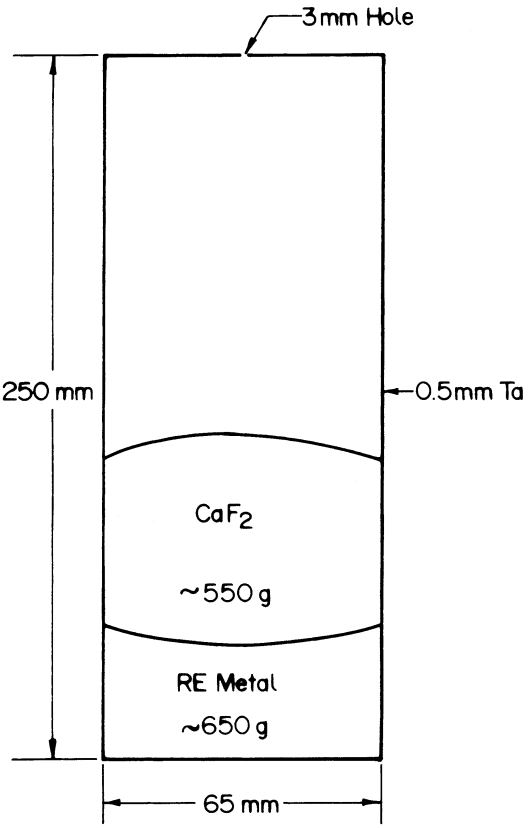

Figure 4.26 Cross section of a typical reduction crucible in calciothermic reduction of rare earth trifluorides (Spedding et al. 1970).

crucibles were used in the semicontinuous operation, which produced 9 to 14 kg of metal in each reduction. Higher thickness prevents erosion through the walls during repeated use of the crucible.

The cross section of a typical reduction crucible used (Spedding et al. 1970) for calciothermic reduction of rare earth fluoride is shown in Figure 4.26. A large crucible is needed because of the low density of the starting materials. The volume occupied by the products of reaction is, however, much lower. Considering these, Daane (1961a) used the apparatus shown in Figure 4.27 to increase the amount of metal made in a heat. The charge was placed in the upper Pyrex hopper and held there while the tantalum crucible was vacuum outgassed. Required quantities of charge were then dropped into the tantalum reaction crucible by lifting the valve control tube and as the charge reacted and melted down, more charge was added so that the crucible might be filled to near its top.

Semicontinuous Reduction The calcium reduction of rare earth fluoride could be carried out on a fairly large scale, as a semicontinuous process, using the reduction and pouring furnace described by Carlson and Schmidt (1961a) for the preparation of yttrium. The principal features of the furnace are shown in Figure 4.28. The charge, which consisted of YF_3 powder mixed with granular calcium (slightly in excess of the stoichiometric amount) was introduced into the reduction crucible from a hopper through a sliding

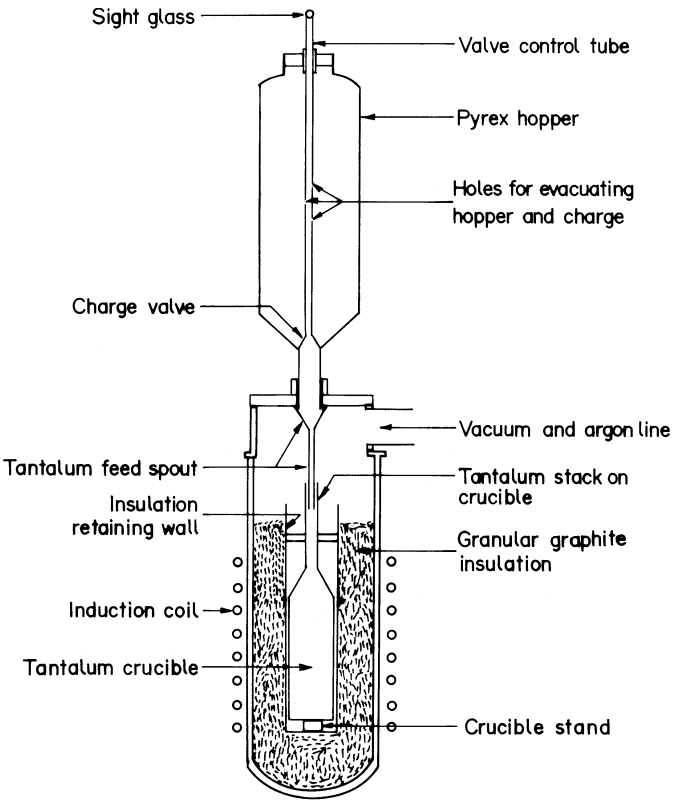

Figure 4.27 Apparatus for reducing rare earth fluorides with calcium (Daane 1961).

vacuum valve. The pouring spout below the hot zone of the graphite heater was sealed by a plug of yttrium metal that flowed into the tube and solidified at the beginning of reduction. Initial charge of the yttrium fluoride–calcium mixture was also placed in the reaction chamber. The system was evacuated and backfilled with argon. After the initial heating of the reaction chamber, to effect a reduction, additional reactants were introduced through the top vacuum valve from the hopper until the reaction chamber was filled with reduced metal and CaF_2 slag. The yttrium slug was then melted out by lowering the induction coil around a graphite focus inductor that heated the pouring spout. The metal and slag ran into the water-cooled mold below. After the pouring operation, a specially designed vacuum valve above the mold was closed so that the mold could be detached and emptied while the next reduction was in progress. The fresh charge of reactants was added to the tantalum crucible from the hopper, while the chamber was still hot. This procedure could be repeated until sufficient metal was obtained or a part of the equipment failed. The reduced yttrium ingot contained 0.15 to 0.5% Ca.

To remove calcium and also the residual fluoride, the as-reduced yttrium was melted into billets using a double arc melting procedure. The analysis of yttrium thus obtained was 0.14 to 0.20% O, 0.05% F, 0.02% N, 0.01% C, 0.03% Fe, 0.001% Ca, and 0.4% Ta.

Goldschmidt Process In the industrial practice described by Herget (1985) for calcium reduction of rare earth fluoride, the fluoride was mixed with granular calcium and the mixture was placed in a tablet form or as rammed material in a steel reactor. The reactor

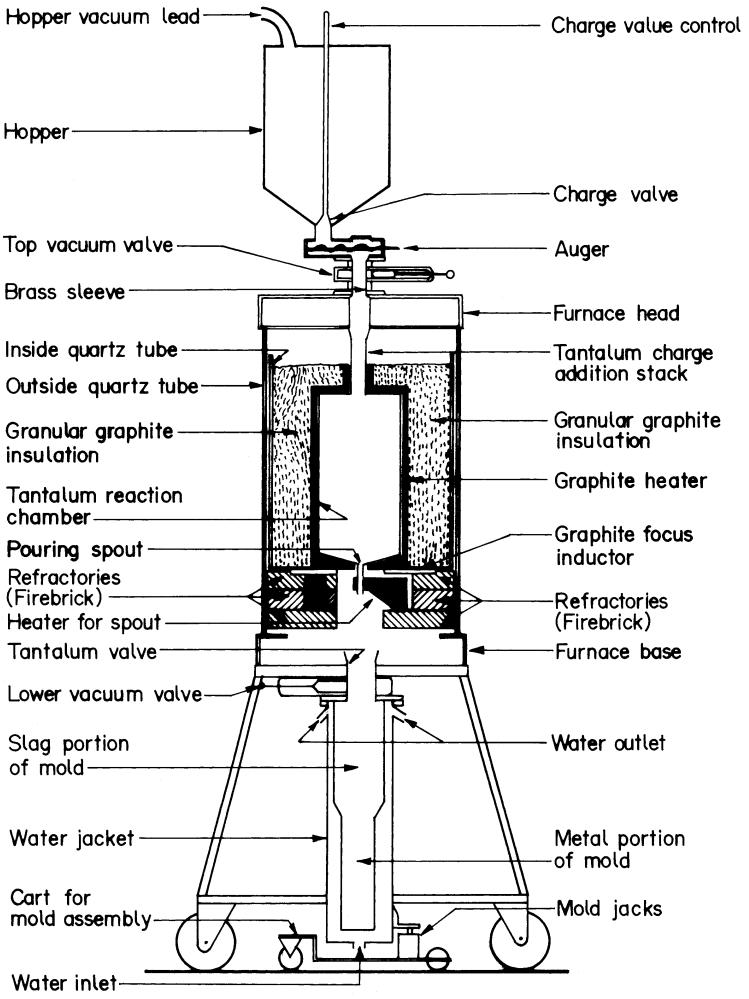

Figure 4.28 Reduction and pouring furnace for semicontinuous preparation of yttrium metal (Carlson and Schmidt 1961a).

was lined on the inside with tantalum, which was coated with a layer of calcium fluoride. After cooling and evacuating the reactor, the metallothermic reduction was initiated by a spark discharge. The reduction proceeded to completion within minutes.

$$2\mathrm{REF_3} + 3\mathrm{Ca} \xrightarrow[\text{vacuum}]{\text{up to } 2000^\circ\mathrm{C}} 2\mathrm{RE} + 3\mathrm{CaF_2}$$

The rare earth metal, collected as an ingot in the bottom part of the reactor, topped by solidified calcium fluoride slag.

The preparation of rare earth metals by reduction of their trifluorides with calcium metal in tantalum crucibles leads to the introduction of up to 0.5% tantalum as impurity. This happens in particular in higher melting rare earths because higher temperatures are reached in their production, and solubility of tantalum in rare earths increases with temperature

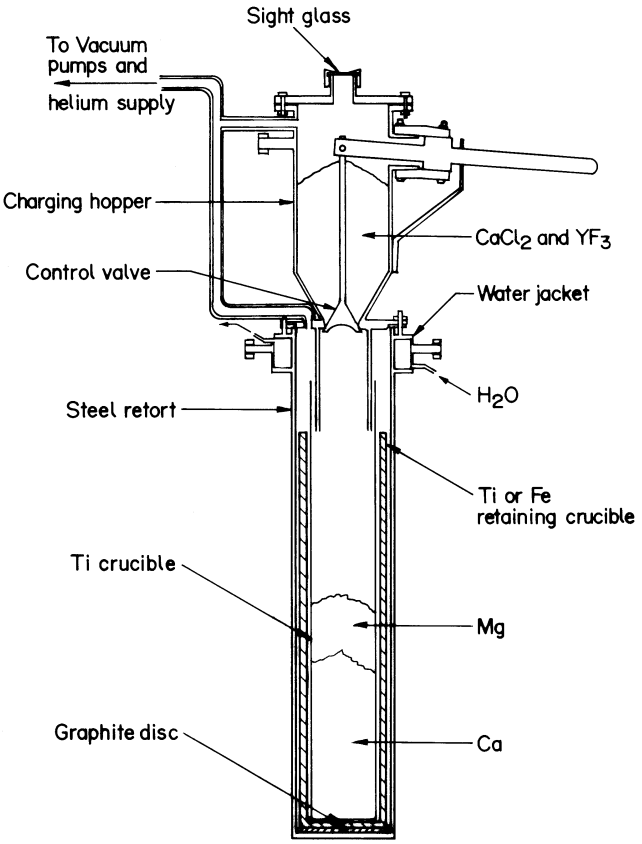

Figure 4.29 Schematic diagram of the reduction retort (Carlson et al. 1960).

(Dennison et al. 1966). In the case of scandium, the tantalum content ranges from 2 to 5%. A solution to this problem was in what is known as the intermediate alloy process.

4.7.3 Intermediate Alloy Process

The temperature necessary for fluoride reduction was lowered and thus the amount of crucible material in the resulting rare earth metal was decreased in the large scale production of yttrium (Carlson and Schmidt 1961a) through the formation of an intermediate low melting alloy with zinc, or more successfully with magnesium. A similar process was applied to scandium also (Spedding et al. 1960).

The first method using the intermediate alloy investigated by Carlson et al. (1956) involved the formation of yttrium–zinc alloy. The process was carried out in a bomb reactor and yttrium trifluoride was reduced with calcium using ZnF_2 as a thermal booster. The product was a low melting Y–Zn alloy that was immiscible with the molten CaF_2 slag. The alloy was eventually heated in a vacuum to volatilize off zinc leaving behind yttrium. Even though the metal prepared was of satisfactory quality, difficulties were encountered in finding a suitable bomb liner in the reduction stage and also in the removal of zinc. This method was investigated no further (Carlson and Schmidt 1961a).

The yttrium–magnesium alloy method was also investigated by Carlson et al. (1960, Carlson and Schmidt 1961a). Yttrium fluoride was reduced by calcium in the presence of calcium chloride to form an Y–24% Mg intermediate alloy. The alloy and the slag formed in the reaction were both molten at 950°C. It was thus possible to carry out the reduction in a refractory metal crucible under an inert gas atmosphere. Calcium chloride not only forms a low melting eutectic with CaF_2 but also decreases the density of the slag, which is an important factor for complete separation between the slag and the alloy phases.

A sketch of the apparatus used for the process is shown in Figure 4.29. Massive pieces of magnesium (290 g) and calcium (680 g) were transferred to the reduction crucible and a mixture of YF_3 (1500 g) and $CaCl_2$ (1350 g) was loaded into the charging hopper. The unit was evacuated by a mechanical pump and then placed into a gas-fired furnace. When the retort temperature had reached 800°C, helium was admitted and a positive pressure of 7 to 35 kPa was maintained in the system throughout the remainder of the run. When calcium and magnesium were molten and reached a temperature of 900°C, the YF_3–$CaCl_2$ mixture was added slowly from the hopper into the molten metals at a rate required to maintain the temperature in the reacting mass above 800°C. The mass was then brought to a temperature of 960°C. At the completion of the run the hot retort was raised from the furnace and allowed to cool in a slightly tilted position. Solidification occurring in this position resulted in easier slag–alloy separation.

The designed composition of the intermediate alloy was 24% magnesium, and a 10% excess calcium reductant gave a metal recovery of over 99% theoretical. The slag composition of 52% $CaCl_2$ gave the best slag metal separation and highest metal yields.

The alloy was crushed into approximately 12 mm pieces in a jaw crusher enclosed in a dry box. Magnesium removal was carried out by sublimation in a 150 mm diameter stainless steel retort equipped with a condenser. The alloy pieces were loaded in a titanium vessel in the vertical retort. The system was evacuated to 10^{-2} Pa at the outset and this pressure was maintained throughout the run. The retort and contents were heated to 900°C in an electric furnace and held for 4 h after which the temperature was raised to 950°C and held for 20 h. Magnesium vapors collected on an air-cooled condenser. The yttrium obtained was in the form of bright porous sponge containing ~0.01% magnesium and calcium. The yttrium sponge obtained in the process was arc melted in an inert atmosphere to form an ingot.

The intermediate alloy method has been used on a large scale for the preparation of yttrium (Carlson and Schmidt 1961a). A titanium or zirconium crucible (510 mm diameter, 1150 mm height, 6 mm wall thickness) was used as the reduction crucible. The crucible was reinforced with a mild steel outer jacket. A thin titanium sheet was inserted between the jacket and zirconium crucible to prevent alloying of steel and zirconium at the reduction temperature. In this process granular calcium (37.6 kg, 10% excess) and granular magnesium (15.8 kg) were used to reduce yttrium trifluoride (82 kg) and $CaCl_2$ (37.6 kg) essentially following the procedure described above.

The analysis of yttrium produced by the above process is given in Table 4.5. The purer sample on the second column was lower in oxygen content because freshly distilled massive calcium was used and the crucible was titanium which has a lower solubility in Y–Mg alloy than does zirconium.

Haefling et al. (1961) conducted experiments to find a reductant for YF_3 using an intermediate alloy process that is more economical than calcium, yet producing yttrium metal of comparable quality. Lithium, calcium–lithium alloy, magnesium, aluminum sodium and zinc were all evaluated.

Table 4.5 Chemical analysis of yttrium produced by the intermediate Y–Mg alloy process (Carlson and Schmidt 1961a)

Crucible	Zirconium	Titanium
Reductant	Calcium granules	Freshly distilled massive calcium
Impurity	Content, %	
Ca	0.001	0.001
Cu	0.010	0.010
Fe	0.015	0.015
Mg	0.003	0.003
Ni	0.035	0.020
N	0.015	0.015
O	0.25–0.40	0.12–0.25
Si	0.01	0.01
Ti	0.005	0.15
Zr	0.7	0.001

Yttrium fluoride was reduced by lithium metal and by Ca–Li alloys in the presence of magnesium to form Y–24% Mg intermediate alloy. The apparatus used in these experiments was the same as that used by Carlson et al. (1960). A typical reaction mixture for lithium reduction of YF_3 consisted of 1500 g YF_3, 288 g Mg, and 235 g Li. The reactants were loaded into the reduction crucible, which was inserted into the steel retort. From then on the run was conducted as described when calcium was used as reductant, except that the reaction temperature was 975°C and duration was one-half hour. The alloy and slag formed were both molten at this temperature. Metal yields of 99% were obtained. The oxygen content was 0.12% in yttrium metal when distilled lithium was used, and it was 0.15 to 0.2% when filtered or ethanol pickled lithium was used.

Calcium–lithium alloys containing 15 to 60% lithium were also used as reductants for YF_3. In each experiment 1500 g of YF_3 and 290 g of magnesium metal were added to form Y–24% Mg alloy. Lithium, calcium, and magnesium were all placed in the reduction crucible and YF_3 was loaded in the feed hopper. The metals was heated to 975°C, as described earlier for runs using calcium as reductant, and YF_3 was added in incremental amounts to the molten Li–Ca–Mg alloy. The reaction mixture was held at 975°C for one-half hour before it was cooled to room temperature, and the Y–24% Mg alloy obtained was processed to yttrium sponge. The yield of yttrium metal was greater than 99% when the reductant alloy contained at least 22% lithium. The oxygen content varied from 0.1 to 0.2%.

Using magnesium as reducing agent, mixtures of Mg, YF_3, and anhydrous $CaCl_2$ were heated to 975°C in a tantalum crucible for various lengths of time. However even after 4 h, the maximum yield was only 17%. The yield was only 18% when aluminum was used as reducing agent at 1000°C, and the yield was only 7% with sodium after reduction at 900°C. No reaction occurred at 900°C with zinc as reducing agent.

The advantage of using lithium as reductant (Haefling et al. 1961) lies in the low melting LiF slag (m.p. 870°C) that is formed. With the reduction temperature 975°C, no fluxing agent was needed when LiF was formed. Lithium is costlier than calcium but the cost difference, when unit weight of yttrium produced is considered, is narrowed because

calcium reactant needs a considerable quantity of $CaCl_2$ to flux the CaF_2 slag produced in the reaction. The use of Ca–Li alloy as reductant for YF_3 offers all the advantages of lithium reductant because all compositions of CaF_2–LiF slag formed were fluid below 975°C. The use of Ca–22% Li alloy was economical because the cost savings not having to use $CaCl_2$ more than offset the extra cost due to lithium in the reductant.

4.7.4 Preparation of Scandium

The use of an intermediate zinc alloy was not very successful with yttrium; however zinc proved to be a suitable element for the intermediate alloy process to produce scandium (Spedding et al. 1960). The process is carried out as follows:

$$2\,ScF_3 + 3\,Ca + 3\,Zn + LiF \rightarrow Sc\text{–}60\%\ Zn\ alloy + 3\,CaF_2\text{–}LiF\ (eutectic\ composition)$$

The alloying of scandium (m.p. 1541°C) and formation of the low melting slag made it possible to carry out the reduction and separation of the products into molten metal and slag layers at 1100°C. In a tantalum crucible, the reactants were sealed under a helium atmosphere by welding. The crucible was in turn sealed inside a stainless steel bomb in a helium atmosphere. On heating the bomb in a muffle furnace to 1100°C, the reaction and subsequent separation of products into alloy and slag layers occurred. When cooled, the crucible was opened and the alloy layer was separated from the slag. The scandium–zinc alloy, which also contained 1 to 2% Ca, was brittle and was easily crushed into small pieces. These pieces were heated very slowly in an induction furnace under high vacuum whereby zinc and calcium sublimed off and a porous scandium sponge was obtained. This was consolidated by arc melting under 1 atmosphere argon. The metal was obtained with an overall yield of 90% and contained trace amounts of tantalum, magnesium, calcium, copper, lithium, iron, silicon, and zinc, less than 100 ppm of carbon, nitrogen, or hydrogen, and probably less than 1000 ppm of residual oxygen.

4.7.5 Reduction of Samarium, Europium, and Ytterbium Halides

The chloride and fluoride reduction methods described so far are applicable to all the rare earth metals except samarium, europium, and ytterbium. This was realized as early as in 1937 by Klemm and Bommer (1937) and corroborated in later investigations (Daane 1961a). When the chlorides or fluorides of samarium and europium or ytterbium reacted with calcium or barium, a very exothermic reaction occurred in which the trihalides were reduced to the dihalides but no metal was obtained.

4.8 OXIDE REDUCTION PROCESSES

Rare earths form highly stable oxides. Among the popular metallic reducing agents, only calcium forms oxide stabler than that of the rare earths. The stability of magnesium oxide is only marginally higher than that of the heavy rare earth oxides and comparable to those

of the light rare earth oxides. Apart from calcium, the only element that can reduce rare earths is carbon. In fact, at about 1700°C and a CO pressure below 100 Pa, carbon is the most efficient reducing agent. In the classical sense, therefore, the possibility of rare earth oxide reduction appears restricted to the use of either calcium or carbon.

The important investigations on oxide reduction are listed in Table 4.6. Early attempts to produce rare earth metals by reduction of their oxides were made between 1890 and 1912 by Winckler (1890, 1891), Matignon (1900), and Hirsch (1912). Using magnesium or calcium as the reducing agent, they invariably ended up with a product mixture consisting of magnesium oxide or calcium oxide and the metal, which could not be separated. Several decades later, Mahn (1950) pursued the magnesium reduction route. Mahn dipped fused oxide blocks of neodymium, gadolinium, or yttrium group elements into molten magnesium heated to 1050°C. The oxide block was rapidly attacked by the magnesium metal, but the products obtained were dilute solutions (<5% RE) of rare earth in magnesium.

The simple and direct attempts to reduce rare earth oxides by calcium and magnesium summarized above were destined to fail for many reasons. The stability of magnesium oxide is almost the same as that of the light rare earths at temperatures up to about 1100°C. Magnesia is stabler than yttrium and other heavy rare earth oxides, but the difference in stability

Table 4.6 Oxide reduction processes

Year	Reactants	Process	Results	Reference
1950	RE_2O_3–Mg (Nd, Gd, Y)	Rare earth oxide blocks dipped in molten magnesium heated to 1050°C	Mg–5%RE alloy	Mahn 1950
1953	RE_2O_3–La (Sm, Yb)	Reduction–distillation in Ta crucible and condenser	Pure RE metal condensate	Daane et al. 1953
1953	RE_2O_3–C	Carbothermic reduction	RE carbide formation	Trombe 1953
1957	Sm_2O_3–C	Reduction–distillation	Impure Sm condensate	Achard 1957
1959	RE_2O_3–Zr (Eu, Sm), La	Reduction–distillation in Mo crucible and condenser	Pure RE metal	Campbell and Block 1959
1959	Sm_2O_3–Ca	Reduction–distillation	Sm containing residual Ca in low yield	Onstatt 1959
1961	RE_2O_3–Ce	Reduction–distillation	Pure RE metal condensate	Daane 1961a
1968	RE_2O_3–La (Sm, Tm, Yb)	Reduction–distillation in Mo crucible and Ta condenser	Pure RE metal condensate	Moriarty 1968
1968	RE_2O_3–La (Dy, Ho)	Reduction–distillation	Residual La, O in condensate	Spedding and Daane 1968
1969	Dy_2O_3–Th	Reduction–distillation	Dy condensate purified by redistillation	Schiffmacher and Trombe 1969
1987	Gd_2O_3–$CaCl_2$–Mg	Heated to reaction temperature and slag leached off	Gd metal powder	Okajima 1987
1987	Nd_2O_3–Ca	Reduction carried out in $CaCl_2$–NaCl bath and metal extracted by Nd–Zn or Nd–Fe alloy pool	Nd–Zn or Nd–Fe alloy	Sharma 1987
1988	Nd_2O_3–Na	Reduction carried out as with Ca	Nd–Zn or Nd–Fe alloy	Sharma and Seefurth 1988, 1988a

is not substantial enough for magnesium to function as a reducing agent for these oxides. Even though the considerable thermodynamic stability of calcia qualifies it as a reducing agent for rare earth oxides, the high melting point of calcia (2600°C) is a definite disadvantage. During the calcium reduction, consolidated rare earth metal is not produced because the enthalpy of reaction is not sufficient to melt both metal and calcia slag and permit their separation by gravity. The reduction, at best, yields rare earth metal dispersed in the slag matrix. Aqueous processing to recover the fine metal powder usually results in oxygen contamination.

The breakthrough in the development of methods for preparation of rare earth metals by oxide reduction came in the 1950s when Daane, Dennison, and Spedding (1953) at Ames succeeded in devising the reduction–distillation process. This method, which is in a way similar to the Pidgeon process for magnesium, has been remarkably useful for the preparation of samarium, europium, and ytterbium, the three metals that could not be obtained by the normal halide reduction route.

4.8.1 Reduction–Distillation — Lanthanothermy

Systematic vapor pressure measurements of the rare earth metals (Habermann and Daane 1961) had indicated that lanthanum was the least volatile of the rare earth metals and that dysprosium had a vapor pressure nearly 300 times that of lanthanum at the same temperature. The metals samarium and europium are also similarly very volatile. Besides, lanthanum oxide was known to have one of the highest (most negative) heat of formation among the rare earth oxides. These observations led Daane et al. (1953) to devise a method for reacting the oxides of samarium, europium, or ytterbium with lanthanum metal and driving this reaction to completion by distilling away the volatile metals in vacuum. The method has since been called lanthanothermic reduction or lanthanothermy.

Preparation of Samarium and Ytterbium Samarium was the first metal to be prepared by the reduction distillation process. Daane et al. (1953) heated a mixture of 20 grams of freshly prepared lanthanum turnings and 20 grams of samarium oxide in a tantalum crucible to 1450°C under 0.1 Pa and held for about half an hour. The crucible was 200 mm long, 25 mm in diameter and 0.6 mm thick. The upper half of the crucible protruded out of the furnace and had a perforated tantalum lid. On opening, the upper walls of the crucible and the bottom of the cap were found to be covered with a silvery crystalline metallic deposit, which analysis showed to be samarium of better than 99% purity with no lanthanum detectable (<0.02%). The yields were 80% from the original oxide. Several subsequent reductions obtained nearly 100 grams of samarium of better than 99.9% purity each time, representing an overall 95% yield.

Preparation of ytterbium by the reduction–distillation process could be done at a lower temperature (Daane et al. 1953, Spedding and Daane 1954), due to its higher volatility compared to samarium, and the yield was similar.

Preparation of Europium The first mention of the preparation of europium metal was made in 1954 by Spedding and Daane (1954). The details of europium preparation and handling appeared in a subsequent paper (Spedding et al. 1958). The schematic of the reduction system is shown in Figure 4.30. The reduction crucible was made from two concentric tantalum cylinders welded together. A mixture of 86.5 g Eu_2O_3 and 73 g lanthanum turnings was charged in the annular space between two concentric tantalum cylinders welded together and shown as the reduction chamber. The chamber was heated

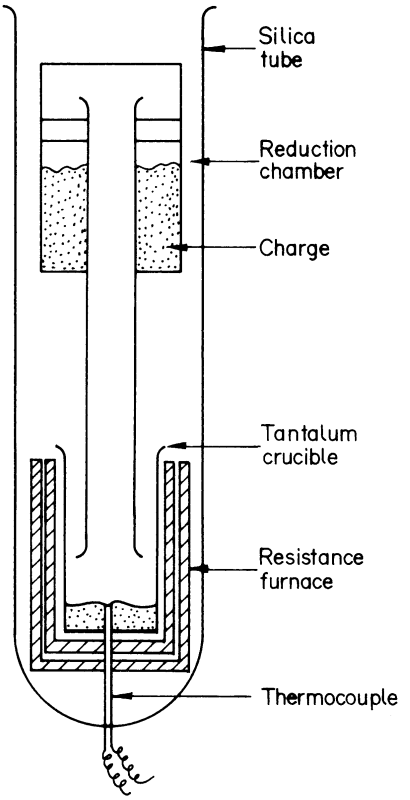

Figure 4.30 Schematic of the apparatus for the reduction of europium (Spedding et al. 1958).

to 1000°C and the pressure was maintained at less than 0.01 Pa. The metal began to distill at 1100°C, and as the temperature reached 1200°C, droplets of europium began to reflux. The evaporated metal condensed in the lower part of the inner cylinder and at intervals, the induction coil was lowered and the metal was melted down into the tantalum crucible below.

An interesting feature of the above process is that the starting materials need not be extremely pure to get pure europium. Samarium is the usual impurity in europium oxide, but it is completely absent in the europium metal produced by the above process because samarium is less volatile than europium, and for the reduction of Sm_2O_3 to metal a higher temperature is needed than that used for Eu_2O_3 reduction. Commercial lanthanum turnings can be used in place of the more expensive very pure lanthanum metal. Any calcium impurity in the charge would, however, be transported to europium.

Preparation of Samarium, Europium and Ytterbium and Terbium Daane (1961a) described the preparation of samarium, europium, and ytterbium. Lanthanum turnings in 10% excess were intimately mixed with the rare earth oxide and the mixture was heated in a tantalum crucible in a high vacuum to effect the reaction

$$2La + RE_2O_3 = La_2O_3 + 2RE$$

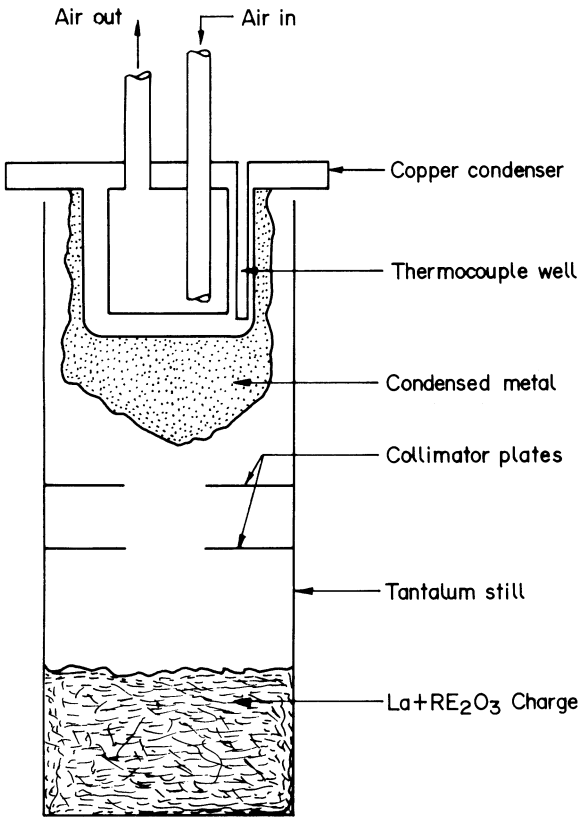

Figure 4.31 Apparatus for preparation of samarium, europium, and yttrium metals (Daane 1961).

Two types of apparatus have been used for carrying out this reaction. One is a simple tantalum crucible, the upper portion of it acting as the condenser. The lower portion of the crucible was maintained at the highest possible temperature so that the volatile metals were recovered as bright crystalline condensates on the walls of the upper part of the crucible. Metal yields were greater than 98%. With a 50 mm diameter reaction chamber, 300 to 400 g metal could be obtained per batch. In another arrangement shown in Figure 4.31, an air-cooled copper condenser was fitted in the upper portion of the reaction chamber. This was first used for the preparation of samarium. The condenser was coated with an alcoholic wash of Sm_2O_3 to provide a barrier to prevent contamination of the metal deposit. A stream of air, controlled by a thermocouple attached to the condenser, was used to maintain the condenser temperature at 300 to 400°C. If the condenser temperature was too low, the metallic deposit was so powdery that it was pyrophoric and difficult to handle. Between 300 and 400°C, good grain growth was maintained in the condensate and a product that was stable in air was obtained. Ytterbium was also prepared under essentially similar conditions. Being a more reactive metal, europium needed to be always handled in an inert atmosphere.

Metals prepared by the above process were found to contain no detectable lanthanum or tantalum. This may be attributed to the great differences in volatility. The contents of other impurities such as carbon, nitrogen, oxygen, and hydrogen were less than 100 ppm.

Somewhat higher temperatures and a larger excess of reductant in the charge were recommended by Beaudry and Gschneidner (1978) who have outlined a procedure for the metallothermic reduction of the oxides of samarium, europium, thulium, and ytterbium. Thulium, like other metals in the group, is volatile and a candidate for preparation by reduction–distillation. The process described by Beaudry and Gschneidner (1978) is as follows. The rare earth oxide was heated in air at 800°C for 15 h to drive off adsorbed compounds such as H_2O and CO_2. Freshly prepared chips or turnings of lanthanum that had been vacuum melted at 1800°C or higher were mixed with freshly ignited oxide. The quantity of lanthanum was 15% more than that needed by the stoichiometry of the reaction

$$2\,La + RE_2O_3 = La_2O_3 + 2\,RE$$

The oxide–lanthanum turnings mixture was packed into a 6.4 cm diameter by 25.4 cm long tantalum crucible that was fitted with a 20 cm long tantalum condenser and a tantalum optical baffle arrangement. The baffles prevent excessive entrainment of oxide particles in the vapor. The crucible and contents were evacuated and heated to a maximum of 1400°C for europium and ytterbium and 1600°C for samarium and held at that temperature for an additional 2 h. The temperature was raised slowly because a fast heating rate could cause lanthanum to melt and run to the bottom of the crucible. On the other hand, in slow heating, as lanthanum reacted with the rare earth oxide, La–La_2O_3 solution was formed and this had a higher melting point than pure lanthanum metal. Once the melting point of the reducing medium was increased, the temperature could be raised to enhance the diffusion rate.

A typical charge for samarium preparation would consist of 550 g Sm_2O_3 and 540 g of lanthanum. The amount of lanthanum was about 15% more than the stoichiometric amount. After reduction–distillation, about 465 g of samarium were obtained representing a yield of 98% which was usual in the process. The reduction crucible could be cleaned, loaded once again with lanthanum and samarium oxide and reused for additional distillation runs.

4.8.2 Reduction–Distillation — Other Reductants

The basic criteria for a successful reduction–distillation process, that the product metal has an appreciable vapor pressure while all other components of the process possess negligible vapor pressure at the reaction temperature, is met in certain systems where in place of lanthanum, metals like cerium or zirconium are used. Both cerium and zirconium have very stable oxides and low vapor pressure and they can be obtained in very pure form. Campbell and Block (1959) investigated the use of cerium and zirconium as reductant for the preparation of europium and samarium.

The diagram of the apparatus used by Campbell and Block (1959) is shown in Figure 4.32. Samarium or europium oxides were mixed with the metal reductant (lanthanum, cerium, or zirconium) and compressed into pellets. The reductants were freshly prepared in a finely divided state as powder or lathe turnings. The pellets were loaded inside the closed end of a molybdenum thimble that was then placed inside a refractory vacuum retort. The evacuated retort was heated overnight at 200°C to remove adsorbed gases from the charge. The temperature was then gradually raised to the operating temperature while maintaining the pressure at less than 25 Pa. At the completion of the run, the pressures were approximately 0.5 Pa. The metal (samarium or europium) collected as bright crystalline

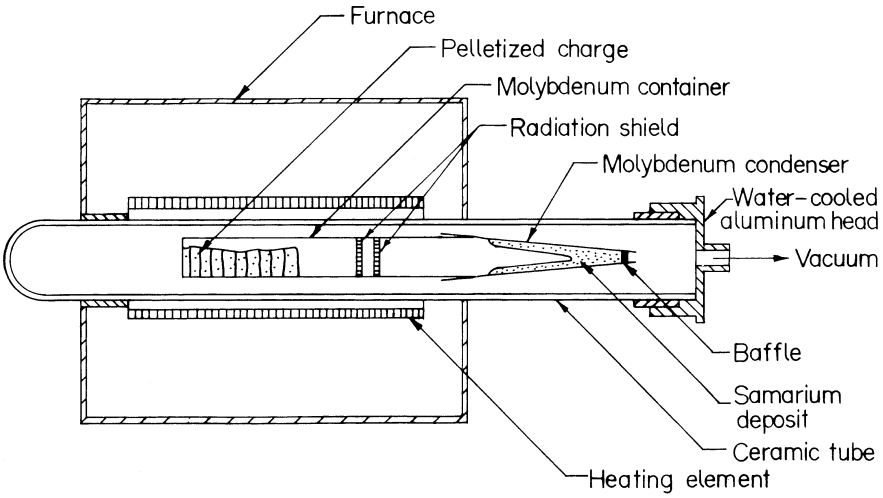

Figure 4.32 Reduction–distillation assembly.

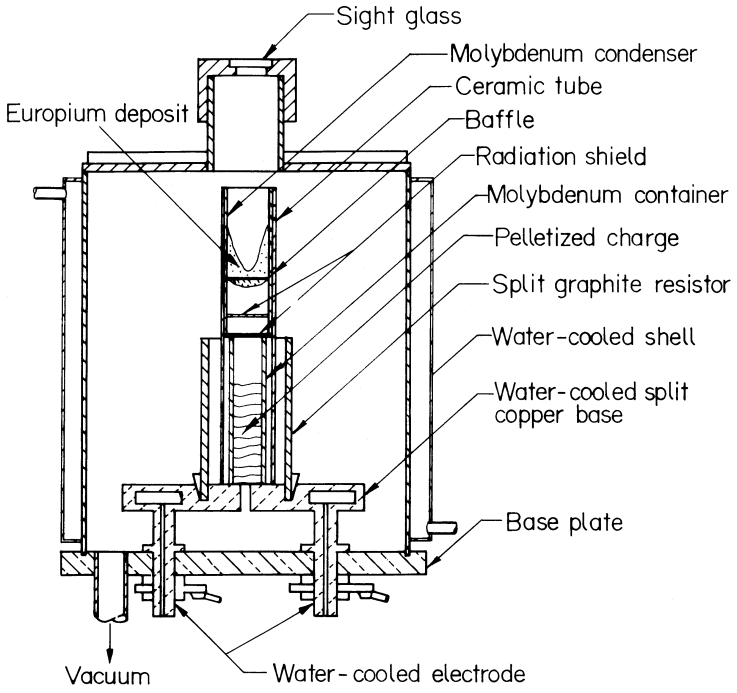

Figure 4.33 Split graphite resistor furnace assembly (Campbell and Block 1959).

deposits in the tapered condenser that was fitted over the open end of the molybdenum thimble, as shown in Figure 4.32. Subsequent operations for collecting the metal deposit were performed under stringent atmosphere control to prevent air contamination. When cool, the condenser was transferred to an inert atmosphere handling chamber. The small end of the condenser was fitted into an expendable 0.125 mm thick tantalum crucible. On

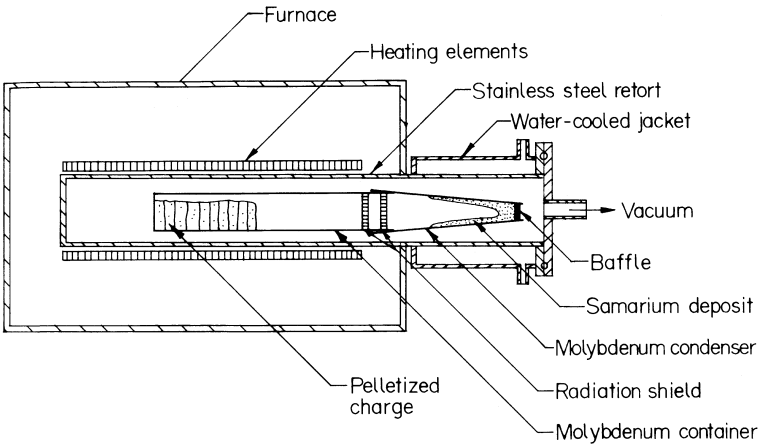

Figure 4.34 Larger scale reduction–distillation assembly (Campbell and Block 1959).

heating the entire assembly under argon, the deposit was melted from the condenser surface and collected in the tantalum crucible, which was subsequently peeled from the cast metal ingot.

Using lanthanum as reductant, high purity europium was obtained in more than 90% yield at reduction temperatures as low as 900°C. This relatively low temperature is attractive for extending the technique to commercial practice. However, the yield was maximum and time needed at maximum operating temperature was minimum when reduction was carried out at 1200°C.

Higher temperature was needed for preparing samarium from its oxide using zirconium as reductant. Campbell and Block (1959) performed this reduction in a high temperature apparatus shown in Figure 4.33. The entire assembly was mounted in a vertical position inside a vacuum furnace, and heat for the reaction was supplied by a hollow split graphite resistor mounted inside the water cooled vacuum furnace shell. After degassing the furnace and reduction equipment at 1000°C until a vacuum of less than 0.1 Pa was obtained, the furnace was cooled under argon and the molybdenum thimble containing the pelletized charge was introduced. The charge had pellets made from 85% Sm_2O_3 and –35 mesh zirconium sponge. The furnace temperature was raised to 1450°C over a 2-h period and maintained at this temperature for 1 h. The retort pressure during reduction was between 0.8 and 1.4 Pa. Crystalline metal deposit thus obtained was recovered from the condenser as described earlier.

Essentially the same operating procedures were adopted by Campbell and Block (1959) in the equipment for larger scale experiments, shown in Figure 4.34.

Apart from lanthanum, cerium, and zirconium aluminum Campbell and Block (1959) tried aluminium also. It was observed that while both cerium and aluminum reduce samarium and europium oxides, they also exert appreciable vapor pressure at the operating temperature and tend to volatilize along with samarium or europium metals. Unlike cerium and aluminum, which tended to carry over into the crystalline deposit, neither lanthanum nor zirconium was detected in the rare earth metals prepared with these reducing agents. Besides, the relatively low cost of zirconium makes it commercially more attractive.

The possibility of using cerium as the reductant in reduction–distillation was also mentioned by Daane (1961a). In addition, he also noted that good results were obtained

with cheaper commercial misch metal; however, the commercial misch metal often contains volatile impurities such as magnesium, aluminum, and various halides. These impurities must be removed by vacuum melting before the use of misch metal for preparation of highly pure samarium, europium, or ytterbium. Thulium has also been prepared using misch metal as reductant for thulium oxide, Tm_2O_3. However, the thulium metal prepared contained a few ppm of neodymium or volatile heavy lanthanides present in the misch metal. This can be attributed to the high temperature involved in the reduction. Lanthanum or cerium was used if high purity thulium was desired.

In addition to the three metals (samarium, europium and ytterbium) described in detail and the metal thulium mentioned earlier, heavy rare earth metals that have vapor pressures significantly greater than lanthanum (but less than Sm, Eu, Tb, and Yb) have also been prepared by reduction distillation. Spedding and Daane (1968) reduced a compacted mixture of the rare earth oxide and lanthanum turnings at approximately 1500°C to prepare dysprosium and holmium metals. The yields were 85 to 94% in these reductions; however, the relatively low vapor pressure difference between lanthanum on the one hand and Dy and Ho on the other manifests in up to 1% lanthanum content in the condensate. The oxygen contents were also higher. Using zirconium in place of lanthanum, Spedding and Daane (1968) obtained a distillate of better quality, less than 1 ppm zirconium and approximately 150 ppm oxygen, but the yields were poor, 20–33%.

The preparation of dysprosium metal by reduction–distillation using thorium was reported by Schiffmacher and Trombe (1969). Thorium filings were used to reduce dysprosium oxide at 1390–1750°C. The distillate was redistilled at 1600°C to obtain metal containing ppm levels of Th and O. The report did not mention the yield of the recoverable metal.

Onstatt (1953) used calcium in place of lanthanum for reduction of Sm_2O_3 and the samarium metal was distilled. Calcium is more volatile than lanthanum. Distillation had to be repeated 3–4 times to reduce the calcium content in the reduced metal to less than 0.1%. The metal yield was only about 40%. The calcium reduction method turned out to be more laborious and less effective than the lanthanum reduction method.

Achard (1957) used carbon in the reduction distillation process for samarium preparation. The distilled product contained considerable oxygen; however, a second distillation in a Ta apparatus at 1 to 10 mPa yielded pure malleable samarium. Europium and ytterbium were also prepared by the above process. Their purities were better.

The oxide reduction–distillation process, also called the direct reduction technique, has been in commercial use since 1959 to produce 99.9% pure (nuclear grade) rare earth metals (Moriarty 1968). The reduction reactor consisted of a molybdenum crucible and a tantalum condenser. It took about 2–3 h of slow heating of a reaction mixture containing 1.4 kg of oxide to get about 1 kg of metal in the condensate. The condensate was consolidated by inert atmosphere melting and casting in an induction furnace. The direct reduction has been commercially used for the preparation of samarium, europium, ytterbium and thulium metals (Daane 1961a, Beaudry and Gschneidner 1978).

4.9 NEW REDUCTION PROCEDURES

Certain modified or new reduction procedures, using magnesium, calcium, or even sodium for reduction of rare earth oxides, have been investigated in recent years. The rare earth

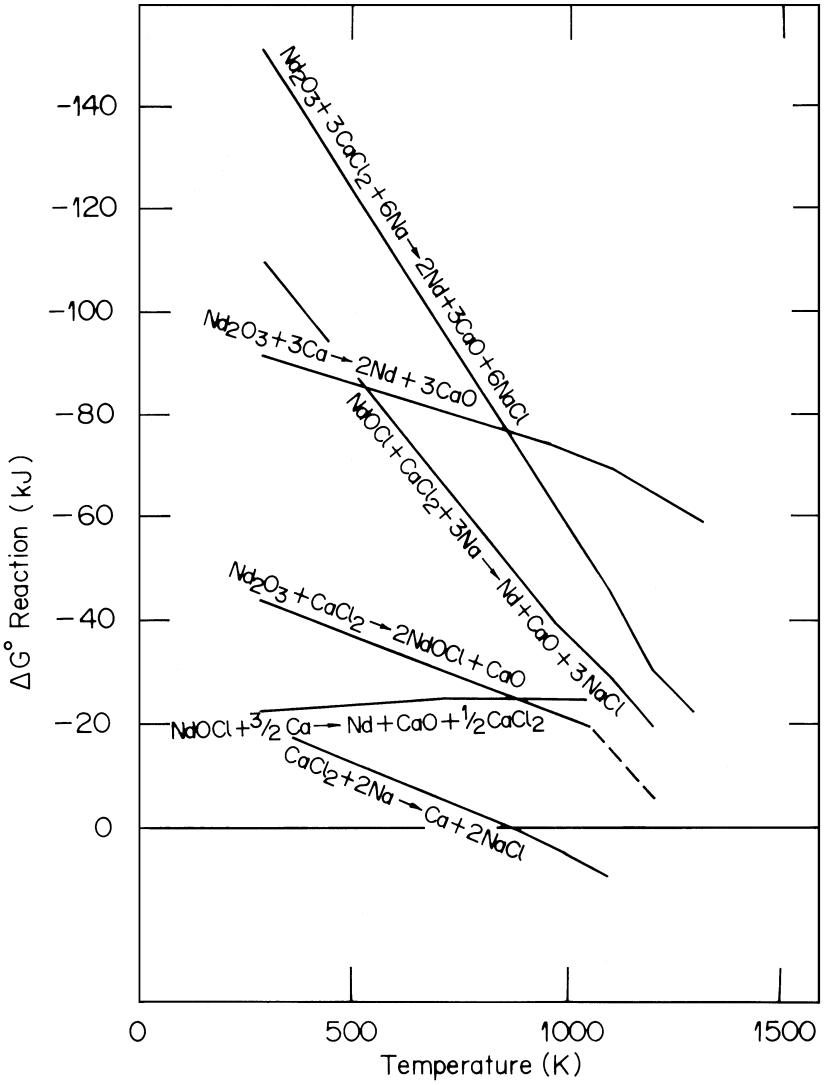

Figure 4.35 Standard free energy change of reactions as a function of temperature (Sharma and Seefurth 1988).

metal product is obtained directly as a powder or as an intermediate alloy that has to be pyrovacuum treated to obtain the metal.

4.9.1 Direct Preparation of Gadolinium Metal Powder

Okajima (1987) described a process for preparing rare earth metal powder by oxide reduction. Fine gadolinium oxide powder was mixed with anhydrous calcium chloride powder and magnesium granules, and the mixture was heated at 1100°C for 1 h. Gadolinium metal powder, at over 90% yield, was obtained from the product by leaching it with

water followed by decantation, alcohol washing, and vacuum drying. The key process modification in this attempt was the use of calcium chloride to flux the slag and reduce its melting temperature.

4.9.2 Metallothermic Reduction in Molten Salt

A novel method for calciothermic reduction of rare earth oxides was investigated at General Motors (Sharma 1987). The method has been applied to the reduction of neodymium oxide. Neodymium metal was produced by metallothermic reduction of Nd_2O_3 with calcium in a $CaCl_2$–NaCl melt, at temperatures between 710 and 790°C by the overall reaction

$$Nd_2O_3 + 3Ca \rightarrow 3CaO + 2Nd$$

The metal was recovered from the salt melt by extraction into a molten Nd–Zn alloy pool. Later on zinc was removed from the alloy by vacuum distillation. The basis of the technique and its application described by Sharma (1987) and Sharma and Seefurth (1988) are as follows.

Neodymium metal cannot be produced by the reduction of Nd_2O_3 with sodium by the reaction

$$Nd_2O_3 + 6Na \rightarrow 3Na_2O + 2Nd$$

But, calcium can reduce Nd_2O_3 according to

$$Nd_2O_3 + 3Ca \rightarrow 3CaO + 2Nd$$

and calcium can be generated by the reaction of $CaCl_2$ with sodium according to the reaction

$$CaCl_2 + 2Na \rightarrow Ca + 2NaCl$$

It therefore follows that Nd_2O_3 can be reduced to neodymium metal according to the reaction

$$Nd_2O_3 + 3CaCl_2 + 6Na \rightarrow 3CaO + 2Nd + 6NaCl$$

The above conclusions were arrived at from the standard free energy change data (Sharma and Seefurth 1988) for the various reactions plotted in Figure 4.35.

A metal in solution of its salt is more corrosive than when in its pure state. Thus, calcium in solution with $CaCl_2$ or $CaCl_2$–NaCl will react with Nd_2O_3 faster than pure calcium. According to Sharma and Seeforth (1988a) at temperatures between 710 and 1100°C, $CaCl_2$–NaCl melts with greater than 70 wt % $CaCl_2$ to provide a high enough concentration of Ca for the reduction to occur at an appreciable rate. That the reduction of Nd_2O_3 is effected by calcium dissolved in the molten salt phase and that calcium metal is

appreciably soluble in $CaCl_2$–NaCl melts are critical to the kinetics of the process. Carrying out the calciothermic reduction in $CaCl_2$–NaCl melts also facilitates separation of Nd from CaO and keeps CaO from interfering with the reaction. Nd_2O_3 can react with $CaCl_2$ to form the oxychloride, NdOCl. However, the neodymium oxychloride so formed is also reduced to the metal by calcium

$$NdOCl + 1.5\,Ca \rightarrow Nd + CaO + 0.5\,CaCl_2$$

Complete separation of the neodymium metal from the salt phase is possible by dissolving neodymium in a liquid metallic pool, which can be a Nd–Zn or a Nd–Fe melt. The density of the molten alloy being greater than that of the salt and CaO, there should be no difficulty in separating the metallic pool from the molten salt. Neodymium, which melts at 1021°C, can be separated from zinc that boils at 907°C by vacuum distillation; the vapor pressure of neodymium is negligible (~10^{-4} Pa) at this temperature. Extraction in a Nd–Fe molten pool is preferred for the Nd–Fe alloy destined for magnetic alloy production.

Sharma (1987) carried out all experimental procedures in a helium atmosphere (<1 ppm O_2, N_2 or H_2O) dry box that had a 130 mm diameter by 550 mm depth furnace extending beneath its floor. A diagram of the apparatus in the furnace well is shown in Figure 4.36. The reduction reaction was carried out in a tantalum crucible, 100 mm diameter by 130 mm depth with a 1.5 mm thick wall.

Calculated quantities of neodymium (99% pure) and zinc (99.9+% pure) metals, enough to make ~300 g of eutectic alloy, were placed in the tantalum crucible and the entire reaction assembly was lowered into the furnace well that was preheated to 550°C. After the zinc melted and diffused into the neodymium pieces, the furnace temperature was raised to 800°C until the alloy melted. At this stage, preweighed salt components (118 g of sodium chloride of 99+% purity and 1060 g of anhydrous calcium chloride of 99.9+% purity) were added and the furnace temperature was decreased to the normal range for reduction (700–725°C). Calculated quantities of Nd_2O_3 (~233 g) were added to the molten bath, the stirrer was lowered into the melt, and the melt was stirred to enhance mixing of the oxide into the melt. Calculated quantities of reductant, calcium metal granules (91.8 g Ca, 10% excess), and sodium (~20 g Na) were added to the melt and the baffle splash guard assembly was put in place. The salt bath and its contents were quickly stirred (300 rpm) for 4 h followed by slow stirring, at 60 rpm, for 1 h.

This sequence improved the mass transfer of the reactants in the first place and promoted good separation of the metallic phase from salt phase. At the end of the reaction, the apparatus was pulled out from the furnace well and quenched. Completion of reaction was ascertained by taking radiographs of the reaction vessel. A clear, sharp interface between the salt and metal pool and an increase in metal pool depth indicated completion of reaction. Salts were washed out of the crucible with warm running water and the alloy product was recovered. The product was 195.7 g of neodymium representing 97.9% of neodymium recovery in the alloy pool. The product analysis (in %) was 90.2 Nd, 9.9 Zn, 0.5 Al, 0.1 Si, 0.03 Ca, 0.05 Mg, and 0.05 Fe. Zinc from the Nd–Zn alloy was removed by vacuum distillation at ~1100°C and high purity neodymium (99+ Nd, 0.002 Zn, 0.4 Al, 0.1 Si, 0.01 Ca, 0.001 Mg, and 0.03 Fe) was obtained.

Using a Nd–Fe pool instead of Nd–Zn pool, Sharma and Seefurth (1988) were able to extract reduced neodymium in the iron alloy using an essentially similar procedure. In another investigation, Sharma and Seefurth (1988) used sodium instead of Ca to reduce neodymium oxide and extract the metal in the iron alloy. Sodium reduction can also be used

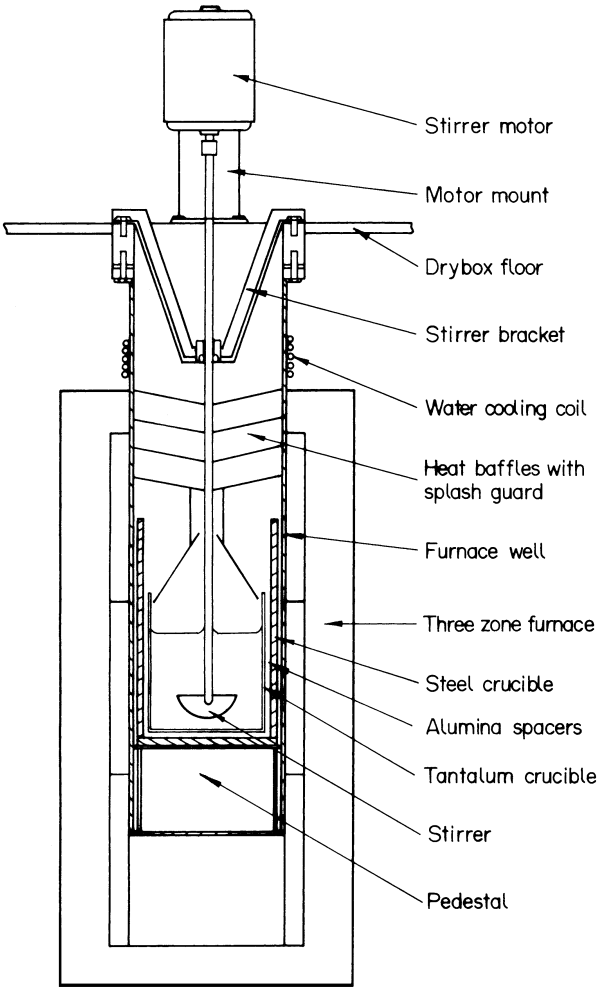

Figure 4.36 Schematic diagram of the reduction apparatus (Sharma and Seefurth 1988).

for obtaining the product first as Nd–Zn alloy and then the metal. This would be commercially more attractive than using calcium.

The molten salt oxide reduction process has not so far been reported for any other rare earth, except neodymium. Its applicability, however, appears wider.

4.10 CARBOTHERMIC REDUCTION

According to the Ellingham diagram, other than calcium, the only element that can reduce the rare earth oxides is carbon. In fact, at about 1750°C and with a CO pressure below 100 Pa, carbon is the most efficient reducing agent (Kruger 1971). Even the reduction of rare earth oxides by carbon is, however, beset with problems. Carbides are formed along with

the reduction. The rare earth carbides are high melting and form extensive and stable solid solutions with oxygen and nitrogen. It is often possible, however, to avoid the formation of carbides in reactive metals reduction by choosing appropriate conditions of temperature, CO/CO_2 ratio, and high vacuum. These conditions are arrived at with the aid of Pourbaix–Ellingham diagrams. These diagrams or thermodynamic data for constructing such diagrams are not available for the rare earths. Besides, many of the rare earths are relatively low melting and/or volatile at high temperatures and the simultaneous vaporization of reduced metal and CO would lead to a reverse reaction occurring and also carbon contamination. These factors have made carbothermic reduction very difficult for rare earth metal production.

An interesting possibility of carbothermic reduction has emerged from the use of a suitable solvent (Anderson and Parle 1976) to dissolve the reduced metal and lower its chemical activity to a level at which no carbides can form. In addition, high temperature refractory attack and vaporization loss are also avoided. The technique is yet to be tried for the rare earths.

4.11 ELECTROLYTIC PRODUCTION OF RARE EARTH METALS

Unlike the chemical reduction processes, all of which basically rely on the availability of reducing agents that form chlorides, fluorides, and oxides which are stabler than those of the rare earth metals, the electrolytic reduction of compound intermediates for the preparation of metals is not limited by considerations of chemical stability. The standard free energy of formation of a compound, which is the measure of its chemical stability, is related to its decomposition potential by the equation $\Delta G^\circ = -n\mathrm{FE}^\circ$, and it can be calculated that an applied voltage as small as 4 V should be more than adequate to dissociate even the stablest chemical compound (Alcock 1976). However in the same way as chemical stability is one of the many qualities of a reducing agent necessary for it to be used in practical processes, theoretical decomposition potential is one of the several requirements of a compound intermediate for it to be electrolytically decomposed in practical processes. When the other requirements are also satisfied, electrolytic reduction offers an effective method for reducing stable rare earth compounds to metals.

The electrolytic process for reducing metals from their salts or compound intermediates is basically simple. The salt of the metal is dissolved in another salt or a mixture of salts that are kept molten in an inert container. Two electrodes — a cathode and an anode — are inserted into the molten bath and an electric current is passed through the circuit, with a voltage sufficient to reduce the salt. The molten salt, known as the carrier electrolyte, first of all serves as a solvent for the metallic salt to be reduced, known as the functional electrolyte. The carrier electrolyte is so chosen as to have a desirable solubility for a functional electrolyte, sufficient conductivity for the electric current, a melting point below the chosen operating temperature of the cell, low vapor pressure, and a greater stability than the functional electrolyte. These properties are normally obtained by using an alkali or alkaline earth fluoride or chloride or a mixture of these fluorides and chlorides. Considerable variety is also observed in the cells used for electrolysis. These pertain to their size, shape, materials of construction, and disposition of the electrodes. Iron, graphite, ceramics such as fire brick and alumina, refractory metals such as molybdenum and tungsten have

all been used as cell materials. The anode is usually made of graphite and the cathode is iron, molybdenum, or tungsten. Often the cell itself serves as the anode or cathode. The temperature in the cell can be maintained in two ways, and on this basis the electrowinning cells associated with rare earth technology have been divided into two types. In one type the electrolytic current is used to supply the heat necessary to keep the bath molten, and in the other type supplemental thermal energy is provided to the bath by a furnace or by an arrangement in the cell independent of the electrolysis circuit.

The largest quantity of rare earth metals commercially produced throughout the world is obtained by electrolytic methods. Lanthanum, cerium, praseodymium, and neodymium have melting points that permit their recovery in the liquid state by electrolysis of relatively inexpensive chlorides at temperatures less than 1100°C. Winning of rare earth elements in the liquid state facilitates slag (electrolyte) metal separation, minimizes contamination of the reduced metal, and enables continuous operation and high volume levels of production. The technical feasibility of preparing limited quantities of high melting rare earth metals such as gadolinium, dysprosium, and yttrium in consolidated form has also been demonstrated by using the fluorides as electrolytes in place of chlorides. These have been carried out in specially designed high temperature cells. The advantages of liquid product recovery and low temperature operation have been realized even in the case of high melting rare earth metals by using metals like cadmium, magnesium, zinc, manganese, chromium, and cobalt as cathode. These metals form liquid alloy with the rare earth metal as it electrodeposits, and liquid product recovery is therefore facilitated.

In the beginning, rare earth chlorides were electrolyzed in fused salt to obtain the metal, and the direct electrolytic reduction of rare earth oxide dissolved in a mixture of rare earth and other fluorides was investigated later (Morrice and Wong 1979).

4.11.1 Chloride Electrolysis

The important investigations on the electrolysis of rare earth chlorides are summarized in Table 4.7.

The possibility of electrolytic reduction of a molten salt for preparation of rare earth metals was first demonstrated in 1875 by Hillebrand and Norton (1875). They prepared a

Table 4.7 Electrolysis of rare earth chlorides

Year	Electrolyte	Electrodes*	Cell	Product	Reference
1902	$RECl_3$–NaCl–KCl	Carbon	Water-cooled copper	Several kg of Ce, La nodules	Muthmann et al. 1902
1912	$CeCl_3$–NaCl	Graphite(A) Cell (C)	Iron	Massive Ce	Hirsch 1912
1923	$LaCl_3$–KF–NaCl	Carbon (A) W (C)	Iron	La metal (0.77% Fe)	Kremers and Stevens 1923
1931	$CeCl_3$–CaF_2	Carbon(A) Mo (C)	Fluorspar	Ce ingot (99.8% pure)	Billy and Trombe 1931
1940	$RECl_3$–NaCl–KCl	Graphite(A) Fe (C)	Refractory lining	La, Ce, Di#, misch metal (99.5–99.9% pure)	Hirschhorn 1968

* A: anode, C: cathode
\# Nd+Pr

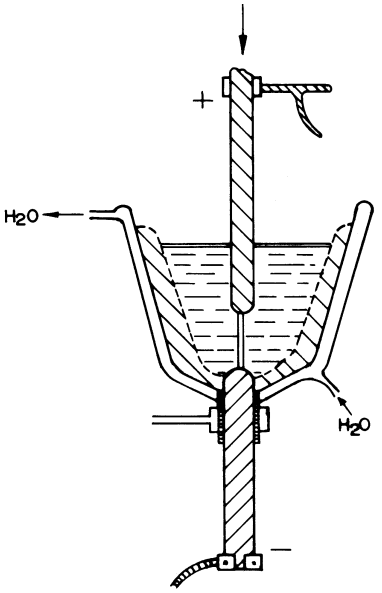

Figure 4.37 Schematic of Muthmann type electrolysis cell (Trombe 1957).

few grams of cerium, lanthanum, and didymium in a coherent form from the electrolysis of fused rare earth chlorides using iron electrodes. The cell consisted of two porcelain crucibles, one of which was porous. The rare earth chloride was melted in the porous crucible, which was then placed into the other porcelain crucible containing the sodium chloride–potassium chloride eutectic mixture. The cathode was placed in the rare earth chloride melt, and the anode, which was an iron cylinder, was located in the sodium chloride–potassium chloride melt. The demonstration by Hillebrand and Norton was followed up by Frey (1876) and by Muthmann et al. between 1902 and 1907. Frey (1876) reported that he had prepared rare earth metals using the fused salt technique developed by Bunsen. Muthmann et al. (1902), Muthmann and Weiss (1904), Muthmann and Scheidemandel (1907) reported the preparation of many metals in the cerium group (cerium, lanthanum, praseodymium, neodymium, and samarium) by electrolyzing fused rare earth chlorides in a water-cooled copper vessel with carbon electrodes. The cell is shown schematically in Figure 4.37. The water-jacketed copper vessel used to hold the fused chloride bath was not part of the electrical circuit. Copper was protected from attack by molten rare earth metal by a thin layer of frozen salt. Through the bottom of the copper vessel the carbon rod cathode projected into the cell. This rod was electrically insulated from the vessel by porcelain rings. The anode, which was also a carbon rod, was introduced into the bath from the top of the cell. This cell arrangement was known as the Muthmann type cell in the early literature. Several pounds of 99.92% cerium were prepared in one experiment in which a molten bath containing cerous chloride and sodium chloride–potassium chloride eutectic mixture was electrolyzed. Cerium and lanthanum were obtained in the form of large nodules. The metals contained some amount of carbon picked up from the cathode. Neodymium was recovered only in very small nodules, and praseodymium could not be electrowon in this cell. The failure was attributed to the form- ation of oxychlorides. As regards samarium, only a thin deposit of samarium metal was obtained on the cerium cathode from a fused bath of $SmCl_3$–$BaCl_2$.

A Muthmann type cell, with graphite instead of copper as cell material, was used by Hirsch (1912) to electrolyze cerium and other rare earth chlorides. This, however, resulted in the formation of carbides, which made the bath viscous and unsuitable for electrolysis. To circumvent this difficulty, Hirsch replaced the graphite container with a wrought iron crucible. Electrolysis of a molten mixture composed of 90% anhydrous $CeCl_3$ and 10% NaCl at 12 to 14 V with an average current of 200 A yielded 580 g of cerium ingot in 4 h. The current efficiency was 41.5%. Iron was the major impurity in the metal which according to analysis was 97.8% cerium.

Cerium was produced in good yield by Thompson (1917) who electrolyzed industrial grade anhydrous fused rare earth chloride in an iron crucible that served as the cathode, with a graphite anode. In addition to cerium chloride, the electrolyte consisted of sodium chloride, potassium chloride, and barium chloride added in small quantities to increase the resistance of the bath and check its decomposition.

Hicks (1918) reported the preparation of "yttrium mixed metal," a mixture of yttrium and higher melting rare earth metals, in a powder form by electrolysis in a chloride bath at 900 to 1100°C. His cell consisted of a graphite container that was the cathode, and a graphite anode. He observed the formation of carbides. This was minimized in later experiments by lining the sides of the crucible with alumina.

Schumacher and Lucas (1924) electrolyzed fused anhydrous rare earth chlorides in a cell consisting of a cathodic graphite crucible and a graphite anode. On finding that much of the reduced metal was dispersed throughout the bath in the form of small particles, they raised the temperature of the bath at the end of each run by increasing the direct current amperage. This was done to permit the metal particles to coalescence at the bottom of the crucible in liquid form. The product was remelted in a magnesia crucible. The authors reported that the cerium prepared by the above procedure was 99.9% pure with only 0.03% carbon and 0.03% iron as impurities. Schumacher and Harris (1926) used the same procedure two years later to prepare small amounts of cerium, lanthanum, praseodymium, neodymium, and samarium metals. For samarium they resorted to external heating at the end of electrolysis to raise the temperature high enough to collect the metal in a coherent mass. The metals were remelted in magnesia crucible. The reported impurity contents in the metals were 0.03% carbon and 0.02% iron. Magnesium content was not, however, reported. Externally heated cells for electrolysis thus began to be used for rare earth metal preparation.

Beginning in 1923, a series of investigations on the electrowinning of rare earth metals was carried out by Kremers and various coworkers (Kremers and Stevens 1923, Thompson and Kremers 1925). A graphite or iron crucible was used as the bath container and cathode and the anode was carbon. The cell was heated in a resistance type muffle furnace to the required temperature. During electrolysis, the bath temperature was kept below the melting point of the rare earth metal. Toward the end of electrolysis, however, the temperature was raised above the melting point to coalesce the cathode product. By electrolyzing the appropriate rare earth chloride–sodium chloride mixtures in iron crucibles, cerium-free misch metal, lanthanum, cerium, and neodymium metals were prepared in quantities ranging up to 60 grams. The metals were heavily contaminated with iron. Lanthanum and cerium contained up to 32% iron and neodymium up to 6.5% iron. Similar contamination resulted when lanthanum was prepared using a graphite crucible — lanthanum carbide was formed.

The metals obtained in the investigations described so far were generally not quite pure. The impurities resulted from cell material, electrodes, electrolyte, and also insufficiently

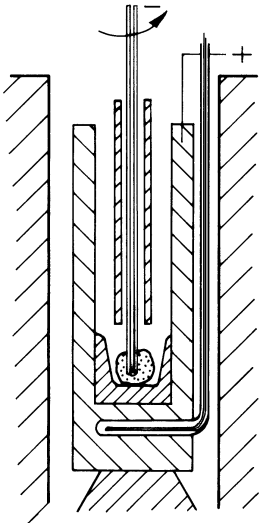

Figure 4.38 Schematic of Trombe type electrolysis cell (Trombe 1957).

separated rare earth starting materials. Initially, attempts were made to find electrode and cell construction materials that were resistant to attack by both the molten electrolyte and molten metal. Later, as high-purity starting materials became available for the electrolysis, contamination from that source was also tackled.

The first directed attempt at reducing electrode contamination in rare earth metals obtained by fused salt electrolysis was made by Kremers and Stevens (1923). They electrolyzed lanthanum chloride in a bath containing sodium chloride and potassium fluoride using a carbon anode and a tungsten cathode. The cell was an iron crucible and this was not part of the electrical circuit. Lanthanum obtained did not contain any tungsten but contained 0.77% iron. Contamination from the electrode was circumvented.

Molybdenum was recognized as a suitable cathode material after Guertler (1923) reported that molybdenum is insoluble in the rare earths at red heat. Molybdenum was used as the cathode in the experiments for the preparation of high purity rare earth metals. A carbon crucible was used as the anode, and the cathode in the form of a rod was spinning. The cell arrangement is shown in Figure 4.38. A fluorspar crucible was placed below the cathode in the melt to collect the product. The cell was heated externally to the required temperature. Fluorspar did not contaminate the rare earth metal product (unlike crucibles made of quartz, graphite, and certain ceramics which contaminated the product), but the chloride–fluoride melts dissolved fluorspar and became more viscous, making the in cell operation difficult. Billy and Trombe (1931) conducted the electrolysis at 850°C using 25 g cerium trichloride and 16 g calcium fluoride as the electrolyte and obtained 9 g of cerium ingot in 90 min. The product contained only a small amount of molybdenum and no calcium. Lanthanum ingots were prepared by Trombe (1932) by electrolysis of $LaCl_3$–KCl–CaF_2 bath at 960–980°C. The ingot contained 0.05% silicon and 0.006% iron. Trombe (1932) also prepared neodymium by electrolysing a mixture of $LaCl_3$–KCl–CaF_2 at 1040 to 1060°C. The neodymium product contained less than 0.05% silicon, 0.02% iron, and a trace of calcium. In this preparation, using a quartz crucible instead of fluorspar resulted in the silicon content in the product rising to 0.6%.

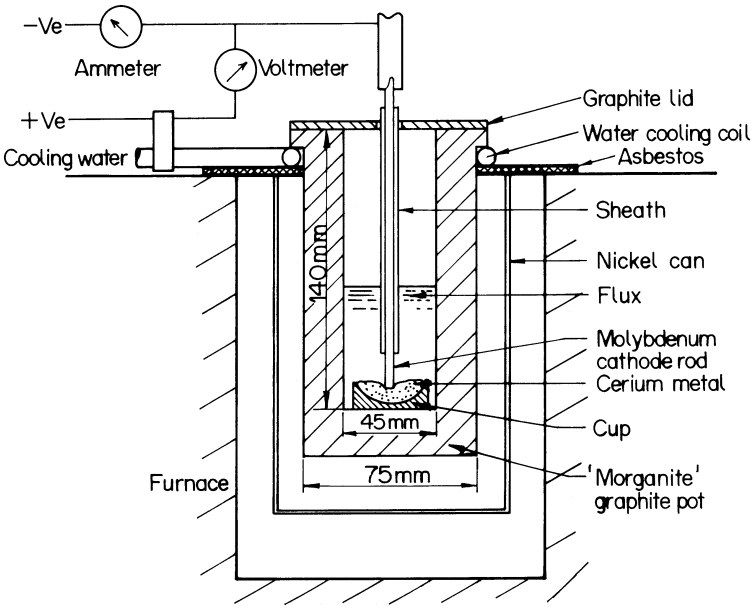

Figure 4.39 Gray's cell for electrolysis of cerium trichloride (Gray 1951).

Weibke (1939) used the Trombe type cell but with a crucible made of alumina instead of fluorspar to collect the metal. The molten salt was a fused mixture of $LaCl_3$–KCl–CaF_2, and molten lanthanum metal of 99.86% purity was collected in the alumina crucible. Gray (1951) essentially repeated Trombe's experiment with cerous chloride and obtained cerium metal that was at best 99.7% pure. His cell is shown schematically in Figure 4.39. He used crucibles made of beryllia, stabilized zirconia and fluorspar to collect the molten cerium metal product. The use of beryllia resulted in 0.01 to 0.1% of beryllium impurity in the metal. Calcium, iron, and magnesium oxides present in stabilized zirconia were found to react with molten cerium metal. Fluorspar was found to dissolve in molten chloride causing an increase in bath viscosity. The increasingly viscous bath rendered the electrolytic process unworkable beyond 30 min.

Kojima and Sato (1954) electrolyzed a molten mixture of 108 g of rare earth chlorides and 99 g of KCl and obtained 22 g of misch metal in about 4 h. They purified their starting bath materials to remove oxygen and also prevented the surface of the melt from contacting air. Current efficiency as high as 77% was achieved by them in some experiments. A LiCl–KCl eutectic containing $CeCl_3$ was kept at a temperature of 850°C by Eastman et al. (1955). Cerium ingot weighing 15 to 100 g was obtained in each run at 80% current efficiency. The metal yield was found to improve from 82 to 97% with exclusion of air from the electrolyte cell. Eastman et al. (1955) used a beryllia or zirconia crucible below the tungsten cathode to collect the molten cerium metal. This cell arrangement was similar to that used by Trombe. The beryllia crucible was not attacked in the chloride system. A molten bath of $LaCl_3$–KCl at 900°C was electrolyzed by Kuroda (1957) to obtain lanthanum ingot. The metal contained 0.041% silicon, 0.034% aluminum, and 0.13% potassium. A high current efficiency of 91.7% was achieved. The effects of variables such as cathode current density, bath temperature, duration of electrolysis, addition of KCl, and distance between electrodes on the current efficiency were all investigated.

Ivanovskii and Ilyushchenko (1961) reported that rare earth metals can be selectively electrodeposited from a melt consisting of mixed rare earth chlorides and potassium chloride. Starting from a rare earth chloride composition of 26% lanthanum, 53.9% cerium, and 21.1% other rare earth elements, they electrodeposited alloys with a low lanthanum content (≤3%) and a cerium content of ≤80%. The melt temperature was 560 to 700°C and cathode current density was 0.25 to 1 A/cm^2.

4.11.2 Electrowinning at Room Temperature

Attempts have been made to prepare rare earth metals at room temperature in both aqueous and nonaqueous media. In aqueous solutions electrolysis is complicated by hydrogen formation even when the cathode displays a high hydrogen overvoltage, as in the case of mercury. The results of efforts in aqueous solutions, alcohols, ethylene-diamine, pyridine, and other organic solvents have been discouraging. However, it was reported by McCoy (1941) that europium and ytterbium amalgams were prepared from potassium citrate solutions.

Starting in 1931, Audrieth, Hopkins, and others (Audrieth et al. 1931, Hopkins and Audrieth 1934, Jukkola et al. 1934, Meints et al. 1937) published a series of reports on the preparation of lanthanum, cerium, samarium, neodymium, and yttrium amalgams from their respective salts by electrolysis in aqueous solution as well as in organic solvents, using a mercury cathode. Electrolysis of concentrated solutions of anhydrous chlorides dissolved in absolute ethyl alcohol yielded the best results. The amalgams were vacuum distilled to remove mercury. The resulting rare earth metal powders were then heated in crucibles lined with the respective rare earth oxides to result in small pellets of lanthanum, neodymium, and cerium.

Sklyarenko and Sakharov (1940) obtained amalgams reportedly containing 0.5 to 1.2 wt % cerium by electrolysis of solutions of $CeCl_3$ in absolute ethyl alcohol, in methyl alcohol and in mixtures of methyl and ethyl alcohols. Moeller and Zimmerman (1954) reported indications of formation of yttrium, neodymium, and lanthanum metals from the electrolysis of anhydrous ethylene-diamine solutions of $Y(OAc)_3$, $NdBr_3$, and $La(NO_3)_2$ using platinum electrodes.

4.11.3 Electrowinning Solid Metal Deposits

Molten rare earth metals are markedly reactive and problems due to this reactivity was sought to be circumvented by some investigators by conducting the electrolysis at temperatures below the rare earth metal melting point. A mixture of $PrCl_3$, NaCl, and KCl, which melts at 535°C, was electrolyzed by Canneri and Rossi (1932) to obtain praseodymium (m.p. 931°C) sponge. The electrolysis temperature was below 600°C. A tungsten cathode and an Acheson graphite anode were used. Mazza (1939) obtained lanthanum (m.p. 918°C), cerium (m.p. 798°C), and praseodymium as solid metals by electrolyzing at 700 and 750°C a bath of rare earth chlorides dissolved in NaCl and KCl. The formation of oxychlorides were avoided by excluding oxygen. Relatively higher levels of purity, namely, 99.7% for lanthanum, 99.8 to 99.9% for cerium, and 99.6% for praseodymium were reported for the product metals obtained.

4.11.4 In situ *Preparation of Electrolyte*

A novel method of introducing rare earth into the molten chloride bath was described in a U.S. Patent of 1959 (Merlub-Sobel 1959). The compacted rare earth oxide – carbon mixture was placed in the hollow graphite anode of the electrolytic cell. Chlorine gas was passed through this mixture in the anode. Rare earth chloride thus formed permeates into the molten bath to be electrolyzed. This method of generating metal chloride *in situ* in the fused salt electrolysis cell was extensively used in later years by the U.S. Bureau of Mines researchers for the electrolytic preparation of vanadium metal (Lei et al. 1967).

4.11.5 Commercial Electrowinning from Rare Earth Chlorides

The rare earth metals that have been produced by fused salt electrolysis of chlorides on a commercial scale (Morrice and Knickerbocker 1961, Hirschhorn 1968) are lanthanum, cerium, and didymium (Nd + Pr). Didymium metal is an alloy of neodymium and praseodymium with minor amounts of lanthanum and other rare earths. The cells had an iron, carbon, graphite, or refractory lined steel vessel to contain the molten bath. The cathode was the bath container itself or an iron or carbon block at the bottom of the container. The anodes were one or more graphite rods extending vertically into the cell through its top. Besides $RECl_3$, the electrolyte contained NaCl, KCl, $CaCl_2$, or other salts as preferred by the various producers, and the bath was molten even at 650°C. The cells were enclosed by steel covers to exclude air to prevent gas pick up in the metal produced.

After loading the mixture of rare earth chloride and NaCl, KCl, or $CaCl_2$ into the cell, in one procedure, the charge was melted by external burners. In another practice, the anodes were lowered until they contacted broken pieces of cerium metal placed at the cell bottom. Solid bath was packed around the bottom of the anode and direct current was turned on to heat and melt the electrolyte. The anodes were then raised to their operating positions. The chloride bath was raised to a temperature between 800 and 900°C by passage of direct current and external heating was normally not required during electrolysis.

During electrolysis the metal collected at the bottom of the cell. The metal could be maintained in the molten state by resistance heating. Alternatively, the metal might be allowed to solidify by use of a cooled cathode, in which case it would be necessary to remelt the metal by internal resistance heating, sometimes supplemented by an external source of heat, prior to its removal from the cell.

The electrolysis was continued as long as the current efficiency or the metal quality was acceptable. The liquid metal product might be removed at fixed intervals by ladling, and additional chloride was introduced as needed to replace that used in the electrolysis. In one practice the product was collected by pouring the entire contents of the cell, including the bath, into molds. After the metal had settled to the bottom of the mold, the liquid bath was returned to the cell and electrolysis was started again.

Lanthanum, cerium, and didymium metals of better than 99% purity have been electrowon commercially from their anhydrous chlorides. The purities of metals obtained are listed in Table 4.8. Metals of high purity could be produced if carefully purified feed materials were used and if cell atmosphere composition was controlled. Current efficiencies of chloride cells were usually between 45 and 50%.

The maximum operating temperature of the chloride cell is 1100°C, and neodymium (m.p. 1021°C) is the highest melting rare earth metal that can be produced by chloride

Table 4.8 Analysis of lanthanum, cerium and didymium metals electrowon commercially from chloride electrolytes (Morrice et al. 1961)

Element	Analysis, %		
	Lanthanum	Cerium	Didymium
La	99.6		0.95
Ce	0.09		0.20
Nd	0.04		72.1
Pr	0.05		27.2
Sm	0.03		0.3
Other rare earth elements	nd	0.10[a]	nd
Al	0.01	0	0.10
Ca	0.01	0.02	0.10
Fe	0.11	0.19	0.05
Mg	0.10	0.02	0.10
Si	0.04	0.002	0.07
Mn	nr	0.02	nr
P	nr	0.001	nr
C	nr	0.05	nr
O	nr	nr	nr
N	nr	nr	nr

[a]includes all rare earth elements other than cerium
nd: not detected
nr: not reported

electrolysis. However, the yield of neodymium in such a cell is very low (Seon and Barthole 1986). At high temperatures in a chloride electrolyte bath, the volatility of bath constituents becomes unacceptable, the solubility of metals in their chlorides increases significantly, and the attack of cell wall materials by the rare earth metals becomes severe. Considerably higher temperature operation, however, is possible in cells using fluoride electrolyte baths.

4.11.6 Oxide–Fluoride Electrolysis

Rare earth metal preparation by electrolysis of a fluoride–oxide bath was first reported 1907. This was followed by many other investigations listed in Table 4.9. Muthmann and Scheidemandel (1907), using a modification of the Muthmann type cell described earlier for chloride electrolysis, prepared cerium ingot by electrolysis of CeF_3–CeO_2. The fluoride was prepared by precipitation with hydrofluoric acid and contained silicates. The cerium metal obtained was reported to be only 86.48% pure and contained 12.49% SiO_2 and 0.87% Fe. They also electrolyzed CeO_2 in mixtures of CeF_3, NaF, and KF, in an attempt to have a lower melting electrolyte and conduct electrolysis at lower temperature. However, these electrolytes yielded only sodium and potassium metals. Electrolysis of rare earth oxy-fluoride baths using carbon and graphite electrodes at temperatures of ~1400°C resulted in the formation of only carbides (Hirsch 1911). The bath melting temperature could not be

Table 4.9 Electrolysis of oxide-fluoride melts

Year	Electrolyte	Electrodes*	Collector	Product	Reference
1951	CeO_2–CeF_3–LiF–BaF_2	Graphite(A) Mo (C)	Mo crucible	Ce(99.7%)	Gray 1951
1960	CeO_2–CeF_3–LiF–BaF_2	Carbon(A) Mo (C)	Electrolyte skull	Ce(99.9%)	Morrice et al. 1960
1962	La_2O_3–LaF_3–LiF–BaF_2	Carbon(A) Mo (C)	Electrolyte skull	La(99.8%)	Morrice et al. 1962
1964	Ce_2O_3–CeF_3–LiF–BaF_2	Graphite(A) Mo (C)	Mo liner	Ce(99.8%), continuous electrowinning	Shedd et al. 1964
1966	La_2O_3–LaF_3–LiF–BaF_2	Graphite(A) Mo (C)	W crucible	La(99.8%), continuous electrowinning	Shedd et al. 1966
1967	RE_2O_3–REF_3–LiF	Graphite(A) W (C)	Electrolyte skull	Pr, Nd, Di nodules (99.83–98.85%)	Morrice and Henrie 1967

*A: anode; C: cathode

lowered by addition of KF. In 1918, Hicks (1918) attempted to prepare a mixture of yttrium with other high melting rare earth metals by electrolyzing either a fused yttrium earths chloride bath or a solution of yttrium earths oxide in cryolite. The cell comprised a graphite container, which was the cathode, a graphite anode and the molten bath, which was operated at temperatures up to 1300°C. The product was some black powders.

Gray's Cell The most successful among the early experiments on oxide–fluoride electrolysis was reported by Gray (1951). In his experiments, CeO_2 was dissolved in a CeF_3–LiF–BaF_2 electrolyte contained in an externally heated 57 mm inside diameter carbon container. A schematic of the electrolysis cell used by Gray is shown in Figure 4.40. The cell pot was made of "Delanium" carbon, which was found to be quite impervious to the melt and protected the nickel can in which it was enclosed. The ash content of (2.3%) of the Delanium carbon was high, and so it was lined on the inside with a high purity (ash content <0.01%), though somewhat porous, graphite. The anode was also made of high purity graphite rod and the cathode was a molybdenum rod; both were suspended from the top and immersed in the melt. The bath, cell materials, electrodes, and the product were all protected from the atmosphere by argon gas, which was continuously flowing around the cathode and over the top of the molten bath. A molybdenum crucible was kept below the cathode to collect the product. Gray chose molybdenum to contain molten cerium because he had found that unless it is oxidized, molybdenum does not dissolve in cerium. The bottom of the cell was lined with a thin sheet of molybdenum to prevent any accidentally spilled cerium reacting with graphite to form cerium carbide. Cerium oxide was added to the bath on the side of the cell opposite to the cup.

The electrolyte, comprising 60.8% CeF_3, 26.9% LiF, and 12.3% BaF_2, was molten at 715°C and dissolved 3–5% CeO_2 at 850°C. Electrolysis was carried out at 880–900°C at cathode current density of 5.0–7.0 amp cm^{-2}. The normal cell voltage was 4.4 V. Molten cerium metal dropped off the cathode and collected in the molybdenum cup kept below. Yields of up to 77% were obtained and the overall purity of the metal was 99.7–99.8% cerium. The product contained 0.1–0.6% calcium and up to 0.3% magnesium as major

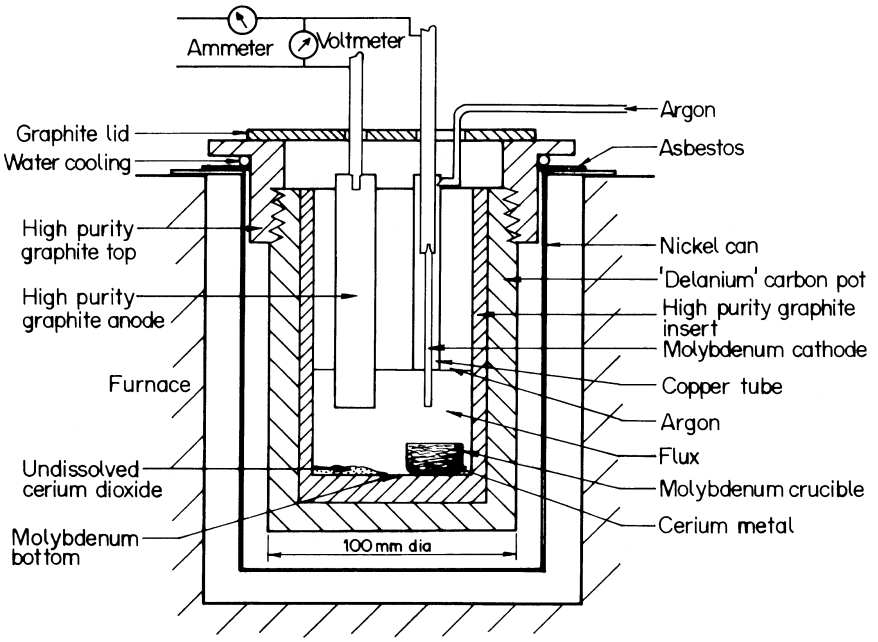

Figure 4.40 Gray's cell for electrolysis of cerium dioxide dissolved in fused fluorides (Gray 1951).

impurities. Much of the later work and further development of the oxide–fluoride electrolysis process was carried out at the Reno Metallurgy Center of the U.S. Bureau of Mines during the 1960s (Morrice and Wong 1979).

Reno Cell Type 6 Many types of electrolytic cells were designed and used at Reno for carrying out oxide–fluoride electrolysis. The first was a 150 mm (6 inch) diameter electrowinning cell, known as cell type 6 (Morrice and Knickerbocker 1961, Morrice et al. 1961). The cell consisted of a 6-inch diameter bath container made of graphite. Three 10-mm diameter molybdenum cathodes and three 25-mm diameter carbon anodes extended down into the container through its top. This electrode arrangement was first used to melt the bath with alternating current and later used for electrolysis with direct current.

The cell was located within a controlled atmosphere temperature pressure (CATP) steel chamber in which atmosphere, temperature, and pressure were controlled. All cell operations, such as feeding, electrowinning, and raising and lowering electrodes, could be conducted while the electrolytic cell and its contents remained under the protected atmosphere within the chamber.

The standard procedure for the electrowinning of high purity cerium using cell type 6 was as follows: first, the solvent phase electrolyte (73% CeF_3, 15% LiF, and 12% BaF_2 powders) was vacuum dried at about 280°C and transferred to the cell chamber. The chamber was evacuated to 2 Pa and back filled with high purity argon or helium. The dried solvent powder was packed into the graphite cell container. A graphite resistor ring was placed on top of the powder and the electrodes were lowered to make contact. On passing alternating current (AC) through the electrodes and the ring, the powder melted and after sufficient melt had been obtained to carry the current, the graphite ring was removed and AC melting was continued until adequate quantity of the melt reached the temperature

Table 4.10 Cell operating data and product analysis in a typical type 6 cell (USBM) run for electrowinning of cerium metal (Morrice et al. 1961)

Electrolysis parameters

Electrolyte composition, %	73 CeF_3–15 LiF–12 BaF_2
Temperature, °C	810–830
Cathode	10 mm diameter Mo rods, 3 nos.
Anode	25 mm diameter carbon rods, 3 nos.
Electrolysis	
Voltage, V	11
Current, A	249
Duration, min	132
Initial cathode current density, $A \cdot cm^{-2}$	10.23
Initial anode current density, $A \cdot cm^{-2}$	4.10
Current efficiency, %	
CeO_2 feed rate, $g \cdot min^{-1}$	7
Cerium nodules recovered, g	800
DC power consumption, kWh per kg of Ce	7.5

Analysis of cerium nodules, %

Element	Content	Element	Content
C	0.016	Li	0.002
N	nr	Ba	nd
O	0.036	Ca + Mg	<0.004
H	0.0003	Al	<0.01
Si	nd	Fe	0.0102
RE other than Ce	nd	Mo	nd

nd: not detected
nr: not reported

sufficient for electrolysis, 810–830°C. The solubility of ceria in the bath at the electrolysis temperature was in the range of 1 to 2%. One of the important features of the cell was the formation of a layer of frozen bath or skull on the interior surface of the graphite container. The skull prevents the molten electrowon rare earth metals from contacting the graphite crucible. The thickness of the insulation on the side walls and bottom of the graphite cell, and the geometry of the electrode with respect to the side wall and bottom of the cell were so chosen as to maintain this electrolyte skull. An automatic vibrating screw feeder was used for continuous feeding of CeO_2 powder into the molten electrolyte. The feeder with hopper was located outside the cell chamber but was so arranged that it operates in the same controlled atmosphere as the cell. The feeder was also refillable without contaminating the cell atmosphere. After melting the bath, the feeder was turned on and 10–20 g of previously vacuum dried CeO_2 powder was added to the bath. The AC supply was disconnected and direct current was turned on for electrolysis to occur. During the electrolysis, CeO_2 was continuously fed to the molten bath at a rate of 7 g per minute. Massive cerium nodules formed as a result of electrolysis and in about 2 h these nodules bridged the gaps between

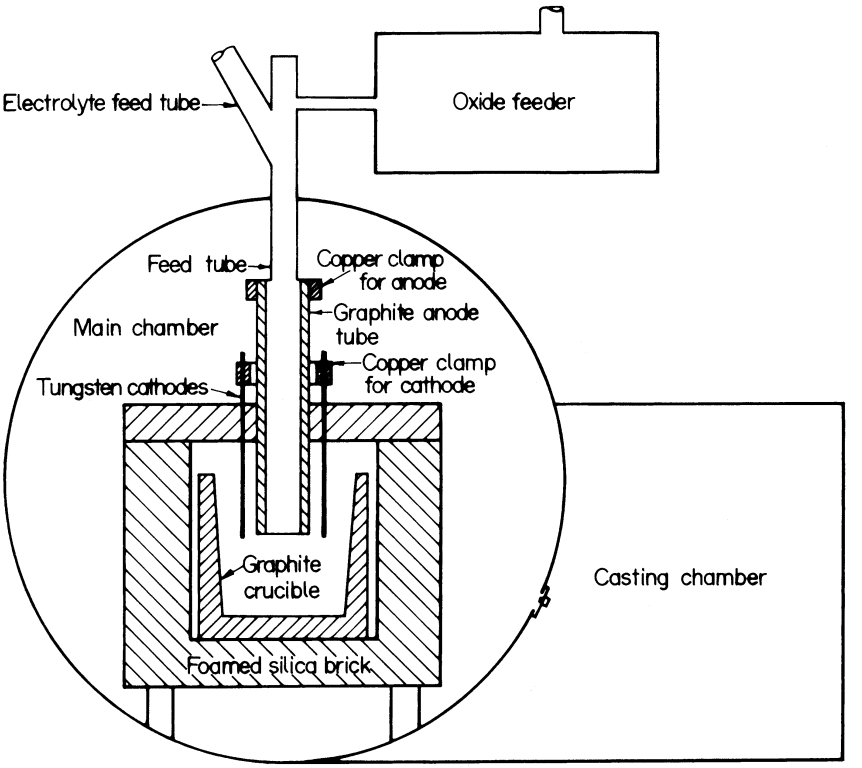

Figure 4.41 Electrolytic cell in protective atmosphere chamber (Shedd et al. 1964).

the electrodes, and electrolysis had to be stopped. After cooling the bath to room temperature within the cell atmosphere, the frozen mass was taken out in open air and broken up to recover the cerium nodules. Details of a sample electrowinning run and the product obtained are summarized in Table 4.10. In the process described, cerium was prepared as a liquid at temperatures very close to its melting point. This circumvented certain difficulties, such as entrapment of electrolyte, which is inherent in recovering the product as a solid, and also minimized contamination of metal with impurities present in molten bath. One major problem, however, was the excessive corrosion of both carbon and graphite anodes at or above the surface of the bath. This was caused by molecular oxygen, generated by the electrolytic reaction and present in the cell atmosphere (Morrice et al. 1961).

Reno Cell Type 12 These are electrolytic cells in which the electrolyte was contained in a ~300 mm (12 inch) diameter graphite crucible. These cells, called type 12 cells, were extensively used at Reno (Shedd et al. 1964). Initially experiments were conducted in which the metal product was collected in an electrolyte skull, and in later experiments cells designed for continuous operation were used. As with the type 6 cell, the electrolyte cell components were all enclosed in a gas-tight chamber.

The arrangement of the type 12 cell components and the electrolyte skull is shown in Figures 4.41 and 4.42. The anode, which is a graphite tube (120 mm outside diameter, 75 mm inside diameter, 560 mm long) suspended vertically in the center of the crucible, also acted as a feed tube for adding electrolyte or cerium oxide to the cell. Molybdenum or

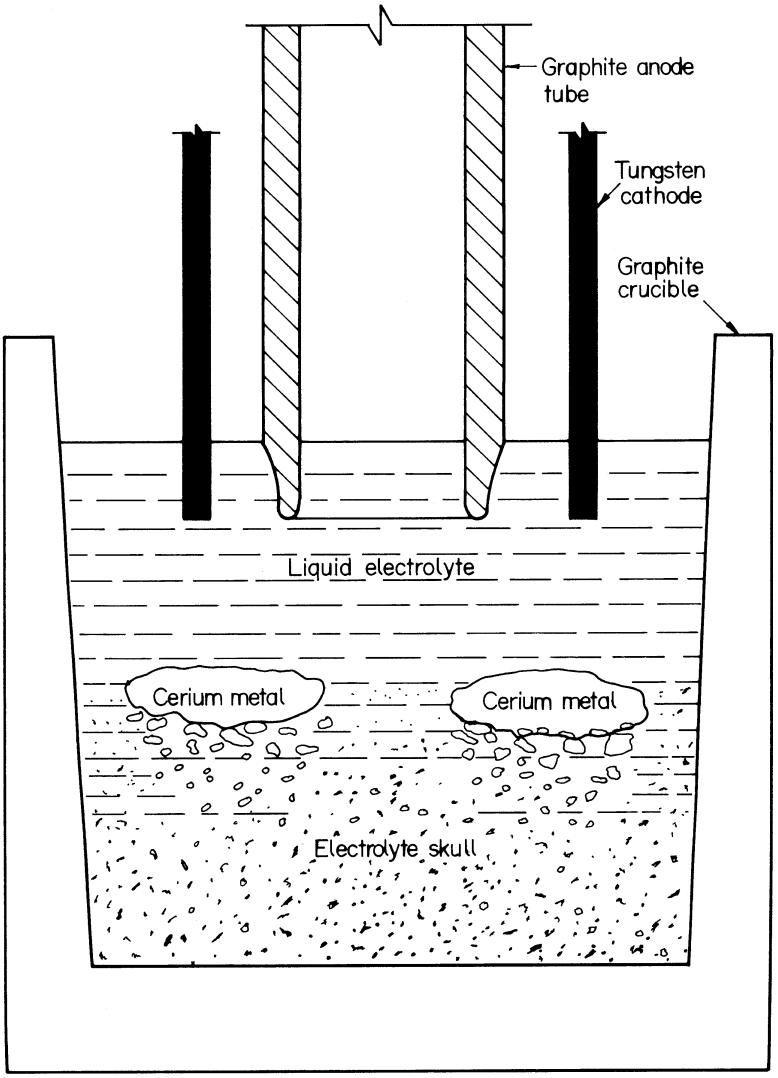

Figure 4.42 Electrolytic cell with electrolyte skull hearth (Shedd et al. 1964).

tungsten rods 10 mm in diameter were used to make the nine cathodes that were arranged in a circle 30 mm from the anode surface.

The vacuum dried electrolyte constituents, 73% CeF_3, 12% BaF_2, and 15% LiF, were fed and packed into the graphite crucible. Cerium was the metal electrowon. The bath was melted initially as described for the type 6 cell, using AC. After the top portion of the electrolyte was liquid and the bottom 100 to 120 mm consisted of sintered electrolyte that provided a skull surface on which electrowon cerium collected, operating temperatures of 850 to 900°C were maintained using AC current for 30 to 45 min to obtain a uniform melt temperature. The cerium oxide feeder was started at a predetermined controlled feed rate of 26 to 30 g/min for 5 min before the power was switched to direct current. With an electrode immersion of 40 mm, the power requirement was 800 to 900 amperes and 7 to 8

volts. This current was sufficient to maintain an operating temperature above 850°C. Cerium was deposited on and dripped from the cathodes and collected as nodules on the electrolyte skull initially in small pieces, and then after 1 h, as temperature profile improved, in large massive pieces weighing 3 to 4.5 kgs.

The oxide content of the electrolyte was kept between 1 and 2% throughout the run and electrolysis was continued for 15 to 20 minutes after termination of oxide feed. Analysis of electrolyte after the run showed the oxide content to be 0.06 to 0.3%.

The metal produced by the above procedure, using an electrolyte skull, had a purity of at least 99.8%. Over 90% of the metal in the oxide feed was recovered at a current efficiency that ranged from 75 to 90%. The analysis of cerium obtained is shown in Table 4.11.

In electrolysis with CeO_2 as feed material, a major problem was excessive burning of the interior of the anode surface, in a nonuniform manner. The nonuniform anode burning was eliminated using cerous oxide, Ce_2O_3, as feed. When Ce_2O_3 was fed to the cell, the corrosion was uniform and limited to the immersed portion. Otherwise the run was similar to that using CeO_2 as feed.

Reno Continuous Cell Type 12 Subsequent to the batch type 12 cell where metal was collected in a frozen electrolyte skull, a new cell design was developed at Reno for continuous electrolysis (Shedd et al. 1964).

The key feature in the cell shown in Figure 4.43 is that the bottom and sides of the graphite crucible were lined with a molybdenum sheet and a tapping pipe was attached to the molybdenum hearth so that the molten metal could be tapped. The tapping pipe extended into an inert atmosphere casting chamber. When the molybdenum hearth or trough was nearly filled with cerium, an auxiliary AC heating circuit could be used to heat the tapping pipe without interrupting the electrowinning sequence. To serve as an electric probe for the AC circuit, a 19 mm diameter molybdenum rod was submerged in the melt. An auxiliary carbon resistance heating unit was located beneath the cell.

Table 4.11 Analysis of cerium metal electrowon from an oxide-fluoride melt (Shedd et al. 1964), %

Element	Cerium collected in electrolyte skull	Tapped cerium metal
C	0.020	0.010
O	0.010	0.016
Al	0.012	0.040
Ba	nd	nd
Ca	0.001	nr
Cu	0.005	0.001
Fe	0.030	0.007
Li	0.002	nr
Mg	0.001	nr
Mo	0.035	0.076
Si	0.005	0.008
W	nr	0.002
Total impurities	0.121	0.160

nd: not detected
nr: not reported

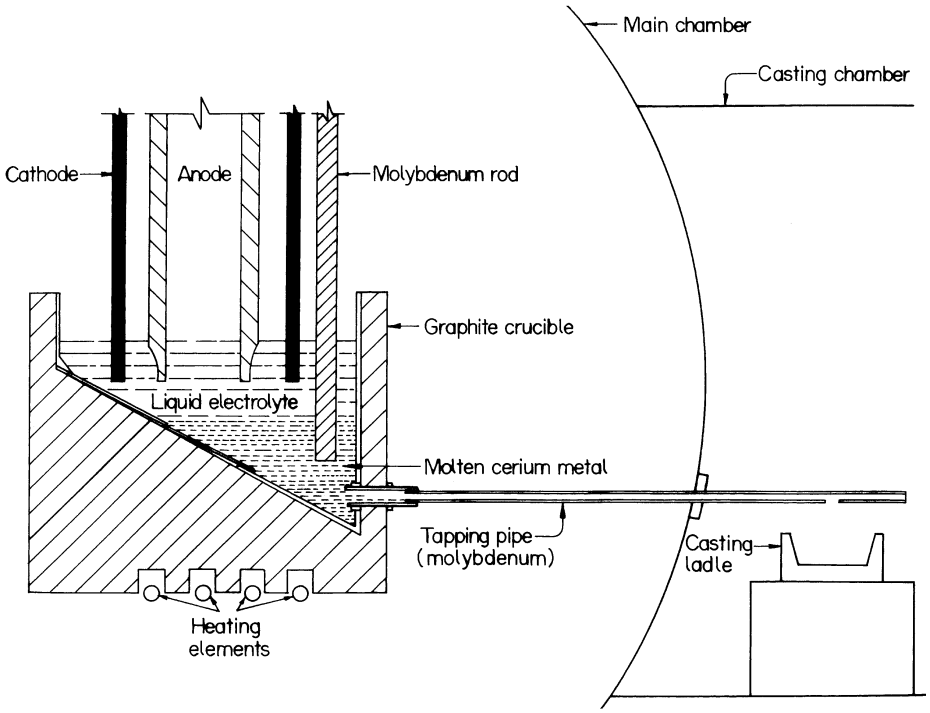

Figure 4.43 Design of cell used to study parameters for continuous operation (Shedd et al. 1964).

The cell for continuous electrowinning of a rare earth metal was first used for the preparation of cerium metal. The dry weight composition of the electrolyte was 63% CeF_3, 16% BaF_2, and 21% LiF and the cell was operated at 900°C. Ce_2O_3 was the cell feed and was fed at a predetermined uniform rate of 30 g per minute during electrowinning.

A typical continuous electrowinning run extended over three days, during which metal was electrowon and several tappings of homogeneous cerium metal were made. The electrolyte was also tapped and recharged to the cell. The anode was changed as needed and electrowinning was resumed. A total of 12 kgs of cerium was tapped. The metal purity was 99.8%, and the impurities in the metal are listed in Table 4.11. Molybdenum figured as a major impurity and was formed due to the hearth's dissolving in cerium during the extended retention time. Tungsten contamination under similar circumstances would be much less, but tungsten sheets in dimensions large enough to make the hearth were difficult to obtain.

Cells for Electrowinning Lanthanum Morrice et al. (1962) attempted to electrowin molten lanthanum metal from lanthanum oxide in a LaF_3–LiF–BaF_2 bath using the same electrode arrangement (Morrice et al. 1960) that worked well in the case of cerium (m.p. 798°C). The direct current (DC) power that this cell could carry was not high enough to maintain the electrolyte temperature needed for the deposition of molten lanthanum (m.p. 918°C). This problem was solved by an improvement in the electrowinning cell as depicted in Figure 4.44. AC was used across the anodes as an auxiliary source of heat to maintain the required bath temperature. The lanthanum electrowinning cell was operated using an arrangement in which AC was imposed on the two anodes, and DC was imposed on one anode and the cathode. The operating data of the cell and analysis of the product

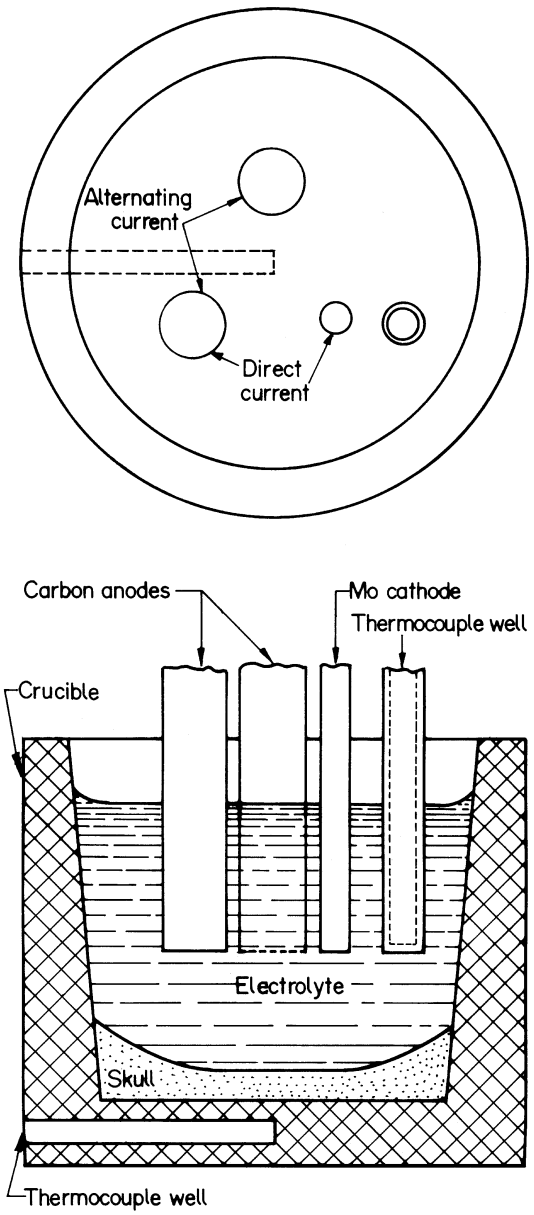

Figure 4.44 Imposed AC cell for electrowinning lanthanum (Morrice et al. 1962).

obtained are listed in Table 4.12. This cell that operated with a current efficiency of about 60% yielded lanthanum nodules containing carbon and oxygen as major impurities. The total impurity content was, however, between 0.1 and 0.2%.

A cell for continuous electrolysis was also developed at Reno (Shedd et al. 1966) for lanthanum metal. The electrode and hearth arrangement in this cell are different from those in the cell used for cerium. Shedd et al. (1966) stated that the ability of cerium to exist in +4 and +3 states permits sustenance of electrolysis even with a small anolyte volume

Table 4.12 Operational data and product analysis in lanthanum electrowinning (Morrice et al. 1962)

Electrolyte composition, %	54.7 LaF_3–30.3 LiF–15 BaF_2
Temperature, °C	
Electrolyte	946
Cell bottom	711
Cathode	Molybdenum
Anode	Carbon
Electrolysis	
Voltage, V	12
Current, A	159
Duration, hr	3
Initial anode current density, A/cm^2	6.2
Cathode current density, A/cm^2	1.5
Current efficiency, %	60
La_2O_3 added to bath before electrolysis, g	1320
La_2O_3 added during electrolysis, g	886
Lanthanum metal recovered, g	451
Metal recovery, %	60
DC power consumed kWh per kg La	17.3
AC power consumed kWh per kg La	17.3

Analyses of lanthanum metal nodules, %.

Al	Ba	Ca	Cu	Fe	Li	Mg	Mn	Mo	Si	C	O	N
0.001	<0.01	0.0009	0.004	0.04	0.016	0.015	<0.0008	0.019	0.01	0.03	0.04	<0.02

Total impurities 0.19%

provided by a single anode. For lanthanum, which has only the trivalent ion species, to achieve sustained electrolysis, a greater proportionate volume of the electrolyte is needed as anolyte. This is possible in the different electrodes arrangement shown in Figure 4.45, where the anodes are placed surrounding the cathode. Increased anolyte volume offered greater opportunity for the electrolyte to dissolve the oxide and make it available to the anode for reaction. Besides, the cerium cell arrangement could not support sufficient current to maintain the higher operating temperature required for molten lanthanum metal.

The cell had eight high purity graphite rods, each 38 mm in diameter, functioning as anodes. There was, however, only a simple cathode made of a 25 mm diameter arc cast molybdenum rod screwed into a graphite plug in the bottom of a central graphite tube. The cone shaped plug had four holes drilled through the tube and the momentum of the particles striking the cone deflected the oxide feed closer to the anode. The electrodes were suspended vertically from copper support clamps that also served as electrical contacts, as shown in Figure 4.46.

Shedd et al. (1966) used a batch type cell shown in Figure 4.46 to establish the electrode geometry, oxide feed rate, and optimum operating parameters. Subsequently, instead of collecting molten lanthanum in the electrolyte skull, a refractory metal crucible was placed in the bottom of the cell directly below the molybdenum cathode. Molten lanthanum was ladled from the tungsten hearth and cast into two-pound ingots. Both frozen electrolyte

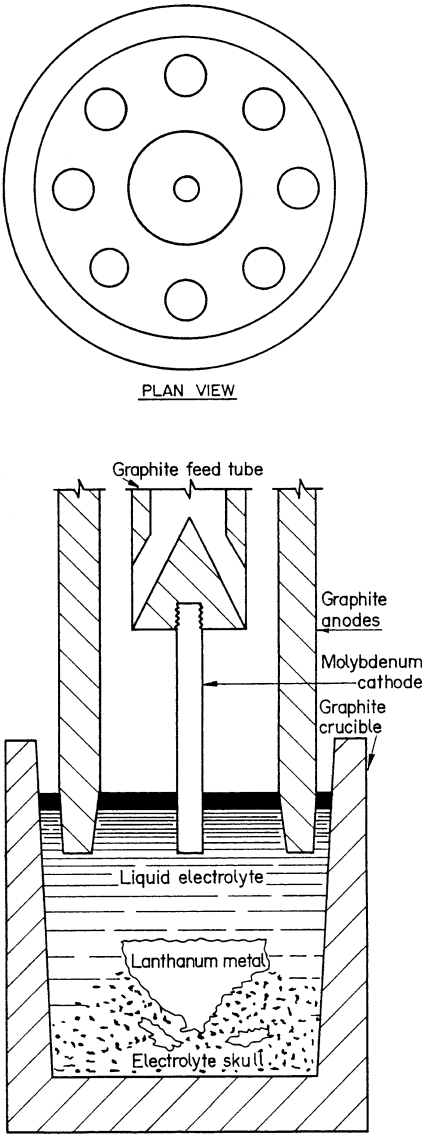

Figure 4.45 Special electrode arrangement in Reno cells for lanthanum electrowinning (Shedd et al. 1966).

skulls and tungsten metal crucibles were found satisfactory for collecting the metal and did not react with molten lanthanum. The chamber was maintained at a partial vacuum (10 kPa) by continuously discharging the carbon oxide gases during the electrowinning. The occurrence of anode effect was found to be markedly reduced under partial vacuum.

The electrolytic cell with tapping facilities for continuous electrowinning of lanthanum is shown in Figure 4.47. The hearth of the cell was a tungsten crucible 100 mm in diameter and 100 mm in depth. A molybdenum pipe was connected to the tungsten crucible through a ½ inch diameter hole drilled in the side of the crucible. The pipe extended about

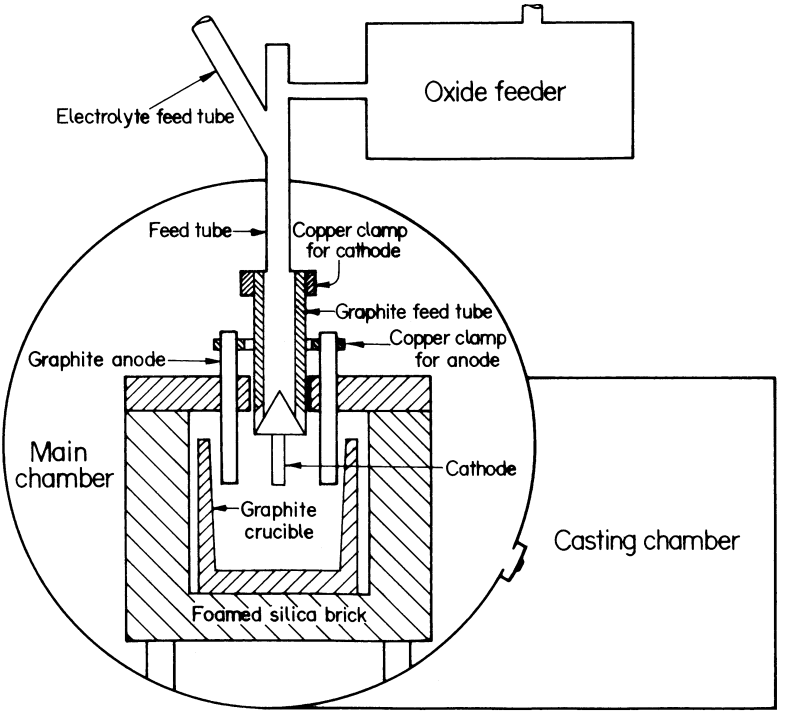

Figure 4.46 Lanthanum electrolysis cell in protective atmosphere chamber (Shedd et al. 1966).

760 mm into the casting chamber. Electrical connections were provided so that the pipe could be heated by passing AC through it and the submerged cathode.

The cell operating parameters and product obtained in continuous electrowinning of lanthanum are listed in Table 4.13 (Shedd et al. 1966). The electrolyte containing 48% LaF_3, 27% BaF_2, and 25% LiF was loaded into the graphite crucible. The La_2O_3 solubility in this electrolyte was 2 wt % at the cell operating temperature. The cell operating temperature of 1000°C was attained by alternating current. During electrolysis, oxides of carbon formed in the cell were continuously removed and flushed out with helium gas. The electrolysis sequence lasted about 2 h, and after every sequence the alternating current was switched on through the tap pipe, auxiliary heat was supplied through the bottom heating elements to maintain the cell bottom at 1000°C, and the metal flowed from the cell through the pipe to the casting chamber where it collected in ladles. Several such tappings of homogeneous lanthanum metal could be made before it was time to tap the electrolyte itself from the cell. Lanthanum produced by the continuous electrowinning process was 99.81% pure. The impurities content (in %) in tapped lanthanum metal are Al 0.03, C 0.033, Fe 0.027, Mo 0.028, O 0.016, and Si 0.055. The elements tungsten, copper, calcium, and barium were not detected. The carbon content of the metal in the first tapping was very low but increased with successive ingots to 0.12% in the last ingot. The other impurities, however, showed a gradual decrease. The rise in the carbon content probably resulted from carbon spalling from the cell components, and this carbon collected on the melt surface contacting the nascent metal.

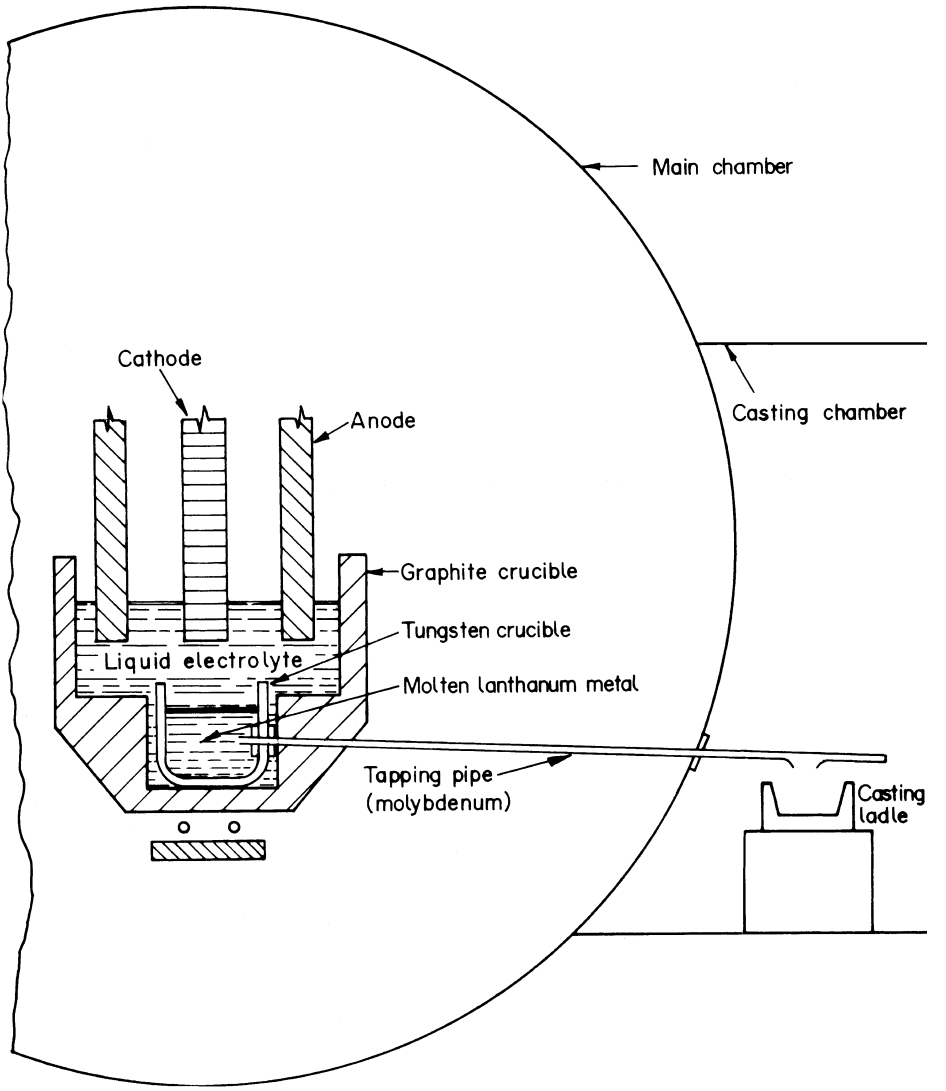

Figure 4.47 Electrolytic cell with tapping facilities for lanthanum electrowinning (Shedd et al. 1966).

Continuous electrowinning has so far been applied to only two rare earth metals: cerium and lanthanum; however, Sharma (1987) indicated the possibility of adopting such a cell to continuously produce neodymium metal. For neodymium, the operating temperature would be 1100°C and the metal produced would probably have higher impurities than lanthanum or cerium, because of higher operating temperature.

Cell for Electrowinning Neodymium, Praseodymium, and Samarium The details of the cell used at Reno (Morrice and Henrie 1967) for electrowinning neodymium, praseodymium and didymium metals are shown in Figures 4.48, 4.49 and 4.50. As in the cases of cerium and lanthanum, these metals and the electrolyte constituents also react with air at the cell operating temperatures. The cell was therefore enclosed in a gas tight steel chamber

Table 4.13 Operational data and product analysis for continuous electrowinning of lanthanum from lanthanum oxide (Shedd et al. 1966)

Electrolyte	48 LaF_3–27 BaF_2–25 LiF
Temperature, °C	975
Average current, A	928
Average voltage, V	11
Power requirement (dc) kWh/kg	8.8
Current efficiency, %	76
Time of electrolysis, min	220
Rate of feed of La_2O_3 g/min	29.5
Total amount of La_2O_3, kg	6.5
Efficiency of oxide utilization, %	78
Rate of metal production, kg/hr	1.2
Anode carbon consumption per kg La, kg	0.12

Analysis, %

Al	0.013
Ba	not detected
Ca	0.002
C	0.500
Cu	0.001
Fe	0.018
Mo	0.017
O	0.009
Si	0.006
W	0.001
Total	0.567

as shown in Figure 4.48. The provision of glove and view ports made it possible to add electrolyte and feed and to adjust the electrodes during the electrowinning experiments. Heat lost from the exposed electrodes and molten bath could raise the ambient temperature within the chamber to >100°C. The refrigeration unit installed in the chamber, however, maintained the ambient temperature at <50°C.

The graphite crucible for holding the molten electrolyte had an inside diameter of 100 to 125 mm and a depth of 150 mm. The cathode was a 5 mm diameter tungsten rod, and the anode was graphite rods 19 to 25 mm in diameter. The cell was internally heated by applying AC between the two anodes. This design is indicated in Figure 4.49. To obtain a thermal gradient in the cell, for developing and maintaining a frozen electrolyte cell in the metal collection zone, while the cell was internally heated, the cell bottom was simultaneously cooled.

To start with, an inert atmosphere was obtained in the cell chambers by pumping down and backfilling with helium. The fluoride electrolyte powder was charged in the cell and melt down was initiated by short circuiting the AC between the anodes and crucible. After obtaining a molten pool of electrolyte, the anodes were raised to electrolysis position, additional electrolyte powder was charged, and heating continued until the required cell temperature was attained. Electrolysis.was then started and the appropriate oxide was

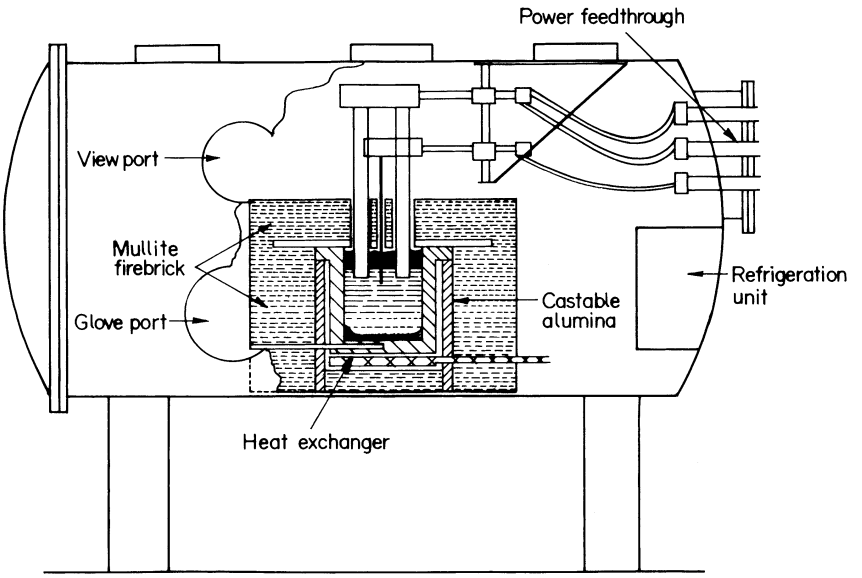

Figure 4.48 Protective atmosphere chamber (Morrice and Henrie 1967).

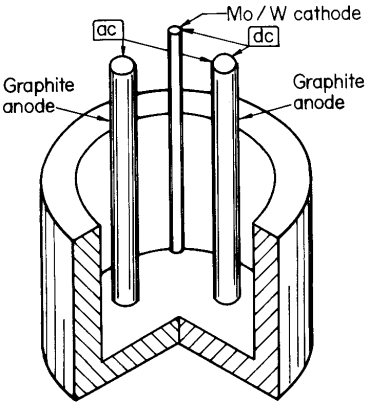

Figure 4.49 Basic features of Reno electrowinning cell (Morrice et al. 1968).

intermittently fed to the cell. By a controlled flow of air or helium through the copper coil located beneath the crucible, the desired temperature gradient between the zones of metal deposition and collection was maintained. After completion of electrolysis, the electrolyte was allowed to cool to ambient temperature before the crucible was removed and crushed, metal nodules recovered, and crushed electrolyte returned for use as bath in the next experiment.

The operational parameters and analysis of product attained in typical electrowinning experiments for neodymium, praseodymium, and didymium (Morrice and Henrie 1967, Morrice et al. 1968) are summarized in Table 4.14.

The results at Reno show the possibility of preparing high purity neodymium, praseodymium, and didymium by electrolysis of the oxides in a medium consisting of the

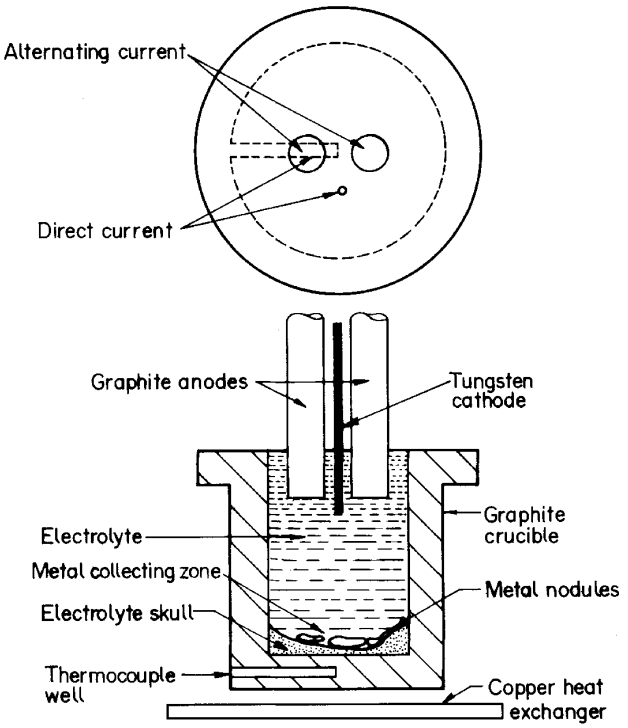

Figure 4.50 Electrowinning cell with AC applied to two anodes (Morrice and Henrie 1967).

respective rare earth fluorides and lithium fluoride. The metals with overall 99.9% purity contained <0.02% each carbon and oxygen and <0.025% tungsten as major impurities. Current efficiencies were upto 83%. In the electrowinning of didymium, the didymium metal product was enriched in neodymium and praseodymium and impoverished in lanthanum, samarium, and yttrium, as compared to the oxide fed to the cell.

High Temperature Electrowinning Cell A high temperature electrowinning cell, also from Reno (Henrie and Morris 1966), operating in the temperature range 1370–1700°C and used for preparation of liquid gadolinium, dysprosium, and yttrium is shown in Figure 4.51.

The electrolyte was contained in a graphite crucible 100 to 125 mm in diameter and 150 mm deep. The anodes were 19 mm diameter graphite rods, and the cathode was a 5 mm diameter tungsten rod. The cell was heated internally by DC and the electrolysis current was supplemented by AC applied between the graphite anodes, which supplied approximately 75% of the total power. The graphite anodes were fluted to provide maximum possible surface area for the anode electrochemical reaction and decomposition of the rare earth oxide to CO, which was the rate-controlling step in the cell operation. The cell bottom could be cooled by passing helium or air through the copper coil placed below the graphite crucible. The cell, like all the others from Reno, was enclosed in an inert atmosphere (CATP) chamber to prevent reaction of the cell components and chemicals with the atmosphere.

In the construction of the high temperature cell, the materials were taxed to the extremes, and Morrice et al. (1968) used a judicious combination of materials to design a satisfactory cell. A shell fabricated from layers of various heat insulating refractory materials surrounded the cell container to help maintain the required heat balance (see

Table 4.14 Cell operating data for electrowinning of neodymium, praseodymium and didymium (Morrice et al. 1968)

Electrolysis parameters	Neodymium	Praseodymium	Didymium
Electrolyte composition, mole %	$50NdF_3$–50 LiF	$50NdF_3$–50 LiF	$50NdF_3$–50 LiF
Temperature, °C			
Electrolyte	1098	1030	1115
Skull (cell bottom)	740	800	770
Cathode	5 mm diameter W rod		
Anode	19 mm diameter graphite (fluted)		
Heating (AC)			
Voltage, V	52	38	45
Current, A	89	130	136
Anode current density, $A \cdot cm^{-2}$	2.0	1.9	2.5
Electrolysis			
Voltage, V	27	19	24
Current, A	55	50	60
Duration, h	2	1.1	1.4
Initial cathode current density, $A \cdot cm^{-2}$	6.9	6.0	9.6
Initial anode current density, $A \cdot cm^{-2}$	0.6	0.3	0.6
Current efficiency, %	77	88	55
REO added, g	312	196	197
Metal recovered, g	151	85	82

Analysis of neodymium and praseodymium nodules[a], %.

Impurity element	Neodymium	Praseodymium
C	0.014	0.010
N	0.001	0.002
O	0.015	0.018
F	0.040	0.030
Si	0.005	0.003
Al	0.002	0.010
Ca	0.005	0.005
Fe	0.012	0.012
Li	0.013	Not determined
Mg	0.005	0.003
W	0.020	0.020
Other RE elements	0.020	0.060
Total	0.150	0.170

[a]The impurity content in didymium was similar to neodymium and praseodymium

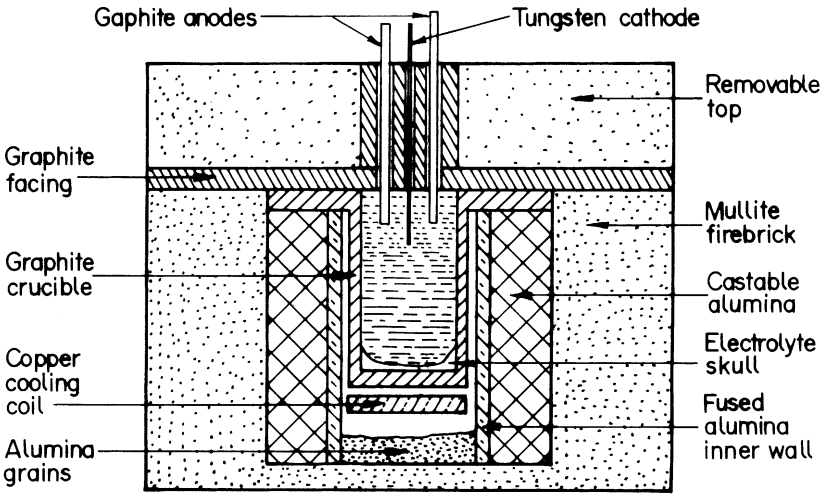

Figure 4.51 High temperature electrowinning cell (Morrice et al. 1968).

Figure 4.51). The inner wall of the shell was made from fused alumina. Castable alumina, 50 mm thick, was then placed around the inner wall. Then there was an outer wall, 100 mm thick, made from mullite brick. Granular alumina was placed below the graphite crucible to a depth of approximately 40 mm. The top of the cell was removable and was also made of mullite firebrick and had a graphite facing to protect the bricks from erosion by the fluoride vapor and splashing electrolyte.

The electrolyte for gadolinium electrowinning consisted of an equimolar mixture of GdF_3 and LiF. Gadolinium oxide was fed to the molten electrolyte maintained at 1370°C. The metal was deposited as liquid at the cathode and dropped down to collect as modules in the frozen electrolyte skull at the bottom of the graphite crucible. The bottom was maintained at 810°C by cooling the bottom of the cell. Such a difference between the temperature of deposition and collection was essential to achieve high recovery and to ensure high purity of the metal product. A typical gadolinium nodule contained 0.05% carbon, 0.01% oxygen, and 0.05% tungsten as major impurities.

Liquid yttrium and dysprosium were also electrowon from their oxides dissolved in melts composed of 50 mole% LiF and 50 mole% YF_3 or DYF_3. The metals were deposited on the cathode at 100 to 200°C above their melting points (m.p. of Dy 1412°C, m.p. of Y 1522°C) and collected at temperatures 400 to 500°C lower. Yttrium and dysprosium nodules thus recovered contained as little as 0.08% carbon and 0.10% oxygen.

The highest temperature at which an electrolysis cell operated was 1700°C for the preparation of liquid yttrium. Morrice et al. (1968) noted that at such temperatures reactions are taking place with energies comparable to those found in arc furnaces. The 100 to 150 mm diameter gadolinium and yttrium cells needed a power input of 12 to 15 kW, which is more than the 9–10 kW power requirement in a typical 300 mm diameter lanthanum or cerium cell (Henrie and Morrice 1966). In addition the yttrium cell volume having a higher power requirement is only one-eighth the volume of the cerium cell. Operating at such high temperatures and power concentration severely stresses the construction materials of the cell, making the process less attractive.

4.12 RECOVERY OF RARE EARTH METALS AS ALLOYS

The earliest attempts at preparation of yttrium and the heavy rare earth metals by chloride electrolysis was frustrated by the formation of metal powder dispersed in the electrolyte, rendering their separation in pure form difficult (Hicks 1918, Thompson et al. 1926). A novel way out of this difficulty appeared to be the recovery of rare earth metal as an alloy that is molten at the electrolysis temperature. The alloy could thus be easily separated from the electrolyte. Metal was subsequently recovered from the alloy by pyrovacuum distillation. This approach attracted a number of investigations and considerable success was achieved. The important investigations are listed in Table 4.15.

4.12.1 Electrolysis of Chlorides

Considerable pioneering work on the electrowinning of rare earth metals from their molten chlorides using a liquid cadmium or zinc cathode was done by Trombe (1935, 1938, 1945) between 1935–1945. The cell arrangement for this purpose was similar to the one he had used for deposition of pure liquid metals except that the cathode was a liquid metal. An electrolyte composed of 44% $GdCl_3$, 44% KCl, and 12% LiCl with a liquid cadmium cathode was used. The bath temperature was held between 625 and 725°C and electrolytic current was maintained for 15 min. A cadmium alloy containing 6% gadolinium was obtained. This alloy was heated in a vacuum to distill away cadmium. Gadolinium thus obtained was melted in a molybdenum crucible at 1240°C to form a semi-agglomerated mass, which was analyzed at 98.4% gadolinium and 0.7% silicon and cadmium. It was a small-scale experiment that used only a total of 4 g of electrolyte. Besides gadolinium, europium

Table 4.15 Electrolytic preparation of rare earth alloys

Year	Electrolyte	Cathode	Product	Reference
1968	RE_2O_3–REF_3–LiF–BaF_2	Consumable metal rod: Cr, Fe, Co	Gd–4Cr Gd–15Fe Dy–18Co Sm–13Fe	Morrice et al. 1968
1969	RE_2O_3–REF_3–LiF	Consumable metal rod: Mn, Cr, Fe	Gd–34Mn Gd–6Cr Dy–16Fe Sm–13Fe Y–37Mn	Morrice et al. 1969
1973	Y_2O_3–YF_3–LiF	Liquid Mg	Y–46Mg alloy	Aamland et al. 1973
1988	$NdCl_3$–KCl	Liquid Mg–Cd Liquid Mg–Zn	Nd–Mg–Cd Nd–Mg–Zn	Chambers and Murphy (1988)

(Trombe 1938) and dysprosium (Trombe 1945) were also prepared using cadmium as liquid cathode. A molten alkali chloride bath was used at 750°C to which praseodymium, yttrium, or samarium chlorides were added. The cathode was a liquid alloy of Mg–Cd. On electrolysis, the liquid cathode collected the rare earth metal. The resulting alloy, which contained up to 35% rare earth metal, was vacuum distilled to remove magnesium and cadmium. Of the three rare earths investigated, only samarium tended to distill together with magnesium.

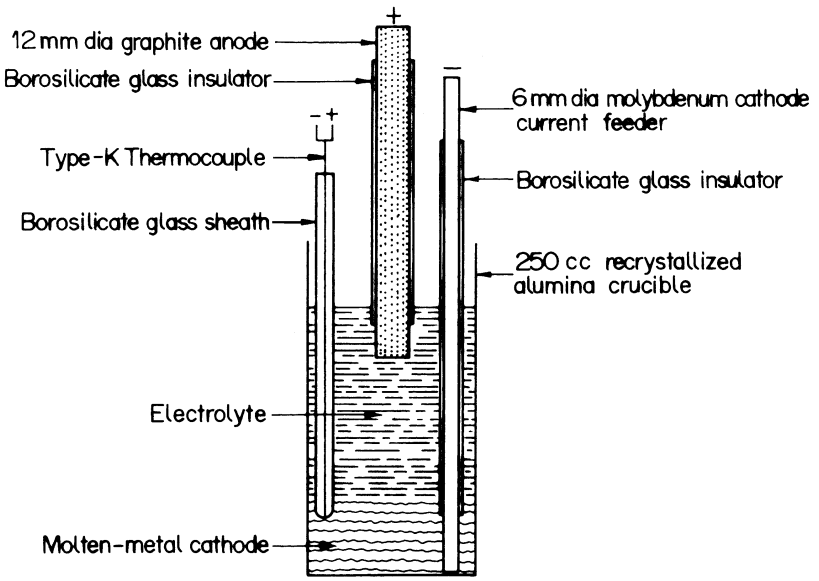

Figure 4.52 Electrolysis cell for reduction of neodymium (Chambers and Murphy 1988).

A scandium–zinc alloy was obtained at the cathode of an electrolysis cell with eutectic KCl–LiCl containing dissolved scandium chloride as electrolyte and molten zinc as the cathode (Fischer et al. 1937). Scandium was recovered after distilling off zinc. An equimolar mixture of $SmCl_3$–NaCl was electrolyzed at 500°C using a liquid zinc cathode, and a $SmZn_{12}$ alloy was obtained (Ishikawa et al. 1974).

Recently, Chambers and Murphy (1988) investigated the fused salt electrolysis of neodymium from a chloride electrolyte using a liquid metal cathode. Even though it was possible to electrodeposit neodymium into a liquid zinc cathode, the current efficiencies averaged only 50% and zinc was dispersed throughout the electrolyte at all current densities. The mobility of zinc in the electrolyte decreased during electrowinning between 500 and 600°C but current efficiencies averaged only 40%. Using a temperature between 600 and 700°C also did not yield satisfactory results. At above 700°C, zinc readily mixed with the electrolyte leading to a very poor metal–salt separation at the end of electrolysis. These problems were circumvented by Chambers and Murphy (1988) by the use of Mg–Zn and Mg–Cd cathodes. The intermetallic compounds MgZn and Mg_3Cd_2 melt between 500 and 550°C, and these were used as cathodes. They used an electrolytic cell shown schematically in Figure 4.52. A recrystallized alumina crucible (55 mm diameter and 105 mm height) was the electrolyte container. The anode was a 12-mm diameter graphite rod and an electrical connection to the liquid metal cathode was made with a 6-mm diameter molybdenum rod. Sheathing the anode and the molybdenum current feeder with borosilicate glass tubes fixed the electrode surface area and enabled accurate control of the current density. The cell was heated externally by a furnace and temperature was measured by a thermocouple sheathed with borosilicate glass and immersed in the molten metal cathode. The electrolyte was a 50:50 mole ratio mixture of $NdCl_3$ and KCl eutectic composition, and its melting point was 480°C. The cell was operated at 650°C and electrolysis lasted for 4 h. In the end, the cell contents were allowed to cool in the alumina crucible after which the crucible was broken and the alloy was separated from the solidified electrolyte.

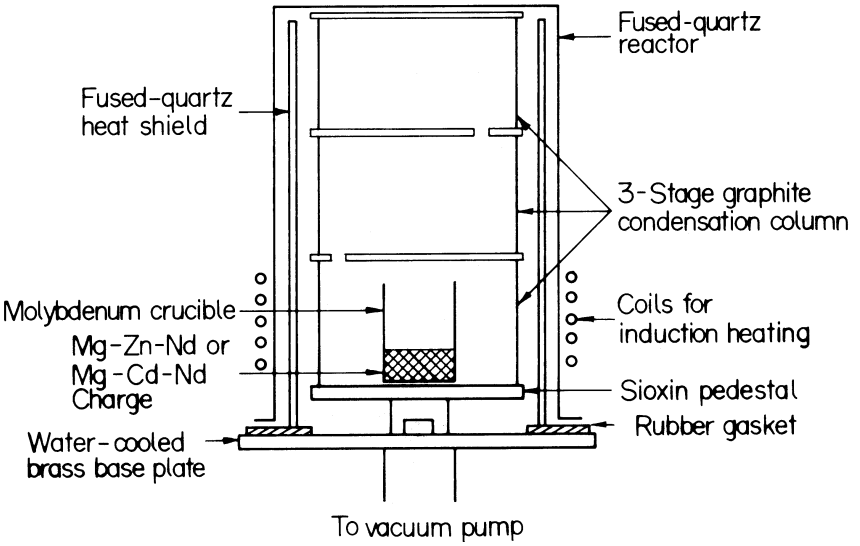

Figure 4.53 Vacuum distillation apparatus (Chambers and Murphy 1988).

Neodymium was recovered from the cathode alloy by distillation. The apparatus used is shown in Figure 4.53. The alloy was contained in a molybdenum crucible placed inside a graphite condenser column. The column was placed in a bell jar that was evacuated. Distillation was carried out at 900°C and 0.1 Pa for 15 min followed by heating at 1100°C and 0.1 Pa for up to 30 min. Magnesium and zinc or cadmium were distilled off leaving behind neodymium in the molybdenum crucible. This was recovered by inverting the crucible and heating under a vacuum, allowing the molten neodymium to drip on to a cold copper hearth.

Between the two liquid alloy cathodes Mg–Zn and Mg–Cd, Chambers and Murphy (1988) considered the Mg–Cd cathode better even though the current efficiency was only 80% as compared to 90% current efficiency when the Mg–Zn cathode was used. The Mg–Cd–Nd alloy yielded purer neodymium product on vacuum distillation. Neodymium metal of 99.9+ purity was recovered from the Mg–Cd alloy cathode whereas about 2% zinc persisted in the neodymium recovered from the Mg–Zn alloy. Besides, the residual chlorine, carbon, and oxygen contents of the neodymium product from vacuum distillation of the zinc alloy cathode were 100, 300, and 180 ppm, respectively, while the corresponding values for the product from the cadmium alloy cathode were 30, 80, and 110 ppm. The Mg–Cd alloy resulted in a cleaner metal–salt separation than did the Mg–Zn alloy. The separation of the Mg–Cd alloy from neodymium by vacuum distillation was achieved more readily than when zinc was involved.

4.12.2 Electrolysis of Oxide–Fluoride Melts

The electrolytic reduction of rare earth oxide dissolved in a fluoride melt to yield the alloy directly has also been investigated. In many cases the alloy can be distilled in vacuum to yield the pure metal as the condensate or as the residue. Two types of cathodes were used. In one type, the cathode was solid at the electrolysis temperature but formed a liquid alloy

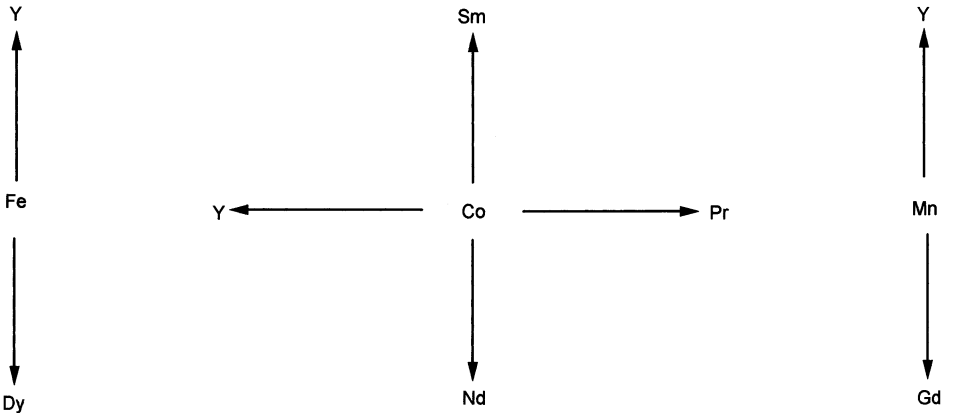

Figure 4.54 Combinations of rare earths and consumable anodes in the electrolytic preparation of alloys (Morrice 1985).

when the rare earth metal was deposited on it. In the other, the cathode was a metal or alloy that was already molten at the electrolysis temperature and formed a molten alloy with the electrodeposited rare earth metal. When the cathode was solid, the temperature of electrolysis was higher than the melting point of the eutectic between the cathode and the rare earth metal but lower than the melting point of the cathode metal (Morrice et al. 1968, 1969). The combinations of rare earth and consumable cathodes investigated at Reno are shown in Figure 4.54 (Morrice 1985). The electrolyte comprised rare earth oxide dissolved in REF_3–LiF–BaF_2, and the cell arrangement is the same as that used for high purity metal preparation. Instead of Mo, a consumable rod of Fe, Ni, Cr, or Co is used as the cathode. Low melting near eutectic alloys of the rare earth and the cathode metal formed and dripped off during electrolysis at the working temperature of 850–1000°C and were collected at the cooled bottom of the cell in a solid form. The consumable cathode rod was lowered into the bath at a controlled rate and semicontinuous operation of the cell was achieved. The alloy could be tapped from the bottom spout after heating the cell to sufficient temperature. The alloys contained about 80–90% REM. Even the difficult to reduce samarium was obtained as Sm–13Fe alloy with about 46% current efficiency, principally because alloy formation effectively prevented back reaction of samarium with the fluoride which results in the formation of Sm(II).

Morrice et al. (1969) investigated the electrodeposition–vacuum distillation process for the preparation of gadolinium, dysprosium, yttrium, and samarium. As high purity liquid metals, the first three are difficult to electrowin because of their high melting points (>1300°C). At the requisite cell operating temperatures (<1400°C), there will be increased carbon contamination of the product. Even though samarium has a comparatively low melting point (1072°C), direct electrowinning of the metal was unsatisfactory because of its reactivity with the electrolyte (Morrice et al. 1968). Electrowinning of these metals as alloys circumvented these problems. Morrice et al. (1969) chose manganese and chromium as alloying elements for gadolinium, manganese for yttrium, and iron for samarium and dysprosium, on the basis of phase diagram information of the corresponding binary alloys and the vapor pressures. The eutectics of the binary systems contain about 75 to 95% of the rare earth metal and, except in the case of gadolinium–chromium, the eutectic temperatures were low enough to permit cell operation in the temperature range of 900 to 1000°C.

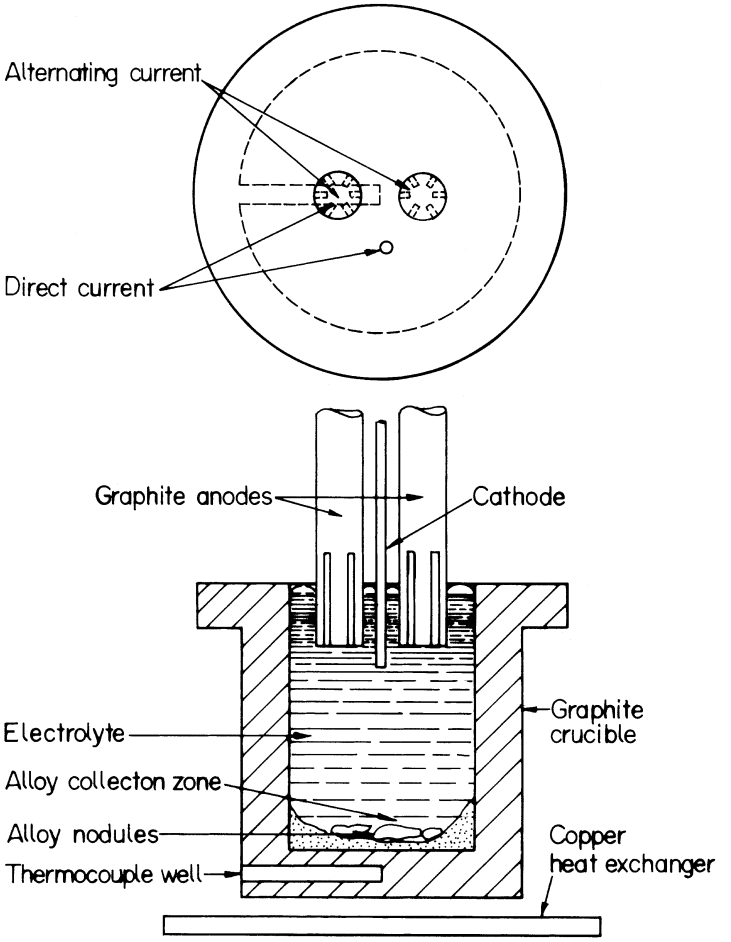

Figure 4.55 Rare earth–ferroalloy electrodeposition cell (Morrice et al. 1969).

The cell used by Morrice et al. (1969) for the electrodeposition of gadolinium, dysprosium, samarium, and yttrium with manganese, chromium, or iron is shown in Figure 4.55. The graphite crucible for holding the molten electrolyte had an inside diameter of 100 mm and a depth of 100 mm. The anodes were two 18 mm diameter fluted graphite rods. The cathode was a 5 to 6.5 mm diameter iron or chromium metal rod or a 15 mm diameter as melted manganese metal bar. The cell was enclosed in an inert gas chamber to avoid atmosphere contamination. Glove and view ports in the chamber permitted addition of cell feed and allowed the raising and lowering of the electrodes during operation.

The electrolytes for the electrodeposition of gadolinium–manganese, gadolinium–chromium, dysprosium–iron, and yttrium manganese alloys contained 50 mol % rare earth fluoride and 50 mol % lithium fluoride. The electrolyte for the electrodeposition of samarium–iron alloy contained 25 mol % SmF_3 and 75 mol % LiF. The solubilities of rare earth oxides in the electrolyte are between 2 and 4 wt %.

In the beginning, melting of the electrolyte was started from the top by striking an arc between two tungsten rods. Subsequently the cell was internally heated by applying AC

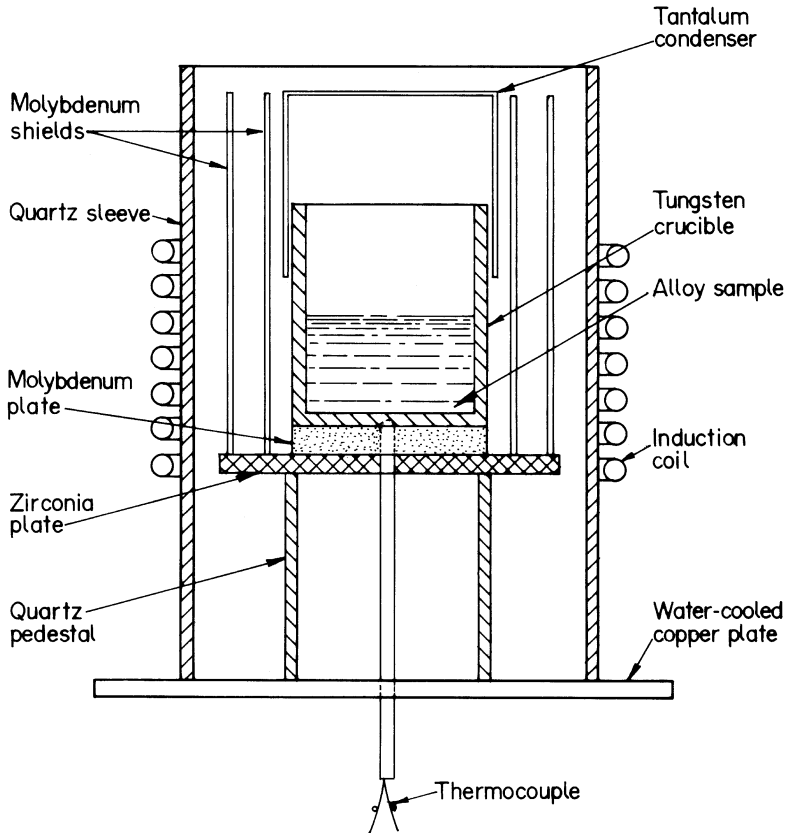

Figure 4.56 Rare earth–ferroalloy distillation apparatus (Morrice et al. 1969).

between the graphite anodes. For electrolysis, DC was applied to the anode and cathode. The rare earth metal was electrodeposited on the manganese, chromium, and iron cathode to form a low melting alloy. The alloy, as it formed, dripped off, the cathode penciled down, and a new section of the cathode was lowered into the electrolyte. The molten alloy descended and collected at the bottom of the cell, where a skull of frozen electrolyte prevented graphite contamination of the alloy. After completion of the experiment, the electrolyte was allowed to freeze, and alloy nodules weighing 2 to 75 grams each were recovered. The operational data for electrodeposition of the various alloys are given in Table 4.16.

The next step of the process, vacuum distillation, was carried out by Morrice et al. (1969) in the apparatus shown in Figure 4.56. In the distillation apparatus, the alloy sample was contained in a 25 mm diameter by 25 mm deep tungsten crucible having a wall thickness of 1.6 mm. The crucible was placed on a 6 mm thick molybdenum disk and was surrounded by two concentric radiation shields made from a molybdenum sheet. This assembly was supported by a zirconia plate on top of a quartz pedestal. To collect the distilled metal, a tantalum condenser was placed above the crucible. The apparatus including the induction furnace for heating the sample was enclosed in a Pyrex bell jar chamber that could be evacuated to 6.6×10^{-5} Pa. The crucible and condenser temperatures were measured using thermocouples.

Table 4.16 Operational data for electrodeposition of alloys (Morrice et al. 1969)

Operational parameters	Values for specific alloys				
	Gd–Mn	Gd–Cr	Dy–Fe	Sm–Fe	Y–Mn
Electrolyte composition, mol %	$50GdF_3$–50LiF	$50GdF_3$–50LiF	$50DyF_3$–50LiF	$25SmF_3$–75LiF	$50YF_3$–50LiF
Average direct current, A	63	71	70	45	64
Average direct current voltage, V	22	27	25	26	30
Initial anode current density, A cm^{-2}	0.7	0.7	0.7	1.1	0.9
Initial cathode current density, A cm^{-2}		18	14	10.1	
Average electrolyte temperature, °C	964	1339	1056	887	1048
Average cell bottom temperature, °C	677	834	707	719	700
Duration of electrolysis, h	0.4	0.8	1.0	1.5	1.0
Alloy recovered, g	58	79	122	67	85
Rare earth metal content, %	66	94	84	87	63
Current efficiency, %	78	67	73	46	76

Distillation was carried out by slowly heating the electrodeposited alloy nodules, about 30 g in each experiment, while maintaining the vacuum at 1.3×10^{-4} Pa. Pure samarium and dysprosium metals distilled off from the iron alloy and collected in the condenser. They were separated from the collector by peeling away the tantalum. Gadolinium and yttrium, being less volatile than the alloying constituents chromium or manganese, remained as residue in the crucible while the alloying constituent distilled off. After completion of experiment, the crucible containing these metals was inverted and the metals melted under vacuum on to a water cooled copper hearth. The details of distillation, starting alloy, and final product analyses are summarized in Table 4.17. After distillation, gadolinium, samarium, and yttrium contained less than 0.02% of ferrous metal. Distillation did not effectively separate dysprosium from iron and high purity dysprosium was not obtained. The difference in vapor pressure between Dy and DyF_3 was not sufficient for effective separation of dysprosium from the fluoride impurity, either.

The method described above for a consumable solid cathode cannot be used to prepare alloys composed of yttrium and low melting constituents such as magnesium, aluminum, or zinc. A suitable method for these was described by Aamland et al. (1973). The method consisted of electroreduction of Y_2O_3 dissolved in molten YF_3–LiF electrolyte and subsequent deposition of yttrium in a floating magnesium cathode. The process was carried out in a specially designed MgO diaphragm cell at a temperature ranging from 780 to 970°C. The product alloys, prepared in batches of ~20 g contained up to 55% yttrium. The cathode current efficiencies were 21 to 60%. The purity of the alloy was comparable to that obtained by metallothermic reduction. On distillation in vacuum, these alloys yielded yttrium metal comparable in purity (0.1 to 0.2% oxygen content) to that obtained by distillation of metallothermic alloys.

Besides Mg, molten aluminum was also used as cathode in the preparation of yttrium–aluminum alloy (Al–20Y) using an electrolyte of Y_2O_3 in YF_3–LiF (Bratland et al. 1972, 1973). Yttrium–aluminum alloy of approximately eutectic composition (91% Y) was electrowon from a mixture of yttria and alumina dissolved in a YF_3–LiF melt (Morrice et al. 1968). This cell used liquid Y–Al cathode and a graphite anode.

4.13 CURRENT EFFICIENCY

Current efficiency in the electrolytic cells described here are determined by several factors. The current efficiency of commercial chloride cells is low, usually below 50%. At the temperature of electrolysis (~900°C), the rare earth metals can react with O_2, H_2, CO_2, and graphite, forming products with low electrical conductivity and a high melting point. The presence of oxychlorides, either from the starting material or by reaction between the trichloride and moisture, is detrimental to the electrolytic process. Oxychlorides have higher melting points than the anhydrous halides and limited solubility in the latter. Their existence causes an increase in viscosity in the molten salt leading to current losses because of lower ionic mobility and a higher temperature for bath operation.

The presence and accumulation of multivalent elements such as Sm, Eu, and other nonreducible components in the electrolyte also lead to lower current efficiency. $SmCl_3$ can easily react with Sm, more readily at higher temperatures, to form soluble divalent chlorides. During electrolysis the oxidation–reduction reaction of Sm^{3+}–Sm^{2+} can occur cyclically at anode and cathode and cause high current consumption and low efficiency.

Table 4.17 Operational data for distillation of alloys containing rare earth and ferrous metals, and analysis of starting alloys and final products (Morrice et al. 1969)

Alloy	Distillation parameters			RE recovered, %	Analyses, %								
	Duration, h	Distillation temperature, °C	Condenser temperature, °C			Al	Ca	C	F	Fe	Mg	O	Si	Ta
Dy–16Fe	2	1300	1095	75	Alloy Distillate	<0.01 <0.01	<0.003 <0.003	0.024 0.002	0.26 0.21	16.2 0.008	0.003 <0.001	0.030 0.021	0.005 <0.005	<0.02 <0.02
Sm–13Fe	3	1000	700	85	Alloy Distillate	<0.01 <0.01	<0.003 <0.003	0.049 0.010	0.58 0.03	13.0 0.005	0.030 0.001	0.050 0.015	0.010 <0.002	<0.02 <0.02
						Al	Ca	C	Cr	F	Mn	O	Si	W
Gd–6Cr	3	1350	*	95	Alloy Residue	<0.01 <0.01	<0.003 <0.003	0.025 0.020	6.2 0.1	0.48 <0.002	<0.003 <0.003	0.027 0.030	0.004 0.008	<0.01 <0.01
Gd–34Mn	0.5	1350	*	96	Alloy Residue	<0.01 <0.01	<0.003 <0.003	0.030 0.050	0.005 0.004	0.39 0.018	33.7 <0.003	0.019 0.020	0.004 0.010	<0.01 <0.01
Y–37Mn	0.1	1550	*	93	Alloy Residue	<0.01 <0.01	<0.003 <0.003	0.045 0.050	0.004 0.004	0.35 0.003	37.0 0.003	0.020 0.060	0.005 0.003	<0.01 0.35

The current efficiencies of molten fluoride systems are better and range from 75 to 95% (Hirschhorn 1968). The fluoride electrolysis investigations, however, have been conducted using high pure starting materials in inert atmosphere electrolytic cells.

Morrice (1985) has commented that low cathode current efficiency could result from reaction of the metal product with the electrolyte and poor coalescence of the electrowon metals. More efficient cell designs to provide cathodic protection and prevent metal products from being contaminated, and the determination of the effects of electrolysis temperature and melt composition have also been suggested by him as a means of improving current efficiency. In addition to low current efficiency, Morrice (1985) had listed anode effect, metal and alloy product contamination, corrosion of cell components, and efficient heat utilization in the cell as areas that need research attention in the molten salt electrowinning of yttrium metals and alloys.

4.14 SUMMARY

Rare earth metals are among those metals that are considered to be most difficult to produce in pure form. Several processes have been developed for the production of rare earth metals of different purities. These include: (i) reduction of anhydrous chlorides or fluorides, (ii) reduction of rare earth oxides, and (iii) fused salt electrolysis of rare earth chlorides or oxide–fluoride mixtures. A qualitative picture as to which reactive element is usable as a reducing agent for rare earth metals preparation is obtained from the free energies of formation of the oxides, fluorides, and chlorides and their dependence on temperature. The data for rare earths and some potential reducing agents indicate that in the oxide systems, the order of stability is $CaO > RE_2O_3 > MgO > Al_2O_3 >> SiO_2$; whereas among the fluorides it is $CaF_2 > REF_3 > LiF > NaF > MgF_2 >> AlF_3$; and among the chlorides, $KCl > NaCl \approx CaCl_2 > RECl_3 > MgCl_2 >> AlCl_3$. The indicated order of stabilities, however, can be changed in real systems by changing the activities of one or more of the reactants or products. When no such change is effected, the above data indicate that calcium is the only choice for the reduction of rare earth oxides and fluorides, whereas chlorides can also effectively be reduced by lithium, sodium, or potassium. Thermodynamic feasibility is at best the first of many factors that determine the practicability of the reduction process. Consideration of the other factors, including the melting point of calcia slag and exothermicity of the reaction, indicated that calciothermic reduction of rare earth oxides is not a suitable process for rare earth metal preparation. It had to be the halide route.

Rare earth metals are highly reactive, particularly at the high temperatures required for their preparation. The halide reduction, which usually involves the metallothermic reduction of pure anhydrous halides with pure metallic reductants, is a standard method of reactive metals preparation and is meant to be an oxygen free process. However, oxygen and other interstitial impurities such as carbon and nitrogen do find entry into the reduced metal in various ways. This is traceable to the extreme stability of the solutions and compounds formed by these elements with rare earth metals. While this cannot be avoided, it can certainly be minimized by suitable choice of container materials and by carrying out all the operations in a controlled environment system.

The methods for producing rare earth metals by chloride reduction processes are summarized in Figure 4.57. Starting from rare earth oxide, the process basically involves two stages. In the first, anhydrous rare earth trichloride is prepared, and in the second stage the

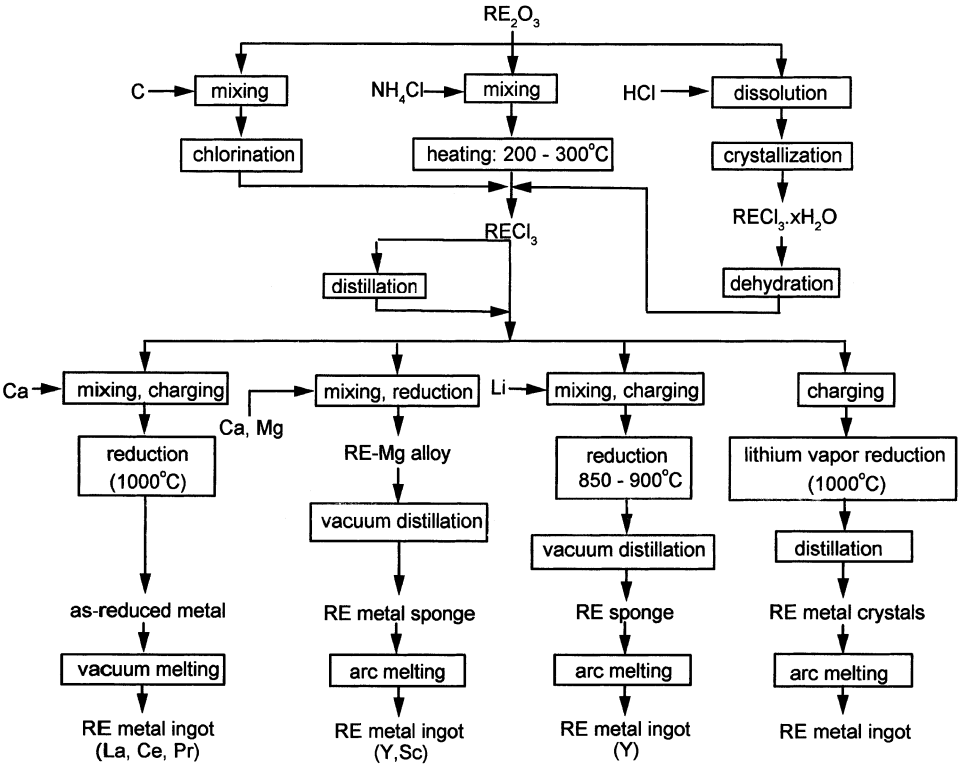

Figure 4.57 Processes for the preparation of rare earth metals through the chlorides.

trichloride is reduced to the metal. The oldest and most widely used process for chloride preparation is the wet route. Rare earth trichloride hexahydrate is crystallized from a HCl solution of rare earth oxide. The hydrated chloride is then dehydrated by heating under dry HCl flow under reduced pressure. Alternatively, dry methods such as chlorination of the oxide by heating with ammonium chloride or chlorination of the oxide or even the rare earth ore concentrate by heating with carbon under chlorine flow have also been used. The chloride can be purified by distillation. The principal reducing agents for rare earth trichloride are calcium and lithium. Calcium reduction has been used at Ames for the production of low melting lanthanides La, Ca, Pr, and also Nd and Gd. For gadolinium and higher melting rare earths, using a higher reaction temperature was complicated by $CaCl_2$ slag frothing and bomb liner attack. Tantalum crucibles were useful. Reduction of rare earth chloride with lithium has been successfully used for most of the rare earths. In the USBM process, the chloride and lithium were heated together in a molybdenum crucible under inert atmosphere. In the Ames process as well as in the commercial process, lithium vapor reduction of rare earth trichloride could yield yttrium and other high melting rare earth metals. Tantalum was used as a container. The LiCl slag was removed by vacuum distillation.

The use of rare earth fluorides as intermediates for reduction to metal circumvents the problems associated with the use of hygroscopic and volatile chlorides. Purer metals are obtained in this elegant process. The methods are summarized in Figure 4.58. Out of the three major alternatives for converting the rare earth oxide to rare earth fluoride,

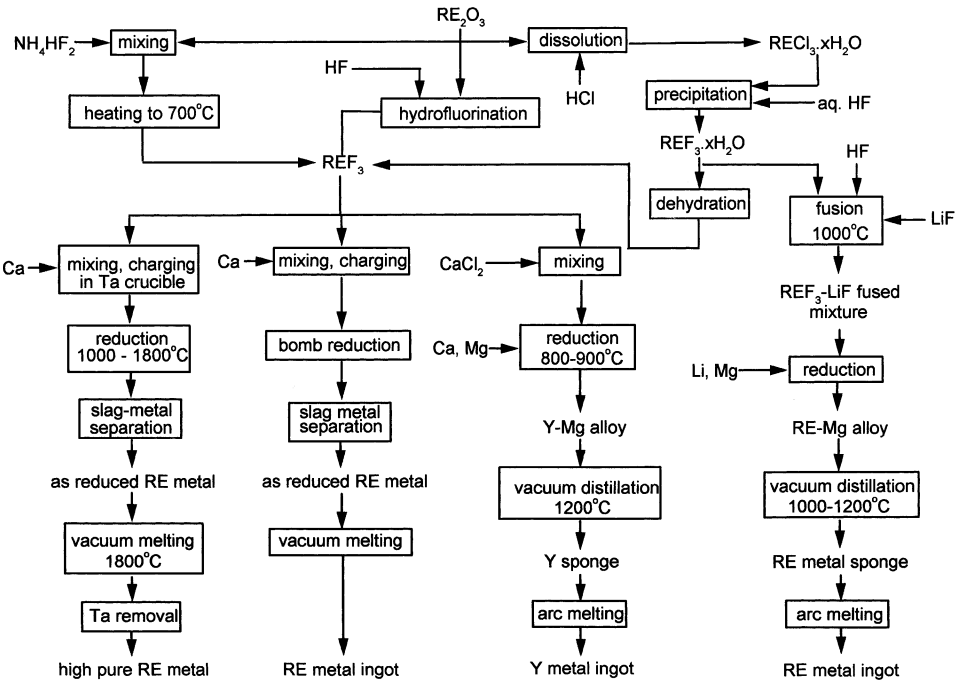

Figure 4.58 Processes for the preparation of rare earth metals through the fluorides.

hydrofluorination at 700°C has been used to prepare the purest fluorides. The Ames process is the technically perfect method for conversion of the fluoride to metal. In this method the rare earth fluoride and calcium loaded in a tantalum crucible are externally heating in an argon atmosphere to about 50°C above the melting point of the highest melting component of the reaction mixture. The reaction goes to completion in a few minutes resulting in good slag–metal separation. The excess calcium and adhering slag are removed from the metal by vacuum melting, and high purity metal is obtained in 97–99% yield. Any rare earth metal, independent of its melting point, except Sm, Eu, and Yb, which form stable divalent halides, can be reduced to metal by this process. Lithium is the only other reductant that has been found to be quite effective, but less than calcium. An important variant of the process, particularly for yttrium, is to conduct the reduction in the presence of magnesium at a low temperature. Magnesium is removed from the Y–Mg alloy by vacuum distillation and the yttrium sponge vacuum melted. A limitation of the fluoride route is the high cost of fluorine chemicals, which end up as low value calcium fluoride.

Even though samarium, europium, and ytterbium cannot be produced by halide reduction, their oxides can be directly reduced to metal in a process that exploits the pronounced volatility of these metals. The technique is quite similar to that used by Pidgeon for magnesium. Lanthanum is among the least volatile of the rare earth metals. Besides, La_2O_3 has one of the most negative values for its heat of formation. In the process, an intimate mixture of lanthanum chips and rare earth oxide is heated in a tantalum crucible fitted with a long tantalum condenser. Lanthanum reduces the rare earth oxide and the rare earth metal produced, being volatile, escapes and collects in the condenser. Metal yield is higher. Certain metals such as cerium, misch metal, zirconium, and thorium, which are

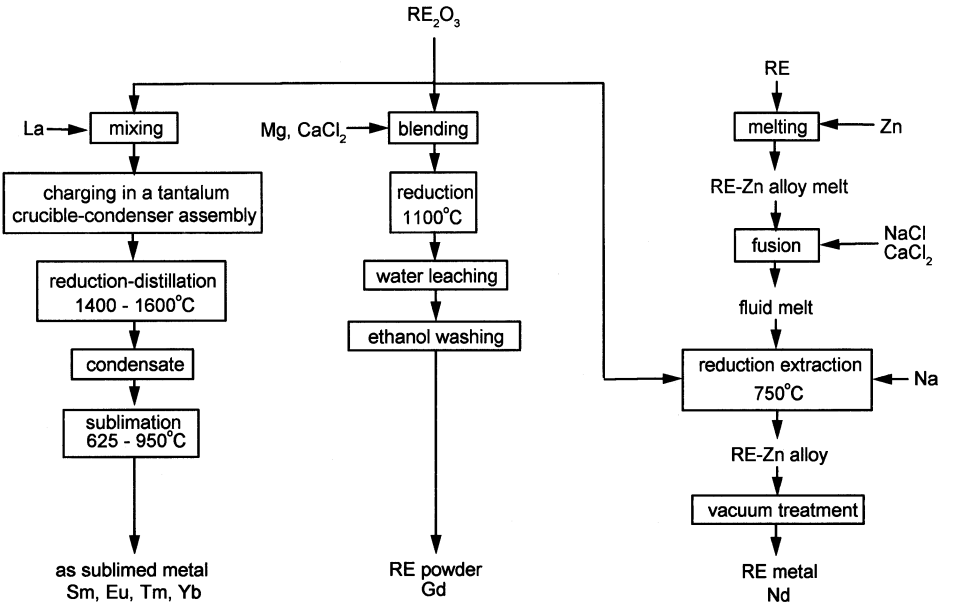

Figure 4.59 Processes for the preparation of rare earth metals by oxide reduction.

similar in the relevant characteristics to lanthanum, have also been used in its place. The process is shown in Figure 4.59 along with certain other specific oxide reduction methods.

A relatively new entrant to the field of metallothermic rare earth production methods is the process of molten salt reduction extraction, developed at General Motors. The reduction is carried out by reacting the Nd_2O_3 with calcium in a molten salt bath ($CaCl_2$–NaCl) and simultaneously extracting the reduced metal into a molten Nd–Zn or Nd–Fe alloy. The Nd–Zn alloy product is treated in a vacuum to remove zinc and produce Nd metal. The process has been made commercially more attractive by the use of sodium instead of calcium as the reducing agent.

The electrolytic methods currently account for the largest quantity of rare earth metals commercially produced throughout the world. Lanthanum, cerium, and praseodymium have melting points that permit their recovery in a liquid state by electrolysis of inexpensive fused chlorides at temperatures less than 1100°C. Winning of the rare earth elements in the liquid state facilitates slag (electrolyte)–metal separation, minimizes contamination of the reduced metal and enables continuous operation and high volume levels of production. Such electrolytic processes are inherently simpler and cheaper compared to complex metallothermic reduction procedures. The technical feasibility of preparing limited quantities of high melting rare earth metals such as gadolinium, dysprosium, and yttrium in addition to neodymium, praseodymium, and didymium (Nd + Pr) in a consolidated form has also been demonstrated by using the fluorides as electrolytes in place of chlorides. These studies have been carried out in specially designed high temperature cells that can operate up to 1700°C. For cerium and lanthanum, cells have been designed and operated at U.S. Bureau of Mines for continuous production of these metals by oxide–fluoride electrolysis. Instead of as pure metals, if the rare earth metals are recovered as binary alloys having melting points in the range 600–1000°C, the electrolytic process has been found applicable to all the rare earth metals with the added advantages of liquid metal recovery

and low temperature operation. Besides, by this process, all the rare earth metals, including those with stable divalency, could be recovered as alloys. If a relatively more volatile metal such as cadmium, zinc, or magnesium is used as the alloying component with a relatively less volatile high melting rare earth, e.g., neodymium, gadolinium, and yttrium, the alloy can be vacuum distilled to pure metal.

The question of a technically perfect reduction process for rare earth metal preparation was answered as early as the 1950s and 1960s with the development of the fluoride reduction process and the lanthanothermic direct reduction process at Ames. But these processes are expensive because of the high cost of chemicals, the expense of the reactor, and the batch nature of the process. The same may be said of electrolytic processes except those for the recovery of lanthanum, cerium, and praseodymium in a chloride bath. The highly effective oxide–fluoride electrolysis has problems of high temperature operation, corrosion, low solubility of oxides in molten fluoride, and limitations on current density to avoid affecting the anode. The field remains open for improvement and new processes that are easy on costs yet provide adequate purity in the final metal product.

CHAPTER 5

Refining Rare Earth Metals

5.1 INTRODUCTION

As-reduced rare earth metals, whether produced metallothermically or by fused salt electrowinning, are generally 98 to 99% pure. It is usually possible in certain cases, if care is taken to use pure raw materials and adopt controlled environment processing, to restrict the total impurities in the as-reduced metals to about 0.5%. More often than not this additional gain in purity is either not technically possible or involves a great increase in process cost, especially in commercial scale operations. The general alternative to improving or modifying the reduction technique itself is first to prepare even a relatively impure metal by a commercially viable reduction method and follow it by a suitable refining procedure. This is important because fairly good grade rare earth metals with purity adequate for many application requirements are usually available at reasonable prices, and the metal that qualifies as ultrapure for one application could be impure for another application. This also highlights the need for customizing the refining procedure for a particular application, with commercial metals as source material. The refining step is, therefore, a necessary and important operation in the extractive flowsheet of the rare earth metals.

A number of processes are used for refining the as-reduced rare earth metals to different levels of purity. The nature and concentration of the impurity to be removed and the final purity level desired in the refined metal generally govern the refining technique that should be used. In the case of rare earth metals, the applicable processes are strongly influenced by the melting points of the metals and their vapor pressure at the melting point. This influence is clearly brought out in Figure 5.1 which depicts the generalized sequence of processes for purification of rare earth metals (Gupta and Krishnamurthy 1992). Complete purification is not achieved by any one refining technique and, as a rule, a sequence of processes has to be applied to remove all the impurities (Jones et al. 1982).

The usefulness of a given technique in the near complete removal of one or more impurities from rare earths is a necessary but not a sufficient criterion for its adoption for large scale or commercial operations. The technique has to be compatible with other demands such as product form, metal yield, batch size, operational simplicity, and economics. On the other hand, in the choice of a technique for small volume metal refining for research purposes, major emphasis is placed on the ultimate purity achievable and considerations such as yield and economics become secondary.

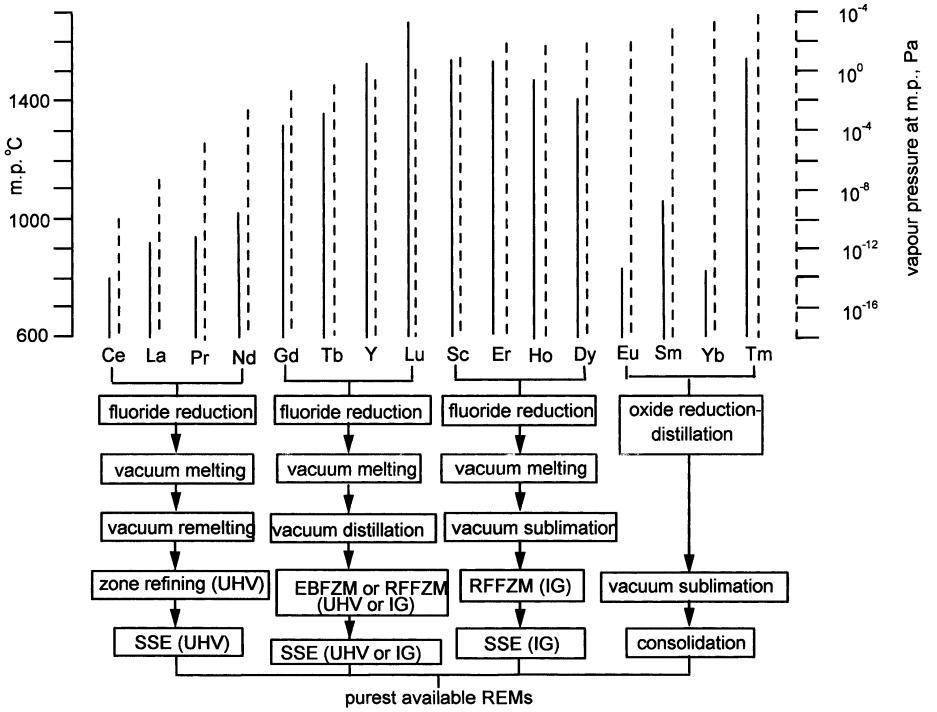

Figure 5.1 Processes for the purification of rare earth metals.

This chapter gives a description of rare earth metal refining processes. It opens with a reference to the origin of various impurities usually associated with as-reduced rare earth metals. Refining by pyrovacuum treatments like vacuum melting, vacuum distillation, and sublimation is then detailed. Fused salt electrorefining has not been applied extensively to rare earth metal refining. The same is true of the iodide or the Van Arkel–de Boer process. Ultrapurification of rare earth metals has been an important operation for certain applications. This is usually carried out by zone refining and its many variations as well as by solid state electrotransport and its variations. The choice of a particular technique, as mentioned earlier, is strongly determined not only by the impurity to be removed, but also by the physical properties of the rare earth metal, particularly its melting point and vapor pressure. Unlike the chemical properties of rare earths, which are well known for their close similarity, the physical properties vary significantly among the rare earths (Gschneidner et al. 1995). This is reflected in the applicable techniques for rare earth metal refining and ultrapurification.

5.2 ORIGIN OF IMPURITIES

It may be recalled and briefly referred to here that the methods useful for rare earth metal production are high temperature controlled atmosphere reduction of halides, either the anhydrous chlorides or fluorides by reductants such as calcium or lithium; fused salts electrolysis of chlorides or oxide–fluoride mixtures; direct reduction of oxides by lanthanum,

cerium, zirconium, or even misch metal; and finally, certain special reduction procedures in molten salts. As-reduced rare earth metals obtained by the above processes are pure enough for certain applications but need further purification for many other applications. Depending on the raw material used and the process adopted, the type and level of impurities in the rare earths vary. Besides, the rare earth metals themselves, because of their inherent characteristics, are selective in picking up certain impurities more than others.

While careful control of rare material purity and process variables will enable preparation of metal that is 99.99+% pure in respect to other metallic atoms, the situation is very different for nonmetallic impurities such as oxygen, nitrogen, carbon, hydrogen, and halides. To get metal better than 99.9% by weight pure with regard to all elements is an extremely challenging task. The rare earths getter nonmetallic elements and they creep into the metal at all stages of manufacture or handling. In addition, these elements, even in small quantities, when in solid solution influence to a significant extent the properties of individual rare earth metals.

In the as-reduced rare earth metals the impurities principally come from the starting materials and the environment in which the process is carried out. The best way to produce the pure metals is to prepare them in such a manner that the impurities do not get into the system. This is best done by producing the reactants in an ultrapure form and keeping the system free at all times from atmospheric gases and adsorbed impurities — a task not always feasible because of technical and/or economic reasons. Any loose nonmetallic elements present in the container materials or on the inner surfaces of the reactor will invariably end up in the metal.

5.2.1 Starting Materials

In the as-reduced metals, the metallic impurities to be considered first are the metallic reductant and any metal added to the charge to form a low melting alloy. A reaction constituent when used in excess of the stoichiometric amount can end up as an impurity. Calcium, lithium, lanthanum, cerium, zirconium, and thorium impurities are all examples in this context. Magnesium and zinc impurities originate from adding alloy constituent. A reaction constituent also ends up as an impurity in the event of incomplete reduction. The presence of residual fluorine or chlorine and residual oxygen in the metal are some examples. The amount of fluorine that remains in the as-reduced metal prepared by fluoride reduction, however, is not the same as the amount of residual chlorine when the metal is obtained by chloride reduction. For example, when Dy, Ho, and Er are prepared by calcium reduction of rare earth fluorides, the metal invariably contains 25–75 ppm fluorine impurity. On the other hand, when these metals are prepared by lithium reduction of their anhydrous chlorides, the chlorine contents in the as-reduced metals are very low, namely, < 3 ppm (Croat 1969). In electrolytic reduction of rare earth metals, for example, the impurities to be anticipated are lithium, fluorine, and oxygen. Lithium and fluorine result from the melt and oxygen comes from the rare earth oxide starting material. Reaction constituents can be the source of impurities in another way also. The impurities present in the compound intermediate or reductant are often quantitatively transferred to the as-reduced metal.

For a long time and until the modern separation methods of ion exchange and solvent extraction were developed for effectively separating the rare earths from one another, one of the difficult problems was to get the rare earth oxide that is pure with respect to all the other rare earths. Using ion exchange, it is possible to get one rare earth so pure that all

other rare earths together amount to less than 10 ppm (Spedding et al. 1970). Solvent extraction methods also can provide such purity in many cases. It should, however, be pointed out that once a certain amount of other rare earth impurity is allowed to be present in the rare earth oxide, it will end up in the metal and usually none of the post-reduction purification techniques are particularly effective in removing these impurities, and they will remain essentially unchanged in the purified metal.

Commercial chemicals frequently used in solvent extraction and ion exchange can be the source of certain metallic impurities found in the rare earth oxides. Lead and calcium are examples. Impurities such as iron, cobalt, nickel, and copper enter the process stream as a result of a chemical attack on reactor materials, such as stainless steel, and end up in the rare earth oxide. Redissolution of this oxide and reprecipitation using very pure chemicals and very pure water usually lead to substantial purification of the oxide from these impurities.

Conversion of highly purified oxides to anhydrous fluorides or chlorides is another stage where impurities can get easily introduced. Hydrogen fluoride (HF) is a very corrosive gas and it can attack the metals of construction, forming volatile fluorides. These lead to introduction of impurities such as molybdenum or iron into the rare earth fluorides. Oxyfluorides and oxychlorides are readily formed by the fluorides and chlorides, and a good part of whatever oxygen is there in the halides will end up in the metal.

Among the many methods used for fluoride preparation, hydrofluorination by reaction between the rare earth oxide and HF can yield the purest product. After preparing the fluoride in the powder form by passing HF over the oxide, in a practice followed at Ames, the fluoride was subjected to a process known as topping to get rid of any trace oxy-compounds (Beaudry and Gschneidner 1978). It was subsequently found (Beaudry et al. 1983) that the oxygen contents of metals prepared from topped and untopped fluorides was nearly the same, particularly for light rare earths. Metallic impurities such as Cu, Ni, Fe, Cr, and Si, which remain in the fluoride after low temperature hydrofluorination, were reduced in the topping process. Topping is not done in commercial practices. The fluorides prepared by the aqueous methods have been found to have slightly higher oxygen contents than the fluorides prepared by hydrofluorination. However, the preparation of fluoride by precipitation of REF_3 from an aqueous solution using 48% HF or by the reaction of RE_2O_3 with NH_4HF_2 are simpler methods and also are useful if certain impurities can be tolerated in the final product. Impurities such as Al, Fe, and Cu are introduced from the NH_4HF_2 (Beaudry and Gschneidner 1978).

Once very pure fluorides have been prepared, they must not be exposed to air because they will react with moisture in the air and form oxyfluoride and will also pick up some air and carbon dioxide. The hygroscopicity of chlorides is more than that of the fluorides and they also have a strong tendency to form oxychlorides. The best fluorides prepared at Ames contain considerably less than 20 parts per million (ppm) oxygen and less than 10 ppm metallic impurities (Spedding et al. 1970).

The impurity levels in the interprocess intermediate, for example, the rare earth fluoride, that can be tolerated for producing metal of certain purity also depend on the process used for reduction. For obtaining low impurity levels in the product, the method of preparing fluoride for use in the electrolytic reduction is not as critical as for the calcium reduction technique (Beaudry and Gschneidner 1978). Similar observations were made by Gray (1951) concerning cerium chloride for metallothermic reduction and cerium chloride for electrolytic reduction. In a calcium reduction, the oxygen content of fluoride is quite critical because any oxide present in the fluoride will end up in the metal. It is not so in

electrolytic reduction. In oxide–fluoride electrolysis, CeO_2 or Ce_2O_3, for example, is added to the fluoride melt and it is the oxide that undergoes reduction to the metal. The fluoride melt can actually extract oxygen and certain impurities such as C, N, F, Mg, and Ni (Carlson et al. 1960). Thus in the electrolytic preparation, it may be anticipated that the long contact time of the metal with the fluoride flux may decrease the level of some impurities in the metal. However, a fluoride flux well loaded or saturated with impurities from the previous runs can also pass on some impurities to the metal.

In the electrolytic preparation of cerium, the method of preparation of CeF_3 influences the purity of the metal obtained. Preparation of the fluoride using NH_4HF_2 introduced impurities such as Al, Fe, and Cu from the bifluoride, and these impurities showed up in the metal. The preparation of CeF_3 by reaction of the oxide with anhydrous HF might lower the levels of these impurities in the metal.

In the same way as impurities in the interprocess intermediates can end up in the metal, impurities contained in the reductant can also find themselves in the as-reduced metal. Calcium is the most important reducing agent for metallothermic reduction of fluorides, and its purity is an important parameter (Spedding et al. 1968). Even the triply distilled commercial calcium invariably contains several hundred ppm oxygen, and when this calcium is exposed to air even for a very short period of time the oxygen content in it will increase to several thousand ppm. It is therefore very necessary to reprocess (distill) calcium just before using and keep it sealed from the atmosphere until use. At Ames, for best results, calcium is sublimed at a low temperature (825°C) under a few millimeters of helium. With such care, calcium containing 10 to 30 ppm oxygen could be produced. Another impurity in calcium is carbon. About 100 ppm carbon persists in the distilled calcium and a part of this carbon will ultimately come into the metal (Spedding et al. 1970).

Even while using lithium as reductant great care has to be taken, as was done for calcium because commercial lithium invariably contains more oxygen than what is acceptable.

5.2.2 Crucible

The materials of construction of the crucible and the reactor in which the metal is prepared come into close contact with the metal and can end up as impurities. A reduction carried out in a tantalum crucible results in an average of 0.05% tantalum in the as-reduced metal (Huffine and Williams 1961). This concentration can be much higher if reduction is carried out at higher temperatures or for longer periods of time. Tantalum crucible was used by Croat (1969) in the preparation of Dy, Ho, and Er. These metals were prepared, as described in the previous chapter, by the reduction of their anhydrous chlorides with lithium as reductant. The temperature of reduction was 900°C, which was well below the melting point of these metals. The tantalum contamination of as-reduced Dy, Ho, and Er was quite low, i.e., <30 ppm. This can be contrasted with the tantalum content of 0.1 to 0.2% which Dy, Ho, and Er have in their as-reduced from when they were obtained by calcium reduction of their fluorides in tantalum crucibles. It may be recalled that these reductions are carried out at high temperatures, above the melting point of the rare earth metals.

Daane (1961) stated that because the solubility of tantalum in liquid rare earth metals increased measurably with increasing temperature, the lowest possible temperature is used in the processes wherein the rare earth metal is processed in contact with tantalum, in order

to keep the tantalum impurity as low as possible. In the reduction of the light rare earth metals (lanthanum through neodymium), the amount of tantalum in the metal is approximately 200 to 300 ppm. For higher melting heavy rare earths and yttrium, this figure increases to about 1000 to 5000 ppm. Among the rare earth metals, tantalum is the most soluble in scandium. As much as 3% tantalum is present in scandium melted in tantalum. As far as dissolution is concerned, tungsten is better as a crucible material. In the liquid rare earth metals, less tungsten dissolves than does tantalum at any temperature (Dennison et al. 1966, 1966a). The refractory metals molybdenum, niobium, titanium, and zirconium are distinctly more soluble in molten rare earth metals than are tantalum and tungsten.

In reduction procedures where an alloying element is used to lower the melting point of the as-reduced metal (for example magnesium in yttrium reduction), titanium or zirconium may be used as crucibles. When yttrium–magnesium alloy is reduced in titanium crucibles, the alloy picked up an average of 0.15% titanium, and when zirconium was used the pickup was 0.58% zirconium (Huffine and Williams 1961).

In the electrolytic preparation of the rare earth metals, cell corrosion can occur extensively and the corrosion products can end up in the metal produced. Carbon impurity in the electrolytically produced metals usually comes from graphite anode and/or cell walls (Beaudry and Gschneidner 1978). Besides carbon, depending on the materials used for cell construction, the metals may be contaminated with iron, silicon, and other metallic impurities. The use of Mo as a liner or for the crucible in the cell leads to pickup of the element in the electrolytic metal. Electrolytic cerium metal obtained using Mo as cell material showed a Mo level of >750 ppm. The use of Ta in place of Mo lowered Mo contamination in the metal and Ta was also not picked up significantly (Shedd et al. 1964).

Experiments at Ames have indicated that even tantalum can be a source of certain interstitial impurities (Beaudry and Palmer 1974). Gadolinium prepared using topped fluoride and high purity calcium, with the reactants and products handled in an inert atmosphere, showed less C, O, and N contents when W was used as crucible than when Ta was used as the crucible.

5.2.3 Environment

A major source of interstitial impurities in the rare earth metals can be the atmosphere used to handle the starting materials and products. This was clearly brought out by the results given by Beaudry and Palmer (1974) for cerium. A batch of cerium was prepared from topped fluoride and high purity calcium, with the reactants and products handled under purified helium. The residual impurity content was (in ppm), O (15), N (40), H (3), C (15), and F (14). When the metal was prepared from topped fluorides and high purity calcium but handled in air, it contained O (350), N (20), H (10), C (75), and F (20). Many nonmetallic interstitial impurities have their origin in the processing atmosphere, which, incidentally, is the factor to be closely monitored and controlled even during the refining processes designed for elimination of impurities from the as-reduced metals.

5.3 METHODS FOR IMPURITY REMOVAL

Impurities once present in the metal can be removed by a variety of techniques (Beaudry and Gschneidner 1978). Two major types of processes can be distinguished. In one, the

impurities and the metal are separated from each other, and in the other type the impurities are not completely separated from the metal but are only redistributed so that one physical portion of the metal is substantially purer than the other portion. The first process usually involves the description of purification methods, and starting from an as-reduced metal, which may be rather crude, they produce a pure metal, eliminating in the process several key impurities. The second type of process usually belongs to the category of ultrapurification methods and starts from a pure metal and converts it to an ultrapure metal. Often the ultrapurification methods work to remove certain impurities introduced into the metal during the purification process. Both in purification and ultrapurification, a high vacuum or ultra high vacuum is used as the environment, not only for preventing atmospheric impurities from coming into contact with the metal undergoing refining, but also to effect removal of impurities from the metal. In ultrapurification, an inert gas effectively equal in purity to high or ultrahigh vacuum is used for certain metals for specific reasons. Generally, however, a vacuum is the natural accompaniment to high temperature in metal purification processes broadly termed as pyrovacuum treatments, which begin with vacuum melting as the first and major step for all but the four most volatile rare earth metals. Purification of the volatile rare earth metals is effected by another pyrovacuum treatment, vacuum sublimation.

5.4 PYROVACUUM TREATMENTS

Pyrovacuum treatments are the most important and effective means available for the purification of rare earth metals with respect to most of the impurities. The process essentially involves heating of the rare earth metal to temperatures up to or above its melting point, under high vacuum. Heating under vacuum at high temperatures is also necessary in certain purification procedures where the purification occurs not exclusively because of high temperature and low pressure but because of other reasons. Examples are the techniques of zone melting and solid state electrotransport. These are generally not grouped as pyrovacuum treatments. Techniques that are called *pyrovacuum refining treatments* or simply *pyrovacuum treatments* are those where purification occurs because the impurity vaporizes leaving behind the metal, or the metal itself vaporizes leaving behind the impurity. In rare earths refining, the first process occurs in techniques grouped as vacuum melting even though the impurities are distilled off. The second process occurs in techniques grouped as vacuum sublimation or vacuum distillation. The term *vacuum distillation* appears to be specifically reserved for processes involving the distillation of the desired metal. During vacuum melting a variety of processes occur that contribute to rare earth refining. The principal mechanisms are simple distillation (of the impurity), degassing, and certain complex deoxidation reactions.

5.4.1 Distillation

Metallic impurities usually present in as-reduced rare earth metals are calcium, magnesium, iron, nickel, silicon, aluminum, chromium, copper, titanium, molybdenum, tantalum, tungsten, and zirconium. When the rare earth metal is subjected to heating/melting under high vacuum, some of these elements simply distill away while others do not. Which of the elements will distill and to what extent they would be so

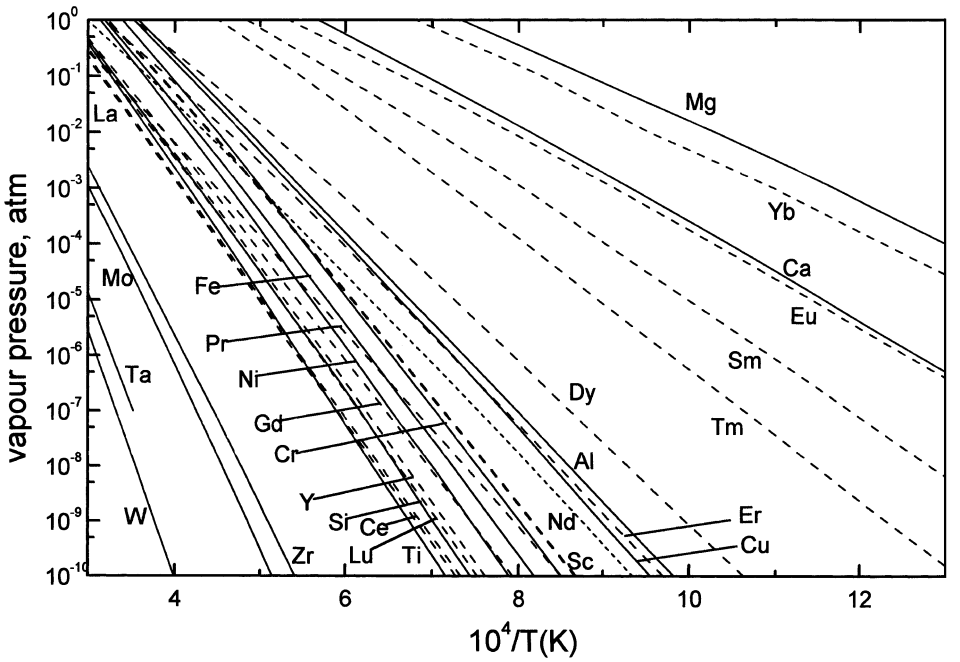

Figure 5.2 Vapor pressures of rare earth and certain impurity elements.

removed depend upon the partial pressures of the impurity metals over the metal/melt. The vapor pressures of pure rare earth metals and also of the impurity metals (Hultgren et al. 1973) are plotted in Figure 5.2. Even at the highest temperature (1850°C) used for vacuum melting of the rare earth metal (Spedding et al. 1968, Beaudry and Gschneidner 1978), among the impurity metals listed, only Ca, Mg, Fe, Si, and Al are more volatile than the least volatile rare earth metals. Nickel and all the refractory metals are substantially less volatile than the rare earth metals. Because impurities are usually present as a dilute solution in the rare earth metals, their partial pressure over the rare earth metals will be considerably less. Taking this into account, the vaporization rate of the impurity element, i, G_i, may be approximated by the following free evaporation equation (Alcock 1976):

$$G_i = 44.32 S_i p_i^0 \sqrt{M_A/T} \text{ g cm}^{-2} \text{ sec}^{-1}$$

when the impurity i is vaporizing from a solution in which its mole fraction is X_i and activity coefficient is γ_i, G_i is given by

$$G_i = 44.32 S_i \gamma_i X_i p_i^0 \sqrt{M_A/T} \text{ g cm}^{-2} \text{ sec}^{-1}$$

Here p_i^0 is the vapor pressure of the pure impurity element i in atmospheres, at the temperature considered, S_i is the vaporization coefficient, which may be equated to 1 as a first approximation, M is the molecular weight of the evaporating species, and T is the temperature in K at which the evaporation is considered. Even though p_i^0 is more, a low

value of X_i and γ_i would seriously limit the vaporization rate. So unless the vapor pressure of the impurity element is quite high, so that p_i ($= \gamma_i X_i p_i^0$) and hence G_i will be substantial at the vacuum melting temperature, no significant refining with respect to the impurity will occur by vacuum melting. These criteria restrict the metallic elements removable from rare earth metals by vacuum melting to Fe, Cu, Al, Mg, and Ca.

The vapor pressures of the rare earth metals are higher or at best of the same order of magnitude as those of the refractory metal impurities. Hence the separation of rare earth metals from these impurities by distilling off the impurities is ruled out. Instead, there is a good possibility of the rare earth metal being distilled off leaving behind the impurities in the residue. This situation arises because of high p_{RE}^0 and hence G_{RE}, forming the basis of rare earth metal purification by distillation.

It is entirely possible that the more volatile impurities are first removed from the rare earth metal by distilling off the impurities by vacuum melting, after which the rare earths are themselves distilled off next from the less volatile impurities. When the vapor pressure of the rare earth is very high, e.g., Sc, Dy, Ho, Er, Lu, even distillation is not necessary. They can be purified by subliming them off from the impurity elements. This applies also to the most volatile of the rare earth metals, Sm, Eu, Tm, and Yb.

5.4.2 Removal of Halogens/Halides

Fluorine and chlorine are the two elements usually found in as-reduced rare earths, and their removal by degassing is important (Croat 1969). They may be present in the rare earth either as unreduced trihalide salt or unremoved reductant salt. Both could either be dissolved in the metal or exist as a second phase adhering to the metal–slag interface or possibly even trapped in pockets beneath the surface of the ingot. For complete removal of these impurities to be possible, their vapor pressures relative to that of the rare earth metal must be sufficiently different.

Dysprosium, holmium, and erbium are the most volatile among all the rare earths prepared by a fluoride or chloride reduction process. The vapor pressures of pure Dy, Ho, and Er relative to the vapor pressure of their pure trifluoride salts and CaF_2 are plotted in Figure 5.3 (Croat 1969). The vapor pressure curves of the metal and the fluoride salts are closely bunched almost at all temperatures, and if the fluorine content removal occurs by fluoride salt evaporation, the chances of metal purification with respect to fluorine impurity does not appear very good.

It must, however, be borne in mind that the relative vapor pressure of components in solution cannot be compared using vapor pressure data for pure components unless the activity coefficients of the system are known. Since the solutions considered in a purification situation are dilute (<0.1%), as a first approximation they may be assumed to follow Henry's law and the partial pressure of the solute or impurity be considered to be proportional to its mole fraction.

In contrast to the trifluoride salts, the trichlorides exhibit considerable vapor pressure, as also shown in Figure 5.3 (Croat 1969). The trichlorides are more volatile by a factor of 1000 than the trifluorides, and the separation of chlorides from the metal should not pose serious problems. The situation is similar regarding the volatility of calcium chloride and lithium chloride vis-à-vis the rare earth metals.

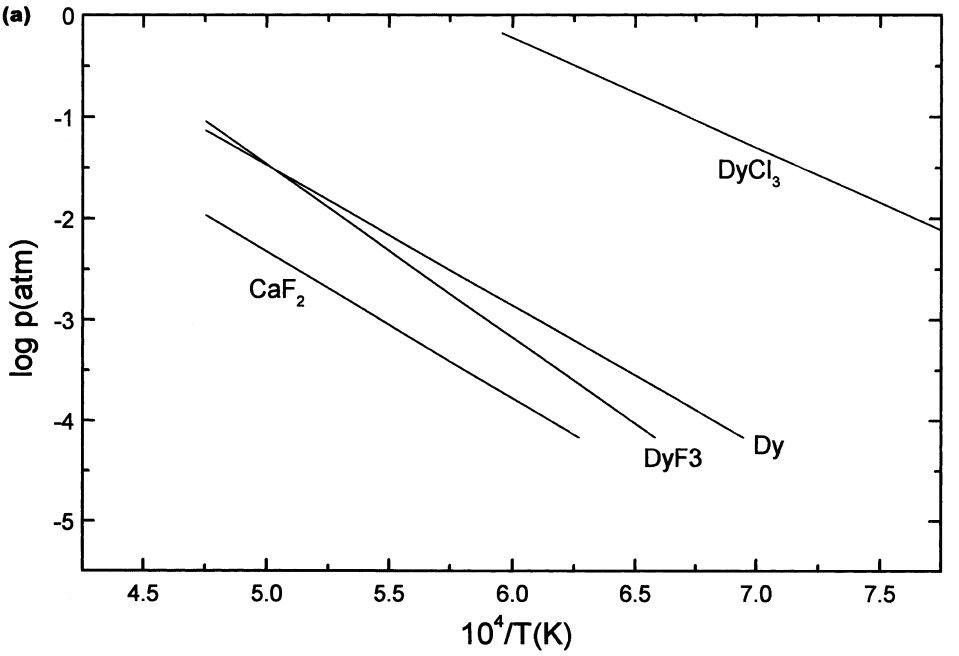

Figure 5.3 Vapor pressures of calcium fluoride, metals and of the trifluoride, trichloride of (a) dysprosium, (b) holmium and (c) erbium (Croat 1969).

5.4.3 Degassing

Among the nonmetallic impurities present in as-reduced rare earth metals, the most critical ones are the gaseous elements hydrogen, nitrogen, and oxygen. Their removal from the rare earths can be termed degassing, and this is one of the most important and also most difficult tasks carried out during pyrovacuum treatment.

The reaction between hydrogen, nitrogen, and oxygen with the rare earth metal can be represented by

$$\frac{1}{2} X_2\,(\mathrm{g}) \leftrightarrow [X]_{\mathrm{RE}}$$

where X stands for H, N, or O and $[X]_{\mathrm{RE}}$ stands for the solution of the gas in the rare earth metal. If these gases have to be removed from solid or liquid rare earths at a useful rate by pyrovacuum treatments, the equilibrium pressure of the gas species over the solution at the degassing temperature must be high. In other words, the following conditions should be satisfied: $p_{X_2} >> p_{\mathrm{RE}}$ and $p_{X_2} >> 1$ mPa.

The first condition is necessary for purification to occur by degassing. The second condition ensures that the degassing occurs at a practically useful rate. Hydrogen, nitrogen, and oxygen behave differently with respect to the above requirements.

Dehydrogenation According to the rare earth metal–hydrogen phase diagrams (Lundin 1961), the composition range of the terminal solid solution between the rare earth metal and

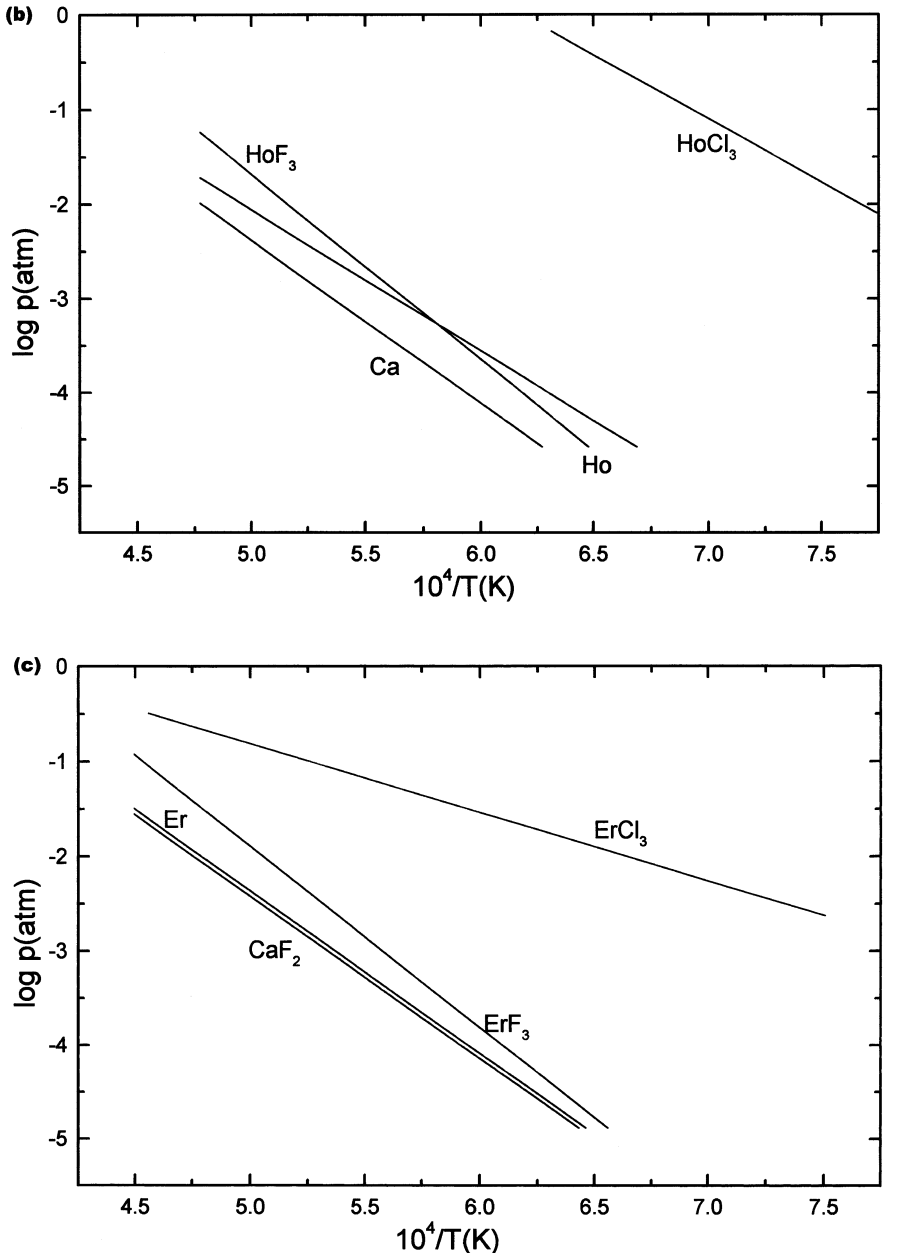

Figure 5.3b, c

hydrogen is considerable, up to ~40 at % hydrogen. In the range of hydrogen concentration usually encountered in as-reduced metals, the hydrogen will invariably be present in the solid solution. Hydrogen elimination will therefore be determined by the pressure–compositional isotherm of the solid solution. These data point to near complete elimination of dissolved hydrogen from the rare earth metals during vacuum melting (Goldschmidt 1967).

Denitrogenation When considering nitrogen removal in as-reduced rare earth metals, it should be noted that the nitrogen content is usually in the range of a few hundred ppm and seldom exceeds 1000 ppm. In this concentration range, nitrogen is present in the rare earths as a solid solution. For example, the solubility limit of nitrogen in cerium at 750°C is 0.3%. Data giving nitrogen pressure in equilibrium with rare earth metal–nitrogen solid solution are sparse. The data on the free energy of formation of rare earth nitrides (Pankratz et al. 1984) indicate that the mononitrides of rare earths are stabler than the lowest nitrides (M_2N) formed by group V metals vanadium, niobium, and tantalum but are not quite as stable as those formed by the group IV metals titanium and zirconium. The decomposition pressures of these nitrides are low. The equilibrium nitrogen pressure over the rare earth metal–nitrogen solid solutions would be considerably lower. The rare earth would not easily degas with respect to nitrogen during vacuum melting (Goldschmidt 1967). Incidentally, the equilibrium nitrogen pressure over the RE–N solid would equal or exceed the vapor pressure of the metal itself for most of the rare earth metals.

Deoxidation Among the nonmetallic impurities in rare earth metals, oxygen is the most important and invariably the nonmetallic element present in greatest concentration in the as-reduced metal. Concentration of a few thousand ppm of oxygen in as-reduced metal is not uncommon and the higher limit of the oxygen content may extend to 1% (Kremers 1961). The solution between the rare earth metal and oxygen has a large range (Massalski et al. 1990) and deoxidation ultimately involves removal of oxygen from the rare earth metal–oxygen solid solution. Even in metal–oxygen solutions of much lower stability than those of the rare earths (e.g., V–O, Nb–O, Ta–O system), equilibrium oxygen pressures over the solution are so low that deoxidation by degassing of oxygen is never considered as a possibility. A look at the oxygen partial pressure data on the V–O, Nb–O, or Ta–O solid solution at any temperature indicates that deoxidation of these metals by evolution of gaseous oxygen is not possible because at all temperatures the partial pressure of oxygen over the solution is considerably lower than the partial pressure of the metal itself (Fromm and Horz 1980). The concentration of oxygen in these metals, however, decreases considerably during pyrovacuum treatments. This has been explained (Smith 1958, Brewer and Rosenblatt 1962, Garg and Sundaram 1974) as due to the formation and evaporation of certain complex oxide species.

Sacrificial deoxidation The formation of volatile suboxides of several reactive and refractory metals and their evaporation from metal–oxygen systems was postulated and experimentally verified by mass spectrometric investigations in the 1950s and 1960s (Smith 1958, Ingram and Drowert 1960). Smith (1958), in his original paper on sacrificial deoxidation, listed yttrium as one of the metals that will deoxidize by suboxide vaporization. It has been verified from experimental observations that several rare earth elements do form suboxides. The formation and evaporation of volatile suboxides of a metal is by itself not a sufficient criterion for a metal to deoxidize. There are other factors, as described below.

The formation of a rare earth metal suboxide, (REO) may be represented as follows:

$$[O]_{RE} + RE = (REO)$$

The square brackets represent the solution and the parentheses represent the gas phase. The standard free energy of formation of the gaseous suboxide becomes more negative with an increase in temperature in the same way as the stability of CO increases with an increase in temperature (Pankratz et al. 1984). When the volatile suboxide forms and evaporates, not only an oxygen atom is removed from the metal, but a metal atom is also lost (or sacrificed).

This process of deoxidation thus earned the name sacrificial deoxidation. Initially Smith (1958) concluded that in all metal–oxygen systems where the ratio of the vapor pressure of the suboxides to that of the metal, p_{MO}/p_M, is more than 1, sacrificial deoxidation can lead to purification of the metal with respect to oxygen. In his original paper, he listed yttrium also as one of the metals amenable to sacrificial deoxidation because p_{yo}/p_y was 10^3 at the vacuum treatment temperature. Several exceptions were subsequently found to this conclusion, and the ability to refine the metal by sacrificial deoxidation was found to depend on the R ratio value as defined (Brewer and Rosenblatt 1962) below:

$$R = \frac{[C_O/C_M]_{vapor}}{[C_O/C_M]_{metal}}$$

where C_O and C_M are the concentration (in at %) of oxygen and metal in the phases indicated by subscript. The R value essentially gives the relative concentration of oxygen in the vapor phase to that in the condensed phase. At a given temperature, the R value changes with a change in the oxygen content. However, Garg and Sundaram (1974) have pointed out that if the monoxide and monatomic metal are the only species in the vapor phase, and if the oxygen is in the concentration range where it obeys Henry's law, the R factor approaches a limiting value independent of concentration at any temperature. The magnitude of the limiting R value determines the possibility of sacrificial deoxidation. If this value is more than 1 then the metal can be purified by sacrificial deoxidation.

The R values for rare earth metal–oxygen systems have not been computed. The requisite data, namely the vapor pressure of suboxide as a function of oxygen content, are not available. Certain conclusions, however, may be derived from experimental observations on deoxidation during pyrovacuum treatment of oxygen containing rare earth metals. There are two other pyrovacuum deoxidation processes that might be useful for residual oxygen removal from the rare earth metals. These are called carbon deoxidation and silicon deoxidation.

Carbon deoxidation Carbon deoxidation is based on the occurrence of the following reaction

$$[O]_{RE} + [C]_{RE} = (CO)$$

between oxygen and carbon dissolved in rare earth metals. Oxygen is present in the metal and a suitable quantity of carbon may be purposely added to encourage carbon deoxidation.

The occurrence of carbon deoxidation basically depends on the reaction given above leading to the establishment of a sufficient CO partial pressure over the RE–C–O system. The partial pressure of CO is related to the thermodynamic properties of the RE–C–O system by the following equation:

$$p_{CO} = \gamma_c X_c \gamma_o X_o \exp(-\Delta G^o_{CO}/RT)$$

where γ_c, γ_o and X_c, X_o are the activity coefficients and atom fractions of carbon and oxygen in the rare earth metals, respectively. If the values of these parameters are such that a sufficient CO pressure is established at the vacuum melting temperatures even at low oxygen contents, oxygen is removable by carbon deoxidation. Here again to estimate the feasibility of carbon deoxidation the thermodynamic parameters γ_c and γ_o must be known. Data are

not available currently for the rare earth systems. The feasibility of carbon deoxidation in RE–C–O systems has to be assessed from experimental observations on deoxidation during pyrovacuum treatments of carbon-doped rare earth–oxygen alloys.

Silicon deoxidation The deoxidation by silicon occurs in certain refractory metal–oxygen–silicon systems through the formation and evaporation of silicon monoxide (Awasthi et al. 1998). The possible occurrence of silicon deoxidation in rare earth–oxygen alloys containing silicon may be represented by

$$[O]_{RE} + [Si]_{RE} = (SiO)$$

Calculation of silicon monoxide pressure and the estimation of silicon deoxidation tendency in the rare earth systems rely on the activity coefficient values for oxygen and silicon being available. The development of good SiO pressure even at low Si and O contents in rare earths is key to the silicon deoxidation's usefulness. In the deoxidation of group V metals, silicon deoxidation is proving to be more efficient than carbon deoxidation. In the case of rare earth metals, the lack of thermodynamic data on the activity of silicon and oxygen in the metals precludes estimation of silicon deoxidation tendencies. Experimental observations on the pyrovacuum treatment of rare earth metal containing oxygen and doped with silicon forms the basis, presently, for assessing the silicon deoxidation tendencies of rare earth metals.

The success of sacrificial, carbon, and silicon deoxidation processes for oxygen removal from the refractory metals like niobium is not only due to favorable values for the activity coefficients of oxygen, carbon, silicon, and also the free energy of formation of niobium monoxide, but also due to the metal's high melting point and low vapor pressure. The last two properties enable the deoxidation treatments to be conducted at high temperatures under conditions of enhanced suboxide stability. Solid state processing enhances the more desirable carbon and silicon deoxidation at the expense of the sacrificial mode of oxygen removal, which incidentally is more favored when the metal is molten (Garg and Sundaram 1975, Kruger 1971). Rare earth metals, in comparison, are low melting and are also more volatile. These two factors limit the extent to which carbon and silicon deoxidation processes can be useful for oxygen removal.

The high volatility of many of the rare earth metals puts the spotlight on another method of refining for freeing the rare earth metal from oxygen. This option is to distill off the rare earth metal while leaving behind an oxygen-enriched residue. Unlike in the deoxidation procedures discussed above where a high volatility of the suboxide and other oxides is desired, when the metal is distilled off from an oxide-enriched residue, the volatility of oxygen containing vapors is unwelcome. However, the enrichment of oxygen in the melt actually encourages the evaporation of the oxygen containing vapors.

Removal of Carbon and Silicon Carbon is very much less volatile than even the least volatile of the rare earth metals. So when a rare earth metal containing only carbon as impurity is pyrovacuum treated, an increase in carbon concentration in the metal will result because of the preferential removal of the metal as vapor. The only method by which carbon can be removed in such a situation is by forming a volatile compound, and carbon monoxide is the compound formed in many refractory metal systems that contain residual carbon impurity to be removed. Carbon deoxidation, when feasible, is not only useful for deoxidizing a metal but also for decarburizing it. By introducing oxygen in carbon-contaminated rare earth metal, the system becomes RE–C–O, and under pyrovacuum conditions the evolution of carbon monoxide can ultimately bring down the

level of residual carbon. The ideal situation exists when carbon and oxygen are removed only by CO evolution, i.e., exclusive carbon deoxidation, because in such a situation a precise quantity of oxygen doping will result in a predictable extent of carbon removal. As mentioned, however, the key factor is the occurrence of carbon deoxidation in RE–C–O solid solution, which has yet to be established. Pure silicon is more volatile than carbon and also some of the rare earths. However, when present in low concentrations, silicon will not distill from the rare earth metals. In the same way that carbon removal can be attempted through the formation of CO, silicon removal can occur through SiO vaporization. The feasibility of silicon removal by this reaction depends on the feasibility of silicon deoxidation from RE–Si–O solid solution.

The process of carbon and silicon removal from rare earth is not so easy as described above; therefore, the alternative of distilling off the rare earth metal and leaving behind a carbon- and/or silicon-enriched residue may be considered. The practicability of this approach depends on the rare earth metal vapor pressure. As noted elsewhere, many of the rare earth metals are rather volatile, and in those cases distilling of the rare earth metal from the carbon and silicon impurities becomes the practically useful approach.

5.5 PYROVACUUM TECHNIQUES

The metallothermic reduction of a rare earth metal is usually completed by pyrovacuum treatment that essentially comprises vacuum melting and/or vacuum distillation. The rare earth metals often contain many impurities that do not volatilize off during vacuum melting. Except perhaps oxygen, however, all these impurities will remain in the residue and possibly not interfere when the metal is distilled off and collected. Thus both the options of pyrovacuum treatment — vacuum melting, which relies on the distilling off of the impurities either in elemental form or as certain compounds, and vacuum distillation, which relies on distilling off of the metal and leaving the impurities behind in the residue — are useful in pyrovacuum refining of the rare earth metals. As may be anticipated, vacuum melting and vacuum distillation are serially combined in the overall process sequence.

The rare earth metals could be divided into four groups primarily on the basis of their volatility. In the post-reduction vacuum treatment, each group is processed somewhat differently.

5.5.1 Lanthanum, Cerium, Praseodymium, and Neodymium

These four light rare earths are characterized by relatively low melting points, very high boiling points and hence extremely low vapor pressures at the melting point. High temperature vacuum melting is the only process by which they are purified. Distillation is ruled out on account of their low vapor pressure.

As-reduced La, Ce, Pr, and Nd from the fluoride process just separated from the CaF_2 slag contain Ca, CaF_2 and F, and H. The rare earth metal containing these impurities readily reacts with moisture, and the as-reduced metal should always be handled under an inert atmosphere. All these impurities are more volatile than the rare earth metals and are removed by melting the metals in a vacuum. Melting at pressures less than 0.1 Pa was

adequate for removing calcium. Calcium content thereby decreased from over 1% to less than 150 ppm. Although removal of Ca and H occurs by heating the metal to just above its melting point, the quantitative removal of fluorine, which can be as high as 500 ppm in the as-reduced metal, required heating to at least 1800°C for 30 min.

In the Ames practice (Beaudry and Gschneidner 1978), vacuum melting of La and Ce was carried out at 1850°C; for Pr the temperature was 1750°C, and for Nd it was 1650°C. The melting lasted at these temperature for 10 min. Heating was done in an induction furnace and a tantalum crucible was used. At the high temperatures used for vacuum melting, the rare earth metals dissolve a considerable amount of tantalum (Dennison et al. 1966, 1966a). However, the solubility of tantalum in these metals decreases with temperature and it is very low at the melting point. This information was utilized in restricting the amount of tantalum impurity in the rare earth metal.

After vacuum melting the metals at high temperature, the furnace was slowly cooled to about 10°C above the melting point of the metal to allow the Ta to precipitate out of the solution and settle to the bottom of the crucible. Empirically the time needed for complete settling of the tantalum was estimated at 24 min per cm height of the liquid metal column (Beaudry and Gschneidner 1978). Later when the ingot was removed from the furnace, the thin tantalum crucible and the dendrites that had settled to the bottom of the crucible were machined off.

Typical analysis of La, Ce, Pr, and Nd prepared by calcium reduction of topped rare earth fluoride, followed by vacuum melting, is given in Table 5.1. During these processes the reactants and products were handled under inert gas cover.

Table 5.1 Preparation method and major impurities in lanthanum, cerium, praseodymium, and neodymium (Beaudry and Gschneidner 1978)

Method: Ames Process

Calciothermic reduction of rare earth trifluoride in a tantalum crucible. As-reduced metal was purified by vacuum melting in a tantalum crucible, and the tantalum ingested into the metal was removed by precipitating it out in the molten metal and machining off the precipitate from the solidified rare earth metal ingot. The entire process was carried out in a protected atmosphere of purified inert gas.

Major Impurities

Impurity element	Content, ppm			
	Lanthanum	Cerium	Praseodymium	Neodymium
C	11	4	7	9
O	35	44	43	35
N	5	7	5	6
H	2	2	1	2
F	10	15	5	3
Ca	<0.1	<0.1	0.1	<0.1
Pt	<0.1	<1	<1	<1
Ta	5	8	12	25

Table 5.2 Typical analysis of as-reduced yttrium metal* (Daane 1961, Huffine and Williams 1961)

Impurity	Metal produced by direct Ca reduction of YF_3	Metal produced by Ca reduction of YF_3 through the Y–Mg alloy process	Arc melted yttrium metal ingot
O	1400 to 2000	1500 to 2000	2750
N	200	150	190
F	500	800	750
C	100	200	110
Ta	4000	–	–
Ti	–	1500	–
Zr	–	–	5800
Ca	10	10	5
Mg	–	30	20
Fe	300	–	620

*These analyses refer to different batches of metals. The metal in column 1 was produced in a tantalum crucible, for the metal in column 2 the crucible was titanium, and the reduction of metal in column 3 was carried out in a zirconium crucible.

5.5.2 Yttrium, Gadolinium, Terbium, and Lutetium

The complete pyrovacuum purification sequence for these metals consists of a high temperature vacuum treatment followed by distillation. The volatile impurities calcium, magnesium, and the fluorides do not pose a serious problem with these metals because they are distilled off during the high temperature vacuum melting.

The analysis of yttrium metal produced by direct calciothermic reduction of YF_3 in the as-reduced form, just separated from CaF_2 slag, is given in Table 5.2. The analysis of the metal produced by the Y–Mg intermediate alloy process after removal of Mg but before any refining treatment is also listed in the table. A variety of pyrovacuum treatments have been investigated for refining as-reduced yttrium. In addition to melting in tantalum crucibles in an induction furnace, other methods of vacuum melting have also been used. Yttrium metal sponge obtained after "demagging" Y–Mg alloy has been purified by consumable electrode arc melting (Daane 1961). The demagged metal sponge has a calcium and magnesium content of 100 ppm each. To arc melt, these granular sponge particles were pressed into sticks that were welded end to end to make the electrode, and this electrode was consumable arc melted into a 100 mm diameter ingot in a vacuum. The 100 mm diameter ingots so obtained were welded together to make a 1525 mm long electrode, which was arc melted in a vacuum into 150 mm diameter ingots. A typical analysis of 150 mm diameter ingot thus obtained was: Ca less than 10 ppm, Mg 30 ppm, and O 500 to 1650 ppm. This ingot had a titanium content of 0.5 to 1.5%, derived mainly from the titanium crucible in which it was demagged. Titanium was not removed from yttrium by arc melting. Consumable electrode arc melting of yttrium, the first melt in an argon atmosphere and the second in a vacuum at a nominal pressure of 0.1 Pa, typically yields a metal with the analysis listed in Table 5.2. There is a decrease in the residual calcium content in the metal to about 5 ppm and that of magnesium to about 20 ppm (Huffine and Williams 1961). Arc melting caused little change as far as other impurities in yttrium are concerned.

Table 5.3 Analyses of yttrium ingot before and after electron bombardment melting (Huffine and Williams 1961).

Impurity	Content, ppm	
	Before melting	After melting*
O	3250	3470
N	200	310
Zr	5000	4000
Cr	150	100
Fe	1000	190
Ni	2000	2000
Cu	–	100

*In the section of the electron bombardment melted ingot having the highest overall purity.

One of the major improvements in the vacuum melting process has been the use of electron bombardment as a method of heating (Smith et al. 1959). Temescal Metallurgical Corporation developed the electron bombardment furnaces for conducting vacuum metallurgical processes, and the process was more often referred to as electron beam melting. This technique was considered a great improvement over arc melting in a vacuum because in electron beam melting it was possible to maintain pressures of about 0.01 Pa or less in the immediate vicinity of the melting metal. Such pressures lead to volatilization processes proceeding more rapidly and to a greater degree of completion. As the melting metal would be made to drop off the feed stock, a large surface of the material was exposed and this also enhanced the purification reactions.

The results of electron bombardment melting of yttrium (Huffine and Williams 1961) are given in Table 5.3. The purpose was to decrease the considerable oxygen content in yttrium by electron beam melting but the results were not encouraging.

A more detailed investigation of electron beam melt refining of yttrium was carried out by Anable and Beall (1965) at the Albany Metallurgy Research Center of U.S. Bureau of Mines. Their purpose was to investigate the purification of commercially available yttrium by melting it in an electron bombardment furnace. Segments of yttrium weighing about 50 grams were melted on a water-cooled copper hearth in the electron beam melting furnace. The samples were melted at power levels corresponding to temperatures in the range 1730 to 1770°C at low pressure (7×10^{-3} Pa to 13×10^{-3} Pa) for 1 to 120 minutes. The samples were cooled in a vacuum before they were removed from the furnace and analyzed.

The results of yttrium purification are listed in Table 5.4. On electron beam melting, except for nickel, silicon, and zirconium, the concentration of all other listed metallic impurities lowered significantly. The aluminum content decreased from 50 to 30 ppm within a few minutes of exposure at all power levels except the lowest power level used. After exposure for 2 h, the Al content decreased to 10 ppm. The iron and copper were removed slowly throughout the two hours of exposure. The iron content came down from 100 to less than 50 ppm, and the copper content was lowered from 40 to 5 ppm. In the minimum exposure period of 20 min, the concentrations of magnesium and manganese decreased from 420 to <5 ppm and from 30 to <5 ppm, respectively. No change occurred in the nickel and zirconium contents, which were originally at 100 and 3000 ppm, respectively.

Table 5.4 Purification of yttrium by electron beam melting (Anable and Beall 1965)

Temperature, °C	Duration of melt, min	Weight loss, %	Analysis, ppm									
			Al	Cu	C	Fe	H	Mg	Mn	N	O	Si
Start material			50	40	545	100	50	420	36	178	5860	100
1730	20	6.2	50	30	310	90	<0.5	<5	<5	220	8000	50
1730	120	24.4	50	5	440	<50	<0.5	<5	<5	240	10000	60
1745	20	10.0	30	30	230	90	<0.5	<5	<5	170	7500	80
1745	120	28.1	10	5	440	50	<0.5	<5	<5	210	12000	90
1760	20	11.1	30	30	240	90	<0.5	<5	<5	190	6000	50
1760	120	37.3	10	5	470	<50	<0.5	8	<5	250	11000	80
1770	20	10.3	30	30	220	90	<0.5	<5	<5	210	5500	50
1770	120	37.5	10	5	510	<50	<0.5	<5	<5	240	12000	60

The nickel and zirconium content remained constant at 100 and 3000 ppm, respectively.

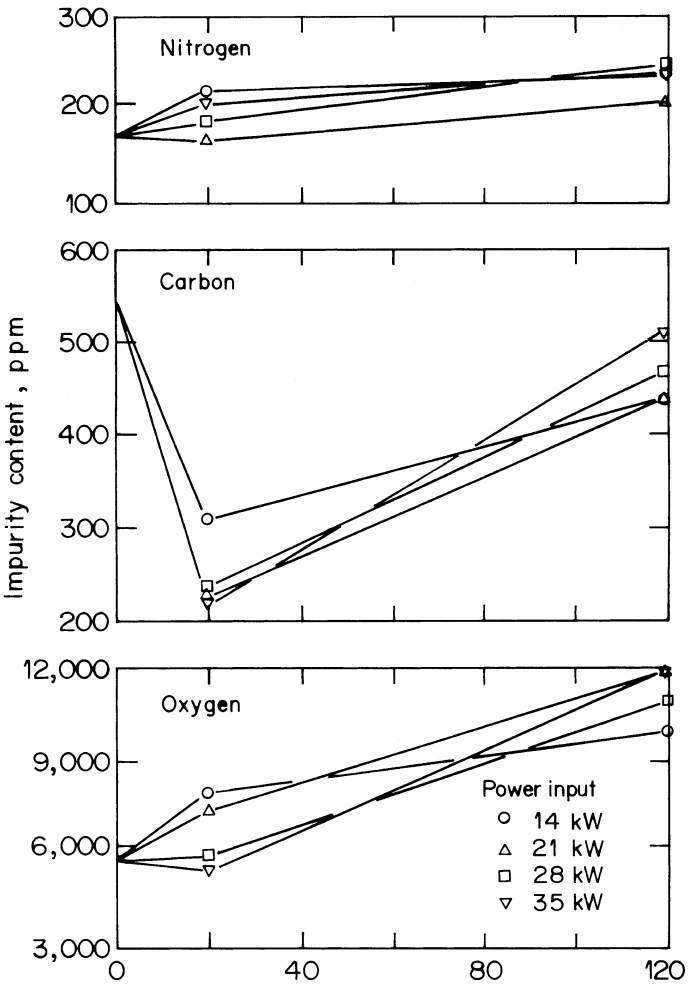

Figure 5.4 Oxygen, carbon and nitrogen contents in electron beam melted yttrium (Anable and Beall 1965).

The silicon contents of all the samples decreased initially, in the first 20 minutes, from 100 ppm to about 50 ppm. The silicon content increased slightly to 60 ppm after 2 h of exposure.

The changes in the oxygen, carbon and nitrogen content in yttrium during electron beam melting at various power levels (temperatures) are shown in Figure 5.4. The oxygen content increased only by electron beam melting. The increase in oxygen content came about partly from the rapid loss of yttrium and partly from oxygen pickup, probably resulting from degassing of the furnace and from the small amount of oxygen that constantly leaked into the furnace. These data do not point to the occurrence of sacrificial deoxidation of yttrium.

The carbon content of yttrium decreased initially from 545 ppm to 220 ppm during electron beam melting at 1770°C but on continued melting increased to a maximum of 510 ppm. This trend points to the possible occurrence of carbon deoxidation in the initial stages

Table 5.5 Behavior of carbon, oxygen, and nitrogen during electron beam melting of yttrium (Anable and Beall 1965)

Temperature, °C	Duration of melt, min	Weight loss, %	Analysis, ppm		
			Carbon	Nitrogen	Oxygen
Start material			545	178	5860
1745	1	7.5	330	190	4950
1745	2	4.0	330	290	5200
1745	3	5.5	350	180	5150
1745	4	6.2	380	270	5100
1745	5	6.5	430	300	5300

of melting. Specific experiments by Anable and Beall (1965) where the duration of melting was up to 5 min (Table 5.5) and samples were analyzed every minute suggested the possibility of a carbon deoxidation in the early phase of the operation: the carbon level came down from 545 to 330 ppm in the first minute and the oxygen content decreased from 5860 ppm to 4950 ppm during this period. A minimum level of oxygen was attained when yttrium was held molten for 1 min. Interestingly, the oxygen content of yttrium during the first 5 min of melting was lower than any value observed between 20 and 120 min. In contrast, the lowest carbon values were consistently obtained after 20 min rather than after 1 to 5 min. Anable and Beall (1965) concluded that a carbon reduction of oxygen was not involved because the oxygen loss is an order of magnitude greater than the carbon loss and the oxygen loss occurred considerably earlier in the operation. It must be noted, however, that the only way carbon can be removed at ~1750°C in vacuum from the yttrium considered here is by forming CO. Secondly, carbon deoxidation need not occur exclusively and thus can result in the removal of only a part of oxygen. The other part of oxygen removed may be accounted for by loss occurring due to suboxide, YO, vaporizing. The possibility of CO and YO vaporizing from the alloy cannot be ruled out. A mass spectrometric work, similar to the one carried out by Anable (1970) for vanadium, could possibly clarify the picture.

The nitrogen content of yttrium remained nearly constant during electron beam melting. Some of the samples showed higher nitrogen content than the original metal. These observations are consistent with the expected behavior of no degassing of nitrogen from yttrium during pyrovacuum treatment. The increased nitrogen content may have the same explanation as increased oxygen content observed in the sample, on a minor scale.

Having concluded that yttrium does not undergo sacrificial deoxidation during electron beam melting, Anable and Beall (1965) attempted doping of oxygen-contaminated yttrium with a small amount of a second metal or compound, so that a volatile compound that could be removed by evaporation might form. They investigated as many as 17 metallic additives and 3 compounds in addition to carbon. Among the metals investigated, titanium and zirconium are known to form volatile suboxides that can be used for refining refractory metals (Garg and Sundaram 1975). Carbon and silicon are already the well-known deoxidizing agents in pyrovacuum treatments. Electron beam melting of doped yttrium was carried out at 1745°C and the metal was held molten for 5 min. The results of doping experiments did not show any decrease in oxygen content. Apparently, yttrium did not deoxidize by the sacrificial mode, nor did it undergo carbon or silicon deoxidation. Other pyrovacuum deoxidants like titanium and zirconium also failed with

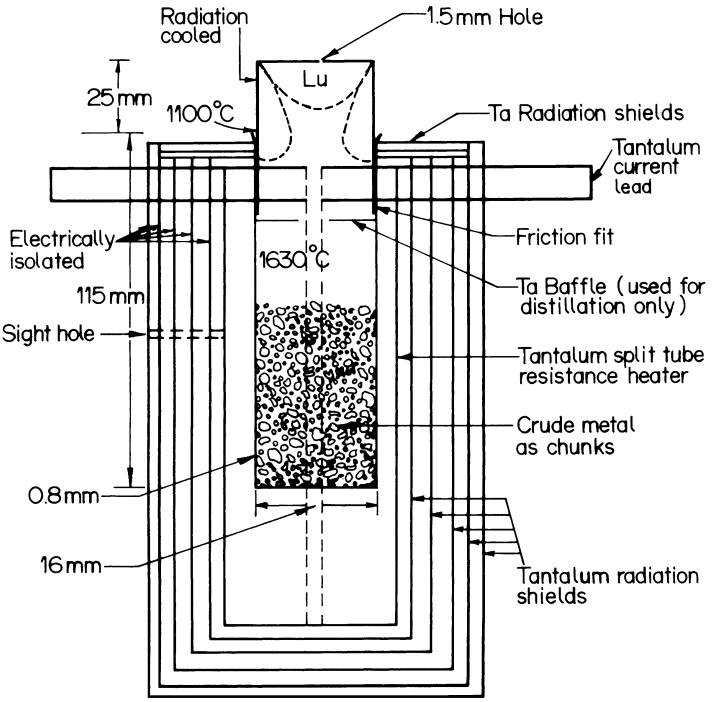

Figure 5.5 Tantalum split resistance furnace used in 1.3×10^{-6} Pa vacuum system to sublime rare earth metals. The temperatures shown are typical for lutetium sublimation (Spedding et al. 1970).

yttrium. Electron beam melting of yttrium decreased the residual fluorine content. The fall in fluorine content in yttrium from 0.06 to 0.002% was attributed to the evaporation of volatile oxyfluorides during electron beam melting (Carlson et al. 1960).

Electron beam melting has also been used for the purification of electrorefined gadolinium (Nagai et al. 1978, Zwilling and Gschneidner 1978). On electron beam melting, the fluorine content decreased from about 0.2% to less than 10 ppm. The hydrogen content also decreased to low levels.

The removal of Ca, Mg, and fluorine has not been a serious problem in these metals, and it is achieved by pyrovacuum treatment by induction melting or electron beam melting. The real challenge is posed by oxygen in these metals. In yttrium and gadolinium the oxygen content is not significantly decreased by induction or electron beam melting.

In the same manner as in the first group of metals (La, Ce, Pr, and Nd) discussed, the use of tantalum crucible in a vacuum melting at ~1800°C leads to the dissolution of a certain amount of tantalum in the metals Y, Gd, Tb, and Lu. Unlike in the four light rare earths, however, the tantalum solubility in Y, Gd, Tb, and Lu does not decrease much on decreasing the temperature to the melting point, and therefore the tantalum in the solution does not precipitate out. The only pyrovacuum way to remove tantalum is by distilling off the rare earth metals, leaving tantalum in the residue. However, under certain circumstances distillation can be avoided. If tungsten crucibles were used instead of tantalum in reduction and vacuum melting, tungsten would dissolve in the rare earth. But after vacuum

melting in these metals, tungsten could be precipitated out in exactly the same way as Ta was allowed to settle in La, Ce, Pr and Nd. This alternative is available if the 0.012 at % W that would persist in the Gd after precipitation can be tolerated. Similarly, at the end of precipitation, 0.03 at % W will remain in Tb and 0.07 at % W in yttrium (Dennison et al. 1966a, Beaudry and Gschneidner 1978).

The distillation of Y, Gd, Tb, and Lu was carried out at Ames in tungsten crucibles because refluxing of some of the distilled metals eroded the tantalum crucibles causing them to leak. A tungsten lined condenser was used since tantalum diffuses into the hot condensate more readily than tungsten. The distillation unit at Ames (Beaudry and Gschneidner 1978, Spedding et al. 1970) is shown in Figure 5.5. The distillation column was prepared from 0.76 mm tantalum and measured 125 mm by 40 mm in diameter. The condensers were prepared from 0.127 mm tantalum and were lined, leaving the lid, with 0.025 mm tungsten foil. The furnace used for distillation was a split tube tantalum resistance furnace 175 mm by 65 mm in diameter. The heater was made from 0.05 mm tantalum and was surrounded by 5 cylindrical radiation shields spaced approximately 6 mm apart. The sublimation column was suspended inside the heater by flaring the mouth of the column and dropping it through a tight-fitting hole in the top radiation shielding.

The reactor chamber housing the furnace system was a stainless steel ball jar, which was double walled for water cooling and had a quartz sight glass for optical temperature measurement. The vacuum system for this chamber consisted of a 400 lps ion pump and a 4000 lps titanium sublimator pump, and these pumps evacuated the system to 1.3×10^{-6} to 1.3×10^{-7} Pa after it was initially evacuated to <0.6 Pa with a 425 lpm fore pump.

The details of pyrovacuum treatment such as temperatures of vacuum melting and distillation, the impurities that usually remained, the temperature of the condenser, the typical size of the run and distillation rate are all summarized (Beaudry and Gschneidner 1978) in Table 5.6. The distillation rate was quite slow (~1 g/h), and in a week only 168 g of metal was purified. However, a slow rate of distillation helped minimize the impurity transfer from the crucible to the distillate. In commercial practices a much higher distillation rate was used. The vacuum required in the distillation assembly was better than 1.3×10^{-6} Pa so that contamination of the distillate was prevented.

The oxygen contents of Y, Gd, and Tb were not decreased even by distillation. This has been reasoned by Spedding et al. (1968) as due to the co-distillation of the volatile oxides YO, GdO and TbO. The vapor pressure of these volatile oxides is high enough in the rare earth matrix that they distill along with the metals. According to Spedding et al. (1968), for each metal at a given temperature of distillation a constant boiling mixture is apparently reached where the two species, metal and suboxide, came over in the same ratio and repeated distillations led to very little improvement. This points to the possibility that the R value of the sacrificial deoxidation is 1 for these metals. In this situation volatile metal suboxides vaporize but there will be no decrease in the oxygen content.

Among all the rare earth metals, yttrium is especially troublesome with oxygen impurity (Spedding et al. 1968). It is the most difficult element from the standpoint that under similar conditions of preparation the oxygen content of the final metal is likely to run the highest of all the rare earths or even rare earth-like elements. The only way out seems to be in preparing the original metal with as little oxygen as possible by starting with very pure raw materials and by taking great pains to carry out all operations in highly purified inert atmosphere.

Table 5.6 Preparation method and major impurities in yttrium, gadolinium, terbium, and lutetium (Beaudry and Gschneidner 1978)

Method: Ames Process

Calciothermic reduction of rare earth trifluoride in a tantalum crucible. As-reduced metal was purified by vacuum melting in a tantalum crucible and the tantalum ingested into the metal was removed by a vacuum distillation step. For vacuum distillation of yttrium, gadolinium, and terbium, tungsten crucibles and tungsten-lined tantalum condensers were used, whereas for lutetium, which could be purified by vacuum sublimation, tantalum crucible and tungsten-lined condenser were used. Pure metal was collected as the condensate. Tantalum impurity remained in the residue. The entire process was carried out in a protected atmosphere of purified inert gas or under high vacuum as appropriate.

Process conditions	Yttrium	Gadolinium	Terbium	Lutetium
Vacuum melting				
Temperature, °C	1850	1800	1750	1800
Vacuum, Pa	1.3×10^{-4}	1.3×10^{-4}	1.3×10^{-4}	1.3×10^{-4}
Vacuum distillation				
Crucible temperature, °C	1725	1725	1575	1645
Condenser temperature, °C	900	900	800	850
Vacuum, Pa	1.3×10^{-6}	1.3×10^{-6}	1.3×10^{-6}	1.3×10^{-6}
Distillation rate, $g\cdot hr^{-1}$	1	1.5	1.5	1
Run size, g	150	250	225	250

Major Impurities

Impurity	Content (ppm)			
	Yttrium	Gadolinium	Terbium	Lutetium
C	20	18	10	16
O	58	48	67	100
N	3	1	8	4
H	4	2	6	3
F	<3	<3	<3	<3
Ca	0.5	<0.5	0.1	<0.1
Pt	<0.1	<0.1	<0.1	<0.2
Ta	2	4	14	<3
W	24	<0.4	7	<24

5.5.3 Scandium, Dysprosium, Holmium, Erbium, and Lutetium

These metals have appreciable vapor pressure at their melting points. The vacuum melting, therefore, had to be relatively brief or much of the metal would be lost by distillation. The temperature and duration of vacuum melting normally practiced (Beaudry and Gschneidner 1978) are listed in Table 5.7.

Fluorine impurity, which was removed relatively easily in the two groups of rare earth metals described earlier, was particularly difficult to remove from this group of metals.

Table 5.7 Preparation method and major impurities in scandium, dysprosium, holmium, and erbium (Beaudry and Gschneidner 1978)

Method: Ames Process

Calciothermic reduction of rare earth trifluoride in a tantalum crucible. As-reduced metal was purified by vacuum melting in a tantalum crucible, and the tantalum ingested into the metal was removed by a vacuum distillation step. Tantalum crucibles and tantalum condensers were used. Pure metal was collected as the condensate. Tantalum impurity remained in the residue. The entire process was carried out in a protected atmosphere of purified inert gas or under high vacuum as appropriate.

Process conditions	Scandium	Dysprosium	Holmium	Erbium
Vacuum melting				
Temperature, °C	1550	1440	1480	1540
Time, min	10	45	45	30
Vacuum sublimation				
Crucible temperature, °C	1425	1175	1220	1300
Condenser temperature, °C	900	700	725	825
Sublimation rate, $g \cdot h^{-1}$	1	2.5	2.1	2.1
Run size, g	100	1000	600	1000

Major Impurities

Impurity	Content (ppm)			
	Scandium	Dysprosium	Holmium	Erbium
C	15	8	4	11
O	95	39	30	22
N	8	1	3	1
H	8	6	4	1
F	8	14	6	5
Ca	0.5	<1	0.5	<0.1
Pt	<0.2	<0.3	<0.1	<0.5
Ta	2	25	<0.8	7
W	77	<1	1	9

When these metals were vacuum melted for the length of time given in the table (this time necessary for quantitative removal of the fluorine impurity) there was substantial metal loss by vaporization. This amounted to 30% for Sc and Dy, 20% for Ho, and 10% for Er. This evaporated metal and the volatilized impurities were, however, collected in a Ta cylinder placed above the crucible to facilitate easy recovery of the metal. The duration of vacuum melting could be shortened and hence metal loss decreased if several hundred ppm impurities can be tolerated in the final product.

The removal of fluorine from Dy, Ho, and Er was also investigated by Croat (1969). A single batch of 1070 gms of as-reduced Dy was vacuum melted at approximately 1450°C for 5 min. In the process, 345 gms (approximately 30%) of the metal distilled out of the crucible but was collected. This distillate contained 6500 ppm fluorine and 3000 ppm Ca.

The remaining undistilled metal was found to contain 119 ppm fluorine and 20 ppm Ca. Similar results were obtained for Er. During vacuum melting, 20% of the metal was removed. The distillate contained 1300 ppm fluorine and the melt had only 32 ppm.

The other part of pyrovacuum treatment in the refining of Sc, Dy, Ho, and Er is sublimation. The high volatility of these metals is an advantage here and purification of metals by sublimation is comparatively easy. Tantalum introduced in the metals during the vacuum melting step was removed by subliming off the metal. The common interstitial impurities N, C, and O formed stable compounds and remained in the residue when these metals were sublimed at a slow rate. Because this operation was so effective, the great care taken to remove oxygen from fluoride and to prevent the introduction of it and other interstitial impurities in the first two groups of metals was not necessary here. Sc, Dy, Ho, and Er metals were purified with respect to these three interstitial impurities during the sublimation step. The major problem on purification of these metals by sublimation is the carryover of fluorine impurity into the condensate. If any fluorides are present, either dissolved in the metal or in the slag trapped in the metal or even attached to the surface, the fluorides distill along with the metal and these metals analyze high in fluoride contamination (Spedding et al. 1968). The solution to this problem is either preparing the metals fairly free from fluoride impurities or in following a reduction process such as the vapor phase rare earth chloride reduction technique (Croat 1969).

Croat (1969) has compared the purity of Dy, Ho, and Er obtained by the chloride process as well as by the fluoride process. He stated that in terms of metal purity, the as-reduced Dy, Ho, and Er from the chloride process are better because the low temperature (900°C) of reduction results in quite low (<30 ppm) tantalum pick up. This may be compared with 0.1–0.2% Ta in the as-fluoride-reduced metal. Also, the chloride process eliminates F as an impurity without at the same time introducing characteristic impurities such as Cl and Li. Comparing Dy, Ho, and Er prepared from both chloride and fluoride methods and sublimed under the same conditions, Croat (1969) concluded that the metals were identical in purity with the exception of 25–75 ppm F in the metal prepared from the fluoride. The analysis data given by Beaudry and Gschneidner (1978) show that the fluorine content even in the fluoride-reduced and sublimed metal is only about 10 ppm or less, see Table 5.7. The sublimation temperatures given in the table are about 100°C lower than the temperatures used by Croat (1969), and the sublimation rates in the table are also only one-fifth of the rate used by Croat (1969).

Lutetium had been purified by distillation as well as by sublimation (Spedding et al. 1968). When distillation was carried out at 1850°C in tantalum crucibles, tantalum dissolved in the refluxing liquid lutetium and the liquid metal often eroded a hole through the tantalum crucible. At such high temperatures oxygen also apparently distilled along with lutetium. Sublimation of lutetium at a temperature slightly below its melting point seemed the better alternative. However, the use of tungsten crucible and tungsten-lined condenser enabled distillation of lutetium without extensive crucible attack (Beaudry and Gschneidner 1978).

5.5.4 Samarium, Europium, Thulium, and Ytterbium

These four metals are prepared by the lanthanothermic or reduction–distillation method. Tantalum is not the major impurity with the metals Sm, Eu, Tm, and Yb because they do not undergo the high temperature vacuum melting step. The reduced–distilled metals

usually contain several hundred ppm La in addition to O and H. These impurities are removed by sublimation. The details of this sublimation and the levels to which the impurities are removed are given in Table 5.8 (Beaudry and Gschneidner 1978).

Table 5.8 Preparation method and major impurities in samarium, europium, thulium, and ytterbium (Beaudry and Gschneidner 1978)

Method: Ames Process: Direct reduction or reduction–distillation

Lanthanothermic reduction of rare earth oxide in a tantalum crucible-tantalum condenser assembly. As-reduced metal distills off simultaneously and collects in the condenser. The condensate was purified with respect to major impurities: lanthanum, oxygen, and hydrogen by vacuum sublimation in a tantalum crucible. The entire process was carried out in a protected atmosphere of purified inert gas or under high vacuum as appropriate.

Process conditions	Samarium	Europium	Thulium	Ytterbium
Vacuum melting				
Temperature, °C	1600	1400	1600	1400
Total time, min	4	4	4	4
Vacuum sublimation				
Crucible temperature, °C	800	700	950	625
Condenser temperature, °C	500	400	550	350
Sublimation rate, $g \cdot h^{-1}$	3	3	3	4
Run size, g	1000	500	500	800

Major Impurities

Impurity	Content (ppm)			
	Samarium	Europium	Thulium	Ytterbium
C	6	100	14	10
O	33	70	8	38
N	20	Not detected	<1	9
H	4	13	9	4
Ca	2	10	0.2	<13
La	3	1	5	4
Ta	30	<0.6	<1	<1
W	<2	<3	<3	<1

The sublimation is carried out in the same crucible in which the reduction–distillation is done. A tantalum optical baffle arrangement is provided in the condenser during reduction–distillation to prevent excessive entrainment of oxide particles. The baffles are removed, and the crucible is leached with acid and then vacuum degassed at 1800°C to remove any volatile impurities before carrying out the low temperature sublimation.

The metals in the as-sublimed condition are composed of many small crystals and possess a large surface area. They are then prone to react with air and pick up impurities. The metal crystals are therefore consolidated as soon as possible. One method is to seal them in a tantalum crucible in an inert gas welder and then heat the crucible in vacuum to

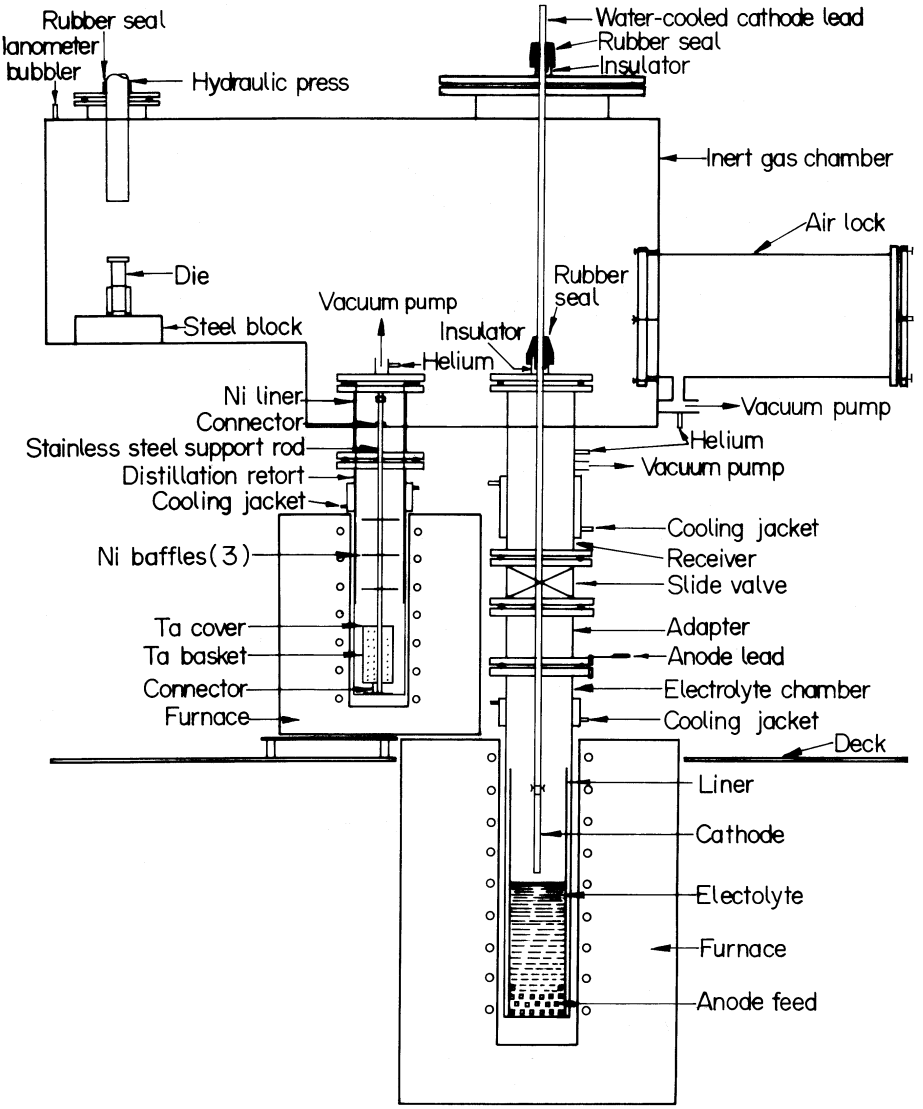

Figure 5.6 Schematic of the electrorefining apparatus (Merrill and Wong 1967).

above the melting point of the metal. The high reactivity of europium necessitates that the as-sublimed metal be handled under an inert atmosphere. Hydrogen remains as an impurity in the as-sublimed metal. This can be removed quantitatively in the consolidation step by holding the temperature above the metals' melting point for 24 h in a dynamic vacuum. Hydrogen diffuses through the Ta and is pumped away.

While the pyrovacuum treatments of vacuum melting and vacuum distillation/sublimation have been the most important methods of as-reduced metal refining, several other methods have been explored for this purification. Electrorefining in a fused salt is one among these methods. This method has been applied particularly to yttrium and gadolinium.

5.6 ELECTROREFINING

Electrorefining as a process for rare earth metal purification has been applied for the purification of yttrium and gadolinium. These are the two metals that are most difficult to obtain in pure form by the exclusive pyrometallurgy route unless great pains are taken to choose very pure materials and carry out all operations in a highly purified inert atmosphere. With gadolinium there is the additional problem of removing dissolved tantalum. Gadolinium has both a low melting point and a low vapor pressure. There is a good amount of refluxing during the distillation process and this causes considerable attack on the W or Ta crucible used (Beaudry and Gschneidner 1978).

5.6.1 Yttrium

Electrorefining of yttrium was investigated by Merrill and Wong (1967) at the Reno Metallurgy Center of U.S. Bureau of Mines. The starting material was an ingot of yttrium containing about 0.57% oxygen, 2.25% zirconium, 0.08% tantalum and several hundred ppm each of carbon, nitrogen, and many other metallic impurities. They used a $LiCl–YCl_3$ electrolyte at 710°C. Adhering electrolyte salt was removed from the electrodeposited metal by vacuum distillation. In their study the affinity of yttrium for oxygen was given major consideration, and emphasis was placed on selecting equipment and procedure that would minimize the contact of the product with air and moisture.

The apparatus shown schematically in Figure 5.6 was used by Merrill and Wong (1967). This system permitted electrorefining and vacuum distillation of the product to be performed under an inert gas, thus minimizing atmosphere contamination.

In the cell, a 12 mm diameter mild steel rod was used as the cathode, and the anode was the electrolyte chamber with crude yttrium charged in the bottom.

The distillation retort, 75 mm in diameter and 430 mm long, was made of mild steel, and had a nickel liner. The charge was contained in a tantalum basket.

At the start of the electrolysis approximately 1200 g of freshly cut pieces of yttrium metal ($50 \times 50 \times 25$ mm) were loaded in the chamber and degassed. Then 1600 g of LiCl were also charged. After evacuating and backfilling with helium, the cell was heated to 710°C. The YCl_3 component in the electrolyte was made *in situ* by reacting HCl gas with yttrium metal, using an *in situ* chlorination apparatus. After the desired concentration of YCl_3 in the electrolyte was attained, chlorination was stopped, the cathode was installed, and electrolysis was commenced. Details of the electrolysis and analysis of the product obtained are listed in Table 5.9.

At the end of each deposition cycle, the cathode deposit was lifted above the electrolyte, allowed to drain, sealed in the receiver, and cooled to room temperature. The deposit was then stripped from the cathode, loaded into a tantalum basket and sealed in the distillation retort. Distillation of the salt from the cathode deposit was carried out at 880°C for 3 h with a final pressure of less than 1.3 Pa. The salt condensed in a ring inside the liner at a level slightly below the external cooling jacket. There was a facility to compact the product metal by a press inside the inert gas chamber before it was sealed in a bottle prior to removal from the chamber.

The results given in Table 5.9 indicate that the electrolysis was effective in lowering all metallic impurities but not the interstitial elements. The nitrogen content in the refined

Table 5.9 Fused salt electrorefining of yttrium (Merrill and Wong 1967)

Electrolysis parameters	
Electrolyte composition, %	(i) 1.7 YCl_3 – 98.3 LiCl (ii) 5.4 YCl_3 – 94.6 LiCl
Temperature, °C	710
Cathode	12.5 mm diameter mild steel rod
Anode	Crude yttrium
Container	Mild steel
Cell	Mild steel
Voltage, V	(i) 0.35 (ii) 0.67
Current, A	(i) 5 (ii) 20
Initial cathode current density, $A \cdot cm^{-2}$	(i) 0.44 (ii) 1.76
Cathode current efficiency, %	(i) 99 (ii) 98
Weight of metal deposited, g	(i) 32,9 (ii) 32,6

Analysis, ppm

Impurity	Anode feed	Electrorefined metal (i)	Electrorefined metal (ii)
Al	60	25	bl
C	135	40	10
Ca	250	<10	10
Cl	nr	1800	2100
Cu	55	15	<10
Fe	360	25	35
Li	<10	25	100
N	140	240	200
Ni	210	<10	bl
O	5750	2400	3400
Si	110	<45	130
Ta	800	<300	<300
Ti	460	<250	<250
Zr	22500	<250	<250

nr: not reported
bl: below detection level

metal was higher than that of the anode feed even though the oxygen content was appreciably lower. Above 5.4 mol % YCl_3 in the electrolyte, the oxygen content in the electrorefined metal increased sharply (to values much more than that in the anode feed) with increase in the proportion of YCl_3 in the electrolyte. For example, when the YCl_3 content was 13.4 mol %, the oxygen content of the electrorefined metal was approximately

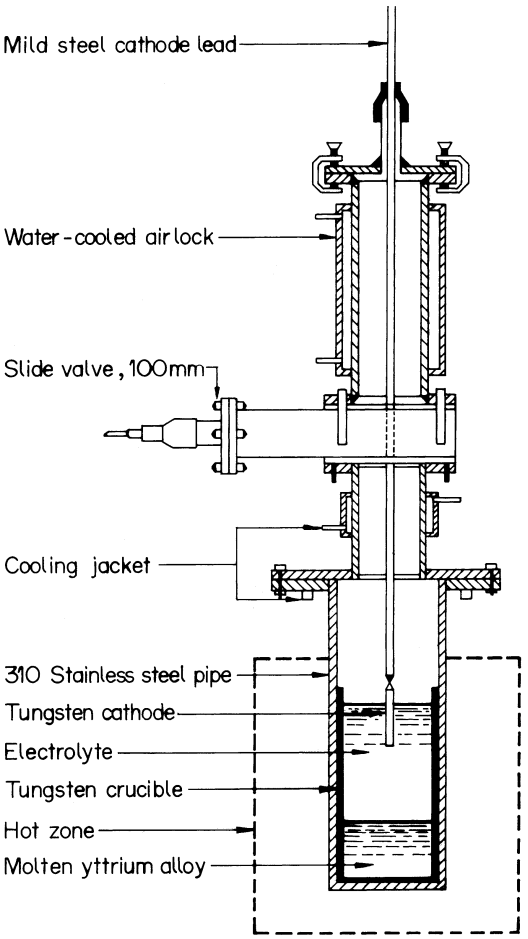

Figure 5.7 Electrorefining apparatus (Fleck et al. 1973).

13,000 ppm, whereas it was only about 5700 ppm in the anode feed. However, an increase in the YCl_3 concentration in electrolyte did not markedly affect the metallic impurity levels. Cathode current efficiency was excellent, always above 90% and in some tests it was 100%. No noticeable effect of the impurity content of the electrorefined metal was observed with variation in initial cathode current density.

The efforts on electrorefining of yttrium were continued at Reno with Fleck et al. (1973) using selected low melting yttrium base alloys as anodes in addition to crude yttrium. Electrolysis in other than $LiCl–YCl_3$ electrolytes was also tried to possibly achieve the difficult refining with respect to oxygen.

The electrorefining apparatus used by Fleck et al. (1973) is shown in Figure 5.7. All the experiments were conducted in a helium atmosphere. The electrolyte consisted of LiCl and YCl_3. A variety of yttrium-containing materials were used as anode. They are listed in Table 5.10.

The results demonstrated that the process results in a substantial decrease in the levels of metallic impurities in the cathode deposit when anodes of yttrium alloys with iron,

Table 5.10 Fused salt electrorefining of yttrium — metallic elements transfer (Fleck et al. 1973)

Electrolysis parameters

Electrolyte composition, wt %: LiCl–7 to 12 YCl_3
Temperature, °C: 900–1000, 825 for 60 Y–40 Mg alloy
Cathode: 6 mm diameter tungsten rod
Anode: Crude yttrium
Container: Tungsten crucible (75 mm in diameter and 150 mm in height)
Cell: USBM inert atmosphere electrorefining apparatus
Voltage, V: 0.35
Initial cathode current density, $A \cdot cm^{-2}$: 0.27

Result summary: Analysis values in ppm

Element	80Y–20Ni			80Y–20Fe			80Y–20Cu			60Y–40Mg		
	Anode	Initial run	Final run	Anode	Initial run	Final run	Anode	Initial run	Final run	Anode	Initial run	Final run
Al	70	22	<20	40	<20	<20	40	<15	15	60	<15	<15
Ca	<20	nd	nd	<20	nd	nd	<20	nd	nd	<20	nd	nd
Cr	150	<3	3	<3	<3	<3						
Co	<30	nd	nd	<30	nd	nd				30	50	nd
Cu	240	27	25	180	18	21	20%	7	2100	120	<20	<20
Fe	220	<15	<15	20%	<15	18	110	<20	<20	180	1800	1800
Mg	14	14	<10	<10	<10	<10	10	25	160	40%	1000	11%
Mn	740	<6	21	120	<6	<6	120	<10	15	200	160	400
Mo	30	<7	<7	30	<7	<7	35	nd	nd	20	10	10
Ni	20%	<10	20	1200	<10	<10	1200	nd	500	900	nd	nd
Si	120	<45	<45	50	<45	<45	50	<10	<10	50	<20	<20
CCE, %		98	69		99	70		88	65		68	13
Y yield, %		95			70			80			nr	

nd, not detected; nr, not reported

nickel, and manganese were used. Yttrium–copper and yttrium–magnesium, however, were not satisfactorily electrorefined because the copper and magnesium transferred to the cathode products in appreciable quantities. No refining with respect to oxygen occurred in electrolysis conducted using LiCl–YCl_3. Fleck et al. (1973) also evaluated electrolytes composed of bromides and fluorides and the results are summarized in Table 5.11. In these systems, the refining of the metallic impurities was the same as that achieved in the LiCl–YCl_3 melt. There is very little, if any, refining with respect to oxygen in the NaBr–KBr–YBr_3 melt. The oxygen content was significantly reduced when yttrium was electrorefined in a LiF–YF_3 or LiCl–LiF–YF_3 system. The main problem, however, in most of these electrolytes was that it was impossible to completely remove the adhering salts from the metal crystals in the cathode deposit.

Table 5.11 Deoxidation in the electrorefining of yttrium (Fleck et al. 1973)

Electrolyte composition, %	LiCl–7–12YCl_3	50.9 KBr–29.3 NaBr–19.8 YBr_3	66 YF_3–35 LiF	70 LiCl–14 LiF–16 YF_3
Temperature, °C	900–1000	750–800	825–925	725–825
Cathode current density, $A \cdot cm^{-2}$	0.027	0.027–0.32	0.027–0.11	0.027–0.11
Oxygen content in the anode material, %	0.4	0.4	0.4	0.4
Oxygen content in the cathode product, %	0.52	0.36	0.11	0.06

5.6.2 Gadolinium

The purification of crude gadolinium by fused salt electrorefining was investigated by Nagai, Beaudry, and Gschneidner (1978) and also by Bratland and Gschneidner (1980).

Nagai et al. (1978) used a fluoride–chloride electrolyte composed of 77.6% LiCl, 11.2% LiF, and 11.2% GdF_3. The function of LiF was primarily to increase conductivity and also to lower the melting temperature of GdF_3 (GdF_3–27% LiF melts at ~625°C). LiCl lowers the melting temperature of the mixture even further. The cathode was pure gadolinium, prepared from distilled gadolinium, in the form of a rod 1.6 mm diameter × 15 cm long. The anode, which was the impure gadolinium to be refined, was prepared from gadolinium made by the calcium reduction of untopped GdF_3 followed by vacuum melting. The anode was in the form of a cylinder 13 mm diameter and 150 mm long.

A tantalum crucible, 65 mm diameter and 130 mm long was used to contain the electrolyte. A schematic diagram of the apparatus used for electrolysis is given in Figure 5.8. The 88 mm diameter and 600 mm long stainless steel tube in which electrolysis was carried out was lined with tantalum to prevent attack by the LiCl and LiF vapors from the electrolyte. After electrolysis, the cleaned cathode deposit was heated in a vacuum induction furnace to 800°C and held for 30 min at 1.3×10^{-4} Pa to remove the adhering electrolyte. The crystals were then arc melted to consolidate them.

The details of electrolysis parameters and purity achieved by Nagai et al. (1978) are summarized in Table 5.12. The purest deposit of Gd was obtained when LiCl and LiF were purified by distillation. The H and F impurities were rather high in the as-arc-melted Gd. Electron beam melting removed both fluorine and hydrogen. Fluorine content in the

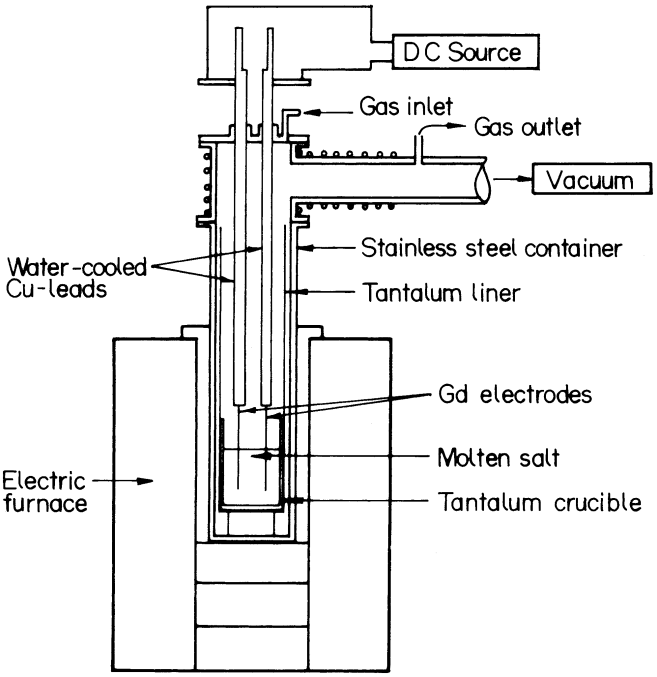

Figure 5.8 Schematic of the electrolysis system (Nagai et al. 1978).

deposit probably came from entrapment of fluoride salt from the electrolyte during the growth of the dendrites.

Gadolinium was electrorefined in an all fluoride electrolyte by Bratland and Gschneidner (1980). The electrolysis cell was essentially the same as that used by Nagai et al. (1978), shown in Figure 5.8. The only difference was that a swing gate valve was mounted in the stainless steel container where the electrolysis cell was located. The advantage, like in the Reno cells, is that with the furnace still hot, the electrode could be removed from the system without admitting air to the hot part of the container, which was kept under argon atmosphere at all times. A viewing glass was provided in the top lid to observe the cell.

The electrolyte consisted of 65 mol % LiF and 35 mol % GdF_3. Commercially available gadolinium metal was used as the starting material for electrowinning. A graphite crucible, 90 mm inside diameter and 100 mm deep, was used to contain the 1.6 kg electrolyte.

The gadolinium to be electrorefined was made in the form of a rod and used as the anode. The cathode was a 6 mm diameter tantalum rod. The electrolysis temperature was 900°C. These and other details of electrolysis are summarized in Table 5.13.

The electrolyte was not subjected to any special purification procedure before charging. It was, however, subjected to pre-electrolysis. The pre-electrolysis was carried out at a constant voltage of 2.7 V and a temperature of 900°C. This step was for removal of dissolved oxide and hydroxide. Bratland and Gschneidner (1980) found that in 2½ h of electrolysis, a 90% decrease in the oxide concentration was achieved and continued pre-electrolysis of the melt for 6 h decreased the terminal oxide concentration further. At this stage, the electrolyte was considered ready for electrorefining the gadolinium metal.

Table 5.12 Fused salt electrorefining of gadolinium (Nagai et al. 1978)

Electrolysis parameters

Electrolyte composition, %	77.6LiCl–11.2LiF–11.2GdF_3
Temperature, °C	700
Current, mA	600
Current density, A/cm^2	0.15
Current efficiency, %	70
Deposition rate, g/h	0.8

Analysis (ppm)

Element	Crude metal	Refined metal		
		1	2	3
O	490	85	180	180
N	89	43	87	98
H	3	60	95	8
F	200	1500	1500	7

1: Arc-melted metal; electrolyte prepared from distilled LiCl, topped GdF_3 and distilled LiF.
2: Electrolyte prepared from distilled LiCl, topped GdF_3 and reagent grade LiF.
3: Metal obtained by electron beam melting of the electrorefined metal in column 2.

In the electrorefining experiments, two cathode arrangements were tried by Bratland and Gschneidner (1980). In one, the cathode was inserted 6 mm into the electrolyte for the entire run. In the second, the cathode barely touched the surface in the beginning of the experiment, and as the metal formed on the cathode it was gradually pulled upward in increments of 5 mm for a total of 35 mm. This was primarily tried to improve the salt drainage of the cathode deposit, which is a problem in all molten salt electrorefining where crystalline deposits are obtained.

The electrorefined gadolinium was consolidated by arc melting. The current efficiency, calculated on the basis of the amount of metal recovered after arc melting two times, was 69.2 and 84.0%, respectively, for the stationary cathode and the retracting cathode. Higher current efficiency in the latter case can be reasoned as due to the more efficient removal of the gadolinium deposit when only the tip of the cathode or metal was exposed to the bath. Besides, when the metal was exposed to the bath for a shorter time, redissolution of the metal was minimized. However, there was no improvement as far as salt drainage was concerned when the cathode was gradually pulled out of the bath.

In addition to higher current efficiency, the product obtained with the retractable cathode was purer, as shown in Table 5.13, indicating that the contaminations originate from the bath and/or the anode metal and not from the furnace atmosphere.

The oxygen content of the metal electrorefined with retracted cathode was lower than any previously electrowon or electrorefined gadolinium metal. This implies that preelectrolysis of the electrolyte was at least as effective as other methods of purification such as treating molten gadolinium fluoride under a dynamic HF – 60% Ar atmosphere. Between the two alternatives, pre-electrolysis appears more attractive because it can be performed *in situ*.

Table 5.13 Purification of gadolinium by electrorefining with pre-electrolysis (Bratland and Gschneidner 1980)

Electrolysis parameters

Electrolyte composition, mole %	$65LiF-35GdF_3$
Temperature, °C	900
Cathode	Pure gadolinium rod
Anode	Crude gadolinium
Container	Graphite crucible
Pre-electrolysis	
Voltage, V	2.7
Duration, h	8
Electrolysis	
Current, A	4
Duration, Ah	5
Cathode current density	
Current efficiency, %	84

Analysis (ppm)

Element	Impure anode	Stationary cathode	Retractable cathode
O	1100	50	34
H	88	50	21
N	400	140	43
C	209	not detected	253

Bratland and Gschneidner (1980) observed that the oxygen contamination of the metal decreased with decreasing oxide concentration in the bath. Electrolysis of an oxide-deficient melt, which probably still contained some oxide, yielded a minimum concentration of about 80 ppm oxygen. Zwilling and Gschneidner (1978) used purified lithium fluoride and gadolinium fluoride containing less than 20 ppm oxygen, and adding no oxide, electrolyzed the melt to obtain gadolinium dendrites that still contained a minimum of 40 ppm oxygen. Comparing these results with those obtained by Bratland and Gschneidner (1980) using pre-electrolysis indicated that pre-electrolysis was attractive not only because it was convenient, but also because it was very effective in decreasing the oxygen content of the bath and hence in the electrorefined metal.

The carbon content of electrorefined gadolinium was more than that of the impure anode. The source was a graphite cell. A small immersed graphite anode might reduce the contamination and eliminate the need for a graphite cell. Zwilling and Gschneidner (1978), however, found that the carbon contamination of gadolinium electrorefined in a Ta crucible was lower (60 to 100 ppm) but still considered more. This resulted from carbon impurity in the lithium fluoride. It was apparently not true after all that the carbon anode was the principal source of carbon contamination in electrorefined gadolinium.

The nitrogen content of the gadolinium electrolyzed by the above procedure was more than what was normally found in gadolinium electrowon in a similar cell. It appeared that nitrogen was very effectively transferred through the electrolyte from anode to cathode.

Table 5.14 Fused salt electrorefining of cerium (Shedd et al. 1964)

Electrolysis parameters

Electrolyte composition, wt %	1 $CeCl_3$–63 $BaCl_2$–17 KCl–19 LiCl
Temperature, °C	700
Cathode	5 mm diameter tantalum rod
Anode	12 mm diameter cerium rod
Cell	graphite
Current, mA	2.5
Voltage, V	0.17

Analysis (ppm)

Impurity	Before refining	After refining
C	350	190
O	40	30
Si	30	50
Fe	340	40
Mo	600	80
Al	250	20
Total impurities	1610	410

Hydrogen and oxygen were also transferred to the electrolyte by anodic dissolution. The *a priori* concentration of these elements as oxide and hydroxide impurities in the electrolyte, however, determined the hydrogen and oxygen contamination of the electrorefined metal.

In their experiments, Bratland and Gschneidner (1980) found that pre-electrolysis was at least as efficient as any other purification method known. While most of the oxygen and hydrogen were removed, the last traces of oxygen and hydrogen were virtually impossible to remove.

Besides yttrium and gadolinium, electrorefining was tried for cerium also. The experiments, mainly to see feasibility, were conducted at Reno by Shedd, Marchant and Henrie (1964).

5.6.3 Cerium

The electrorefining of relatively impure cerium metal in a chloride electrolyte was demonstrated by Shedd, Marchant, and Henrie (1964) at Reno. The electrolysis parameters and results are summarized in Table 5.14. An electrolyte composed of 64% $BaCl_2$, 17% KCl, and 19% LiCl was melted in a graphite lined 100 mm diameter inert atmosphere electrorefining cell. Cerium chloride was generated *in situ* in the electrolyte by chlorinating a cerium bar with HCl gas. When the electrolyte contained 1% $CeCl_3$, the chlorination was stopped and the cerium bar was removed. A 5 mm diameter tantalum cathode and a 12 mm diameter cerium anode were inserted 75 mm in the bath. Electrorefining was conducted at 0.17 V and 2.5 A, and the operating temperature was 700°C (about 100 degrees lower than the melting point of cerium). Very fine crystals of cerium were deposited on the cathode. This deposit and adhered salt were melted at 900°C under an inert atmosphere in a boron

nitride crucible. After melting, the contents were poured on a tungsten crucible and the cerium button and salt were readily separated.

The analysis of the starting material and refined metal is given in Table 5.14. Shedd et al. (1964) noted that the anode was made by consolidating the small, impure, pea-size cerium nodules obtained during electrowinning. After refining this material, a purer product than the electrowon metal was obtained.

5.7 ULTRAPURIFICATION METHODS

After the pyrovacuum or electrorefining treatments for removing a variety of metallic and nonmetallic impurities from as-reduced rare earth metals, certain purification techniques may be applied to the purified metals for several reasons: (i) to further decrease the contents of impurities that have already been removed by the purification techniques, (ii) to remove impurities whose concentration had not decreased by the purification techniques, and (iii) to remove impurities that have inevitably been introduced by the purification techniques. These methods are known as ultrapurification methods. Two techniques of ultrapurification have been widely applied for the rare earth metals. They are zone refining and solid state electrotransport.

5.8 ZONE REFINING

The process of zone refining involves generating a thin molten zone of the metal by localized melting and passing the zone slowly along the length of the metal rod to be purified in one direction several times. Purification takes place at the traveling solid–liquid interface. The solubility of an impurity element in the coexisting solid and liquid phases is usually different. Impurities more soluble in the molten metal will move in the direction in which the molten zone is moved and therefore concentrate in the zone to solidify last and accumulate in the finishing end of the rod. On the other hand, impurities more soluble in the solid phase concentrate in the crystallizing solid and so ultimately accumulate in the starting end of the rod. The liquid soluble and solid soluble impurities apparently move in opposite directions. Zone refining is essentially a technique for impurity redistribution within the sample rather than impurity removal (Pfann 1966), and only a portion of the rod ends up as pure metal in the process. Since the extent of purification depends on the solubility of the impurities in the solid metal, those impurities that are soluble in the solid cannot be removed to below the equilibrium concentration. As a result, the interstitial impurities that are quite soluble in the solid rare earth metal just below its melting point cannot be removed completely. Generally, zone refining is more useful for substitutional impurity removal and less effective for the interstitial impurities. The use of a vacuum in the process combines the benefits of conventional zone refining with those of pyrovacuum treatments. In the zone refining of rare earth metals, the use of high vacuum or an equally pure inert atmosphere is mandatory to prevent the metal from picking up impurities from the gaseous atmosphere.

Basically two techniques are used for passage of molten zones. The simpler technique involves the use of a crucible to hold the metal. The metal is contained in a long horizontal

trough or crucible and the zone is moved in a horizontal direction. As mentioned earlier, the rare earth metals are so reactive that they reduce ceramic container materials at their melting points and get contaminated. Attempts have been made to overcome this problem by using a water-cooled container in which an unmolten skin of the metal being purified is maintained, and this thin skin acts as the true container of the molten metal. The other technique is the vertical floating zone technique in which the metal is supported vertically from the ends without a container, the narrow molten zone being maintained because of the surface tension of the metal. Heating in either method is by induction and this mode of heating can have either an inert atmosphere or vacuum. Better control and narrower zones are obtained by electron beam heating but this requires a high vacuum.

5.8.1 Preliminary Studies

At the time of the first review on zone refining of rare earths by Huffine and Williams (1961), zone refining had been reported on only two metals. Kendall in General Electric had purified gadolinium by using the conventional horizontal induction heating technique with a tantalum crucible in a purified argon atmosphere (Huffine and Williams 1961). He made 10 passes of a 45 mm wide zone at a rate of 38 mm/h. The product was evaluated only by metallography. The purified ingot showed substantial concentration of impurities at the ingot ends with corresponding purification of the middle of the ingot.

Yttrium was subjected to purification by zone melting at the General Electric Company's Aircraft Nuclear Propulsion Department (GE–ANPD), and the results were summarized by Huffine and Williams (1961). The refining was done by the floating zone technique with induction heating, and a 9.5 mm diameter rod was processed in a continuously pumped vacuum. Three heating passes were made (below the melting point) in order to remove the volatile impurities sufficiently to prevent the arcing of the heating coil. The main impurity, magnesium, and a considerable amount of yttrium oxyfluoride were vaporized. Following this, six zone passes were made at the rate of 64 mm/h, and the analysis of the purified metal is given in Table 5.15.

Table 5.15 Purification of yttrium by zone refining (Huffine and Williams 1961)

Impurity	Content, ppm			
	Before processing	After processing		
		Beginning	Middle	End
O	5800	7600	6170	5310
N	270	280	250	250
Fe	500	500	300	100
Cr	10	10	<1	<1
Cu	10	2	0.5	0.5
Ni	50	50	50	50
Ti	100	100	100	100
Zr	4700	4300	3100	2750

The results given in Table 5.15 indicate no significant change in O, N, Ni and Ti contents and only a marginal movement of the metallic impurities Cr, Cu, Fe, and Zr. Other indicators of purity such as microstructure and hardness also did not reveal any significant variation with location in the zone-refined rod. It appeared that zone refining was not a useful purification process for yttrium.

Two other early attempts at zone refining of yttrium were reported. An yttrium rod containing 0.052% oxygen and 0.065% fluorine was zone refined in two passes by Carlson et al. (1960). However, no significant change in oxygen content was observed although there was a decrease in the fluorine content. The decrease in fluorine was attributed to the evaporation of oxyfluoride.

Necker (1961) zone refined yttrium and observed that metallic impurities could be decreased from 4300 to 1800 ppm after six zone passes. This observation did not agree with that of Huffine and Williams (1961).

Revel et al. (1974) carried out the zone refining of cerium in an induction-heated cold crucible. They found that 12 passes of a molten zone decreased a number of metallic impurities to the part per billion range. The purification with respect to interstitial impurities during the zone refining was not determined. Beaudry and Gschneidner (1978) noted that it was not likely that purification with respect to interstitial was attained during the experiments of Revel et al. (1974) because the vacuum used was inadequate and the interstitial impurities exhibit high solubility in solid cerium. They, however, stated that from impure cerium, many metallic impurities could be decreased by zone refining.

Two years later, Hukin and Jones (1976) zone refined terbium under an atmosphere of pure argon in a horizontal cold crucible with induction heating. They observed that O, N, and C moved in the direction opposite to that of the molten zone. Significant purification with respect to the interstitial as well as the metallic impurities was reported.

Jones et al. (1978) reported that in much of the earlier work on zone melting, the ingot underwent degradation during processing particularly by oxygen and nitrogen rather than undergoing any possible improvement from the treatment. In fact, they were corroborating the statement of Revel et al. (1974) that zone refining of cerium would fail to remove nonmetallic elements (N, O) and that one should be satisfied not to increase their amount during the treatment. This state of affairs was changed by the work of groups at the University of Birmingham and at the Ames Laboratory (Jones et al. 1978, Fort et al. 1981).

Making use of technological developments associated with cold boat crucibles together with advances in vacuum technology, particularly the use of ultrahigh vacuum equipment, the groups of D. Fort at the University of Birmingham and K.A. Gschneidner, Jr. at Ames were able to handle molten rare earth without degradation during processing, and contributed to much of the current knowledge on zone refining of rare earth metals.

5.8.2 Lanthanum, Gadolinium, and Terbium

Commercially available lanthanum, gadolinium and terbium metals were zone refined by Jones et al. (1978) in water-cooled boats using radiofrequency heating. The lanthanum was zone refined in ultrahigh vacuum (working pressure $\sim 10^{-8}$ Pa) while purified argon of equivalent purity was used for gadolinium and terbium. The use of argon moderated the vaporization problems, particularly with terbium. The configuration of the boats was such that melting occurred right through the ingot.

In the zone melting of lanthanum ~15 g pieces of the metal were consolidated in the cold boat by a general melting. The start material outgassed badly, and outgassing was

considered complete when the whole rod could be held molten in a vacuum better than 10^{-7} Pa. The ingot length was 120 mm, zone width was ~15 mm, and the zoning speed was 180 mm/h. After 33 zone passes, the ends were cropped for mass spectrographic analysis and the remaining rod (now 104 mm long) was treated further. The rod was replaced inverted and subjected to a further 30 zone passes at an average speed of 150 mm/h, while the vacuum remained better than 10^{-7} Pa during the whole zoning procedure.

Table 5.16 Analysis of zone refined lanthanum, gadolinium, and terbium (Jones et al. 1978)

Impurity	Analysis, ppm		
	Beginning	Middle	End
	Lanthanum		
H	900	759	526
O	11829	7450	5248
N	690	776	204
Tb	15		3
Y	30		10
Ni	75		160
S	31		100
Na	5		0.3
Li	30		10
	Gadolinium		
H	17	17	17
O	933	593	341
N	39	24	14
Tb	10	27	60
La	6	7.5	20
Cu	4	6.5	65
Ni	2	3	30
Fe	40	49	190
Ti	1.5	3	8
Si	32	49	65
Al	15	95	450
S	7	20	26
	Terbium		
H	13	10	13
O	1999	640	348
N	140	69	29
Pb	0.4	1	1.5
Cu	6.5	7	32
Ni	0.5	2.5	4.5
Fe	6.5	27	75
Ti	5	3	4
Al	6	50	170

At the completion of zoning, samples were removed from the beginning, end, and middle portions of the refined rod. The beginning and end samples were actually cut 10 cm from the extremities of the ingots. The analysis of the zone-refined lanthanum is given in Table 5.16.

In the refining of gadolinium and terbium, 120 g start material was consolidated and outgassed to a constant vacuum better than 1.3×10^{-5} Pa, as described for lanthanum. The ingots were then zone refined under static high purity argon. The zoning width was 15 mm, zoning speed was 250 mm/h, and the number of passes in each case was 25. The analysis after zone refining appears in Table 5.16.

The results in the table show that in lanthanum, gadolinium, and terbium, zone refining results in redistribution of oxygen and nitrogen. After zoning, in each of the three cases, the maximum impurity concentration occurred at the start end, thus indicating that these impurities had moved in the opposite direction to that of zone travel. The hydrogen content showed no consistent segregation effects, possibly because of the reversible nature of the rare earth/hydrogen reaction. Most of the metallic impurities had moved in the direction of the zone. The results indicated that zone refining can result in a greatly improved product, perhaps even on a commercial scale.

5.8.3 Lanthanum, Cerium, and Gadolinium

In experiments jointly conducted by groups from the University of Birmingham and the Ames Laboratory (Fort et al. 1981), a zone-refining apparatus constructed to ultrahigh vacuum standards was used to ultrapurify high pure Ames metals. The metals were lanthanum, cerium, and gadolinium. Only three rare earths — lanthanum, cerium, and praseodymium — have vapor pressures that are low enough at the melting points of the metals to allow conventional cold-boat zone refining in vacuum, and all other rare earth elements require an inert gas environment to suppress volatilization. The use of inert gas can result in contaminant introduction, but such contamination could be kept to acceptable levels provided no gaseous impurities leaked into the system during refining and provided that negligible degassing from the system walls into the argon occurred. The use of ultrahigh-vacuum-rated equipment and pumping the system to a high vacuum before admitting argon help keeping contamination to acceptable levels.

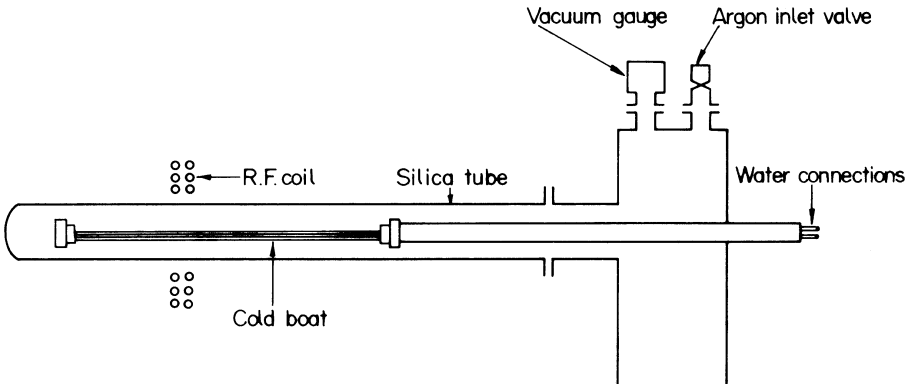

Figure 5.9 Schematic drawing of the cold-boat zone refining assembly (Fort et al. 1981).

A schematic diagram of the cold boat zone refining assembly used by Fort et al. (1981) is given in Figure 5.9.

The assemblies were constructed using stainless steel ultrahigh vacuum components and copper gaskets throughout. One assembly was evacuated using ion and sublimation pumps and the whole system was bakeable to 400°C. It has a base pressure of 2.6×10^{-8} Pa. This system was used for zone refining both in vacuum and under argon. Another cold boat assembly was evacuated by a diffusion-pumped vacuum system with a cryogenic trap. The assembly was leak tested initially to 2.6×10^{-8} Pa, but the actual pumps had a base pressure of only 6.6×10^{-6} Pa. This assembly was used for zoning runs under argon. For zoning runs under inert gas, the systems were filled with argon (to 1 atm) via an inert gas purifier specified to reduce the total amount of impurities to less than 1 vol. ppm. To induce the molten zone, induction heating at 350 kHz was used. A "double-pancake" type coil with six turns in two layers was used. The radiofrequency power output was regulated to keep the molten zone lengths at approximately 10% of the total bar length.

Cerium has the lowest vapor pressure of all the rare earth metals and would therefore exhibit the optimum potential for purification with respect to oxygen, nitrogen, or hydrogen when zone refined under ultrahigh vacuum conditions. During ultrahigh vacuum zone refining of cerium, Fort et al. (1981) experienced severe trouble in stabilizing the molten zone. The zone kept vibrating and touching the cold boat where it would freeze, then remelt, touch the boat, and freeze again. This stability problem was overcome when the cerium rod was zone refined under 1 atm pressure argon. The rod was loaded into the diffusion pumped cold boat, the rod was degassed by melting in a vacuum (initially 6.6×10^{-6} Pa but rising to 5×10^{-4} Pa during melting), and then purified argon was admitted to a pressure of 1 atm. The molten zone became well defined (the melting–freezing cycles ceased) and a constant length and controlled zone refining was possible. At the rate of 12.7 cm h^{-1}, a total of 15 zones were passed.

The zone stability problem exhibited by cerium in ultrahigh vacuum was also displayed by lanthanum (Fort et al. 1981) experiments. However, previously commercial purity lanthanum had been zone refined (Jones et al. 1978) in ultrahigh vacuum without problems in stabilizing the molten zone. Stability of the molten zone appeared to be connected to material purity. The impurities in the metal influence the surface tension of the molten metal and hence affect the molten zone stability. An inert gas atmosphere may stabilize the molten zone by making the temperature profile across the zone much sharper by increasing the heat losses from the nonheated parts of the bar and also by altering the surface characteristics of the molten metal.

Fort et al. (1981) proceeded with zone refining of lanthanum in ultrahigh vacuum in spite of not achieving a stable molten zone. The refining run was composed of 14 zone passes at 18.7 cm h^{-1} and then 11 zone passes at 11.7 cm h^{-1}. During zoning, the vacuum improved from 1.3×10^{-5} Pa during the initial pass to 5.3×10^{-7} Pa for the final 10 passes.

Gadolinium could not be cold boat zone refined in ultrahigh vacuum because of the metal's high vapor pressure and hence its excessive volatilization. Fort et al. (1981) zone refined Gd under inert gas. Two different vacuum treatments were given to Gd before argon was let in. In one, the starting material was degassed at red heat (~800°C) to a vacuum of 2.6×10^{-5} Pa before it was cooled to room temperature and purified argon was admitted, and at 25.2 cm h^{-1}, 20 zone passes were made. In the other treatment, the starting material was degassed to a vacuum of 2.6×10^{-7} Pa before admission of argon. Nine zones were run at 18.7 cm h^{-1} followed by 11 passes at 11.7 cm h^{-1}. In another run, gadolinium containing 190 atomic ppm tungsten was zone refined, principally to redistribute this impurity. The

Table 5.17 Analysis of Ce, La, and Gd before and after zone refining (Fort et al. 1981), values in at. ppm

Element	Start	After zone refining				
		Beginning	¼	½	¾	End
Lanthanum						
O	295	434	434	1215	564	174
H	275	965	1100	2338	2062	688
N	30	30	20	80	50	20
Ta	3.4	41	40	33	36	220
Cu	10	37	20	16	15	120
Fe	10	5	4	4	9	66
Ni	2	2	1	1	2	10
Co	<0.2	2	1	1	7	15
Cl	3	10	10	7	7	5
Cerium						
O	395	1226	683	823	455	341
H	556	1668	973	1112	417	139
N	260	260	240	230	130	60
Gadolinium						
O	864	1770	894	648	432	304
H	1092	780	780	780	468	312
N	34	190	101	101	45	56
C	367	262	367	524	616	1087
W	190	<1	<1	55	33	1433
Fe	38	3	10	20	5	160
Al	10	<0.04	1	4	8	100
Ta	11	<0.03	1	24	23	10
Si	5	<0.03	10	10	2	20
Co	2	<0.03	<0.05	<0.1	0.2	5
Ni	3.2	<0.3	<0.3	3	0.8	10

diffusion pumped cold boat system was used. After degassing the starting metal (to 6.6×10^{-6} Pa), purified argon was filled to 1 atm and first 20 zones were passed at 12.7 cm h^{-1} followed by 1 zone pass at 2.5 cm h^{-1}. The last pass was to promote grain growth.

The analyses of cerium, lanthanum, and gadolinium before and after zone refining are listed in Table 5.17. The results show that in cerium and gadolinium, under the conditions used, the impurity levels rise or fall progressively from the beginning of the bar to the end. The results for lanthanum and cerium are shown in Figure 5.10. Unlike cerium, the results for lanthanum do not show a consistent trend, and this is traceable to the unstable molten zone. A stable molten zone is necessary for worthwhile refining.

Redistribution of Interstitial Impurities Fort et al. (1981) observed that in the zone refining of gadolinium, terbium and lanthanum, the impurities oxygen, hydrogen, and

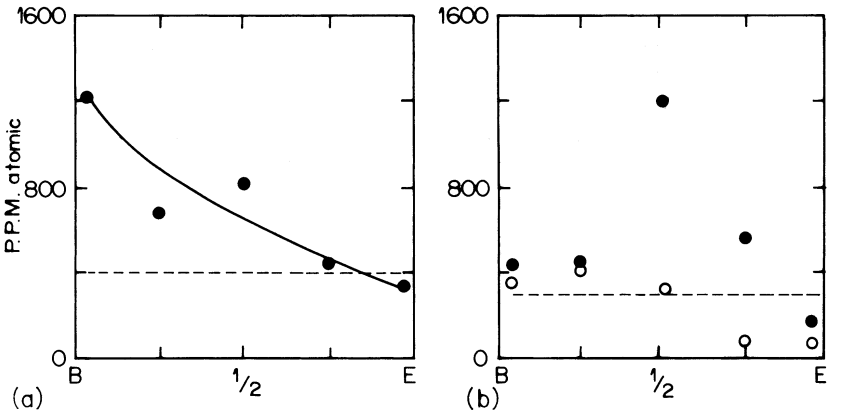

Figure 5.10 Oxygen concentration profiles along the zone-refined bar from beginning B to the end E for (a) cerium and (b) lanthanum. Dotted line indicates starting concentrations. In (b), solid circles represent values at the top of the bar, and hollow circles represent the values at the bottom of the bar (Fort et al. 1981).

nitrogen moved against the zone directions. The impurity profiles for oxygen and carbon are shown in Figure 5.11. It is seen that unlike oxygen, carbon was found to move in the zone direction in gadolinium. It is thus not possible to decrease the levels of all four major interstitial impurities at one end of a gadolinium bar by zone refining. Also, the lowest levels of oxygen, hydrogen, carbon, and nitrogen achieved by Fort et al. (1981) did not represent significant improvements over the starting concentrations. They also observed in the zone refining of gadolinium that ultrahigh vacuum degassing was advantageous before zoning under vacuum.

Redistribution of Metallic Impurities Metallic impurities were found to be markedly redistributed in gadolinium by zone refining (Fort et al. 1981). The impurity profile in gadolinium after zone refining is shown in Figure 5.12. All three metallic impurities shown — aluminum, iron, and tungsten — have undergone redistribution by zone refining and have concentrated at the end, leaving the portion from the beginning to three-fourths of the bar enhanced in purity. Tungsten, iron, and aluminum move well, but zone refining has not been particularly effective for zirconium. In fact, the metallic impurities were so effectively redistributed by zone refining of gadolinium that Fort et al. (1981) achieved the total metallic impurity level in the beginning section — the lowest ever recorded in a rare earth metal. From a starting concentration of 190 at ppm, zone refining left at least one-quarter of the bar with a tungsten content of less than 1 at ppm. In lanthanum, despite the instability of the molten zone, useful transport of metallic impurities was observed (Fort et al. 1981).

In the zone refining of rare earth metals, Fort et al. (1981) observed that the majority of the metallic contaminants were transported in the zone direction. This was observed for iron, copper, cobalt, nickel, tantalum, tungsten, and aluminum. Such behavior can be anticipated because the binary phase diagrams of each of these metals with the rare earths showed eutectics adjacent to the pure rare earths due partly to the low solubility of most of these elements within the matrix of the large rare earth atoms. The lowering of the melting point of the host rare earth metal by small amounts of impurities led to the distribution coefficient (k_{eff}) becoming less than one and, as a consequence, movement of impurity in the zoning direction.

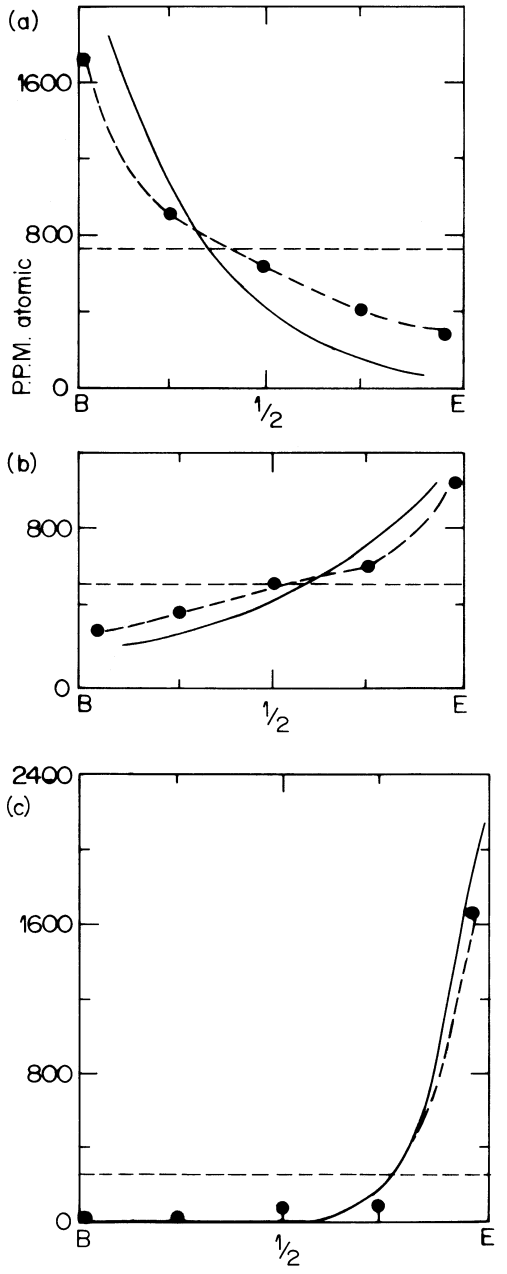

Figure 5.11 Impurity profiles in zone-refined gadolinium after 20 passes. (a) oxygen, (b) carbon, and (c) tungsten + iron + aluminum. ------- starting concentrations, —— calculated ultimate concentration distribution profile (Fort et al. 1981).

In gadolinium, many of the common metallic impurities have been amenable to considerable transportation by zone refining. Interestingly, the direction of transport of oxygen, hydrogen, and nitrogen, which are present in considerable concentrations besides not

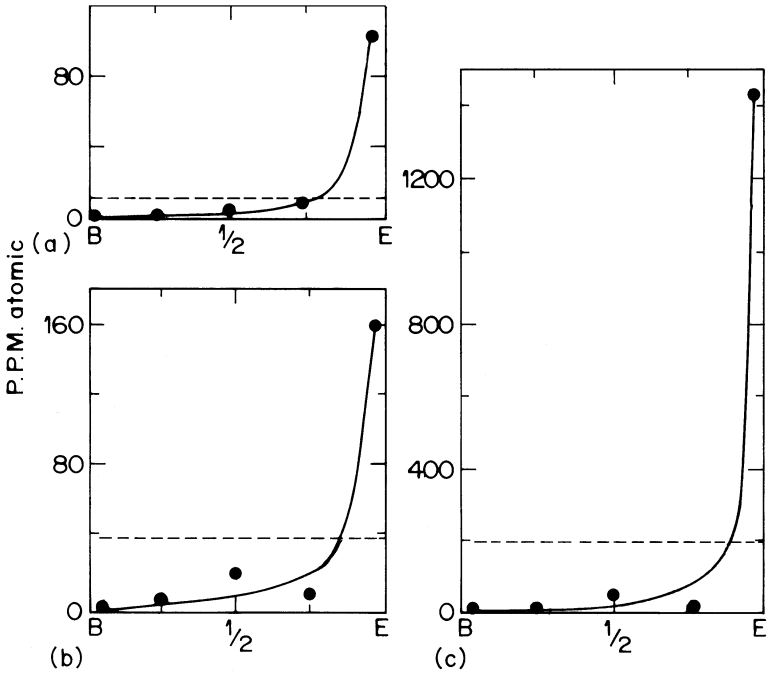

Figure 5.12 Profile of metallic impurities (a) aluminum, (b) iron and (c) tungsten in zone refined gadolinium. -------- starting levels (Fort et al. 1981).

transporting very effectively, is opposite to the direction of transport of common metallic impurities which are present in relatively low concentrations but transport very efficiently. As a result, no part of the zone-refined bar is of greatly improved overall purity compared to the starting metal. This was stated clearly by Fort et al. (1981), see Figure 5.13. The inevitable conclusion is that zone refining is not a particularly viable method of refining rare earth metals with respect to all impurities.

The ability of zone refining to refine rapidly with respect to metallic impurities makes the technique still useful, particularly in combination with another technique that can refine with respect to the interstitial impurities. Zone refining in combination with solid state electrotransport should enable production of very pure rare earth metals.

5.9 SOLID STATE ELECTROTRANSPORT

It has been known for many years that foreign ions in a metal lattice that is subjected to a direct current field display mobility (Jost 1952). The mobility is more pronounced for the nonmetallic atoms, which can possibly migrate interstitially in the metal, even though metallic impurities also move (Seith and Wever 1953). The remarkable mobility of oxygen in zirconium was reported as early as 1940 by De Boer and Fast (1940). Inspired by this fact, Williams and Huffine (1959) at the Aircraft Nuclear Propulsion Department of General Electric Co. (ANPD–GE) examined the technique in 1959 for the purification of yttrium.

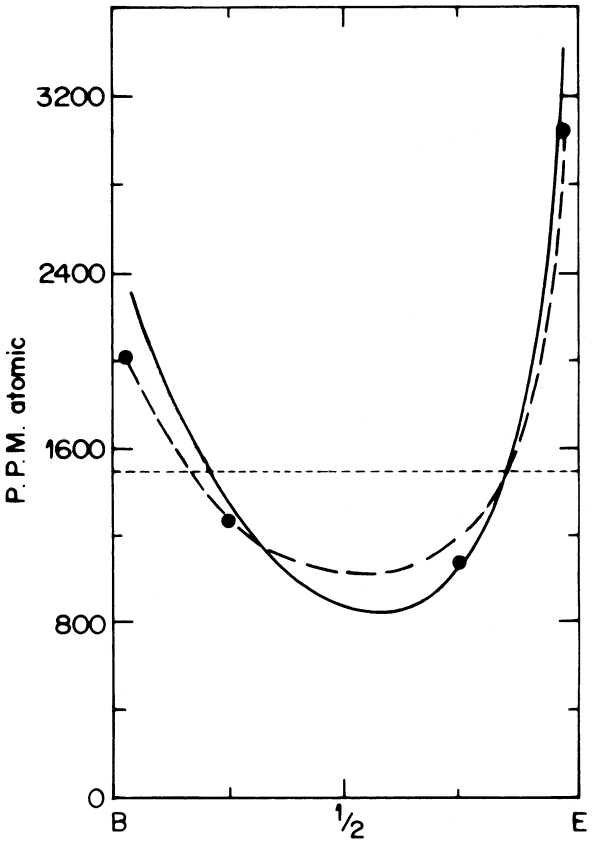

Figure 5.13 Sum of the oxygen, carbon, tungsten, iron and aluminum impurity levels in zone refined gadolinium after 20 passes. --------- starting concentrations, —— calculated ultimate concentration distribution profile (Fort et al. 1981).

Williams and Huffine (1959) electrolyzed yttrium bars of 9.5 mm and 19 mm in diameter in static argon using the vacuum chamber of an arc melting furnace. The temperatures were 1370 and 1270°C, respectively, and the electrolysis lasted for 200 h. Water-cooled electrodes were fixed to the bars, and the bars were heated by the passage of direct currents of approximately 300 to 700 A.

The results of electrolysis at the two temperatures were similar, but the overall transport of impurities was better at the higher temperature. This could be anticipated for a diffusional process. Data obtained at 1230°C are shown in Table 5.18. The movement of oxygen toward the anode was very marked. The movement of nitrogen, though in the same direction, was less pronounced. Many metallic impurities also moved toward the anode.

The solubility of oxygen in yttrium is low; however, the mobility of what is dissolved is quite high. This leads to the situation where the high mobility of dissolved oxygen results in dissolution of oxygen from the insoluble inclusion, resulting finally in the removal of the inclusion itself. The inclusions completely removed near the cathode appeared near the anode.

These encouraging initial observations of Williams and Huffine (1959) laid the foundation of future work on this technique of purification of rare earth metals at Ames by

Table 5.18 Electrotransport purification of yttrium (Williams and Huffine 1959)

Impurity	Content before processing, ppm	Content after processing, ppm		
		Near cathode	Center	Near anode
O	3330	665	3100	10900
N	510	366	570	700
Si	55	100	10	140
Fe	150	60	50	600
Mn	9	<1	<1	6
Mg	5	10	<5	6
Zr	9000	9000	9000	7000
Ni	250	50	100	10000
Cr	80	20	20	30
B	7	3	6	15
Ti	9	<3	<3	30
Co	1	<1	<1	6

Verhoeven, Carlson, Schmidt, Beaudry, and Gschneidner and at the University of Birmingham by Fort and Jones (Fort 1987; Fort et al. 1987, 1990; Jones et al. 1982).

The solid state electrolysis (SSE) described by Huffine and Williams (1961) is more popularly known by the name solid state electrotransport. In solid state electrotransport a direct current is passed through a rod or strip of metal held between two electrodes in an appropriate container. Those impurities are amenable to transport and migrate to one end of the rod leaving the remainder enhanced in purity.

During electrotransport, the impurities move under the influence of the electric field to one end of the bar. A greater electric field makes the impurities move faster. Jones et al. (1982) states this as the electron flow sweeping the impurities (particularly the interstitial impurities O, H, N, and C) toward the anode end. The same electric current also (resistance) heats the metal rod (to near the melting point), enhancing the impurity transport rates. Since the passage of the electric current heats the rod, however, the maximum field becomes limited by the rate at which the heat can be removed from the bar. The use of a higher electric field without leading to a rise in temperature to unacceptable levels is favorable for SSE. The maximum temperature that can be acceptable for using a higher electric field is limited by two factors. One is the melting point of the metal. The other is the vapor pressure of the metal being purified. When SSE is carried out under high vacuum, the heat is lost by radiation. When an inert atmosphere is used, cooling also occurs by conduction. When the rod is of a smaller diameter, the surface-to-volume ratio is greater, and this increases the cooling per unit length and permits an increase in the electric field. A rod of smaller diameter also means processing less material.

The extent of purification is often determined by the surroundings. A vacuum of 1.3×10^{-7} Pa or an equally pure inert gas is the minimum requirement for realizing the movement of gaseous impurities to one end of the metal by electrotransport faster than they enter the metal from the surroundings.

The ends of the rod being purified by electrotransport are usually cooler, and in this portion the transport would be slower. As a result there is a danger that the cooler end, from which the impurities are removed, will release or feed the impurities at a rate slower than

the rate at which the impurities are transported through the rest of the material. This end can continue to act as an impurity source even after other portions have been purified. This limitation has been circumvented by butt welding a previously electrotransport purified rod to the end from which impurities are being removed.

A concentration and chemical potential gradient is established along the length of the rod during electrotransport. This gradient will encourage back diffusion and this is another source of impurity.

Verhoeven (1966) derived a theoretical expression to estimate the degree of purification attainable in SSE for a specified set of conditions. There are major limitations, however, as described above, in achieving experimentally what has been predicted by theory. In any case, purification by electrotransport can be enhanced by maximizing transport by an electric field, thereby minimizing contamination from the surroundings and the cold end and finally minimizing diffusion of impurities. Another item is that solute mobilities are considerably higher in the bcc phase and when possible it is preferable to process the metal in the bcc phase.

Following the initial work of Huffine and Williams (1961), many investigations have been carried out on the electrotransport purification of rare earth metals. A summary of electrotransport purification studies presented by Carlson and Schmidt (1976) has been updated with the later works and is given in Table 5.19.

SSE has emerged as one of the major methods for purifying rare earth metals to the highest levels. It is practically indispensable in this role because the major contaminants in rare earth metals are invariably oxygen, hydrogen, carbon, and nitrogen. These four elements usually account for more than 95% of the impurities found in commercially obtainable rare earth metals. These interstitial impurities are exactly those that are most amenable to electrotransport purification. Table 5.19 also summarizes purification achieved with respect to these impurities.

5.9.1 SSE System

In SSE, ultrahigh vacuum rated equipment is always used to reduce environmental contamination risks even when processing under inert gas. Fort et al. (1987) used the hot chuck technique to maintain the sample at a uniform temperature throughout its length. Here the sample holders were at a temperature similar to the sample. While the basic ultrahigh vacuum chambers and power generators used for SSE have not changed much since the early days of SSE, the electrodes (or clamps or chucks or adaptors) that provide electrical contact between the sample and the main power feed through the chamber have become more sophisticated. The section of chuck adjoining the sample should operate at within 100 K of the sample temperature, should not contaminate the sample, should allow for length changes in the sample while heating and cooling, and should also carry high currents (~300 A). Tantalum is the preferred chuck material because, among other things, in this metal oxygen, hydrogen, and nitrogen electromigrate from anode to cathode in the opposite direction to that of the rare earths. So, electromigration of these impurities from the chucks into the purer (cathode) ends of the rare earth samples is ruled out.

The sample for solid state electrorefining was prepared by induction melting in a cold boat either under vacuum or purified argon followed by mechanical swaging. Single crystal rods grown by electron beam float zoning (EBFZ) in a vacuum (for Gd, Tb, and Y) or radio-frequency float zoning (RFFZ) under argon (for Gd, Tb, Y, Ho, and Dy) were also used.

Table 5.19 Electrotransport purification of rare earth metals

Rare earth	Atmosphere	Temperature, °C	Time, h	Initial concentration, ppm			Initial RRR	Final concentration, ppm			Final RRR	Reference
				C	N	O		C	N	O		
Pr	UHV			Ames metal							400	Fort 1987
Nd	UHV	860	1237	13	54	45			1	16	116	Carlson and Schmidt 1976
Nd	Ar	800–863	1250	7	2	40		5		20	40	Fort et al. 1987
Gd	UHV	1000–1050	2600	21	2	51		5	2	3	800	Fort et al. 1987
Tb	UHV	1050	350		30	380	17.5		15	25	60	Jordon and Jones 1975
Tb	UHV	985–1075	900	Ames metal					400			Fort 1987
Dy	Ar	1050–1100	500	Ames metal					125			Fort 1987
Ho	Ar	1100	200	Ames metal					90			Fort 1987
Lu	UHV	1150	168	70	15	475	21	60	6	42	150	Peterson and Schmidt 1969
Y	Ar	1230–1370	200		510	3330			90	340		Williams and Huffine 1961

When SSE processing was to be carried out under purified argon, the procedure (Fort 1987) involved (i) pumping and backing the system and sample assembly until the base pressure was 10^{-5} Pa, (ii) outgassing the sample and electrodes by passing a current through them, the temperature designed to be attained being determined by the volatility of the element, (iii) admitting argon into system to a pressure of about 70 kPa via an inert gas purifier designed to reduce the total of all gaseous impurities to below one volume ppm, (iv) performing the SSE processing, and (v) evacuating the system to make sure no leaks had developed during processing.

5.9.2 Residual Resistivity Ratio

The electrical resistivity, ρ, of metals at low temperatures is an excellent tool to determine impurity concentration in them (Schulze 1981). The residual resistivity ratio, RRR, is calculated as

$$\text{RRR} = (\rho_{298\ \text{K}} - \rho_{4.2\ \text{K}})/\rho_{4.2\ \text{K}}$$

where ρ is the resistivity at the temperature given as subscript. RRR is related to the impurity concentration, C_i, by

$$C_i = \text{K/RRR}$$

where K is a constant of proportionality. A high value of RRR is seen to indicate a low value of C_i and vice versa.

5.9.3 Lanthanum

The solute mobilities are high in the bcc phase and this phase is stable in lanthanum above 1138 K. Fort (1987) conducted SSE processing of lanthanum above this temperature. To achieve steady state distribution of C and N, processing for 500 h was necessary. Oxygen distributes relatively more quickly in lanthanum. It is interesting to note that an attempt to SSE process a relatively impure lanthanum start material led to run failure because a build up of impurities at the anode end led to a decrease in the melting temperature of the region. After 120 h of SSE, the anode portion melted even at 1033 K.

In an earlier investigation, Ames lanthanum metal was SSE refined by Pan et al. (1980). The metal was refined to a resistance ratio of 260.

5.9.4 Praseodymium

SSE processing has been carried out on praseodymium by Fort (1987) using commercial metal as well as Ames metal as the start material. When refining standard grade commercial praseodymium, impurity transport and precipitation resulted in failure by melting at that point. On the other hand, high purity commercial metal as well as Ames metal could be refined to RRR values of approximately 250 and over 400, respectively.

5.9.5 Neodymium

The vapor pressure of neodymium at SSE processing temperatures is about two orders of magnitude higher than that of praseodymium. At temperatures approaching 1150 K, however, losses by volatilization were still not too high. In a SSE-refined material starting from commercially available neodymium, analytical and metallographic evidence indicated impurity transport by SSE, but the RRR values showed no gradient along the length of the sample. The flat RRR profile was attributed to a minor substitutional impurity that had a disproportionate effect on RRR and that was not significantly transported during SSE. If the same material were zone refined and the substitutional impurity removed prior to electrotransport, RRR gradient appeared. As could be anticipated, SSE processing of Ames neodymium resulted in a product having RRR gradients with or without preliminary zone refining (Fort 1987).

5.9.6 Gadolinium

Early work on successful purification of gadolinium by the electrotransport technique was carried out by groups at the Ames Laboratory and the Materials Science Center, University of Birmingham. Using a purified helium atmosphere at 1245°C, Peterson and Schmidt (1972) obtained metal with a resistance ratio ($R_{300\ K}/R_{4.2\ K}$) of 405. Somewhat lower temperature and an ultrahigh vacuum were used by Jordon and Jones (1975) and the metal refined had a resistance ratio of 175.

Fort (1987) noted that in the SSE purification of gadolinium, two of its properties had to be allowed for. One is its comparatively high volatility and the other is the closeness of the hcp to bcc transformation temperature to the melting point. He estimated that several hundred hours of SSE at 1320 K would be required for oxygen to approach steady state conditions. Typically the SSE program for gadolinium consisted of 500 to 1000 h at 1273–1323 K followed by slow cooling to room temperature over about 100 h. Using a previously zone-refined Ames metal, the highest RRR value of 800 was obtained.

5.9.7 Terbium

Jordon and Jones (1975) refined terbium by SSE under ultrahigh vacuum at 1050°C for 350 h. They prepared terbium of better than 99.9 at % purity from metal of commercial purity. The highest resistivity ratio obtained for the refined metal was 60 after a double processing treatment and 90 for the triple processed metal.

Fort (1987) used single crystal rods grown by electron beam float zone melting (EBFZ) and radiofrequency float zone melting (RFFZ) of Ames metals, as starting material. For terbium, the highest RRR attained was more than 400 with initial SSE processing at 1348 K for 200 h followed by approximately 600 h at 1273–128 K and 100 h at 1258 K. At these temperatures, volatilization rates were controllable.

5.9.8 Yttrium

As described earlier, the technique of electrotransport was first used by Williams and Huffine (1959) for a rare earth metal to refine yttrium. A purer grade of yttrium containing

lower interstitial impurity resulted from refining at a lower temperature under nearly 10^{-5} Pa vacuum, as compared to the product obtained from the first attempt (Carlson et al. 1966). Murphy et al. (1975) performed an interesting experiment in the electrotransport purification with a Y–2% Fe alloy. The alloy was electron transport purified at 1200°C for only 60 h. Even by this, the iron content of the entire cathode section decreased to below 0.01%. Carlson and Schmidt (1976) stated that electrotransport should be a feasible method for purifying yttrium with respect to silver, nickel, and other fast diffusing metallic elements besides iron. The interstitial impurities carbon, nitrogen and oxygen also have favorable mobilities in yttrium and are removable to very low concentration if ultrahigh vacuum was used and end effects and surface reactions were minimized.

Fort (1987) considered 1390–1420 K as the temperature at which the volatilization rates in a vacuum were acceptable for a processing time of 1000 h required for carbon and nitrogen impurities to closely approach steady state. Oxygen reached this state quickly. The highest RRR value of 800 (extrapolating to well over 1000 at the cathode end) was obtained with a high purity metal initially grown into a single crystal rod using RFFZ. The RFFZ processing program, in turn, consisted of 750 h at 1373–1423 K, 300 h at 1273–1373 K, and cooling to room temperature over 240 h.

5.9.9 Dysprosium and Holmium

Both dysprosium and holmium have moderately high vapor pressures. Fort (1987) noted that in processing them by SSE, an inert gas environment is necessary. However, even with 100 kPa gas pressure, problems due to volatilization did not disappear. One problem is whisker formation. During SSE, vaporization and recondensation onto the samples resulted in formation of dendritic whiskers on the sample surface. The 2–4 mm long whiskers form in dense clusters on parts of the sample and in these parts marked reduction in temperature was noticeable because of the cooling effect of the large surface area. Such whiskering, usually most severe toward the top of the sample, could be greatly reduced by slanting the sample at about 45° to the vertical, so that the vapor originating at the sample bottom rose away from the rest of the rod. Holding the sample horizontal was suspected to induce grain boundary sliding and hence not attempted.

SSE processing of dysprosium, under 70 kPa argon pressure, was carried out by Fort (1987) keeping the temperature between 1323 and 1373 K and processing time to 500 h. Prior to and after the main processing under argon, the sample and clamps were degassed at 1073–1173 K in vacuum. A commercially pure start metal, resublimed under ultrahigh vacuum conditions, was refined by SSE as above to obtain the lightest RRR of 125.

In the case of holmium, an Ames metal, SSE processed at 1373 K for 200 h refined to RRR of 90.

5.9.10 Erbium

The SSE of erbium has been described in detail by Fort et al. (1990). Ames metal was used as the start material. The metal was cast into a crude rod in a cold boat using arc melting. The rod was mechanically swaged to a uniform diameter of 7.1 mm except for one end, which was left slightly thicker. This thicker section, which would run cooler during SSE and was less likely to melt in the event of excessive impurity build up, was intended to be

the anode. The swaged rod was thoroughly cleaned, degassed, and stress relieved at 850°C and mounted in the SSE equipment. To prevent whisker formation, as explained in dysprosium processing, the sample was held at a 45° angle to the vertical.

The entire SSE processing was carried out in six stages. Some of these stages were carried out in ultrahigh vacuum and some under argon.

By SSE purification, the total impurity content in erbium decreased from 921 ppm atomic in the start material to 338 ppm atomic in the purest (cathode) section. This represents a 63% decrease in the overall impurity level. The resultant purity in the cathode end was 99.97 at % or 99.996 wt % compared to the start level purity of 99.91 at % or 99.988 wt %. In fact, the cathode end of the SSE refined rod represents the lowest impurity concentration ever reported for erbium.

Oxygen, nitrogen, and hydrogen electromigrated in erbium, as expected, toward the anode. Oxygen was the main contaminant at 640 ppm atomic in the start material. This level decreased in the cathode end to 200 at ppm after three stages of processing and to 168 ppm after six stages. The start value of nitrogen was 48 ppm atomic (4 ppm weight) and after six stages of processing, the N content at the cathode was below the limit of detection (1 wt ppm) and there was a progressive increase along the length of the sample from the cathode to the anode. In the start metal, the H content was below the detection limit. But at the end of SSE, the H level was 1500 ppm atomic (9 ppm weight) at the anode end while the H contents at other positions were below the detection limit. Some H contamination had occurred during SSE and H had then migrated toward the anode. Carbon concentration in the start metal was 97 ppm atomic, but at the end of SSE the value at the cathode was 111 ppm atomic. Carbon did not show a progressive increase in concentration from cathode to anode even though the level was lowest at the anode. Some carbon contamination of the sample had occurred during the SSE procedure, most likely during the preparation of the SSE rod and by the degassing of carbonaceous gases from the furnace walls. The final high carbon value was 306 at ppm in the center section and 195 ppm atomic at the anode.

Fluorine is another intractable impurity in erbium, and its content in the SSE refined erbium rod showed no constant trend along the rod length. This, most probably, is connected with possible inhomogeneous distribution of fluorine in the start metal. Fluorine contamination is a factor in erbium because the vapor pressures of ErF_3 and Er are comparable. Therefore during pyrovacuum refining, the fluoride tends to cosublime, and the sublimate collected first will have a higher F content than the one collected later.

For the metallic impurities, no consistent trend was generally apparent, possibly due to their presence in relatively low concentrations. Overall SSE is significant as the final step in the preparation of high purity erbium.

5.9.11 Lutetium

Carlson et al. (1973) purified lutetium by SSE. A rod of lutetium, 2.5 mm in diameter and 153.5 mm long was SSE purified at 1150°C for 168 h in an all-metal ultrahigh vacuum chamber under 3.3×10^{-8} Pa. The impurities profile of the rod and corresponding resistance ratios obtained by Carlson et al. (1973) are shown in Figure 5.14. They noted that there is a correlation between the resistance ratio and oxygen content of lutetium because the carbon and nitrogen content remained constant along the length of the rod. Peterson and Schmidt (1969) had predicted a favorable purification factor but low mobility for carbon at a temperature of 1150°C resulting in a long time for carbon to reach steady state. Even

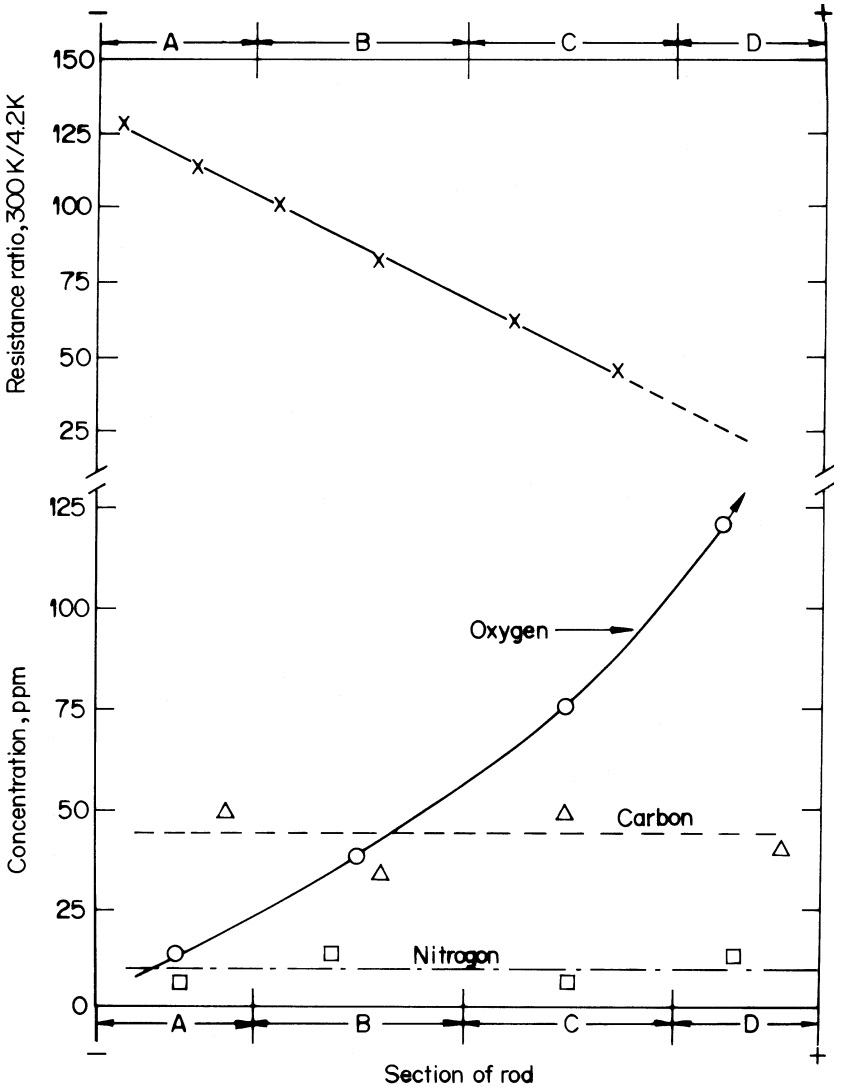

Figure 5.14 Concentration profile and resistance ratio of lutetium rod after purification by electrotransport at 1175°C for 160 h (Carlson et al. 1973).

though conditions for the removal of oxygen and nitrogen were stated to be favorable, as shown in Figure 5.14, the only redistribution of oxygen was actually observed.

5.9.12 Samarium

Samarium is volatile. Its vapor pressure at its melting point is approximately two orders of magnitude higher than dysprosium and holmium. Even under 70 kPa argon, the maximum temperature at which SSE processing of Sm could be carried out was 710–720°C, more than 350°C below its melting point. At these relatively low temperatures, whisker

formation was a problem, and even after 200 h no significant purification was detected by Fort (1987). In other words, SSE was not successfully applied to samarium because volatilization could not be sufficiently suppressed.

Electrotransport refined the maximum number of rare earth metals and in the process obtained some of the rare earths in their purest known states. However, Fort (1987) stated that SSE was a viable method of turning good quality metal into very good quality metal but was not a successful method for improving the purity of poorer quality start metals because the build up of impurities resulted in melt-through. While commenting on the potential of SSE processing for rare earth elements in the context of vaporization problems encountered, Fort (1987) observed that the vapor pressure should be 10^{-4} Pa or less when processing under vacuum and 0.5 Pa or less when processing under 70 kPa of argon, at the chosen SSE processing temperature. Among the rare earth elements not covered above, cerium and possibly scandium should be amenable to SSE processing in vacuum. Refining of scandium and europium under 70 kPa argon should be possible. It is not possible to SSE refine thulium and ytterbium.

5.10 ZONE REFINING AND ELECTROTRANSPORT

Electrotransport is the ultrapurification method effective for redistribution of interstitial impurities, and zone refining redistributes substitutional or metallic impurities effectively. In the ultrapurification of rare earth metals, refining has to be accomplished with respect to both the metallic and nonmetallic (interstitial) impurities. For this, in the overall sequence of ultrapurification, zone refining is followed by electrotransport. This sequence has been extensively investigated by Fort et al. (1987) for neodymium and gadolinium metals.

5.10.1 Neodymium

Fort et al. (1987) have described the ultrapurification of neodymium by zone refining followed by electrotransport. A bar of neodymium weighing about 92 g was degassed in the cold boat (of zone-refining equipment) at red heat and 2.6×10^{-7} Pa. The system was then filled with purified argon and subjected to zone refining (25 molten zones were passed at the rate of 11.7 cm h^{-1}). Matter transport also occurred during the process and the beginning of the rod became significantly thicker than the end. It was removed, swaged to a diameter of 8 mm, and its ends were cropped because zone transported impurities would have accumulated in the ends. The rod was then cleaned, placed in the cold boat, degassed in vacuum to red heat, backfilled with argon and zone refined (14 molten zones were passed at 11.7 cm h^{-1}). It was again removed, swaged to a diameter of 6.4 mm, its ends cut off because impurities had accumulated there, and the remaining, middle portion, of the rod was subjected to SSE.

The "beginning" end from zone refining was made the cathode in SSE because during zone refining most metallic impurities would have transported to the "end" end. Moreover, interstitial impurities would migrate from the cathode end to the anode end during SSE. Purification of neodymium by SSE was done under purified argon. The SSE processing consisted of an initial outgassing of the sample in a vacuum at 830°C for 144 h followed by the main run in 50×10^{3} Pa purified argon at >863°C, 820–863°C, and 800°C, for a total

Table 5.20 Analysis of zone refined and electrotransported neodymium (Fort et al. 1987)

Element	Start, at ppm	After zone refining and SSE, at ppm		
		Cathode	Center	Anode
O	360	180	239	360
H	571	bl	bl	143
N	21	bl	31	165
C	84	64	312	480
Ta	88	60	40	21
Fe	11	<0.6	1	16
Cu	3	2	3	0.7
Cr	2.6	<0.5	<0.06	<0.4
Se	4.3	8	5.4	8.2
Ce	3.6	4.7	6.3	5
Tb	<2	4	5	4
Si	<6	4	2	4
Gd	<3	<2	3	1.6
Cl	6	10	4	4
All impurities	<1166	<336	<652	<1212
Metallic impurities	<124	<82	<66	<60
O+H+N+C	1036	244	582	1148
Atomic percent	99.88	99.97	99.93	99.88

bl: below limits of detection.

of 755 h SSE under argon. The processing did not result in any dramatic increase of RRR. After cropping the anode end where impurities had accumulated, Fort et al. (1987) processed by SSE in a vacuum. The run lasted for a total of 1060 h of which for 412 h the sample temperature was above 863°C. The analysis is given in Table 5.20.

Among the metallic impurities, iron migrated to the anode end while tantalum had also distributed. The tantalum content of the start material was 88 at ppm. This content decreased to 60 at ppm at the cathode and to progressively lower levels in the center and the anode end. The indication is that tantalum was transported against the zone direction during zone refining. The decrease in iron content from an initial 11 at ppm to a final 0.6 at ppm at the cathode could have occurred by zone refining, but this conclusion could not be stated with certainty because iron is known to electromigrate rather quickly for a substitutional solute in many rare earth metals.

The interstitial impurities migrated toward the anode, as expected, during SSE. The carbon content indicated possible pick up of carbon from swaging and cleaning operations involving the use of hydrocarbons as lubricants or solvents. The overall impurity content decreased from about 1160 at ppm in the start material to approximately 330 at ppm at the cathode section after SSE. This corresponds to an improvement in purity from 99.88 at % to 99.97 at %. Much of the impurity content was as interstitial impurities O, H, N, and C. They together constituted 1036 at ppm and by combined zone refining and SSE, principally by the latter, their content decreased to 244 at ppm, at the cathode end. As pointed out earlier, the low impurity content of neodymium is not reflected in its RRR of the

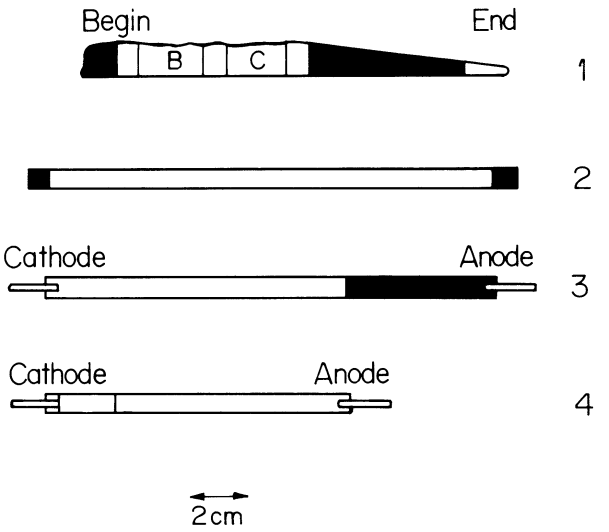

Figure 5.15 Schematic diagrams showing the size and shape changes of the gadolinium sample (1) after zone refining, (2) after remelting parts B and C and swaging, (3) after first stage of SSE, and (4) after final stage of SSE. Sections marked black were discarded before the next stage of processing. The tantalum end rods screwed onto the sample to act as current carriers during SSE are also shown (Fort et al. 1987).

purified samples, values that probably remain low because of reasons other than impurity concentration.

5.10.2 Gadolinium

Fort et al. (1987) have purified gadolinium by zone refining followed by electrotransport, enhancing, in the process, the purity from 99.75 at % to 99.94 at %. The procedure adopted is similar to that used for neodymium, using ultrahigh vacuum rated equipment.

A bar of gadolinium (Ames metal) weighing 110 g was degassed at red heat in a cold boat to a vacuum of 2.6×10^{-7} Pa. The system was backfilled with pure Ar to 100 kPa, and zone refining was conducted with nine successive molten zone passes at a rate of 18.7 cm h^{-1} followed by nine passes at 11.7 cm h^{-1}. A significant amount of material transport back toward the beginning of the bar occurred during zone refining and this is shown schematically in Figure 5.15. Portions marked A in the figure accumulated impurities transported to the "beginning" end of the zone-refined bar and had the highest O and N levels. That section was discarded. Virtually all iron, tungsten, aluminum and copper impurities accumulated in sections D and E and these were also discarded. Parts marked B and C had the lowest overall impurity contents after zone refining. Those portions were cut, remelted into a rod about 100 mm long, swaged to a diameter of 6.4 mm, cleaned, degassed, and again remelted in one quick zone pass. This rod was taken for refining by SSE.

Gadolinium is a relatively volatile metal which restricts the temperature and/or duration of SSE refining in vacuum. The electromigration velocities of oxygen, carbon and nitrogen are higher in the bcc phases (above 1235°C), but at such temperatures vaporization

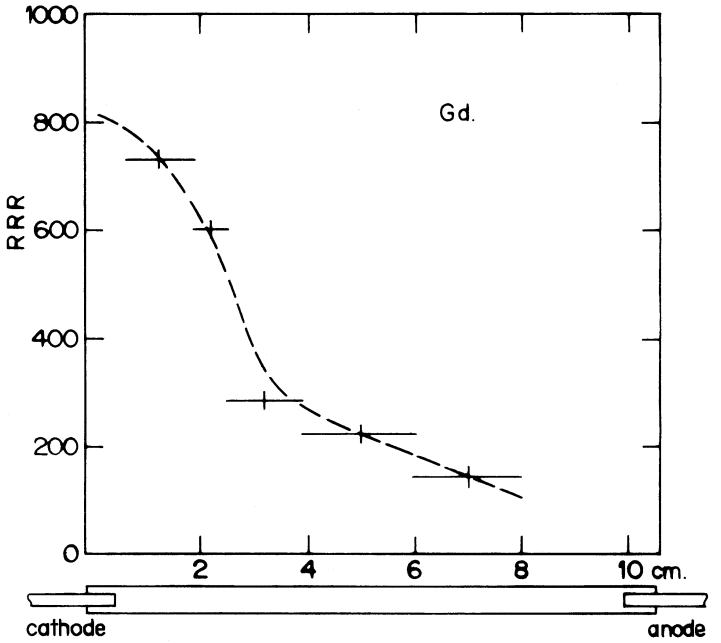

Figure 5.16 The final resistance ratio ($\rho_{293\ K}/\rho_{4.2\ K}$) profile along the zone refined and electrotransport purified gadolinium (Fort et al. 1987).

of gadolinium would severely curtail run duration. Hence processing has to be done in the α hcp phase, and the temperature chosen by Fort et al. (1987) was 1030–1040°C. The total processing time for the entire run, which was done in two parts, including initial degassing, warming up, and cooling down, was 2600 h.

The RRR profile of the SSE refined gadolinium rod is given in Figure 5.16. The measured best value of RRR near the cathode was 730 and the extrapolated value at the extreme cathode end was 800, the highest resistance ratios reported for gadolinium. The purest portion was the cathode end. The analysis of gadolinium purified by zone refining followed by SSE is given in Table 5.21.

By zone refining followed by SSE, the overall impurity level in gadolinium had decreased from 2480 at ppm (in the start metal) to 597 at ppm at the cathode section. In other words, the gadolinium purity had improved from 99.75 at % to 99.94 at %. Much of the impurity content given above is due to hydrogen, which in the start material was 1560 at ppm (10 wt ppm) and decreased to 468 (3 wt ppm) at ppm. If impurities other than hydrogen are considered, the initial value was 921 at ppm, and after zone refining and after SSE it was 129 at ppm.

The oxygen content was 550 at ppm in the start material. It decreased marginally to 500 at ppm in the purest region after zone refining, and came down to as low as 29 at ppm at the cathode end after SSE. Carbon zone refined in the zoning direction and electromigrated toward the anode. The effects of both these techniques worked in the same direction. Yet the content decreased from 320 at ppm in the start material to only 60 at ppm, at the cathode end. Maximum purification with respect to carbon occurred during SSE. If metallic impurities alone were considered, the improvement was from 40 at ppm to less than 17 at ppm. Iron was transported by both these techniques and decreased from 10 at ppm

Table 5.21 Analysis of gadolinium purified by zone refining and electrotransport (Fort et al. 1987)

Values in at ppm

Element	Start	After zone refining					After SSE cathode end
		Begin	¼	½	¾	End	
O	550	658	457	378	304	363	29
H	1560	468	390	468	390	780	468
N	11	39	17	11	11	11	22
C	320	210	288	341	419	563	60
Fe	10	1	0.3	2.5	68	900	0.22
W	5	<2	<1	<1	8	140	4.3
Al	4	<0.2	0.6	1	6	50	<0.07
Si	2	<0.5	<0.4	<0.4	2	40	0.84
Ti	2	<0.2	<0.1	0.9	7	18	<0.08
Cr	2	<0.5	<0.6	<0.6	4	10	0.37
Ni	8	0.3	0.03	0.1	<0.4	20	0.17
Zr	9	12	9	15	60	60	5.7
Cu	2	0.4	0.2	0.3	10	200	0.13
Ce	0.4	0.4	0.1	0.2	0.6	0.6	1.7
Hg	1	2	<0.02	<0.05	<0.3	1	2.1
Ta	2	<0.4	<0.3	<0.3	3	6	1.9
Cl	nd	5	6	4	20	9	0.63
All impurities	2481	<1398	<1171	<1224	1318	3171	597
Metallic impurities	40	<18	<13	<22	169	1445	18
O+H+N+C	2441	1375	1152	1198	1129	1717	579
Atomic percent	99.75	99.86	99.88	99.88	99.87	99.68	99.94

in the start material to 0.22 at ppm at the cathode end. Zirconium moved in both zone refining and electrotransport, but these had not markedly decreased its content.

5.11 IODIDE REFINING

The iodide refining process, developed in 1925 by Van Arkel and de Boer (1925), has been successfully applied to the refining of several reactive and refractory metals. The process is carried out by heating the impure metal with iodine in a closed system. A volatile iodide of the metal is formed, and this iodide is decomposed on contact with a hot wire whereby the pure metal deposits on the wire and the released iodine returns to react with more of the crude metal.

Two general criteria must be met before a metal is considered for iodide refining (Loonam 1959). One is that the metal must be capable of existing as a condensed phase (solid or liquid) at some temperature and pressure in equilibrium with a gas (gaseous

iodide) of high atomic ratio of iodine to metal. The second criterion is the capability of the metal to react readily with the gaseous product of the deposition reaction at the same pressure but a different temperature to yield a gaseous product of low atomic ratio of iodine to metal. It is also desirable that the metal have a high melting point and low vapor pressure. These aid in the deposition of the metal as a solid. The iodide refining is most likely to be feasible with metals that form tri-iodide and tetraiodide because the large positive entropy changes on dissociation lead to an overall decrease in free energy of dissociation with increasing temperature. In other words, the metals least likely to be amenable to refining are those that form monoiodides that remain monomeric and stable in the vapor phase. According to Loonam (1959), the monoiodides of rare earth metals would be sufficiently stable to prevent dissociation, and this observation has been confirmed by the data of Scaife and Wylie (1958). In addition, the generally high volatilities of rare earth metals are not very favorable for iodide refining because at the high temperature needed for the dissociation of the iodide the deposited metal would vaporize.

Foster et al. (1952) used a modified Van Arkel–de Boer process for deposition of lanthanum, the least volatile of the rare earths. The iodide was formed by reaction of iodine and aluminum on lanthanum oxide. At 1000°C the dissociation of iodide was negligible and only slightly improved at 1800°C. Only small amounts of lanthanum were detected on the wire, and even this deposit was contaminated with aluminum.

The deposition of yttrium from both bromide and iodide was also attempted by Frazier (Huffine and Williams 1961). The bulb temperature (iodide formation) was between 300 to 350°C, and the molybdenum filament temperature (iodide decomposition) was between 600 and 1600°C. No deposit was formed which suggested that it was not possible to deposit rare earth metals by the Van Arkel–de Boer process.

5.12 MISCELLANEOUS PROCESSES

Many techniques, not covered above, have been applied for the purification of one or more rare earth metals. One is based on amalgamation of rare earth metals or the hydrides. This technique has been used by Schumacher and Harris (1926) and Audrieth (1939). While mercury wets the rare earth metals and hydrides and forms amalgams, the oxides, carbides, and halides remain insoluble in mercury and could be separated by underpouring or filtration. Warf et al. (1953, 1957) have shown that the hydrides of lanthanum, cerium, and ytterbium were wetted by mercury, whereas the oxide and other impurity inclusions floated on the amalgam. The metal has to be in a finely divided form for efficient amalgamation, which can be accomplished by forming the brittle hydride and grinding. After the flotation, mercury and hydrogen were removed by vacuum distillation and pure rare earth metal powder was obtained.

Rare earth metals readily form relatively stable hydrides. This fact was sought to be exploited in a technique where hydrogen was to be introduced into a low melting rare earth alloy to selectively precipitate the rare earth hydride. The hydride would then be separated from the melt by filtering or decantation and vacuum distilled to remove hydrogen and produce the metal powder. This technique was used successfully for thorium, but the experiments of Frazier (Huffine and Williams 1961) with a low melting alloy of yttrium, aluminum, and magnesium were inconclusive.

5.13 SUMMARY

As-reduced rare earth metals are usually 98 to 99% or at best 99.5% pure. A number of processes may be used to refine and ultrarefine these metals to as high as 99.99 at % purity. The nature and concentration of impurity to be removed, the final purity level desired in the refined metal, and the physical properties of the metal itself determine the refining techniques to be used. Complete purification is not achieved by any one refining technique and, as a rule, a sequence of processes has to be applied to remove all the impurities.

Impurities in the as-reduced rare earth metals originate from many sources. The most important sources are the starting materials, namely, the rare earth compound intermediate and the reductant. Also important is the environment in which reduction is carried out, namely, the gaseous atmosphere or the residual gases in the atmosphere if the process is conducted in a vacuum, as well as the container for reduction. Any other rare earth present in the rare earth that is currently processed is also an impurity, but the presence of such impurity rare earths in a given rare earth metal has to be controlled in the separation stage itself before the metal reduction. The impurities originating from the starting materials are calcium, lithium, magnesium, cerium, zirconium, thorium, zinc, iron, cobalt, nickel, copper, fluorine, chlorine, and oxygen. The impurity content of the final metal is determined by the purity of the raw materials, the processes used for converting raw materials to interprocess intermediates for reduction, and the reduction process itself. The impurities oxygen, nitrogen, hydrogen, and carbon usually originate from the atmosphere in which the processes are carried out. Crucibles for reduction come into intimate contact with the metal being reduced, undergo corrosion or dissolution, and end up as an impurity in the metal. Iron, silicon, carbon, titanium, zirconium, molybdenum, and tantalum are examples of impurities that end up in the metal this way.

There are two major methods of impurity removal from as-reduced metals. In the first type to which most of the conventional purification techniques belong, the impurities are eliminated from the metal. In the second type, to which most of the ultrapurification techniques belong, the impurities are not completely separated from the metal but are redistributed so that one physical portion of the metal is substantially purer than the other portion. Both in purification and ultrapurification, high vacuum or ultrahigh vacuum is used as the environment not only for preventing atmospheric impurities from coming into contact with the metal undergoing refining, but also to effect removal of impurities from the metal.

Pyrovacuum treatment, in which the metal is heated to temperatures up to and above its melting point under high vacuum in a tantalum crucible, is the most important and effective means available for the purification of rare earth metals. In vacuum melting, purification occurs because the impurities vaporize, leaving behind the purer metal. In vacuum distillation or sublimation, the metal itself is vaporized off to condense as a purer product, leaving behind impurities in the residue. The rare earths lanthanum, cerium, praseodymium, and neodymium all have very low vapor pressures, and vacuum melting and vacuum remelting complete the purification operation. In the case of gadolinium, terbium, yttrium, and lutetium, the vapor pressures are relatively higher and vacuum melting is followed by vacuum distillation. The metals scandium, erbium, holmium, and dysprosium are more volatile and can be purified by vacuum melting followed by vacuum sublimation. In the case of the four most volatile rare earth metals, europium, samarium,

ytterbium, and thulium, no vacuum melting is done and purification is effected exclusively by vacuum sublimation. The pyrovacuum treatments are carried out in induction- or resistance-heated furnaces using tungsten or tantalum as a container for most of the metals and also in electron beam melting furnaces for yttrium.

Electrorefining in an inert atmosphere electrolysis cell, as a process for rare earth metal purification, has been applied for the purification of yttrium and gadolinium, the two metals that are most difficult to obtain by exclusive pyrometallurgy routes. When refined in a $LiCl-YCl_3$ bath the metallic impurities were removed, whereas refining in a $LiF-YF_3$ bath led to the removal of oxygen in addition to the metallic impurities. In the electrorefining of gadolinium the electrolyte invariably contained GdF_3 in addition to LiF. The electrorefined metal contained less oxygen, but the final oxygen concentration is determined by the oxide and hydroxide impurities in the electrolyte.

Further removal of impurities, the bulk of which have already been eliminated in pyrovacuum treatments, is achieved by the ultrapurification techniques of zone refining and electrotransport. Zone refining is useful for bringing down the levels of metallic impurities, particularly tantalum and tungsten picked up by the metals during pyrovacuum refining. In zone refining of rare earth metals, the use of a high vacuum or an equally pure inert atmosphere is mandatory to prevent the metal from picking up impurities from the gaseous atmosphere. Two techniques have been used. In one the metal is contained in a long horizontal trough or crucible, and the zone is moved in a horizontal direction. In the other, the metal is supported vertically from the ends without a container, the narrow molten zone being maintained because of the surface tension of the metal. Heating is by induction or preferably by an electron beam.

Much of the early work on zone refining was done on yttrium but later works focused attention on lanthanum, cerium, gadolinium, and terbium. Metallic impurities such as iron, copper, cobalt, nickel, tantalum, tungsten and aluminum are transported efficiently in the zone direction. As it is, these elements are not originally present in high concentrations. The direction of transport of oxygen, hydrogen, and nitrogen is opposite to the direction of transport of common metallic impurities. These three impurities are usually present in considerable concentration and also do not transport efficiently. As a result, no part of the zone-refined bar is of greatly improved overall purity compared to the starting metal. The ability of zone refining to refine rapidly with respect to metallic impurities, however, makes the technique useful particularly in combination with another technique that can refine with respect to the interstitial impurities. Zone refining in combination with solid state electrotransport enabled production of rare earth metals with the lowest possible impurity content.

In solid state electrotransport, a direct current is passed through a rod or strip of metal held between two electrodes in an ultrahigh vacuum rated container. During electrotransport the impurities move under the influence of the electric field and when held for sufficient time accumulate at one end or another of the bar, leaving the remainder enhanced in purity. The electric current also heats the metal rod to near the melting point, and the high temperature enhances the impurity transport rates. The vapor pressure of the metal at the electrotransport temperature determines whether the process is carried out in ultrahigh vacuum or under an equivalently pure inert gas cover. The technique was first applied to purify yttrium and subsequently to purify lanthanum, praseodymium, neodymium, gadolinium, terbium, erbium, and lutetium, cerium, and scandium. Purification by this technique is very difficult for samarium and europium and impossible for thulium and ytterbium.

Oxygen, hydrogen, carbon, and nitrogen account for more than 95% of the impurities found in commercially obtainable rare earth metals and these are the elements most amenable to electrotransport purification. It is a slow process and works on relatively small samples, and only a portion of the sample is left in a highly purified condition. Zone refining is also a process of refining by impurities redistribution, particularly of substitutional impurities, and the combined zone refining electrotransport operation finally results in only a small portion of the metal in a highly purified state with respect to all impurities. Such very high purity metals have been invaluable for research.

Some more techniques including iodide refining have been attempted for rare earth metals, but the results were unsuccessful or inconclusive. The sequence of vacuum melting, vacuum distillation/vacuum sublimation, zone refining, and electrotransport remains the technically perfect route for the conversion of as-reduced rare earth metals to the purest possible rare earth metals.

CHAPTER 6

Rare Earth Materials

6.1 INTRODUCTION

Rare earths-containing end product materials for commercial use or for research applications are numerous. A complete description of the most important of these materials was given in the section on applications of rare earths in Chapter 1. These materials can be basically divided into two groups. One group comprises commercially used rare earth compounds, alloys, and metals, while the other group comprises rare earth-bearing products obtained using rare earth compounds, alloys, and metals as the interprocess intermediates. This chapter focuses on the preparation of the commercially used rare earth compounds, alloys, and metals. Several materials, for example, rare earth compounds such as the chloride, hydroxide, fluoride, oxide, and carbonates, figure as intermediates obtained during routine processing or by processes readily branched from the regular flowsheet. The preparation of these compounds was therefore included in the chapter on resource processing. Preparation of elemental rare earths was covered in the preceding two chapters, which also included certain references to the preparation of rare earth alloys either because the processes used were very similar or because the alloys happened to be intermediates for the preparation of pure metals.

The materials covered in this chapter are specific specialty alloys of rare earths, starting from misch metal and including rare earth–iron–silicon alloys, yttrium–aluminum alloys, lanthanum–nickel alloys, permanent magnet materials based on samarium and on neodymium, and magnetostrictive, and magnetocaloric materials. Many rare earth compounds have emerged as special performance materials in a range of new technology areas. Their preparative aspects have also been described.

6.2 MISCH METAL

Misch metal is the material containing, in metallic form, the mixed light rare earths in the same or slightly modified ratio as found in the resource minerals. The composition of the

misch metal depends on the source from which it is derived. Misch metal obtained from a monazite source is relatively high in neodymium and praseodymium, whereas the misch metal from a bastnasite source is high in lanthanum but low in neodymium and praseodymium.

Traditionally, monazite was the source of rare earths (Morrice and Knickerbocker 1961). In the 1890s monazite was processed for the extraction of thorium as thorium nitrate, which was used in Auer gas mantles. The residue remaining after thorium extraction contained cerium, lanthanum, neodymium, praseodymium, and other rare earth compounds in minor amounts but was discarded. Auer Von Welsbach first found that a pyrophoric metal (misch metal) could be prepared from this residue. In 1908 he founded the Treibacher Chemical Works in Austria and started commercial production of misch metal. The metal's pyrophoric properties were of use in making lighter flints. Soon, monazite was processed principally as a source for misch metal. Starting in 1949, when a large bastnasite deposit was discovered in Mountain Pass, California, bastnasite was also processed as a source for misch metal. Presently, misch metal is obtained from both monazite and bastnasite sources. The processes used are fused salt electrolysis or thermal reduction.

Misch metal is commercially produced in tonnage quantities by fused salt electrolysis of anhydrous chlorides (Hirschhorn 1968). Specific details of these commercial operations have not been revealed, but several descriptions of procedures and equipment have been published.

6.2.1 Preparation of Mixed Rare Earth Chlorides

Commercial production of misch metal is based on the use of mixed rare earth chloride, $RECl_3$. In the past, all mixed rare earth chloride was obtained by wet chemical treatment of monazite and bastnasite, in the form of a hydrated product. This hydrated product contained about 30% H_2O and was treated to yield an anhydrous product with low oxychloride content, for electrowinning. Dehydration was accomplished using methods that minimize oxidation or hydrolysis.

Typically, dehydration techniques involved the use of vacuum heating of hydrated mixed rare earth chloride or heating them in air with an admixture of certain nonrare earth salts. The additives were meant to reduce hydrolysis. During World War II, one supplier to the German misch metal industry (the Auergesellschaft in Berlin) used rotary iron vacuum drum dryers that were steam heated to 350°C at a vacuum level of 93×10^3 Pa. The anhydrous chloride was reported to contain 1.5% oxychlorides (Livingston and Kent 1946).

In another method, the chloride was melted in a cast iron, steel or ceramic vessel from which air was largely excluded (Kremers 1954). Heating was carried on until a porous, solid, nearly anhydrous product was obtained. The product had up to 10% of water insoluble basic chloride content.

Heating a mixture of rare earth chloride with $CaCl_2$ in air for 2 to 2½ h was practiced at Prometheus in Bavaria (Hirschhorn 1968). The yield was usually 62%. This indicates that there was obviously substantial oxychloride content in the product. A two-stage vacuum drying process was used at Treibacher Chemische Werke in Austria. The hydrate was heated first at 170°C and then at 350°C (Livingston and Kent 1946).

In certain commercially adopted dehydration techniques (Hirschhorn 1968), ammonium chloride was added to the hydrated chloride to reverse the hydrolysis, according to the following reactions:

$$RECl_3 + 3H_2O \rightarrow RE(OH)_3 + 3HCl$$

$$RE(OH)_3 + 3NH_4Cl \rightarrow RECl_3 + 3NH_3 + 3H_2O$$

In an industrial practice, to carry out dehydration ($RECl_3 \cdot 6H_2O$) was quickly heated to 400 to 500°C with NH_4Cl in an inert atmosphere.

Some producers used sodium or calcium chloride to retard hydrolysis on the basis of the common chloride ion mass action effect. The addition of NaCl and/or $CaCl_2$ to the electrolyte was usually desirable, and their incorporation into the feed during dehydration was convenient.

Apart from the route that involves preparation of a hydrated chloride and its subsequent dehydration, there are other processes for obtaining the anhydrous chlorides directly from the mineral. Th. Goldschmidt AG at Essen in Germany uses chlorination of monazite or bastnasite to produce anhydrous rare earth chlorides (Brugger and Greinacher 1967). The product is suitable, without any further processing, for electrolysis to misch metal. The analysis of this chloride (Hirschhorn 1967) is given in Table 6.1 along with the analysis of chlorides from the wet processing of both monazite and bastnasite.

6.2.2 Electrolysis of Chlorides

Two types of cells have been used for the production of misch metal by chloride electrolysis (Singer et al. 1945, Livingston and Kent 1946). Details of these cells are given in Figures 6.1 and 6.2 and listed in Table 6.2.

Table 6.1 Typical analysis of rare earth chlorides (Hirschhorn 1967)

Component	Hydrated chloride from monazite	Hydrated chloride from bastnasite	Anhydrous chloride from chlorination of bastnasite
Total RE oxide[a]	46.2	46.0	66
CeO_2	47.6	50.3	49.1
Pr_6O_{11}	5.0	4.2	4.7
Nd_2O_3	17.3	11.2	12.7
Sm_2O_3	2.9	1.3	1.6
La_2O_3 and other RE oxides	27.1	32.8	29.5
H_2O	28.5	29.0	0.5
Fe_2O_3	0.04	0.002	<0.01
P_2O_5	<0.04	<0.03	<0.01
Na_2O	0.1	0.15	0.16
MgO	0.1	0.1	0.09
CaO	0.9	0.19	1.3
SrO		0.2	0.3
BaO		0.24	1.1
Insoluble residue	0.05	0.04	5.4[b]

[a]The individual rare earth oxide contents are given as the percentage of total rare earth oxide present. The contents of other components are in percentage.
[b]Mainly rare earth fluoride.

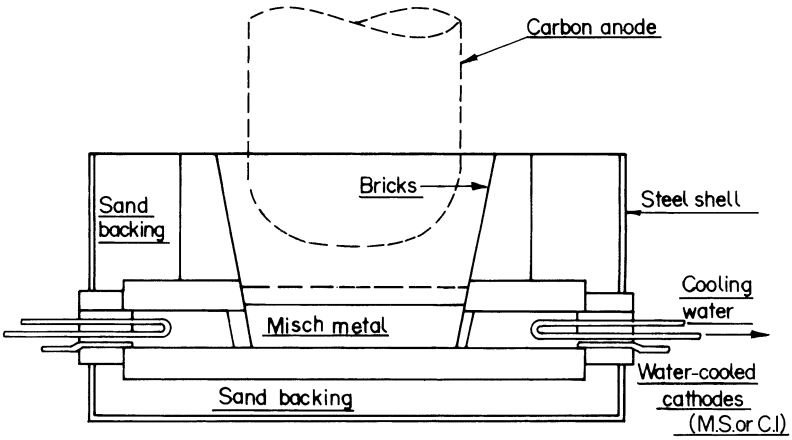

Figure 6.1 Electrolysis cell at Treibacher Chemische Werke, Austria (Morrice and Wong 1979).

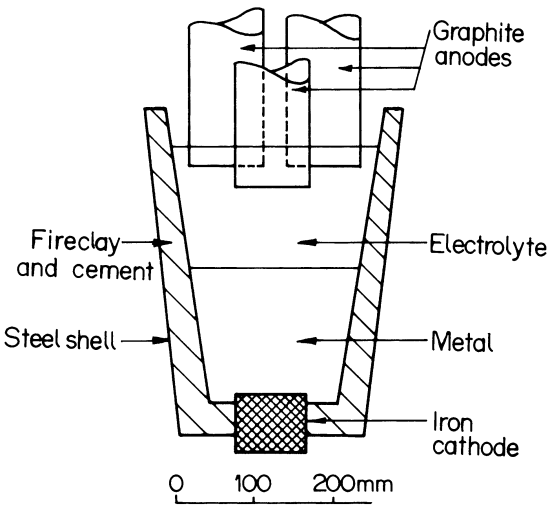

Figure 6.2 Electrolysis cell at Prometheus, Bavaria (Hirschhorn 1967).

The type of cells shown in Figure 6.1 are ceramic cells. The container for the molten electrolyte and for the molten misch metal cathode is made of fire brick. The electrical connection to the cathode was given through two water-cooled steel blocks inserted in the cell walls. The anode was 50 cm in diameter and 1 meter long and was made of amorphous carbon. The anode could be raised and lowered into the electrolyte. They were usually operated in series to facilitate semicontinuous production. Molten electrolyte was transferred from one cell to another for rapid start up. During operation, misch metal collected at the bottom of the cell where it was kept in the molten state by the flow of direct current through it to the cathode. At suitable intervals, the metal that was covered with a layer of molten electrolyte was ladled out and poured into molds. The metal solidified in the mold

Table 6.2 Characteristics of some fused salt electrolytic cells for preparation of misch metal (Hirschhorn 1967)

	Treibacher cell	Prometheus cell
Electrolyte	$RECl_3$–NaCl	$RECl_3$–$CaCl_2$
Anode	Carbon	Graphite
Cathode	Iron	Iron
Bath temperature, °C	850	850
Cell atmosphere	Cell gases + air	Cell gases + air
Average DC current, A	2300	1500
Average DC voltage, V	14	12
DC power consumption, kWh/kg	15.6	13.6
Current efficiency, %	45	50
$RECl_3$/Metal ratio	2.3	2.8
Capacity, kg metal/hr	1.86	1.32

under the protective layer of electrolyte. After cooling, the solidified electrolyte was broken off and the metal was separated and washed.

The cell shown in Figure 6.2 also has a refractory lined steel vessel to contain the molten bath (Hirschhorn 1967). The cathode was an iron block at the bottom of the container. Several graphite rods extended vertically into the cell through its top and served as anodes. Unlike the cell given in Figure 6.1, the cell in Figure 6.2 was tiltable (Livingston and Kent 1946). This arrangement simplified pouring of the product into molds.

Contamination of the misch metal product due to iron and silica could be decreased by constructing cells of graphite. When misch metal contaminated with iron was acceptable, as for example, misch metal for ferrous alloy applications, iron pots could be used instead of graphite (Greinacher 1970).

Before electrolysis a mixture of anhydrous rare earth chloride, NaCl, KCl, or $CaCl_2$ was charged into the pot. In one procedure, the charge was melted by external burners. In another procedure, the anodes were lowered into the cell until they contacted broken pieces of cerium kept at the bottom of the pot. The solid bath constituents were then packed around the bottom of the anodes. The direct current was turned on and after sufficient electrolyte had been melted, the anodes were raised to begin electrolysis. The chloride bath temperature was raised to 800 to 900°C by passage of electric current. During electrolysis additional external heating was not required.

The cells could be enclosed by steel covers so that air was excluded. This would decrease gas content in the misch metal produced. The gaseous products of electrolysis, comprising mainly chlorine mixed with gaseous carbon compounds, were drawn off and treated by absorption in a suitable off-gas treatment system to decrease air pollution.

The electrolysis was usually continued as long as the current efficiency remained high and metal quality was satisfactory. Generally, the current efficiencies of the commercial cells described for misch metal production are low. This is in part due to the energy consumption for maintenance of cell temperature and also due to the accumulation of compounds of samarium, europium, and other nonreducible rare earth compounds in the electrolyte (Hirschhorn 1967). The product was collected at the bottom of the cell where it could be maintained in the molten state by resistance heating or allowed to solidify by using

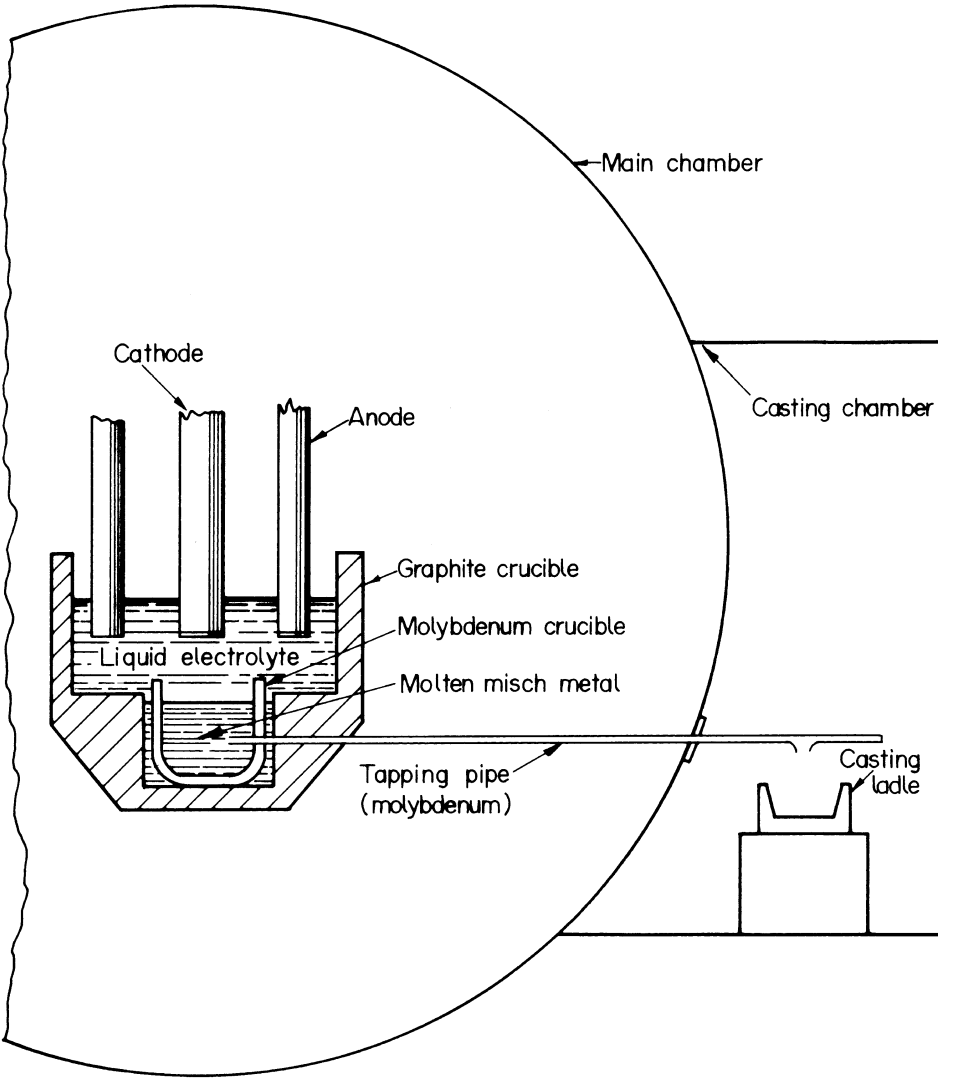

Figure 6.3 Electrolytic cell with provision for tapping metal product (Shedd et al. 1970).

a cooled cathode. In the latter case, the solidified metal was melted again by internal resistance heating, supplemented, if needed, by an external source of heat before it was removed from the cell. These were many ways by which the misch metal was recovered from the cell. One procedure was to scoop the liquid metal with a ladle. The other procedure was to pour the entire contents of the cell, electrolyte bath included, into molds in which it was kept molten. After the misch metal had settled to the bottom of the mold, the liquid bath was returned to the electrowinning cell and the electrolysis was started again. The analysis of misch metal commercially produced by chloride electrolysis is given in Table 6.3.

Commercial production of misch metal has been carried out primarily by chloride electrolysis, however, in the U.S. and Japan, the procedure followed (Thomas 1977, Kudo 1988) used oxide as the feed to the electrolytic cell and a mixed fluoride electrolyte was

Table 6.3 Analysis of commercially produced misch metal (Hirschhorn 1967)

Element	Content in MM, %
Ce	53
La	23
Nd	16
Pr	5
Dy	Trace
Gd	2
Y	Trace
Other RE	Not detected
Cr	0.034
Fe	0.035
Mg	0.032
Mn	0.006
Si	0.010
C	0.008
O	0.002
N	0.003

used. This procedure was essentially developed by the U.S. Bureau of Mines (USBM) at the Reno Metallurgy Research Center. The USBM process of electrowinning misch metal directly from mixed rare earth oxides dissolved in a fluoride electrolyte was adopted by the Rare Earth Metal Corp. of America, a joint venture of Alcoa and Molycorp in the U.S. and by Santoku Metal Industry Co. in Japan. As early as 1977, the Rare Earth Metal Corp. successfully completed operation of a pilot electrolytic cell using mixed rare earth oxide and began construction of a 20,000 amp cell for a production rate of about 100,000 kgs of misch metal per year. Santoku switched over from chloride electrolysis to the USBM process and operates several 20,000 amp cells for misch metal production (Thomas 1977).

6.2.3 Electrolysis of Oxide–Fluoride Melts

The electrolysis of a mixed rare earth oxide feed obtained by processing of bastnasite concentrate in a REF_3–LiF–BaF_2 electrolyte was investigated at the Reno center of the U.S. Bureau of Mines for preparing misch metal (Shedd et al. 1970). The process was carried out in a 300 mm diameter cell for continuous electrolysis, shown in Figure 6.3.

The cell had a 300 mm inside diameter with a 50 mm diameter molybdenum cathode surrounded by eight 50 mm diameter graphite rod anodes. The spacing between the cathode and anode was 65 mm. The feed material was added to the cell through a 25 mm diameter tube positioned between two anodes. A molybdenum crucible was placed below the cathode to collect the misch metal product. A molybdenum pipe attached to the molybdenum collecting crucible extended out of the cell 760 mm into a casting chamber where a mold was kept to collect the molten misch metal.

The cell was internally heated. Initial melting of the bath and heating to electrolysis temperature were done by applying alternating current (AC) to a graphite resistor positioned

Table 6.4 Analysis of treated bastnasite concentrate (Shedd et al. 1970)

Element	Content, %
Ba	4.7
Ca	0.3
C	0.6
Ce	42.3
Eu	Not detected
F	2.0
Gd	0.01
Fe	0.7
La	23.9
Nd	9.8
Pr	3.2
Sm	0.6
Si	1.0
S	0.07
Th	Not detected
Y	0.2

between the cathode and the two anodes. Once the electrolyte reached the temperature of 950°C, the resistor was removed and the direct current (DC) used for electrolysis provided sufficient heat to maintain the cell at 950°C.

The cell was insulated by refractory bricks and was located in a gas-tight steel chamber, 1220 mm in diameter and 1220 mm long. The chamber was equipped with a glove and view and access ports. It was evacuated and back filled with helium four times before start of each operation.

The feed material for electrolysis was derived from bastnasite. It was prepared as follows. The bastnasite concentrate was leached with dilute hydrochloric acid to remove $CaCO_3$ and $SrCO_3$. The leach residue was roasted with Na_2CO_3 at 700°C to convert the barite impurity to $BaCO_3$ and to decompose the carbonate. The material was then leached in water to remove Na_2SO_4 and dried at 400°C. The bastnasite concentrate thus treated was a mixture of oxides with a small amount of fluorides. The analysis is given in Table 6.4.

The electrolyte was composed of REF_3, LiF (99.6% pure), and BaF_2 (98.2% pure). The mixed rare earth fluoride was prepared from the treated bastnasite concentrate by hydrofluorination. The oxygen content of the fluoride was 0.64% and the sulfur content was 0.04%. All the electrolyte components were dried at 300°C for 24 h before use. Based on preliminary experiments with a 75 mm diameter experimental cell, Shedd et al. (1970) chose an electrolyte containing 50% REF_3, 20% BaF_2, and 30% LiF. Forty-five kgs of electrolyte were used. The cell operating data are listed in Table 6.5. The cell was maintained at the operating temperature throughout the duration of electrolysis during which many electrodepositions were carried out. At times when electrolysis was not conducted, the electrolyte was kept molten by passing AC through the electrodes.

After electrolysis, the metal product was tapped. To tap the metal, the cathode was raised out of the electrolyte and an AC of 1500 amperes at 9 volts was passed between the anode and the molybdenum tapping pipe. Metal flowing from the pipe was collected in the

iron mold in the casting chamber. Tapping lasted until all the metal had drained and electrolyte began to flow through the pipe. The AC was then turned off and the electrolyte was allowed to freeze in the tapping pipe. The analysis of the tapped metal is also given in Table 6.5.

Table 6.5 Data for operation of electrowinning and tapping of misch metal (Shedd et al. 1970)

Electrolyte composition, %	50 REF_3–20 BaF_2–30 LiF
Temperature, °C	950
Anode	50 mm diameter graphite rods, 8 nos.
Cathode	50 mm diameter molybdenum rod, 1 no.
Average voltage, V	8,5
Current, A	980
Initial anode current density, A/cm^2	1.04
Cathode current density, A/cm^2	8.32
Treated bastnasite concentrate fed, g	8630*
Feed rate of treated bastnasite concentrate, g/min	14.4
Duration of electrolysis, h	10
Misch metal product, g	6359
Current efficiency, %	37
REO utilization, %	98

Analysis of tapped misch metal product

Element	Al	C	Fe	Mo	O	Si	S	Ce
Content, %	0.17	0.15	0.56	0.38	0.02	0.20	0.005	60.0

Element	La	Nd	Pr	Sm, Gd, Y, Th
Content, %	18.4	15.2	6.0	not detected

*contained rare earth value as RE_2O_3 6481 g.

Shedd et al. (1970) noted that several electrodepositions could be conducted in the electrolyte, and the electrolyte system would sustain prolonged use if periodic additions of salts were made to readjust the electrolyte composition.

Even though misch metal is commercially prepared by the fused salt electrolysis methods described above, and the product is suitable for most of its applications such as alloying additive for ductile iron and steels and as a lighter flint, there are a number of applications where misch metal can be potentially useful as a replacement for the relatively more expensive individual rare earth metals, and a purer misch metal is desirable. A method based on metallothermic reduction of the fluoride has been described by Palmer et al. (1982) of the Ames group for preparation of pure misch metal.

6.2.4 Ames Process

The flowsheet for the production of pure misch metal starting from mixed rare earth carbonate obtained from bastnasite or monazite processing (Palmer et al. 1982) is shown in Figure 6.4. The term "purity" used here refers to the absence of the non rare earth elements

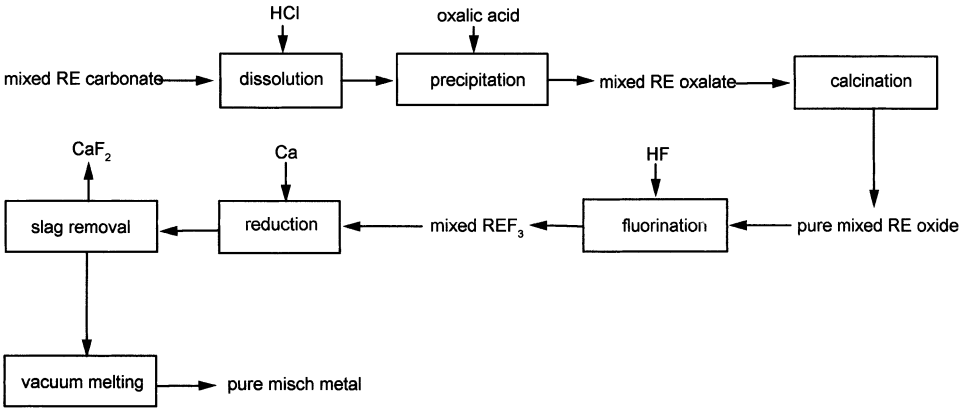

Figure 6.4 Flowsheet for the preparation of pure misch metal.

from this mixed rare earths alloy. The purity in the product was achieved by using purified start materials. As-received mixed rare earth carbonates from bastnasite and monazite origin were first purified by dissolution in HCl and precipitation of the rare earths as oxalate. The oxalate was calcined to the oxide in fused silica trays. This treatment brought down the levels of almost all the impurities originally present in the rare earth carbonate and resulted in pure mixed rare earth oxide. The values are given in Table 6.6.

Oxalate precipitation is a well-known analytical procedure to recover pure rare earths from solution. Along with thorium and the alkaline earths, calcium, strontium, and barium, the rare earths also form the most insoluble oxalates. Oxalates of most of the non-rare-earth metals are not precipitated from dilute acid solutions. As a result, oxalate precipitation, using oxalic acid, leads to complete partition between the rare earths on the one hand and silicon, manganese, iron, copper, and zinc on the other (Palmer et al. 1982). Use of a strongly acidic media will result in some calcium, strontium, barium, thorium, and uranium being left behind in the aqueous phase.

Table 6.6 Analyses REO from bastnasite and monazite before and after purification (Palmer et al. 1982)

Impurity	Bastnasite		Monazite	
	As-received	Purified	As-received	Purified
Si	50	7	20	<2
Ca	22000	1400	820	100
Mn	3	<0.5	1000	1
Fe	500	20	400	20
Cu	800	<0.1	400	<0.1
Zn	60	<2	60	<1
Sr	7000	20	2	<2
Ba	200	<0.4	10	<0.4
Th	6.5	<4	120	50
U	1.4	<0.2	100	6

The oxides were converted to fluorides in 300 g batches. The oxide loaded in a platinum tray was heated to 650°C under a flow of 8 lph anhydrous HF and 20 lph argon for 24 h. The fluorides were then reduced with high purity calcium in tantalum crucibles as described in Chapter 4 for metal preparation. From the reduced mass, CaF_2 slag was removed and the misch metal was vacuum melted at 1000°C. The misch metal thus obtained contained H 1 ppm, C < 10 ppm, N < 6 ppm, and O ≤ 30 ppm. The residual fluorine content varied from ~60 to ~250 ppm. Vacuum melting at 1700°C, instead of 1000°C, brought down the residual fluorine content drastically to ~10 ppm.

As regards the composition of the misch metal with respect to constituent rare earths, Palmer et al. (1982) anticipated and also observed certain composition changes between the mixed rare earth oxide/fluoride, as-reduced metal and the vacuum cast metal. In the reduction step, the samarium trifluoride SmF_3 will at best reduce to SmF_2, and this very stable difluoride will remain with CaF_2 slag. Samarium metal is thus lost as it does not end up in the misch metal. Even in the electrolytic production of misch metal, samarium content in the mixed rare earth chloride feed was found to concentrate in the slag, and this slag, incidentally, was one of the prime sources of samarium for use in $SmCo_5$ permanent magnets. Another significant composition change, regarding the proportion of the various rare earth metals in misch metal, occurs during vacuum melting. Vacuum melting at 1700°C leads to the loss of a quarter to half of the neodymium contained in the as-reduced or 1000°C vacuum cast metal. The analysis of misch metals prepared at Ames and commercially available from Ronson metal are listed in Table 6.7 (Palmer et al. 1982).

The Ames experiment of thermal reduction as a method for preparation of misch metal is the second highly refined attempt at the process. The first attempt was made by Decroly et al. (1953) in Brussels, Belgium in 1952, using a thermit type reaction.

6.2.5 Thermal Reduction Process

Starting from mixed rare earth oxides prepared by processing of bastnasite and monazite ores from the Belgian Congo, Decroly et al. (1953) at the University of Brussels prepared mixed rare earth fluoride and reduced it by calcium to misch metal.

The mixed oxide was converted to the fluoride by using ammonium bifluoride. The reaction was carried out in the apparatus shown in Figure 6.5. An intimate mixture of rare earth oxide and excess ammonium bifluoride was loaded in the crucible made of aluminum but lined on the inside with slightly sintered CaF_2. The crucible was placed in an electric furnace and a copper or aluminum collector was put over the crucible to recover the gases that evolved in the reaction. The collector was connected with a silica tube where some volatilized ammonium bifluoride could be condensed and recovered. The charge was heated at 150°C for several hours and a solid double fluoride product was obtained.

$$RE_2O_3 + 4NH_4HF \rightarrow 2REF_3 \cdot NH_4F + 2NH_3 + 3H_2O$$

In the second step, the double fluoride was decomposed by heating to 400°C.

$$REF_3 \cdot NH_4F \rightarrow REF_3 + NH_4F$$

The decomposition was carried out in the apparatus shown in Figure 6.6. A silica tube placed in an electric furnace was the decomposition vessel. This vessel was connected to another

Table 6.7 Composition (at %) of various misch metals

Source	Vacuum casting temperature, °C	La	Ce	Pr	Nd	Sm	Gd	Y	Fe	Mg	Si	C	N	O	F
Monazite	1000	20.1	49.7	6.4	20.4	<0.5	1.8	1.6	0.009	<0.0001	<0.0001	7	4	21	86
Monazite	1700	22.5	52.2	6.2	15.5	<0.5	2.0	1.6	0.008	<0.0001	<0.0001	7	6	22	8
Bastnasite	1000	39.8	37.5	6.2	16.5	<0.5	<0.2	<0.05	0.006	<0.0001	<0.0001	23	1	15	132
Bastnasite	1700	42.1	40.8	6.5	10.6	<0.5	<0.2	<0.05	0.006	<0.0001	<0.0001	<2	3	29	13
Ronson	as-received	23.6	54.4	5.4	12.1	0.5	0.4	0.1	4.3	2.8	0.2				
Ronson	1700	24.4	53.3	5.3	11.9	0.5	0.4	0.1	2.6	0.01	0.2	13	55	740	20

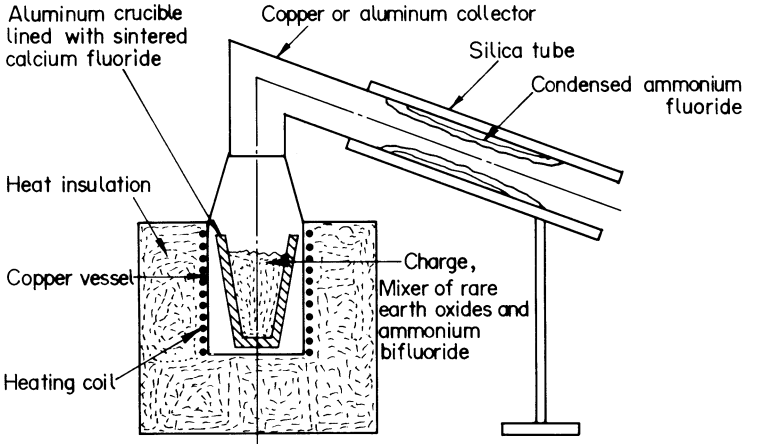

Figure 6.5 Apparatus for the fluorination of mixed rare earth oxide (Decroly et al. 1953).

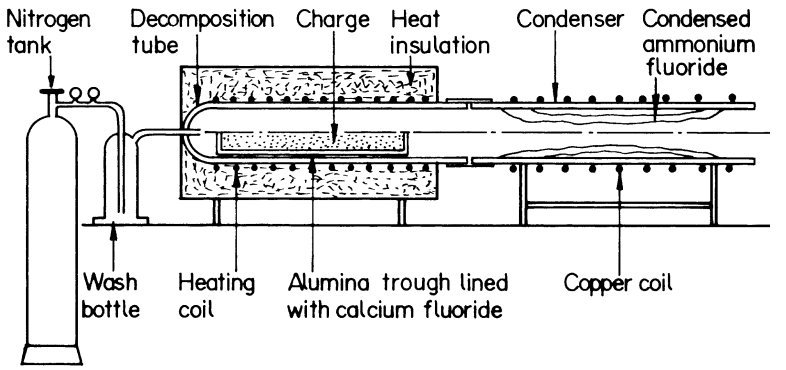

Figure 6.6 Apparatus for the decomposition of ammonium rare earth double fluoride (Decroly et al. 1953).

silica tube by a rubber connection. The second tube was cooled by a copper coil in which water was circulated. To sweep away the ammonium fluoride vapors and to keep an inert atmosphere in the reactor, dry nitrogen was introduced into the decomposition vessel. Ammonium fluoride collected in the condensation tube and was easily recovered.

The double fluoride was loaded in a calcium fluoride-lined aluminum trough and the trough was placed in the decomposition vessel. Keeping a nitrogen flow, the temperature was raised to 400°C. The double fluoride decomposed. The decomposition of 1000 g of double fluoride took 10 to 12 h. The completion of the double fluoride decomposition was checked by determining nitrogen content of the residue, and decomposition was considered complete when the nitrogen content was 10 ppm. Chemical analysis for fluorine confirmed the quantitative formation of rare earth trifluoride.

Calcium was used as the reducing agent for the mixed rare earth trifluorides, but the heat available from the heat of reaction alone for $2REF_3 + 3Ca \rightarrow 2RE + 3CaF_2$ was not sufficient to heat and melt the reduced metals and slag in a typical thermit type reduction. The use of iodine as booster was necessary.

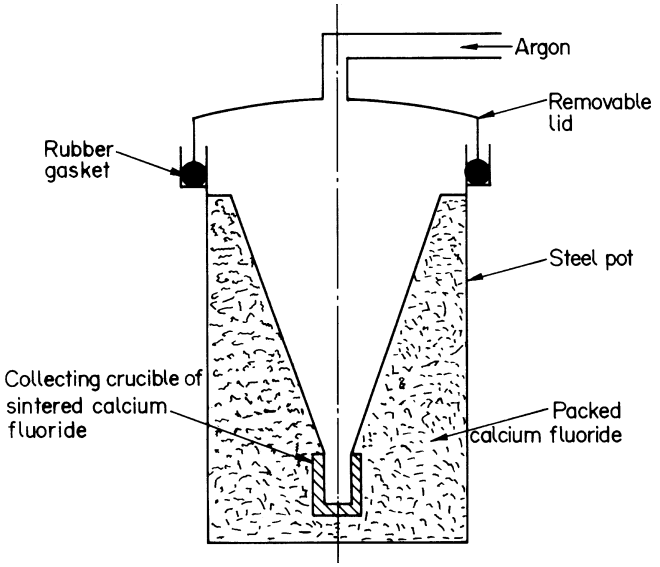

Figure 6.7 Apparatus for thermit type reduction of rare earth trifluoride by calcium (Decroly et al. 1953).

The apparatus used by Decroly et al. (1953) to carry out the reduction of mixed rare earth fluoride with calcium is shown schematically in Figure 6.7. It comprised a steel pot with removable lid. To obtain air tightness when the lid was closed, a water-cooled circular rubber gasket was used. This gasket was placed in a circular trough welded at the top of the steel pot. The wall of the reaction chamber was made of packed CaF_2 powder, and the chamber was conical in shape. At the bottom of this chamber was a cylindrical crucible of sintered CaF_2. An electric heating coil provided in the pot was used for drying the lining and crucible. The use of pure calcium fluoride as refractory material eliminated the possibility of contamination of the produced metal except by elements already present in the charge.

The reaction mixture had 150 gms of mixed fluorides, 70 gms of iodine, and an amount of calcium chips 15% in excess of the quantity theoretically needed to reduce the fluorides and combine with iodine. After loading this mixture, the reaction was started by a burning magnesium ribbon. The reaction proceeded very smoothly and lasted only a few seconds. When the reduction was through, the vessel was closed with the lid, which had a tube that allowed pumping off all the air present in the reactor and replacing it with pure argon. The product was cooled under a positive pressure of argon. After cooling, the slag was easily separated and the metal collected in the lower crucible as a small ingot, which was recovered.

The analysis of the misch metal obtained is given in Table 6.8. It was not quite pure but good enough for preparing pyrophoric alloy. Even in the small-scale experiments, the yield of misch metal was 78 to 80%.

6.3 RARE EARTH–SILICON–IRON ALLOYS

Rare earths are added to steel mostly in the form of rare earth–silicon–iron alloy or as misch metal. The alloy is often preferred over misch metal because of its low cost.

Table 6.8 Analysis of misch metal prepared by thermit reduction (Decroly et al. 1953)

Element	Content, %
RE metals	98.2*
Ca	0.32
Si	0.09
Fe	1.04
Cu	0.28
Not determined	0.07

*47.9% Ce, 50.3% La, Nd etc.

Commercially, the rare earth–silicon–iron alloy is prepared by carbothermic reduction of a mixture of rare earth compounds, silica, and iron at above 1930°C (Staggers 1977). An alloy composed of approximately 1/3 misch metal, 1/3 silicon, and 1/3 iron was obtained in a submerged electric arc furnace by the direct reduction of bastnasite ore concentrate, iron ore, and quartz. In the commercial production process, the rare earth recovery is not more than 60%.

Many other techniques have been reported (Marchant et al. 1980) for the preparation of rare earth–silicon–iron alloys. They rely on the use of calcium–silicon (~30% Ca) alloy or calcium silicide as reducing agents for mixed rare earth oxides prepared from monazite or bastnasite sources. Many variations of the reduction technique have been patented (Krismer and Smetana 1968, Hirschhorn and Klein 1969, Kallenbach and Bungardt 1969). In one, up to 50% of the calcium–silicon alloy was replaced by either calcium or silicon (Krismer and Smetana 1968). Calcium carbide was also used as a partial replacement of the calcium–silicon alloy (Kallenbach and Bungardt 1969). In yet another process, mixed rare earth oxides were reduced with calcium silicide at 1500°C, and iron scrap was added to the molten charge to get a product containing 30% RE, 29% Si, 40% Fe, and 1% Ca (Hirschhorn and Klein 1969). The use of calcium silicide, ferrosilicon, silicon, and aluminum as reductants for mixed rare earth oxides prepared from bastnasite flotation concentrate were investigated at the Reno Center of USBM to obtain rare earth–silicon–iron–aluminum alloys (Marchant et al. 1980).

6.3.1 Reno (USBM) Process

The flowsheet of the process is shown schematically in Figure 6.8. The starting materials were mixed rare earth oxide, aluminum turnings and ferrosilicon alloy. The mixed rare earth oxide was commercially available leached and calcined bastnasite concentrate. The total rare earth content of the concentrate was 78.6 wt %, and this comprised the percentages 40.5 Ce, 25.1 La, 9.3 Nd, 3.25 Pr, and < 0.4 other RE. The ferrosilicon was also a commercially available product with a nominal composition of 25% Fe–75% Si. The reduction procedure involved blending the mixed rare earth oxide with aluminum turnings and 6 mm fragments of ferrosilicon alloy and loading the mixture in a densified silicon carbide crucible. A flux of lime (CaO) and magnesia (MgO) was added on top of the reduction charge. The flux was necessary, because if it were absent a significant amount of rare earth–silicon–iron alloy became entrapped in a viscous slag. As a result, complete

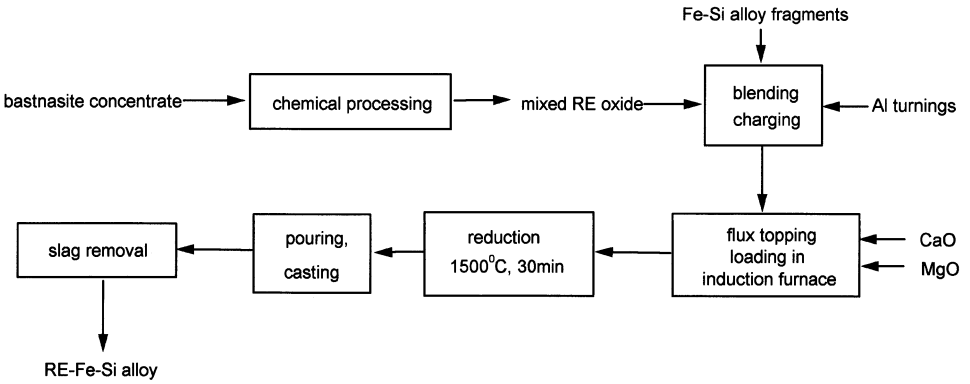

Figure 6.8 Schematic flowsheet for the preparation of rare earth–iron–silicon alloy.

separation of slag from the alloy became difficult when attempts were made to pour the molten product. The reduction was carried out in an induction furnace. The charge and flux were melted and held at 1500°C for 30 min to complete the reaction. The melt was then poured into an iron mold. The rare earth–silicon–iron alloy was recovered by allowing the melt to freeze and breaking the slag away. The product analysis is given in Table 6.9.

The following reactions were also investigated by Marchant et al. (1980) for preparing rare earth–silicon, rare earth–silicon–aluminum and rare earth–silicon–aluminum–iron alloys.

$$RE_2O_3 + 3CaSi_2 \rightarrow 2RESi_2 + 2Si + 3CaO$$

$$2RE_2O_3 + 11Si \rightarrow 4RESi_2 + 3SiO_2$$

The use of ferrosilicon in place of silicon resulted in iron reporting to the alloy product. The rare earth recovery was highest (98%) when 120% of the stoichiometric amount of calcium silicide was used. For an industrial operation, however, calcium silicide is not very suitable as a reductant because of its limited availability and high cost. The rare earth recovery in the alloy was very low (~40%) when silicon or ferrosilicon was used even at 120% of the stoichiometric amount. The use of aluminum in addition to silicon or ferrosilicon improved the rare earth recovery to ~70%, however ~600% of the stoichiometric amount of aluminum had to be used.

$$3RE_2O_3 + 15Si + 2Al \rightarrow 6RESi_2 + 3SiO_2 + Al_2O_3$$

The resulting alloy contained ~18% aluminum. When silicon was used in the above reaction, the product was a rare earth–silicon–aluminum alloy, and a problem with the rare earth–silicon–aluminum alloy was that the alloy disintegrated into powder even after a short time exposure to air. On the other hand, when ferrosilicon was used in place of silicon the resulting rare earth–silicon–aluminum–iron alloys remained intact in air. The rare earth alloy in the disintegrated form would be undesirable as a ladle addition because of a dusting problem.

Table 6.9 Results for ferrosilicon–aluminum reduction of mixed rare earth oxide in an induction-heated reactor (Marchant et al. 1980)

Charge weight, g	1170
Reactants:	
Mixed rare earth oxide, g	681
Fe–78 Si alloy, g	309
Aluminum	182
Flux:	
CaO, g	681
MgO, g	45
Alloy product weight, g	812
Slag weight, g	1100

Analysis:

Alloy			Slag	
Components	Content, wt %	Recovery, %	Component	Content, wt %
RE	52.6	80	RE_2O_3	12.7
Si	27.6	93	SiO_2	4.7
Fe	10.7	85	FeO	1.2
Al	3.8	16	Al_2O_3	28.9
Ca	5.0		CaO	49.3
P	0.05		MgO	2.3
S	0.003		P	0.15
O	0.28		S	0.24

The major advantages of the USBM process are the higher rare earth content in their alloy product (53% RE, 28% Si, 11% Fe, and 4% Al) and a higher (80%) rare earth recovery. This compares well with the commercial process figures of 30% rare earth in alloy and 60% rare earth recovery. Functionally, the USBM alloys were as good as the commercial rare -earth–silicon–iron alloys (Marchant et al. 1980).

6.3.2 BARC Process

The preparation of rare earth–silicon–iron alloy by metallothermic reduction was also investigated at the Metallurgy Division of BARC (Bose et al. 1985). A mixed rare earth oxide (REO) concentrate of monazite origin, obtained from Indian Rare Earths in Alwaye, was used as the source of rare earths. The RE_2O_3 content of the mixed oxide was 95% and the ratio of CeO_2 to RE_2O_3 in the oxide was about 48%. Commercially available 80% grade ferrosilicon and aluminum rod scrap (>99% Al) were used as reductants. Two types of fluxes were used. One was a CaO–MgO flux and the other was a CaO–CaF_2 flux. The details of charge and products are listed in Table 6.10.

The charge comprising mixed REO, 25 mm pieces of ferrosilicon, and aluminum was loaded in a 250 mm graphite crucible and covered on top with CaO–MgO flux mixture.

Table 6.10 Metallothermic reduction of mixed REO (Bose et al. 1985)

Charge			Flux				Product				
REO	Fe–80Si	Al	CaO	MgO	CaF_2	RE–Si–Fe alloy recovered	REM	Si	Fe	Al	REM recovered, %
5000	2670	1336	5000	330	–	5610	54.2	33.2	5.5	4.0	76
4000	2600	1070	5050	–	7000	5000	55.0	33.0	5.0	4.0	82

The reduction was carried out by heating the charge to 1550°C in an induction furnace and keeping it at that temperature for 30 min. The molten RE–Si–Fe alloy that was formed was tilt poured and cast in cast iron molds.

When $CaO–CaF_2$ flux was used, the procedure was different. Calcium fluoride was first melted in the crucible. Mixed rare earth oxide and then CaO were added to the melt to form a molten bath of $REO–CaO–CaF_2$. Ferrosilicon and aluminum in lump form were added to the bath at 1500°C, and the reaction was allowed to proceed for 30 min. The alloy product was finally cast.

The rare earths loading in the rare earth–silicon–iron alloy and the recovery of rare earths in the alloy were similar in the experiments conducted at USBM and at BARC. The mixed rare earth oxide derived from monazite was used at BARC and a bastnasite source material was reacted at USBM. The product obtained at BARC was higher in Si content and relatively low in iron. BARC experiments pointed to $CaO–CaF_2$ as the more favorable flux mixture in view of better slag fluidity, lower temperature of operation, and better rare earth recovery in the alloy. The REO losses into the slag phase were also limited to below 10%.

6.3.3 Baotou Process

Caiquan et al. (1985) used the rare earth containing blast furnace slag, obtained on smelting of the Bayan Obo iron–rare earth ore at the Baotou blast furnaces, as the source of rare earths for reduction to the rare earth–silicon–iron alloy. The composition of the slag and the alloy obtained from it are both given in Table 6.11.

Table 6.11 Composition of the Baotou slag and RE FeSi alloy obtained (Caiquan et al. 1985)

Baotou slag								
Elements	REO	Fe	P	F	CaO	SiO_2	MnO	Alkalinity
Content, %	10–16	≤1	≤0.1	10–16	38–42	20–24	≤2	1.0

RE–Si–Fe alloy						
Elements	RE	Si	Mn	Ca	Ti	Fe
Content, %	18–47	45–50	5–2	6–2	3–0.5	Balance

The alloy was obtained by reduction of the blast furnace REO slag in an arc furnace using lime as flux and ferrosilicon as reductant. The recovery of REM was in the 60–70% range and many different grades of alloys, including 30% RE–Si–Fe alloy, could be prepared.

6.4 RARE EARTH–MAGNESIUM–SILICON ALLOYS

The rare earth–Mg–Si alloys have been used as additives in the making of nodular iron. The conventional methods for production of these alloys have disadvantages such as consumption of large amounts of metallic magnesium and the loss of magnesium due to vaporization. Shumao and Mingqin (1985) carried out direct preparation of rare earth–Mg–Si alloys by a silicothermic reduction process.

The rare earths-bearing raw materials were from the Bayan Obo deposit. One of the two materials is the Baotou blast furnace slag containing >10% REO, and the other is the rare earth concentrate containing about 30% REO. The other components of the charge were calcined dolomite containing 34% MgO and reducing agents such as ferrosilicon calcium and silicon. Reductions were carried out in an electric arc furnace. The optimum smelting conditions were smelting temperature >1550°C, CaO + MgO ≈ 35–45%, and silicon content of the reducing agent >85%. The composition of the alloy obtained was Mg 3–5%, (Ca + Mg) >10%, RE 6–17%, Si 50–55%, and the balance was Fe. Shumao and Mingqin (1985) noted that controlling the voltage and current in the operation and timely tapping of the alloy were necessary for the success of the process.

6.5 RARE EARTH–ALUMINUM–ZINC ALLOY

A galvanizing zinc alloy containing 5% aluminum and small amounts of lanthanum and cerium has been considered to offer much better protection to underlying steel than does normal zinc cover (Radtke and Herrschaft 1983). Xujun et al. (1985) have investigated a molten salt electrolysis method as an alternative to conventional methods of melting together the components or thermal reduction of compound intermediates.

The electrolyte consisted of 20–30% $RECl_3$ in an equimolar mixture of KCl–NaCl, with CaF_2 1%, NaF 1% as additives. A cylindrical graphite crucible, which was also the anode, was used to contain the molten salt. The cathode was molten Al–Zn alloy (Al:Zn = 60:40) contained in a porcelain crucible and placed in the cell. Electrolysis was conducted at 650–680°C and the bath was continuously stirred. Cathode current density was kept at 2–2.5 A/cm^2. After electrolysis was completed, the cathode product was removed and cooled, and the electrolyte on the alloy surface was washed away.

Under the conditions mentioned, an alloy containing 8% RE was obtained. The current efficiency was as high as 81% and the rare earth recovery was quantitative. In their experiments Xujun et al. (1985) produced up to 375 g of the alloy per batch.

6.6 YTTRIUM–ALUMINUM ALLOY

Both yttrium and aluminum are constituents in several oxidation resistant alloys useful for high temperature service. Yttrium–aluminum master alloy is convenient for introducing the constituent elements in the high temperature alloys. Methods mainly based on fused salt electrolysis have been developed for the production of these alloys (Morrice et al. 1973).

In one method (Bratland et al. 1972), yttrium–aluminum alloys were made by electrolysis of yttrium oxide in yttrium fluoride–lithium fluoride melts using floating cathodes of

liquid aluminum In this arrangement, the maximum concentration of yttrium recovered in the alloy was only 22%.

Yttrium–aluminum alloys of higher yttrium content were prepared at Reno by electrolyzing mixtures of yttrium oxide and aluminum oxide dissolved in yttrium fluoride–lithium fluoride melts and codepositing the metals to form liquid alloys.

The 120 mm diameter cell used at Reno for electrowinning Y–Al alloy using a liquid Y–Al alloy cathode is shown in Figure 6.9 (Morrice et al. 1973). The anode as well the crucible used to contain the molten electrolyte were made of graphite. The cell was placed inside a shell of mullite bricks to provide thermal insulation. To furnish heat to melt the electrolyte and to maintain the desired operating temperature, a graphite resistance heater was located below the graphite crucible. To protect cell components, the alloy product, and the graphite resistor from air oxidation at the operating temperature, the entire assembly was placed inside a chamber under helium. As usual, glove ports and view ports were provided in the chamber to facilitate the cell operation.

Yttrium fluoride was prepared by fluorinating 99.9% pure Y_2O_3 powder with ammonium bifluoride (Carlson and Schmidt 1961). The rare earth fluoride contained 0.1 to 0.2% residual oxygen. Lithium fluoride, yttrium oxide, aluminum oxide, yttrium metal, and aluminum metal used by Morrice et al. (1973) were all 99.9% pure.

The starting alloy pool was a 91% Y–9% Al liquid alloy (at the operating temperature), and it covered the bottom of the graphite crucible. This alloy was obtained by arc melting the alloy components together. This liquid alloy pool was the cathode. The anode, a 75 mm diameter 12 mm thick horizontal graphite disk, was immersed into the electrolyte, and it was 12 to 19 mm above the alloy pool surface. The electrolyte was prepared by mechanically mixing the required amounts of yttrium fluoride and lithium fluoride to obtain the composition 80% YF_3–20% LiF. The electrolyte temperature was 1025°C. An oxide mixture comprising 87% Y_2O_3–13% Al_2O_3 (this mixture has the same Y/Al ratio as that of the eutectic alloy) was fed to the cell and electrolysis was conducted at 4 volts and 70 to 80 amperes for 3 h. Yttria and alumina were electrolytically reduced, and the resulting metals formed alloy in the alloy pool, which increased in quantity without major change in composition, as the electrolysis progressed.

The composition of the alloy formed needed to be closely controlled because if the aluminum content of the cathode pool increased, it would tend to float and interfere in

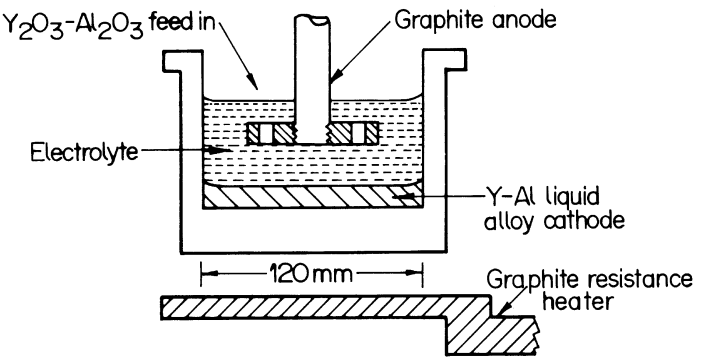

Figure 6.9 Electrolytic cell for production of Y–Al alloy at a Y–Al liquid cathode (Morrice et al. 1973).

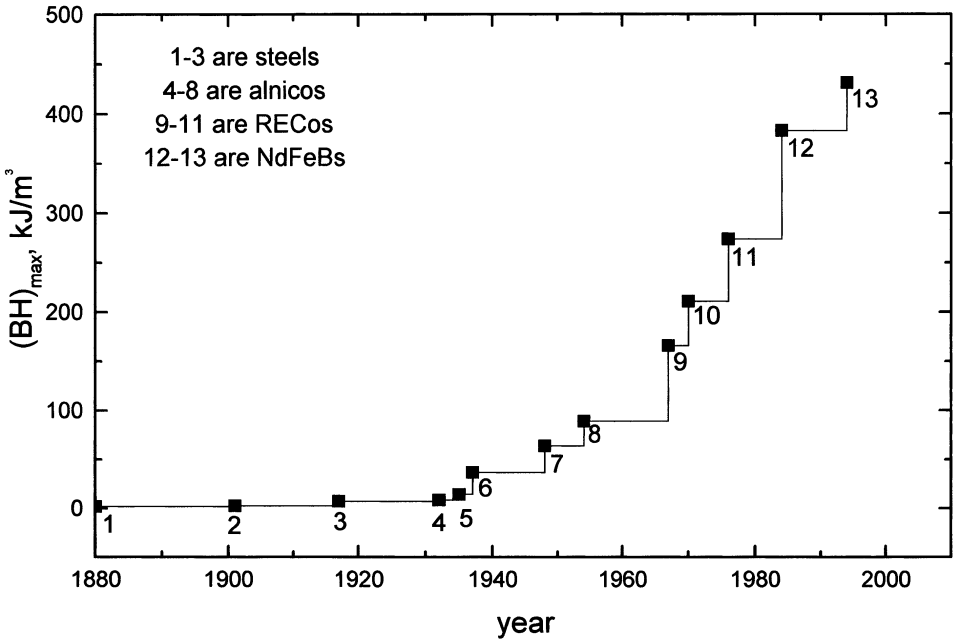

Figure 6.10 Permanent magnet development since 1880.

electrolysis. On the other hand, if the yttrium content in the cathode pool increased, the melting point of the alloy pool would rise and the pool would solidify.

The operation of the liquid cathode has been investigated for 12 to 15 h (Morrice et al. 1973). The current efficiency and Y–Al alloy recovery were maximum at 68 and 89%, respectively, when 85% Y_2O_3–15% Al_2O_3 oxide mixture was fed to the cell. The electrowon alloy was approximately of eutectic composition (91% Y).

6.7 PERMANENT MAGNET MATERIALS

There are numerous permanent magnet materials and those that have been commercially important are listed in Table 6.12 (Strnat 1985). Permanent magnets are rated on the basis of several key properties. The foremost among these properties are the energy product and coercivity. The attractive characteristics of good permanent magnet materials are high coercivity (resistance to demagnetization) and high energy product. The energy product $(BH)_{max}$ is a measure of the useful strength of a permanent magnet and is the most often quoted figure of merit for comparing permanent magnets. The progression of the maximum energy product in various permanent magnet materials during this century (Strnat 1985) is shown in Figure 6.10. The figure illustrates the 100-fold increase of the magnetic energy that can be stored in a volume unit and the enhancement of the coercivity by an even larger factor. Many of these enhancements began in the late 1960s with the discovery and development of rare earth based permanent magnet materials. These materials are based on either the rare earth–cobalt system or the neodymium–iron–boron system.

Table 6.12 Important permanent magnet materials (Strnat 1985)

Magnet	Energy product $(BH)_{max}$, kJ/m^3	Remanence, Br mT	Coercivity at 20°C, kA/m		Temperature coefficient of remanence, % per °C	Curie temperature °C	Maximum temperature for practical use, °C	Density, g/cm^3
			${}_BH_C$	${}_JH_C$				
BaFe, plastic bonded anisotropic	17.9	245	175	207	−0.20	450	100	3.7
BaFe anisotropic	25.5	365	175	180	−0.20	450	~200	5.0
AlNiCo 500 precision casting	36	1150	48	50	−0.20	860	450	7.4
Sm−Co plastic bonded	56−64	550−590	360−416	600	−0.04	725	80	5.1
Sm−Co	180	950	720	1800	−0.04 (20−1000°C)	725	~250	8.3
Sm_2Co_{17}	195−225	1000−1100	690−820	1200−2070	−0.03 (20−100°C)	750−800	~300	8.4
NdFeB plastic bonded	80	680	460	820	−0.10 (25−90)	340	150	6.0
NdFeB	225−800	1100−1250	720−930	800−1120	−0.10	310	100−150	7.4

6.8 RARE EARTH–Co PERMANENT MAGNETS

During the past three decades, the rare earth transition metal (RE–TM)-based magnets have evolved into a family of commercial products of considerable variety and constantly growing technological importance. The first group of rare earth magnets developed in the 1960s and commercially produced in the 1970s were based on the intermetallic compounds $RECo_5$ and RE_2Co_{17}. These intermetallic compounds possess the ideal combination of magnetic and structural properties for magnet applications. The first and most widely used magnet of this type was $SmCo_5$. The structure of $SmCo_5$ is hexagonal ($CaCu_5$ structure), its saturation induction is moderate, and it has extremely large positive values of magneto-crystalline anisotropy. The magnets based on $SmCo_5$ are single phase and magnetic property values achieved in the laboratory are Br = 1 T, H_{cj} = 3200 kA/m, and $(BH)_{max}$ = 200 kJ/m^3. The $(BH)_{max}$ in commercial $SmCo_5$ magnets are in the range 130–160 kJ/m^3. In other words, $SmCo_5$ magnets offer energy per unit volume 2 to 3 times more than that of the old generation magnets such as PtCo and AlNiCo and also exhibit 5 to 20 times greater resistance to demagnetization. In single phase $SmCo_5$ magnets the mechanism of coercivity is based on nucleation and/or pinning of domain walls at surfaces or grain boundaries. To achieve large values of coercivities it is necessary to have particle form (1–10 μm) or fine grained sintered magnets prepared from such powders. Magnet production techniques are, therefore, based on powder metallurgical procedures and include field pressing, i.e., alignment in a magnetic field during the pressing operation as a key process.

Less expensive alternatives to $SmCo_5$ have also been widely investigated (Wernick 1995). These include the use of Pr, Ce, and Ce–MM in combination with samarium. $(Pr, Sm)Co_5$ have higher values of saturation induction than $SmCo_5$. The Sm–Ce and Sm–MM combinations are cheaper, but the magnetic properties are also lower.

The addition of copper to certain $RECo_5$ alloy (partial substitution of Cu for Co) and proper heat treatment can result in a finely distributed two phase structure and high coercive force, even in bulk (Nesbitt and Wernick 1973). Low copper Sm or $SmCo_5$ based alloys are magnetically hardened by a Cu rich 1–5 phase precipitated within the grain. The precipitate impedes domain wall motion and gives ${}_mH_c$ in the range 400–560 kA/m. Copper additions strongly broaden the high temperature homogeneity range of the 1–5 phase toward 2–17 and permit incorporation of iron into the lattice. It has therefore been possible to prepare precipitation hardened magnet alloys (Sm, Ce) (Co, Cu, Fe)$_z$ up to z = 6.8 and (Sm, Y) (Co, Cu, Fe)$_z$ up to z = 7.2 with excellent properties. These may be considered as 1–7 alloys. The magnetic data for selected magnets are listed in Table 6.13.

The RE_2TM_{17} compositions have basic properties that could lead to magnets of energy products of 480 kJ/m^3 or more. Sm_2Co_{17} ($SmCo_{8.5}$) has the highest anisotropy and best potential. Commercial magnets based on $SmCo_{8.5}$ contain, in addition to Co, the metals Cu, Fe, and Zr to replace some of the Co. The preparation of sintered magnets very close to the 2–17 stoichiometry, having energy products exceeding the highest for the 1–5 composition; have been reported (Strnat 1978). For example, $Sm_2(Co,Fe,Mn,Cr)_{17}$ and $Sm_2(Co,Fe,Cu,Nb)_{17}$ have an energy product of 225 kJ/m^3 while, $Sm_2(Co,Fe,Cu, Zr)_{17}$ have energy products of 240 kJ/m^3 each. The attractive hard magnetic properties of these materials arise from microstructural precipitates that pin domain walls.

Table 6.13 Magnetic data of selected 1–7 or 2–17 alloys (Strnat 1978)

Alloy type	Production method	$(BH)_m$ kJ/m^3	Br T	$_MH_C$ kA/m	α % per °C (temp. range)
$SmCo_5$	Sintering	192	0.98	955	−0.04 (−50 to +100)
$(MM_{0.8}Sm_{0.2})Co_5$	Sintering	128	0.82	1194	−0.055 (−50 to +100)
$Sm(Co,Fe,Cu)_7$	Sintering, precipitation annealing	211	1.04	494	−0.03 (20 to 120)
$Sm_2(Co,Fe,Cu,Zr)_{17}$	Sintering, precipitation annealing	242	1.12	533	−0.03 (−50 to +150)
$(Sm,Ho)Co_5$	Sintering	99	0.71	>200	~0 (−90 to +50)
$SmCo_5$	Polymer bonding	112	0.75	>1195	−0.04 (−35 to +100)

α is the approximate value of the temperature coefficient of remanence per 1°C.

6.8.1 Preparation

The preparation of RE–Co magnets involves two major stages. The first is the preparation of the RECo alloy and the next is the production of the magnets from the alloy. The RECo alloy has been prepared by many routes. They are (i) direct melting of the alloy components, (ii) co-reduction or reduction diffusion using the metal oxides as start materials, and finally (iii) the direct production of the alloy by fused salt electrolysis using cobalt as the consumable anode.

Direct Melting Rare earth–cobalt alloys for magnet production can be prepared by melting together the alloy components. The melting can be carried out either in cold crucible by means of high frequency induction heating or in crucibles such as boron nitride and alumina (Kirchmayr and Poldy 1979). The latter, however, is slowly attacked by the melt. A survey of the various techniques for preparing RE–Co alloys has been given by Herget and Domazer (1975). For melting a mixture of samarium or other rare earth and cobalt, either small ready-made crucibles or crucibles that are rammed and fired *in situ* using an inner graphite core have been used. Vacuum induction melting is a particularly clean method for preparing these alloys. If small quantities of alloys are to be prepared, the components can be melted in an arc furnace. Walkiewicz et al. (1973) prepared Sm–Co compounds by nonconsumable arc melting of 99.9% pure metals. About 80-g charges of these metals were melted under helium. To achieve homogeneity, the arc melted buttons were inverted and remelted a total of five times. An excess of samarium was provided in the charge to compensate for samarium loss due to vaporization. To obtain the stoichiometric $SmCo_5$ composition of 33.8% samarium, a charge composition of 37% samarium and 63% cobalt was used. A blending method was also used as an alternative to the above approach, which essentially involved obtaining a particular alloy composition by adding controlled amounts of Sm and Co to the charge before melting. In this method, two separate compounds, near stoichiometric $SmCo_5$ and Sm_2Co_{17}, were first prepared. These compounds were then blended in the required ratio and melted to obtain the optimum composition of 36.7±0.3% samarium. Walkiewicz et al. (1973) found the blending method to be superior

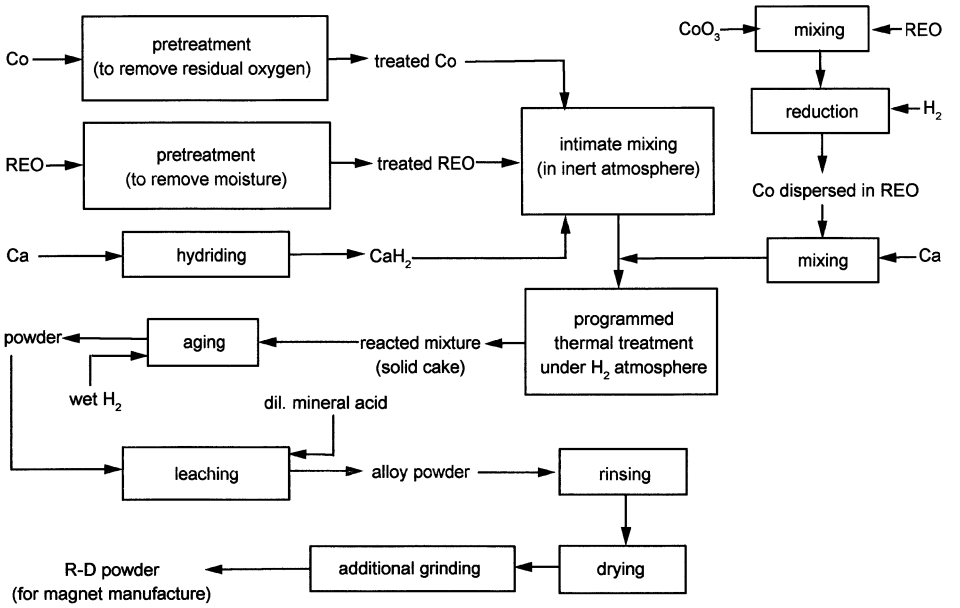

Figure 6.11 Schematic of the reduction diffusion process.

to the direct melting method in which samarium content was directly controlled during melting.

At the beginning of the 1970s when alloys of the type $RECo_5$, particularly $SmCo_5$, assumed great importance as new permanent magnet materials of extraordinary performance, development of new economic methods of alloy preparation began apart from the route of melting samarium metal with cobalt in vacuum induction furnaces. It was discovered that calciothermic reduction of Sm_2O_3 in the presence of cobalt powder, and eventually of additional alloy components, yielded the required alloy directly in the powder form. There are two variants of this method and they are known as reduction diffusion and co-reduction.

Reduction Diffusion Process The process was invented in 1969 by Cech (1974) working at the General Electric Corporate R&D Center in Schenectady, New York. The flowsheet of the process is given in Figure 6.11. Cobalt powder, rare earth oxide, and calcium hydride were used as the starting materials. They were first pretreated. The pretreatment sequence consisted of removal of residual oxygen from the cobalt powder, removal of moisture from the rare earth oxide, and conversion of metallic calcium to the hydride form. As an alternative, Cech (1974) suggested that cobalt oxide and RE oxide could be mixed first and then the dispersed cobalt oxide could be reduced to the metallic state with hydrogen. The pretreated starting materials were then intimately mixed under an inert atmosphere and subjected to a programmed thermal treatment in a hydrogen atmosphere furnace.

The reacted mixture, which was in the form of a solid cake, was aged in wet nitrogen. This treatment permitted excess calcium dispersed in the product to react with moisture and led to the spontaneous disintegration of the product cake into powder. The powder was treated with a dilute mineral acid to leach out calcium oxide. The powder was then rinsed, dried, and subjected to additional grinding to refine the particle size to that needed for the fabrication of magnets.

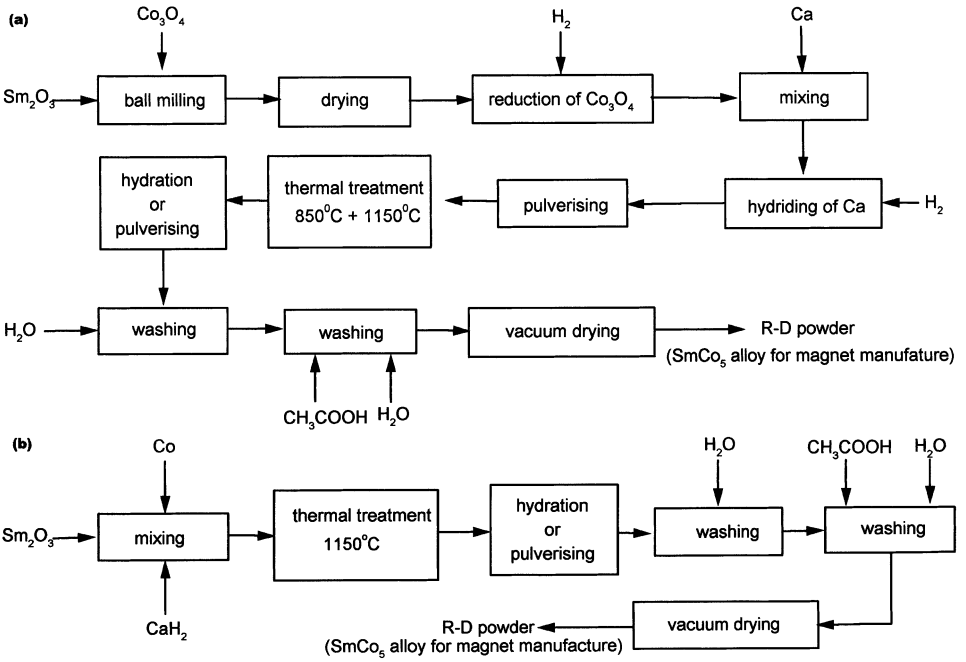

Figure 6.12 Original (a) and modified (b) reduction diffusion processes (McFarland 1973).

In his experiments, Cech (1974) prepared the cobalt powder by hydrogen reduction of the cobalt oxide after it was first dispersed in the rare earth oxide. He also prepared calcium hydrate "in-house" from commercial grade calcium nodules. He dispersed calcium nodules in the cobalt metal–rare earth oxide mixture before converting them to hydride. Hydriding of calcium required only a brief furnacing treatment. The mixture was then homogenized by passing through a double disk pulverizer and then repacked in a covered iron boat for the chemical reduction treatment.

The chemical reduction treatment consisted of heating the charge at 850°C for 2 h followed by three 30-min holding periods at 900, 950, and 1000°C and finally a 2-h holding at 1050°C. The charge was then drawn into a water-cooled chamber to facilitate rapid cooling. Slow cooling, in a hydrogen atmosphere, it was observed, led to the formation of Sm_5CoO type material by the reversal of the second reaction given below.

Cech (1974) suggested that the following reactions closely describe the reduction diffusion process for $RECo_5$ alloy formation.

$$10Co + RE_2O_3 + CaH_2 \rightarrow 2RECo_5O + CaO + H_2\ (850°C)$$

$$2RECo_5O + 2CaH_2 \rightarrow 2RECo_5 + 2CaO + 2H_2\ (1050°C)$$

According to Cech (1974), carrying out the reduction step directly at 1050°C led to undesirable complications arising out of formation of low-melting rare earth-rich intermetallic phases. The reduction should occur at such a rate that the rare earth formed should at the same time be removed by solid state diffusion into cobalt.

The maximum overall yield of rare earth in the alloy obtained by Cech (1974) was 97+% using the following stoichiometry.

$$10Co + Sm_2O_3 + 12(3CaH_2) \rightarrow 2SmCo_5 + 3CaO + 0.6CaH_2$$

The yield decreased both at lower and higher proportions of CaH_2. The batch size of the experiments were 2.7 kg of $SmCo_5$.

In addition to $SmCo_5$, other alloys containing 75% Pr and 25% Sm in the rare earth part of the alloy have been prepared by the reduction diffusion. This fine powder alloy was processed to magnets that were as good as or superior to those made from conventional melt cast powder.

The original reduction diffusion developed by Cech (1974) at General Electric was modified by McFarland (1973) from the same laboratory, and the schematics of both processes are shown in Figure 6.12.

Cech (1974) was attempting to generate a powder in the 5 μ to 10 μ size range to avoid an expensive fluid energy milling step. The work on magnet fabrication by Cech as well as by Benz and Martin (1970) had indicated that superior magnets could be made with powders of 6 μ to 8 μ size and this size was not achieved without milling. McFarland (1973) therefore decided to do away with particle size controlling steps in the Cech process and to mill the final powder to the desired size. This led to process simplification by eliminating the initial wet ball milling step, the subsequent drying step, and a final screening step for removing oversize particles. In addition, cobalt oxide (Co_3O_4), which was chosen by Cech (1974) as the source of cobalt and also to provide many nuclei for the formation of fine particle Co–RE alloy, was replaced by commercially available cobalt metal powder. Commercially available CaH_2 was used instead of generating it *in situ*. These changes eliminated the four steps following the first drier, namely the steps that required careful handling of freshly reduced, pyrophoric cobalt, and a complicated heating, cooling, and grinding schedule to generate and blend in the CaH_2. Thus all the early steps are telescoped into one step in McFarland's modification. The modified process, which was also scaled up, was carried out as follows.

The starting materials were weighed and loaded into a blender. Cobalt and rare earth oxides, in stoichiometric quantities, were mixed first and then the calcium or calcium hydride up to 1.5 times the theoretically required quantity was added. The blending continued until a uniform mixture was obtained. The mixture was loaded into boats with loose fitting covers. A glove box flushed with nitrogen gas was routinely used for the CaH_2 addition and boat filling operations.

The loaded boats were introduced into an electrically heated retort with a hydrogen atmosphere. The retort was initially heated at 850°C for 2 to 3 h and the temperature was then raised to 1150°C and maintained for 2 to 3 h before the boats were moved to the cooling zone, still under hydrogen atmosphere.

After cooling to room temperature, the medium-hard lumpy product material in the boat was transferred to a glove bag containing a moist hydrogen atmosphere. The material decrepitated, following the exothermic reactions,

$$CaH_2 + H_2O \rightarrow CaO + 2H_2$$

$$CaO + H_2O \rightarrow Ca(OH)_2$$

to a fine powder. Depending primarily on the excess CaH_2 present, this hydration treatment required 1 to 5 days.

The bulk of the slaked lime was removed from the hydrated material by purely mechanical means. The hydrated powder was slurried in water, the alloy was allowed to settle, and suspended lime was removed by decanting. An AC magnetic field was found to be useful to agitate the magnetic powder but to hold it in the bottom of the container for easy separation. Finally, the powder was rinsed with water and then with alcohol and transferred to a vacuum filter. The moist powder with about 3 to 5% alcohol was placed in trays in a vacuum oven drier and dried overnight at 50°C. The dry powder was stored in a sealed container preparatory to magnet manufacture. Following the above procedure, McFarland (1973) produced several compositions — from near stoichiometric $SmCo_5$ to $(Sm_{0.5}Pr_{0.5})Co_5$ and $(Sm_{0.6}MM_{0.25}Pr_{0.15})Co_5$.

Jones et al. (1976) have described a scaled-up reduction diffusion process for the production of $RECo_5$ and RE_2Co_7, followed at Hitachi Magnetics Corporation MI, since 1973.

The general reaction of the reduction diffusion process

$$x\mathrm{Co} + \frac{y}{2}\,\mathrm{RE_2O_3} + \frac{3y}{2}\,\mathrm{Ca} \rightarrow \mathrm{Co}_x\mathrm{R}_y + \frac{3y}{2}\,\mathrm{CaO}$$

was adopted for the production of the stoichiometric samarium compounds $SmCo_5$ and Sm_2Co_7 as per the reactions

$$5\mathrm{Co} + \frac{1}{2}\,\mathrm{Sm_2O_3} + \frac{3}{2}\,\mathrm{Ca} \rightarrow \mathrm{SmCo_5} + \frac{3}{2}\,\mathrm{CaO}$$

$$7\mathrm{Co} + \mathrm{Sm_2O_3} + 3\mathrm{Ca} \rightarrow \mathrm{Sm_2Co_5} + 3\mathrm{CaO}$$

An excess of calcium, about 1.2 to 1.4 times the theoretically needed amount, was used in carrying out the reactions in practice.

Calculated quantities of cobalt powder, samarium oxide, and calcium granules (the raw materials) were mechanically mixed to form a uniform charge. The charge was heated in dry hydrogen at 1160°C for 4 h to complete the calcium reduction and rare earth diffusion. The reacted mass, which consisted of the Sm–Co alloy, CaO, and CaH_2 was placed in a high humidity environment to slack the lime and decompose the CaH_2. The resulting $Ca(OH)_2$ was separated by magnetic and gravimetric means. The alloy powder was washed with dilute acetic acid to remove remaining traces of hydroxide, vacuum filtered, and dried. It was then sealed in metal cans and stored.

Two compositions for the final alloy were selected for production. One was the stoichiometric alloy with 33.8% Sm. This was the base alloy powder. The other was an alloy with 42.2% Sm. This was used as the additive. The base alloy powder and additive were used for magnet fabrication. The additive powder being richer in rare earth content, a blend of the two resulted in an overall composition hyperstoichiometric to the $RECo_5$ after correction for the oxygen content (as RE_2O_3). The particle size and particle size distribution of these alloy powders depend upon the cobalt powder used.

Magnets made entirely from reduction diffusion powder display permanent magnetic properties, which are equivalent to those of magnets made from ingot material. In either case, the properties attained were strongly dependent upon the unit processes used to make

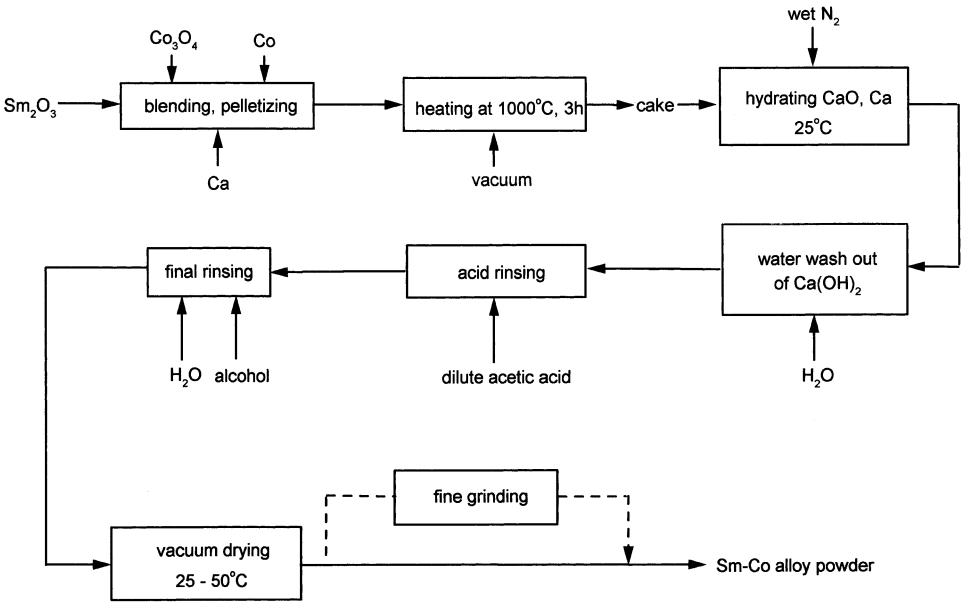

Figure 6.13 Schematic flowsheet of the co-reduction process (Strnat 1988).

the magnets. In this context excellent reproducibility was possible for the products from reduction diffusion powders.

Jones et al. (1976) refer to the impact of the reduction diffusion process on the cost of producing the rare earth cobalt magnet alloys. Even though calcium metal used as reductant in the process is expensive, it is at least cheaper by a factor of two than the alternative misch metal used to produce the samarium metal. Besides, a costly controlled atmosphere melting step was also eliminated. Overall, the raw material and process cost reductions associated with the reduction diffusion process resulted in an eight-fold reduction in the published price of Sm–Co magnet alloys between 1971 and 1976.

Co-reduction The co-reduction process developed at Th. Goldschmidt AG (Domazer 1976, Herget 1982) also leads to the direct preparation of samarium–cobalt alloy from the metal oxides. Calcium was used as the reductant, a part of the cobalt in the final alloy was derived from cobalt oxide used to function as thermal booster in the reaction mixture, and the process was carried out in a vacuum at 1100–1200°C according to the overall reaction

$$Sm_2O_3 + Co_3O_4 + 7Co + 7Ca \xrightarrow[\text{vacuum}]{1100-1200^\circ C} 2SmCo_5 + 7CaO$$

The schematic flowsheet of the process is shown in Figure 6.13. A palletized mixture of Sm_2O_3, Co_3O_4, Co, and Ca in stoichiometric quantity was heated at 1100–1200°C. Co-reduction, like reduction diffusion, occurred rather quickly after initiation at high temperatures. However, it was necessary to keep the charge at the temperature indicated for about 2 to 4 h to permit full alloy formation between just formed but still partly isolated Sm and Co particles. Solid CaO product particles form very early in the reaction, and by remaining interspersed between the metal particles they slowed down alloy formation by diffusion. The high melting point of CaO precluded the formation of a molten slag and

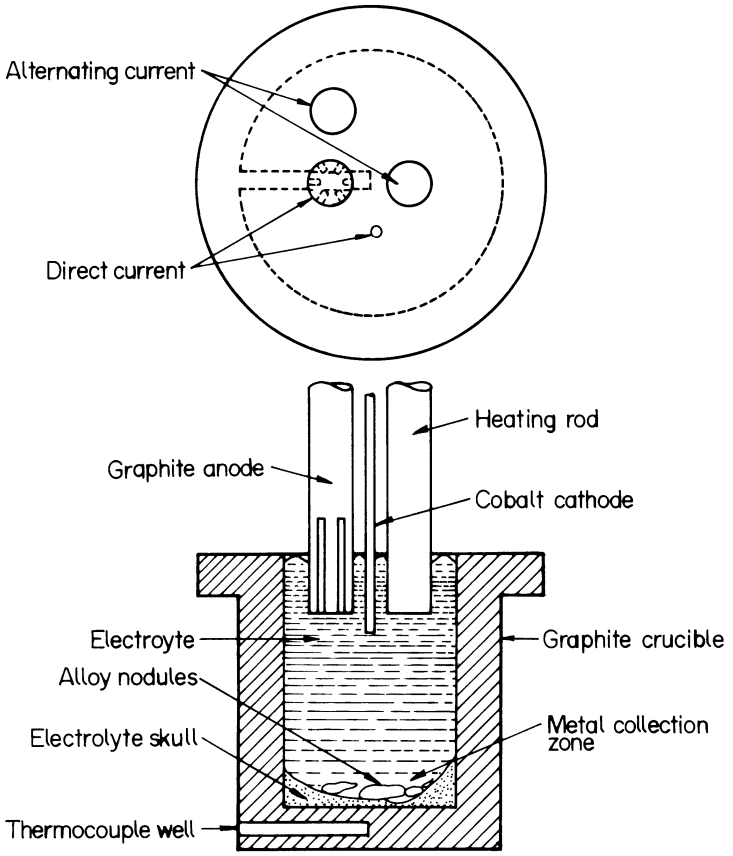

Figure 6.14 Electrolysis cell for RE–Co alloy preparation-I (six inch diameter cell) (Morrice et al. 1969).

hence metal–slag separation. As the result, the alloy came out as a powder and not as an ingot. This was desirable because all the rare earth–transition metal alloys were being processed into magnets by powder metallurgical methods, and even if an ingot were first produced it would have to be pulverized to obtain the alloy as powder.

As metal did not coalesce and thus did not collect separately from the slag during the above process, a separation step for powder product collection was necessary. This was carried out by first reacting the CaO and excess calcium metal with moist nitrogen, mechanically removing most of the $Ca(OH)_2$, and leaching the remainder away with a mild acid (acetic acid).

Electrolysis Apart from the reduction diffusion and co-reduction methods described, electrolytic methods have been investigated at the U.S. Bureau of Mines, Reno Center (Morrice et al. 1969), for the preparation of rare earth cobalt alloys for magnet use. Morrice et al. (1969) have described the following process for preparing high purity cobalt alloys containing individually samarium, yttrium, praseodymium, cerium, lanthanum, gadolinium, dysprosium, neodymium, didymium mixture, mixed yttrium group metals, and mixed cerium group metals. Because the relatively high prices of high purity rare earth metals are an important factor for producing rare earth–cobalt magnet materials, the

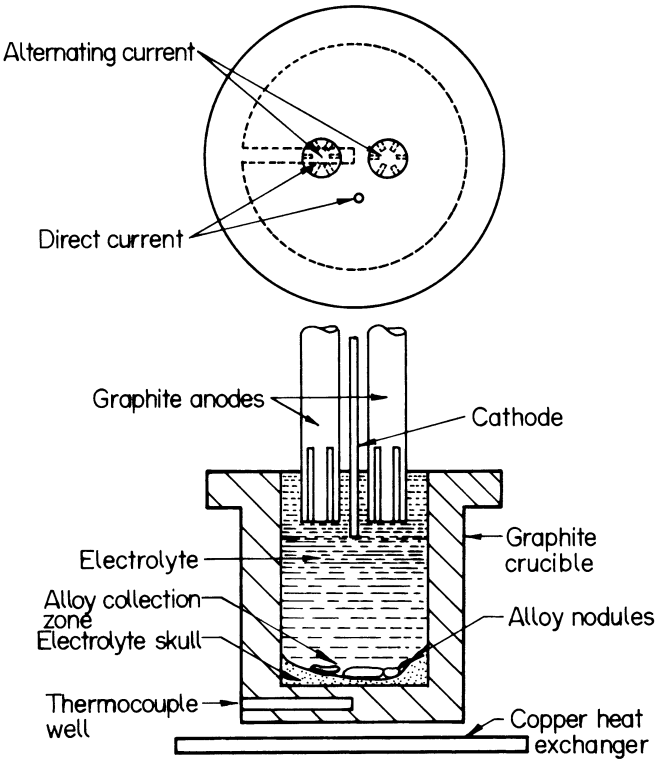

Figure 6.15 Electrolysis cell for RE–Co alloy preparation-II (four inch diameter cell) (Morrice et al. 1969).

electrolytic process uses oxides, a relatively cheap source of high purity rare earth metals, as feed materials.

Two internally heated thermal gradient cells were used for electrolysis. They are shown in Figures 6.14 and 6.15. The cells were enclosed in inert gas chambers to prevent atmospheric contamination. In both the cells the electrolyte was contained in a graphite crucible, and the crucible was placed inside a shell fabricated from insulating bricks to enable it to maintain the requisite heat balance. The cathode in each cell was a 6 mm diameter cobalt rod.

The first cell, shown in Figure 6.14, used a 150 mm diameter and 175 mm deep graphite crucible. The anode was a fluted 38 mm diameter graphite rod. For supplementary heating, AC was applied between two 32 mm diameter graphite rods. Approximately 9 kg of electrolyte was used in the cell. The cell was used to prepare cobalt alloys of cerium, praseodymium, lanthanum, neodymium, didymium mixture, and the mixed cerium group metals.

The second cell, shown in Figure 6.15, used a 100 mm diameter and 125 mm deep graphite crucible. For supplementary heating, alternating current was applied between two 19 mm diameter fluted graphite rods. These fluted graphite rods were also connected to a direct current source and functioned as anodes during electrolysis. Generally 4 kg of electrolyte was contained in the cell. This cell was used to prepare cobalt alloys of samarium, yttrium, gadolinium, dysprosium, and mixed yttrium group metals.

The electrolytes used comprised LiF and the respective rare earth fluoride. The electrolyte used for cobalt didymium alloy preparation contained BaF_2 as an additional component. This was necessary for increasing the resistance of the electrolyte so that the desired electrolyte temperature could be maintained. For the preparation of mixed rare earth–cobalt alloys, the proportion of individual rare earth fluorides in the electrolytes corresponded approximately to the proportions in the respective mixed oxides used as cell feed.

Before commencing electrolysis, the inert atmosphere chamber was evacuated and backfilled with helium. The required electrolyte temperature was attained by applying AC to the heater rods and heating. Once the bath reaches the required electrolysis temperature, electrolysis was started and the rare earth oxide was intermittently fed to the cell at a rate determined by the rate of rare earth metal production. At the cathode zone, the temperature was maintained at above the melting temperature of the eutectic formed between cobalt and rare earth metals. The cathode was consumed as the molten alloy formed and dripped off and successive new sections of the cathode were lowered into the electrolyte. The alloy was collected in the form of nodules in a skull of frozen electrolyte and rare earth oxide at the bottom of the cell. At the conclusion of electrolysis, the cell was allowed to cool in the inert atmosphere chamber. The solidified electrolytic cake was then removed from the crucible and broken to recover the alloy nodules. The adhering electrolyte on the nodules was cleaned off by grinding.

The summary of operating data for preparing all the cobalt alloys are listed in Table 6.14.

There are two major benefits to using this cell arrangement. The electrolysis takes place at a temperature above the melting temperature of the eutectic between cobalt and the rare earth but below the melting point of cobalt, and the low melting alloy formed dripped off the cathode to the cell bottom which is at a lower temperature than the cathode zone. One benefit is that the reaction between the rare earth alloy and the electrolyte is minimized; the other benefit is that the frozen electrolyte skull prevents contact between the product and graphite crucible.

During electrolysis the alloy product coalesced well and nodules weighing as much as 60 g each were formed. The compositions of the alloys formed are also given in Table 6.14. The proportions of cobalt and rare earth metals in the alloy products corresponded to the lowest melting eutectics in the RE–Co system and in any given experiment, the concentration of cobalt usually varied by less than 3% among the nodules. In the products obtained using mixed oxide feed, the concentrations of certain rare earth metals contained in the alloy products did not correspond to their proportions in the oxide feed. The reason may be traceable to the difference in the concentrations of the individual rare earths in the electrolyte, the difference in their readiness to form alloys with cobalt at a given temperature, and the difference in their reaction rates with the electrolyte.

The rare earth cobalt alloys directly produced by electrolysis were relatively low in impurities. They were rich in rare earth metals and were found to be suitable for the preparation of rare earth cobalt compounds with the addition of more cobalt by melting. Then the compounds can be processed into fine particle permanent magnets by pulverization and consolidation.

It is seen in Table 6.14 that the cathode current efficiency varied widely among the various rare earth alloys. Low current efficiency is probably caused by reactions between the rare earth metals and the electrolytes. This was rather prevalent in the electrolytic preparation of samarium cobalt alloy. Samarium metal reacts with the SmF_3–LiF electrolyte

Table 6.14 Cell operating data and product analyses for electrolytic preparation of selected rare earth cobalt alloys (Morrice et al. 1969)

	Co–Ce	Co–Pr	Co–Sm	Co–Y
Electrolyte composition, %	35LiF–65CeF_3	32LiF–68PrF_3	27LiF–73SmF_3	15LiF–85YF_3
Current, A	50	39	53	59
Voltage, V	6	7.5	31	26
Anode current density*, A cm^{-2}	0.6	0.5	0.7	0.8
Cathode current density*, A cm^{-2}	5.1	4.0	10	11
Electrolyte temperature, °C	775	875	945	910
Cell bottom temperature, °C	685	835	660	715
Duration of electrolysis, h	3.2	2.0	1.4	1.6
Alloy recovered, g	174	175	50	135
Rare earth content, %	89	69	74	67
Cathode current efficiency, %	74	88	27	87
Major impurities, %				
Al	0.020	0.010	0.010	0.003
C	0.002	0.010	0.014	0.008
Fe	0.010	0.015	0.030	0.030
O	0.003	0.002	0.028	0.020
Ni	0.01	0.015	0.015	0.040
Si	0.005	0.010	0.010	0.010

*Based on initial electrode area

$$2SmF_3 + Sm \rightarrow 3SmF_2$$

resulting in not only low yield but also a coating of dark red salt that was rich in SmF_2, on the alloy nodules. In some experiments, BaF_2 was added to the electrolyte for improving the product recovery, but it was found that Sm also reacted with SmF_3–LiF–BaF_2 electrolyte. Morrice and Wong (1978) found that the rate of reaction of electrowon samarium with the electrolyte (SmF_3–LiF eutectic) increased markedly with increase in the temperature of the electrolyte. To reduce the amount of back reaction, it was desirable to deposit samarium on the consumable cobalt cathode and to collect the samarium cobalt alloy product at as low a temperature as possible. However, high temperature increases the solubility of Sm_2O_3 in the electrolyte and augments the formation of samarium cobalt alloy at the cathode. It therefore follows that to obtain the best cell operation for Sm–Co alloy preparation, the cell will have to be a thermal gradient cell.

Morrice and Wong (1978) obtained samarium cobalt alloy by fused salt electrolysis in a thermal gradient cell. The electrolyte was a SmF_3–LiF eutectic with a composition of 25 mole % (73%) SmF_3 and 75 mole % (27%) LiF and a eutectic temperature of 690°C. The cell enabled the following conditions to be realized. (1) At the Sm_2O_3 feed zone the temperature of the electrolyte was such that (high) sufficient dissolved Sm_2O_3 was available for electrolysis, (2) at the cathode zone the temperature was such that the liquid samarium cobalt alloy formed and dripped off the cathode, and (3) at the alloy collection zone the temperature was such that the reaction rate between samarium cobalt alloy product and the electrolyte was minimum.

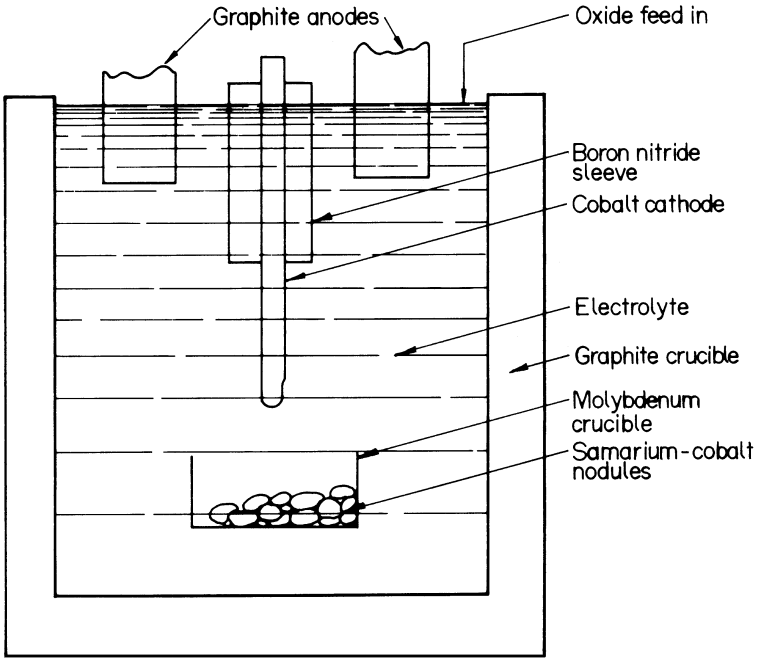

Figure 6.16 Schematic of the thermal gradiant electrolytic cell for Sm–Co alloy preparation (Morrice and Wong 1978).

A schematic of the thermal gradient cell is shown in Figure 6.16. The electrolyte was contained in a 125 mm diameter by 150 mm deep graphite crucible. The cell was heated internally by passing AC between two fluted 19 mm diameter anodes. As much as 6 kW of AC power could be applied to the upper 25 to 38 mm of the molten electrolyte, and this arrangement enabled maintaining a temperature difference of 300°C between the upper and lower portions of the bath. A 6 mm diameter cobalt rod was used as the cathode. The cathode rod was electrically insulated from the top or anolyte portion of the bath by a boron nitride sleeve. To collect the samarium cobalt alloy product, a perforated molybdenum basket was suspended in the electrolyte directly below the cathode. The temperature at which the samarium cobalt alloy was prepared and collected could thus be selected by raising or lowering the cathode and the product collection basket. After electrolysis, the basket containing alloy product as nodules would be lifted off the molten bath to drain out the excess electrolyte.

The optimum cell operating data for the thermal gradient cell and product analysis are given in Table 6.15. The current efficiency achieved was 50+% which is approximately double the current efficiency achieved for Sm–Co alloy in a usual oxide fluoride electrolysis cell.

6.8.2 Preparation of Magnets

In the attempts, beginning in 1968, to produce usable high density permanent magnets from $RECo_5$ alloys, the initial approach was to grind the alloys, $SmCo_5$, $La_{1-x}RE_xCo_5$, and

Table 6.15 Operating data and product analysis for Sm–Co alloy preparation in the thermal gradient cell (Morrice and Wong 1978)

Electrolyte composition, %	73 SmF_3–27 LiF
Direct current, A	40
Direct current, V	36
Alternating current*, A	66
Alternating current*, V	55
Initial anode current density**, A cm^{-2}	0.6
Initial cathode current density**, A cm^{-2}	5.2
Oxide feed zone temperature, °C	953
Cathode zone temperature, °C	720
Time of electrolysis, min	50
Cobalt cathode consumed, g	13
Samarium-cobalt recovered	42
Samarium content, %	79
Cathode current efficiency, %	53

Analysis of remelted samarium cobalt alloy product

Element	Al	C	Cr	Co	Cu	Fe	Mg	Mo	Mn	Ni	O	Sm
Content	0.04	0.17	0.003	43.5	0.04	0.02	0.003	0.46	0.07	0.15	0.05	55.6

*Supplemental powder applied to anode.
**Calculated using the initial cathode surface area.

$MMCo_5$, which was followed by alignment and pressing of the powders mixed with chemical binders (Buschow et al. 1968, Velge and Buschow 1968, Strnat et al. 1968, Westendorp and Buschow 1969). However, the interest in the plastic bonded magnets decreased after the first successful preparation of sintered magnets in 1969. In the mid-seventies, the plastic bonded magnets attracted attention once again (Menth et al. 1978) because they are not brittle and are easy to handle and machine. There are two types of magnets sintered and plastic bonded, which are made from $RECo_5$ magnetic materials.

Sintered Magnets The sintered magnets were first reported by Das (1969). Several subsequent investigations focused on sintering and the sintering technology was eventually optimized for $SmCo_5$ as well as for other $RECo_5$ alloys (Menth et al. 1978). A schematic representation of the production steps involved are given in Figure 6.17. The starting alloy may be obtained either by direct melting or by the direct alloy processes of reduction diffusion or co-reduction.

In general, the major steps in the preparation of these magnets are blending of the starting alloys, milling of the mixture, sintering of the green powder compact, and the post-sintering heat treatment.

Blending During the blending, samarium loss can occur due to evaporation and oxidation; therefore, the process should begin with a starting composition having an excess of Sm. This is done either by starting with an alloy of composition $SmCo_{5-x}$ or by starting with a mixture of two alloys with different Sm contents, for example, $SmCo_5$ and a Sm-rich sinter additive (e.g., 60% Sm–40% Co). As another alternative, a mixture of two alloys, $SmCo_{5+x}$ and $SmCo_{5-x}$, may be used (Naastepad et al. 1973). The important point is that

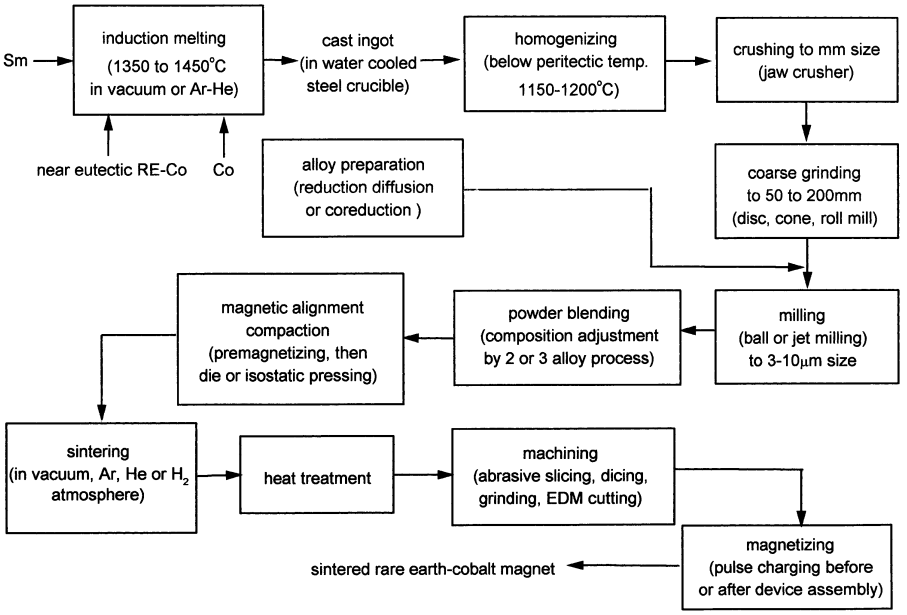

Figure 6.17 Flowsheet for sintered rare earth-cobalt permanent magnet production (Strnat 1988).

the samarium content must be so chosen that no Sm_2Co_{17} phase is present in the final $SmCo_5$ magnets. Similarly, in the production of Sm_2Co_{17} magnets, the starting composition must ensure that no Co phase is present in the final sintered magnet. Inclusions of such a second phase would adversely affect the coercivity field.

Milling Many critical parameters need to be controlled during the milling process. They are grain size, grain size distribution, damage to crystal structure, and the loss of Sm due to oxidation. The loss of Sm is kept low by exclusion of air and water vapor. The techniques of milling that fulfill the stated conditions are ball milling under toluene or petroleum ether, and jet milling with dry nitrogen as working gas. The resulting average grain size of the powder should be comparable to the initial diameter for a single domain particle. Usually the alloys are milled into particles of about 3–7 μm average size. In the final magnets, a good magnetic homogeneity is achieved if the grain size distribution is narrow. Grains that are too small have a high structural defect density and an unfavorable surface to volume ratio giving rise to a high oxidation rate. Grains that are too large no longer exhibit single domain character and may not be single crystals, resulting in poor magnetic alignment of the powder.

Aligning and pressing The powder is compacted in a die to 60–70% of bulk density, usually with a ~800–2400 kA/m magnetic field applied to achieve grain orientation. Sometimes the die pressing is followed by further isostatic compaction.

Sintering The aligned green compacts are sintered under an atmosphere of argon, helium, or vacuum. The objective is to obtain an optimum combination of high density (i.e., high remanence) and high coercive field. It is necessary to have a constant and well-defined sintering temperature to ensure that the magnet has no open porosity and that no grain growth occurs that would have a detrimental effect on the coercive field. For $SmCo_5$ the sintering temperature is 1120°C, and for $MM_{0.85}Sm_{0.15}Co_5$ it is 1050°C. Sintering usually

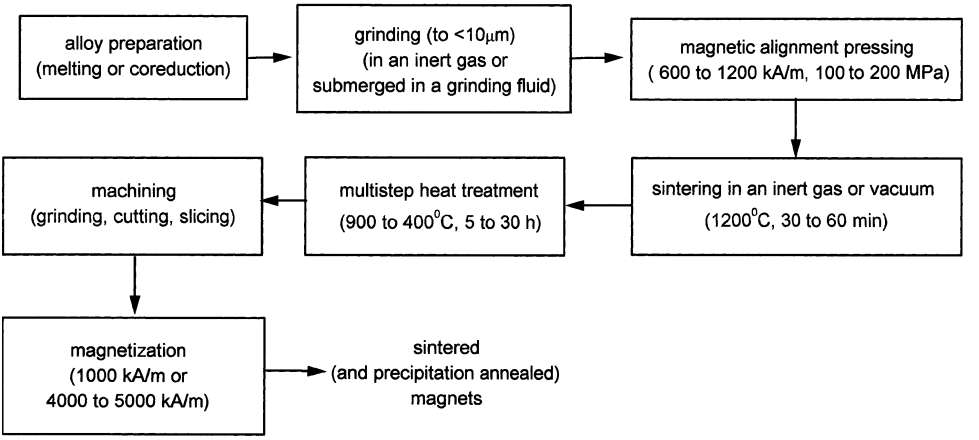

Figure 6.18 Flowsheet for the preparation of precipitation hardened magnets.

lasts for 30 min to 1 h. Sintering in H_2 above 1100°C is also possible if suitable precautions are taken to avoid hydride formation (Jones et al. 1977). Hot pressing has also been used to prepare good magnets (Strnat 1978).

Heat treatment A post-sintering heat treatment is used to increase the coercive field of $RECo_5$ as well as RE_2Co_{17} magnets. For $SmCo_5$, the optimum annealing temperature is 900°C, and for $MM_{0.85}Sm_{0.15}Co_5$ it is 950°C. The beneficial effects of annealing $RECo_5$ magnets include (1) gradual removal of the lattice defects that determine the nucleation of the reversed domains, (2) decrease of local inhomogeneities in composition, and (3) partial precipitation in the grain boundaries of the oxygen that is dissolved in the magnetic phase during sintering.

Following annealing, the magnet has to be cooled to room temperature at a carefully controlled rate depending on its mass and shape. Cooling too slowly can result in the eutectoidal decomposition of the 1:5 phase to the 2:17 phase and associated lattice defects, adversely affecting the coercive field. Cooling too fast, on the other hand, can create microscopic cracks and internal stresses that adversely influence both the stability of the magnets against oxidation and the coercivity.

The magnetic properties of the products obtained in the above procedure depend greatly on the many parameters, including composition, particle size, alignment, sintering conditions, and the final heat treatment. Close quality control for all the processing steps is important as its presence or absence is made obvious by the product magnet's hysteresis loop shape, the spread of properties in a production lot, the magnitude of irreversible flux losses on heating, and the long term stability of the magnets (Strnat 1978). A well-sintered magnet at high mass density and a high H_k (the reverse field that reduces the flux density to 0.9 Br) displays low irreversible losses during short-term heating and good long-term aging stability, especially at elevated temperatures in air.

Precipitation Hardened Magnets The copper containing rare earth magnets can in principle be produced by casting (Naastepad et al. 1973) followed by processing by zone melting or recrystallization to promote directional grain growth. Such magnets are brittle and are not in commercial use. All commercial magnets of the copper type, near the 1–5, 1–7, or 2–17 compositions, are made by the powder metallurgical route shown in Figure 6.18. Only a single powder (no Sm–Co additive or sintering aid) is used. For these magnets,

milling and sintering are less critical compared to the procedure for fine particle magnets. The powder particles have to be single crystals so that they can be aligned easily in a magnetic field; however, they need not be single domain particles as is necessary for nucleation type magnets. The choice of grain size can be based on requirements of minimal oxidation and optimum sintering kinetics. No negative influence on the hard magnetic properties comes from grain growth during sintering. The sintering temperature of the $Sm(Co,Cu,TM)_{5<z<7.5}$ alloys must be below the peritectic temperature. TM here represents a transition metal. For example, for $Sm(Co_{0.84},Cu_{0.16})_{7.2}$ the sintering temperature of 1180°C (peritectic temperature ≈ 1220°C) results in an almost 100% theoretical density for the magnet. The coercive field in these alloys is relatively low, at about 72 kA/m, after sintering. The coercive field can be improved by up to a factor of six by an appropriate annealing that results in an optimum density and precipitate size.

Machining, handling, and magnetizing Sintered RE–Co magnets present certain problems in machining, handling, and magnetizing. They are hard and brittle. Machining them involves slicing with diamond blades, and surface grinding or cutting on spark erosion machines in a demagnetized state. The high H_C and low recoil permeability of rare earth permanent magnets (REPM) allows precharging and manipulation in an open circuit and they will not self-demagnetize. For larger high energy magnets, however, machining, shipping, and handling in the magnetized state are difficult. It is therefore often necessary to magnetize after partial assembly of a device. This can be problematic. High H_C 2–17 magnets and $SmCo_5$, first charged and then field demagnetized, need up to 4 MA/m for saturation. This demands expensive magnetizing equipment and may not be at all possible for larger assemblies. Incompletely magnetized $SmCo_5$ magnets can display severe thermal instabilities of the flux. Some of these limitations are circumvented in the bonded magnets, which are also attractive for many more reasons.

Bonded Magnets The RE–TM based bonded or matrix magnets were first introduced in the late 1960s, but their commercial development was slow. There were difficulties relating to chemical reactivity of the powder and inexpensive manufacturing methods. Earlier products were made from 5–20 μm particles of $SmCo_5$ bonded with epoxy, polyethylene chloride, or ethylene vinyl acetate. These deteriorated very quickly at temperatures above 50°C and were not magnetically very stable even at room temperature (Strnat et al. 1976). Much improvement was brought about by coating the particles with metallic or organic diffusion barriers and with careful selection of compatible polymeric binders. The most important development was the introduction of alloys bulk hardened with copper. Used as coarse powders (≈ 20–200 μm), these did not suffer the severe sensitivity of H_c to the particle surface condition. They were, therefore, much more stable. Another way of improving the elevated temperature stability was to use a soft metal matrix. Alloys with compositions close to the 2–17 stoichiometry and with higher Fe content were developed particularly for bonded magnets. Methods developed for producing ingots with a coarse columnar grain structure obviated the need for presintered blocks for making bonded magnets. Moreover, the adaptation of inexpensive molding methods such as extrusion and injection molding in an orienting field encouraged large-scale production and industrial applications of the bonded rare earth permanent magnets.

The schematic flowsheet for the production of polymer bonded RE–Co magnets is given in Figure 6.19 (Strnat et al. 1976). The RE–Co alloy was converted to a powder comprising mostly single crystal particles of sufficiently high coercive force. The powder was stabilized and/or magnetically hardened before sizing and blending with a binder. Then the blend was exposed to a magnetic field that magnetizes and orients the particles, the mass

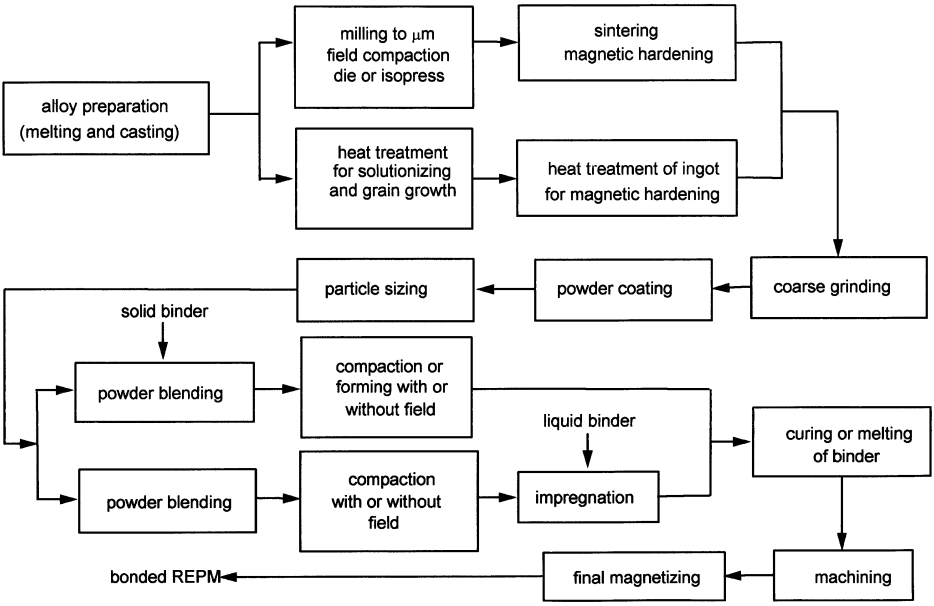

Figure 6.19 Schematic flowsheet for the production of bonded RE–Co magnets.

was compacted, and the binder was hardened. In an alternative procedure, the magnetic powder alone was compressed into a porous body that was then infiltrated with a liquid binder that subsequently solidified. The polymer bonded magnets were produced in two basic forms. One form was as rigid bodies with thermosetting or chemically hardened resin binder, and the other was as flexible sheets or strips with a thermoplastic or rubber binder (Strnat et al. 1976). Such magnets were generally made from $SmCo_5$ powder and were anisotropic by field alignment of the particles. The energy products of plastic bonded magnets ranged from 25 to >135 kJ/m^3. The 2–17 alloys were used in the upper end, $SmCo_5$ in the middle, and alloys with MM substitution in the low Br region. As regards the magnetic properties of the bonded magnets, the best compression molded 2–17 matrix magnets offer room temperature properties equivalent to medium grade sintered $SmCo_5$. They are, however, far superior to any non-RE magnet type. Injection molded magnets are commercially attractive because of the low cost of processing but they had significantly poorer Br, H_{ci} and loop shape. Metal matrix magnets with 2–17 alloy, a Sn–Pb binder and Cu filler have been prepared to obtain magnet sets with precisely controlled variable saturation (Strnat and Strnat 1991).

The most important advantage of matrix bonding is inexpensive mass production. This comes about because of the possibility of molding magnets or even subassemblies to final shapes with close tolerances. There is little cutting scrap or grinding loss, and machining, when necessary, can be done with conventional machine tools. Compared to sintered magnets, there are fewer handling problems with bonded magnets. As regards mechanical behavior, the bonded magnets are somewhat ductile (metal matrix) and elastic or even flexible (plastic or rubber binders). At dense packing they are moderately brittle. The bonded magnets can be conveniently produced in much larger sizes than the sintered ones without ending up with property inhomogeneities, or cracking and warping by uneven shrinkage, which are size-limiting factors for the sintered bodies.

The samarium cobalt magnets proved to be attractive replacements for the older ferrites, Pt–Co and Alnico permanent magnets, and also for electromagnets in many applications. Their use has all along been constrained by economic disadvantages. Among the light rare earths, samarium is the least abundant and hence most expensive, and this unfavorable situation is aggravated by the fact that the price and availability of cobalt are subject to largely unpredictable excursions. The bulk of the world's cobalt is mined in Zaire and the 1978 civil war there dried up the supplies. This drastically intensified the worldwide search for alternative RE–TM systems having economically more acceptable elemental constituents. Neodymium–iron–boron magnets were discovered and developed as a consequence.

6.9 NEODYMIUM–IRON–BORON MAGNETS

Even though iron-based materials having the characteristics of samarium–cobalt had long been desired, no suitable compounds were known. RE–Fe phases having $CaCu_5$ structure do not exist and $REFe_{17}$ compounds in which RE is a light rare earth have an unusually low Curie temperature. Two lines of research, one relying on the rapid solidification by melt spinning of rare earth–iron–metalloid alloys and the other based on conventional powder metallurgy gave encouraging results by the early 1980s. Croat et al. (1984, 1984a) reported energy products as large as 112 kJ/m^3 in melt spun ribbons of $Nd_{0.135}Fe_{0.817}B_{0.048}$, and Sagawa et al. (1984) applied traditional sintering methods to ternary light rare earth–iron systems and obtained $(BH)_{max} \sim 288$ kJ/m^3 for $Nd_{0.15}Fe_{0.77}B_{0.08}$. Both of these high $(BH)_{max}$ materials, rapidly solidified as well as sintered, contained a novel ternary crystalline compound $Nd_2Fe_{14}B$. The larger energy product reported by Sagawa et al. (1984) came from the crystalline orientation provided by the powder metallurgy procedure. $Nd_2Fe_{14}B$ immediately attracted considerable technological interest because of its excellent intrinsic magnetic properties [$(BH)^*_{max} \sim 512$ kJ/m^3, $H_a \sim 5840$ kA/m] as well as economic advantages over samarium–cobalt materials. Practical magnets with energy products in the range of 320–400 kJ/m^3, values that are significantly larger than any attained previously, were prepared from melt spun (Croat 1989, Lee 1985) and sintered (Sagawa et al. 1987) alloys. Large-scale production programs following both the approaches have been subsequently implemented.

The overall process for the production of Nd–Fe–B magnets has two major stages. One is the production of magnetic alloy and the other is processing of the Nd–Fe–B alloy into permanent magnets.

6.9.1 Production of Nd–Fe–B Alloys

Many methods have been developed for the production of neodymium iron robon (Nd–Fe–B) alloys (Agarwal et al. 1988). They include direct melting, co-reduction, and several special techniques that make use of reduction extraction or thermit type processes for directly making the Nd–Fe or Nd–Fe–B alloys.

Direct Melting The direct melting method was used by Ormerod (1985) at Philips Electronic Components and Materials Division, The Netherlands, to prepare the Nd–Fe–B alloy. The target composition in their vacuum induction melting was 15 at % Nd, 77 at %

Fe, and 8 at % B, which was the composition reported by Sagawa et al. (1984) as giving the optimum magnetic properties. The alloy was prepared from 99.9% Fe, 99.9% Nd, and 99.8% B. The iron and boron was initially melted in an alumina crucible under argon. After degassing under vacuum, the melt temperature was allowed to come down to just above the liquidus and neodymium was added. Corrections were made for any anticipated melting losses. The melt was then cast in a thick walled copper mold with a 5 mm cavity. The advantage of vacuum induction melting is that it can yield a wide range of alloy compositions with very low (<200 ppm) oxygen contents; however, pure elemental starting materials are needed.

Kaneko and Ishigaki (1994) have used ferroboron as the source of boron in the preparation of Nd–Fe–B alloy by direct melting. Using 99.5% pure rare earth metals, 99.9% pure electrolytic iron and ferroboron, as raw materials, the $(Nd,Pr,Dy)_{12.5-15}Fe_{77-81.5}B_{6-8}$ alloys were prepared by induction melting in an argon atmosphere. The as-cast alloy was subsequently put through a homogenization treatment by heating for 5 h at 1000°C, before it was converted to powder.

Nd–Fe–B alloys have also been made by arc melting. For example, an alloy of 81.5 at % Fe, 13 at % Nd and 5.5 at % B was prepared by arc melting Nd–17.5% Fe master alloy, electrolytic iron and crystalline boron, under a continuous flow of ultrapure argon. To minimize segregation and achieve compositional homogeneity in the alloy, the arc melted ingot was remelted four times. The arc melted alloy was subsequently induction melted before processing by rapid solidification.

Co-reduction In continuation of their earlier work on Sm–Co alloys, efforts were on at Th. Goldschmidt AG in Germany to make the Nd–Fe–B type of materials by the calciothermic reduction technique soon after the first announcement of the Nd–Fe–B magnets at the 29th MMM Conference in Pittsburgh in November 1983 (Sagawa et al. 1984). The technique was successfully applied the first time in October 1984 (Herget 1985). Co-reduction was based on the following overall reaction.

$$7.5Nd_2O_3 + 50.7Fe + Fe_2O_3 + 0.143Fe_{44}B_{56} + 52.5Ca \xrightarrow[\text{vacuum, 4 h}]{1100-1200^\circ C} Nd_{15}Fe_{77}B_8 + 52.5CaO$$

The source of boron used in the above reaction was commercial ferroboron powder containing 20% boron. The conditions for carrying out the above reaction were essentially similar to those used for co-reduction of Sm_2O_3 and Co_3O_4 because the difference of the free energies of formation between Sm_2O_3 and CaO on the one hand and between Nd_2O_3 and CaO on the other are similar. Calculated quantities of the starting materials were thoroughly mixed, pressed into pellets, and loaded in crucibles made of high temperature resistant steel. The crucibles were closed by welding except for an opening for evacuation and put in a vertical position into electric furnaces. These furnaces were evacuated and heated to reaction temperature.

The Nd–Fe–B alloy exhibits a much greater tendency for oxidation compared to $SmCo_5$ (Herget 1985), and this introduces differences in the process used for separation of the alloy powder from the CaO slag. A new and proprietary leaching procedure was developed and used by Th. Goldschmidt AG for the separation of alloy and CaO, and this process kept the oxygen content at 0.20% or even less in alloys with >40% Nd.

The co-reduction process has been used by Herget (1985) not only to achieve a neodymium content of above 40% in the Nd–Fe–B alloy, but also to add/incorporate rare earth or alloying elements such as Dy, Al, Nb, or Co in the product. The alloy powders

produced typically contained O: 0.12–0.25%, C: 0.03–0.04%, Ca: 0.03–0.06%, and Al: 0.01–0.20% as residual impurities. The Al impurity was derived from the aluminum content of ferroboron, which was itself produced by an aluminothermic reduction process. If elemental boron were used instead of the aluminothermic ferroboron, the Al content could have been avoided.

Herget (1985) noted that the alloy powder picked up oxygen, and its oxygen content tended to increase even when stored in sealed plastic bags.

The calciothermic production of Nd–Fe–B alloys has also been used by a group at the Beijing University of Iron and Steel Technology (Herget 1985). The reduction process was carried out at ambient pressure under argon. The details of the procedure for aqueous treatments for alloy–CaO separation were not disclosed in these investigations.

The advantages of the calciothermic technique are high alloy yields, immediate production of powder that is so fine that it can be directly fed into the fine milling stage without prior crushing, wide variability regarding the number of components as well as alloy compositions, and cost advantages because of using commercial oxide as the starting materials. There are certain disadvantages also. They are the high cost of the calcium reducing agent, the batch-wise nature of the reduction operation, and interestingly, the powder form of the product. Alloy in the form of powder hampers its use for the magnet manufacturing process originally adopted by General Motors. The neodymium alloy powders with their high surface area and hence possibility of quick oxidation are not very suitable to melting, and melting precedes melt spinning and quenching as practiced by the General Motors process. Lump metals are preferred.

Production of Consolidated Alloys There are two basic routes to production of metallic rare earth alloys and several companies have developed their own proprietary modifications of these basic routes to make neodymium alloys for magnets (Agarwal et al. 1988). The two major routes are based on oxide as the starting material but differ in the reduction step. Oxide reduction can be carried out by using calcium as the reductant for the oxide or after converting the oxide to fluoride, or the reduction is achieved by a fused salt electrolysis technique. The modifications and the major unit operations involved are summarized in Figure 6.20 and Figure 6.21. The outlined processes and their modifications have been used for making neodymium alloys by Molycorp Research Chemicals, Comurhex, Goldschmidt, General Motors, Ronson, and Santoku.

Molycorp The schematic flowsheet of the Molycorp process is shown in Figure 6.20. The process used was calciothermic reduction of neodymium fluoride prepared from the carbonate by a wet process.

Neodymium nitrate was made from the carbonate by an aqueous process. The nitrate was fed to a batch precipitation reactor at a controlled rate with excess hydrofluoric acid. The solution pH was controlled by adding sodium hydroxide solution. At the end of the reaction, the reactor contents were passed through a continuous filter where the neodymium fluoride precipitate was removed and thoroughly washed. The filtrate was neutralized, and excess fluoride was precipitated from it by the addition of lime.

Water was removed from the neodymium fluoride precipitate by first feeding it to a dryer for removal of adhering moisture and then feeding it to a calciner for removing water of hydration. Calcination was carried out in an atmosphere of hydrogen fluoride, which was obtained from an HF still. The off-gases were scrubbed and neutralized. The calcined product was stored under nitrogen.

Anhydrous neodymium fluoride was blended batch-wise with an excess of calcium granules. The mixture was loaded in tantalum crucibles and reduced in an induction furnace

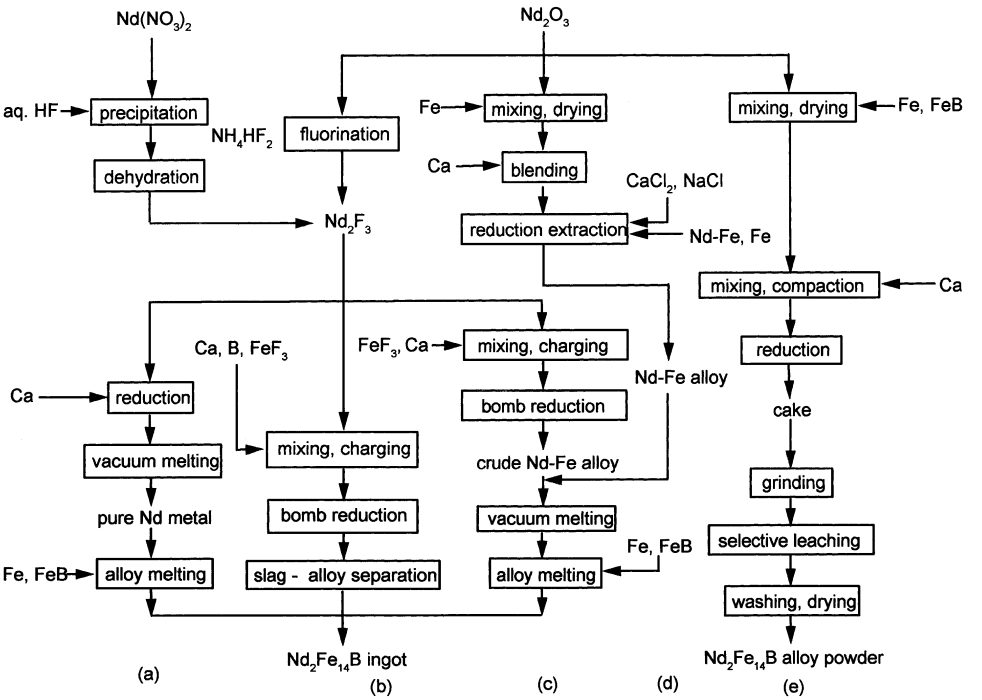

Figure 6.20 Preparation of Nd–Fe–B alloys-I (a) Molycorp process, (b) Ames process, (c) Comurhex process, (d) General Motors process, (e) Goldschmidt process.

under a nitrogen atmosphere. The furnace was provided with a solids charging system and a crucible tilting mechanism. Thus, portions of calcium fluoride/calcium slag could be poured off and the crucible recharged twice during the course of reduction. The decanted slag was solidified and disposed of, and the reduced neodymium was cast into molds for purification.

As-reduced neodymium metal was purified by vacuum melting in an induction furnace. Purification needed high vacuum and a long duration. The purified neodymium was cast into molds for alloying. Alloying was carried out by adding iron and ferroboron in controlled amounts to pure neodymium metal and alloy melting was carried out in a nitrogen atmosphere. The alloy was cast in molds and analyzed. "Off-spec" material was recycled and acceptable material was sold for magnet manufacturing.

Research chemicals The route followed is calciothermic reduction of neodymium fluoride and the fluoride was prepared from the oxide by a dry process. The schematic flowsheet is shown in Figure 6.20 as the Ames process. Neodymium oxide was blended with a large excess (100%) of ammonium bifluoride and the mixture was charged to a drum type fluorinating reactor. This batch reactor was operated with a programmed temperature cycle. The charge was heated to first convert the oxide to the complex fluoride and then to remove the unreacted excess bifluoride. The complex fluoride was then decomposed by heating in vacuum and the product fluoride was calcined. The drum was rotated during the reaction period to effect mixing of the phases. The calcined fluoride was cooled, removed from the reactor, and stored under nitrogen. The fluoride was processed to the magnet alloy using the same equipment and procedure as that described for the Molycorp process.

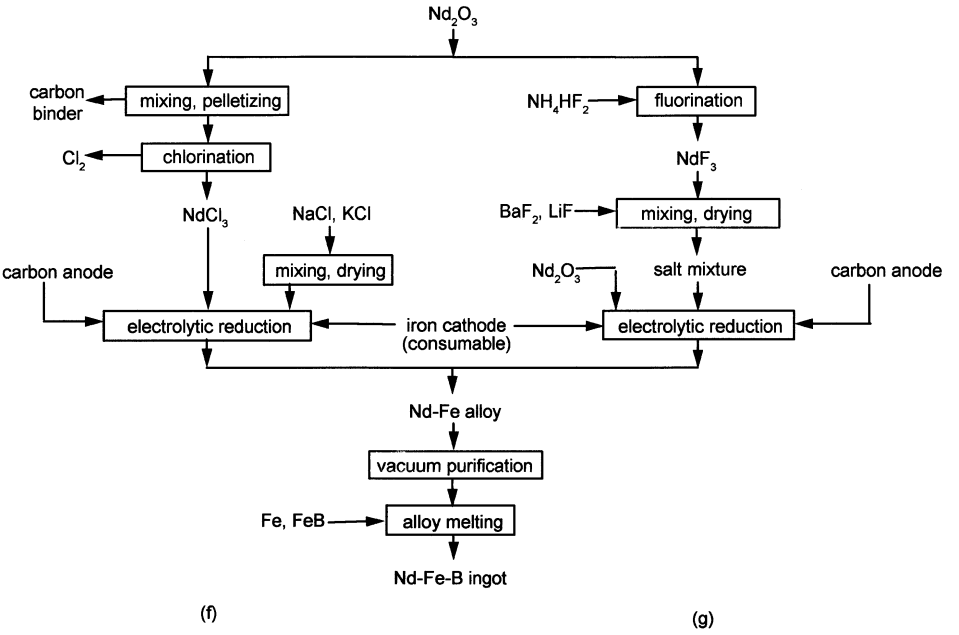

Figure 6.21 Preparation of Nd–Fe–B alloys-II (f) Ronson process, (g) Santoku process (IMR).

During fluorination, the initial gaseous reaction products, ammonium fluoride, water, and unreacted hydrogen fluoride, were removed from the reactor in a stream of nitrogen and were scrubbed with water for disposal. At the time of excess bifluoride removal, the off gases passed through switching condensers where the bifluoride was collected as a solid. This was scrubbed and the scrub solution was treated with sufficient lime to bring the pH to near neutral. The solution was then clarified, the overflow discharged, and the sludge disposed.

The condensers that had collected the bifluoride were heated sequentially to above the solid's (ammonium bifluoride) melting point and the liquid was pumped to a scrapped surface heat exchanger for solidification. The bifluoride was recycled.

Comurhex The schematic flowsheet of the Comurhex process is shown in Figure 6.20. The key step was an adiabatic calciothermic reduction of a mixture of neodymium and iron fluorides.

The wet process described earlier for the Molycorp flowsheet was used for the preparation of neodymium fluoride. Iron fluoride was prepared by reaction of iron chloride with gaseous hydrogen fluoride that was obtained by stripping a portion of the hydrofluoric acid used in neodymium nitrate precipitation. Hot and dry iron chloride, obtained by feeding iron chloride continuously to a dryer/preheater, was fed to a fluoridizing reactor in which excess hydrogen fluoride was fed countercurrently. The reactor was staged and cooled to control the temperature profile. The reactor off-gas contained hydrogen chloride, excess hydrogen fluoride, and some iron chloride. It was scrubbed with water and then disposed. The scrub solution was discharged after fluoride removal by liming and clarification. The iron fluoride was cooled in the final reactor stage and collected warm for storage. It was stored under nitrogen.

Neodymium fluoride, iron fluoride, and excess calcium were mixed in a proportion sufficient to produce a reaction product mass at a temperature between 1100 and 1200°C, adiabatically. The mixture was loaded around a mandrel and compressed into steel reactor vessels. These vessels were jacketed and were designed to withstand an internal pressure of 7 MPa. A tantalum cup was fitted below the charge to collect the alloy product. An ignitor charge comprising calcium and iron fluoride was placed over the top of the charge.

After loading the reactor, it was purged with nitrogen and the charge was ignited. The reaction proceeded rapidly from the core to the outside where it was quenched by the cold material in contact with the wall. The reduced iron–neodymium alloy has a relatively low melting point and drained through the calcium fluoride slag into the tantalum cup. After cooling, the reactor was opened, the alloy was retrieved from the tantalum cup, and the slag was removed from the reactor for disposal. The unreacted charge adhering to the wall was separately collected and recycled for blending with fresh material.

The crude NdFe alloy was purified by vacuum melting and adjusted to the required final composition in alloy melting furnaces by the procedure described for the Molycorp process.

Th. Goldschmidt The schematic flowsheet of the Th. Goldschmidt process for producing neodymium iron boron alloy is shown in Figure 6.20. Neodymium alloy powder of desired composition was directly produced by a calciothermic reduction of a proportional mixture of neodymium oxide, iron, and ferroboron.

Neodymium oxide was mixed with a slight excess of iron and ferroboron and the mixture was heated to remove traces of moisture and kept in a nitrogen atmosphere. Calcium, in a suitable excess quantity, was blended with this mixture and the charge was fed to the press for compaction. The pellets were loaded into holding vessels and the vessels were closed and purged with nitrogen and then with argon. These vessels were then transported to electrically heated furnaces, where they were heated to the reaction temperature. After completion of the reaction, the vessels were removed from the furnace, allowed to cool and the contents were discharged into holding bins under an argon atmosphere.

The reduced alloy was liberated from the slag by grinding the reaction product in a closed circuit ball mill under liquid hexane. From the finely ground material, hexane was removed by evaporation in a wiped surface evaporator and the ground material was transferred to surge bins under argon atmosphere. The material now contained unreduced reactant, excess calcium, and calcium oxide in addition to the product alloy. The other materials were separated from the alloy by a proprietary leaching process in which pH and E_h were carefully controlled and nitric acid, a chelating agent, or other chemicals were probably used for selective leaching. The leach effluent was filtered to recover the solid product. The product was washed with deoxygenated water, dried, and stored under argon. The filtrate was treated with lime to neutralize excess acid and precipitate dissolved neodymium and iron as hydrous oxides. The effluent was clarified and the overflow discharged. The sludge was also disposed.

The product was quality controlled, and "on-spec" material was stored in lined containers under inert gas. The off-spec material was either used for blending or was converted to ingot in an alloy furnace after the addition of required boron or ferroboron.

General Motors The schematic flowsheet of the process is shown in Figure 6.20. The key process is the calciothermic reduction of a mixture of neodymium oxide and iron that takes place in a molten salt mixture in a stirred tank reactor.

Neodymium oxide was blended with iron and the mixture was heated to remove traces of moisture. The dried material was stored under an inert atmosphere. The quantities of

neodymium oxide and iron were chosen so that on reduction of the oxide, neodymium and iron would form an alloy of eutectic composition. Calcium and sodium chlorides were also blended and heated before loading them into the reduction reactor as make up. The iron–neodymium mixture was blended with excess calcium and the charge was kept in surge bins under an inert atmosphere for feeding to the reactor.

The reduction was carried out in a tantalum-lined electrically heated stirred tank reactor. The reactor was charged with the required amount of salt mixture, and a heel of eutectic alloy and solids was melted. The temperature was raised to ~750°C, and the neodymium oxide–iron charge was fed to the reactor at a controlled rate with high agitation for a predetermined period. Charge feeding was then interrupted, agitation was decreased and then stopped to permit the phases to settle, and the molten alloy product was removed by bottom tapping. This cycle was repeated many times while the unreacted calcium and neodymium oxide and the calcium oxide slag were being retained within the reactor. At the conclusion of the cycles, all of the eutectic was removed and the salt, which contained large amounts of solids, was discharged for disposal. The NdFe eutectic was vacuum purified and alloyed to the final composition by the same procedure as described for Molycorp.

Ronson The schematic flowsheet of the process used by Ronson is shown in Figure 6.21. The process is an electrochemical reduction of neodymium chloride by electrolysis in a mixture of fused chloride salts using a consumable iron cathode.

Neodymium chloride was prepared from neodymium oxide by chlorination in the presence of carbon. The oxide was mixed with excess carbon and a binder, and the mixture was compacted into pellets. The green pellets were dried and screened. The undersize pellets were recycled and the others held in surge. Chlorination was carried out in a shaft furnace. The pellets fed to the top of the shaft furnace descend against a countercurrent flow of heated chlorine gas. The neodymium chloride formed is molten at the prevailing temperature. It drained from the reactor into a heated enclosed receiver. Unreacted oxide and excess carbon were settled and skimmed in the receiver. The furnace off-gas containing excess chlorine and carbon oxides was scrubbed with off-gas from the electrolytic cells to remove chlorine.

The liquid neodymium chloride from the chlorination furnace was transferred under inert atmosphere to an exchanger for solidification. The solid chloride was held warm under nitrogen for charging to the electrolytic cells. The electrolyte components, sodium chloride, and potassium chloride were mixed, heated under an inert atmosphere to remove moisture, and were held for changing to the cell. Electrolysis was carried out in cells with carbon anodes and a consumable iron cathode. Neodymium–iron alloy formed at the cathode was collected at the cell bottom and tapped periodically. Chlorine was evolved at the anode. The gas was scrubbed in an oxidizing solution of calcium hydroxide, and the resulting solution of soluble chloride salt was released. During electrolysis impurities in the charge materials, especially the oxychlorides, accumulated in the electrolyte and the electrolyte must be purged to remove them.

The crude alloy obtained from the electrolytic cell was purified by vacuum melting to remove volatile chlorides and was then alloyed with iron and ferroboron as in the Molycorp process.

Santoku The schematic flowsheet of the Santoku process is given in Figure 6.21. The process involves electrolytic reduction of the neodymium oxide in a fused fluoride electrolyte and recovery of the metal as the iron alloy.

Neodymium oxide was dried by heating to remove the moisture, and the dry oxide was stored under an inert atmosphere for charging to the cell. A portion of the oxide was

converted to the fluoride, using ammonium bifluoride as the fluorinating agent under conditions described for the Research Chemicals/Ames flowsheet. Neodymium fluoride was mixed with barium fluoride and lithium fluoride, and the mixture was dried by heating to remove the trace amounts of water. The dry fluorides mixture was stored under inert gas cover for charging to the cells.

Electrolysis was carried out in cells equipped with carbon anodes and iron cathodes. The cathode was consumable as the reduced neodymium metal alloys with the iron forming a low melting eutectic that was collected in tantalum liners at the cell bottom. Oxides of carbon were formed at the carbon anode. These gases were vented and scrubbed for discharge.

The cells were loaded with the fluoride electrolyte mixture and heated to melt the electrolyte and attain the cell operating temperature. The oxide was charged at a controlled rate and the molten alloy product was bottom tapped periodically. Unreacted oxide and other impurities collected in the electrolyte and they were purged. The neodymium–iron alloy obtained from the cell was first purified mechanically to remove adhering electrolyte and then charged to the alloy melting furnace. This furnace was equipped with a vacuum system and was used first to purify the alloy from volatile impurities by vacuum melting after which alloying additions were introduced to obtain the final composition.

Among the processes listed above, neodymium recovery of about 90% was possible when calcium was the reducing agent and neodymium fluoride was the intermediate starting compound. The yield was only about 70 to 75% in the electrolytic processes because of losses caused by bleeding of the electrolyte to control its chemical composition. The primary alloy product contained about 30 to 32% neodymium. This neodymium was actually 96% neodymium and 4% other rare earth metals.

The processes for alloy production of rare earth metals are considered fairly straightforward up to the primary alloy stage. Both the yield and quality control become major concerns when these primary alloys are processed to fabricate the final magnet product.

6.9.2 Production of Nd–Fe–B Magnets

Prior to the production of Nd–Fe–B magnets, the Nd–Fe–B alloys that have been prepared by one or another of the above processes are first converted to a metallurgical or physical form suitable for further processing to magnets. The most important processing in this context is the reprocessing of the magnet alloy by the rapid solidification technique of melt spinning. In another route the cast alloy ingot is converted to fine powder before a modified powder metallurgical consolidation to magnets. The second is known as the sintering route.

Melt Spinning The melt spinning procedure involves ejection of molten Nd–Fe–B alloy through a crucible orifice onto the surface of a substrate disc. The apparatus is shown schematically in Figure 6.22. The disc is usually made of copper because of its high thermal conductivity, and it rotates with surface velocity v_s. A fine jet or stream of molten alloy is directed onto the surface of the rapidly spinning quench wheel. While the jet feeds a pool of liquid metal, at its point of contact with the wheel the spinning wheel extracts the metal as a thin rapidly quenched ribbon or flake. The process is carried out in an inert atmosphere, usually argon, because the rare earths are very reactive chemically and need to be protected from oxidation during high temperature processing. In melt spinning the cooling or quench rate attained is estimated to be of the order of 10^5 °C/s, and this rate can be varied by

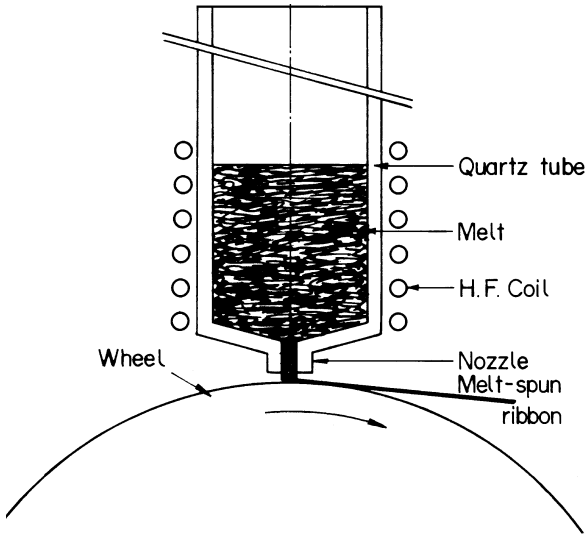

Figure 6.22 Schematic of the melt spinning apparatus (Ormerod 1985).

changing ν_s. The cooling rate is directly proportional to ν_s. The quenched material is inherently brittle and the products are obtained in the form of ribbons typically 30–50 μm thick, 1–3 mm wide and having lengths on the millimeter or centimeter scale, depending on ν_s.

The microstructure and magnetic properties of melt-spun Nd–Fe–B ribbons are sensitively dependent upon the quench rate (Herbst and Croat 1991), which in turn depends upon ν_s. Plotted as a function of ν_s, H_{ci} and $(BH)_{max}$ each exhibit a maximum. At high quench rates ($\nu_s \geq 30$ m/s) essentially amorphous, "overquenched" materials with negligible H_{ci} and $(BH)_{max}$ are obtained. At quench rates $\nu_s = 19$ m/s, ribbons consisting of spheroidal $Nd_2Fe_{14}B$ grains with an average diameter of 30 nm are obtained. These ribbons have the highest coercivities ($H_{ci} \approx 1120$ kA/m) and energy products [$(BH)_{max} \sim 112$ kJ/m^3]. These are optimally quenched ribbons. At ν_s below the value resulting in optimally quenched ribbons, ribbons composed of progressively larger $Nd_2Fe_{14}B$ crystallites and characterized by decreasing H_{ci} and $(BH)_{max}$ are formed. It is interesting and technologically significant that the largely amorphous, overquenched ribbons melt spun at quench rates required only to exceed a minimum value instead of confining to a narrow interval, can be suitably annealed to nearly duplicate the properties of optimally quenched materials obtained directly. The quenched ribbon or flake is usually ground down to a fine powder before processing to consolidated magnets.

Consolidation The production of bulk magnets by consolidation of melt-spun ribbons (Lee 1985, Lee et al. 1985) is accomplished by the procedures outlined in Figures 6.23a and 6.23b. The first procedure yields what are known as "bonded magnets," and the second procedure results in the so-called "hot pressed magnets."

Bonded magnets Bonded Nd–Fe–B magnets are manufactured from the rapidly solidified magnetic powder (Lee 1985, Lee et al. 1985, Croat 1998). This is done in many ways. The melt-spun ribbon or flake is typically ground down into a finer powder before being processed into bonded magnets. At present nearly 90% of the bonded neodymium magnets is produced using a compaction molding process. The magnetic powder is blended

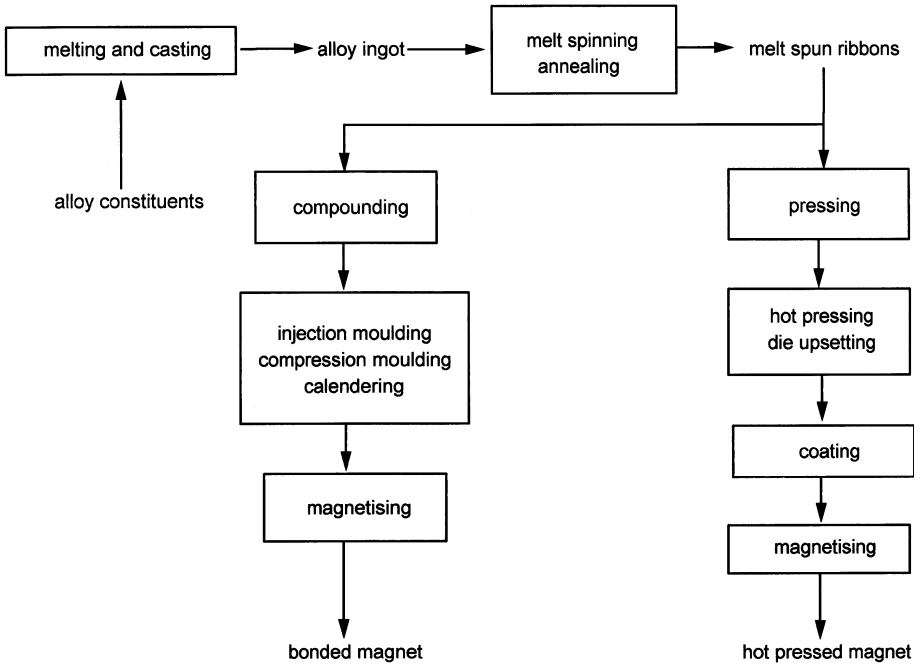

Figure 6.23 Processes for magnets from melt-spun ribbons (Tourre 1998).

with an epoxy dissolved in a suitable organic solvent. While blending of the mixture is continuing, the solvent is drawn off resulting in a coating or encapsulation of the magnetic powder particles. The encapsulated powder is dried and then fed into a conventional powder metal press and compacted into the required shape. After compaction, the parts are heated in an oven to cure the epoxy. The energy products obtained in magnets made by compaction molding are usually in the range of 80 to 88 kJ/m^3.

Bonded neodymium magnets are also produced from melt-spun powders by injection molding. This is the second most common method. The powder is first mixed or "compounded" with a thermoplastic material such as nylon. It is then fed to a conventional injection molding machine. The energy products of injection molded magnets are lower, in the range of 40 to 48 kJ/m^3, because these magnets have a higher percentage of resin.

The bonded neodymium magnets are given a coating before final assembly. The coating prevents surface oxidation and also loss of magnetic particles. Melt-spun ribbons are very desirable for bonded magnet production. Due to the extremely fine particle size, no degradation of the properties accompanies pulverization. The flat geometry of the ribbon fragments (~0.5 mm×0.5 mm×40 μm) facilitates efficient packing so that densities of approximately 85% with respect to $Nd_2Fe_{14}B$ can be obtained even with modest pressures of 600–700 MPa. The bonded magnet, like its constituent ribbons, is magnetically isotropic.

Hot pressed magnets The procedure based on hot pressing affords complete densification of melt-spun ribbons. The temperatures and pressures needed for hot pressing depend on the starting alloy composition. For composition near $Nd_{0.135}Fe_{0.817}B_{0.048}$, full density was achieved using $p \sim 100$ MPa and $T \sim 700$°C. Most desirable grain size was developed by hot pressing "overquenched" ribbons. Energy products of the hot pressed

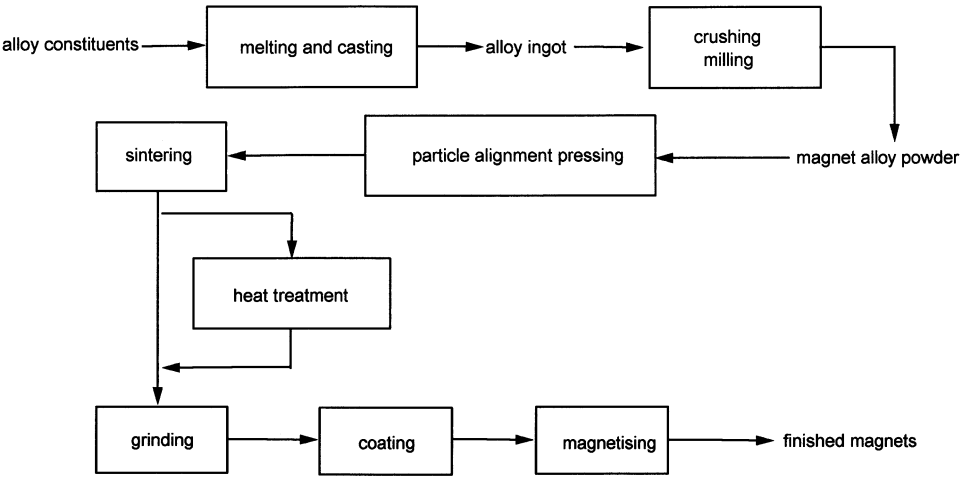

Figure 6.24 Process steps for the production of sintered rare earth permanent magnets.

magnets were in the range of 80 to 160 kJ/m^3. Only a slight (~10%) crystallographic alignment of the easy C axis parallel to the press direction was introduced by the uniaxial hot pressing.

Another variant of the hot pressing method, called die upsetting, results in a greater (~75%) crystallographic alignment of the easy C axis and consequently much larger energy products. In this method an initial hot press is followed by another in a die cavity of larger diameter. The second hot press in the larger die, called die upsetting, causes bulk lateral plastic flow and an accompanying reduction in ribbon thickness. It has been found (Nozawa et al. 1988, Tokunaga et al. 1989) that the greatest magnetic alignment was achieved only if the original sample height was reduced by at least a factor of four during die upsetting. Like their hot pressed precursors, the die upset magnets are fully dense and possess energy products as high as 360 kJ/m^3.

Compositional modifications in magnet materials offer opportunities for altering the intrinsic properties of the major component and/or the nature of secondary phases and their influence on coercivity. The Curie temperature increases monotonically with x in the stoichiometric $RE_2Fe_{14-x}Co_xB$ compounds, and melt spun Nd–(Fe,Co)–B materials containing $Nd_2Fe_{14-x}Co_xB$ as the principal constituent have been prepared (Wecker and Schultz 1990). In $Nd_2Fe_{14-x}Co_xB$, the Curie temperature increases from 312°C for $x = 0$, through 427°C for $x = 2$, to 727°C, which is the T_c of $SmCo_5$, when $x = 14$, i.e., for $Nd_2Co_{14}B$. For $x \geq 9$ in the $Nd_2Fe_{14-x}Co_xB$ system; however, Br, H_{ci} and $(BH)_{max}$ all vanish as T approaches a temperature T_s (which is less than T_c), and this intrinsic behavior limits the practical magnets (Herbst and Croat 1991).

The coercivity of melt spun Nd–Fe–B materials is significantly increased by doping (at concentrations <5 at %) with other elements (Herbst and Croat 1991). Niobium and zirconium are known to improve H_{ci} of melt-spun ribbons (Kohmoto et al. 1987, Wecker and Schultz 1990). Enhancement of H_{ci} by 10–90% has been found (Fuerst and Brewer 1990, 1991) in hot pressed and die upset magnets containing Ag, Au, Cd, Cu, Ir, Mg, Ni, Pd, Pt, Ru, or Zn.

Sintered Magnets Of the two major types of Nd–Fe–B magnets, namely bonded magnets and the sintered magnets, the second is produced and consumed in quantities that

are approximately four times that of the first. For example, in 1997 in Japan, the world's largest producer of Nd–Fe–B, 3300 tons of sintered magnets were produced compared to only 830 tons of bonded magnets (Yan and Xiong 1998).

The magnets prepared through the sequence of orient, press, sinter operations on finely divided alloy powders are designated as "sintered." Sagawa et al. (1984) were the first to apply this method to Nd–Fe–B. Their procedure was as follows. Neodymium–iron–boron alloy having the composition $Nd_{0.15}Fe_{0.77}B_{0.08}$ was prepared by induction melting. It may be noted that this composition was substantially enriched in Nd and B relative to both stoichiometric $Nd_2Fe_{14}B$ (corresponding to $\approx Nd_{0.12}Fe_{0.82}B_{0.06}$) as well as the optimum melt spinning composition of $\approx Nd_{0.13}Fe_{0.82}B_{0.05}$. The ingot was crushed, milled, and pulverized to powder with a particle size of ~3 μm. The powder was aligned in a magnetic field (800 kA/m) and pressed ($P \sim 200$ MPa) perpendicular to the alignment direction. The compact obtained was sintered in argon gas at ~1100°C for 1 h and cooled quickly. It was then subjected to a post-sinter anneal at ~625°C under argon to improve the coercivity to its maximum value. By the sintering route, which is quite similar to the process for preparing $SmCo_5$ magnets, Nd–Fe–B magnets with energy products up to 360 kJ/m^3 have been prepared (Kirchmayr 1985).

In general, the steps for the production of sintered rare earth permanent magnets are as given in Figure 6.24. The Nd–Fe–B alloy, after vacuum melting and casting, is in the form of chill cast lumps. These are crushed, under a nitrogen atmosphere, in a high energy hammer mill to <500 micron particles. The premilled (crushed) magnet alloy is milled to produce a narrow size distribution of single crystal particles. Milling is carried out, for example, by vibration ball milling in an organic liquid under an inert atmosphere. In the next step, the powder particles are magnetically aligned and pressed such that the easy axes of magnetization of the particles are parallel. The compaction is done by die pressing or isostatic pressing. The applied field is either DC or some combination of DC and pulsed. The compaction pressure is kept sufficient to give the powder compact enough mechanical strength for handling but not high enough to cause particle misorientation. The compacted magnets are sintered in the region of 1100°C in inert gas atmospheres or under vacuum to over 95% of theoretical density. The optimum sintering temperature range for Nd–Fe–B magnets (Sagawa et al. 1984) is much wider (approximately 120°C) than that for $SmCo_5$ magnets. In the as-sintered form itself, the properties obtained with a Nd–Fe–B magnet are such that the material forms a useful permanent magnet.

A post-sintering heat treatment, usually an isothermal heat treatment in the region of 630°C for 1 h, was reported by Sagawa et al. (1984) to increase the coercivity of the Nd–Fe–B magnets. However, heat treatment does not appear as a necessary procedure in the overall process scheme for making the sintered Nd–Fe–B magnets.

Generally the rare earth magnets, particularly the SmCo magnets, are hard and brittle. The Nd–Fe–B magnets, however, are tougher and less prone to breakage and chipping. After sintering and heat treatment, the magnets are ground, and, in the case of large blocks, they are divided into even, very small magnets by cutting and slicing. The sintered pieces are ground on conventional grinding machines fitted with silicon carbide or diamond grinding wheels. The Nd–Fe–B magnets combine relative recoil permeability close to unity and high coercivity and may be magnetized prior to assembly without flux loss. Because of the difficulty in handling magnetized and brittle material, it is usual that magnetization is carried out during system assembly.

RE magnets are, in general, prone to corrosion. They get exposed to aggressive media such as acids, alkalis, salts, lubricants, and also gases. They need to be protected. High

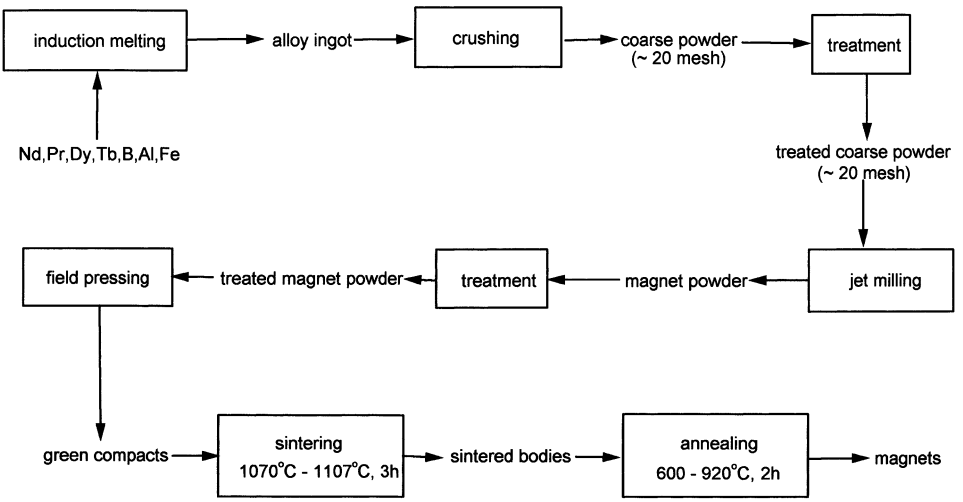

Figure 6.25 Process steps for sintered Nd–Fe–B magnets with additives (Liang et al. 1998).

humidity or dew formation is sufficient to cause corrosion in the case of Nd–Fe–B. The magnets are protected from corrosion by coating them. Metallic coatings, for example, of nickel or tin, are applied by galvanic processes. Coating also ensures that the magnets can be cleaned thoroughly free of all magnet dust.

After the magnet is put into its final shape, it is magnetized to saturation. This is done using very high magnetic fields, using capacitor discharge magnetizers. Magnetization is done only parallel to the magnetic orientation set during particle alignment pressing.

The powder metallurgical fabrication of Nd–Fe–B magnets is facilitated not only by the superior intrinsic properties of $Nd_2Fe_{14}B$ but also by the fact that $Nd_2Fe_{14}B$, Nd, and the tetragonal compound $Nd_{1+\epsilon}Fe_4B_4$ form a ternary eutectic which makes possible liquid phase sintering resulting in high densification without significant grain growth (Sagawa et al. 1987). The highest energy product $(BH)_{max}$ ~405 kJ/m^3 for a sintered Nd–Fe–B magnet was reported by Sagawa et al. (1987). The composition was $Nd_{0.15}Fe_{0.82}Be_{.05}$. Ge et al. (1998) have noted that an improved method for casting molten Nd–Fe–B alloy can help in making better magnets. One of the key factors is to bring down the Nd content in the alloy to as close to 27% (stoichiometric composition of $Nd_2Fe_{14}B$: 26.69% Nd, 72.31% Fe, 1.00% B) without at the same time precipitating the α-Fe phase.

Sintered RE–Fe–B magnets with $(BH)_{max}$ ~320 kJ/m^3 have been obtained (Kirchmayr 1985) by using 5Ce–didymium (Nd–15% Pr–5% Ce). Many investigations (Herbst and Croat 1991) have been directed at finding substitutions in and additions to sintered Nd–Fe–B magnets essentially to extend their useful operating temperature range. This is achievable via enhancement of T_c and H_{ci}, decrease of the temperature coefficients of Br and H_{ci}, and diminution of the irreversible flux losses accompanying high temperature exposure. Sagawa et al. (1984a) demonstrated that cobalt substitution increases T_c and decreases the temperature coefficient of Br, however, cobalt substitution is accompanied by a loss of coercivity. Partial replacement of Nd by Dy substantially enhances H_{ci} and the reduces temperature coefficient of H_{ci}, although it lowers Br somewhat. The largest room temperature coercivity ever observed in a neodymium based sintered magnet was achieved

in $(Nd_{0.53}Dy_{0.47})_{0.15}Fe_{0.77}B_{0.08}$ by Sagawa et al. (1987a). The $(BH)_{max}$ was 160 kJ/m^3 and H_{ci} = 3980 kA/m. Combined Dy and Co substitution has been found to be effective in raising T_c and H_{ci} and in decreasing the temperature coefficient of Br and the irreversible flux losses. Other elements that have been found to have beneficial effects on coercivity and thermal stability are Al, Ga, and Nb. By a process described by Liang et al. (1998), Nd–Fe–B magnets with $(BH)_{max}$ = 334–358 kJ/m^3, $H_{cj} \geq$ 1114 kA/m, Br = 1.33–1.37 T were produced starting from a magnet alloy of composition $Nd_{9.5}Pr_{3.4}Dy_{0.4}Tb_{0.4}B_{6.1}Al_{0.7}Fe_{79.5}$. The process outline as given by them is shown in Figure 6.25. The authors, however, did not present details of the "treatments" given to the magnet powder before pressing.

Nd–Fe–B magnets are exemplary as regards the swift progress from the laboratory discovery to commercialization. The largest energy products realized so far, ~400 kJ/m^3, are substantially short of $(BH)_{max}$ ~512 kJ/m^3. Alloy modification and alternate preparation methods are being explored to bridge this gap. New preparation methods include mechanical alloying (Schultz et al. 1989), hot deformation of ingots (Shimoda et al. 1988), and the hydrogenation, disproportionation, desorption process (McGuiness et al. 1990).

Super High Energy Magnets The theoretical maximum energy product $(BH)_{max}$ for Nd–Fe–B magnets is calculated to be 512 kJ/m^3 on the basis of saturation magnetization of $Nd_2Fe_{14}B$ single crystal (Sagawa et al. 1985). Many groups have attempted to achieve this value. In 1987 Sagawa et al. (1987) obtained, as mentioned above, 405 kJ/m^3 for $Nd_{128}Fe_{80.7}B_{6.5}$ [in wt %, 27.4 Nd–70.17 Fe–1.08 B] by controlling the oxygen content to less than 1000 ppm. In 1990, Otsuki et al. (1990) achieved a higher value of 416 kJ/m^3 by a special procedure in which they added neodymium rich alloy powder prepared by the rapid solidification technique to the alloy powder having a stoichiometric composition ($Nd_2Fe_{14}B$) and then sintered the powders. In 1994, Kaneko and Ishigaki (1994) succeeded in developing Nd–Fe–B sintered magnets, having the highest magnetic properties of Br = 1.495 T, $(BH)_{max}$ = 431 kJ/m^3, and H_{ci} = 845 kA/m. The procedure adopted by them aimed at densification of magnets up to theoretical value, increasing the volume fraction of the $Nd_2Fe_{14}B$ (T_1) phase and achieving a high degree of alignment of the T_1 grains. It was carried out as follows. The alloy corresponding to the overall composition 29.2% Nd –69.80% Fe –1.00% B ($Nd_{13.1}Fe_{80.9}B_{6.0}$) was made by induction melting of 99.5% pure rare earth metal, 99.9% pure electrolytic iron, and ferroboron. As-cast alloys were homogenized by heating in vacuum at 1000°C for 5 h; the cast alloys were crushed using a jaw crusher and a disc mill to coarse powder (< 200 μm). Fine powders of about 3 μm mean particle size were then obtained by pulverizing the coarse powder in a jet mill. The particle size distribution of the resulting powder was more uniform than those found in currently mass produced magnets. A new compacting method for fine powder was used to improve the degree of alignment of the T_1 grains up to 95% or more. The isostatic press was carried out with three steps: (1) filling powders into a cylindrical mold in which the packing density was 2000 kg/m^3, (2) aligning with the pulse magnetic filed of 6400 kA/m, and finally (3) compacting by isostatic pressing at a pressure of 200 MPa. The compacts thus obtained were sintered at about 1060 ~ 1080°C for 3 h in an argon atmosphere and were subsequently annealed at about 500–600°C for 1 h, also in argon.

The mean particle size measured by a Fisher subsieve sizer is the same, i.e., 3 μm for the alloy powders obtained by Kaneko and Ishigashi (1994) and for the commercially used alloy powders. Particle size distribution of the former, however, is more uniform, and, as a result, the microstructure of the sintered magnet obtained under the improved pulverizing conditions became finer and the grain size became smaller, than under conventional

conditions. This finer microstructure results in an increase of H_{ci}. The degree of alignment of T_1 grains improves with the strength of the pulse magnetic field and exceeds 95% for a magnetic field of 6400 kA/m. The improvement of Br and $(BH)_{max}$ in the new magnets is due to the high degree of orientation of T_1 crystals.

Kaneko and Ishigaki (1994) state that the making of a super high energy product magnet is dependent upon controlling the chemical composition, increasing the volume fraction of the $Nd_2Fe_{14}B$ matrix phase, improving particle size distribution, and adopting the isostatic pressing method to get better alignment of fine particles.

The highest grade sintered Nd magnets in large-scale production have an energy product of 320 kJ/m^3 and the coercivity is also insufficient. To be able to obtain a higher residual magnetization (Br), iron rich composition close to a 2–14–1 compound is necessary. There are, however, difficulties in achieving this composition at production level. The problems are powder oxidation and a decrease in Br. The Nd–Fe–B alloys in the form of fine powders with diameters of 3 to 4 μm easily oxidize in air to form Nd_2O_3. The oxygen content in sintered Nd magnets ranges from 0.5 to 0.7%. Oxidation consumes neodymium and the nonmagnetic Nd_2O_3 lowers the magnetic property of the material. In sintered Nd–Fe–B magnets, additions used to increase coercivity decrease residual magnetization. To obtain a high performance Nd magnet, a balance between oxidation protection and decreased use of additives is necessary. The poor corrosion resistance of sintered Nd magnets necessitates the use of coating for actual use. Honshima and Ohashi (1994) have developed a two alloy method for producing sintered neodymium iron boron magnets. Their method addresses the twin problems of oxidation resistance and minimum use of additives.

Two alloy process The process flowsheet of the two-alloy method of Honshima and Ohashi (1994) is shown in Figure 6.26. This is a powder metallurgy procedure that used two alloys as starting material. One alloy, the main alloy, had a composition closely approximating the 2–14–1 compound, and the other alloy, called the suballoy, had a composition rich in rare earth elements and cobalt. The main alloy was responsible for the intrinsic magnetic properties. The suballoy was a sintering aid and was responsible for the densification of the sintered body and the cleaning of sintered particle grain boundaries during the sintering process. The two alloys were melted and cast individually and crushed to 200 μm size. After the coarse pulverization, they were mixed and processed further. In the present process, the pressing of fine powder in a homogeneous magnetic field was accomplished in air.

The main alloy composition was $Nd_{12.3}Fe_{81.8}B_{5.9}$. In the as-cast alloy, a large amount of primary iron exists and a solid solution heat treatment was necessary to obtain the single 2–14–1 phase. The suballoy was rich in cobalt and this improved the corrosion resistance of the fine powder and the sintered body. Dysprosium, praseodymium, and gallium added via the suballoy enhanced coercivity. The main and suballoys mixing ratio was approximately 90:10, and after sintering the final composition of the magnet was $Nd_{11.3}Pr_{1.6}Dy_{0.8}Fe_{76.9}Co_{3.1}B_{5.9}Ga_{0.3}$.

The magnet produced by the two alloy method was superior to that produced by the conventional (one alloy) method. Using the two alloy method, sintered Nd magnets with energy products of 360 kJ/m^3 and moderate coercivity were mass produced. The oxidation stability of fine powder of two alloy magnets was excellent. For example, after exposure of the powder to air at 24°C and 40% relative humidity for 3 days, the coercive force of the sintered magnet produced by the two alloy method remained almost constant. In contrast, even after one day of exposure, the coercive force of the sintered magnet produced

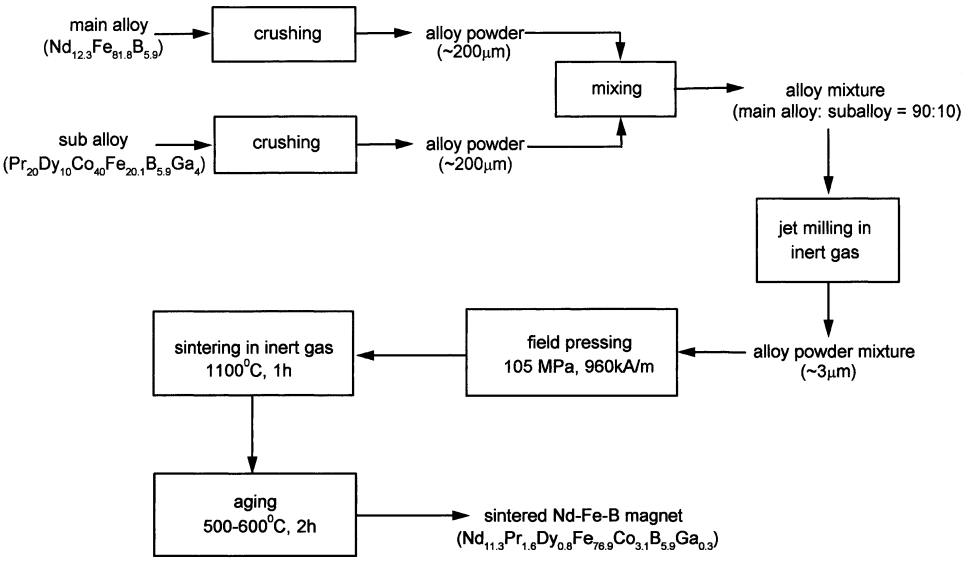

Figure 6.26 Flowsheet of the two alloy method for making Nd–Fe–B magnets (Honshimo and Ohashi 1994).

conventionally decreased considerably (to less than half of the original value). The low oxidation level of the fine powder is attributed to cobalt base compounds. The two alloy method thus allows the fine powder to be handled in air during the pressing process, obviating the need for special processing under vacuum or inert gas. The method is therefore attractive for use in mass production. The two alloy method also resulted in less oxygen in the sintered body and improved its corrosion resistance. The cobalt addition to the 2–14–1 alloy suppressed oxidation further.

Improved magnetic properties of the two alloy product were attributed primarily to the dysprosium distribution and partially to praseodymium distribution. Even though dysprosium increased coercivity, it decreased saturation magnetization. In the processing method described, however, dysprosium was distributed mainly near the grain boundaries of the sintered 2–14–1 particles. Its presence near grain boundaries increased coercivity and its absence in the center region reduced the decrease in saturation magnetization, thus yielding a high performance Nd magnet.

Even though fine powder oxidation and corrosion resistance of the sintered magnet body were improved by the two alloy process, the improvement in corrosion resistance was not sufficient. Thus, like in the case of conventional sintered Nd magnets, a coating was necessary for corrosion protection (Minowa et al. 1989). An electroless copper layer, which has good contact with the Nd magnet was first provided, and over this copper underlayer an electroless nickel upper layer was provided. The total thickness was about 10 μm. While coating adhesion was ensured by the copper underlayer, the electroless plating method ensured that film thickness was uniform throughout, including the magnet edges (Honshima and Ohashi 1994).

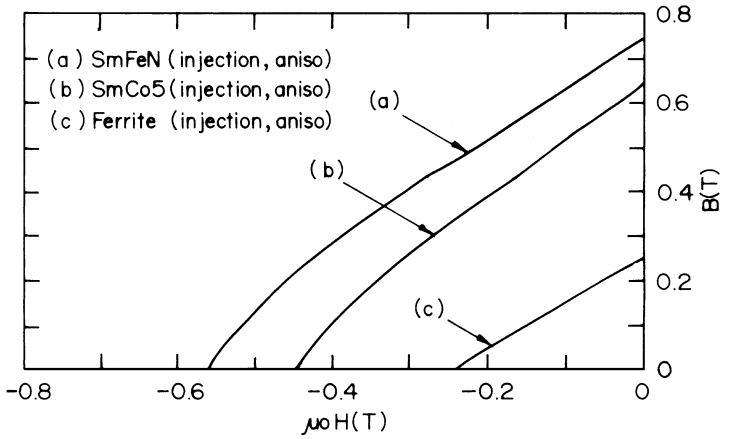

Figure 6.27 Comparison between injection molded Sm–Fe–N and other bonded magnets (Ohmori 1998).

6.10 Sm–Fe–N MAGNETS

In addition to the well-known Sm–Co and Nd–Fe–B series of magnets, several other RE–TM magnets have been evaluated for their attractive magnetic properties. These include Tb–Fe–Co and Sm–Fe–N magnets. The properties of bonded Sm–Fe–N (Ohmori 1998) are shown in Figure 6.27. The Sm–Fe alloy has been prepared by reduction diffusion and the bonded magnet has been made by injection molding. The production process followed at Sumitomo is shown in Figure 6.28.

6.11 NANOCOMPOSITE PERMANENT MAGNET MATERIALS

A new type of magnet material described as nanocomposite permanent magnetic materials consisting of exchange coupled hard and soft magnetic phases (exchange spring magnets) has been attracting attention, particularly because of their low temperature coefficients of Br and H_{cj} (Coehoorn et al. 1989, Chang and Hsing 1996). Nanocomposite magnets have been synthesized by melt spinning, mechanical alloying, and milling (Guo et al. 1998).

6.12 TERFENOL-D

Investigations carried out in the mid-1960s on the magnetic properties of pure rare earth metals revealed that some of them exhibited large magnetostriction at low temperatures (Clark 1979). When a magnetic field is applied to a magnetostrictive material, it will expand or contract. Similarly, when stress is applied to the material, a magnetic pulse is generated. In 1971 Clark and Belson (1972) from the Naval Ordnance Laboratory

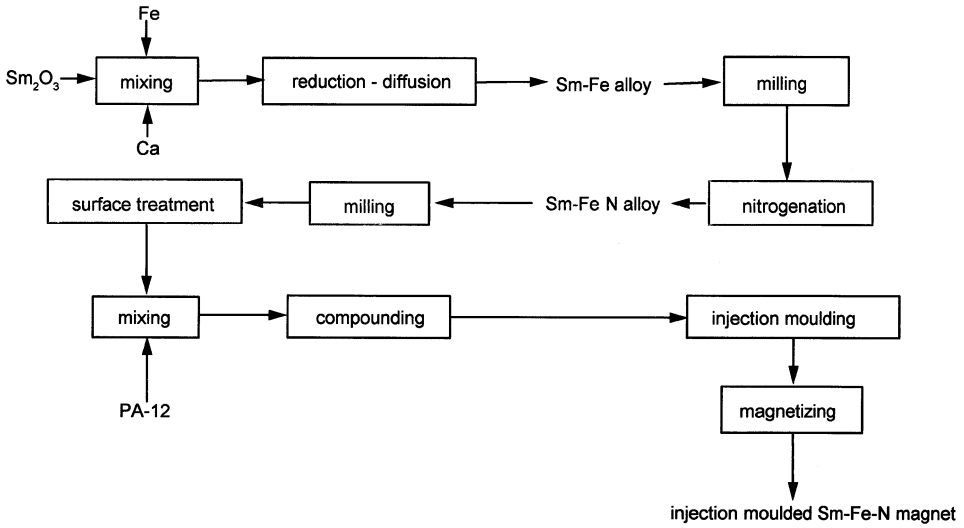

Figure 6.28 Production process for injection molded Sm–Fe–N magnet (Ohmori 1998).

announced that $TbFe_2$ exhibited magnetically induced strains at room temperature that were larger, by a factor of ten, than that of any other magnetostrictive materials like Ni, ferrites, known until then. This was almost simultaneously confirmed by Koon et al. (1971). Much of the work on developing the optimum properties of the $TbFe_2$ materials was carried out by Clark and coworkers at the Naval Ordnance Laboratory and the materials were named "terfenol" after terbium–iron (Fe) and the initials of the Naval Ordnance Laboratory. It was subsequently found that dysprosium added to the $TbFe_2$ compound allowed the use of lower magnetic fields to produce the strain, but this led to some degradation in the total strain. The optimum composition arrived at was $Tb_{0.3}Dy_{0.7}Fe_{1.9}$, and this is now known as "terfenol-D." Terfenol-D exhibits giant magnetostriction in an applied field, ~100 times larger than in nickel.

Schmidt et al. (1986) prepared terfenol-D by a thermit reduction process. Appropriate amounts of TbF_3, DyF_3, and FeF_3 plus 10% excess calcium were mixed together and loaded into a heavy walled iron crucible lined with CaF_2. The crucible was closed and the reaction was triggered electrically using a hot iron filament. The exothermic reaction proceeded quickly, and with the alloy and slag forming immiscible liquids they settled giving terfenol-D, which was well separated from the CaF_2 slag on cooling. The yield of terfenol-D was 94%. This method is a less expensive alternative to the conventional method of preparation of the material by arc melting.

In arc melting, the high purity metals, Fe–99.98%, Dy–99.97%, and Tb–99.97% were alloyed together. Initial alloying by arc melting in a water-cooled copper hearth is followed by several meltings to prepare homogeneous alloy (Verhoeven 1987).

Experiments on the growing terfenol-D crystals and directionally solidified polycrystalline materials were carried out at the Ames Laboratory by McMasters et al. (1986). To achieve the optimum magnetostrictive characteristics, attempts were directed to obtain (1) single crystals oriented with ⟨111⟩ along the crystal axis, (2) a minimum amount of defect structure and impurity content, and (3) a constant stoichiometry along the crystal axis.

Terfenol-D has many applications in sensor and control devices in industry.

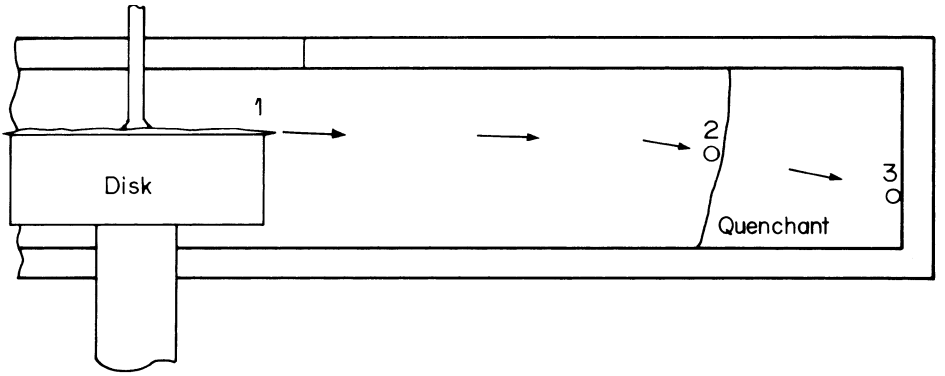

Figure 6.29 Schematic diagram of the rotating disc atomizer. Cross section of the quench bath. Position 1 indicates the atomization skull, 2 a particle before contacting the quenchant, and 3 a particle before contacting the container (Osborne et al. 1993).

6.13 MAGNETIC REFRIGERANTS

Initially GdPd and later the intermetallics $(Dy_{0.5}Er_{0.5})Al_2$ and $TbNi_2$ have been found useful as magnetic refrigeration materials used for cooling gases or systems to temperatures as low as 4 K. Magnetic refrigerators have been considered more efficient than most cryogenic cooling systems particularly below liquid nitrogen temperature (Anonymous 1989).

The magnetic refrigerant rotates through a magnetic field, and while doing so warms or cools itself. As the refrigerant enters the magnetic field, it warms up and when it leaves the magnetic field it cools down. This behavior permits heat exchange and cooling of a gas or a system. The gadolinium refrigerant, for example, is rotated at ~5 rpm.

The refrigerator using the magnetic refrigerant is called the active magnetic regenerative (AMR) magnetic refrigerator (MR) (Gschneidner et al. 1994a). A current design of the AMR–MR refrigerator for the liquefaction of hydrogen gas is based on a modified Joule–Brayton cycle and uses GdPd as the active component for the low temperature range. The problems associated with GdPd are the cost of Pd and the ductility of the compound, which makes crushing the intermetallic to a fine powder difficult. The refrigerant in the form of a fine powder is necessary for efficient heat transfer during various heating and cooling cycles.

The intermetallic $(Dy_{0.5}Er_{0.5})Al_2$ is not only cheaper and more brittle than GdPd but also has a much larger (30% more than GdPd) magnetocaloric effect. It is an excellent replacement for GdPd (Gschneidner et al. 1994a). The magnetocaloric effect of $TbNi_2$ is also 15% larger than GdPd (Gschneidner et al. 1994).

For attaining extremely low temperatures, the intermetallic compound $PrNi_5$ has been used as the key material in an adiabatic demagnetization refrigerator, in conjunction with the nuclear magnetic cooling of copper (Gschneidner et al. 1995). In the two-stage adiabatic demagnetization unit, $PrNi_5$ was used as the first stage and copper as the second stage. In the presence of two magnetic fields, one around the $PrNi_5$ stage and the second around the copper, the entire unit was cooled down by a dilution refrigerator to ~25 mK. Then as the ~6 T field was slowly removed from the $PrNi_5$ stage, the entire unit cooled down to ~5 mK.

A temperature of ~30 μK could then be reached when the field around copper in the second stage was reduced.

The preparation of magnetic refrigeration materials is usually accomplished by arc melting 99.8 at % pure rare earth metals and >99.99% pure nickel or aluminum in correct proportions on a water-cooled copper hearth (Gschneidner et al. 1994). When more than one rare earth metal was in the alloy, the rare earths were melted first, and then in the second step the non-rare earth metal component was melted in. The methods described earlier for rare earth intermetallics and metals or the atomization technique described below for making cryogenic cooler materials could be used for powder preparation.

Cryogenic coolers used for applications in present and emerging technologies such as magnetic resonance imaging, Josephson circuitry, and magnetic levitation utilize packed bed heat exchangers for transferring heat from a load to a sink. The packed beds are composed of rare earth–metal compounds (RE_xM_y) such as Er_3Ni, DyCo, and $(Er_{0.9}Yb_{0.1})Ni$ or pure rare earth metals such as Nd. The diameter of the particles used in the packed beds is ~200 μm. Osborne et al. (1993) have used centrifugal atomization with a rotating disk to produce high quality spherical particles of RE_xM_y compounds and pure metals.

In the process used by Osborne et al. (1993) for the preparation of Er_3Ni powder, the starting Er_3Ni compound was first prepared. Stoichiometric amounts of Er and Ni were alloyed by arc melting in a water cooled copper hearth. The Er_3Ni intermetallic thus obtained contained 89.5% Er, 10.5% Ni, 45 ppm O, 4 ppm N, and 18 ppm C.

Alumina crucibles were used to contain molten Er_3Ni prior to atomizing. The alumina crucible had a 3.2 mm hole drilled in it for bottom pouring. The charge (Er_3Ni) was melted under UHP (ultra high pure) Ar atmosphere, heated to 50–100°C above the melting point, held for 5 min for complete homogenization and then poured onto a rotating 50 mm diameter atomization disk made of low density alumina with an erosion resistant coating. A schematic of the system is shown in Figure 6.29. The atomized particles were quenched in a 2 liter volume of a low viscosity (100 centistokes) silicone oil. The oil was held in a container and the container was also rotating concentrically at a lower rpm, in the same direction as the atomization disk. The oil was preheated to 170°C in air to improve dehydration of the quenchant.

The particles were collected from the quenchant by filtration. They were cleaned with heptane and methyl alcohol. Even though the purity of the powder obtained was high and its shape was spherical, Osborne et al. (1993) did not consider the particle shape optimal. In the ideal case, the superheat must be so high that the particles have time to respherodize in the quenchant, yet low enough that complete solidification occurs before contacting the container wall.

Particles of Nd metal were also prepared by a similar technique. The important difference was that in place of alumina as container, tantalum was used and prior to use it was baked at 1300°C for 8 h under 10^{-4} Pa.

Prior to the development of the centrifugal atomization technique for making $ErNi_5$ powder, the Ames group (Anderson et al. 1993) had investigated a high pressure gas atomization approach (HPGA) to produce uniform spherical powders of high purity $ErNi_3$. The system used is shown in Figure 6.30.

The starting $ErNi_3$ alloy was prepared by arc melting weighed amount of Er and Ni in a water cooled copper hearth. The major impurities in Er (at ppm) were H 828, C 97, N 60, O 546, F 246, Cl 14, and Fe 19 (all the remaining impurities <10 at. ppm and most <1 at. ppm), and the major impurities in Ni in ppm atomic were H-330, C-580, O-107, Cl-1, and Mn-2 (all the remaining impurities were <1 at. ppm).

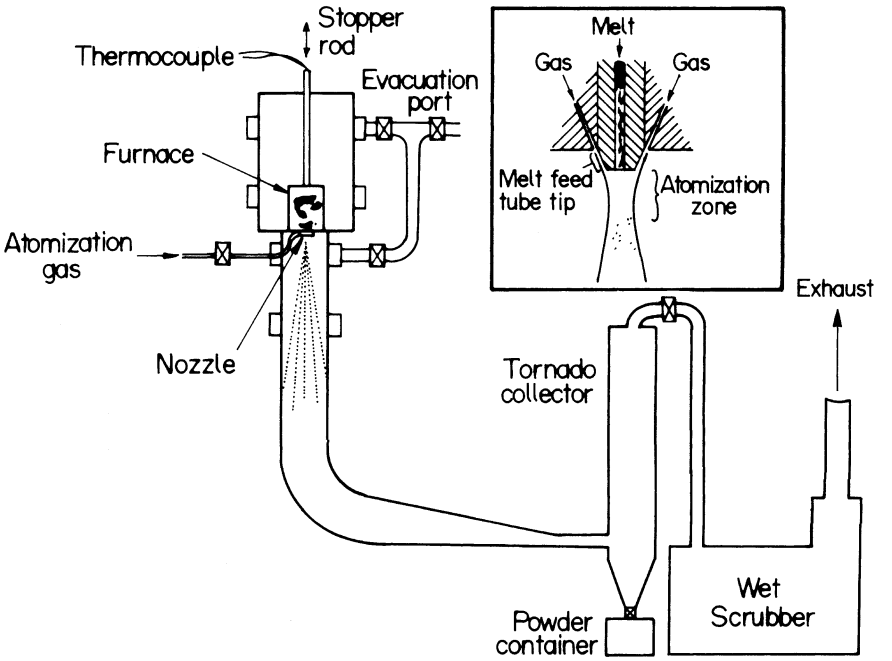

Figure 6.30 Schematic diagram of the high pressure gas atomization (HPGA) apparatus at Ames. Inset sketches the nozzle/pour tube configuration (Anderson et al. 1993).

The HPGA system consisted of a melting system with a high purity (99.55%) controlled porosity (21.0% porosity) alumina crucible, a high purity (99.8%) hard fired alumina stopper rod, and a boron nitride (93% BN) pour tube. The Er_3Ni alloy was heated to 1100°C (about 200°C above the estimated liquidus temperature of Er_3Ni) to promote effective alloy homogenization and atomization. The melting and atomization chamber, shown in Figure 6.30, had been evacuated to 6 Pa and backfilled with UHP (99.998%) argon to a positive pressure of 110 kPa prior to melting and atomization operations. A gas pressure of 3 MPa with UHP Ar was used to operate the atomization nozzle. The melt tip configuration used promoted production of large (0.15 to 0.35 mm) powder particles. Besides, an *in situ* passivation process was used during the atomization of the powder to condition it against atmospheric degradation.

The atomizer yielded both spherical powders and flattened splat flakes, and they were separated using a fluidized bed sorter. Uniform spherical powders of Er_3Ni, between 0.15 and 0.35 mm in diameter, were obtained, after sorting. The nominal alloy composition of the Er_3Ni charge remained unchanged in the resulting powder. In the as-atomized (unsorted) powder the contents of gaseous impurities were 63 ppm H, 67 ppm N, and 2600 ppm O. Anderson et al. (1993) attributed the high oxygen content to the formation of splat flakes, which have a large surface to volume ratio. A fairly large fraction of as-atomized powder yield (~10 to 20%) consisted of splat flakes. The average yield of high quality spherical powders was only about 16% of the initial atomizer charge weight.

Other techniques for obtaining rare earth metals and intermetallic compounds in powder form are (1) mechanical grinding of cast ingots into powder, (2) spark erosion and (3) rotating electrode pressing. These techniques have one or more limitations relating to

powder shape, purity and composition. Among all the techniques, centrifugal and high pressure gas atomization procedures appear better.

6.14 THIN FILM DEPOSITION PROCESSES

For many applications rare earth-bearing materials are required in the form of a thin film deposited on a suitable substrate. The techniques used for the preparation of bubble domain memory materials and magnetooptic storage media illustrate the techniques used.

6.14.1 Bubble Domain Memory Materials

In 1970, Bobeck et al. (1970) discovered that many rare earth garnet crystals grown from fluxes possess sufficient unaxial anisotropy to maintain bubble domain stability. Subsequently it was shown that films of magnetic garnets could be readily deposited by liquid phase epitaxy from molten $PbO–B_2O_3$ solutions on to gadolinium gallium garnet, $Gd_3Ga_5O_{12}$, (GGG) substrates. A large number of substrates, 30 at a time, can be simultaneously dipped into the melt under near isothermal conditions at temperatures ranging from 750°C to 1100°C, and melt compositions can be adjusted to yield garnet films of required specifications. The substrate GGG is prepared as follows.

The GGG melts congruently at 1740°C and is grown by the well-known Czochralski or pulling technique. Crystals are grown from melts contained in indium crucibles in an atmosphere of nitrogen containing 2% O_2 (Brandle and Valentino 1972, Brandle et al. 1972). Large crystals of GGG, 75 mm diameter and weighing up to 75 g, are grown routinely (Nielsen 1981). The crystals are sewed, lapped, and polished to prepare substrates onto which the magnetic garnet films are deposited.

6.14.2 Magnetooptic Storage Media

Magnetooptic storage media (Buschow 1988, Kryder 1993) consist of a thin film of magnetic material deposited on a transparent substrate, usually glass or plastic. The thin film is made in such a way that it is energetically most favorable for the magnetization to lie perpendicular to the plane. The most common magnetooptic storage media consist of amorphous alloys of the rare earth elements gadolinium and terbium and the transition metal elements iron and cobalt. The amorphous alloys, e.g., $Tb_{25}(Fe_{0.9}Co_{0.1})_{75}$, are deposited onto substrates by some form of sputtering process (to a thickness of 500 μ).

A sputtering system typically consists of a vacuum chamber in which a target and the substrates to be coated are located. The target consists of the magnetic material to be deposited onto the substrates. The target is biased with a strong negative voltage (about 1000 V) relative to the ground potential of the vacuum chamber itself. When an inert gas, such as argon, is leaked into the chamber at a low pressure, the large voltage potential in the system causes the electrons to be stripped from the argon atoms and a plasma is formed. Then the positive argon ions are accelerated toward the negatively biased target and strike it with high energy. The ensuing transfer of momentum from the argon ions causes atoms or clusters of atoms of the target material to be sputtered away from the target. These sputtered atoms diffuse away from the target. If a substrate is in close proximity to the target, it gets coated with a thin film of the target material.

The rare earth transition metal thin films deposited by such a sputtering method are typically amorphous. This fact has proved to be important to their performance as low noise recording media. In spite of their amorphous structure, the rare earths transition metal thin films exhibit anisotropic properties such that the lowest energy orientation for magnetization is perpendicular to the film plane. This is necessary for a good magnetooptic storage medium.

Rare earth transition metal alloys are prone to corrosion and must be protected from the environment. This is done in magnetooptic media by using a thin dielectric that is impervious to both water vapor and oxygen, between the substrate and magnetic film. Suitable materials are Si_3N_4 or AlN. The top surface of the film is protected by a similar dielectric and a reflective metal overcoat, such as aluminum. The rare earth transition metal media manufactured this way have design lifetimes of over 10 years.

The rare earth transition metal thin films used as storage medium in modern magnetooptic disks include GdTbFe and TbFeCo with the total rare earth content of about 20%.

6.15 $LaNi_5$

The hydrogen absorption characteristics of $LaNi_5$ type compounds were first revealed by Zijlstra and Westerdorp (1969) and elaborated further by Van Vucht et al. (1970) at the Philips Research Laboratories in Eindhoven, The Netherlands. $LaNi_5$ behaves like a hydrogen sponge. When hydrogen is introduced into a finely divided alloy of $LaNi_5$, it will be absorbed resulting in the formation of lanthanum nickel hydride

$$LaNi_5 + 3H_2 = LaNi_5H_6$$

The absorption reaction is exothermic, and this will limit the reaction rate at a fixed H_2 pressure if heat is not removed. When heat is removed the hydrogen adsorption rate remains high, and the quantity that could be absorbed is remarkable. Because the hydrogen is actually chemically bound within the hydride crystal lattice, when fully loaded, $LaNi_5H_6$ has a volumetric density of hydrogen that is significantly greater than even liquid hydrogen. $LaNi_5$ hydride is more attractive as a hydrogen storage system than many alternatives because (1) it operates at ambient temperature, (2) it stores H_2 at low pressure, comparable to liquid, (3) it is comparable in weight efficiency to compressed gas, and (iv) it is comparable in volumetric efficiency to cryogenic liquid. The only disadvantage of $LaNi_5$ is the high cost, compared to, for example, FeTi.

In the $LaNi_5$–H system, the hysteresis of the adsorption–desorption cycle is small. Like adsorption, the desorption kinetics is also fast. There is a 25% increase in volume in LaNi5 on full hydrogen loading. Desorption at a comfortable rate can be accomplished at temperatures around 150°C.

For an actual application the $LaNi_5$ alloy was prepared by arc melting to the proper stoichiometry from lanthanum and nickel charge metals of at least 99.5% purity (Lundin 1973). The arc-melted alloy ingot was broken to granule size in a hardened steel mortar and pestle. The grinding operation could be conducted in air. The size of the granules was approximately 0.75 to 3 mm.

As regards hydrogen adsorption–desorption, the behavior of (La, Ce) Ni_5 and $MMNi_5$ alloys is basically similar to that of $LaNi_5$.

Genshi et al. (1985) prepared $MMNi_5$ compound by chemical synthesis. The chlorides of $Ni(NiCl_2)$ and $MM(MMCl_3)$ were dissolved in water and then precipitated as $MM_2(CO_3)_2 \cdot 5Ni_2(OH)_2 \cdot CO_3 \cdot xH_2O$. The precipitate was dried and heated under H_2 at about 750°C to reduce Ni^{2+} to Ni and obtain misch metal carbonate–nickel mixture. This powder was reduced with Ca at 1000°C to yield misch metal nickel intermetallic compounds.

One of the problems with the use of rare earth–nickel hydride forming materials is pulverization of alloys into a very fine powder upon repetitive hydriding–dehydriding cycles and very poor thermal conductivity of the powdered alloys. To prevent such disintegration and also improve thermal conductivity, Ishikawa et al. (1985) proposed a microcapsulation method. In this method, fine particles of hydride forming alloys such as $LaNi_5$ and $MMNi_{4.5}Mn_{0.5}$ were coated with a thin layer of metallic copper by a chemical plating method. Hydrogen storage capacities of alloys were not appreciably affected due to the plating. The encapsulated alloy powders was easily pressed into pellets. The pellets had high thermal conductivity and sufficient porosity to permeate hydrogen leading to fast reaction kinetics. The encapsulation is done as follows.

As-cast $LaNi_5$ and $MMNi_{4.5}Mn_{0.5}$ were crushed and then pulverized by repeating the hydrogen adsorption–desorption cycle up to 10 times. After the final dehydrogenation, the powders were ground and screened to 20 μm average particle size, in air. The surfaces of alloy particles were activated by treating with the aqueous $SnCl_2$ and HCl solution and then with $PdCl_2$ + HCl aqueous solution. The powders were then immersed in the Cu^{2+}–tartaric acid complex + CH_2O + NaOH aqueous solution to form a metallic copper layer of ~ 1 μm thick. The coated alloy powders were pressed into pellets at 100 MPa at room temperature. The encapsulated alloy powder in the pellets was easily reactivated by evacuating and then heating at ~100°C under 10 atm hydrogen pressure. The encapsulated particles were able to withstand more than 5000 repeated hydriding–dehydriding cycles without disintegrating.

6.16 SUPERCONDUCTORS

Superconductivity was discovered in 1911 by Kammerlingh Onnes who showed that mercury loses all of its electrical resistance (becomes superconducting) when cooled to liquid helium temperature (4 K). Between that time and 1986 a variety of materials were found to be superconducting, but the highest known critical temperature, T_c, was 23.3 K for Nb_3Ge. The critical temperature is the upper limit of the temperature range in which the material is still superconducting. The critical current and critical magnetic field are similarly defined because superconductivity is destroyed by too much current and too great a field, and these three critical variables characterize the superconductor. It is technologically and commercially advantageous to have materials that have high critical values.

In 1986 a new group of materials known as high temperature superconductors was discovered by Bednorz and Mueller. They (Bednorz and Mueller 1986) originally reported work on a multiphase Ba–La–Cu–O compound with a T_c below 30 K. As work continued in several groups, it was revealed that the superconducting phase had a perovskite-like structure and that the T_c could be pushed up to 40 K by replacing barium ions in the compound with strontium. The widely accepted BCS (Bardeen, Cooper and Schrieffer) theory of superconductivity had predicted a maximum possible T_c of about 40 K. As shown in Figure 6.31 this limit as well as the liquid nitrogen temperature of 77 K was quickly

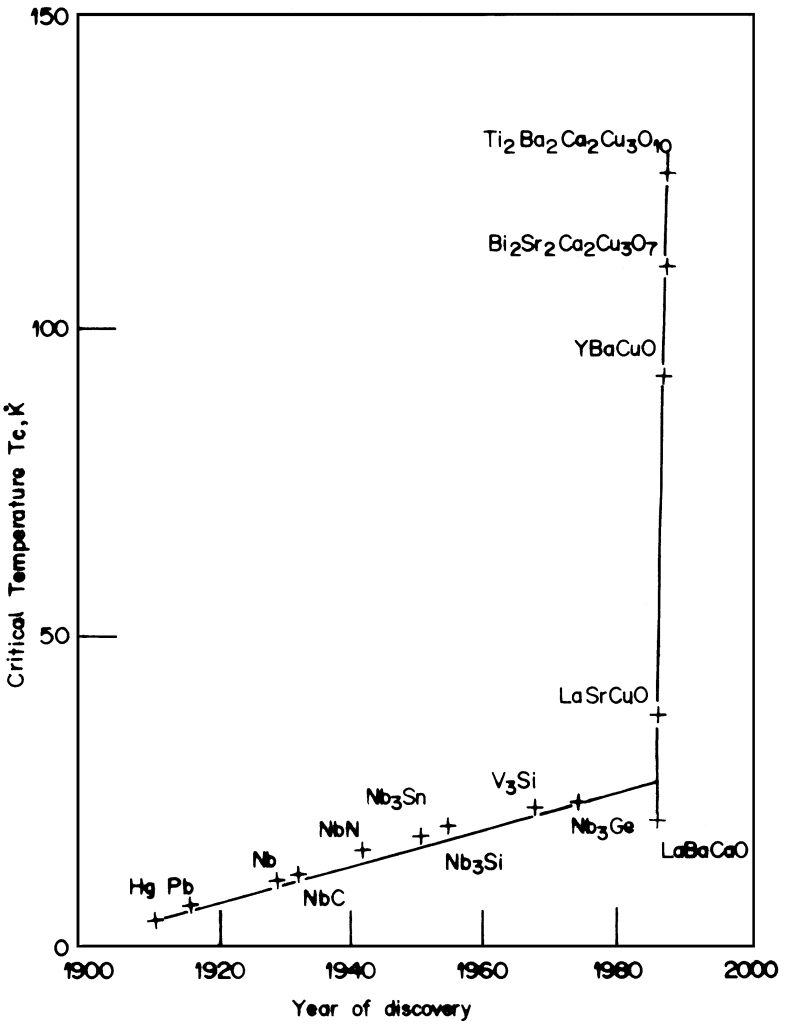

Figure 6.31 Development of high temperature superconducting alloys.

crossed with the discovery of newer ceramic superconducting compounds (Fox 1996, Fisher 1988, Alford 1992). Most significant of these was the discovery in February 1987 by Chu's group at Houston that a multiphase Y–Ba–Cu–O compound (YBCO) had a T_c of 92 K. It was subsequently shown that the YBCO phase responsible for superconductivity was perovskite-like with a composition of $Y_1Ba_2Cu_3O_{7-x}$ (commonly referred to as the 1–2–3 phase).

The Ginzburg and Landau (known as GL) theory explains many features of high temperature superconductivity. One conclusion from the GL theory, particularly relevant to the processing of superconductors, is that all high T_c superconductors, already discovered and yet to be discovered, should have very short coherence lengths of typically atomic scale dimensions. Coherence length is the distance over which paired electrons (carrying supercurrent) interact. In high temperature superconductors, the coherence length is about 1–3 nm, which is less than that for a conventional superconductor.

The very short coherence length of the electron pair in all high–T_c superconductors implies that, in polycrystalline material, grain boundaries must be sharp and contain no amorphous phases. If the grain boundary width exceeds coherence length the electron pairs will be strongly scattered. Generally, the crystalline defects, other than those that pin fluxoids without scattering electron pairs, must be minimized. The coherence length is comparable with the spacings of the copper–oxygen layers in YBCO. Thus the critical current in a direction perpendicular to these layers will be low. This is confirmed in that high J_c is obtained in directions parallel to a–b planes but not parallel to the c-axis. Texturing, therefore, becomes essential to obtain high critical current densities in polycrystalline materials. Besides, to obtain ceramic superconductors with sufficient strength for winding, for example, into coils and to withstand the Lorentz force originating from a high current in a high magnetic field, the size of pores and cracks must be minimized.

In $YBa_2Cu_3O_{7-x}$, the highest critical density is achieved when $x = 0$, but the material remains superconducting down to $YBa_2Ca_3O_{6.5}$. In the production of bulk $YBa_2Cu_3O_7$, the tetragonal phase $YBa_2Cu_3O_6$ is formed first and then annealed in oxygen to produce the tetragonal to orthorhombic phase transformation to $YBa_2Cu_3O_7$.

These are three main techniques for making high-T_c superconductors. In the first, the materials can be deposited onto a single crystal structure by methods such as evaporation, laser ablation, or sputtering so that epitaxial growth occurs. In the second, thick films can be made by mixing the powder with various polymers and solvents and applying it to a suitable polycrystalline ceramic or metallic substrate. In the third method, bulk materials can be made by sintering a powder of right stoichiometry, for example, Y_2O_3, $BaCO_3$, and CuO mixed in the molar proportions 1:2:3. The fracture toughness of superconducting ceramics is so low that making bulk ceramics in complex shapes requires rather sophisticated processing techniques.

Thin films of high-T_c superconductors are produced because they have major potential application in electronic devices, and for basic scientific measurements single crystal thin films are relatively easy to grow. The best superconducting thin films have been obtained by growing them epitaxially on substrates closely lattice matched to the superconductor. As regards methods for producing the thin films, if $Y_1Ba_2Cu_3O_7$ is used as a target, it can be sputter deposited onto a substrate held at about 400°C. The YBCO layer will be oxygen deficient and in amorphous or polycrystalline form. Subsequent annealing in oxygen results in epitaxial growth that nucleates at the substrate–film interface. Alternatively, the materials can be directly sputtered onto a single crystal substrate held at 650°C. A tetragonal epitaxial film of approximate composition $YBa_2Cu_3O_6$ is formed and oxygen annealing leads to orthorhombic superconducting $YBa_2Cu_3O_{7-x}$. Thin film deposition can also be done by laser ablation, molecular beam epitaxy (MBE), metal organic chemical vapor deposition (MOCVD), and metallorganic molecular beam epitaxy (MOMBE). Thin film (0.5 μm) superconductors are capable of carrying large amounts of current (10 million amps per cm^2), but they are not suitable for many practical applications because of their fragility. Bending of the thin film material can damage the YBCO grain structure and misalignment in the grain structure, hampers the flow of current.

Thick film tapes (1–2 μm thickness) conduct one million amps per cm^2 and can retain half of their current carrying ability in magnetic fields as high as nine tesla. In a process developed in 1995 at the Superconductivity Technology Center of the Los Alamos National Laboratory, a three-layer tape made of YBCO compound and zirconium oxide placed in a pliable nickel alloy tape was made. The zirconium oxide layer prevents interaction between the YBCO compound and nickel and also forces the YBCO into a regular crystalline order

that promotes superconductivity. Ion beam deposition is used to apply the zirconium dioxide layer. One beam of ions lays down a few hundred thousandths of an inch of zirconium oxide, while the second beam orients the crystals as they form on nickel. This results in an orderly symmetrical surface on which the YBCO layer can be affixed.

By pulsed layer deposition of thick films (6–10 μm) of Y-123, researchers at Los Alamos National Laboratory have reported J_c values greater than 1 MA/cm^2 at 77 K (Foltyn et al. 1993). This potentially scaleable technique may be used to prepare superconductor coated continuously on long lengths of metal or ceramic substrates with suitable buffer layers.

Bulk superconducting YBaCuO can be made by sintering Y_2O_3, CuO, and BaO and annealing in oxygen. However, careful control is needed in the annealing temperature and cooling rate, in reducing the particle size, and in eliminating impurities. It is then possible to produce a material that is 99% pure superconducting $Y_1Ba_2Cu_3O_{7-x}$, having 99% of grain boundaries atomically sharp with no traces of impurities. Critical current values in the pure polycrystalline materials typically exceed 10^7 Am^{-2}.

To obtain $YBa_2Cu_3O_{7-x}$ that has sufficient strength to be fabricated into wires and coils, the density must be above 85% and the larger the better, and crack size should be less than 10 μm. The critical current density increases with an increase in the density of the material. In addition to good mechanical properties, high density materials also have longer life and do not degrade.

Typically, the density of a sintered body can be increased by raising the sintering temperature. In the Y-123 system, if special precautions such as vacuum calcination are not taken during powder preparation, often a low melting (~900°C) Ba–Cu–O liquid forms. While sintering above this temperature leads to more rapid liquid phase sintering resulting in improved density and increased grain size, it also results in an insulating phase along the grain boundaries thereby decreasing the critical current density (McGinn 1994).

To obtain bulk superconductor with good mechanical properties, high purity starting material in the form of submicrometer powder is essential (Masur et al. 1994). Using viscous processing routes, coils and shapes can then be fabricated.

To achieve high current densities in polycrystalline wires and thick films of ceramic superconductors, texturing is essential. Texturing or texture processing leads to improved J_c in polycrystalline Y-123 by avoiding or minimizing many of the weak link limitations to J_c. Some of the primary causes of weak link behavior can be minimized by having a microstructure where the current flow is directed primarily in the basal plane and by minimizing the occurrence of high angle grain boundaries. In bulk Y-123, formation of texture has been achieved by a number of different techniques, including compaction processes, magnetic alignment of particles, and directional solidification of particles. Transport J_c values exceeding 10 kA/cm^2 in applied fields of several tesla have been achieved by solidification routes described by the term "melt texturing" (Jin et al. 1988, 1989). In the case of Y-123, melt texturing describes directional solidification from the melt or partially melted state. Texturing is achieved in various ways such as melt texturing, rolling, and solidification in high magnetic fields.

A process known as the metallic precursor (MP) approach has been used to prepare long lengths of high T_c ceramic superconducting wires (Sandhage et al. 1990). The MP approach is particularly attractive for fabrication of high filament count, fine filamentary composite conductors because most of the wire-forming process is performed while the material is in its metallic state. In the process described by Masur et al. (1994) of the American Superconductor Corporation, high filament count silver-sheathed composite

wires of $YBa_2Cu_4O_8$ were prepared. The process starts with the preparation of homogeneous alloy powder by mechanical alloying of the metallic elements. The alloy powder is packed into a silver can that is sealed and extruded into a hexagonal rod. Cut pieces of the rod are stacked into a multirod bundle that is again packed into a can and extruded into a hexagonal rod. This process is repeated many times. In the final step, the can is extruded with a reduction ratio of up to 300:1 into a rectangular tape or round wire. The extruded metal tapes were internally oxidized to form silver–suboxide composites. The suboxides consisted of Y_2O_3, BaO, CuO and $Ba_2Cu_3O_x$. They were then reacted to form the Y-124 phase. The finely divided suboxides that form from the oxidation process react quickly to form Y-124 even at ambient oxygen pressure. Following oxidation, the tapes were subjected to thermomechanical treatments (TMT) to convert the suboxides into textured polycrystalline Y-124 grains. The TMT involved multiple iterations of heat treatment in the range of 600–825°C followed by uniaxial pressings of up to 2 GPa and a final heat treatment at 750°C for 100 h in 1 atm of oxygen. Tapes containing up to 962,407 filaments with filament dimensions as fine as 0.25 μm thick and 1 μm wide with significant biaxial crystallographic texture were thus made. These wires exhibited transport current densities in the oxide filament of 69,500 A/cm^2 at 4.2 K in self-field with decreased weak link behavior in applied field, better critical current retention during binding, and in general some of the best properties for a polycrystalline, sintered wire of YBCO in an applied magnetic field.

6.17 SUMMARY

There are numerous rare earth-containing end-product materials suitable for commercial applications or research uses. Many of these are compounds, alloys, and metals that are produced either as end products of ore processing or as interprocess intermediates in the preparation of rare earth metals. Many rare earth materials, however, have to be produced specifically starting from interprocess intermediates or metals. These processes have been covered in this chapter.

The first commercial rare earth material was the gas mantle produced by Carl Auer von Welsbach. The production method was mentioned in Chapter 1. To light the gas mantles, a lighter flint based on misch metal was also invented by Welsbach. As early as 1908, he used fused salt electrolysis of mixed rare earth chloride as the method to obtain misch metal. This method to date remains the most important process for misch metal production. In the U.S. and Japan, the USBM process of oxide–fluoride electrolysis has also been adopted for commercial production of misch metal. Thermal reduction processes based on calcium reduction of mixed rare earth fluoride have been investigated in Brussels and at Ames.

The addition of rare earths to steel results in several advantages. Rare earths are added in the form of misch metal or as rare earth–iron–silicon–iron alloys. The rare earth–iron–silicon alloys are commercially prepared by a carbothermic reduction of a mixture of rare earth compounds or ore concentrate, iron or iron ore, and silica in a submerged electric arc furnace. Many other processes that result in higher rare earth loading in the alloy and better rare earth recovery have also been developed. These include the USBM process in which a mixed rare earth oxide of bastnasite origin was reduced by calcium silicide, ferrosilicon, silicon, and aluminum, and the BARC process in which a mixed rare earth oxide of monazite origin was reduced with ferrosilicon and aluminum scrap. In the Chinese practice,

rare earth-containing blast furnace slag from Baotou was reduced with ferrosilicon using lime as flux in an arc furnace. Electric arc furnace reductions have also been used to produce rare-earth–magnesium–silicon alloy starting from rare earth containing blast furnace slag, calcined dolomite–ferrosilicon, calcium, and silicon. Electrolytic processes have been used to prepare rare earth–aluminum–zinc and yttrium–aluminum alloys.

Rare earth transition metal-based magnets are a family of commercial products of considerable variety and constantly growing major technical importance. The first group of rare earth magnets developed in the 1960s and 1970s were based on the intermetallic compounds $RECo_5$ and RE_2Co_{17}. These compounds possess an ideal combination of magnetic and structural properties for high performance magnet applications. They were prepared by the simple technique of direct melting of alloy components or by using more sophisticated methods such as co-reduction or reduction diffusion using metal oxides as start materials. The technique of direct production of alloy by fused salt electrolysis using cobalt as consumable anode was also used. The alloys were ground to a powder, mixed with a chemical binder, and pressed under a magnetizing field to produce the plastic-bonded magnets. The adoption of inexpensive molding methods such as extrusion and injection molding in an orienting field facilitated large-scale production and industrial application of the bonded rare earth permanent magnets. Instead of plastic, a soft metal matrix has also been used as the binder and metal matrix bonded magnets have better elevated temperature stability. Sintered magnets were prepared by following the sequence of blending, milling, aligning and pressing, sintering, and finally a post-sintering heat treatment. As regards the magnetic properties the sintered magnets are superior, but bonded magnets also have numerous practical advantages.

Cost and supply problems of samarium and cobalt were serious disadvantages of the samarium–cobalt magnets, and the search for suitable alternatives culminated in the development of neodymium–iron–boron magnets in the 1980s. Like in the case of the samarium cobalt, the overall process for the production of Nd–Fe–B magnets comprises two major stages. One is the production of magnetic alloy, and the other is the processing of the Nd–Fe–B type alloys into permanent magnets.

Many methods have been developed for the production of Nd–Fe–B alloys. They include direct melting, co-reduction, and certain special techniques that make use of reduction extraction or thermit type processes for directly making the Nd–Fe or Nd–Fe–B alloys. The alloys are converted to magnets by two basically distinct routes. One route involves the rapid solidification technique of melt spinning and the other follows the traditional pressing and sintering route. The melt spinning procedure involves ejection of molten Nd–Fe–B alloy through a crucible orifice onto the surface of a spinning substrate disc. The product so obtained is in the form of ribbons typically 30–50 μm thick, 1–3 mm wide. The melt-spun ribbons are consolidated into a dense form to produce either a bonded magnet or a hot pressed magnet. Fine tuning of magnetic properties to desired values is also achieved by doping the magnet alloy with elements such as niobium, zirconium, and many others.

The "sintered Nd–Fe–B magnets" are prepared starting from finely divided alloy powders obtained from pulverizing of cast ingots or directly reduced powders, and following the sequence of orient, press, sinter operations. In spite of the numerous cost and magnetic property advantages of the Nd–Fe–B magnets over the rare earths–cobalt magnets, the Nd–Fe–B magnets have one major limitation. Their Curie temperature is low. Attempts have been made to overcome this problem through partial replacement of neodymium by cobalt and/or dysprosium. Other beneficial elemental additives are aluminum and gallium.

Attempts to realize in practical magnets the theoretical maximum energy product for Nd–Fe–B magnets, namely, 512 kJ/m^3, led to the development of what are known as the super high energy magnets. The making of such magnets was found to be dependent upon controlling the chemical composition, increasing the volume fraction of the $Nd_2Fe_{14}B$ phase, improving particle size distribution, and adopting the isostatic pressing method to get better alignment of fine particles.

Another limitation of neodymium iron boron magnets is the susceptibility of the fine powder magnet alloy to oxidation. Oxidation lowers the magnetic property Br. Certain additives for increasing coercivity also decrease Br. The twin problems of oxidation resistance and decreased use of additives were addressed in the process known as the "two alloy method" for the manufacture of the magnet. A main alloy with the composition $Nd_{12.3}Fe_{81.8}B_{5.9}$ was mixed with a suballoy rich in cobalt and also having dysprosium, praseodymium and gallium in the ratio 90:10, and after sintering the final composition of the magnet was $Nd_{11.3}Pr_{1.6}Dy_{0.8}Fe_{76.9}Co_{3.1}B_{5.9}Ga_{0.3}$. This magnet was superior to that produced by the conventional (one alloy) method, in terms of energy product, coercivity, and also oxidation resistance. The corrosion resistance of the magnet was still not sufficient for final service conditions, and multilayer coating was needed for corrosion protection of the magnet.

Rare earths are not only important materials for permanent magnets, but also versatile magnetic materials. The alloy $Tb_{0.3}Dy_{0.7}Fe_{1.9}$, called "terfenol-D," is a remarkable magnetostrictive material. Terfenol-D has been produced either by the conventional method of direct melting of the constituents in an arc furnace or by a thermit type reduction of appropriate amounts of TbF_3, DyF_3 and FeF_3 with calcium, in a crucible lined with CaF_2. Initially GdPd, and later the intermetallics $(Dy_{0.5}Er_{0/5})Al_2$ and $TbNi_2$, were identified as magnetic refrigeration materials for cooling gases and systems to as low as 4 K. These materials have been usually prepared by arc melting of 99.8 at % pure rare earth metals and >99.99% pure nickel or aluminum in correct proportion. A process known as centrifugal atomization has been used to produce ~200 μm size fine particles of cryocooler materials such as Er_3Ni, DyCo, and $(Er_{0.9}Yb_{0.1})Ni$. High pressure gas atomization has also been used to produce uniform spherical powders of high purity Er_3Ni. Both these techniques are superior in powder shape, purity, and composition, to methods such as mechanical grinding of cast ingots into powder, spark erosion, and rotating electrode pressing. Another special application of rare earth as magnetic materials is in magnetooptic storage media. Here thin films (500 μ thick) of amorphous alloy such as $Tb_{25}(Fe_{0.9}Co_{0.1})_{75}$ is deposited onto a transparent plastic substrate by some form of sputtering process. Storage medium in modern magnetooptic discs can also be the amorphous alloy GdTbFe.

The intermetallic $LaNi_5$ behaves like a hydrogen sponge. When hydrogen is introduced into a finely divided alloy of $LaNi_5$, it will be absorbed at room temperature and bound in the lanthanum nickel hydride $LaNi_5H_6$ that is formed. At a higher temperature, e.g., 150°C, the hydrogen is desorbed at a comfortable rate. This property of $LaNi_5$ has led to numerous applications. The preparation of $LaNi_5$ is done by arc melting together the pure metals in the proper stoichiometry. The arc melted alloy ingot is broken to granule size in a hardened steel mortar and pestle. The alloy granules are coated with a metallic copper thin layer by a chemical plating method to prevent their crumbling to fine powder due to repeated hydriding–dehydriding. In addition to $LaNi_5$, (La, Ce)Ni_5 and $MMNi_5$ alloys have also been used. All these alloys have also been directly prepared by calcium reduction of coprecipitated $RE_2(CO_3)_2 \cdot 5Ni_2(OH)_2 \cdot CO_3 \cdot 2H_2O$.

One of the most recent and remarkable applications of rare earths is in the new

generation high-T_c superconductors. High T_c was first reported in a multiphase Ba–La–Cu–O compound, and one of the most important compositions that has T_c above liquid nitrogen temperatures is a Y–Ba–Cu–O (YBCO) compound. The YBCO phase responsible for superconductivity is perovskite-like with a composition of $Y_1Ba_2Cu_3O_{7-x}$ (commonly referred to as 1–2–3 phase). There are three main techniques for making high-T_c superconductors. First, the materials can be deposited onto a single crystal structure by methods such as evaporation, laser ablation, or sputtering so that epitaxial growth occurs. Second, thick films can be made by mixing the powder with various polymers and solvents and applying it to a suitable polycrystalline ceramic or metallic substrate. Third, bulk materials can be made by sintering a powder of right stoichiometry.

Thin film (0.5 μm) superconductors are capable of carrying large amounts of current (10 million amps cm^{-2}), but they are not suitable for many applications because of their fragility. Thick film tapes (1–2 μm thick) conduct one million amps cm^{-2} and can retain half of its current-carrying ability in magnetic fields as high as nine tesla. In one process developed at the Los Alamos National Laboratory, a three-layer tape comprising YBCO compound and zirconium oxide placed on a pliable nickel alloy tape was made. By pulsed layer deposition of thick films (6–10 μm) of Y-123, Los Alamos researchers have obtained J_c values greater than 1 MA/cm^2 at 77 K. This potentially scaleable technique may be used to prepare superconductor coated continuously on long lengths of metal or ceramic substrates with suitable buffer layers. Bulk superconducting YBaCuO can be made by sintering Y_2O_3, CuO, and BaO under carefully controlled conditions. To obtain bulk superconductor with good mechanical properties, high purity starting materials in the form of submicrometer size powder is essential. Using various processing routes, coils and shapes can then be fabricated. To achieve high current densities in polycrystalline wires and thick films of ceramic superconductors, texturing is essential. Texturing is achieved in various ways such as melt texturing, rolling, and solidification in high magnetic fields. A process known as the metallic precursor approach has been used to prepare long lengths of high T_c ceramic superconducting wires. The process proceeds through the stages of mechanical alloying of metallic precursor elements, repeated extrusion and compound forming by internal oxidation, and thermomechanical treatments.

A great variety in applications and an equally wide range of methods for processing mark the role of rare earth materials in modern technology. New techniques of materials synthesis such as mechanical alloying, self-propagating high temperature synthesis, various thin and thick film production techniques, and also techniques for production and control of materials structures at the nanometer scale, popularly known as "nano-processing," when applied to the production and processing of rare earth materials will open up more new possibilities of applications as well as newer challenges to rare earth materials processing. These will keep up the new tradition of advanced rare earth materials evolution to fulfill the newer needs of humankind in the new millennium.

CHAPTER 7

A Sojourn in the World of Rare Earths

The authors have, through the preceding chapters, provided a comprehensive account of the rare earths family members in their collective as well as individual forms. This final chapter offers a concise description of the rare earths that will be not only informative, but also enlightening for general readers and those who wish to have a look into the world of the rare earths out of inquisitiveness. The perusal of this chapter, on the whole, will provide the reader with a substantial fund of knowledge.

It will be useful to begin this chapter with a general introduction to the elements, and this is best accomplished by dealing first with the electronic structure of atoms.

The behavior of each of the electrons that surround the nucleus of an atom of an element is described by a wave function that represents a solution to the Schrödinger wave equation. These wave functions define the spatial distribution of electron density about the nucleus, i.e., the probability of locating an electron at a particular point at a particular instant in time. Boundary surfaces enveloping the regions of high electron density are called atomic orbitals. The overall wave function, providing a total description of the state of an electron in an atom of an element, is expressed in terms of quantum numbers. The quantum numbers result from the solution of the Schrödinger equation for the hydrogen atom. Although the results for this atom represent only an approximation for atoms of elements containing more than one electron, the hydrogen atom forms the model for discussing multi-electron atoms of elements. There are four quantum numbers, each of which can assume only certain permitted numerical values: n, the principal quantum number, is a positive integer (1, 2, 3, 4,... but not 0); l, the azimuthal quantum number, can only be a positive integer less than n (0, 1, 2;3,..., $(n-1)$); m, the magnetic quantum number, can possess all integral values from +1 to –1; s, the spin quantum number, can have only the values $+\frac{1}{2}$ or $-\frac{1}{2}$.

As already mentioned, the hydrogen atom orbitals provide the basis for the treatment of multi-electron atoms of elements. Each electron in a multi-electron atom is considered as moving in an atomic orbital that is qualitatively like the hydrogen atom orbitals. Four quantum numbers are required to designate each of the orbitals, as in the hydrogen atom case, and the quantum numbers possess the same physical significance. An additional stipulation is required to comprehend the linkage between the electron structure of atoms

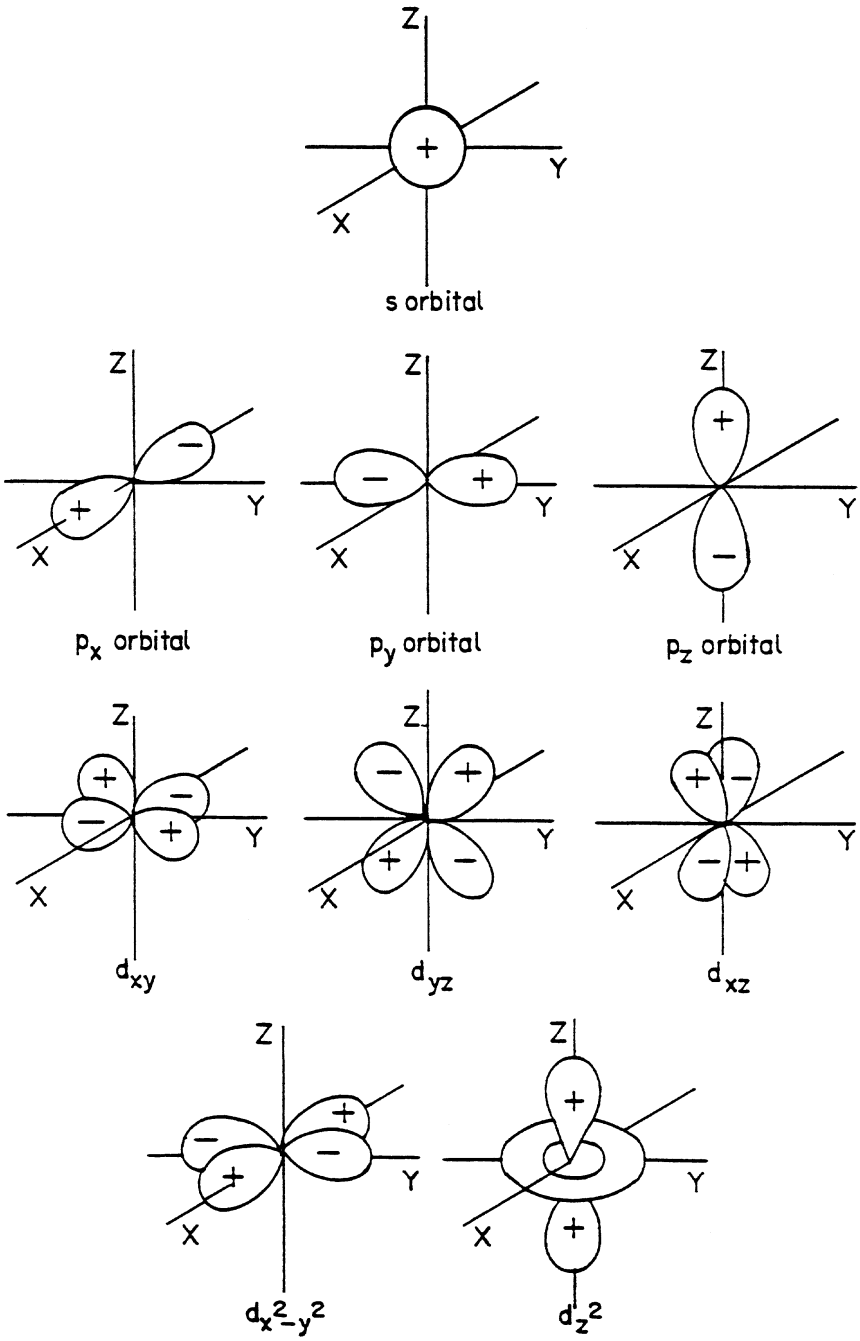

Figure 7.1 The *s*, *p*, and *d* atomic orbitals.

and the physicochemical behavior of elements. This condition, which was proposed by Wolfgang Pauli and has come to be known as Pauli's exclusion principle, has far-reaching consequences in chemistry.

Pauli's exclusion principle stipulates that each electron in an atom of an element is characterized by its own unique set of quantum numbers and that no two electrons belonging to that atom can possess the same set of quantum numbers. The Pauli principle is a fundamental principle. It finetunes the conduct of electrons over and above the Schrödinger equation. The first of the quantum numbers, n, relates to the average distance of the electron from the nucleus (hence the size of the orbital). It is the most important factor deciding the energy of an electron. Electrons with $n = 1, 2, 3, 4,...$ are said to occur in the K, L, M, N,... shells of the atom and are located at progressively increasing distances from the nucleus. The second quantum number, l, can be considered to be a measure of the angular momentum of the electron. It is related to the shape of the orbital. Azimuthal quantum numbers are normally designated s, p, d, f rather than 0, 1, 2, 3 (hence a 3s orbital has $n = 3$, $l = 0$). The third quantum number, m, is also called the orbital quantum number. This is because it indicates the orientation of the orbital in space. For example, in a 2p orbital, $n = 2$, $l = 1$ and m can take the values +1, 0, –1. Hence, there are three kinds of p orbitals, p_x, p_y, and p_z, which differ in their orientations but are equivalent in energy (degenerate). Each orbital may hold only two electrons, one with $s = +\frac{1}{2}$ and the other with $s = -\frac{1}{2}$. The spin quantum number indicates that an electron may be regarded as spinning either clockwise or counterclockwise about an axis and producing a magnetic field that may be in either one of two opposite directions.

The shapes and orientations of the s, p, and d atomic orbitals are shown in Figure 7.1. The s orbitals are spherically symmetrical; the 1s orbital ($n = 1$; $l = 0$; $m = 0$; $s = \pm\frac{1}{2}$) is the lowest-energy atomic orbital and may contain one A electron (as in hydrogen) or two electrons with opposite (paired) spins (as in helium and all heavier elements). The next orbital to be filled is the 2s orbital, which can similarly contain one or two electrons. Following this there are the three 2p orbitals ($n = 2$; $l = 1$; $m = +1, 0, -1$; $s = \pm\frac{1}{2}$), which are dumbbell-shaped orbitals directed along the three Cartesian axes (i.e., along three mutually perpendicular directions). Two lobes of high electron density are separated by a nodal plane of zero density, and the sign of the wave function is positive in one lobe and negative in the other. The 3s and 3p orbitals succeed the 2p orbitals in energy and are in turn followed by the 3d orbitals (also shown in Figure 7.l).

Prior to defining the status of the electron distribution in a multi-electron atom, it is important to gain an understanding of the energy level sequence of the orbitals. The starting reference may be drawn to the hydrogen atom. The energies of the hydrogen atom orbitals depend only on n, and the corresponding energy level sequence is shown in Figure 7.2(a). In atoms of the other elements, the occurrence of more than one electron induces electron repulsion effects, which bring about a modification in this orbital energy pattern. The initial task, therefore, is to ascertain the sequence of the energies of the orbitals in multi-electron atoms. Once the sequence of the energies of the orbitals is established, the electronic structure of the atoms of various elements is delineated simply by placing one electron at a time in the lowest energy orbital available, subject to, of course, compliance with the Pauli principle. The origin of the periodicity in the properties of elements then becomes very obvious. The orbital energy pattern and the Pauli principle are essential for understanding the structure of the periodic table.

In order to comprehend why and how the energy level scheme of the hydrogen atom gets modified, one may consider the ground state distribution of electrons in the atoms of the three elements hydrogen, helium, and lithium, which possess one, two, and three electrons, respectively. In hydrogen, the electron belongs to the lowest energy orbital, 1s; the electron in the orbital is arbitrarily designated by an "up" ($m = +\frac{1}{2}$) spin. This particular

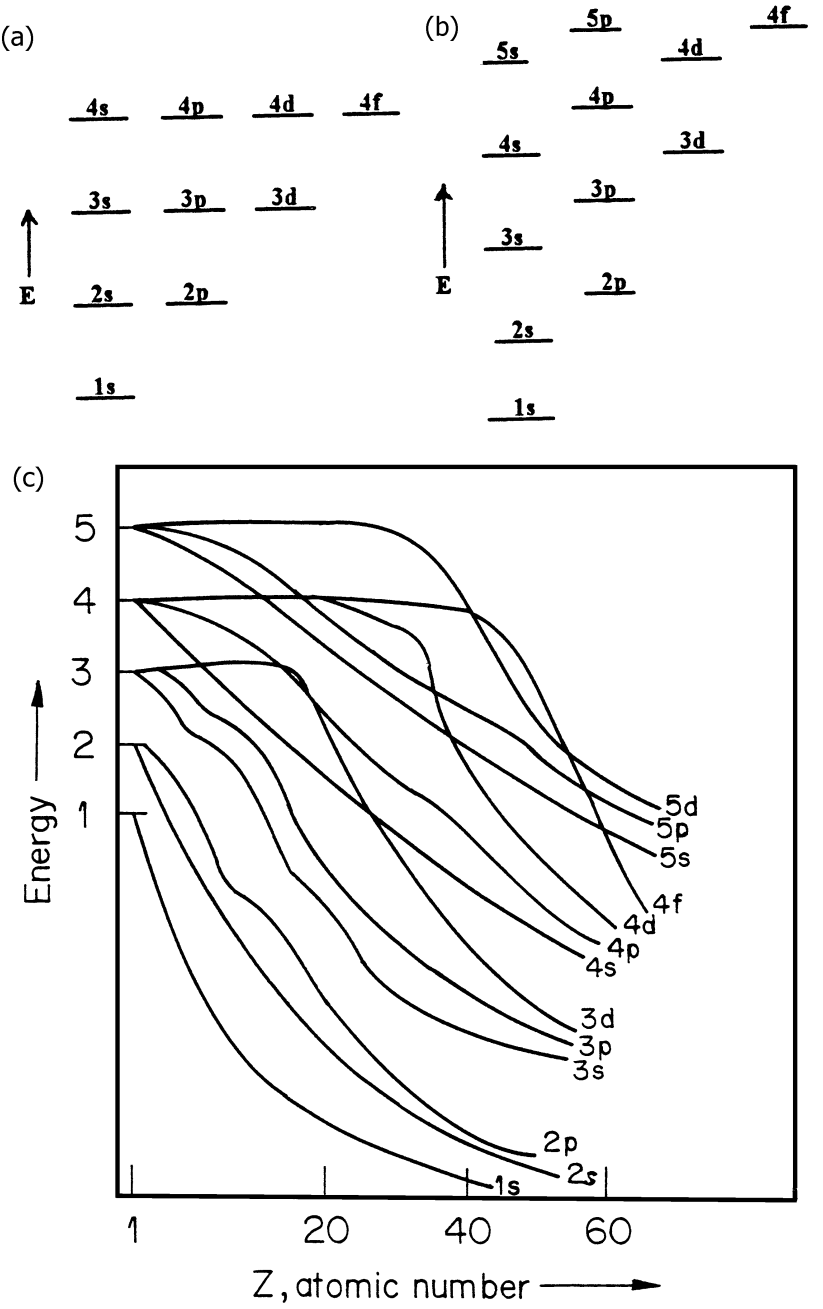

Figure 7.2 The energy level diagram valid for (a) the hydrogen atom and (b) multi-electron atoms; (c) the variation of orbital energies with atomic number (Z).

orbital can host the second electron of helium only if it possesses the opposite spin. If the two electrons were to possess the same spin, the three orbital quantum numbers (n, l, and m) as well as the spin quantum number (s) would be the same. This is not allowed according

to Pauli's principle. Thus, there being no room in the 1*s* orbital for further electrons, the third electron of lithium has to go to the next higher energy orbital. The question now arises as to where the third electron may be placed: in the 2*s* orbital or in the 2*p* orbitals? If the hydrogen atom energy level pattern were to hold good for multi-electron atoms, it would have made no difference since all these orbitals would have the same energy. It, however, so happens that the 2*s* orbital has a lower energy than the *2p* orbitals in lithium. The maxima or peaks of the 2*s* and the 2*p* orbitals have been found to be at distances greater than the 1*s* maximum. Therefore, an electron in the 2*s* or the 2*p* orbitals in lithium will be further outside as compared to the two 1*s* electrons. The third electron will not feel the pull due to the full nuclear charge because the shielding effect of the inner 1*s* electrons. The shielding experienced by a 2*s* electron, however, is less than that experienced by a 2*p* electron, since the 2*s* orbital approaches closer to the nucleus. This implies that a 2*s* electron experiences a greater attraction from the nucleus than a 2*p* electron does. It may, in other words, be said that a 2*s* electron is more tightly held or bound than a 2*p* electron. The 2*p* orbitals, therefore, have more energy than the 2*s* orbital.

In general, orbitals with the same n but different l do not possess the same energy in multi-electron atoms. Within a set of orbitals with a given n, the energy increases as l increases. This is a consequence of the fact that as the value of l increases, the extent of approach of the orbital to the proximity of the nucleus decreases and the shielding due to the inner electrons becomes more dominating. It may, therefore, be said that an electron with a large l experiences less nuclear charge. The energy level pattern, which is qualitatively true for nearly all multi-electron atoms, is provided in Figure 7.2(b). The variation in orbital energy with atomic number is shown in Figure 7.2(c). To sum up, it may be pointed out that (1) the energies of the *np* orbitals are higher than that of the *ns* orbital, but considerably lower than that of the $(n + 1)s$ orbital; (2) the energies of the *nd* orbitals are comparable with the energy of the $(n + 1)s$ orbital, but less than the energies of the $(n+1)p$ orbitals; and (3) the *nf* orbitals are comparable in energy to the $(n + 1)d$ orbitals. Once the energy level sequence is derived, it becomes quite simple to delineate the electron configuration in atoms making use of the Aufbau principle, which simply states that electrons should be placed, one at a time, in the lowest energy orbital available, without violating the Pauli principle. In addition, two rules, known as Hund's rules, are taken into account in arriving at the electronic configurations of multi-electron atoms. These rules are as follows: (1) in filling a group of orbitals of equal energy, it is energetically preferable to assign electrons to empty orbitals rather than placing them in orbitals that are partly occupied; and (2) when two electrons are placed in two different orbitals, the energy is lower if the spins are parallel.

The carbon atom and the boron atom (corresponding to atomic numbers six and five, respectively), will be used here as examples. The electron configuration in the latter atom is $1s^2\ 2s^2\ 2p^1$ and that in the former is $1s^2\ 2s^2\ 2p^2$. It is known that the pair of electrons in the 1*s* orbital must have opposed spins. The same is true of the two electrons in the 2*s* orbital. There are three orbitals in the 2*p* sublevel ($2p_x$, $2p_y$ and $2p_z$). The single 2*p* electron in boron could be placed in any of these orbitals. Its spin could be either "up" ($m = +\frac{1}{2}$) or "down" ($m = -\frac{1}{2}$). The orbital diagram is ordinarily drawn with the first electron in an orbital arbitrarily designated by an "up" arrow, ↑:

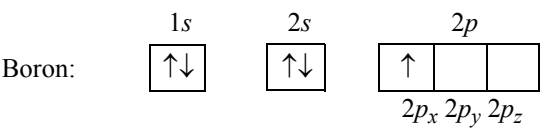

With the next element, carbon, a complication arises. Where should the sixth electron be placed? One could put it in the same orbital as the other 2*p* electron, in which case it would have to have the opposite spin, ↓. It could also be placed in one of the other two orbitals ($2p_y$ or $2p_z$), either with a parallel spin, ↑, or an opposed spin, ↓. Experiments reveal that there is an energy difference between these arrangements. The most stable configuration is the one in which the two electrons are in different orbitals with parallel spins. The orbital diagram of the carbon atom is thus:

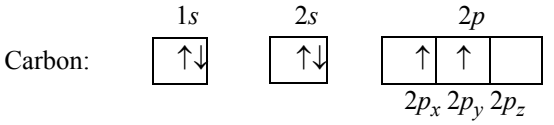

One could see that the above procedure is prescribed by Hund's rules. The examples dealt with representatively provide the general outline of the procedure by which one derives the ground state configuration of atoms.

7.1 THE PERIODIC TABLE OF ELEMENTS

The foregoing descriptive matter regarding the electron distribution in multi-electron atoms points to the origin of periodicity in the properties of elements. The most orderly and well-founded presentation reflecting this periodic feature is the periodic table of elements, which is a classically outstanding chemical portrayal of elements. No parallel or alternative mode of presentation that is as comprehensive has been suggested. The table provides an arrangement of elements in the order of increasing atomic number in horizontal rows of such lengths that elements with similar chemical properties appear in the same vertical column. If one examines the long form of the periodic table in different textbooks, one will notice such vertical columns of elements; each column is referred to as a group and the different groups are numbered or labeled across the top for identification.

From the time of Mendeleev, whose name is synonymous with the periodic table, there has been no general agreement as to the numbering system to be adopted. Most chemists use a system of Roman numerals (I to VIII) and the letters A and B. The International Union of Pure and Applied Chemistry (IUPAC) has recommended that the 18 groups should be numbered consecutively from left to right, 1 to 18. This is also a common numbering system used in some texts. This system refers to the main-group elements (i.e., elements in the two groups at the far left and the six groups at the right) as Groups 1 through 8. The transition elements, to which reference will be made later, in the center of the periodic table, are not assigned group numbers. Of the systems mentioned above, the first labeling scheme will be used here, but the other two notations will be shown in parentheses in the order mentioned. The group on the left side of the table, labeled IA (or 1 or 1) is called the alkali metals group. The elements of the next group, labeled IIA (2 or 2) are the alkaline earth metals. The elements of group VIIIA (18 or 8) are called the noble gases because they are not reactive. To the left of the noble gases are the halogens labeled VIIA (17 or 7). The elements in groups labeled A (1, 2, 13–18 or 1, 2, 3–8) are called the representative or main group elements and those labeled B (3–11 or group numbers not assigned) are called the transition metals. This is the description of the table that one generally comes across.

Having described the group classification, it is only appropriate that reference is drawn

to the significance of the (horizontal) rows. The elements within a row (sometimes called a period) exhibit a gradual variation in behavior, which implies that any particular element shows some similarity with its neighbors, but appreciable dissimilarity with those who are not neighbors. These vertical–horizontal characteristics of the periodic table indicate that the table can be "construed" like a crossword puzzle. In addition, the periodic "puzzle" contains, at many positions, diagonal patterns, which also highlight certain patterns of physicochemical behavior.

Next, the table can be regarded from the electron configuration point of view. With this particular term of reference, the periodic table separates the elements into blocks in which *s*, *p*, *d*, and *f* orbitals are filled up. It is interesting to describe the classification of elements on this basis. It turns out that the elements can be classified into four general types. Elements of the first type are the inert (or noble) elements. They are all characterized by a completely filled outer shell with the configuration ns^2np^6, helium being an exception. Helium also has a completely occupied outer shell but the configuration is $1s^2$. The second class is made up of the representative elements. They are the elements of the *s*-block and the *p*-block, with the exception of the inert elements. They all possess incomplete outermost shells. The electronic configuration ranges from ns^1 to ns^2np^5. The third type of element is the transition elements, which have the two farthest incomplete shells with the general configuration $(n-1)d^{1-9}ns^{1 \text{ or } 2}$. There are three transition series corresponding to the incompletely filled 3*d*, 4*d*, and 5*d* orbitals. These elements reside in the center of the table, in the nine columns from group IIIB through group 1B (3–11 or no group number assigned). The elements in group IIB (12 or no group number assigned), the zinc family (zinc (Zn), cadmium (Cd), and helium (Hg)), are not transition metals according to the definition. Even though they are found in the "*d*-block" of the table, their *d* orbitals are always completely filled. The fourth type of element is similar to the transition elements but differ from the regular transition elements in that they have three outermost incomplete shells. Called "inner transition elements," they not only have incomplete *d*-levels, but they also have incomplete *f*-levels. There are two sets or series of such elements, each consisting of 14 elements. The filling of *f*-sublevels with a principal quantum number that is two less than the period number occurs in these. The elements of the first set or series, the lanthanides (cerium (Ce) through lutetium (Lu)) are the elements that follow lanthanum (La) in period 6; in these the 4*f*-sublevels get filled up. The second set or series of elements, the actinides (thorium (Th) through lawrencium (Lr)), fitting in period 7 after actinium (Ac), are associated with the filling of the 5*f*-sublevel. It has been mentioned earlier that in one of the forms of presentation of the periodic table, the transition elements, at the center of the table, are not assigned group numbers. The same is true of the inner transition elements in that they do not belong to any of the groups labeled at the top of the table. While all the elements, but one, belonging to the former family are naturally available, only a few of the elements of the latter family are naturally occurring. Moreover, the members of the latter family, unlike those of the former, are all radioactive.

7.2 RADIATION

A brief account of radiation is relevant here in recognition of the fact that monazite, one of the industrial sources of rare earths, with varying amounts contain thorium, which is radioactive. In fact, in some countries of the world monazites serve as the principal

suppliers of rare earths. Processing of monazites for the recovery of their contained rare earths necessitates the consideration of radioactivity arising due to thorium. Radiation comprises energy traveling through space. It is essential to the environment of human beings and includes visible light and radio waves as well as radiant heat from the sun. Life on earth has evolved with an ever-present background of radiation. Natural background radiation is the sum total of the contributions from cosmic rays; radiation from soil, rocks and building materials; as well as ingested radioactive isotopes. Living organisms appear to be able to cope well with this radiation, provided the levels are not too high.

Radiation originates from atoms — the basic building blocks of matter. Everything in the universe is made of atoms. A thousand million atoms side-by-side might just fill up the space occupied by a period on this page.

Most atoms are stable; an oxygen-16 atom remains an oxygen-16 atom forever. Some atoms, however, eventually disintegrate to yield totally new atoms. Such atoms are said to be "unstable" or "radioactive." An unstable atom possesses more internal energy than is strictly required with the result that the nucleus can undergo a spontaneous rearrangement to a more stable form. This is called "radioactive decay." When an unstable atom undergoes radioactive decay, it emits some of its extra energy as radiation in the form of gamma rays or as fast moving particles. Radioactive decay may occur in several successive stages, all the time progressing to a stable state where the final product atom is no longer radioactive.

Radiation of only one type, namely, ionizing radiation, will be considered now. This comes in two forms, rays and particles. Ionizing radiation is special because it has the ability to affect the large chemical molecules of which living organisms are made and thereby may implement alterations that are biologically important. The list of several types of ionizing radiation includes x-rays and gamma rays, alpha particles, beta particles, cosmic rays, and neutrons. Apart from its generation from natural sources, ionizing radiation is also generated in a range of medical, commercial, and industrial activities. The most familiar of these sources is medical x-ray equipment. In terms of exposure to this radiation, natural sources account for about 87% of the annual dose to the population, while medical procedures account for nearly all of the balance.

Each radioactive species decays at a characteristic rate. The time involved in the decay, the number of steps in the process and the kinds of radiation released in each step are by now well known. In the context of radioactive decay, the term "half-life period" is widely used. This term is defined as the time taken for half of the atoms of a given assemblage of atoms of a radioactive species to decay. Half-life periods can range from less then a millionth of a second to millions of years, depending on the radioactive species under consideration. After one half-life, the level of radioactivity of a substance is halved; after two half-lives it comes down to one quarter; after three half-lives to one eighth, and so on.

Many of the endowments of nature can be of great benefit to humanity but may also have associated risks when misused. Radiation is no exception. Radioactive materials should be used only when the benefits significantly outweigh the risks. Ionizing radiation, like a multitude of other agencies, may cause serious health effects in human beings. The degree of damage caused by this radiation depends on many factors — dose, dose rate, type of radiation, the part of the body exposed, age, health of the person subjected to exposure, and so on.

We have a range of simple, sensitive instruments capable of detecting minute amounts of radiation, from natural and man-made sources. In the context of protection from radiation, it is equally important to know that there are four ways in which we can protect ourselves. These are time, distance, shielding, and containment.

7.3 LANTHANIDE AND ACTINIDE ELEMENTS

We'd like to resume with a discussion of the lanthanide and the actinide elements. These elements, while assigned no group numbers, are placed separately and shown below the main body of the periodic table. This mode of representation gives a compact appearance and, more importantly, helps to place similar elements in their appropriate abodes in a single column in the table.

It is interesting to point out an additional feature arising from the periodic arrangement of the elements; this pertains to the trends that are observed in respect of atomic radii. The trends regarding the atomic radii of the main group elements are very regular. Across a period there is a decrease in the atomic radius as one moves from left to right, while proceeding down a group there is an increase in this parameter. These trends are explained by considering the two major factors that influence the atomic size — the effective nuclear charge and the principal quantum number of the outermost electron orbital. In the case of the *d*-block elements, the decrease in size across a row is not as significant as with the main group elements. The trends observed down transition metal groups are somewhat unusual. There is an increase in radius between the fourth and the fifth period transition metals, as expected from the increase in the principal quantum number of the outermost electrons. However, there is an unexpected similarity among the radii of the fifth and the sixth period transition elements. The explanation for this phenomenon lies in the lanthanide series of elements (from cerium, atomic number 58, to lutetium, atomic number 71), which appear between the elements lanthanum and hafnium in the sixth period. The electrons in the completely filled 4*f*-sublevel in hafnium and the other elements of the sixth row transition metals do not completely shield the valence electrons, thus causing a larger effective nuclear charge to be experienced by the outermost electrons. A consequence of this increase in the effective nuclear charge is a reduction in the atomic radii, called the lanthanide contraction. This contraction nearly cancels or nullifies the expected increase in the atomic radius between the fifth and the sixth period transition metal elements.

An important consequence of the lanthanide contraction is that many of the fifth and sixth period transition elements show remarkable similarities in their physical and chemical properties. For example, hafnium is very similar to zirconium in atomic radius and their chemistries are nearly identical, but these are quite different from those of titanium. The chemical behaviors of zirconium and hafnium are so similar that it took more than a hundred years for chemists to realize that hafnium occurred as an impurity in all samples of zirconium. Until 1923, when hafnium was finally identified, every published atomic weight of zirconium was wrong. All the physical constants that were assigned to zirconium actually applied to the naturally occurring mixtures of zirconium and hafnium. Even with today's superior technology, the two elements are difficult to separate from one another. The lanthanide contraction effects exert a similar influence on two other pairs of elements: tantalum and niobium, and tungsten and molybdenum.

The lanthanide contraction also has other consequences. One physical property that is directly influenced is the density of the elements of the sixth period. These elements possess unusually high densities because their atomic radii are virtually the same as those of the fifth period elements in the same group, while their atomic masses are almost twice as large. Osmium and its neighbor iridium have the highest densities among all naturally occurring elements. The chemical activity of the sixth period elements is also influenced by the lanthanide contraction. Because of the high effective nuclear charge experienced by

their valence electrons, sixth period elements such as platinum, gold, and mercury are relatively inert. Because of this chemical inactivity, platinum and gold are among the few metallic elements that occur in nature in an uncombined state. All told, the lanthanide contraction not only causes the periodic table's orderly progression to be interrupted, but also is instrumental in producing chemical effects in other elements.

According to the definition provided by the International Union of Pure and Applied Chemistry (IUPAC), the element lanthanum (La), the 14 elements starting from cerium (atomic number 58) and ending with lutetium (atomic number 71), and the 2 group IIIB (3) elements, scandium and yttrium, with atomic numbers 21 and 39, respectively, form what are termed the rare earths. The inclusion of the two group IIIB elements in the list of the rare earths is based on the invariable occurrence of the former with the latter in nature and the similarity in ionic radii. Significant scandium enrichment, however, is seldom found in rare earth minerals although very minor amounts are widely distributed in many minerals. The rare earths are divided into two groups on the basis of differences in properties: the light or cerium group comprising the first seven members lanthanum to europium (atomic numbers 57 through 63), and the heavy or yttrium group comprising the elements with atomic numbers ranging from 64 to 71 (gadolinium to lutetium), plus yttrium and scandium. Despite its low atomic weight, yttrium is placed in this group because its occurrence, ionic radius, and properties are similar to those of the other members belonging to this group.

From the preceding account, it is clear that the term "rare earths" is a collective name for a group of 17 elements of which 16 are naturally occurring. They are all metals in the elemental state and form salts that are strong electrolytes. While "rare earths" is the common name for these elements, earths is an old name for what are now known to be oxides, and these elements are not truly rare. The most plentiful amongst the family, cerium, is more abundant than lead in the earth's crust and thulium, the least plentiful member of the family, is more abundant than cadmium, silver, gold, or platinum. The light group members (La through Eu) are more abundant than the heavy group members (Gd through Lu). In this context it may also be pointed out that elements with even atomic numbers are found to be more abundant than their neighbors with odd atomic numbers. Thus the rare earths are neither rare nor earths. Truly speaking, the word "rarity" stems from the difficulty experienced in separating the rare earths into individual elements and not from their relative abundance. All the rare earths occur naturally except one. This member is promethium. It should be produced artificially from neodymium by bombardment with neutrons. The process yields a neodymium isotope, which decays by beta emission to promethium, which is radioactive with a half-life of 3.7 years. It may be mentioned here that this radioactive element possesses many amazing nuclear and chemical properties. It has been compared with an entity in a sealed envelope, with many more mysteries to be unraveled in the future. The rare earths are finally a community of 16 naturally occurring elements since promethium does not occur naturally.

The description of the classification of the elements made on the basis of electronic configuration provided earlier brings out the fact that there is a close linkage between the electronic structure and the chemical behavior of the elements. Thus, all the inert gases have similar electronic structures (fully filled *ns* and *np* orbitals) and they behave alike chemically. Similarly, the chemically alike alkali metals have a single *s* electron outside the closed shell. All halogens have the ns^2np^5 electronic configuration while oxygen, sulfur and selenium, with a strong chemical resemblance to each other, have the configurations $2p^4$, $3p^4$, and $4p^4$, respectively. The classification of the elements as metals and nonmetals also bears a correlation with the electronic structure. Most metals, such as sodium, beryllium,

and aluminum, have one to three electrons more, and most nonmetals, such as fluorine, oxygen and nitrogen, have one to three electrons less, as compared to the corresponding closed-shell configuration. The striking similarity in chemical behaviour exhibited by the lanthanides and the actinides is also understandable, as the outer orbital structure in each of these groups is the same, differences occurring only in the 4*f*- and 5*f*-levels. The same reasoning applies for the three transition series where the differences are only in the number of *d* electrons. The elements belonging to this class show a significant resemblance to each other; e.g., they form colored ions, possess several valence states, form coordination compounds, and so on. Introductory textbooks, while dealing with the rare earths, often view them as being chemically so similar to one another that collectively they are treated as one element. To a certain degree this is correct, and many of their uses are based on this close similarity. However, important differences in their behavior and properties do exist; for example, the melting points of the end members of the series differ by a factor of almost two (lanthanum (La): 918°C, lutetium (Lu): 1663°C).

The very similar chemical properties of the individual members of the rare earths family should, in no way, be construed to imply that they will always remain inseparably together. Separation between the rare earths family members is entirely possible, though not easy. Mention must be made here of an important feature that has made such separation feasible. Knocking out three electrons from the neutral atom in the rare earths elements causes the liberation of ions having slightly different sizes. The size or the ionic radius decreases with increasing atomic number. Lanthanum has the largest (0.12 nm) and lutetium has the smallest (close to 0.10 nm) ionic radius. These differences in ionic radii bring about differences in ionic potentials and consequently differences in their hydrated radii in aqueous solutions. This helps in a graded separation of the rare earths family members through chromatography. The small differences in their solubility are exploited in a separation technique known as fractional crystallization, which implements separation between the rare earths. There are, of course, other well-developed techniques by which rare earths separation is accomplished.

More than 95% of the rare earth oxides (REO) occur in three minerals: (1) bastnasite, a fluorocarbonate ($REFCO_3$), which theoretically contains about 75% REO and very minor amounts (0.05%) of yttrium; (2) monazite, a rare earth phosphate ($(RE,Y)ThPO_4)_2$, which can theoretically contain up to 70% combined REO, including about 2% yttrium oxide (but most concentrates contain about 55 to 65% REO); and (3) xenotime, an yttrium rich phosphate mineral ($(Y,RE)PO_4$) that can theoretically contain about 67% yttrium oxide. Among these, the first two, bastnasite and monazite, are the sources of the light group of the rare earths. Xenotime and also uranium tailings are sources of the heavy group and of yttrium. Bastnasite is the world's major source of REO; it is mined as a primary product by Molycorp from the Mountain Pass deposit in California and as a by-product of iron ore mining in China. The five major countries producing monazite are Australia, Brazil, Malaysia, China, and India. The major producers of xenotime are Malaysia, China, and Australia. World production in concentrate, intermediate, and final product forms is approximately 60,000 t/a of REO. The industry is dominated by China, Europe, and the U.S., with several small producers of high value products in Japan. Australia was the dominant producer of monazite in the 1980s, the source being Western Australia's titanium minerals industry, but the scenario has changed in recent years due to the availability of cheaper ores from China. Currently, the rare earths are not produced in Western Australia. Some relevant projects are, however, under consideration. Some salient features of these projects have been presented in Table 7.1. There is certainly an abiding interest in the rare

Table 7.1 Proposed Western Australian projects

Producer	General description and information
Name: Aston Rare Earths Ltd. *Location:* Mt. Weld, 15 km south of Laverton *Capacity:* Cerium oxide, 2,500 t/a (proposed) *Ownership:* Aston Mining Ltd. (100%)	The Mt. Weld Rare Earths Project is based on a large monazite resource (with low radioactivity) containing nearly 1.3 Mt of ore with a REO content of 23.6%, capable of supplying 10% of the world's demand for rare earths for a period of over 20 years. When developed, the project envisages operation at two locations. A mine and a concentrator at Mt. Weld is to produce 12,000 t/a of monazite concentrate. A second, plant, capable of producing rare earth oxide products, is to be located at Meenaar Industrial Park, 20 km east of Northam. The deposit is rich in cerium, which constitutes about 50% of the contained rare earth oxides. Initially, Aston Rare Earths has decided to focus on the production of cerium products, as they have the greatest growth potential in the near future. Applications include cerium concentrates for polishing powder production; high grade cerium concentrates for use in specialty glasses; cerium carbonate for the autocatalyst market; high grade cerium oxide for the specialty glass/ceramic market. In addition, Aston Rare Earths is to produce a "cerium depleted concentrate" which is to be marketed to rare earths processors in Asia and Europe. In the long term, these concentrates will be processed to separate the following rare earths: lanthanum, for rare earth nickel hydride batteries; neodymium, for rare earth magnets; europium, for rare earth phosphors.
Name: Rhodia Pinjarra Pty Ltd. *Location:* Pinjarra, 100 km south of Perth *Capacity:* 15,000 t/a (proposed) *Ownership.* Rhodia Chimie (France) (100%)	Rhodia Pinjarra Pty Ltd. (formerly Rhône-Poulenc Chimie Australia Pty Ltd.) envisages development of a rare earths plant on a location adjacent to the company's existing gallium plant. The project involves processing of monazite ore to produce rare earth nitrate for export. The plant is to be designed to receive, store, and process up to 12,000 t/a of monazite to produce 15,000 t/a of rare earth nitrates and 6000 t/a of residue. The rare earth nitrates are to be shipped to the U.S. and France for further separation and purification. An estimated 23,000 t/a of tri-calcium phosphate is proposed to be sold for fertilizer production. Monazite is produced in Australia as a co-product from the processing of titanium minerals. It is a rare earth phosphate, which also contains small amounts of other elements, including thorium, uranium, iron, and titanium metals. The monazite feedstock for the proposed processing plant is to be obtained from the existing titanium mineral separation plants at Narngulu (near Geraldton), Eneabba, Capel and Bunbury.

earths in the countries of the world that are endowed with rare earths resources and reserves of commercial significance.

7.4 PROCESSING RARE EARTHS

What follows is a presentation of the ways by which rare earth resources are processed. Attention is first focused on bastanasite. The mined product is comminuted and subjected to a flotation process. The concentrate ensuing from the process is thickened, filtered, and rotary kiln dried to produce a rare earth oxide (REO) concentrate. The concentrate can be further upgraded to 70% REO by leaching with 10% hydrochloric acid to remove calcite. This 10% acid treatment does not affect bastanasite. A concentrate with 85% REO is

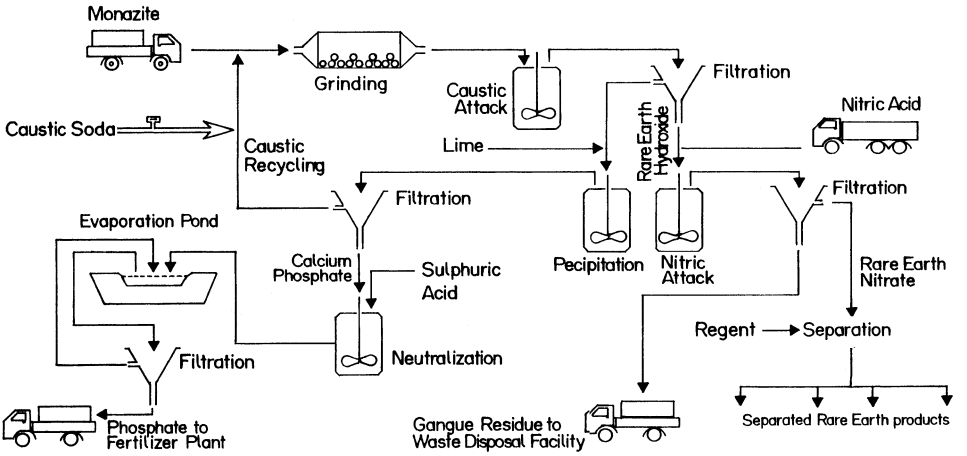

Figure 7.3 A scheme for monazite processing.

typically produced by roasting the leached concentrate. This is carried out to remove carbon dioxide from the carbonate. The concentrate is leached with concentrated hydrochloric acid for conversion to soluble rare earths chlorides. The cerium component, which is oxidized to its higher valence insoluble oxide during the calcination step, is passed through a countercurrent decantation and thickening circuit and then filtered, resulting in a filter cake composed of about 70% REO, more than 90% of which is ceric oxide. This precipitate is reprocessed, dried, and marketed as a cerium concentrate. The rare earths in the thickener overflow with a cerium-free rare earth chloride solution, which is separated by solvent extraction into a lanthanum (La), praseodymium (Pr), and neodymium (Nd) concentrate and a samarium (Sm), gadolinium (Gd), and europium (Eu) concentrate. Each of these concentrates is subjected to additional solvent extraction and proprietary processes to produce various mixed rare earth compounds and individual oxides.

The processing aspects of two other resources, monazite and xenotime, may be considered next. Both these resources are usually digested in an autoclave at 150°C with a 70% sodium hydroxide solution for several hours. Hydroxides of the rare earths and of thorium, formed in the reaction, are insoluble, while trisodium phosphate (TSP) and excess sodium hydroxide remain in solution. Water is added, and after settling the insoluble hydroxides are recovered by filtration; sodium hydroxide is recycled to digestion and TSP is recovered by crystallization. The filtered hydroxides are washed, and the thorium fraction is removed by using one of several methods. One chemical process involves the mixing of the precipitated rare earths and thorium hydroxides with water; the mixture is brought to a pH of 3.4 by the addition of hydrochloric acid. At this pH the rare earths hydroxides get selectively dissolved, forming a rare earths chloride solution. Undissolved thorium hydroxide is removed by filtration and thermally treated to produce thorium oxide. Here again additional processes are introduced into the rare earths stream with the objective of producing purified forms of separated rare earths products. A scheme of the processing of monazite is shown in Figure 7.3. The scheme produces essentially two commodities: rare earth nitrates and phosphates for use in fertilizer manufacture. There are five main processing steps:

(1) Mixing the monazite with hot caustic soda to dissolve phosphates from the mineral, leaving rare earth hydroxides.

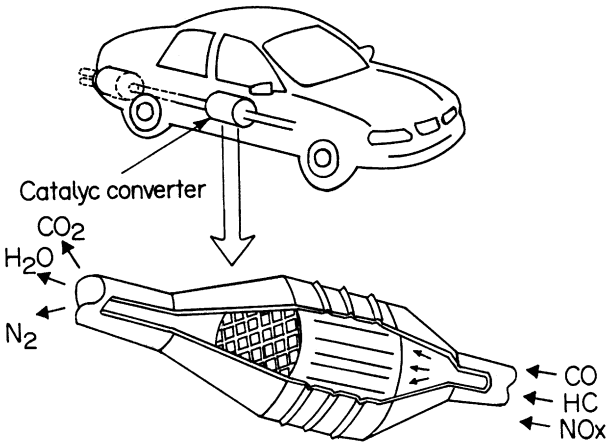

Figure 7.4 Catalytic converter in automobiles.

(2) Filtering hydroxides from the solution, allowing the remaining phosphates to be utilized for agriculture fertilizer. The caustic soda is recycled. Tricalcium phosphate is stored temporarily in the evaporation ponds before the material goes to fertilizer makers.

(3) Reacting the rare earth hydroxides with nitric acid and barium salt, then filtering the solution to remove insoluble radioactive elements — thorium, uranium, radium — and other inert materials. Evaporation ponds on site store wash waters.

(4) Processing the resulting rare earth nitrates into separated rare earth products.

(5) Transporting the radioactive waste arising in the whole processing scheme.

It should be clear from the brief coverage provided for the processing routes adopted for the different resources that the rare earths end up (1) as unseparated (or mixed) as direct products of processing or as a result of further chemical processing; or (2) as separated individuals in the form of different chemical intermediates such as chlorides, oxides, and fluorides, the most popular usable forms for a variety of purposes.

7.5 APPLICATIONS OF RARE EARTHS

A voluminous body of literature testifies to the fact that the rare earths are enormously useful. This presentation attempts to provide just an illustrative account, and it is hoped that through this the reader will get interested in the acquisition and dissemination of information as regards the importance of the rare earths in present-day science and technology. The presentation first concerns itself with applications in the form of compounds and then those in the form of metals.

An important application pertains to the use of europium oxide in phosphors for color television picture tubes and other cathode ray tube (CRT) displays. In combination with yttrium oxide, yttrium oxysulfide, or yttrium orthovanadate, a superior red color is produced. The application of fluorescent materials for lighting with regard to a three-wavelength lamp has been successful, and this lamp is widely used in the market as the only lamp that simultaneously achieves high efficiency and high color rendering. The lamp derives its white light through the combination of red color from Y_2O_3:Eu^{3+}; green color from

(lanthanum (La), cerium (Ce)) $PO_4:Tb^{3+}$, etc.; and blue color from $BaMg_2Al_{16}O_{27}:Eu^{2+}$ and others.

A typical use of the rare earths is as petroleum cracking catalysts. The petroleum fluid cracking catalysts (FCC) consist of three main constituents: an amorphous silica–alumina refractory binder, a generally inert filler, and a rare earth containing zeolite (sodium aluminosilicate). Lanthanum and cerium chlorides are the principal compounds that are used in a mixture form in the production of these catalysts. Automobile exhaust emission is another important example of the catalytic application of the rare earths. A catalytic converter is incorporated in automobiles. Its role is to transform the primary pollutants in the exhaust gas — carbon monoxide (CO), unburnt hydrocarbons (HC), and nitrogen oxides (NO_x) into nontoxic compounds: carbon dioxide (CO_2), water (H_2O), and nitrogen (N_2). The exhaust gas is passed through a honeycomb monolith (metallic or more often ceramic), the interior surface of which is coated with the catalyst formulation consisting of three key ingredients: precious metals (platinum, palladium, rhodium), alumina, and rare earth-based materials containing cerium and lanthanum oxides. Rare earths improve the durability of the catalyst and enhance its catalytic activity. Figure 7.4 shows the catalytic converter in place.

Although the theoretical basis for the efficacy of the rare earths as polishers is not clear, it appears that besides mechanical pulverization, chemical reactions contribute to the effect. The sources of polishers are largely confined to bastnasite and the rare earth chlorides, which include cerium oxide polishers. They are used for polishing the CRTs of televisions and the substrates of photomasks for integrated circuits. The use of rare earth compounds for polishing purposes is very well founded. A brief description of polishing powders will be presented here. Morphological characteristics of the powders have an influence on the polishing performance in terms of the quantity of glass removed and the quality of the polished surfaces. The three morphological characteristics of powders are (1) specific surface area, which reflects the degree of particle strength and porosity; (2) degree of external sintering, which influences the grain boundaries; and (3) particle size distribution, which influences the stability of the suspension. Powder characteristics are carefully controlled throughout processing to ensure quality. The term "polishing efficiency" (PE) is often used to qualify polishing. It is expressed by the formula, $PE = M/sxt$, where PE is polishing efficiency in $mg/dm^2/min$, M is weight of glass removed in milligrams, s is surface of glass in dm^2, and t is polishing time in minutes. It decreases with time as the polishing particles are broken down and the suspension becomes loaded with glass particles. An improvement in the polishing efficiency occurs when the polishing bath concentration is increased. The bath concentration depends mainly on the type of polisher or pad used. When pads are changed from polyurethane (PU) or nonwoven types to felt or pitch types or to hard polyurethane, the suspension concentration should accordingly be increased. It is generally seen that PE is proportional to speed, regardless of the type of polisher and operating conditions used. Therefore, operation at the maximum speed available, while remaining within the values compatible with the type of pad used, is recommended. An important consideration is the influence of the applied pressure on the object to be polished. This is the pressure applied on the glass to be polished, which is not the same as that indicated by the spindle manometer. At high rotating speeds (>250 rpm), the effect of pressure is very significant up to 0.8 to 1 bar. Beyond this, the PE remains unchanged. When high production rates are sought (in the polishing of standard spectacle glass, for instance), it becomes mandatory to operate at high rotation speeds (>1000 rpm) and high pressures (>1 bar). There are two other factors, namely, the water hardness and the suspension temperature, on which the PE depends. Moderately hard water and operating

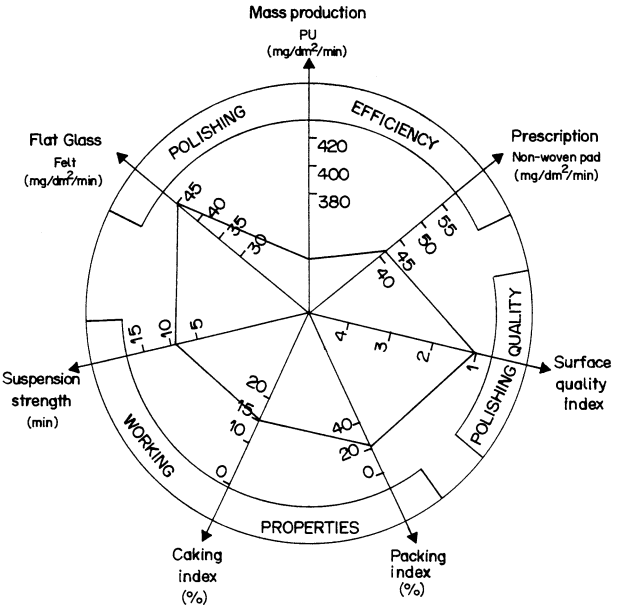

Figure 7.5 Monogram to determine fields of application of a given polishing powder.

temperatures between 15 to 30°C are generally the recommended parameters. The efficiency of a polishing powder can be evaluated by two series of tests: the first series of tests concerns the polishing efficiency and quality; and the second series of tests concerns the properties of the suspended powder before and after use. In some plants, storage containers are located some distance away or remote from machines. This may result in the powder settling out of solution. It is therefore important to measure the suspension strength. If the suspension is not used immediately after preparation, sedimentation may take place. This can be measured by permitting the suspension to settle for 24 h. It is then stirred and the supernatant liquid is decanted. The resulting deposit is then dried and weighed. All these events are covered in what is known as packing. There is one additional thing that could occur called "caking." This is when a deposit is formed in the suspension following the polishing operation. The composite picture of a polishing powder can be graphically established from the following five parameters: polishing efficiency, surface quality, suspension strength, packing, and caking (Figure 7.5). With this method or monogram as it may be called, it becomes possible to compare rapidly the various product properties and determine their fields of application.

The use of the rare earths as glass additives constitutes a well-known application field. Neodymium oxide is used to color decorative glass from light pink to blue-violet. It is also added to welding glasses to protect the eyes from the yellow flare emitted by sodium vapor. Optical glasses are incorporated with lanthanum oxide to increase the index of refraction and decrease the dispersion of light. Camera lenses and other applications needing a high degree of light transmission may be cited as other important examples of uses of lanthanum oxide. Yttrium oxide and gadolinium oxide are used as additives for lenses. Cerium oxide is used as an achromatic agent, and neodymium oxide is used as an additive to the CRT front glass of TVs. The use of the rare earths in laser glasses must be added to this list of applications in glasses.

Thin layer single crystals of yttrium–iron–garnet (YIG) show vertical magnetic anisotropy and are used for magnetic domain memory. Yttrium–iron garnets and gadolinium–iron garnets (GIGs) are widely used as ferrite materials in microwave applications. These garnets can be operated in low magnetic fields in the lower microwave frequencies.

The rare earths play an important role in the realm of new high strength, high temperature ceramics. The stabilization of cubic zirconia (ZrO_2) by the addition of yttria (Y_2O_3) is well known. Stabilized zirconia has several major applications. Its use in oxygen sensors in the air–fuel ratio control systems of automobiles can be cited as just one example. As regards the development of new materials, special mention may be made of silicon nitride (Si_3N_4) doped with yttria (Y_2O_3) and Si_3N_4–Al_2O_3 (SiAlON = Sialon) doped with Y_2O_3. These materials are already being used in cutting tools and in turbine blades in exhaust gas streams and are being considered for use in engine blocks and other engine parts.

Magnetic refrigeration makes use of the entropy change in a magnetic spin system under the influence of an external magnetic field, which is utilized for cooling. Two major breakthroughs have been reported in magnetic refrigeration. The first one has been the successful demonstration of the fact that sub-room-temperature magnetic refrigeration is a viable technology and that it may be competitive with conventional gas cycle compression/expansion refrigeration. A cooling power equivalent to about 600 watts has been obtained in a laboratory prototype refrigerator using three kilograms of gadolinium spheres as the magnetic refrigerant in a magnetic field of 5T. The second breakthrough is the discovery of the giant magnetocaloric effect (MCE) materials Gd_5 $(Si_xGe_{1-x})_4$, which have MCEs better (ranging from 25 to 200%) than those associated with known prototype magnetic refrigerants, depending on the temperature range.

The application fields of the rare earths, both in their metallic and alloyed forms, will be discussed next.

The major uses of the rare earths are as additives to ductile iron, steels, and nonferrous metals, such as magnesium, and superalloys; as lighter flints; in ordnance, and in research. In most of these applications the rare earths are used as mixed metals in which they are present in their natural proportions. In this form they are popularly known as misch metal. The rare earths, in their separated metallic forms, are used only as additives to superalloys and in research.

The ductile iron market is quite sizeable for the rare earths; additions to the extent of about 0.2 wt % serve to spheroidize graphite, to counteract the effects of deleterious impurities, and to enhance liquid fluidity. The acceptance of misch metal over magnesium, even though the former costs more, is due to the fact that magnesium volatilizes from the melt, making it difficult to control the quality of the ductile iron, while the rare earths do not volatilize and thus the quality of the final product is easier to control. The addition is generally made as a ferro-misch metal silicide or ferro-cerium silicide.

The addition of rare earths to steels is continually gaining acceptance. The extent of addition in this particular area of application amounts to about 0.2 wt %. The addition of rare earths helps in controlling the sulfur concentration and thus brings about improvements mainly in the workability and the transverse impact values. The major use of the rare earths in the steel sector has been as additives to plate and pipeline steels. Sulfidic forms of the rare earths constitute the most stable sulfides known; only calcium sulfide has a comparable free energy of formation. Additions are generally made in the form of a ferro-misch metal (or cerium) silicide.

The addition of rare earths to magnesium improves its strength, creep resistance, and

fatigue properties, especially at elevated temperatures. Minor nonferrous uses of the rare earths include their addition to copper-based and aluminum-based alloys and bronzes.

The rare earths, in their pure metallic states, are incorporated in a number of chromium-based, cobalt-based and nickel-based superalloys. Essentially yttrium, lanthanum, or cerium, of about 0.1 wt %, is added to improve the high temperature oxidation and/or corrosion resistance in various corrosive environments including saltwater, combustion atmospheres containing sulfur, and in some other environments where superalloys without rare earths added exhibit relatively inferior properties. The rare earths are believed to form a protective complex oxide coating that inhibits surface attack. In the case of sulfur-bearing environments, the formation of stable rare earth oxysulfides is believed to provide protection.

The pyrophoric nature of the light rare earths, especially cerium, accounts for two important uses: lighter flints and ordnance. A variety of misch metal–iron compositions (60 to 80% misch metal with the remainder mostly iron plus additional minor alloying agents) are used in lighter flints and industrial sparking tools.

Fundamental and applied research accounts for the major use of the rare earths in their pure, separated metallic state. Some research is directed toward obtaining more information about the fundamental properties and nature of these metals and their alloys. It is from these results that new applications are likely to be generated. The remaining research is oriented towards translating some of the more promising ideas and developments into commercial realities.

To sum up, it may be pointed out that on a volume basis, approximately 95% of the usage of the rare earths is in the mixed form; the individual elemental forms of the rare earths account for the remaining 5% of the total volume, but this component represents over 50% of the monetary value. It must be borne in mind that as in the case of many other materials, the markets for the rare earths also have been mixed. There were years when the markets showed a worldwide recession. The use of the rare earths in steels has dropped considerably due to economical factors and to strong competition from other desulfurizing and shape control processes. The glass and glass polishing areas have also shrunk somewhat, but the catalysts market was reasonably favorable. The bright spot has been the sales of the individual rare earths, i.e., the high technology component of the rare earths market, which is nearly recession proof. It may, in general, be added that it is apparent to anyone following the literature pertaining to the rare earths that research on rare earths, especially the applied type, has greatly expanded, even in those countries that have experienced cutbacks in the funding of science. There used to be a time when most of the research on the rare earths was concentrated in the U.S. That is no longer the case today. Both these trends are healthy and should continue to engender a keen worldwide competition in science, technology, and industry involved with the rare earths. The future appears to be bright for new innovations and new applications of the rare earths at the industrial level.

It will be of interest to refer to the applications of permanent magnets and the impact of rare earths based magnets. Permanent magnet materials are used throughout the industrialized world in an enormous variety of applications. Some of the broad fields of application include motors and generators (domestic and industrial motors, starter motors, and stepper motors); acoustic devices (loudspeakers, headphones, microphones, pick-ups); magneto-mechanical applications (holdings, couplings, bearings, magnetic separation, actuators), and information technology (IT), telecommunications, measurement and control (switches, sensors, traveling wave guides, transducers, MRI tomography). Among the broad fields of

application cited, the largest share goes to motors and generators, amounting to some 35% of the total usage. The most widely used permanent magnetic materials, accounting for about half of the total market in value terms, are the ferrites. Although they have relatively low energy products, they are and will remain the cheapest source of permanent magnetic fields. The introduction of rare earth permanent magnets based on samarium–cobalt around 1970 and of neodymium–iron–boron magnets in the mid-1980s ushered in a new era with regard to hard magnetic materials. Samarium–cobalt magnets possess a better temperature stability as compared to neodymium–iron–boron magnets and will continue to be used in most thermally demanding applications. This better temperature stability results from the high Curie temperature of samarium–cobalt magnets, 700–800°C, as against only 312°C for neodymium–iron–boron magnets. Applications that demand a high magnetic strength to weight (or volume) ratio and that do not need operation at high temperatures, say, above 150°C, are served well by neodymium–iron–boron magnets. Substitution of neodymium–iron–boron for samarium–cobalt has been particularly evident, for example, in computer peripheral drives, personal stereos, camera motors, and compact disc players.

In automotive applications needing the use of permanent magnets, either ferrites (for their low cost) or Alnico magnets (for their temperature stability) have been used to date. The development of cost-effective, hot-pressed neodymium–iron–boron magnets has made possible a reassessment of the benefits of a change over to smaller and lighter, albeit more expensive, magnets on the basis of improved total system performance and cost. For example, the replacement of the wound field stator in the starter motor by a permanent magnetic field brings down the load on the battery and the alternator, permitting them to be smaller and thus cheaper.

A potentially voluminous market for neodymium–iron–boron magnets is in magnetic resonance imaging (MRI) tomography, both in whole-body scanners and in smaller systems. Ferrites would give the cheapest means of generating a permanent magnetic field, but the weight (~100 tonnes for a whole body magnet) of material renders them unsuitable for many applications. Although more expensive, neodymium–iron–boron magnet systems are much lighter and more compact and, in some circumstances, can even compete with superconducting solenoids in producing the required magnetic fields. A forecast has been made that MRI scanners may become as commonplace as x-ray scanners in the course of the next decade, and many of these are likely to contain neodymium–iron–boron magnets.

The development of neodymium–iron–boron magnets is having a widespread impact on the way permanent magnets are used, because they offer the very high strength of samarium–cobalt magnets at much lower costs and without the prospect of supply limitations. Most of the next decade's growth in permanent magnets will be in neodymium–iron–boron magnets, much of which will be supplied as polymer-bonded and hot-pressed magnets. The search for new permanent magnet materials has led to further interest in rare earth–iron intermetallic compounds modified by the introduction of interstitials such as nitrogen or carbon. Interstitial modification results in an expansion of the lattice, an enhancement of the Curie temperature, and, in some alloys, the development of a strong uniaxial anisotropy.

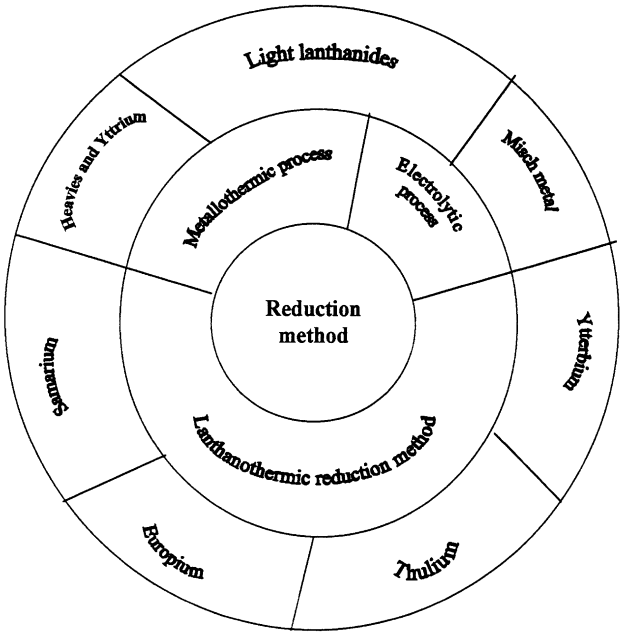

Figure 7.6 Different metallurgical processes for producing rare earths in their metallic forms.

7.6 METHODS OF PREPARING ELEMENTAL AND COMPOUND FORMS OF RARE EARTHS

The final part of this chapter will give an account of the different methods by which the rare earths are prepared in their elemental forms from their different compounds. There are principally three methods, the metallothermic, the electrolytic, and the lanthanothermic (Figure 7.6), which are usually adopted.

The metallothermic method is used to prepare the light lanthanide metals, lanthanum (La), cerium (Ce), praseodymium (Pr) and neodymium (Nd). The reductant normally used is calcium. Rare earth fluorides serve as the source. Presently rare earth fluorides are made by various methods. Conventionally these can be divided into two main groups. The first group comprises methods based on the precipitation of fluorides from soluble salts of the corresponding metals by hydrofluoric acid (aqueous methods) followed by thermal decomposition of the hydrated fluorides until an anhydrous state is reached. The second group, called dry, gaseous, or nonaqueous methods, comprises methods based on direct fluoridizing (by hydrogen fluoride, fluorine, or other fluorinating agents). These methods have several important advantages compared with the aqueous methods: the fluorides obtained are anhydrous; the operations involving fluoride precipitation, washing, decantation, and filtration are bypassed as well as the drying and calcination of the fluoride. The calcination process is, of course, associated with pyrohydrolysis. The products obtained by precipitation are inferior to those obtained by nonaqueous means. Both groups of methods are used in world production practices. Nevertheless, the method of gaseous hydrofluorination is

preferable. In all nonaqueous processes the starting materials are rare earth oxides, which interact with gaseous hydrogen fluoride. The starting materials, i.e., the oxides, are produced by the thermal decomposition of carbonates, hydroxides, oxalates, and so on. One of the best equipment to implement thermal decomposition is a horizontal ring-shaped vibrating apparatus with direct heating. The rare earth fluorides are synthesized by the reaction of rare earth oxides with hydrogen fluoride at 200–550°C in a single continuous operation: $(RE)_2O_3 + 6HF \rightarrow 2(RE)F_3 + 3H_2O$. Hafnium (HF) is preferred over NH_4HF_2 as a fluorinating agent since with the former there is less residual oxygen in the resultant fluoride. The latter, moreover, introduces some iron into the fluoride, which eventually reports to the metal. For obtaining fluorides with the lowest oxygen content it is necessary to melt them under a HF gas cover before the reduction step. Every stage of production and processing of fluorides involves the use of platinum wares. Fluorides thus prepared are mixed with 10% excess calcium metal and charged into a tantalum crucible, which is then heated inductively to about 1400°C or to a temperature that is about 100°C above the lanthanide metal's melting point, whichever is higher. The denser lanthanide metal settles to the bottom, and the calcium fluoride slag floats on top of it. The slag is easily removed at room temperature and the metal is then vacuum cast at 1000–1200°C to remove the excess calcium. For obtaining metals of the highest purity, freshly prepared, multiple distilled calcium is used as the reductant, and the vacuum casting is implemented at a much higher temperature (about 1800°C). The high vacuum casting temperature, however, causes the lanthanide metals to dissolve significant amounts of tantalum, but if the sample is slowly cooled and maintained just above its melting point, most of the dissolved tantalum precipitates along the tantalum crucible wall. The high-tantalum zone in the peripheral regions of the ingot is machined off, leaving behind the essentially tantalum free lanthanide metal. Other variations of this process involve the use of chloride intermediates instead of fluorides and the substitution of lithium for calcium as the reductant. The chloride intermediates bear the disadvantage of being hygroscopic. The fluoride intermediates do not suffer from this drawback. A literature survey would provide the readers with a few other variations, but the route involving fluoride–calcium interaction continues to be one of the most universally chosen metallurgical routes.

The metallothermic means of the preparation of the light lanthanides described above is also used for the preparation of the heavy lanthanides and of yttrium. There exists, however, one difference in that the high temperature vacuum casting operation is replaced by vacuum distillation or sublimation. Due to the fact that the heavy lanthanides show appreciable tendencies for dissolving tantalum even at the melting point, it is important that these metals are distilled.

The electrolytic method is the exclusive choice for the light lanthanides, using chloride, fluoride, or oxide. For the reduction of the oxide, a complex fluoride solvent, which dissolves about 5% of the oxide at the operating temperature, is used. The electrolytic cell walls are usually constructed of ceramic (e.g., firebrick) or graphite or molybdenum; the anode is made of graphite and the cathode of iron or molybdenum or tungsten. The choice of material is governed by the purity desired for the final product. Typical operating conditions are a temperature of 800–1000°C, a high current (200 to 2500 A), a voltage of 4 to 15 V, and a current density of 2 to 10 A/cm^2. The advantage of the electrolytic method over the metallothermic one is that the lanthanide metal can be produced at a much lower cost. In general, the purities of the electrolytically produced metals are inferior to those of the metallothermically produced ones, although in principle it should be possible to produce high purity metals electrolytically. A limitation of the electrolytic

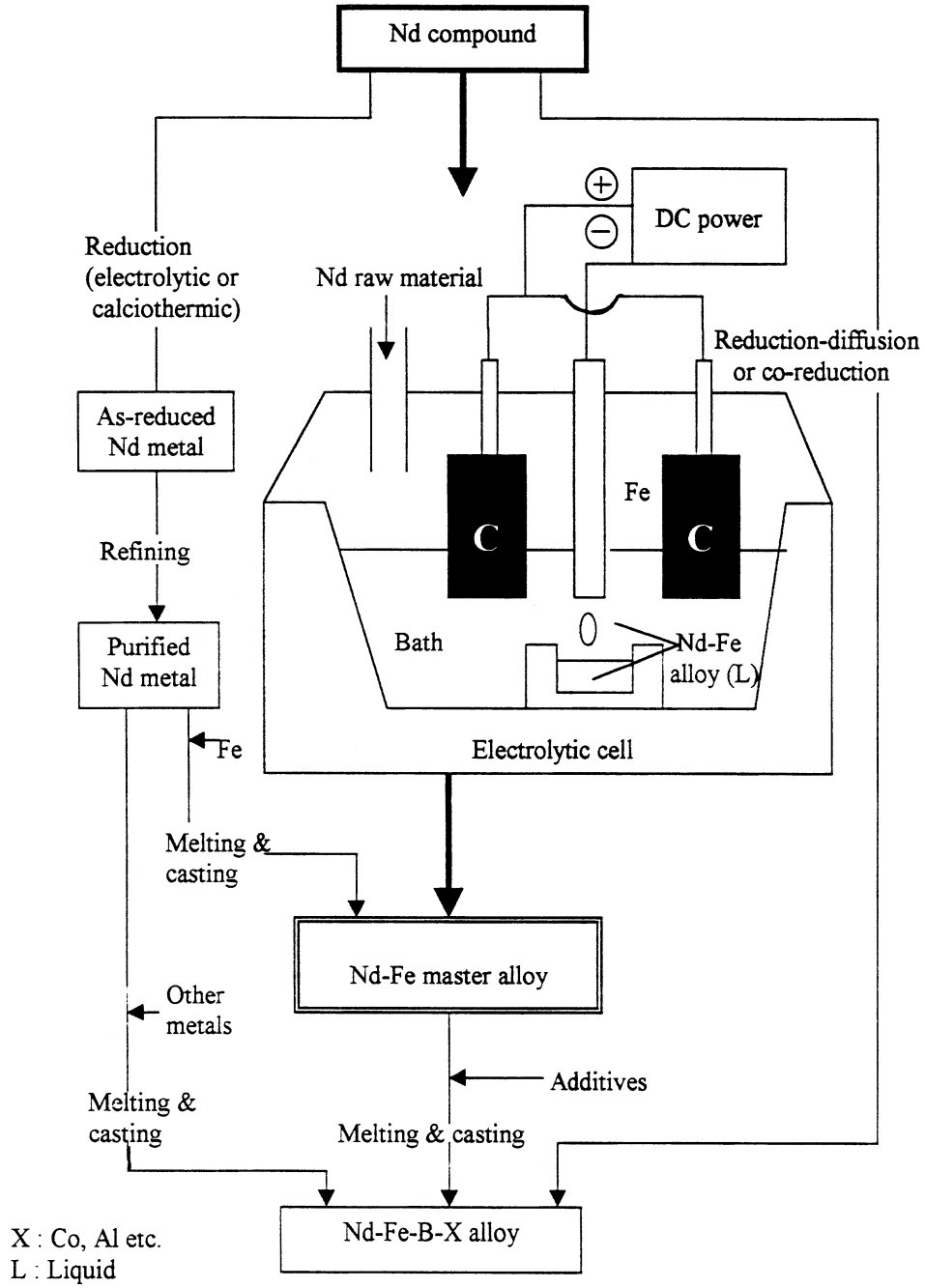

Figure 7.7 Different metallurgical processes combined to produce rare earth-based alloy system.

method is that it cannot be (or at least, to date, it has not been) deployed to produce heavy lanthanides in their pure forms. The primary reason for this is that the cell and electrode

materials are not capable of withstanding the high temperatures needed because of the high melting points of the heavy lanthanides.

Besides the light lanthanides, there is one more product, called misch metal, that is produced by the electrolytic method. In order to keep the production price low, the cells and the electrodes are constructed of the cheapest workable materials. In general, the quality of the misch metal produced is 98% or less pure. In part, this is due to the addition of magnesium to reduce the oxidation of misch metal at room temperature. The misch metal also contains appreciable amounts of other metallic impurities such as iron, aluminum, silicon and lead. Some of these impurities are from the original chloride used as the starting material, and the remainder are introduced during the metal reduction process. Since the primary use of misch metal is as an alloying agent or as lighter flints, the relatively high impurity contents do not appear to be a major deterrent for the process to be adopted in the industry. However, in specific applications such as misch metal ordnance devices (projectile liners), the influence of impurities is much more critical.

Strictly speaking, the third method should be known as a metallothermic method; however, in view of the special features involved, a special name is given to it. It is called the lanthanothermic method, named after the reductant, lanthanum (La), used in the process. The physicochemical principles of the process are very similar to the well-known Pidgeon process for the production of magnesium, involving vacuothermal reduction of calcined dolomite with ferrosilicon as the reductant. Like magnesium metal, the rare earths elements samarium (Sm), europium (Eu), thulium (Tm), and ytterbium (Yb) have relatively high vapor pressures. The reductant used is lanthanum. It has a low vapor pressure, which permits its use to perform this duty. It is an illustration of the use of one rare earth to produce a select group of rare earths. The process is implemented by mixing oxides of Sm, Eu, Tm, or Yb with lanthanum chips and loading the mixture into what may be called a tantalum distillation container. The mixture is heated and lanthanum reduces the rare earth oxide. At the temperature used in the reduction process, the rare earth metal that is yielded has a very high vapor pressure. It evaporates, leaving the reaction site, and thus the reaction is driven to completion. The oxide of lanthanum is left behind. The volatile rare earth metal is usually subjected to redistillation for accomplishing further purification. Although other reactive metals with high boiling points such as cerium, zirconium, and thorium can be utilized, lanthanum is the more popular and the classically accepted reductant in the metallurgical preparation of the particular group of rare earth metals with which we have been concerned.

It will be of interest to have a look at Figure 7.7 which shows, in essence, the various methods adopted to produce an industrially important rare earth-based alloy system.

7.7 CONCLUSION

The rare earths industry is one of the most fascinating and challenging industries in the world. The industry is a fast moving one that is regularly shaken up by swings in supply and demand and the appearance of new applications. China, at present, is by far the largest producer and exporter of all kinds of rare earths products; it is also the second largest consumer of the rare earths in the world. At present about 75% of the rare earths consumed in the world originate in China. China will continue to dominate the supply of the rare earths in the international market in the future. Information about the rare earths in China

is disseminated by China Rare Earths Information, an important organization located in Baotou, Inner Mongolia, P.R. China. This region in China is reputed to be endowed with exceptionally rich resources of the rare earths and to have the necessary infrastructure for rare earths products development. At the present time, challenges facing the Chinese production of the rare earths include limited funds, marketing/distribution arrangements, and preference for domestic production equipment.

In the future, attention will be focused on new rare earth materials that will be in phase with the rapid growth and development of hi-tech industries, especially information technology. Among the emerging rare earths materials, the potential of sulfides as good candidates for plastic coloration represents a very striking example of new developments as regards the uses of rare earths compounds. It may be mentioned in this context that very few yellow to red inorganic pigments are in use at present besides cadmium sulfoselenides and lead molybdates. Organic substitutes have limitations such as those pertaining to thermal stability and ultraviolet stability. Concerted research has gone into the development of red pigments for plastic coloration based on safe materials, and in this respect the rare earths have a considerable advantage since they are nontoxic elements. The choice of a rare earth sulfide matrix is a consequence of its desirable intrinsic optical properties. In this context it is important that one recognizes and accepts the fact that the path can often be a long one before such intrinsic properties can be made amenable for commercial exploitation, eventually leading to large scale applications.

This concluding chapter, which has captured in one shot a portrait of the rare earths may be brought to conclusion with a final salutation to these fantastic elements. They are in the limelight today and hold the promise of continuing to be so in the days to come. The prevailing status and the projected future of the rare earths are all due to their special properties, which can be put to good use in the service of humankind. Rare earth magnetic materials, rare earth hydrogen storage materials, rare earth phosphors, rare earth magnetostrictive materials, rare earth magnetic refrigeration materials, the applications of the rare earths in agriculture and in low energy lighting, and some others have already made significant progress. The emergence of neodymium–iron–boron ($Nd_2Fe_{14}B$) magnets, for example, has resulted in a dramatic improvement in permanent magnet performance because these magnets have a magnetic energy product up to an order of magnitude higher than those of Alnico and ferrite magnets. Let us all, belonging to different institutions and organizations the world over, join to work with a common goal to make the rare earths dream come true.

This sojourn, starting with an introduction to mineralogy, occurrences and resources processing, then moving to applications along with a general description with regard to polishing powders, and finally to extraction, with the text sequence diverted at some point to deal generally with radiation, all interwoven into one presentation, should prove to be as interesting and enjoyable to the readers as it has been to the authors.

References

Aamland, E., MacDonald, D.J., and Kerterke, D.G. (1973) Molten salt electrowinning of magnesium–yttrium alloys, Bureau of Mines Report of Investigations 7722, U.S. Department of the Interior, Washington, D.C.

Achard, J.C. (1957) Separation de certains elements des terres rares par voie seche. Application au samarium et a l' europium, *CR Acad. Sci.*, 245: 1064–1066.

Adams, J.W. (1971) In Parker, J.G. and Baroch, C.T. (eds.), *The Rare Earth Elements, Yttrium and Thorium — A Materials Survey*, pp. 22–39, Bureau of Mines Information Circular 8476, U.S. Department of the Interior, Washington, D.C.

Adams, J.W. and Staatz, M.H. (1973) Rare earth elements, United States mineral researches, U.S. Geol. Survey Prof. Paper 820: 547–556.

Agarwal, J.C., Loreth, J.M., and Katrak, F.E. (1988) Economics of production of rare earth metals alloys. In Bautista, R.G. and Wong, M.M. (eds.), *Rare Earths,* pp. 281–289, The Minerals, Metals and Materials Society, Warrendale, PA.

Alcock, C.B. (1976) *Pyrometallurgy*, pp. 239–239, Academic Press, New York.

Alford, N.M. (1992) Applications of high temperature superconductors, *Chemistry & Industry* (2 November 1992): 808–812.

Altschuler, Z.S., Berman, S., and Cuttitta, F. (1967) Rare earths in phosphorites — geochemistry and potential recovery, U.S. Geol. Survey Prof. Paper 575B: B1–B9.

Anable, W.E. (1970) Purification of vanadium by vacuum melting, *J. Vac. Sci. Technol.*, 7(6): 574–581.

Anable, W.E. and Beall, R.A. (1965) Electron beam melting of yttrium, U.S. Bureau of Mines Report of Investigations 6661, U.S. Department of the Interior, Washington, D.C.

Anderson, L. (1986) Occurrence and processing of rare earth minerals, *Erzmetall*, 39(4): 152–157.

Anderson, I.E., Osborne, M.G., Takeya, H., and Gschneidner, Jr., K.A. (1993) Gas atomized $ErNi_3$ powder for cryocooler applications. In *Proceedings of the 7th International Cryocooler Conference*, Santa Fe, New Mexico, 17–19 Nov., pp. 1120–1132, 1992, Phillips Laboratory, Air Force Material Command, Kirtland Air Force Base, New Mexico.

Anderson, R.N. and Parlee, N.A.D. (1976) Carbothermic reduction of refractory metals, *J. Vac. Sci. Technol.*, 13: 526–529.

Anonymous (1989) Magnetic refrigeration, *Supercond. Ind.*, 2: 34–41.

Aplan, F.F. (1988) The processing of rare earth minerals. In Bautista, R.G. and Wong, M.M. (eds.), *Rare Earths*, pp. 15–34, The Minerals, Metals and Materials Society, Warrendale, PA.

Appleton, D.B. and Selwood, P.W. (1941) Fractional partition of the rare earths, *J. Am. Chem. Soc.*, 63: 2029.

Argall Jr., G.O. (1980) Three iron ore bodies of Bayan Obo, *World Min.*, 33(1): 38–46.

Audrieth, L.F. (1939) Preparation of amalgams. In Booth, H.S. (ed.), *Inorganic Syntheses*, Vol. 1, Chapter 2, McGraw Hill, New York.

Audrieth, L.F., Jukkola, E.E., Meints, R.E., and Hopkins, B.S. (1931) Observations on the rare earths XXXVII. Electrolytic preparation of rare earth amalgams — Preparation of amalgam of lanthanum and neodymium, *J. Am. Chem. Soc.*, 53: 1805–1809.

Auzel, F. and Goldner, P. (1999) Rare earth ions in the glass amplifying medium: a proposal for new doping precursors, *Materials Science Forum*, 315–317: 34–41.
Awasthi, A., Krishnamurthy, N., Bhatt, Y.J., Venkataramani, R., and Garg, S.P. (1998) Refining of tantalum by silicon deoxidation, *J. Alloys and Compounds*, 265: 190–195.
Bagchi, D.C. (1988) The use of rare earths in cinema arc carbons. In Gupta, C.K. and Krishnan, T.S. (eds.), *Rare Earths — Applications and Technology*, pp. 265–268, Trans Tech Publications, Switzerland.
Banks, C.V., Carlson, O.N., Daane, A.H., Fassel, V.A., Fisher, D.W., Olsen, E.H., Powell, J.E., and Spedding, F.H. (1959) Studies on the preparation, properties and analysis of high purity yttrium oxide and yttrium metal at the Ames Laboratory, IS-1, National Technical Information Service, Springfield, Virginia.
Barghusen, J.J. and Smutz, M. (1958) Processing of monazite sands, *Ind. Eng. Chem.*, 50: 1754–1755.
Bashir, V.S. (1988) Monazite, the basic raw material for rare earths beneficiation from beach sands. In Gupta, C.K. and Krishnan, T.S. (eds.), *Rare Earths — Applications and Technology*, pp. 33–44, Trans Tech Publications, Switzerland.
Bauer, D.J. (1959) Development of equipment and processes for extracting cerium (IV), Bureau of Mines Report of Investigations 5536, U.S. Department of the Interior, Washington, D.C.
Bauer, D.J. and Lindstrom, R.E. (1964) Naphthenic acid solvent extraction of rare earth sulphates, Bureau of Mines Report of Investigations 6396, US Department of the Interior, Washington, D.C.
Bauer, D.J. and Lindstrom, R.E. (1971) Differential extraction of rare earth elements in quaternary ammonium salt chelating agent systems, Bureau of Mines Report of Investigations 7524, US Department of the Interior, Washington, DC.
Bauer, D.J., Rice, A.C., and Berber, J.S. (1960) Liquid–liquid extraction of rare earth elements, Bureau of Mines Report of Investigations 5570, U.S. Department of the Interior, Washington, D.C.
Bautista, R.G. (1995) Separation chemistry. In Gschneidner, Jr., K.A. and Eyring, L. (eds.), *Handbook on the Physics and Chemistry of Rare Earths*, Vol. 21, pp. 1–28, North Holland, Amsterdam.
Beaudry, B.J. and Gschneidner, Jr., K.A. (1978) Preparation and basic properties of rare earth metals. In Gschneidner, Jr., K.A. and Eyring, L. (eds.), *Handbook on the Physics and Chemistry of Rare Earths*, Vol. 1, pp. 173–232, North Holland, Amsterdam.
Beaudry, B.J. and Palmer, P.E. (1974) The use of inert atmospheres in the preparation and handling of high purity rare earth metals. In Haschke, J.M. and Eick, H.A. (eds.), *Proc. 11th Rare Earth Research Conf.*, Traverse City, Michigan, Conf-741002, Part 2, pp. 612–620, National Technical Information Service, Springfield, Virginia.
Beaudry, B.J., Palmer, P.E., and Gschneidner, Jr., K.A. (1983) The effect of fluoride preparation on the purity of the rare earth metals, *J. Less Common Metals*, 93: 277.
Bednorz, J.G. and Muller, K.A. (1986) Possible high-T_c superconductivity in the Ba–La–Cu–O system, *Z. Phys. B Condensed Matter*, B64: 189–193.
Benz, M.G. and Martin, D.L. (1970) Cobalt–samarium permanent magnets prepared by liquid phase sintering, *Appl. Physics Lett.*, 17(4): 176–177.
Berber, J.S., Shaw, V.E., Rice, A.C., Lindstrom, R.E., and Bauer, D.J. (1960) Technology of bastnasite, Bureau of Mines Report of Investigations 5599, U.S. Department of the Interior, Washington, D.C.
Billy, M. and Trombe, F. (1931) Préparation de cerium pur, *Compt. Rend.*, 193: 421–423.
Block, F.E. and Campbell, T.T. (1961) Rare earth and yttrium halides for metal production – chlorides, bromides and iodides. In Spedding, F.H. and Daane, A.H. (eds.), *The Rare Earths*, p. 89–101, John Wiley, New York.
Block, F.E., Campbell, T.T., Mussler, R.E., and Robidart, G.B. (1960) Preparation of high purity yttrium by metallic reduction of yttrium trichloride, Bureau of Mines Report of Investigations 5588, U.S. Department of the Interior, Washington, D.C.
Bobeck, A.H., Spencer, E.G., Van Vitiert, L.G., Abrahams, S.C., Barns, R.L., Grodkiewicz, H., Sherwood, R.C., Schmidt, P.H., Smith, D.H., and Walters, E.M. (1970) Uniaxial magnetic garnets for domain wall "bubble" devices, *Appl. Phys. Lett.*, 17: 131–134.
Bochinski, J., Smutz, M., and Spedding, F.H. (1953) Separation of individual rare earths by liquid–liquid extraction from multicomponent monazite rare earth nitrates I. Undiluted TBP and concentrated aqueous rare earth nitrate systems at low acid concentrations, U.S. Atomic Energy

Commission Report ISC-348, National Technical Information Service, Springfield, Virginia.
Bochinski, J., Smutz, M., and Spedding, F.H. (1958) Separation of monazite rare earths by solvent extraction, *Ind. Eng. Chem.*, 50: 157–160.
Bose, D.K., Mehra, O.K., and Gupta, C.K. (1985) Preparation of rare earth–iron–silicon alloys by metallothermic reduction, *J. Less Common Metals*, 110: 239–242.
Brandle, C.D. and Valentino, A.J. (1972) Czochralski growth of rare earth–gallium garnets, *J. Cryst. Growth*, 12: 3–8.
Brandle, C.D., Miller, D.C., and Nielsen, J.W. (1972) The elimination of defects in Czochralski grown rare earth–gallium garnets, *J. Cryst. Growth*, 12: 195–200.
Bratland, D. and Gschneidner, Jr., K.A. (1980) Electrorefining and electrowinning of gadolinium in a molten fluoride electrolyte purified by pre-electrolysis, *Acta Chemica Scandinavica*, A 34, 683–686.
Bratland, D.G., Boe, H., and Grjotheim, K. (1973) On electrowinning of yttrium-aluminium and yttrium - magnesium alloys from molten fluorides, *Rev. Chim. Miner.*, 10: 347–353.
Bratland, D., Boe, G.H., Grjotheim, K., Rensvik, H., and Aamland, E. (1972) Some introductory investigations on electrolytic deposition of Y–Al and Y–Mg alloys, *Rev. Roum. Chim.*, 17(1–2): 41–48.
Brewer, L. and Rosenblatt, G.M. (1962) Thermodynamics of suboxide vaporization, *Trans. AIME*, 224: 1268–1271.
Bril, K.J. (1964) In Eyring, L. (ed.) *Progress in the Science and Technology of Rare Earths*, Vol. 1, pp. 30–61, Pergamon, Oxford.
Brown, C.G. and Sherrington, L.G. (1979) Solvent extraction used in industrial separation of rare earths, *J. Chem. Technol. Biotechnol.*, 29: 193–209.
Brugger, W. and Greinacher, H. (1967) A cracking process for rare earth ores by direct chlorination at high temperature on a production scale, *J. Metals*, 19(12): 32–35.
Buckingham, S., Maheswaren, J., Meehan, B., and Peverill, K. (1999) The role of applications of rare earth elements in enhancement of crop and pasture production, *Materials Science Forum*, 315–317: 339–347.
Bureau of Mines Staff (1975) Classification of Resources. In Mineral Facts and Problems, 1975 Edition, pp. 16–17, Bureau of Mines, U.S. Department of the Interior, Washington, D.C.
Buschow, K.H.J. (1984) Hydrogen absorption in intermetallic compounds. In Gschneidner, Jr., K.A. and Eyring, L. (eds.), *Handbook on the Physics and Chemistry of Rare Earths*, Vol. 6, pp. 1–112, North Holland, Amsterdam.
Buschow, K.H.J. (1988) Magnetooptical properties of alloys and intermetallic compounds. In Wohlforth, E.P. and Buschow, K.H.J. (eds.), Vol. 4, p. 595, Ferromagnetic Materials, North Holland, Amsterdam.
Buschow, K.H.J., Luiten, W., Nastepad, P.A., and Westendorp, F.F. (1968) Magnet material with $(BH)_{max}$ of 18 million Gauss Oersteds, *Philips Tech. Rev.*, 29: 336.
Caiquan, Li, Zeguang, T., and Zaizhang, L. (1985) Rare earth ferrosilicon alloy. In Xu Guangxian and Xiao Jimei (eds.), *New Frontiers in Rare Earth Science and Application*, pp. 1190–1193, Vol. II, Science Press, Beijing.
Callow, R.J. (1967) *The Industrial Chemistry of Lanthanum, Yttrium, Thorium and Uranium*, pp. 108–119, Pergamon, New York.
Campbell, T.T. and Block, F.E. (1959) Europium and samarium reduction, *J. Metals*, 11, 744–746
Canneri, G. and Rossi, A. (1932) On the preparation of metallic praseodymium, *Gazz. Chim. Ital.*, 62: 1160–1163.
Cannon, J.G. (1974) Rare earth elements and metals. In Considine, D.M. (ed.), *Chemical and Process Technology Encyclopedia*, pp. 961–969, McGraw Hill, New York.
Carbonneau, C. and Carbon, J.C. (1965) The production of pyrochlore concentrates at St. Lawrence columbium and metals corporation, *CIM Trans.*, 68: 71–79.
Carlson, O.N. and Schmidt, F.A (1961) Preparation of the rare earth fluorides. In Spedding, F.H. and Daane, A.H. (eds.), *The Rare Earths*, pp.79–88, John Wiley, New York.
Carlson, O.N. and Schmidt, F.A. (1961a) Metallothermic preparation of yttrium metal. In Spedding, F.H. and Daane, A.H. (eds.), *The Rare Earths*, pp.113–125, John Wiley, New York.
Carlson, O.N. and Schmidt, F.A. (1967) Metallurgy Division Research and Development Report IS-1600, p. M-10, Ames Laboratory, USAEC, Iowa State University, Ames, IA, National Technical Information Service, Springfield, Virginia.
Carlson, O.N. and Schmidt, F.A. (1976) Electrotransport of solutes in rare earth metals. In Lundin,

C.E. (ed.), *Proc. 12th Rare Earth Research Conference*, 18–22 July, 1976, Vail, Colorado, pp. 460–469, University of Denver, Denver Research Institute.
Carlson, O.N., Haefling, T.A., Schmidt, F.A., and Spedding, F.H. (1960) Preparation and refining of yttrium metal by Y–Mg intermediate alloy process, *J. Electrochem. Soc.*, 107: 540–545.
Carlson, O.N., Schmidt, F.A., and Peterson, D.T. (1966) Electrotransport of interstitial atoms in yttrium, *J. Less Common Metals*, 10: 1–11.
Carlson, O.N., Schmidt, F.A., and Peterson, D.T. (1973) Purification of rare earth metals by electrotransport. In Kevane, C.J. and Moeller, T. (eds.) (1973) *Proc. 10th Rare Earth Research Conf.*, pp. 701–710, Carefree, AZ, May 1973, Conf-730402, P2, National Technical Information Service, Springfield, Virginia.
Carlson, O.N., Schmidt, F.A., and Spedding, F.H. (1956) Preparation of yttrium metal by reduction of yttrium trifluoride with calcium**,** Report ISC-744, U.S. Atomic Energy Commission, National Technical Information Service, Springfield, Virginia.
Cech, R.E. (1974) Cobalt–rare earth intermetallic compounds produced by calcium hydride reduction of oxides, *J. Metals*, 26(2): 32–35.
Chambers, M.F. and Murphy, J.E. (1988) Molten salt electrolysis of neodymium from a chloride electrolyte. In Bautista, R.G. and Wong, M.M. (eds.), *Rare Earths*, pp. 369–376, The Minerals, Metals and Materials Society, Warrendale, PA.
Chang, W.C. and Hsing, D.M. (1996) Magnetic properties and transmission electron microscopy microstructures of exchange coupled $Nd_{12-x}Fe_{82+x}B_6$ melt spun ribbons, *J. Appl. Phys.*, 79(8, Pt. 2A): 4843–4845.
Charlot, G. (1976) Process for treatment of pyrochlore concentrates, U.S. Patent 3,947,542.
Chem. Eng. (1953) Rare earths now medium rare, *Chem. Eng.*, 60(1): 120–124.
Chem. Eng. News (1965) 43(19): 78.
Clark, A.E. (1979) Magnetostrictive RFe_2 intermetallic compounds. In Gschneidner, Jr., K.A. and Eyring, L. (eds.), *Handbook on the Physics and Chemistry of Rare Earths*, Vol. 2, pp. 231–258, North Holland, Amsterdam.
Clark, A.E. and Belson, H.S. (1972) Giant room temperature magnetostriction in $TbFe_2$ and $DyFe_2$, *Phys. Rev. B*, 5: 3642–3644.
Clark, A.L. and Zheng, S. (1991) China's rare earth potential, industry and policy. In Siribumrungsukha, B., Arrykul, S., Sanguan Sai, P., Pungrassami, T., Sikong, L., and Kooptarnon, K. (eds.), *Proc. Int. Conf. Rare Earth Minerals and Minerals for Electronic Uses*, Jan. 1991, Hat Yai, Thailand, pp. 577–662, Prince of Songkla University, Thailand.
Clark, A.L. and Zheng, S. (1991) *Materials Science Forum*, 8: 577.
Coehoorn, R., Duchateau, J.P.W.B., and Denissen, C.J.M. (1989) Permanent magnet materials based on neodymium iron carbide ($Nd_2Fe_{14}C$) prepared by melt spinning, *J. Appl. Phys.*, 65(2): 704–709.
Coey, J.M.D., Hong Sun and Hurley, D.P.F. (1991) Intrinsic magnetic properties of new rare earth iron intermetallic series, *J. Mag. Magnetic Mat.*, 101: 310–316.
Collins, J.F., Calkins, V.P., and McGurty, J.A. (1961) Applications of rare earths to ferrous and nonferrous alloys. In Spedding, F.H. and Daane, A.H. (eds.), *The Rare Earths*, pp. 499–511, John Wiley, New York.
Collocott, S.J., Dunlop, J.B., Lovatt, H.C., and Ramsden, V.S. (1999) Rare earth permanent magnets: new magnet materials and applications, *Materials Science Forum*, 315–317: 77–83.
Coon, V.T., Wallace, W.E., and Craig, R.S. (1978) Methanation by rare earth intermetallic catalysts. In McCarthy, G.J. and Rhyne, J.J. (eds.), *The Rare Earths in Modern Science and Technology*, Vol. 1, Plenum, New York.
Crawford, M.K., and Brixner, L.M. (1991) Phospholuminable phosphorus for x-ray imaging: applications and mechanisms, *J. Lumin.*, 488, 49: 37.
CREI (1998) Rare earth industry in Baotou, China Rare Earth Information, 4(5): October 1998.
Croat, J.J. (1969) The preparation of high purity dysprosium, holmium and erbium by the lithium reduction of their trichloride salts, Report No. IS-T-346, Ames Laboratory, ERDA, Iowa State University, Ames, IA, National Technical Information Service, Springfield, Virginia.
Croat, J.J. (1989) Manufacture of Nd–Fe–B permanent magnets by rapid solidification, *J. Less Common Metals*,148: 7–15.
Croat, J.J. (1998) The current status of bonded NdFeB permanent magnets. In *Preprints of the Conference, China Magnets*, held on 18–21 October 1998 at Beijing, PR China.
Croat, J.J., Herbst, J.F., Lee, R.W., and Pinkerton, F.E. (1984) High energy product Nd–Fe–B

permanent magnets, *Appl. Phys. Lett.*, 44: 148–149.
Croat, J.J., Herbst, J.F., Lee, R.W., and Pinkerton, F.E. (1984a) Pr–Fe and Nd–Fe based materials: A new class of high performance permanent magnets, *J. Appl. Phys.*, 55: 2078–2082.
Cross, W.M. and Miller, J.D. (1988) Bubble attachment time measurements for selected rare earth phosphate minerals in oleate solutions. In Bautista, R.G. and Wong, M.M. (eds.), *Rare Earths*, pp. 45–55, The Minerals, Metals and Materials Society, Warrendale, PA.
Cuthbertson, R.E. (1952) Froth flotation of monazite from heavy gravity minerals, U.S. Patent 2,610,738.
Daane, A.H. (1961) Metallothermic preparation of rare earth metals. In Spedding, F.H. and Daane, A.H. (eds.), *The Rare Earths*, Wiley, New York, pp. 102–112.
Daane, A.H. (1961a) Yttrium. In Hampel, C.A. (ed.), *Rare Metals Handbook*, pp. 653–666, Reinhold, New York.
Daane, A.H. and Spedding, F.H. (1953) Preparation of yttrium and some heavy rare earth metals, *J. Electrochem. Soc.*, 100: 442–444.
Daane, A.H., Dennison, D.H., and Spedding, F.H. (1953) The preparation of samarium and ytterbium metals, *J. Amer. Chem. Soc*., 75: 2272–2273.
Das, D.K. (1969) Twenty million energy product samarium–cobalt magnet, *IEEE Trans Magn.*, MAG-5: 214–216.
Davies, K.E. (1981) Industrial applications of pure rare earth metals and related alloys. In Gschneidner, Jr., K.A. (ed.), *Industrial Applications of Rare Earth Elements*, pp. 165–175, ACS Symposium Series 164, American Chemical Society, Washington, D.C.
Dayton, S.H. (1958) Radioactive black sand is yielding columbite concentrate at Idaho Mill, *Min. World*, 20(5): 36–41.
De Boer, J.H. and Fast, J.D. (1940) Electrolysis of solid solutions of oxygen in metallic zirconium, *Rec. Trav. Chim.*, 59: 161.
de Rhoden, C. and Peltier, M. (1957) U.S. Patent 2,783,125.
Decroly, C., Tytgat, D., and van Impe, J. (1953) Preparation of misch metal by thermal reduction, *J. Electrochem. Soc.*, 100: 388–391.
Dennison, D.H., Tschetter, M.J., and Gschneidner, Jr., K.A. (1966) The solubility of tantalum in eight liquid rare earth metals, *J. Less Common Metals*, 10: 108–115.
Dennison, D.H., Tschetter, M.J., and Gschneidner, Jr., K.A. (1966a) The solubility of Ta and W in liquid rare earth metals, *J. Less Common Metals*, 11: 423–435.
Desai, G.C. (1988) Use of rare earths in paints and pigments, *Materials Science Forum*, 30: 259–264.
Diatloff, E., Asher, C.J., and Smith, F.W. (1999) The effect of rare earth elements on the growth and nutrition of plants, *Materials Science Forum*, 315–317: 354–360.
Domazer, H.G. (1976) In Strnat, K.J. (ed.), Proc. 2nd Int. Workshop on R–Co Permanent Magnets, pp. 348–363, University of Dayton, Dayton.
Douglas, D.A. and Bauer, D.J. (1959) Liquid–liquid extraction of cerium, Bureau of Mines Report of Investigations 5513, U.S. Department of the Interior, Washington, D.C.
Drew, L.J., Qingrun, M., and Weijun, S. (1991) The geology of Bayan Obo iron–rare earth–niobium deposits, Inner Mongolia, China. In Siribumrungsukha, B., Arrykul, S., Sanguan Sai, P., Pungrassami, T., Sikong, L., and Kooptarnon, K. (eds.), *Proc. Int. Conf. Rare Earth Minerals and Minerals for Electronic Uses*, Jan. 1991, Hat Yai, Thailand, Prince of Songkla University, Thailand, pp. 13–31.
Duncan, L.K. (1970) Cerium oxide for glass polishing, *Glass Industry*, 41: 387–393.
Eastman, E., Fontana, B., Thurmond, C., and Wilmarth, W. (1955) The preparation of cerium by electrolysis of molten salts, U.S. Atomic Energy Commission Report TID-5212, National Technical Information Service, Springfield, VA.
Ellingham, H.J.T. (1944) Reducibility of oxides and sulphides in metallurgical processes, *J. Soc. Chem. Ind*., 63: 125–133.
Emley, E.F. (1966) *Principles of Magnesium Technology*, Pergamon, Oxford.
Evans, J.R. (1966) California's Mountain Pass mine now producing europium oxide, *Mineral Information Service*, 18(2): 23–32.
Eyring, L. and Cunningham, B. (1948) In Chemistry Division Quarterly Report for September, October and November 1948, US Atomic Energy Commission Report UCRL-264, National Technical Information Service, Springfield, VA.
Falconnet, P.G. (1988) Rare earths production and marketing opportunities. In Gupta, C.K. and Krishnan, T.S. (eds.), *Rare Earths — Applications and Technology,* pp. 1–12, Trans Tech

Publications, Switzerland.
Fangji, L., Juing, W., and Xinglan, Z. (1988) A process for the recovery of RE minerals with a chelating collector. In Bautista, R.G. and Wong, M.M. (eds.), *Rare Earths*, pp.71–79, The Minerals, Metals and Materials Society, Warrendale, PA.
Farr, M.B. (1982) Rare earths, *Min. Ann. Rev.*, 94–95.
Ferron, C.J., Bulatovic, S.M., and Slater, R.S. (1991) Beneficiation of rare earth oxide minerals. In Siribumrungsukha, B., Arrykul, S., Sanguan Sai, P., Pungrassami, T., Sikong, L., and Kooptarnon, K. (eds.), *Proc. Int. Conf. Rare Earth Minerals and Minerals for Electronic Uses*, Jan. 1991, Hat Yai, Thailand, pp. 251–269, Prince of Songkla University, Thailand.
Fischer, W., Dietz, W., and Jubermann, O. (1937) Ein neues Verfahren zur Trennung der seltenen Erden, *Naturwissenschaften*, 25: 348.
Fisher, G. (1988) Superconductor mysteries unravel as developments proceed, *Am. Ceram. Soc. Bull.*, 67: 725–735.
Fisher, R.W. and Olson, D.G. (1959) Vibrating tray hydrofluorination furnace, AEC Document IS-2 (July 1959), National Technical Information Service, Springfield, VA.
Fjellvag, H., Karen, P., Kjekshus, A., Lyng, S., and Bratten, O. (1988) Is mutual separation of rare earth elements crucial for preparation of high T_c materials?, *Physica C*, 153–155: 1421–1422.
Fleck, D.C., Kleespies, E.K., and Kesterke, D.G. (1973) Purification of yttrium by electrorefining, U.S. Bureau of Mines Report of Investigations 7710, U.S. Department of the Interior, Washington, D.C.
Foltyn, S.R., Tiwari, P., Dye, R.C., Le, M.Q., and Wu, X.D. (1993) Pulsed laser deposition of thick $YBa_2Cu_3O_{7-\delta}$ films with $J_c \geq 1$ MA/cm^2, *Appl. Phys. Lett.*, 63: 1848–1850.
Foos, R.A. and Wilhelm, H.A. (1954) Separation of yttrium and some rare earths by liquid–liquid extraction, U.S. Atomic Energy Commission Report ISC–695, National Technical Information Service, Springfield, VA.
Fort, D. (1987) The purification and crystal growth of rare earth metals using solid state electrotransport, *J. Less Common Metals*, 134: 45–65.
Fort, D., Beaudry, B.J., and Gschneidner, Jr., K.A. (1987) The ultrapurification of rare earth metals, gadolinium and neodymium, *J. Less Common Metals*, 134: 27–44.
Fort, D., Beaudry, B.J., and Gschneidner, Jr., K.A. (1990) Solid state electrotransport purification of erbium, *J. Less Common Metals*, 134: 27–44.
Fort, D., Jones, D.W., Beaudry, B.J., and Gschneidner, Jr., K.A. (1981) Zone refining of rare earth metals: lanthanum, cerium and gadolinium, *J. Less Common Metals*, 81: 273–292.
Foster, K.W., Pish, G., Schamp, H.W., Goode, J.M., and Eyles, T.E. (1952) Preparation of lanthanum metal by the de Boer process, Mound Laboratory, AEC Report MLM-686, National Technical Information Service, Springfield, VA.
Fox, G.J. (1996) High temperature superconductors open door to advanced technology, *Elements*, August/September 1996: 22–26.
Frey, E. (1876) Notice of the preparation of the earth metals in the chemical plant of Dr. Schuchardt in Gorlitz, *Ann*., 183: 367–368.
Fromm, E. and Horz, G. (1980) Hydrogen, nitrogen, oxygen and carbon in metals, International Materials Reviews, 25: 269–311.
Fuerst, C.D. and Brewer, E.G. (1990) Enhanced coercivities in die-upset Nd–Fe–B magnets with diffusion alloyed additives (Zn, Cu, and Ni), *Appl. Phys. Lett.*, 56: 2252–2254.
Fuerst, C.D. and Brewer, E.G. (1991) Diffusion alloyed additives in die-upset Nd–Fe–B magnets, *J. Appl. Phys*., 69: 5826–5828.
Fuerstenau, D.W. and Pradip, K. (1986) The role of inorganic and organic additives in bastnasite ore flotation. In *Flotation Heute*, Heft 48, pp. 19–38, GDMB, Clausthal–Zellerfeld, Germany.
Fujita, M. and Leepawpanth, Q. (1991) Thai–Japan research cooperation on the recovery of rare metals from tin tailings. In Siribumrungsukha, B., Arrykul, S., Sanguan Sai, P., Pungrassami, T., Sikong, L., and Kooptarnon, K. (eds.), *Proc. Int. Conf. Rare Earth Minerals and Minerals for Electronic Uses*, Jan. 1991, Hat Yai, Thailand, pp. 537–556, Prince of Songkla University, Thailand.
Garg, S.P. and Sundaram, C.V. (1974) Thermodynamics of sacrificial deoxidation, BARC Report 777, Bhabha Atomic Research Center, Bombay.
Garg, S.P. and Sundaram, C.V. (1975) Thermodynamics of C- and Al-deoxidation of refractory metals, BARC Report, 822, Bhabha Atomic Research Center, Bombay.
Garg, S.P., Venkataraman, M., Krishnamurthy, N., and Krishnan, R. (1996) Phase diagrams of binary

tantalum alloys, pp. 173–189, Indian Institute of Metals, Calcutta.
Ge, Z., Sun, C., and Luo, Y. (1998) Progress in preparing magnet alloy. In *Preprints of the Conference, China Magnets*, held on 18–21 October 1998 at Beijing, PR China.
Genshi, W., Daxin, Z., Deying, S., Xianglong, W., and Panwan, S. (1985) Chemical synthesis and hydrogen storage characteristics of misch metal–nickel compounds. In Xu Guangxian and Xiao Jimei (eds.), *New Frontiers in Rare Earth Science and Application*, pp. 1062–1065, Vol. II, Science Press, Beijing.
Goldschmidt, H.J. (1967) *Interstitial Alloys*, Plenum, New York.
Gray, P.M.J. (1951) The production of pure cerium metal by electrolytic and thermal reduction processes, *Trans. Inst. Min. Met.*, 61 (Oct. 1951–Sept. 1952): 141–170.
Greinacher, E. (1970) *Seltene Erden.* Chemische Technologie Vol. 2, Anorganische Technologie II, pp. 218–222, Hanser Verlag, Munich.
Greinacher, E. (1981) History of rare earth applications, rare earth market today: Overview. In Gschneidner, Jr., K.A. (ed.), *Industrial Applications of Rare Earth Elements*, pp. 3–18, ACS Symposium Series 164, American Chemical Society, Washington, D.C.
Greskovich, C.D., et al. (1992) Ceramic scintillators for advanced X ray detectors, *Ceram. Bull.*, 71: 1120–1126.
Greskovich, C. and Duclos, S. (1997) Ceramic scintillators. *Ann. Rev. Materials Science*, 27: 69–88.
Gruzensky, W.G. and Engel, G.T. (1959) Separation of yttrium and rare earth nitrates with the solvent extraction system tri-N-butylamine-3-methyl-2-butanone, *Trans. Met. Soc. AIME*, 215: 738–742.
Gschneidner, Jr., K.A. (1975) Derivation, extraction and preparation. In Horovitz, C.T. (ed.) *Scandium*, pp. 66–75, Academic Press, London.
Gschneidner, Jr., K.A. (1981) *Industrial Applications of Rare Earth Elements*, ACS Symp. Ser. 164, American Chemical Society, Washington, D.C.
Gschneidner, Jr., K.A. (1990) Physical properties of rare earth metals, *Bull. Alloy Phase Diagrams*, 11: 216–224.
Gschneidner, Jr., K.A. and Daane, A.H. (1988) Physical metallurgy. In Gschneidner, Jr., K.A. and Eyring, L. (eds.), *Handbook on the Physics and Chemistry of Rare Earths*, Vol. 11, pp. 409–484, North Holland, Amsterdam.
Gschneidner, Jr., K.A., Beaudry, B.J., and Capellen, J. (1995) Rare earth metals. In ASM Metals Handbook, pp. 720–732, ASM International, Metals Park, OH.
Gschneidner, Jr., K.A., Pecharsky, V.K., Pecharsky, A.O., and Zimm, C.B. (1999) Recent developments in magnetic refrigeration, *Materials Science Forum*, 315–317: 69–76.
Gschneidner, Jr., K.A., Takeya, H., Moorman, J.O., and Pecharsky, V.K. (1994a) $(Dy_{0.5}Er_{0.5})Al_2$: a large magnetocaloric effect material for low temperature magnetic refrigeration, *Appl. Phys. Lett.*, 64(2): 253–255.
Gschneidner, Jr., K.A., Takeya, H., Moorman, J.O., Pecharsky, V.K., Malik, S.K., and Zimm, C.B. (1994) New magnetic refrigeration materials for the liquifaction of hydrogen. In Kittel, P. (ed.), *Advances in Cryogenic Engineering*, Vol. 39, pp. 1457–1465, Plenum, New York.
Guertler, W. (1923) Molybdenum as a constituent in alloys, *Z. Metallkd.*, 15: 151–154.
Gunasekaran, N. (1988) Mixed rare earth oxides and their catalytic applications. In Gupta, C.K. and Krishnan, T.S. (eds.), *Rare Earths — Applications and Technology*, pp. 117–124, Trans Tech Publications, Switzerland.
Guo, A.H., Yu, X.J., and Li, W. (1998) Rare earth permanent magnets with low temperature coefficients. In *Preprints of the Conference*, *China Magnets*, 18–21 October 1998, Beijing, PR China.
Gupta, C.K. and Krishnamurthy, N. (1992) Extractive metallurgy of rare earths, International Materials Review, 37(5): 197–248.
Haberman, C.E. and Daane, A.H. (1961) Vapour pressure of rare earth metals, *J. Chem. Phys.*, 41: 2818–2827.
Haefling, J.A., Schmidt, F.A., and Carlson, O.N. (1961) A study of several metals as reductants for yttrium fluoride, Research and Development Report ISC-374, Ames Laboratory, USAEC, National Technical Information Service, Springfield Virginia.
Hampel, C.A. (ed.) (1961) *Rare Metals Handbook*, 2nd ed., pp. 1–14, Reinhold, London.
Harrah, H.W. (1967) Rare earth concentration at Molybdenum Corporation of America, Part 2, Solvent extraction plant, *Deco Trefoil*, 31(5): 9–16.
Harrison, E.E. (1952) Vapour pressure of some rare earth halides, *J. Appl. Chem.*, 2: 601–602.
Hart, K.P. and Levins, D.M. (1988) Management of wastes from the processing of rare earth minerals, *Chemca* 88.

Hartley, F.R. (1952) The preparation of anhydrous lanthanum chlorides by high temperature chlorination of monazite, *J. Appl. Chem.*, 2: 24–31.
Hashimoto, T., Numasawa, T., Shino, M., and Okada, T. (1981) Magnetic refrigeration in the temperature range from 10K to room temperature: the ferromagnetic refrigerants, *Cryogenics*, 21: 647–653.
Haskin, L.A. and Paster, T.P. (1979) Geochemistry and mineralogy of rare earths. In Gschneidner, Jr., K.A. and Eyring, L. (eds.), *Handbook on the Physics and Chemistry of Rare Earths*, Vol. 3, pp. 1–80, North Holland, Amsterdam.
Hatfield, W.E. and Miller, J.H. (1988) *High Temperature Superconducting Matrials Preparation, Properties and Processing*, Marcel Dekker, New York.
Haughten, J.L. and Prytherch, W.E. (1937) *Magnesium and its Alloys*, His Majesty's Stationary Office, London.
Heartling, G.H. (1981) PLZT electrooptic ceramics and devices. In Gschneidner, Jr., K.A. (ed.), *Industrial Applications of Rare Earth Elements*, pp. 3–18, 265–283, ACS Symposium Series 164, American Chemical Society, Washington, D.C.
Heartling, G.H., and Land, C.E. (1971) Hot pressed $(Pb,La)(Zr,Ti)O_3$ ferroelectric ceramics for optoelectronic applications, *J. Am. Ceram. Soc.*, 54: 1–11.
Hecht, H., Jander, G., and Schlapmann, H. (1947) The influence of thionyl chloride on oxides, *Z. anorg. Chem.,* 254, 259–264.
Hedrick, J.B. (1985) Rare earth elements and yttrium. In *Minerals Facts and Problems*, Bureau of Mines Bull. 675, pp. 647–664, U.S. Department of the Interior, Washington, D.C.
Hedrick, J.B. (1985a) Rare earth minerals and metals. In *Minerals Yearbook*, Vol. 1, pp. 791–803, U.S. Department of the Interior, Washington, D.C.
Hedrick, J.B. (1986) Rare earth minerals and metals. In *Minerals Yearbook*, Vol. 1, pp. 771–782, U.S. Department of the Interior, Washington, D.C.
Hedrick, J.B. (1988) Availability of rare earths, *Ceram. Bull.*, 67(5): 858–861.
Hedrick, J.B. (1991) Rare earths: The lanthanides, yttrium and scandium. *Minerals Yearbook 1991*, pp. 1211–1237, Vol. 1, Bureau of Mines, U.S. Department of the Interior, Washington, D.C.
Hedrick, J.B. (1992) Rare earths: The lanthanides, yttrium and scandium. *Minerals Yearbook 1992*, pp. 1035–1061, Bureau of Mines, U.S. Department of the Interior, Washington, D.C.
Hedrick, J.B. (1995) Rare earths. *Minerals Yearbook 1995*, Vol. 1, 1–11, Bureau of Mines, U.S. Department of the Interior, Washington, D.C.
Hedrick, J.B. (1997) Rare earth metal prices in the U.S. ca. 1960 to 1994, *J. Alloys and Compounds*, 250: 471.
Hedrick, J.B. (1998) Rare earths. Minerals yearbook 1998, Vol. 1, 61.1–61.14, U.S. Geological Survey, U.S. Department of the Interior, Washington, D.C.
Hedrick, J.B. (2000) Rare earths. *U.S. Geological Survey Minerals Yearbook 2000*, Vol. 1, 62.1–62.17, U.S. Department of the Interior, Washington, D.C.
Hedrick, J.B. (2001) Rare earths. *U.S. Geological Survey Minerals Yearbook 2001*, Vol. 1, 61.1–61.17, U.S. Department of the Interior, Washington, D.C.
Hedrick, J.B. (2002) Rare earths. *U.S. Geological Survey Minerals Yearbook 2002*, Vol. 1, 61.1–61.16, U.S. Department of the Interior, Washington, D.C.
Hedrick, J.B. (2004) Rare earths. U.S. Geological Survey, Mineral Commodity Summaries, January 2004.
Hedrick, J.B., Sinha, S.P., and Kosynkin, V.D. (1997) Loparite, a rare earth ore $(Ce, Na, Sr, Ca)(Ti,Nb,Ta,Fe^{3+})O_3$, *J. Alloys Compounds*, 250: 467.
Henderson, A.W., May, S.C., and Higbie, K.B. (1958) Chlorination of euxenite concentrates, *Ind. Eng. Chem.*, 50: 611–612.
Henrie, T.A. (1964) Electrowinning of rare earth and uranium metals from their oxides, *J. Metals*, 16: 978–981.
Henrie, T.A. and Morrice, E. (1966) A high temperature electrowinning cell for rare earths, *J. Metals*, 18: 1207–1208.
Herbst, J.F. and Croat, J.J. (1991) Neodymium–iron–boron permanent magnets, *J. Magn. Magn. Mater.*, 100: 57–78.
Herget, C. (1982) Production and properties of rare earth–cobalt permanent magnet alloy powders, *Met. Powder. Rep.*, 37(1): 34–36.
Herget, C. (1985) Metallurgical ways to NdFeB alloys, permanent magnets from coreduced NdFeB. In Strnat, K.J. (ed.), *Proc. 8th International Workshop on Rare Earth Magnets and their Applica-*

tions, 6–8 May 1985, University of Dayton, Magnetics, KL-365, Dayton, OH, pp. 407–422.
Herget, C. and Domazer, H.G. (1975) Methods for the production of rare earth–3d metal alloys with particular emphasis on the cobalt alloys, *Goldschmidt Informiert*, 4/75(35): 13–22.
Hicks, J.F.G. (1918) The preparation and properties of yttrium mixed metal, *J. Am. Chem. Soc.*, 40: 1619–1626.
Highley, D.E., Slater, D., and Chapman, G.R. (1988) Geological occurrence of elements consumed in the electronics industry, *Trans. Instn. Min. Metall.*, Section C, 97 (March 1988): C34–C41.
Hill, W.H. (1951) Rare Earth Inc. redredges Idaho gold placer for monazite, *Min. World*, 13(2): 12–14.
Hillebrand, W.F. and Norton, T.H. (1875) Electrolytic deposition of cerium, lanthanum and didymium, *Ann. Phys. U. Chem.*, 155: 633–639.
Hirsch, A. (1911) *Ind. Eng. Chem.*, 3: 880–896.
Hirsch, A. (1912) The preparation of metallic cerium, *J. Electrochem. Soc.*, 20, 57–102.
Hirschhorn, I.S. (1967) Commercial production of rare earth metals by fused salt electrolysis. In Koehler, W.C. (ed.), *Proc. 6th Rare Earth Research Conf.*, May 3–5, 1965, Gatlinberg, TN, Available on Report AFOSR–67–1214, National Technical Information Service, Springfield, Virginia, pp. 728–738.
Hirschhorn, I.S. (1968) Commercial production of rare earth metals by fused salt electrolysis, *J. Metals*, 20(3): 19–22.
Hirschhorn, I.S. and Klein, E.A. (1969) Rare earth metal and silicon alloys, German Patent 1,800,701 (April 30, 1969).
Holocombe, C.E., et al. (1982) Stable materials for fluorine rich environments, *Ind. Eng. Chem. Prod. Res. Dev.*, 21(4): 673–677.
Honshima, M. and Ohashi, K. (1994) High energy NdFeB magnets and their applications, *J. Materials Engineering and Performance*, 3(2): 218–222.
Hopkins, B.S. and Audrieth, L.F. (1934) The electrolysis of rare earth metal salts in nonaqueous solvents, *J. Electrochem. Soc.*, 66, 135–142.
Hopkins, B.S. and Quill, L.L. (1933) Use of non-aqueous solvents in the study of the rare earth group, *Proc. Natl. Acad. Sci. US*, 19: 64–68.
Horrigan, R.V. (1981) Rare earth polishing compounds. In Gschneidner, Jr., K.A. (ed.), *Industrial Applications of Rare Earth Elements*, pp. 95–100, ACS Symposium Series 164, American Chemical Society, Washington, D.C.
Houot, R., Cuif, J.P., Mottot, Y., and Samama, J.C. (1991) Recovery of rare earth minerals with emphasis on flotation process. In Siribumrungsukha, B., Arrykul, S., Sanguan Sai, P., Pungrassami, T., Sikong, L., and Kooptarnon, K. (eds.), *Proc. Int. Conf. Rare Earth Minerals and Minerals for Electronic Uses*, Jan. 1991, Hat Yai, Thailand, Prince of Songkla University, Thailand, pp. 301–324.
Huffine, C.L. and Williams, J.M. (1961) Refining and purification of rare earth metals. In Spedding, F.H. and Daane, A.H. (eds.), *The Rare Earths*, Wiley, New York, pp. 145–162.
Hukin, D.A. and Jones, D.W. (1976) Rare earths — a growth industry. In Lundin, C.E. (ed.), *Proc. 12th Rare Earth Research Conference*, 18–22 July, 1976, Vail, Colorado, pp. 891–904, University of Denver, Denver Research Institute, Denver.
Hultgren, R., Desai, P.D., Hawkins, D.I., Gleiser, M., and Kelley, K.K. (1973) Selected values of the thermodynamic properties of binary alloys, American Society for Metals, Metals Park, OH.
Hussin, K., Aziz, A., Ibrahim, M., and Sulaiman, M.Y. (1991) The content of rare earth elements in amang from selected mines in Malaysia. In Siribumrungsukha, B., Arrykul, S., Sanguan Sai, P., Pungrassami, T., Sikong, L., and Kooptarnon, K. (eds.), *Proc. Int. Conf. Rare Earth Minerals and Minerals for Electronic Uses*, Jan. 1991, Hat Yai, Thailand, Prince of Songkla University, Thailand. pp. 81–89.
Huston, E.L. and Sheridam, J.J. (1981) Applications for rechargeable metal hydrides. In Gschneidner, Jr., K.A. (ed.), *Industrial Applications of Rare Earth Elements*, pp. 223–250, ACS Symposium Series 164, American Chemical Society, Washington, D.C.
Ingraham, M.G. and Drowart, J. (1960) Mass spectrometry applied to high temperature chemistry, Proc. Symp. on High Temperature Technology, pp. 219–240, McGraw Hill, New York.
Ishikawa, H., Oguro, K., Kato, A., Suzuki, H., and Ishii, E. (1985) Microcapsulated rare earth–nickel hydride forming materials. In Xu Guangxian and Xiao Jimei (eds.), *New Frontiers in Rare Earth Science and Application*, pp. 1058–1061, Vol. II, Science Press, Beijing.
Ishikawa, H., Utsunomiya, T., Hatano, T., Hoshino, Y., and Sato, M. (1974) Preparation of samarium

metal by molten salt electrolysis with a fused zinc cathode, *Bull. Tokyo Inst. Technol.*, 20: 103–118.
Ito, T. (1991) The MMAJ rare earth R&D project. In Siribumrungsukha, B., Arrykul, S., Sanguan Sai, P., Pungrassami, T., Sikong, L., and Kooptarnon, K. (eds.), *Proc. Int. Conf. Rare Earth Minerals and Minerals for Electronic Uses*, Jan. 1991, Hat Yai, Thailand, Prince of Songkla University, Thailand, pp. 325–336.
Ivanovskii, L.E. and Ilyushchenko, E.G. (1961) Separation of rare earth metals by electrolysis of fused salt. Trudy Inst. Elektrokhim. Uralskogo Filiala Akad. Nauk SSSR, 2: 131–134.
Iya,V.K. (1953) Preparation of pure scandium, *CR Acad. Sci.*, 236: 608–610.
Jackson, W.D. and Christiansen, G. (1993) International Strategic Minerals Inventory Summary Report – Rare Earth Oxides, U.S. Geological Survey Circular 930-N, U.S.Geological Survey, Map Distribution, Denver CO.
Jantsch, G., Jawurek, H., Skalla, N., and Ganalouski, H. (1930) Halides of the rare earths VI. Halides of the terbium and erbium earth groups, *Z. anorg. allgem. Chem.*, 193: 391–405.
Jantsch, G., Skalla, N., and Jawurek, H. (1931) Halides of the rare earths V. The halides of ytterbium, *Z. anorg. allgem. Chem.*, 201: 207.
Jiles, D.C. (1994) The development of highly magnetostrictive rare earth iron alloys, *J. Phys. D., Appl. Phys.* 27: 1–11.
Jin, S., Sherwood, R.C., Gyorgy, E.M., Tiefel, T.H., van Dover, R.B., Nakahara, S., Schneemeyer, L.F., Fastnacht, R.A., and Davies, M.E. (1989) Large magnetic hysteresis in a melt textured Y–Ba–Cu–O superconductor, *Appl. Phys. Lett.*, 54:584–586.
Jin, S., Tiefel, T.H., Sherwood, R.C., Davies, M.E., van Dover, R.B., Kammlott, G.W., and Fastnacht, R.A. (1988) High critical currents in Y–Ba–Cu–O superconductors, *Appl. Phys. Lett.*, 52: 2074–2076.
Jones, D.W., Abell, J.S., Fort, D., and Hulbert, J.K. (1982) Preparation of rare earth materials, crystals and specimens, *J. Magn. Magn. Mater.*, 29: 20–30.
Jones, F.G., Doser, M., and Nezu, T. (1977) Hydrogen atmosphere sintering of cobalt–samarium magnets, *IEEE Trans. Magn.*, MAG-13: 1320–1322.
Jones, D.W., Fort, D., and Hukin, D.A. (1978) Zone refining of rare earth metals. In McCarthy, G.J. and Rhyne, J.J. (eds.), *The Rare Earths in Modern Science and Technology*, Vol. 1, pp. 309–314, Plenum Press, New York.
Jones, F.G., Thoe, J.H., Lehman, H.E., and Downs, R.B. (1976) Production of RCo_5 and R_2Co_7 powders by the R/D process. In Lundin, C.E. (ed.), *Proc. 12th Rare Earth Research Conferenc*e, 18–22 July, 1976, Vail, Colorado, pp. 1054–1062 University of Denver, Denver Research Institute, Denver.
Jonsson, A., Harris, D.R., Chang, R.Y., and Thomsen, O.J. (1992) Analysis of critical experiments with erbia–urania fuel. *Trans. Am. Nucl. Soc.*, 65: 415–417.
Jordon, R.G. and Jones, D.W. (1975) The purification of rare earth metals II. Solid state electrotransport purification of terbium, *J. Less Common Metals*, 42, 101–110.
Jost, W. (1952) *Diffusion in Solids, Liquids and Gases*, Academic, New York.
Jukkola, E.E., Audrieth, L.F., and Hopkins, B.S. (1934) Observations on the rare earths XLI. Electrolytic preparation of rare earth amalgams. 3. Amalgam of lanthanum, neodymium, cerium, samarium, and yttrium. Metallic lanthanum, neodymium and cerium by thermal decomposition of their amalgams, *J. Am. Chem. Soc.*, 56, 303–304.
Kaczmarek, J. (1981) Discovery and commercial separations. In Gschneidner, Jr., K.A. (ed.), *Industrial Applications of Rare Earth Elements*, ACS Symp. Ser. 164, American Chemical Soc., Washington D.C., 135–166.
Kallenbach, R. and Bungardt, W. (1969) Low phosphorus alloys of silicon with rare earth metals, German Patent 1,274,801 (March 13 1969).
Kanazawa, Y. and Miyawaki, R. (1991) Rare earth minerals and their crystal structures. In Siribumrungsukha, B., Arrykul, S., Sanguan Sai, P., Pungrassami, T., Sikong, L., and Kooptarnon, K. (eds.), *Proc. Int. Conf. Rare Earth Minerals and Minerals for Electronic Uses*, Jan. 1991, Hat Yai, Thailand, Prince of Songkla University, Thailand. pp. 43–79.
Kaneko, Y. and Ishigaki, N. (1994) Recent developments of high performance NEOMAX magnets, *J. Materials Engineering and Performance*, 3: 228–233.
Karl, A. (1934) Chemical preparation of cerium and its alloys, *Bull. Soc. Chim.*, 1: 871–877.
Kaschuk, V.A. and Svetlov, M.B. (1982) Investigation of some properties of VT5L alloy with rare earth additions. In Williams, J.C. and Belov, A.F. (eds.), *Titanium and Titanium Alloys —*

Scientific and Technological Aspects, Vol. III, pp. 2201–2208, Plenum Press, New York.
Kasey, J.B. (1959) British Patent 825,305.
Kennard, F.L. (1981) Oxygen sensors. In Gschneidner, Jr., K.A. (ed.), *Industrial Applications of Rare Earth Elements*, pp. 251–263, ACS Symposium Series 164, American Chemical Society, Washington, D.C.
Ketelle, B.H. and Boyd, G.E. (1947) The exchange absorption of ions from aqueous solutions by organic zeolites IV. The separation of yttrium group rare earths, *J. Am Chem. Soc.*, 69: 2800–2812.
Kilbourn, B.T. (1988) Metallurgical applications of yttrium and the lanthanides, *J. Metals*, 40(5): 22–25.
Kilbourn, B.T. (1990) Rare earths: Lanthanides and yttrium, *Amer. Ceram. Soc. Bull.*, 69: 874–877.
Kirchmayr, H.R. (1985) Magnetic properties of rare earth intermetallics. In Xu, Guangxian and Xiao, Jimei (eds.), *New Frontiers in Rare Earth Science and Applications*, pp. 879–886, Science Press, Beijing.
Kirchmayr, H.R. and Poldy, C.A. (1979) Magnetic properties of intermetallic compounds of rare earth metals. In Gschneidner, Jr., K.A. and Eyring, L. (eds.), *Handbook on the Physics and Chemistry of Rare Earths*, Vol. 2, pp. 55–230, North Holland, Amsterdam.
Kleber, E.V. and Love, B. (1963) *The Technology of Scandium, Yttrium and the Rare Earth Metals*, Pergamon, Oxford.
Kleirheksal, J.H. and Kremers, H.E. (1928) Observations on the rare earths XXIX: The preparation and properties of anhydrous rare earth chlorides, *J. Am. Chem. Soc.*, 50: 959–967.
Klemm, W. and Bommer, H. (1937) Contribution to the knowledge of the rare earths, *Z. anorg. allg. Chem.*, 231: 138–171.
Knudsen, I.E. and Levitz, N.M. (1959) Preparation of yttrium fluoride in fluidized beds, AEC Document ANL–6011.
Koch, C.W. (1953) Thermodynamics of the trichlorides and oxychlorides of some of the lanthanide and actinide elements (Thesis), UCRL–2286 (September 1953).
Koch, D.F.A. (1987) Rare earth extraction and separation. In Rare Earth Horizon 1987, *Proceedings of a Conference at National Measurement Laboratory*, April 1987, pp. 73–85, Lindfield.
Kohmoto, O., Yoneyama, T., and Yajima, K. (1987) Magnetic properties of rapidly quenched $Nd_{10}Fe_{85-x}T_xB_5$ (T = Zr, Nb) alloys, *Jap. J. Appl. Phys.*, Part 1, 26: 1804–1805.
Kojima, T. and Sato, M. (1954) Metallurgical research on cerium metal (part 10), Application: on the fused salt electrolysis of $CeCl_3$·2KCL–KCl eutectic mixture, *J. Electrochem. Soc. Japan*, 22, 303–306.
Koon, N.C., Schindler, A.I., and Carter, F.L. (1971) Giant magnetostriction in cubic rare earth iron compounds of the type RFe_2, *Phys. Lett.*, 37A: 413–414.
Koppiker, K.S. (1990) In Pai, B.C., Pillai, R.M., and Damodaran, A.D. (eds.), *Advances in Rare Earths Research*, Regional Research Laboratory, Trivandrum, pp. 47–53.
Kosynkin,V.D., Moiseev, S.D., Peterson, C.H., and Nikepelov, B.V. (1993) Rare earth industry in the Commonwealth of Independent States, *J. Alloys and Compounds*, 192: 118–120.
Kremers, H.E. (1925) The preparation and some properties of metallic neodymium, *Trans. Am. Electrochem. Soc.*, 47: 365–371.
Kremers, H.E. (1954) Rare earth metals. In Hampel, C.A. (ed.), *Rare Metals Handbook*, pp. 329–346, Reinhold, New York.
Kremers, H.E. (1953) Rare earth metals. In Kirk, R.E. and Othmer, D.F. (eds.), *Encyclopedia of Chemical Technology*, Vol. 11, pp. 503–521, Interscience, New York.
Kremers, H.E. (1961) Rare earth metals. In Hampel, C.A. (ed.), *Rare Metals Handbook*, 2nd edn., pp. 393–417, Reinhold, New York.
Kremers, H.E. and Stevens, R.G. (1923) Observations on the rare earths XIV. The preparation and properties of metallic lanthanum, *J. Am. Chem. Soc*., 45: 614–617.
Krikorian, O.H., and Curtis, P.G. (1988) Synthesis of CaS and interaction with molten metals, *High Temp. High. Proc.*, 20: 9.
Krishnamurthy, N., Kundu, T., Awasthi, A., and Garg, S.P. (2000) Derived thermodynamic properties and phase diagrams of the rare earth–tungsten systems, *Z. Metallkd.*, 91(3): 234–240.
Krismer, B. and Smetana, O. (1968) Alloys of silicon with scandium, yttrium, rare earth metals and thorium, Austrian Patent 259,881 (February 12, 1968).
Kroll, W.J. (1959) The present status of titanium extractive metallurgy, *Trans. Met. Soc. AIME*, 275: 546.

Kruesi, P.R. and Duker, G. (1965) Production of rare earth chloride from bastnasite, *J. Metals*, 17: 847–849.
Kruger, J. (1971) Extractive Metallurgy. In Winkler, O. and Bakish, R. (eds.) *Vacuum Metallurgy*, Elsevier, Amsterdam, pp. 145–335.
Krumholz, P. (1957) Brazilian practice for monazite treatment. In *Proc. Symp. Rare Metals*, Bombay, December 1957, pp. 78–82, The Indian Institute of Metals and Bhabha Atomic Research Centre.
Kryder, M.H. (1993) Magnetooptical storage media. In *Encyclopedia of Materials Science and Engineering*, Supplementary Volume 3, pp. 1773–1778, Pergamon, Oxford.
Kudo, Y. (1988) Industrial applications of rare earths in Japan. In Gupta, C.K. and Krishnan, T.S. (eds.), *Rare Earths — Applications and Technology*, pp. 243–258, Trans Tech Publications, Switzerland.
Kuroda, T. (1957) The preparation of lanthanum by fused salt electrolysis and its application, Denki Shikenjo Kenkyu Hokoku, 561, 103.
Laferty, J.M. (1951) Boride cathodes. *J. Appl. Phys.*, 22: 299–309.
Lee, R.W. (1985) Hot pressed neodymium–iron–boron magnets, *Appl. Phys. Lett.*, 46: 790
Lee, R.W., Brewer, E.G., and Schaffel, N.A. (1985) Processing of neodymium–iron–boron melt spun ribbons to fully dense magnets, *IEEE Trans. Magn. MAG*, 21: 1958–1963.
Lei, K.P.V., Cattoir, F.R., and Sullivan, T.A. (1967) Electrolytic process for producing ductile vanadium, Bureau of Mines Bulletin 6972, U.S. Dept. of the Interior, Washington, D.C. Lever, F.M. and Payne, J.B. (1968) Separation of the rare earth and production of the metals. In *Advances in Extractive Metallurgy*, The Institution of Mining and Metallurgy, London, pp. 789–804.
Lever, F.M. and Payne, J.B. (1968) Separation of the rare earth and production of the metals.In Advances in Extractive Metallurgy, pp. 789–804, The Institution of Mining and Metallurgy, London.
Levine, A.K. and Palilla, F.G. (1965) YVO_4:Eu, A new red emitting phosphor for colour television. *Trans. N.Y. Acad. Sci.*, Ser. II, 27: 517.
Li, W., Jiang, L., Wang, D., Sun, T., and Zhu, J. (1986) Rare-earth–transition-metal–boron permanent magnets with smaller temperature coefficients, *J. Less Common Metals*, 126: 95–100.
Liang, S., Hui, Y, Chen, F, Li, W., and Zhong, X. (1998) High performance NdFeB magnets. In *Preprints of the Conference*, *China Magnets*, held on 18–21 October 1998 at Beijing, PR China.
Lide, D.R. (1997) Abundance of elements in the earth's crust and sea, *CRC Handbook of Physics and Chemistry*, 78th edn, p. 14, CRC Press, Boca Raton, Florida.
Lindstrom, R.E. and Winget, J.O. (1962) Hydrogen as retaining ion for rare earth separation by ion exchange, Bureau of Mines Report of Investigations 6131, U.S. Department of the Interior, Washington, D.C.
Linebarger, H.F. and McCluhan, T.K. (1981) The role of rare earth elements in the production of nodular iron. In Gschneidner, Jr., K.A. (ed.), *Industrial Applications of Rare Earth Elements*, pp.19–42, ACS Symposium Series 164, American Chemical Society, Washington, D.C.
Little, H.F.V. (1921) In Friend, J.N. (ed.), *A Textbook of Inorganic Chemistry*, Charles Griffini, London, Chaps. 10–14.
Livingston, J. and Kent, H. (1946) The cerium metal and light flint industry in Germany and Austria, Final Report No. 909, Office of the Military Government for Germany, Field Information Agency, Technical, pp. 5–18.
Loonam, A.C. (1959) Principles and application of the iodide process, *J. Electrochem. Soc.*, 106, 3, 238.
Love, B. and Kleber, E.V. (1960) Rare earths: sixteen new metals are ready to use, *Mater. Des. Eng.*, 52(5): 134–137.
Lucas, B.H. and Ritcey, G.M. (1975) Examination of a rare earth solvent extraction circuit for possible upgrading of the thorium product, *CIM Bull.*, 68 (753): 124–130.
Lundin, C.E. (1961) Rare earth metal phase diagrams. In Spedding, F.H. and Daane, A.H. (eds.), *The Rare Earths*, Wiley, New York, pp. 224–385.
Lundin, C.E. (1973) The use of LaNi5 as a hydrogen source for fuelling a nonpolluting internal combustion engine. In Kevane, C.J. and Moeller, T. (eds.), *Proc. 10th Rare Earth Research Conf.*, pp. 662–669, Carefree, AZ, May 1973, Conf–730402, P1 and P2, National Technical Information Service, Springfield, Virginia.
Luo, J. and Clin, X. (1988) Selective flotation of fluorite, barite and calcite. In Xu, G. (ed.), *Proc. Int. Conf. Rare Earth Dev. & Appl.*, Vol. 1, pp. 67–70.
Luo, J. and Clin, X. (1985) A new development of mineral processing flowsheet for the treatment of

a complex ore containing Fe, rare earths, Nb and F, XVth ZMPC, Vol. 3, p. 474–485, Cannes, France.
Luyckx, L.A. (1981) The rare earth metals in steel. In Gschneidner, Jr., K.A. (ed.), *Industrial Applications of Rare Earth Elements*, pp. 43–78, ACS Symposium Series 164, American Chemical Society, Washington, D.C.
Mackey, T.S. (1986) Recent developments in U.S. rare earth technology. In Somasundaram, P. (ed.), *Advances in Mineral Processing*, pp. 509–534, Society of Mining Engineers Inc., Littletown, CO.
Magnetic refrigeration (1989) *Supercond. Ind.*, 2: 34–41.
Mahajan, Y.R. and Rama Rao, P. (1988) Rare earths in new materials. In Gupta, C.K. and Krishnan, T.S. (eds.), *Rare Earths — Applications and Technology*, pp. 125–146, Trans Tech Publications, Switzerland.
Mahn, F. (1950) *J. Recher. CNRS*, 10: 28–31.
Malunga, G.W.P., Samama, J.C., and Houot, R. (1991) Rare earth potential in Malawi. In Siribumrungsukha, B., Arrykul, S., Sanguan Sai, P., Pungrassami, T., Sikong, L., and Kooptarnon, K. (eds.), *Proc. Int. Conf. Rare Earth Minerals and Minerals for Electronic Uses*, Jan. 1991, Hat Yai, Thailand, pp. 193–203, Prince of Songkla University, Thailand.
Marchant, J.D., Morrice, E., Herve, B.P., and Wong, M.M. (1980) Preparing rare earth–silicon–iron–aluminum alloys, Bureau of Mines Report of Investigations 8445, U.S. Department of the Interior, Washington, D.C.
Marinsky, J.A., Glendenin, L.E., and Coryell, C.D. (1947) The chemical identification of radioisotopes of neodymium and element 61, *J. Am. Chem. Soc.*, 69: 2781–2785.
Marsh, J.K. (1942) Rare earth metal amalgams. Part I: The reaction between sodium amalgam and rare earth acetate and chloride solutions, *J. Chem. Soc.*, 398–401.
Marsh, J.K. (1943) Rare earth metal amalgams. Part IV: The isolation of europium**,** *J. Chem. Soc.*, 531–535.
Marsh, J.K. (1955) Separation of lanthanons with the aid of ethylene diamine NNN′N′ tetraacetic acid ('Enta' acid). Part V: The solubilities of some alkali lanthanon enta salts, *J. Chem. Soc*., 451–452.
Marsh, J.K. (1957) Isolation of samarium, europium and ytterbium materials by means of sodium amalgam, *Inorg. Syn.*, 5: 32–37.
Massalski, T., Okamoto, H., and Subramanyam, R. (eds.) (1990) *Binary Alloy Phase Diagrams*, 2nd ed., Vols. 1 and 2, American Society for Metals, Meterials Park, OH.
Masur, L.J., Podtburg, E.R., Craven, C.A., Otto, A., Wang, Z.L., and Kroeger, D.M. (1994) Advances in the processing and properties of $YBa_2Cu_4O_8$, *J. Metals*, 46(12): 28–30.
Matignon, C. (1900) *CR Acad. Sci.*, 131: 837–839, 891–892.
Mazza, I. (1939) On the electrometallurgy of lanthanum, cerium and praseodymium, *Atti Congr. Intern. Chim.*, 10th Congr., Rome, 1938, 3, 604–609.
McCallum, R.W. (1998) New or novel applications of rare earth materials, *Rare Earths'98*, Abstracts, p. 26, Free Mantle, Western Australia.
McColl, J.R. and Palilla, F.C. (1981) Use of rare earths in television and cathode ray phosphors. In Gschneidner, Jr., K.A. (ed.), *Industrial Applications of Rare Earth Elements*, pp. 177–193, ACS Symposium Series 164, American Chemical Society, Washington, D.C.
McCoy, H.N. (1936) Contribution to the chemistry of europium, *J. Am. Chem. Soc.*, 58: 1577–1580.
McCoy, H.N. (1941) Europium and ytterbium amalgams, *J. Am. Chem. Soc.*, 63: 1622–1624.
McFarland, C.M. (1973) Cobalt–rare earth powders by the reduction–diffusion process. In Kevane, C.J. and Moeller, T. (eds.) *Proc. 10th Rare Earth Research Conf.*, Carefree, AZ, May 1973, Conf–730402, P2, pp. 701–710, National Technical Information Service, Springfield, Virginia.
McGill, I. (1993) Rare earth elements. In Elvers, B., Hawkins, S., Russy, W., and Schulz, G. (eds.), *Ullmann's Encyclopedia of Industrial Chemistry*, Vol., A22, pp. 607–649, VCH, Weinheim.
McGill, I. (1997) Rare earth metals. In Habashi, F. (ed.), *Handbook of Extractive Metallurgy*, Vol. III, pp. 1695–1741, Wiley–VCH, Weinheim.
McGinn, P.J. (1994) Progress in the melt texturing of RE-123 superconductors, *J. Metals* (12): 31–33.
McGuiness, P.J., Zhang, X.J., Forsyth, H., and Harris, I.R. (1990) Disproportionation in $Nd_{16}Fe_{76}B_8$-type hydrides, *J. Less Common Metals*, 162: 379–387.
McKeown, F.A. and Klamic, H. (1959) Rare earth bearing apatite, at Mineville, Essex Co., N.Y., *U.S. Geol. Survey Bull.*, 1046B: 9–23.
McMasters, O.D., Verhoeven, J.D., and Gibson, E.D. (1986) Preparation of terfenol-D by float zone solidification, *J. Magn. Magn. Mater.*, 54–57(2): 849–850.
Meechumna, P. (1991) Separation of microlite from cassiterite and zircon. In Siribumrungsukha, B.,

Arrykul, S., Sanguan Sai, P., Pungrassami, T., Sikong, L., and Kooptarnon, K. (eds.), *Proc. Int. Conf. Rare Earth Minerals and Minerals for Electronic Uses*, Jan. 1991, Hat Yai, Thailand, pp. 211–220, Prince of Songkla University, Thailand.
Meints, R.E., Hopkins, B.S., and Audrieth, L.F. (1937) Electrolytic preparation of rare earth amalgams II, Decomposition of lanthanum amalgam for the preparation of the free metals, *Z. anorg. allgem. Chem.*, 231: 54–62.
Menth, A., Nagel, H., and Perkins, R.S. (1978) New high performance magnets based on rare earth transition metal compounds, *Ann. Rev. Mater. Sci*., 8: 21–47.
Merlub-Sobel, M. (1959) Preparation of fused salt electrolytes. U.S. Patent 2,870,072 (January 20).
Merrill, C.C. and Wong, M.M. (1967) Electrorefining yttrium, U.S. Bureau of Mines Report of Investigations 7018, U.S. Department of the Interior, Washington, D.C.
Merritt, R.R. (1990) High temperature methods for processing monazite: I Reaction with calcium chloride and calcium carbonate, *J. Less Common Metals*, 166: 197–210.
Merritt, R.R. (1990a) High temperature methods for processing monazite. II. Reaction with sodium carbonate, *J. Less Common Metals*, 166: 211–219.
Mialki, W. (1965) Seltene Erden in der Kerntechnik, *Metall*, 19: 16–21.
Miao, M.W. and Horng, J.S. (1988) Decomposition of Taiwan black monazite by hydrothermal and sodium fusion methods. In Bautista, R.G. and Wong, M.M. (eds.), *Rare Earths*, pp. 195–206, The Minerals, Metals, and Materials Society, Warrendale, PA.
Mineral Facts and Problems (1985) "Resource Reserve Definitions", Minerals Facts and Problems 1985, Bureau of Mines Bulletin 675, pp. 2–7, U.S. Department of the Interior, Washington, D.C.
Mining Journal (1994) Malaysian Rare Earth Plants to Close, Mining Journal (London), February 11, 1994 Issue, 322(8262): 106.
Minowa, T., Yoshikawa, M., and Honshima, M. (1989) Improvement of the corrosion resistance on Nd–Fe–B magnet with nickel plating, *IEEE Trans. Magn.*, 25: 3776–3778.
Minh, N.Q. (1993) Ceramic fuel cells, *J. Amer. Ceramic. Soc.*, 76(3): 563–588.
Moeller, T. (1961) Chemistry of rare earths. In Spedding, F.H. and Daane, A.H. (eds.), *The Rare Earths*, Chapter 2, John Wiley, New York.
Moeller, T. (1963) *The Chemistry of Lanthanons*, Reinhold, New York.
Moeller, T. (1967) Lanthanide elements. In Hampel, C.A. (ed.), *Encyclopedia of Chemical Elements*, pp. 338–349, Reinhold, New York.
Moeller, T. (1971) The lanthanides. In Bailer, K., Emeleus, H.J., Nyholm, R., and Trotman Dickenson, A. (eds.), *Comprehensive Inorganic Chemistry*, Vol. 4, Pergamon, Oxford.
Moeller, T. and Kremers, H.E. (1945) The basicity characteristics of scandium, yttrium and the rare earth elements, *Chem. Rev.*, 37: 97–159.
Moeller, T. and Zimmerman, P.A. (1954) Electrolysis of rare earth metal salts in basic solvents, *Science*, 120: 539–540.
Moldenhauer, M. (1914) *Chem. Z.*, 38: 147.
Molycorp Application Report (1964–1970) A bibliography. Six years of research in catalysis with rare earth elements, Vol. 1, No. 7101.
Molycorp Application Report (1971–1976) A bibliography of the research in catalysis with rare earth elements, Vol. 2, No. 7907.
Molycorp, Inc. (1993) *A Lanthanide Lanthology*, Molycorp, Inc., Mountain Pass, CA, U.S.
Morey, G.W. (1938) *The Properties of Glass*, pp. 435–436, Reinhold Publishing Corporation, New York.
Moriarty, Jr., J.C. (1968) The industrial preparation of the rare earth metals by metallothermic reduction, *J. Metals*, 20 (11): 41–45.
Morrice, E. (1985) Molten salt electrowinning of rare earth and yttrium metals and alloys. In Xu Guangxian and Xiao Jimei (eds.), *New Frontiers in Rare Earth Science and Application*, Vol. II, pp. 1099–1106, Science Press, Beijing.
Morrice, E. and Henrie, T.A. (1967) Electrowinning of high purity neodymium, praseodymium and didymium metals from their oxides, Bureau of Mines Report of Investigations 6957, U.S. Department of the Interior, Washington, D.C.
Morrice, E. and Knickerbocker, R.G. (1961) Rare earth electrolytic metals. In Spedding, F.H. and Daane, A.H. (eds.), *The Rare Earths*, pp.126–144, John Wiley, New York.
Morrice, E. and Wong, M.M. (1978) Effect of temperature on the electrolytic preparation and recovery of samarium–cobalt alloy, Bureau of Mines Report of Investigations, 7556, U.S. Department of the Interior, Washington, D.C.

Morrice, E. and Wong, M.M. (1979) Fused salt electrowinning and electrorefining of rare earth and yttrium metals, *Miner. Sci. Eng.*, 11(3): 125–136.
Morrice, E. and Wong, M.M. (1982) Flotation of rare earths from bastnasite ore, Bureau of Mines Report of Investigations 8689, U.S. Department of the Interior, Washington, D.C.
Morrice, E, Darrah, J., Brown, E., Wyche, C., Headrick, W., Williams, R., and Knickerbocker, R.G. (1960) Metallurgical laboratory data on reduction and refining of ceric oxide and cerous fluoride to cerium ingot, RI 5549, U.S. Department of the Interior, Washington, D.C.
Morrice, E., Porter, B., Brown, E.A., Wyche, C., and Knickerbocker, R.G. (1961) Electrowinning of cerium group and yttrium group metals, Bureau of Mines Report of Investigations 5868, U.S. Department of the Interior, Washington, D.C.
Morrice, E., Shedd, E.S., and Henrie, T.A. (1968) Direct electrolysis of rare earth oxides to metals and alloys in fluoride melts, Bureau of Mines Report of Investigations 7146, U.S. Department of the Interior, Washington, D.C.
Morrice, E., Shedd, E.S., Wong, M.M., and Henrie, T.A. (1969) Preparation of cobalt rare earth alloys by electrolysis, *J. Metals*, 21(1): 34–37.
Morrice, E., Whisler, N., and Wong, M.M. (1973) Electrowinning of yttrium–aluminium alloy from yttria alumina mixtures. In Kevane, C.J. and Moeller, T. (eds.), Proc. 10th Rare Earth Research Conf., Carefree, AZ, May 1973, Conf-730402, P1 and P2, pp. 682–691, National Technical Information Service, Springfield, Virginia.
Morrice, E., Wyche, C., and Henrie, T.A. (1962) Electrowinning of molten lanthanum from lanthanum oxides, Bureau of Mines Report of Investigations 6075, U.S. Department of the Interior, Washington, D.C.
Morton, J.R. and James, D.B. (1967) Effect of temperature on the HEDTA and EDTA elution position of yttrium in the rare earth sequence. In Proc. 6th Rare Earth Research Conference, Report No. AFOSR-67-1214, pp. 667–677, National Technical Information Service, Springfield, Virginia.
Mosander, C.G. (1827) The preparation of cerium by reduction of $CeCl_3$ with potassium, *Pogg. Ann.*, 11: 406–416.
Mueller, R.M., Buchal, Chr., Folle, H.R., Kubota, M., and Pobell, F. (1980) A double stage nuclear demagnetization refrigerator. *Cryogenics*, 20(7): 395–407.
Murphy, A.J. and Payne, R.J.M. (1947) Magnesium–cerium–zirconium alloys: properties at elevated temperatures, *J. Inst. Met.*, 73: 105–127.
Murphy, J.E., Adams, G.H., and Cathey, W.N. (1975) Electrotransport and diffusion of iron in α yttrium, *Metall. Trans.*, 6A: 343–348
Muthmann, W. and Scheidemandel, J. (1907) On the extraction of the rare earth metals by electrolysis of the fluorides, *Ann*, 355: 116–136.
Muthmann, W. and Weiss, L. (1904) Investigations on metals of the cerium group, *Liebigs Ann.* 331: 1–46.
Muthmann, W., Hofer, H., and Weiss, L. (1902) On the preparation of metals of the cerium group by molten electrolysis, *Ann. Chem*., 320: 231–269.
Naastepad, P.A., den Broeder, F.J.A., and Wassink, R.J.K. (1973) *Powder Metall. Int.*, 5: 61–65.
Nagai, H., Beaudry, B.J., and Gschneidner, Jr., K.A. (1978) Purification of gadolinium by electrorefining, *Metall. Trans.*, 9B: 25–28.
Narayanan, N.S., Thulasidoss, S., Ramachandran, T.V., Swaminathan, T.V., and Prasad, K.R. (1988) Processing of monazite at the rare earths division, Udyogamandal. In Gupta, C.K. and Krishnan, T.S. (eds.), *Rare Earths — Applications and Technology*, pp. 45–56, Trans Tech Publications, Switzerland.
Necker, W.C. (1961) The zone purification of yttrium. In Bunshah, R.F. (ed.), *Trans. Vac. Metallurgy Conf.*, pp. 289–298, Interscience, New York.
Nesbitt, E.A. and Wernick, J.H. (1973) *Rare Earth Permanent Magnets*, Academic Press, New York.
Nielsen, J.W. (1981) Bubble domain memory materials. In Gschneidner, Jr., K.A. (ed.), *Industrial Applications of Rare Earth Elements*, pp. 219–222, ACS Symposium Series 164, American Chemical Society, Washington, D.C.
Nininger, R.D. (1956) *Exploration for Nuclear Raw Materials*, D. Van Nostrand, Princeton, N.J.
Noblitt, H.C. (1965) Development of a process for the concentration of Oka pyrochlore. In A. Roberts (ed.), *Minerals Processing*, pp. 669–678, Pergamon, Oxford.
Nolting, H.J., Simmons, C.R., and Klingenberg, J.J. (1960) Preparation and properties of high purity yttrium metal, *J. Inorg. Nucl. Chem.*, 14, 208–216.
Nozawa, Y., Iwasaki, K., Tanigawa, S., Tokunaga, M., and Harada, H. (1988) Nd–Fe–B die upset

and anisotropic bonded magnets, *J. Appl. Phys.*, 64: 5285–5289.
O'Driscoll, M. (1991) An overview of rare earth minerals supply and applications. In Siribumrungsukha, B., Arrykul, S., Sanguan Sai, P., Pungrassami, T., Sikong, L., and Kooptarnon, K. (eds.), *Proc. Int. Conf. Rare Earth Minerals and Minerals for Electronic Uses*, Jan. 1991, Hat Yai, Thailand, pp. 409–420, Prince of Songkla University, Thailand.
Ohmori, K. (1998) The use of reduction diffusion process (R/D) in magnet industry. In *Preprints of the Conference, China Magnets*, held on 18–21 October 1998 at Beijing, PR China.
Okajima, Y. (1987) Rare earth metal powder, Japanese Patent 62 13 506 91987 (CA 106, 217418).
Olson, J.C., Shaw, D.R., Pray, L.C., and Sharp, W.N. (1954) Rare earth mineral deposits of the Mountain Pass district, San Bernandino Country CA, U.S. Geol. Survey Prof. Paper 261, U.S. Govt. Printing Office, Washington, D.C.
Omachi, R. (1988) Hi-tech applications of rare earths. In Gupta, C.K. and Krishnan, T.S. (eds.), *Rare Earths — Applications and Technology*, pp. 147–154, Trans Tech Publications, Switzerland.
Onstatt, E.I. (1953) Preparation of massive samarium metal, U.S. Atomic Energy Commission Report LA-1622, National Technical Information Service, Springfield, Virginia.
Onstatt, E.I. (1959) Separation of lanthanons by amalgam cathodes. III Electrochemical fractionation of the lanthanons at a lithium amalgam cathode, *J. Am. Chem. Soc.*, 81: 4451–4458.
Ormerod, J. (1985) The physical metallurgy and processing of sintered rare earth permanent magnets, *J. Less Common Metals*, 111: 49–69.
Osborne, M.G., Anderson, I.E. and Gschneidner, Jr., K.A. (1993) Centrifugal atomization of rare earth metal and intermetallic compounds. In Lawley, A. and Swanson, A. (eds.), *Advances in Powder Metallurgy and Particulate Materials – 1993 Powder Characterization, Testing and Quality Control*, Vol. 1, pp. 65–73, Metal Powder Industries Federation — American Powder Metallurgy Institute, Princeton, NJ.
Otsuki, E., Otsuka, T., and Imai, T. (1990) Processing and magnetic properties of sintered Nd–Fe–B magnets. In *Proceedings of the 11th International Workshop on Rare Earth Magnets and their Applications*, Vol. 1, pp. 328–340, Pittsburg, PA.
Overstead, W.C., Theobold, P.K., and Whitlow, J.W. (1959) Thorium and uranium resources in monazite placers of the western Piedmont, North and South Carolina, *Trans. AIME*, 214: 709–714.
Palmer, P.E., Burkholder, H.R., Beaudry, B. J., and Gschneidner, Jr., K.A. (1982) Preparation and some properties of misch metal, *J. Less Common Metals*, 87: 135–148.
Pan, P.H., Fennemore, D.K., Berolo, A.J., Shanks, H.R., Beaudry, B.J., Schmidt, F.A., and Danielson, G.C. (1980) Heat capacity of high purity lanthanum, *Phys. Rev. B*, 21: 2809–2814.
Panditharatna, L. (1991) The Ceylon mineral sands industry: Profile and prospects. In Siribumrungsukha, B., Arrykul, S., Sanguan Sai, P., Pungrassami, T., Sikong, L., and Kooptarnon, K. (eds.), *Proc. Int. Conf. Rare Earth Minerals and Minerals for Electronic Uses*, Jan. 1991, Hat Yai, Thailand, pp. 481–500, Prince of Songkla University, Thailand.
Pankratz, L.B., Stuve, J.M., and Gokcen, N.A. (1984) Thermodynamic Data for Mineral Technology, Bureau of Mines bulletin 677, U.S. Department of the Interior, Washington, D.C.
Parker, J.G. and Baroch, C.T. (eds.) (1971) The Rare Earth Elements, Yttrium and Thorium — A Materials Survey, Bureau of Mines Information Circular 8476, U.S. Department of the Interior, Washington, D.C.
Pasto, A.E. and Tennery, V.J. (1977), Synthesis and fabrication of EuB_6, *Trans. Am. Nucl. Soc.*, 26(1): 176.
Payne, R.J.M. and Bailey, N. (1959–60) Improvement of the age hardening properties of magnesium–rare earth alloys by addition of silver, *J. Inst. Met.*, 88: 417–427.
Peppard, D.E., (1964) Fractionation of rare earths by liquid extraction using phosphorus based extractants. In LeRoy Eyring (ed.), Progress in the Science and Technology of Rare Earths, Vol. 1, pp. 89–108, Pergamon, Oxford.
Peppard, D.E., Faris, F.J., Gray, P.R., and Mason, G.W. (1953) Studies of the solvent extraction behavior of transition elements. I. Order and degree of fractionation of the trivalent rare earths, *J. Phys. Chem.*, 57: 294–301.
Peppard, D.E., Driscoll, W.J., Siromen, R.J., and Mason, G.W. (1958) Acidic esters of organophosphoric acids as selective extractants for metallic cations – tracer studies, *J. Inorg. Nucl. Chem.*, 7: 276–285.
Peppard, D.E., Mason, G.W., Maier, J.L., and Driscoll, W.J. (1957) Fractional extraction of the lanthanides as their di-alkyl organophosphates, *J. Inorg. Nucl. Chem.*, 4: 334–343.

Peters, A.W. and Kim, G. (1981) Rare earths in noncracking catalysts. In Gschneidner, Jr., K.A. (ed.), *Industrial Applications of Rare Earth Elements*, pp. 117–131, ACS Symposium Series 164, American Chemical Society, Washington, D.C.

Peterson, D.T. and Schmidt, F.A. (1969) Electrotransport of carbon, nitrogen and oxygen in lutetium, *J. Less Common Metals*, 18: 111–116.

Peterson, D.T. and Schmidt, F.A. (1972) Electrotransport of carbon, nitrogen and oxygen in gadolinium, *J. Less Common Metals*, 29: 321–327.

Pfann, W.F. (1966) *Zone melting*, 2nd edition, Wiley, New York.

Pidgeon, L.M. and King, J.A. (1948) Vapour pressure of magnesium in the thermal reduction of magnesium oxide by ferrosilicon, *Discussions Faraday Soc*. (4): 197–206.

Pierce, T.B. and Peck, J.F. (1963) The extraction of the lanthanide elements from perchloric acid by di-(2-ethyl hexyl) hydrogen phosphate, *Analyst*, 88: 217–221.

Pilkington, E.S. and Wylie, A.W. (1952) Production of lanthanum and thorium compounds from monazite II, *J. Appl. Chem. (London)*, 2: 265–273.

Poirer, R.H., Calkins, G.D., Lutz, G.A. and Bearse, A.E. (1958) Ion exchange separation of uranium from thorium, *Ind. Eng. Chem.*, 50: 613–616.

Powell, A.R. (1939) Treatment of rare earth minerals, British Patent 510,198.

Powell, A.R. (1957) Discussion on the paper: The extraction of thorium from monazite. In *Extraction and Refining of the Rarer Metals*, pp. 376–379, The Institution of Mining and Metallurgy, London.

Powell, J.E. (1961) Separation of rare earths by ion exchange. In Spedding, F.H. and Daane, A.H. (eds.), *The Rare Earths*, Chap. 6, John Wiley, New York.

Powell, J.E. (1964) The separation of rare earths by ion exchange. In Eyring, L. (ed.), *Progress in the Science and Technology of Rare Earths*, Vol. 1, pp. 62–84, Pergamon, Oxford.

Powell, J.E. (1979) Separation chemistry. In Gschneidner, Jr., K.A. and Eyring, L. (eds.), *Handbook on the Physics and Chemistry of Rare Earths*, Vol. 3, pp. 81–110, North Holland, Amsterdam.

Powell, J.E. and Spedding, F.H. (1956) Basic principles involved in the macro separation of adjacent rare earths from each other by means of ion exchange, U.S. Atomic Energy Commission Report ISC–857, National Technical Information Service, Springfield, Virginia.

Powell, J.E. and Spedding, F. H. (1959) The separation of rare earths by ion exchange, *Trans. AIME*, 215: 457–463.

Powell, J.E. and Spedding, F.H. (1959a) Basic principles involved in the macroseparation of adjacent rare earths from each other by means of ion exchange, *Chem. Eng. Prog. Symp. Ser.*, 55(24): 101–113.

Pradip, K. and Fuerstenau, D.W. (1988) Alkyl hydroxamates as collectors for the flotation of bastnasite rare earth ores. In Bautista, R.G. and Wong, M.M. (eds.), *Rare Earths*, pp. 57–70, The Minerals, Metals and Materials Society, Warrendale, PA.

Preston, J.S. (1996) The recovery of rare earth oxides from a phosphoric acid byproduct. Part 4: The preparation of magnet-grade neodymium oxide from the light rare earth fraction, *Hydrometallurgy*, 42: 151–167.

Preston, J.S. and Du Preez, A.C. (1988) The solvent extraction of cobalt, nickel, zinc, copper, calcium, magnesium and the rare earth metals by organophosphorus acids, *Mintek Report* M 378, 30 pp.

Preston, J.S. and Du Preez, A.C. (1990) Solvent extraction processes for the separation of rare earth metals. In Sekine, T. (ed.), *Solvent Extraction*, pp. 883–894, Elsevier, Amsterdam.

Preston, J.S., Cole, P.M., Craig, W.M., and Feather, A.M. (1996) The recovery of rare earth oxides from a phosphoric acid byproduct. Part 1: Leaching of rare earth values and recovery of a mixed rare earth oxide by solvent extraction, *Hydrometallurgy*, 41: 1–19.

Preston, J.S., du Preez, A.U., Cole, P.M., and Fox, M.H. (1996a) The recovery of rare earth oxides from a phosphoric acid byproduct. Part 2: The preparation of high purity cerium dioxide and recovery of a heavy rare earth oxide concentrate, *Hydrometallurgy*, 42: 21–44.

Pungrassami, T. and Sanguansai, P. (1991) An overview on rare earth mineral resources/reserves of active tin mines in Thailand. In Siribumrungsukha, B., Arrykul, S., Sanguan Sai, P., Pungrassami, T., Sikong, L., and Kooptarnon, K. (eds.), *Proc. Int. Conf. Rare Earth Minerals and Minerals for Electronic Uses*, Jan. 1991, Hat Yai, Thailand, pp. 557–575, Prince of Songkla University, Thailand.

Qui,L.F., Kang, X.H. and Wang, T.S. (1991) A study on photochemical separation of rare earths: The separation of europium from an industrial concentrate material of samarium, europium, and gadolinium, *Sep. Sci. Technol.*, 26: 199–221.

Rabatin, J.G. (1981) Rare earth x-ray phosphors for medical radiography. In Gschneidner, Jr., K.A. (ed.), *Industrial Applications of Rare Earth Elements*, pp. 203–218, ACS Symposium Series 164, American Chemical Society, Washington, D.C.
Radtke, S.F., and Herrschaft, D.C. (1983) Role of misch metal in galvanizing with a Zn–5%Al alloy, *J. Less Common Metals*, 93: 253–259.
Reed, J.B., Hopkins, B.S., and Audrieth, L.F. (1935) Observations on the rare earths XLIV. Preparation of anhydrous rare earth compounds by the action of fused and solid "orium" salts on the oxides, *J. Am. Chem. Soc.*, 57: 1159–1160.
Reed, J.B., Hopkins, B.S., and Audrieth, L.F. (1939) Anhydrous rare earth chlorides. In Booth, H.S. (ed.), *Inorganic Syntheses*, Vol. 1, Chapter 11, McGraw Hill, New York.
Revel, G., Rouchand, J.C., and Pastol, J.L. (1974) Preparation and neutron activation analysis of high purity cerium. In Haschke, J. and Eick, H.E. (eds.), *Proc. 11th Rare Earth Research Conf.*, Traverse City, MI, Conf.–741002, Part 2, pp. 602–612, National Technical Information Service, Springfield, Virginia.
RIC Insight (1990) 3 (1, 6, 12).
RIC News (1993) XXVII (2).
RIC News (1995) XXX (3).
RIC News (1997) XXXII (1).
Rice, A.C. (1959) Preparation of rare earth chloride solutions, Bureau of Mines Report of Investigations 5540, U.S. Department of the Interior, Washington, D.C.
Rice, A.C. and Stone, C.A. (1962) Amines in liquid–liquid extraction of rare earth elements, Bureau of Mines Report of Investigations 5923, U.S. Department of the Interior, Washington, D.C.
Richardson, F.D. and Jeffes, J.H.E. (1948) The thermodynamic of substances of interest in iron and steel making from 0 to 2400°C. I. Oxides, *J. Inn Steel Inst. (London)*, 160: 261–270.
Riker, L.W. (1981) The use of rare earths in glass compositions. In Gschneidner, Jr., K.A. (ed.), *Industrial Applications of Rare Earth Elements*, pp. 81–94, ACS Symposium Series 164, American Chemical Society, Washington, D.C.
Ritcey, G.M. and Ashbrook, A.W. (1979) Solvent Extraction Principles and Applications to Proess Metallurgy, Part 2, pp. 398–420, Elsevier, Amsterdam.
Ritcey, G.M. and Pouskouleli, G. (1987) In Schulz, W.W., et al. (eds.), *Science and Technology of Tributyl Phosphate*, Vol. 2, Part A, pp. 65–121, CRC Press, Boca Raton, FL.
de Rhoden, C. and Peltier, M. (1957) U.S. Patent 2,783,125.
Robjohns, N. (1989) Rare Earths, *Min. Ann. Rev.*, C83–C84.
Ronda, C.R., Kynast, U.H., Dingen, W.P.M., and Van Hal, H.A.M. (1993) Optimizing bY_2SiO_5:Tb for projection television applications, *J. Alloys and Compounds*, 192: 55–56.
Rosynek, M.P. (1977) Catalytic properties of rare earth oxides, *Catal. Rev. Sci, Eng.*, 16: 111–154.
Ryanson, P.R. (1977) U.S. Patent 4,105,517.
Sabot, J.L. and Maestro, P. (1995) Lanthanides. In Kroschwitz, J.I. and Grant, M.H. (eds.), *Kirk–Othmer Encyclopedia of Chemical Technology*, 4th edn, Vol. 14, pp. 1091–1115, John Wiley, New York.
Sagawa, M., Fujimura, S., Yamamoto, H., and Matsuura, Y. (1984) New material for permanent magnets on a base of Nd and Fe, *J. Appl. Phys.*, 55: 2083–2087.
Sagawa, M., Fujimura, S., Yamamoto, H., and Matsuura, Y. (1984a) Permanent magnet materials based on the rare earth–iron–boron tetragonal compounds, *IEEE Trans. Magn.*, MAG-20: 1584–1589.
Sagawa, M., Fujimura, S., Yamamoto, H., Matsuura, Y., and Hirosawa, S. (1985) Magnetic properties of rare earth iron boron permanent magnets, *J. Appl. Phys.*, 57: 4094–4096
Sagawa, M., Hirosawa, S., Yamamoto, H, Fujimura, S., and Matsuura, Y. (1987) Nd–Fe–B permanent magnet materials, *Jap. J. Appl. Phys.*, 26: 785–800.
Sagawa, M., Hirosawa, S., Tokuhaara, K.,Yamamoto, H, Fujimura, S., Tsubokawa, Y., and Shimitzu, R. (1987a) Dependence of coercivity on the anisotropy field in the $Nd_2Fe_{14}B$ type sintered magnets, *J. Appl. Phys.*, 61: 3559–3561.
Sandhage, K., et al. (1990) The metallic presursor approach to long lengths of $YBa_2Cu_3O_{7-x}$ superconducting wire. In Whang, S., Dasgupta, A., and Collings, E. (eds.), *High Temperature Superconducting Compounds III*, pp. 347–362, TMs, Warrendale, PA.
Sauerwald, F. (1947) The magnesium–zirconium composition diagram, *Z. anorg. allgem. Chem.*, 255: 212–220.
Scaife, D.E. and Wylie, A.W. (1958) A carbide–iodide process for high purity thorium. Preprint of

Paper A/CONF 15/P/1098 presented at the Second United Nations International Conference on Peaceful Uses of Atomic Energy, 58 pp., United Nations, Geneva.
Schiffmacher, G. and Trombe, F. (1969) Preparation du dysprosium metallique par reduction de son oxyde alaide du thorium, *CR Acad. Sci.*, 268: Ser. C, (2): 159–162.
Schmidt, F. A. and Carlson, O.N. (1974) Method for preparing scandium metal, U.S. Patent 3,846,121.
Schmidt, F.A., Peterson, D.T., and Wheelock, J.T. (1986) U.S. Patent 4,612,047.
Schultz, L., Schnitzke, K., and Wecker, J. (1989) Preparation and properties of mechanically alloyed rare earth permanent magnets, *J. Magn. Magn. Mater.*, 80: 115–118.
Schulze, K.K. (1981) Preparation and characterisation of ultrahigh purity niobium, *J. Metals*, 33(5): 33–42.
Schumacher, E. and Harris, J. (1926) Investigations of the thermoionic properties of rare earth elements, *J. Am. Chem. Soc.*, 48: 3108–3114.
Schumacher, E. and Lucas, F. (1924) Photomicrographic evidence of the crystal structure of pure cerium, *J. Am. Chem. Soc.*, 46: 1167–1169.
Seith, W. and Wever, H. (1953) A new effect in the electrolytic transfer in solid alloys, *Z. Elektrochem.*, 57: 891.
Sharma, R.A. (1987) Neodymium production processes, *J. Metals*, 39(2): 33–37.
Sharma, R.A. and Seefurth, R.N. (1988) Metallothermic reduction of Nd_2O_3 with Ca in $CaCl_2$–NaCl melts, *J. Electrochem. Soc.*, 135: 66–71.
Sharma, R.A. and Seefurth, R.N. (1988a) A molten salt process for producing neodymium iron alloys by reduction of Nd_2O_3 with sodium. In Bautista, R.G. and Wong, M.M. (eds.), *Rare Earths*, pp. 355–368, The Minerals, Metals and Materials Society, Warrendale, PA.
Shastri, L.V., Mittal, J.P., Krishnan, N.P.K., and Murthy, T.K.S. (1988) Development of a photochemical route for upgrading europium from aqueous lanthanide mixtures. In Gupta, C.K. and Krishnan, T.S. (eds.), *Rare Earths — Applications and Technology*, pp. 57–60, Trans Tech Publications, Switzerland.
Shaw, V.E. (1959) Extraction of yttrium and rare earth elements from Arizona euxenite concentrate, Bureau of Mines Report of Investigations 5544, U.S. Department of the Interior, Washington, D.C.
Shaw, V.E. and Bauer, D.J. (1959) Extraction and separation of rare earth elements Idaho euxenite concentrate, Bureau of Mines Report of Investigations 6577, U.S. Department of the Interior, Washington, D.C.
Shaw, K.G., Smutz, M., and Bridger, G.L. (1954) A process for separating thorium compounds from monazite sands, U.S. Atomic Energy Commission Report ISC–407, National Technical Information Service, Springfield, Virginia.
Shedd, E.S., Marchant, J.D., and Henrie, T.A. (1964) Continuous electrowinning of cerium metal from cerium oxides, Bureau of Mines Report of Investigations 6362, U.S. Department of the Interior, Washington, D.C.
Shedd, E.S., Marchant, J.D., and Henrie, T.A. (1966) Electrowinning and tapping of lanthanum metal, Bureau of Mines Report of Investigations 6882, U.S. Department of the Interior, Washington, D.C.
Shedd, E.S., Marchant, J.D., and Wong, M.M. (1970) Electrowinning misch metal from a treated bastnasite concentrate, Bureau of Mines Report of Investigations 7398, U.S. Department of the Interior, Washington, D.C.
Sherrington, L. (1983) Commercial processes for rare earths and thorium. In Lo, T.C., et al. (eds.), *Handbook of Solvent Extraction*, pp.712–723, Wiley, New York.
Shibata, J. (1991) Solution chemistry and separation of metal ions in leached solution. In Siribumrungsukha, B., Arrykul, S., Sanguan Sai, P., Pungrassami, T., Sikong, L., and Kooptarnon, K. (eds.), *Proc. Int. Conf. Rare Earth Minerals and Minerals for Electronic Uses*, Jan. 1991, Hat Yai, Thailand, pp. 365–377, Prince of Songkla University, Thailand.
Shimoda, T., Akioka, K., Kobayashi, O., and Yamagami, T. (1988) High energy cast Pr–Fe–B magnets, *J. Appl. Phys.*, 64: 5290.
Shumao, X. and Mingqin, W. (1985) Preparation of RE–Mg–Si alloys by silicothermic reduction of dolomite. In Xu Guangxian and Xiao Jimei (eds.), *New Frontiers in Rare Earth Science and Application*, Vol. II, pp. 1185–1189, Science Press, Beijing.
Singer, R., Airey, H., Grimmett, L., Leech, H., and Bennett, R. (1945) The cerium industry in German territory including reports on radium and mesothorium, British Intelligence Subcommittee, Final

Report 400, Item 21, pp. 1–118.
Singh, S.S. (1988) Rare earths in laser technology. In Gupta, C.K. and Krishnan, T.S. (eds.), *Rare Earths — Applications and Technology*, pp. 155–172, Trans Tech Publications, Switzerland.
Sklyarenko, S.I. and Sakharov, B.A. (1940) The electrochemical preparation of cerium amalgam, *J. Appl. Chem. USSR*, 13: 841–845.
Smith, H.R. (1958) Electron bombardment melting techniques. In Bunshah, R.F. (ed.), *Vacuum Metallurgy*, pp. 221–235, Reinhold, New York.
Smith, H.R., d'A Hunt, C., and Hanks, C.W. (1959) Electron bombardment melting, *J. Metals*, 11(2): 112.
Smutz, M. (1956) In F.R. Bruce et al. (ed.), Progress in Nucl. Energy, Ser. 3, Vol. 1, pp. 36–39, McGraw Hill, New York.
Smutz, M., Bridger, G.L., Shaw, K.G., and Whatley, M.E. (1954) The Ames process for separation of monazite, *Chem. Eng. Prog. Symp. Ser.,* No 13, 50: 167–170.
Spedding, F.H. (1978) Prologue. In Gschneidner, Jr., K.A. and Eyring, L. (eds.), *Handbook on the Physics and Chemistry of Rare Earths*, Vol. 1, pp. xv–xxv, North Holland, Amsterdam.
Spedding, F.H. (1982) Rare earth elements. In Grayson, M. and Eckroth, D. (eds.) Kirk-Othmer Encyclopedia of Chemical Technology, Vol. 19, pp. 833–854, Wiley, New York.
Spedding, F.H. and Daane, A.H. (1952) The preparation of rare earth metals, *J. Am. Chem. Soc.*, 74: 2783–2785.
Spedding, F.H. and Daane, A.H. (1954) Production of rare earth metals in quantity allows testing of physical properties, *J. Metals*, 6: 504–510.
Spedding, F.H. and Daane, A.H. (1956) The preparation and properties of rare earth metals. In Finniston, H.M. and Howe, J.P. (eds.), *Prog. Nucl. Energy Ser.*, 5, Vol. 1, pp. 413–432, Pergamon, New York.
Spedding, F.H. and Daane, A.H. (eds.) (1961) *The Rare Earths*, John Wiley, New York.
Spedding, F.H. and Daane, A.H. (1968) Metallurgy Division Research and Development Report IS-1900, Ames Laboratory, USAEC, Iowa State University, Ames, Iowa, National Technical Information Service, Springfield, VA.
Spedding, F.H. and Henderson, D.C. (1971) High temperature heat contents and related thermodynamic functions of some trifluorides of the rare earths: Y, La, Pr, Nd, Gd, Ho, and Lu, *J. Chem. Phys.*, 54: 2476–2483.
Spedding, F.H. and Powell, J.E. (1954) A practical separation of yttrium group rare earths from gadolinium by ion exchange, *Chem. Eng. Prog. Symp. Ser.*, 50(14): 7–15.
Spedding, F.H., Beaudry, B.J., Croat, J.J., and Palmer, P.E. (1970) The preparation and properties of ultrapure metals. In *Les Elements Des Terres Rares* 1, p. 25, Centre National de la Recherche Scientifique, Paris. Also R&D Report IS-2283, Ames Laboratory, USAEC, May 1970.
Spedding, F.H., Beaudry, B.J., Croat, J.J., and Palmer, P.E. (1968) The properties, preparation and handling of pure rare earth metals. In *Materials Technology — An Interamerican Approach*, p. 151, Am. Soc. Mech. Eng., New York.
Spedding, F.H., Daane, A.H., Wakefield, G., and Dennison, D.H. (1960) Preparation and properties of high purity scandium metal, *Trans. Met. Soc. AIME*, 218: 608–611.
Spedding, F.H., Fulmer, E.I., Butler, T.A., Gladrow, E.M., Gobush, M., Porter, P.E., Powell, J.E., and Wright, J.M. (1947) Separation of rare earths by ion exchange. III. Pilot plant separations, *J. Am. Chem. Soc.*, 69: 2812–2818.
Spedding, F.H., Gschneidner, Jr., K.A., and Daane, A.H. (1959) The lanthanum–carbon system, *Trans. Met. Soc. AIME*, 215: 192–197.
Spedding, F.H., Hanak, J.J., and Daane, A.H. (1958) The preparation and properties of europium, *Trans. AIME*, 212: 379–383.
Spedding, F.H., Powell, J.E., and Wheelwright, E.J. (1954) The use of copper as the retaining ion in the elution of rare earths with ammonium ethylene diamine tetraacetate solutions, *J. Am. Chem. Soc.*, 76: 2557–2560.
Spedding, F.H., Wilhelm, H.A., Keller, W.H., Ahmann, D.H., Daane, A.H., Hach, C.C. and Ericson, R.P. (1952) Production of pure rare earth metals, *Ind. Eng. Chem.*, 44: 553–556.
Staggers, J.O. (1977) Rare earth metal silicide alloys, U.S. Patent 4,018,597.
Strnat, K.J. (1978) Rare earth magnets in present production and development, *J. Magn. Magn. Mater.*, 7: 351–360.
Strnat, K.J. (1985) A review of rare earth permanent magnets, applications and prospects. In Xu Guangxian and Xiao Jimei (eds.), *New Frontiers in Rare Earth Science and Application*,

pp. 872–878, Vol. II, Science Press, Beijing.
Strnat, K.J. (1988) R–Co permanent magnets. In Buschow, K.H.J. (ed.), *Ferromagnetic Materials*, Vol. 4, pp. 131–209, North Holland, Amsterdam.
Strnat, K.J. and Strnat, R.M.W. (1991) Rare earth–cobalt magnets, *J. Magn. Magn. Mater.*, 100: 38–56.
Strnat, K. J., Olson, J.C. and Hoofer, G. (1968) Coercivity of misch metal–cobalt alloy powders, *J. Appl. Phys.*, 39: 1263–1265.
Strnat, K.J., Wong, K.M.D., and Blaettner, H. (1976) Bonded rare earth–cobalt permanent magnets. In Lundin, C.E. (ed.), *Proc. 12th Rare Earth Research Conference*, 18–22 July, 1976, Vail, Colorado, pp. 31–40, University of Denver, Denver Research Institute, Denver.
Strnat, R.M.W., Clarke, J.P., Leupold, H.A., and Tauber, A. (1987) Metal matrix magnets for new TWT applications, *J. Appl. Phys.*, 61: 3463–3465.
Sulaiman, M.F. (1991) An overview of the rare earth mineral processing industry in Malaysia. In Siribumrungsukha, B., Arrykul, S., Sanguan Sai, P., Pungrassami, T., Sikong, L., and Kooptarnon, K. (eds.), *Proc. Int. Conf. Rare Earth Minerals and Minerals for Electronic Uses*, Jan. 1991, Hat Yai, Thailand, pp. 389–395, Prince of Songkla University, Thailand.
Szabadvary, F. (1988) The history of the discovery and separation of the rare earths. In Gschneidner, Jr., K.A. and Eyring, L. (eds.), *Handbook on the Physics and Chemistry of Rare Earths*, Vol. 11, pp. 33–80, North Holland, Amsterdam.
Taniguchi, J.R., Doty, A.W., and Byers, C.H. (1988) Large scale chromatographic separation using continuous displacement chromatography. In Bautista, R.G. and Wong, M.M. (eds.), *Rare Earths*, pp.147–161, The Minerals, Metals and Materials Society, Warrendale, PA.
Templeton, C.C. (1949) The distribution of rare earth nitrates between water and *n*-hexyl alcohol at 25°C, *J. Am. Chem. Soc.*, 71: 2187–2190.
Templeton, C.C. and Peterson, J.A. (1948) Fractionation of lanthanum and neodymium nitrates by solvent extraction, *J. Am. Chem. Soc.*, 70: 3967–3968.
Taylor, R.K.A. (1991) Australian rare earth resources for the electronics industry. In Siribumrungsukha, B., Arrykul, S., Sanguan Sai, P., Pungrassami, T., Sikong, L., and Kooptarnon, K. (eds.), *Proc. Int. Conf. Rare Earth Minerals and Minerals for Electronic Uses*, Jan. 1991, Hat Yai, Thailand, pp. 125–136, Prince of Songkla University, Thailand.
Thakur, N.N. (2000) Separation of rare earths by solvent extraction. Private communication.
Thomas, R. (1977) Rare earths: new production processes based on oxides. In Thomas, R. (ed.) Operating Handbook of Mineral Processing, p. 51, McGraw Hill, New York.
Thompson, A. (1917) *Met. Chem. Eng.*, 17: 213.
Thompson, A. and Kremers, H.E. (1925) The preparation and properties of cerium free misch metal, *Trans. Am. Electrochem. Soc*., 47: 345–352.
Thompson, A.P., Holte, W.B., and Kremers, H.E. (1926) The electrolytic preparation and some properties of metallic yttrium, *Trans. Am. Electrochem. Soc.*, 49: 277–289.
Thornton, W.A. (1981) Lamp phosphor. In Gschneidner, Jr., K.A. (ed.), *Industrial Applications of Rare Earth Elements*, pp. 195–201, ACS Symposium Series 164, American Chemical Society, Washington, D.C.
Tirnh, X.B. (1991) Mineralogical characteristics of Nam Nam Xe rare earth deposit in Vietnam. In Siribumrungsukha, B., Arrykul, S., Sanguan Sai, P., Pungrassami, T., Sikong, L., and Kooptarnon, K. (eds.), *Proc. Int. Conf. Rare Earth Minerals and Minerals for Electronic Uses*, Jan. 1991, Hat Yai, Thailand, pp. 636–643, Prince of Songkla University, Thailand.
Tokunaga, M., Nozawa, Y., Iwasaki, K., Tanigawa, S., and Harada, H. (1989) Magnetic properties of isotropic and anisotropic Nd–Fe–B bonded magnets, *J. Magn. Magn. Mater.*, 80: 80–87.
Topp, N.E. (1965) *The Chemistry of Rare Earth Elements*, Elsevier, Amsterdam.
Tourre, J.M. (1998) Rare earths 1998 Market Update. In *Preprints of the Conference, China Magnets*, held on 18–21 October 1998 at Beijing, PR China.
Trombe, F. (1932) Preparation of metallic lanthanum free from iron and silicon, *Compt. rend.*, 94: 1653–1655.
Trombe, F., (1933) Préparation du néodyme métallique exempt de fer et de silicium, *CR Acad. Sci.*, 196: 704–706.
Trombe, F. (1935) The isolation of gadolinium, *CR Acad. Sci.*, 200: 459–461.
Trombe, F. (1938) On the isolation of metallic europium, *CR Acad. Sci.*, 206: 1380–1383.
Trombe, F. (1945) On the isolation of metallic dysprosium, *CR Acad. Sci.*, 220: 603–604.
Trombe, F. (1953) The vapor pressures of the rare earth metals, their separation and purification, *Bull.*

Soc. Chim. Fr., 20: 1010–1012.
Trombe, F. (1957) Preparation of rare earth metals, In *Proc. Symp. Rare Metals*, Bombay, December 1957, pp. 402–444, The Indian Institute of Metals and Bhabha Atomic Research Center.
Trombe, F. and Mahn, F. (1943) Preparation du cerium, du neodyme et du gadolinium metalliques a partir de leurs alliages avec le magnesium, *CR Acad. Sci.*, 217: 603–605.
Trombe, F. and Mahn, F. (1944) The preparation and thermal dissociation of alloys of magnesium with cerium, neodymium and gadolinium, *Ann. Chim.*, 19: 345–361.
Turner, H. (1998) Radiolanthanides in Nuclear Oncology, *Rare Earths' 98*, Abstracts p. 27, Free Mantle, Western Australia.
USGS (2003) U.S. Geological Survey, Mineral Commodity Summaries, Jan 2003.
Van Arkel, A.E. and de Boer, J.H. (1925) Preparation of pure titanium, zirconium, hafnium and thorium metals, *Z. anorg. allgem. Chem*., 148: 345.
Van Vucht, T.H.N., Kuijpers, F.A., and Brunning, H.C.A.M. (1970) Reversible room temperature absorption of large quantities of hydrogen by intermetallic compounds, *Philips Res. Rep*., 25: 133–140.
Velge, W.A.J.J., and Buschow, K.H.J. (1968) Magnetic and crystallographic properties of some rare earth cobalt compounds with $CaZn_5$ structure, *J. Appl. Phys.*, 39: 1717–1720.
Venuto, P.B. and Habib, E.T. (1979) *Fluid Catalytic Cracking with Zeolite Catalysts*, Marcel Dekker, New York.
Verhoeven, J.D. (1966) Electrotransport arc means of purifying metals, *J. Metals*, 18(1): 26–31.
Verhoeven, J.D., Gibson, E.D., McMasters, O.D., and Baker, H.H. (1987) The growth of single crystal terfenol-D crystals, *Metall. Trans.*, 18A: 223–231.
Vickery, R.C. (1955) The extraction and purification of scandium, *J. Chem. Soc.*, 245–251.
Villani, F. (1980) Recovery of rare earth and thorium oxides from pyrochlore, *Rare Earth Technology and Applications*, Noyes Data Corporation, NJ, Chemical Technology Review No. 154, pp. 6–7.
Viswanathan, P. (1957) Studies on Travancore beach sands, *Indian Mining Journal*, Special Issue, 109–139.
Vogt, T. (1998) Neutron and x-ray diffraction studies on AB_5 rare earth metal hydrides, *Rare Earths' 98*, Abstracts p. 37, Free Mantle, Western Australia.
Walkiewicz, J.W., Winston, J. S., and Wong, M.M. (1973) Preparation of samarium cobalt permanent magnets, Bureau of Mines Report of Investigations 7784, U.S. Dept. of the Interior, Washington, D.C.
Wallace, D.N. (1981) The use of rare earth elements in zeolite cracking catalysts. In Gschneidner, Jr., K.A. (ed.), *Industrial Applications of Rare Earth Elements*, pp. 101–116, ACS Symposium Series 164, American Chemical Society, Washington, D.C.
Wallace, W.E., Craig, R.S., Gupta, H.O., Pedziwiatr, A., Oswald, E., and Schwab, E. (1988) High energy $PrCo_5$ permanent magnets, *Materials Science Forum*, 30: 177–186.
Warf, J.C. (1949) Extraction of cerium (IV) nitrate by tributyl phosphate**,** *J. Am. Chem. Soc*., 64: 3257–3258.
Warf, J.C. and Kerst, W.K. (1953) Studies of the rare earth hydrides, Technical Rept. II on Project NR 356-290 Contract No. 228 (03) Chemistry Department Univ. of Southern California, Office of Naval Research.
Warf, J.C., Donahue, J., and Hardcastle, K. (1957) Chemistry Department, Univ. of Southern California, Office of Naval Research, Technical Rept. II on Project NR 052–390 Contract Nonr. 228 (15).
Wauby, P.E. (1978) Rare earth additions to steel, *Int. Met. Rev.*, 23(2): 74–98.
Weaver, B. (1974) In Marinsky, A. and Marcus, Y. (eds.), *Ion Exchange and Solvent Extraction*, pp. 196–210, Marcel Dekker, New York.
Weaver, B., Kappelmann, F.A., and Topp, A.C. (1953) Quantitative separation of rare earths by liquid–liquid extraction. I. The first kilogram of gadolinium oxide, *J. Am. Chem. Soc.*, 75: 3943–3945.
Weber, M.J. (1979) Rare earth lenses. In Gschneidner, Jr., K.A. and Eyring, L. (eds.), *Handbook on the Chemistry and Physics of Rare Earths*, Vol. 4. pp. 275–316, North Holland, Amsterdam.
Wecker, J. and Schultz, L. (1990) Effect of Zr and Nb additions on the microstructure and the magnetic properties of melt spun Nd–Fe–B and Nd–Fe–Co–B, *J. Magn. Magn. Mater.*, 83: 189–191.
Weeks, M.E. (1956) *Discovery of the Elements*, 6th edn., pp. 695–727, American Chemical Society, Easton (PA).
Weibke, F. (1939) Preparation of lanthanum by electrolysis of its fused chloride, *Z. Elektrochem.*, 45,

518–520.
Welker, T. (1991) Recent developments on phosphors for fluorescent lamps and cathode ray tubes, *J. Lumin*., 48–49: 49–56.
Wernick, J. (1995) Magnetic materials. In Kroschwitz, J.I. and Grant, M.H. (eds.), *Kirk–Othmer Encyclopedia of Chemical Technology*, 4th edn, Vol. 15, pp. 723–788, John Wiley & Sons, New York.
Westendorp, F. F. and Buschow, K.H.J. (1969) Permanent magnets with energy products of 20 million Gauss Oersteds, *Solid State Commun.*, 7: 639–640.
Weterings, K. and Janssen, J. (1985) Recovery of uranium, vanadium, yttrium and rare earths from phosphoric acid by a precipitation method, *Hydrometallurgy*, 15: 173–190.
Wheelwright, E.J. (1973) *Promethium Technology*, American Nuclear Society, Hinsdale, IL.
Williams, J.M. and Huffine, C.L. (1959) Solid state electrolysis of yttrium metal, *Trans. Am. Nucl. Soc.*, 2(1): 29.
Williams, J.M. and Huffine, C.L. (1961) Solid state electrolysis in yttrium metal, *Nucl. Sci. Eng.*, 9: 500–506.
Wilson, T.A. (1991) Mining, refining and marketing of bastnasite and its separated products. In Siribumrungsukha, B., Arrykul, S., Sanguan Sai, P., Pungrassami, T., Sikong, L., and Kooptarnon, K. (eds.), *Proc. Int. Conf. Rare Earth Minerals and Minerals for Electronic Uses*, Jan. 1991, Hat Yai, Thailand, pp. 271–277, Prince of Songkla University, Thailand.
Winckler, C. (1890) *Ber. Deutsch. Chem. Gesell.*, 23: 772.
Winckler, C. (1891) *Ber. Deutsch. Chem. Gesell.*, 24: 873.
World Mining (1966) Molycorp uses solvent extraction to separate europium oxide from rare earths, *World Mining* 2(3): 16–19.
Wu, P.C.S. (1978) Europia as nuclear control material, *Nucl. Tech*., 39: 84.
Wu, C.S., and Segre, E. (1942) Artificial radioactivity of some rare earths, *Phys. Rev.*, 61: 203.
Wu, M.K., Ashburn, J.R., Tong, C.T., Hor, P.H., Meng, R.L., Goa, L., Huang, Z.L., Wang, Q., and Chu, C.W. (1987) Superconductivity at 93 K in a new mixed phase Y–Ba–Cu–O compound system at ambient pressure, *Phys. Rev. Lett.*, 58: 908–910.
Xuefang, X. (1985) In Xu, G. and Xiao, J. (eds.), *New Frontiers in Rare Earth Science and Applications*, vol. 1, pp. 5–10, Science Press, Beijing.
Xujun, W., Xiuzhi, X., Falun, F., and Yongcheng, C. (1985) A study on the Zn–Al–Re alloy preparation by using molten salt electrolysis. In Xu, G. and Xiao, J. (eds.), *New Frontiers in Rare Earth Science and Application*, Vol. I, pp. 476–479, Science Press, Beijing.
Yan, J. and Xiong, J. (1998) Correlation between global NdFeB industry and Chinese rare earth industries. In *Preprints of the Conference, China Magnets*, 18–21 October 1998, Beijing, PR China.
Yntema, L.F. (1930) The separation of europium by electrolytic reduction (Observations of the rare earths XXXV), *J. Am. Chem. Soc.*, 52: 2782–2785.
Yost, R.M., Russel, H., and Garner, C.S. (1947) *The Rare Earth Elements and Their Compounds*, Wiley, New York.
Zadorozhnyi, V.G. (1965) Industrial flotation of sands from titanium–zirconium deposits, *Tsvetnye Metally*, 6 (August): 7–12.
Zadorozhnyi, V.G. (1967) Industrial tests of acid still residues for flotation of titano zirconium sands, *Tsvetnye Metally*, 8 (July): 25–27.
Zhang, B.Z., Lu, K.Y., King, K.C., Wei, W.C., and Wang, W.C. (1982) Rare earth industry in China, *Hydrometallurgy*, 9: 205–210.
Zijlstra, H. and Westendorp, F.F. (1969) Influence of hydrogen on the magnetic properties of $SmCo_5$, *Solid State Commun.*, 7: 857–859.
Zintl E. and Neumayr, S. (1933) Metals and alloys. VIII. Crystal structure of β lanthanum, *Z. Elektrochem.*, 39: 84–86.
Zuttel, A., Chartouni, D., Nutzenadel, Ch., Schlapbach, L., Guether, V., Otto, A., Bartsch, M., and Kotz, L. (1999) Comparison of the electrochemical and gas phase hydrogen sorption processes, *Materials Science Forum*, 315–317: 84–93.
Zwilling, G. and Gschneidner, Jr., K.A. (1978) Fused salt electrorefining of gadolinium, an evaluation of three electrolytes, *J. Less Common Metals*, 60: 221–230.